Equal-order Finite Elements of Hydrostatic Flow Problems

Dissertation
zur Erlangung des Doktorgrades
der Mathematisch-Naturwissenschaftlichen Fakultät
der Christian-Albrechts-Universität zu Kiel

vorgelegt von

Madlen Kimmritz

Kiel, 2013

Erster Gutachter: Prof. Dr. Malte Braack

Zweiter Gutachter: Prof. Dr. Steffen Börm

Tag der mündlichen Prüfung: 08.02.2013

Zum Druck genehmigt: 14.03.2013

gez. Dekan Prof. Dr. Wolfgang J. Duschl

Abstract

Subject of this thesis is the issue of equal-order finite element discretization of hydrostatic flow problems. These flow problems typically arise in geophysical fluid dynamics on large scales and in flat domains. This small aspect ratio between the depth and the horizontal extents of the considered domain allows to efficiently reduce the complexity of the incompressible three dimensional Navier-Stokes equations, which form the basis of geophysical flows. In the resulting set of equations, the vertical momentum equation is replaced by the hydrostatic balance, which thus decouples the vertical pressure variations from the dynamic system, and the dynamically relevant pressure becomes two dimensional. Moreover, the vertical velocity component can be explicitely determined by the horizontal velocity components. Concomitant with this reduction is the replacement of the divergence constraint by a suitably modified version of it. As in the classical framework, it is known that these *hydrostatic flow problems* also show a saddle point structure, and there is a similar uncertainty concerning existence and uniqueness of solutions as is apparent for the classical case.

Although the variational framework has been intensively treated, the issue of the discretization, in particular the finite element discretization of hydrostatic problems has hardly been considered yet. The present work dedicates to this topic. We indicate the tight relation between a finite element discretized hydrostatic flow problem and its two dimensional counterpart with respect to inf-sup stability.

Moreover, we elaborate stabilization techniques in order to result to inf-sup stable schemes and to suitably treat the case of dominant advection. For each of these cases we can draw on classical stabilization schemes. For the isotropic hydrostatic Stokes problem we thus derive and examine residual-based as well as symmetric stabilization schemes. In the appropriate Oseen case we restrict to symmetric stabilization schemes.

Beside the isotropic case, we also consider hydrostatic problems on vertical anisotropic meshes, i.e. although the mesh may be anisotropic, the surface mesh still shows isotropic structure. Therefore we derive an interpolation operator, which has suitable projection and stability properties in three dimensions. An appropriate operator for the two dimensional case for bilinear finite element spaces has been developed in [Bra06]. In this vertical anisotropic context we restrict to symmetric stabilization schemes for both problems, the hydrostatic Stokes and the hydrostatic Oseen problem.

Further, we also examine the hydrostatic Stokes problem on meshes with anisotropy occurring also in the surface mesh. This may be necessary in regions with strong flows in one horizontal direction, e.g. in the Bering strait or along coastlines.

In a following chapter we *shortly* discuss on the time discretization approach, particularly on the issue of pressure correction schemes. These schemes are discussed already in a couple of works for classical flow problems. But a proper analysis is still missing.

Finally, after considering algorithmic aspects, which also includes the topic of parallelization, we numerically validate our theoretical results and numerically illustrate apparent physical phenomena occurring in ocean circulation regimes.

Zusammenfassung

Die vorliegende Arbeit widmet sich der Thematik der Diskretisierung von hydrostatischen Strömungsproblemen mittels Finiter Elemente gleicher Ordnung. Hydrostatische Strömungsprobleme treten typischerweise im Bereich der geophysikalischen Fluiddynamik auf grossen Skalen und in flachen Gebieten auf. Mathematische Grundlage bilden die inkompressiblen dreidimensionalen (3D) Navier-Stokes Gleichungen. Das kleine Aspektverhältnis zwischen der Gebietstiefe und der horizontalen Ausdehnung des Gebietes erlaubt es, die Komplexität der inkompressiblen 3D Navier-Stokes Gleichungen merkbar zu reduzieren. Anwendung der sogenannten *hydrostatischen Approximation*, welches das kleine Aspektverhältnis ausnutzt, führt dazu, dass die vertikale Gleichung der Impulserhaltung durch die hydrostatische Balance ersetzt wird. Dadurch wird der dynamisch relevante Druck zweidimensional (2D) und die vertikale Geschwindigkeit bestimmt sich direkt aus den horizontalen. Einhergehend mit dieser Reduktion ist eine Modifikation der Bedingung der Divergenzfreiheit. Das resultierende *hydrostatische* Strömungsproblem weist bekanntermaßen eine Sattelpunktstruktur auf, ähnlich dem klassischen Problem. Desweiteren herrscht auch im hydrostatischen Kontext eine ähnliche Unsicherheit bezüglich Existenz und Eindeutigkeit von Lösungen vor, wie sie auch in der klassischen Navier-Stokes-Thematik anzutreffen ist.
Obwohl hydrostatische Probleme im variationellen Rahmen intensiv untersucht worden sind und werden, ist das Feld der Diskretisierung dieser Probleme, insbesondere die Finite-Elemente-Diskretisierung, größtenteils unbearbeitet. Die vorliegende Arbeit widmet sich dieser Thematik. Wir zeigen die enge Beziehung auf, die bezüglich der Inf-sup-Stabilität zwischen dem diskreten hydrostatischen Strömungsproblem und seinem 2D Pendant existiert. Desweiteren erarbeiten wir Stabilisierungsverfahren, um Inf-sup-Stabilität zu erlangen und den Fall der dominanten Advektion adäquat zu behandeln. Hierbei können wir auf klassische Stabilisierungsverfahren zurückgreifen.
Neben dem isotropen Fall betrachten wir hydrostatische Probleme auf anisotropen Gittern. Für die Analyse entwickeln wir einen Interpolationsoperator, der passende Projektions- und Stabilitätseigenschaften in 3D besitzt. Ein entsprechender Operator für den 2D Fall für bilineare Finite Elemente wurde in [Bra06] entwickelt. Für die Stabilisierung beschränken wir uns auf symmetrische Verfahren. Die Druckstabilisierung bleibt aufgrund der Dimension des Drucks auf vertikal anisotropen Gitter, d.h. obwohl Gitteranisotropie auftreten kann ist das Oberflächengitter isotrop, isotrop. Im Fall auftretender Gitteranisotropie auch im Horizontalen greifen wir auf anisotrope Druckstabilisierung zurück.
Desweitern diskutieren wir kurz die Thematik der Zeitdiskretisierung. Insbesondere gehen wir auf Druckkorrektur-Verfahren ein. Diese Verfahren wurden bereits für klassische Strömungsprobleme diskutiert. Jedoch fehlt bislang eine Analyse dieser Thematik im hydrostatischen Kontext.
Anschließend betrachten wir algorithmische Aspekte und gehen dabei auch auf die Thematik der Parallelisierung ein. Wir schließen die Arbeit mit einer numerischen Validierung der theoretischen Ergebnisse ab und illustrieren einige Phänomene der Ozeanzirkulation.

Table of Contents

Chapter 1

Introduction

This work is devoted to the issue of stabilization of equal-order finite element discretized hydrostatic flow problems. The set of equations which is largely applied in ocean circulation models is a prominent example of hydrostatic flow problems, such are e.g. the finite difference models MOM3 [GHPR07] and SPEEDO [SH09] or the finite element ocean model described by Danilov et al. [DKS04]. Let me open this topic with the words of the internationally recognized German climate researcher Mojib Latif:

> *"Twentieth century climate exhibits a strong warming trend. There is a broad scientific consensus that the warming contains a significant contribution from enhanced atmospheric greenhouse gas (GHG) concentrations due to anthropogenic emissions. The climate will continue to warm during the 21st century [...], but by how much remains highly uncertain. This is mainly due to three factors: natural variability, model uncertainty, and GHG emission scenario uncertainty. [...] Model uncertainty is important at all lead times. Furthermore, our understanding of the Earth System dynamics is incomplete. Potentially important feedbacks [...] are not well understood and not even taken into account in many model projections. Yet the scientific evidence is overwhelming that global mean surface temperature will exceed a level toward the end of the 21st century that will be unprecedented during the history of mankind, even if strong measures are taken to reduce global GHG emissions. It is this long-term perspective that demands immediate political action." [Lat11]*

We observe the following from this illustrative example of application: There is an eminent interest in reliable predictions concerning the developments in climate, in which the oceanic behavior plays a crucial role. However there is also a variety of uncertainties concerning the (numerical) results of global circulation models. These uncertainties range from the lack of knowledge of the underlying physics to uncertainties with respect to the applied numerical models, e.g. stemming from the parameterization of the scale processes, which are not resolved by the model. To go a step further into the field of uncertainties, the Clay Mathematics Institute put out a reward of one million US$ on "considerable progresses" in the context of existence and uniqueness results of a solution of the 3D Navier-Stokes equations, see also [Son09, Fef], which form the

mathematical fundament of hydrostatic flow equations and are tightly related to the hydrostatic equations occurring in climate and oceanic circulation models. Thus, it is advisable to keep in mind, that results of ocean circulation and climate models are an *attempt* to describe the behavior of the nature as good as possible. Regarding the quality of such models we refer to e.g. [MSB+04, RJ08]. In this work we restrict our attention to the oceanic case and to simplifications of it.

The 3D Navier-Stokes equations with additional diffusion-convection equations for potential temperature and salinity are assumed to describe ocean circulations sufficiently accurate. However, these set of equations are extremely expensive due to the variety of scales in oceanic regimes. Several millions of degrees of freedom are necessary if relevant scales are aimed to be adequately resolved. For oceanic flows, an established approach to reduce this vast amount of degrees of freedom while taking maintainable error is the application of the hydrostatic approximation. This leads to the widely used set of *primitive equations*, see Pedlosky [Ped86]. Due to the assumption of a large aspect ratio between horizontal and vertical scales (which applies to relatively flat domains), the hydrostatic balance, i.e. the effects of gravity, dominates all other components occurring in the vertical part of the momentum balance. Two effects can be observed. First, the vertical velocity component can be eliminated from the dynamical system, demanding the horizontal velocity field to be divergence free in vertical mean. Second, the three dimensional pressure field decomposes into a hydrostatic and a two dimensional hydrodynamic one. The hydrostatic pressure compensates gravitational forces. In hydrostatic equilibrium, it varies only vertically and is dynamically irrelevant. The vertical velocity component can be determined by a set of ordinary differential equations.

Once the set of equations is formulated, the issue of numerical realization arises. Frequently, the finite different approach is applied in ocean circulation models, which mainly is reasoned historically and by their low computational costs. However, the finite element approach enjoys increasing popularity due to its robustness with respect to irregular and rough boundaries of the underlying domain. Moreover, the possibility to use stabilized equal-order finite elements is attractive in terms of higher-order schemes. Up to now, little work has been published on the analysis of such discrete problems. The publications concerning the finite element approach of hydrostatic flow problems known to the author are the following: In the context of inf-sup stable finite elements, in [GR05b] Guillen and Rodriguez designed and analyzed a consistent finite element method for the primitive equations of the ocean. Analysis of stabilized finite element schemes for the hydrostatic approximation of flow problems is done in [CGS12], where the authors considered the orthogonal sub-scales VMS method applied to the hydrostatic approximation of the Oseen problem. Moreover, in [KB12] we constructed several stabilization schemes for the hydrostatic Stokes system and studied them with respect to stability and error estimates. In [Kim12], we dealt the construction and analysis of symmetric stabilization schemes for the hydrostatic Oseen system, which are attractive as they do not exhibit surplus coupling like residual-based schemes.

As already mentioned, the hydrostatic approximation is justified due to the thinness of the domain. In the context of discretization this means, that the applied decomposition

of the domain (grid) either has a very fine resolution in each direction, which cellwise are of similar magnitude, or the resolution is much larger in the horizontal extends than in the vertical one. In the former case we call such a grid *isotropic*. In the latter (*anisotropic*) case, which is the recommendable approach in order to prevent numerical overheads, application of the deductions and the stabilizations of the isotropic case to the anisotropic does not lead to optimal results. Moreover, the applied interpolation operators come up against their limitations. In [Bec95] Becker introduced an interpolation operator for the 2D anisotropic case and bilinear finite element spaces. In [Ape98], Apel dedicated to the field of anisotropic interpolation operators in 2D and 3D for finite elements of arbitrary polynomial order. The issue of inf-sup stable finite elements in the anisotropic framework has been treated in [AM08, AR01, AC00, SSS99, SS98], extensively for the 2D case. Analysis in the anisotropic framework of a linear (non hydrostatic, i.e. *classical*) flow problem in two dimensions, which already shows important characteristics of the Navier-Stokes problem, i.e. the Stokes problem, has been done by [AM08, AR01, AC00, Ric05, BT06a, MPP02]. The appropriate Oseen problem in two dimensions has been treated in [Bra08a], the authors of [LAK06] also treated the three dimensional case. To the authors knowledge, appropriate analysis of stabilized equal-order finite element discretized problems in the hydrostatic framework has not been published yet. We start to close this gap in this work.

In order to algorithmically treat the discretized hydrostatic problems, one can take advantage of the differing dimensions of the three dimensional velocity field and the dynamically relevant hydrodynamic two dimensional pressure. On the one hand, an Uzawa approach can be used or splitting schemes can be applied. These schemes have been invented by [Cho68, Tem68] as time stepping schemes. Several splitting schemes have been invented and analyzed since then, see e.g. [BC08, GMS06, Pro97, Ran92, NP05] in the classical (i.e. non hydrostatic) framework. An analytical extend to the hydrostatic case is not known to the author. In this work, we give an intention of the applicability of a suitable class of splitting schemes in the hydrostatic context. An extensive analysis on this issue however still seems to be missing. A different approach is the coupled solving, which has been done in [CGS12].

Another important issue we touch in this work is the thematic of parallelization, which provides the possibility to handle the vast complexity by distributing the problem to several computing units.

In the following we introduce the structure of the thesis by presenting a short survey of the remaining chapters.

The Primitive Equations of the Ocean

In Chapter 2 we introduce basic notations, such as the definition of the domain or relevant operators, which we apply throughout the work. Starting from a short discussion on our spatial and temporal window of interest, we then introduce the governing equations of hydrodynamics. Afterwards, we present common and important approximations of the oceanic geophysical fluid dynamics regime, which lower the complexity

of the underlying set of equations, one effective approximation being the hydrostatic approximation. We give appropriate initial and boundary conditions and collect important dimensionless numbers, which are used to characterize geophysical flows. The considerations and deductions concerning the primitive equations are collections from the textbooks [Ped86, CRB11, OWE12].

Variational Formulation of Hydrostatic Flow Problems

In Chapter 3 we turn to the variational formulation of the resulting set of equations. We introduce basic notations in the variational context. We consider different hydrostatic problems of different complexity, starting with the stationary Stokes system, turning over to the stationary hydrostatic Oseen problem and to the stationary Navier-Stokes problem and finally consider the appropriate evolutionary cases.
Moreover, we sketch known mechanisms to validate existence and uniqueness in the classical framework and indicate appropriate proving mechanisms for the hydrostatic framework. Within this context we collect regularity results of the appropriate hydrostatic problems and compare those statements to the classical problems. This survey has been done due to two reasons: On the one hand the effect of the hydrostatic approximation on the regularity of the problems is figured out. On the other hand these existence and uniqueness results form the basis in the argumentation in the discrete framework, particularly in the field of error estimates.
The collection of propositions and statements is taken from textbooks and appropriate articles, see the referenced literature in the respective sections. Besides, in Section 3.1.3 we examine and prove relevant properties of the averaging operator and the modified inf-sup constraint, and argue on the impact of the domain anisotropy on the inf-sup constant. The appropriate propositions and remarks are a generalization of the propositions and proofs we did in [KB12] to the common Sobolev spaces of order p. In [KB12] we validated existence and uniqueness of the stationary hydrostatic Stokes problem for $p = 2$ in a classical manner. In the present work we join the results to the results also known from literature.
Moreover, we validate a generalization of the classical Poincaré – Friedrichs inequality to the $\mathrm{W}_0^{1,p}(\Omega)$. We apply this in the Oseen framework.

Equal-Order Finite Element Discretization of Stationary Systems

Chapters 4 and 5 form the heart of this work. In Chapter 4 we start with an introduction of fundamental notations in the finite element framework, ranging from the notions of triangulations and finite element spaces to suitable interpolation operators, which are essential in the proofs of *a priori* error estimates. We describe the mesh restrictions in the hydrostatic framework. Similar to the variational case we examine the discrete counterparts of the averaging operator and the modified inf-sup constraint, both being analyzed in [KB12] and here being generalized to the case of Sobolev spaces of order $p \in (1, \infty)$, which has been done due to the regularity demands in the Oseen framework.

In Sections 4.2 and 4.3 we give an introduction of the stabilization of the 2D Stokes and the 3D Oseen problem, collecting relevant estimates and elaborating propositions, which are applied in the hydrostatic case. Sections 4.4 and 4.5 are devoted to the hydrostatic Stokes and hydrostatic Oseen problem. In each of these cases we introduce the appropriate Galerkin formulation, consider the inf-sup stability property of the equal-order finite element discretization, introduce suitable stabilizations, validate stability and prove optimal *a priori* error estimates. The deductions concerning the hydrostatic Oseen problem is the core of the submitted article [Kim12].

Equal-Order Finite Element Discretization of Stationary Systems on Anisotropic Meshes

Chapter 5 treats the hydrostatic problems formulated on (vertical) anisotropic meshes. As already indicated, these examinations and elaborations demand application of different interpolation operators and stabilization schemes. Section 5.1.1 introduces the notion of anisotropic meshes. In particular, we elaborate an inverse estimate for anisotropic tensor product type meshes, which we apply in the construction of an H^1-stable projection operator in 3D. Section 5.1.2 presents important interpolation operators in the anisotropic framework. In the context of the anisotropic Scott-Zhang interpolation operator we present the 2D anisotropic H^1-stable projection operator for bilinear finite element spaces as developed in [Bra06] and transfer the deductions to the 3D case on finite element spaces of arbitrary polynomial order r on tensor product type meshes. These deductions use the results and proofs of [Ape98]. In Section 5.1.3 we once again turn to the examination of the vertical averaging operator and the modified inf-sup condition. Section 5.2 and 5.3 then treat the hydrostatic Stokes and the hydrostatic Oseen problem in the vertical anisotropic framework. This means, that we presume an isotropic surface mesh and allow for anisotropy in the vertical direction.

Discretization of Evolutionary Hydrostatic Systems

Chapter 6 examines the algorithmic treatment of evolutionary flow problems. We introduce the topic of splitting schemes, as they provide an approach to deal with the different dimensions occurring in hydrostatic flow problems. Due to their suitability in the hydrostatic framework, we go further into the topic of pressure correction schemes. In Section 6.3 we examine the adaption of pressure correction schemes to the hydrostatic framework. We introduce the treatment of the modified inf-sup constraint and examine the questions, whether the ideas and functionalities of pressure corrections schemes (designed for classical flow problems) are transferable to the hydrostatic case. We finally introduce a suitable adaption of the pressure correction schemes to stabilized hydrostatic problems.

Algorithmic Issues

In Chapter 7 we recall the algorithmic realization of the deduced problems, introducing the Uzawa approach as well as the possibility to resort to the concept of pressure correction schemes. The fundamentals of the appropriate sections are given in Appendix B, which in turn are based on the textbooks [Mei11, Hac93, BBC+94, Saa03].

We also consider concepts of parallelization in the hydrostatic framework. A further background on the topic of parallelization can be found in [KR11], where we discuss the parallel multigrid smoother and prove the smoothing property of the parallel iteration for a simple model example.

Numerical Examples

In Chapter 8 we validate the theoretical results of Chapter 4, consider physical phenomena, which are apparent in ocean circulation and use one of the schemes deduced in Chapter 6. Finally, a presentation of an application of the parallelization to the hydrostatic framework can be found in [KR11], where we adapted the concept of parallelization to a hydrostatic flow problem.

Conclusions and Perspectives

This work closes with Chapter 9, in which we summarize the core results of the thesis and discuss open questions and show possible future work on this topic.

Chapter 2

The Primitive Equations of the Ocean

The basic equations of hydrodynamics suitably describe the flows in the air, the ocean and on land, each regime having its own special features. Moreover, dependent on the area of interest, different characteristics of the considered flow come to the fore, while others take a back seat. Before starting to model the set of equations we thus have to clarify our focus of interest. Regarding the underlying scheme, appropriate, relevant processes then can be figured out.

This chapter is structured as follows: Preliminary, we introduce basic notations, such as the definition of the domain or relevant operators. Starting from a short discussion on our spatial and temporal window of interest, we then introduce the governing equations of hydrodynamics. Afterwards, we present common and important approximations of the oceanic geophysical fluid dynamics regime, which lower the complexity of the underlying set of equations. We give appropriate initial and boundary conditions and collect important dimensionless numbers, which are used to characterize geophysical flows.

The following deductions are based on the text books [Ped86, CRB11, OWE12]. As we do not aim to go too deep into details, we refer to the cited literature for deeper insights into this topic.

Without loss of generality we use the Eulerian representation, i.e. alterations of fluid particles are observed from a fix point in space, instead of following that particle (Lagrangian representation). For ease of simplified argumentation, we apply Cartesian coordinates, which corresponds to mapping the problem onto a plane. This is sufficiently accurate, if the dimension of the considered domain is much less than the radius of the earth. Due to [CRB11], this approach is maintainable for domains with dimension up to about 1000 km.

2.1 Preliminaries

Throughout this work we consider the domain

$$\Omega \;:=\; \{\boldsymbol{x} = (x, y, z) \in \mathbb{R}^3 \mid (x, y) \in \omega \text{ and } z \in (-d(x, y), 0)\}$$

with the 2D surface domain $\omega \subset \mathbb{R}^2$and a positive depth function $d : \overline{\omega} \to \mathbb{R}_{\geq 0}$. The minimal depth of Ω is denoted as

$$\delta_{min} := \min\{d(x, y) \,|\, (x, y) \in \omega\}\,,$$

the maximal depth as

$$\delta_{max} := \max\{d(x, y) \,|\, (x, y) \in \omega\}\,.$$

If $\mathrm{diam}\omega/\delta_{max} \ll 1$, we denote Ω as *flat*. We classify the following boundary parts:

(a) the upper surface $\Gamma_u := \omega \times \{0\}$,

(b) side walls $\Gamma_s := \{\boldsymbol{x} \in \mathbb{R}^3 \,|\, (x, y) \in \partial\omega \text{ and } z \in [-d(x, y), 0]\,\}$ and

(c) the bottom $\Gamma_b := \{\boldsymbol{x} \in \mathbb{R}^3 \,|\, (x, y) \in \omega \text{ and } z = -d(x, y)\,\}$.

The latter two boundary parts are united to $\Gamma_w = \Gamma_s \cup \Gamma_b$. In particular, the changes in the sea surface height are not considered in the definition of Ω. For ease of simplicity, these are completely neglected in the upcoming and the approximation of a rigid lid is applied. For a more differentiated approach, the reader is referred to [CRB11]. Moreover, we assume a basin, which has no influx and no out flux, i.e. the side walls Γ_s are assumed to be rigid.

The time span of interest is denoted as $(0, \mathcal{T})$.

The gradient of a scalar field $v \in \mathcal{C}^1(\overline{\Omega}, \mathbb{R})$ is denoted as $\nabla v := (\partial_x v,\, \partial_y v,\, \partial_z v)$. Given a vector field $\boldsymbol{v} \in \mathcal{C}^1(\overline{\Omega}, \mathbb{R}^3)$ with components v_1, v_2 and v_3, the divergence operator is defined as $\mathrm{div}\ \boldsymbol{v} := \partial_x v_1 + \partial_y v_2 + \partial_z v_3$. For any scalar field $v \in \mathcal{C}^2(\overline{\Omega}, \mathbb{R}^3)$, the Laplacian operator Δ is given as $\Delta v := \mathrm{div}\,\nabla v$.

We introduce a different notation for the two dimensional (2D) case: Given a scalar field $w \in \mathcal{C}^1(\overline{\omega}, \mathbb{R})$, the gradient is given by $\nabla' w := (\partial_x w,\, \partial_y w)$. The 2D divergence operator is denoted as $\mathrm{div}'\,\boldsymbol{w} := \partial_x w_1 + \partial_y w_2$for any $\boldsymbol{w} \in \mathcal{C}^1(\overline{\omega}, \mathbb{R}^2)$ with components w_1 and w_2. Appropriately, the 2D Laplacian is defined as $\Delta' w := \mathrm{div}'\nabla' w$ for any $w \in \mathcal{C}^2(\overline{\omega}, \mathbb{R}^2)$.

Given a vector $\boldsymbol{\alpha} := (\alpha_1,\, \alpha_2,\, \alpha_3)^\top$, $\alpha_i \geq 0$ for $i \in \{1, 2, 3\}$, and a vector valued, sufficiently regular $\boldsymbol{\varphi} := (\varphi_1, \varphi_2, \varphi_3)^\top$, the modified divergence operator $\mathrm{div}_{\boldsymbol{\alpha}}\cdot$ and the gradient operator $\nabla_{\boldsymbol{\alpha}}\cdot$are given by

$$\mathrm{div}_{\boldsymbol{\alpha}}\,\boldsymbol{\varphi} := \partial_x(\alpha_1^{1/2}\varphi_1) + \partial_y(\alpha_2^{1/2}\varphi_2) + \partial_z(\alpha_3^{1/2}\varphi_3) \tag{2.1}$$

$$\nabla_{\boldsymbol{\alpha}}\varphi := (\alpha_1^{1/2}\partial_x\varphi,\ \alpha_2^{1/2}\partial_y\varphi,\ \alpha_3^{1/2}\partial_z\varphi)^\top\,. \tag{2.2}$$

The modified Laplacian is defined as

$$\Delta_{\boldsymbol{\alpha}}\varphi := \operatorname{div}_{\boldsymbol{\alpha}}\nabla_{\boldsymbol{\alpha}}\varphi\,, \tag{2.3}$$

imposing sufficient regularity for φ. The vector valued modified Laplacian is also denoted by $\Delta_{\boldsymbol{\alpha}}$.

Moreover, we abbreviate the pointwise vertical integration as $\mathbf{M} : \mathcal{C}(\overline{\Omega}) \to \mathcal{C}(\overline{\omega})$, which is defined by

$$\mathbf{M}\, v\,(x,y) := \int\limits_{-d(x,y)}^{0} v\,(x,y,\widehat{z})\, d\widehat{z}\,. \tag{2.4}$$

The vector-valued operator is also denoted as $\mathbf{M}$.

2.2 Scales

The ocean exhibits a wide range of processes, which show very different temporal and spatial variating behavior. In order to describe them, the notion of *scales* is applied. *Scales of motions* are dimensional quantities, which represent the quantitative magnitude of the variable of interest. They are rather estimates, than precisely defined.

In [CRB11], the notion of scales is given as follows: For a given variable v, the time scale T is the time period, in which v changes significantly by a typical value V . The spatial scale L is denoted similarly. E.g. considering an oceanic gyre, we could fix T as the time, a particle in this gyre needs to carry out one cycle, V as the mean velocity of that particle and L as the diameter of that cycle. In [SDT06], the authors present a more sophisticated approach via spatio-temporal correlation functions.

Figure 2.1 illustrates the vast amount of different acting processes occurring in the ocean. Such are e.g. turbulent eddies, which last from seconds to minutes and vary centimeterwise, and the oceanic conveyor belt, which acts over thousands of kilometers and exhibit temporal cycles, which may span centuries.

No model can include all these processes. This can be highlighted by the following: Assume a set of equations, which describes ocean physics down to a minimal length scale of 1 cm with appropriate initial value. The earth's surface is about $5,1 \times 10^8 km^2$, the ocean covers 70.8%, i.e. $361 \times 10^{16} cm^2$. Thus, already the storage of one single 2D variable at a particular time necessitates 28.8 PB memory on a 64 bit architecture. Compare this to the memory capacity of the NASA *Columbia Supercomputer* [1], which currently has a filesystem capacity of 9.3 PB [2]. The attempt to model *all* physics from small to large scale over centuries in order to gain suitable climate forecast is impracticable.

[1] see http://www.nas.nasa.gov/hecc/resources/columbia.html

[2] see http://www.nas.nasa.gov/assets/pdf/papers/2011_NAS_User_Survey_Results.pdf

An alternative is given by the fact, that due to the phenomena of interest, certain physical processes are relevant, while others are negligible: Modeling oceanic flows is always based on a certain question of interest. This may be microscale turbulent structures, see e.g. [WCd+11], or, of currently prominent interest, the spread of radioactive water originating from the Fukushima nuclear reactor disaster, see e.g. [BSLB12]. Clearly, in the former case microstructural processes are important, whereas major currents with spatial scales of hundreds of kilometers are no matter of concern. However, in the latter case, tides have insignificant impact but major currents are the focus point. Note, that processes of different scales interact. To prevent computational overhead treating this interaction suitably, parameterizing the effects of the non considered scales is a common approach.

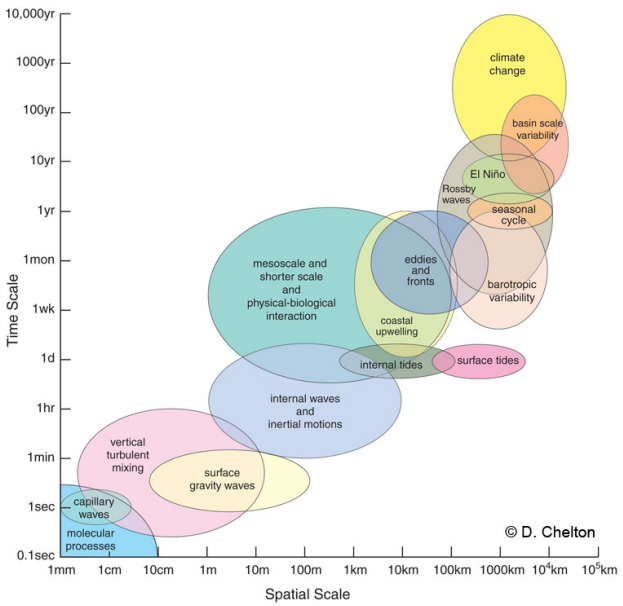

Figure 2.1: Time and spatial scales of oceanic processes. Figure courtesy of Dudley Chelton, Oregon State University

Concluding, dependent on the underlying question, different sets of equations evolve, and before beginning to model oceanic flows, the question of scales has to be clarified.

Oceanic geophysical fluid dynamics, i.e. our regime of interest, take place in domains whose horizontal expansions are much larger than the vertical one. E.g., the Atlantic Ocean has widths ranging from 1 500 km at its narrowest region to more than 13 000 km in its north-south extend, while its typical depth is 3-4 km. Thus, the vertical length scale H is expected to be much larger than the horizontal length scale L. [CRB11] present typical scales, see also Table 2.1.

Scale	horizontal length scale L	vertical length scale H	time scale T
Value	10 km	100 m	$\geq$ 1 day

Table 2.1: Typical spatial and time scales for oceanic flows.

2.3 Conservation laws and equation of state

In this section we introduce the major physical principles, fluid dynamics are based on. We deduce a complete set of equations, which describes geophysical flows, comprising the momentum equation and the equation of mass conservation, but also the equation

of state, which determines the density and involves two further equations for salinity and temperature.

2.3.1 Conservation laws

Oceanic flows are covered by two major physical principles, *conservation of mass* and *conservation of momentum*. Conservation laws are of the following structure: Let ψ be a (conservative) property of interest. Given a mass element of arbitrary but fix volume V of the fluid, the time variation, i.e. the total derivative ($D_t \cdot := \partial_t \cdot + (\boldsymbol{v} \cdot \nabla)\cdot$), of ψ

$$\int_V D_t(\rho\psi)dV = \int_V \left(\partial_t(\rho\psi) + (\boldsymbol{v} \cdot \nabla)(\rho\psi)\right) dV \text{ (per volume } V) \quad \text{and} \tag{2.5}$$

$$\int_V D_t\psi dV = \int_V \left(\partial_t\psi + (\boldsymbol{v} \cdot \nabla)\psi\right) dV \quad (\text{per mass } \textstyle\int_V \rho dV) \tag{2.6}$$

can either vary due to

1. *transport* $\int_V -\text{div}\,(\rho\psi\boldsymbol{v} + \boldsymbol{J}_\psi)dV$ (per volume) and $\int_V -\text{div}\,(\psi\boldsymbol{v} + \boldsymbol{J}_\psi)dV$ (per mass), or
2. *sources and sinks* $\int_V C_\psi dV$.

The terms $\rho\psi\boldsymbol{v}$ and $\psi\boldsymbol{v}$ denote advective fluxes and $\boldsymbol{J}_\psi$ the non-advective one. Thus, changes in the total amount of ψ can be described by

$$\partial_t \int_V \rho\psi dV = \int_V \left(-\text{div}\,(\rho\psi\boldsymbol{v} + \boldsymbol{J}_\psi) + C_\psi\right) dV \quad \text{and} \tag{2.7}$$

$$\partial_t \int_V \psi dV = \int_V \left(-\text{div}\,(\psi\boldsymbol{v} + \boldsymbol{J}_\psi) + C_\psi\right) dV,$$

respectively. As V is arbitrarily chosen, equations (2.5) and (2.6) can be replaced in a limiting process by the *conservation laws*

$$\partial_t\rho\psi = -\text{div}\,(\rho\psi\boldsymbol{v} + \boldsymbol{J}_\psi) + C_\psi \quad \text{and} \quad \partial_t\psi = -\text{div}\,(\psi\boldsymbol{v} + \boldsymbol{J}_\psi) + C_\psi, \tag{2.8}$$

respectively.

2.3.2 Mass budget

In the ocean, the only mass exchange takes place at boundaries, e.g. at the air-sea interface, where precipitation and evaporation take place, and boundaries with in- and outflows, e.g. due to rivers. Thus, in the inner part of the ocean no mass sinks, sources or non-advective fluxes are apparent and the conservation law (per volume) for mass becomes

$$\partial_t\rho = -\text{div}\,(\rho\boldsymbol{v}).$$

2.3.3 Momentum budget

Momentum is defined as mass × velocity. Due to *Newton's 2nd law of motion* (force = mass × acceleration), the conservation law (per mass) of momentum can be described as

$$D_t(\rho \boldsymbol{v}) = \boldsymbol{f},$$

whereas $\boldsymbol{f}$ collects volume and surface forces. In the scale ranges of ocean circulation models, the *volume force* is governed by gravity and rotation, i.e. we set

$$\boldsymbol{f}^v = -\rho \boldsymbol{g} - \boldsymbol{\Theta} \times \boldsymbol{v}$$

with acceleration of gravity $\boldsymbol{g} = (0,\, 0,\, \mathrm{g}\,)^\top m s^{-2}$ and an angular velocity of the earth $\boldsymbol{\Theta} = (0\,, 0\,, \mathrm{f}\,)^\top s^{-1}$. The constant of gravity acceleration is given by $\mathrm{g} = -9.81$, the Coriolis parameter by $\mathrm{f} = 7.29 \times 10^{-4} \sin\varphi$ with latitude φ. Note, that both, $\boldsymbol{g}$ and $\boldsymbol{\Theta}$, are approximately given.

The *surface force* occurs due to deformation of the mass element and is given by $\boldsymbol{f}^s = \operatorname{div} \Pi$ with symmetric stress tensor Π. The mean normal force per area is given by $p = -\frac{1}{3}\mathrm{trace}(\Pi)$, i.e. the pressure. The tangential stresses are denoted by the friction tensor Σ. For Newtonian fluids, such as the ocean, the friction force can be sufficiently accurate formulated as

$$\operatorname{div} \Sigma = \operatorname{div}(\mu \nabla \boldsymbol{v}) + \frac{\mu}{3} \nabla(\operatorname{div} \boldsymbol{v})$$

with molecular viscosity μ. Thus, the equation for conservation of momentum finally reads

$$D_t(\rho\, \boldsymbol{v}) = -\rho \boldsymbol{g} - \boldsymbol{\Theta} \times \boldsymbol{v} - \nabla p + \operatorname{div}(\mu \nabla \boldsymbol{v}) + \frac{\mu}{3} \nabla(\operatorname{div} \boldsymbol{v}).$$

Remark 2.1. *In [CRB11] it is anticipated, that the rotation of the earth has to be taken into account, only if the motion of the fluid evolves on a time scale T, which is larger than the time of one rotation, i.e. if $T \geq 2\pi/|\boldsymbol{\theta}| \approx 24h$.*

2.3.4 Equation of state

For completeness of the given problem, an equation for the density field ρ is still missing, the equation of state. In the ocean, ρ varies due to fluctuations of pressure p, temperature T and salinity S, i.e. $\rho = \rho(p, T, S)$, see [Gil82]. However, as water is almost incompressible, $\rho = \rho(T, S)$ is assumed for most applications with

$$\rho = \rho_0 \big\{ 1 - \alpha(T - T_0) + \beta(S - S_0) \big\}.$$

The coefficients and reference values are the thermal expansion coefficient $\alpha = 1.7 \times 10^{-4} K^{-1}$, the saline contraction coefficient $\beta = 7.6 \times 10^{-4}\, psu^{-1}$ and reference values $\rho_0 = 1028 kg\, m^{-3}$, $T_0 = 10°C = 283K$ and $S_0 = 35\, psu$.

2.3.5 Energy and salt budget

The temperature equation is based on the principle of energy conservation, i.e. the *1st law of thermodynamics*. It states, that the internal energy e of an element is the difference between the received heat Q and the mechanical work W performed by the element onto the ambient fluid, i.e.

$$D_t e = Q - W.$$

The relation between e and T is given by $e = c_V T$ with heat capacity $c_V = 3990 J\, kg^{-1} K^{-1}$ at constant volume.

In oceanic regimes no internal heat sources are apparent, i.e. the received heat Q solely consists of that heat, the considered element gains from its ambience by dissipative processes, i.e. $Q = k_T \rho^{-1} \Delta T$ with thermal conductivity constant k_T.

As seawater is almost incompressible, the mechanical work W, performed by the considered element, is neglected, i.e. the temperature equation becomes

$$\rho c_V D_t T = k_T \Delta T.$$

For the derivation of an equation for the salt budget, it is assumed, that seawater elements conserve their salt budgets, except for diffusive transport, i.e.

$$D_t S = \kappa_S \Delta S$$

with coefficient κ_s of salt diffusion.

2.4 Approximations

In this section we introduce the most relevant approximations, applied in the framework of geophysical fluid dynamics. These are first, the Boussinesq approximation, where the "almost incompressibility" of the fluid is of advantage. Second, the Reynolds average and parameterization of turbulence are applied, where small-scale processes are filtered out of the governing set of equations (Reynolds averaging) and the impact of the processes of the unresolved scales on the resolved processes are modeled (parameterization of turbulence). Third, the hydrostatic approximation is applied, in which the vertical momentum equation reduces to the equation of the hydrostatic balance, which adjusts, when the fluid is in equilibrium. This approximation effects, that the dynamically relevant pressure and the vertical velocity field become diagnostical, i.e. can be determined by the remaining ones. Under the assumption of a constant density (note, that the oceanic flow is almost incompressible), this approximation even effects, that the pressure becomes completely 2D.

Note, that there are lots of approximations, which are not mentioned in this chapter, such as the plane approximation or the representation of the different potentials occurring in the body forces of the momentum equations. For more detailed information on these issues we refer to [Ped86, CRB11, OWE12].

2.4.1 Boussinesq approximation

In the ocean, the variations of the density ρ are small compared to its constant mean value ρ_0:

$$\rho = \rho_0 + \widetilde{\rho} \quad \text{with} \quad \rho_0 = 1028\, kg\, m^{-3} \quad \text{and} \quad |\widetilde{\rho}| \leq 3\, kg\, m^{-3}.$$

Note, that ρ_0 is supposed to be the density, which adjusts, if the fluid is in equilibrium state, also called the *state of rest*. Applicating the Boussinesq approximation means to replace each occurrence of ρ by its approximative mean ρ_0, unless $\widetilde{\rho}$ is dynamically relevant. A first application converts the equation for the mass budget,

$$D_t\widetilde{\rho} + \widetilde{\rho}(\text{div } \boldsymbol{v}) + \rho_0(\text{div } \boldsymbol{v}) = 0\,, \tag{2.9}$$

into volume conservation: The total derivative $D_t\widetilde{\rho}$ is observed to be smaller than the second term on the left hand side of (2.9), see [CRB11], which again is of the order 10^{-3} times smaller than the last term, due to $\widetilde{\rho}/\rho_0$ being of order 10^{-3}. Thus, the first two terms of (2.9) can be neglected and the velocity field can be regarded as divergence free (or volume conserving):

$$\text{div } \boldsymbol{v} = 0\,. \tag{2.10}$$

This equation is also called *continuity equation* in the mathematical framework. Considering the total derivative $D_t(\rho\ \boldsymbol{v}) = \rho\, D_t\, \boldsymbol{v} + (D_t\widetilde{\rho})\ \boldsymbol{v}$ of the momentum equation, the latter term can be neglected, using the scaling arguments for $D_t\widetilde{\rho}$ as presented above, and the equation of volume conservation (2.10). Approximating $\rho\, D_t\, \boldsymbol{v}$ by $\rho_0\, D_t\, \boldsymbol{v}$ and recalling volume conservation results in

$$\rho_0 D_t\, \boldsymbol{v} = -\rho \boldsymbol{g} - \boldsymbol{\Theta} \times \boldsymbol{v} - \nabla p + \text{div}\,(\mu \nabla \boldsymbol{v}).$$

Due to $\boldsymbol{g} = (0\,, 0, \mathrm{g}\,)^\top m\, s^{-2}$, the remaining impact of the non constant density $\rho = \rho_0 + \widetilde{\rho}$ on the momentum solely acts on the vertical momentum equation by the terms $\rho_0 \mathrm{g} + \widetilde{\rho}\mathrm{g}$. The former term, $\rho_0\mathrm{g}$, accompanies a pressure p_0, that, in the state of rest, adjusts due to the gravity force, and is given by

$$p_0(z) = P_0 - \rho_0 g z \tag{2.11}$$

with surface pressure P_0 and $p = p_0 + \widetilde{p}$. The pressure p_0 is called *hydrostatic* and $\widetilde{p}$ *hydrodynamic*. The relation between ρ_0 and p_0 becomes comprehensive, if the momentum equation is considered in the state of rest, in which the velocity field is $\boldsymbol{v}_0 = \boldsymbol{0}$. Thus, the momentum equation becomes

$$D_t\, \boldsymbol{v} = -\frac{\widetilde{\rho}}{\rho_0}\boldsymbol{g} - \frac{1}{\rho_0}\boldsymbol{\Theta} \times \boldsymbol{v} - \frac{1}{\rho_0}\nabla\widetilde{p} + \text{div}\,(\nu \nabla \boldsymbol{v})$$

with kinematic viscosity $\nu := \mu\rho_0^{-1}$.

In a similar fashion, the temperature equation can be approximated as

$$D_t T = \kappa_T \Delta T$$

with heat kinematic diffusivity $\kappa_T = k_T(\rho_0 c_V)^{-1}$. Note, that the equation of salt conservation resulted from a conservation law, formulated per mass. Thus, the Boussinesq approximation is not applied for this equation. For the choice of appropriate values for κ_S and κ_T, the authors of [CRB11] state, that molecular diffusion mainly effects small-scale processes. The authors suggest to account for the apparency of turbulence and to set the diffusivity coefficients κ_S and κ_T to the frequently applied larger value $\kappa_S = \kappa_T = \kappa := 10^{-2} m^2 s^{-1}$.

2.4.2 Reynolds average and parameterization of turbulence

Recall that, on the one hand, oceanic flows contain a broad and interacting spectrum of scales of motion, and that on the other hand, the focus of oceanic fluid dynamics is clearly on large scale behavior, not on small-scale ones. In contrast, the deduction of the present set of equations occasionally resulted from considerations on molecular scale.

Two tasks arise: a) to filter out the small-scale processes of the present set of equations and b) to parameterize the impact of those small-scale processes, which are relevant for the large-scale scenario.

To meet the first task, a given field u is decomposed, such that

$$u = \langle u \rangle + u' \quad \text{with} \quad \langle\langle u \rangle\rangle = \langle u \rangle \quad \text{and} \quad \langle u' \rangle = 0 \tag{2.12}$$

applies, whereas $\langle u \rangle$ denotes a mean, e.g. the temporal average with sufficiently large and small enough time interval, and fluctuations u' from that mean value. Quantity $\langle u \rangle$ is called *Reynolds average of* u and is the quantity of interest in the upcoming model. For different common averaging techniques see [SDT06].

Due to (2.12), Reynolds averaging the linear terms results in swapping the involved quantity $\boldsymbol{\phi}$ by $\langle \boldsymbol{\phi} \rangle$. Applying the averaging to the nonlinear terms results in

$$\langle \boldsymbol{\phi}\, \boldsymbol{\psi} \rangle = \langle \boldsymbol{\phi} \rangle \, \langle \boldsymbol{\psi} \rangle + \langle \boldsymbol{\phi}'\, \boldsymbol{\psi}' \rangle \,.$$

Thus, the Reynolds-averaged set of equation is

$$\begin{aligned}
\operatorname{div} \langle \boldsymbol{v} \rangle &= 0 \\
\partial_t \langle \boldsymbol{v} \rangle + (\langle \boldsymbol{v} \rangle \cdot \nabla) \langle \boldsymbol{v} \rangle + \nabla \langle \boldsymbol{v}'\, \boldsymbol{v}' \rangle &= -\frac{\langle \widetilde{\rho} \rangle}{\rho_0} \boldsymbol{g} - \frac{1}{\rho_0} \boldsymbol{\Theta} \times \langle \boldsymbol{v} \rangle - \frac{1}{\rho_0} \nabla \langle \widetilde{p} \rangle + \operatorname{div} \left(\nu \nabla \langle \boldsymbol{v} \rangle \right) \\
\partial_t \langle T \rangle + (\langle \boldsymbol{v} \rangle \cdot \nabla) \langle T \rangle + \operatorname{div} \langle \boldsymbol{v}'\, T' \rangle &= \kappa \Delta \langle T \rangle \\
\partial_t \langle S \rangle + (\langle \boldsymbol{v} \rangle \cdot \nabla) \langle S \rangle + \operatorname{div} \langle \boldsymbol{v}'\, S' \rangle &= \kappa \Delta \langle S \rangle \\
\langle \widetilde{\rho} \rangle &= \rho_0 \big\{ \beta (\langle S \rangle - S_0) - \alpha (\langle T \rangle - T_0) \big\},
\end{aligned}$$

which basically coincides with the non-averaged set, except for the additional terms $\nabla \langle \boldsymbol{v}'\, \boldsymbol{v}' \rangle$, $\operatorname{div} \langle \boldsymbol{v}'\, T' \rangle$ and $\operatorname{div} \langle \boldsymbol{v}'\, S' \rangle$. These terms represent the effect of the turbulent,

unresolved scales on the resolved ones. The term $\nabla\langle \boldsymbol{v}'\,\boldsymbol{v}'\rangle$ is given by

$$\nabla\langle \boldsymbol{v}'\,\boldsymbol{v}'\rangle = \begin{pmatrix} \partial_x\langle u'u'\rangle + \partial_y\langle v'u'\rangle + \partial_z\langle w'u'\rangle \\ \partial_x\langle u'v'\rangle + \partial_y\langle v'v'\rangle + \partial_z\langle w'v'\rangle \\ \partial_x\langle u'w'\rangle + \partial_y\langle v'w'\rangle + \partial_z\langle w'w'\rangle \end{pmatrix}.$$

At this point, the second task, i.e. parameterizing the unresolved but relevant small-scale processes, is imposed. This task opens the challenging field of turbulence parameterization. A survey of and insight into this topic is given by [SDT06]. A frequently used approach is proposed by Smagorinsky. We do not discuss this approach here, but refer to [Sma63].

We apply the approach of replacing the terms $\nabla\langle \boldsymbol{v}'\,\boldsymbol{v}'\rangle$, $\operatorname{div}\langle \boldsymbol{v}'\,T'\rangle$ and $\operatorname{div}\langle \boldsymbol{v}'\,S'\rangle$ with the primary turbulent effect, diffusion (or dissipation) of the resolved quantities, see also [Ped86, CRB11]. Due to the anisotropic behavior of large-scale oceanic flows, the appropriate eddy viscosity coefficients are distinguished between horizonal and vertical ones. Both are considered to be much larger than the kinematic viscosity ν. [CRB11] suggests to assume one common horizontal eddy viscosity $\mathcal{A}_h$ for each of the horizontal small-scale parameterizations. Due to the different turbulent behavior of salinity and temperature on the one hand and velocity on the other hand, a vertical eddy diffusivity κ_E is introduced for the former state variables, and a vertical eddy viscosity ν_E for the velocity. Both, κ_E and ν_E are much smaller than $\mathcal{A}_h$, i.e. $\kappa, \nu_E \ll \mathcal{A}_h$. [Ped86] suggests the estimates $10^5 - 10^8 cm^2 s^{-1}$ for $\mathcal{A}_h$ and $1 - 10^3 cm^2 s^{-1}$ for ν_E.

For ease of presentation, we skip the brackets of the Reynolds averaging in the upcoming and denote the Reynolds averaged quantities as $\boldsymbol{v}, \widetilde{p}, T, S, \widetilde{\rho}$. Defining the eddy viscosity vector $\boldsymbol{\mathcal{A}}_\nu := (\mathcal{A}_h,\, \mathcal{A}_h,\, \nu_E)^\top$ and the diffusivity vector $\boldsymbol{\mathcal{A}}_\kappa := (\mathcal{A}_h,\, \mathcal{A}_h,\, \kappa_E)^\top$, we apply the notation (2.3). The Reynolds averaged set of equations with the introduced parameterization of unresolved small-scale processes is given by:

$$\begin{aligned} \operatorname{div} \boldsymbol{v} &= 0 \\ \partial_t \boldsymbol{v} + (\boldsymbol{v}\cdot\nabla)\,\boldsymbol{v} &= -\frac{\widetilde{\rho}}{\rho_0}\boldsymbol{g} - \frac{1}{\rho_0}\boldsymbol{\Theta}\times\boldsymbol{v} - \frac{1}{\rho_0}\nabla\widetilde{p} + \Delta_{\boldsymbol{\mathcal{A}}_\nu}\boldsymbol{v} \\ \partial_t T + (\boldsymbol{v}\cdot\nabla)T &= \Delta_{\boldsymbol{\mathcal{A}}_\kappa} T \\ \partial_t S + (\boldsymbol{v}\cdot\nabla)S &= \Delta_{\boldsymbol{\mathcal{A}}_\kappa} S \\ \widetilde{\rho} &= \rho_0\big\{\beta(S - S_0) - \alpha(T - T_0)\big\}. \end{aligned}$$

2.4.3 Hydrostatic approximation

The set of equations received at the end of the preceding section is also known as the 3D incompressible Navier-Stokes equations, here formulated in a rotating frame, with anisotropic viscosities and coupled with convection - diffusion equations for temperature and salinity, which in turn couple to the Navier-Stokes equations via the forcing of the momentum equations. Although this set of equations already went through a lot of approximations (lots of them not being mentioned here), this set is still too complex for applications in geophysical fluid dynamics. In order to reduce this system

noticeably while maintaining the basic physical structure we do some scale analysis, see also [Ped86, CRB11], and, at the end of this section, end up in the hydrostatic approximation of the 3D incompressible Navier-Stokes equations.

As introduced in Section 2.2, the ratio between vertical and horizontal length scales is small, i.e. $a := HL^{-1} \ll 1$. For oceanic flow scenarios a is of order 10^{-2} to 10^{-3}. A consequence of this ratio results if the continuity equation is considered:

$$\frac{\partial v_1}{\partial x} + \frac{\partial v_2}{\partial y} + \frac{\partial v_3}{\partial z} = 0.$$

Let U be the scale of the horizontal velocities v_1 and v_2, W be the scale of the vertical velocity v_3 and L and H be the horizontal and vertical length scales, respectively. Moreover, P denotes the scale of the pressure p. The first two terms are both of order U/L. The last one is of order W/H, which in turn is of order U/L. Due to the small aspect ratio we observe

$$W = aU\,.$$

Furthermore, let T be the time scale and have a look at the momentum equations. Each term in momentum equations we assign the appropriate scale in a subsequent line:

$$\begin{array}{lllllllll}
\dfrac{\partial v_1}{\partial t} & +v_1\dfrac{\partial v_1}{\partial x} & +v_2\dfrac{\partial v_1}{\partial y} & +v_3\dfrac{\partial v_1}{\partial z} & -\mathcal{A}_h\dfrac{\partial^2 v_1}{\partial x^2} & -\mathcal{A}_h\dfrac{\partial^2 v_1}{\partial y^2} & -\nu_E\dfrac{\partial^2 v_1}{\partial z^2} & -\mathrm{f}\,v_2 + \dfrac{1}{\rho_0}\dfrac{\partial \widetilde{p}}{\partial x} = 0 \\
\dfrac{U}{T} & \dfrac{U^2}{L} & \dfrac{U^2}{L} & \dfrac{UW}{H} & \mathcal{A}_h\dfrac{U}{L^2} & \mathcal{A}_h\dfrac{U}{L^2} & \nu_E\dfrac{U}{H^2} & \mathrm{f}\,U \quad \dfrac{P}{\rho_0 L}
\end{array}$$

$$\begin{array}{lllllllll}
\dfrac{\partial v_2}{\partial t} & +v_1\dfrac{\partial v_2}{\partial x} & +v_2\dfrac{\partial v_2}{\partial y} & +v_3\dfrac{\partial v_2}{\partial z} & -\mathcal{A}_h\dfrac{\partial^2 v_2}{\partial x^2} & -\mathcal{A}_h\dfrac{\partial^2 v_2}{\partial y^2} & -\nu_E\dfrac{\partial^2 v_2}{\partial z^2} & +\mathrm{f}\,v_1 + \dfrac{1}{\rho_0}\dfrac{\partial \widetilde{p}}{\partial y} = 0 \\
\dfrac{U}{T} & \dfrac{U^2}{L} & \dfrac{U^2}{L} & \dfrac{UW}{H} & \mathcal{A}_h\dfrac{U}{L^2} & \mathcal{A}_h\dfrac{U}{L^2} & \nu_E\dfrac{U}{H^2} & \mathrm{f}\,U \quad \dfrac{P}{\rho_0 L}
\end{array}$$

$$\begin{array}{lllllllll}
\dfrac{\partial v_3}{\partial t} & +v_1\dfrac{\partial v_3}{\partial x} & +v_2\dfrac{\partial v_3}{\partial y} & +v_3\dfrac{\partial v_3}{\partial z} & -\mathcal{A}_h\dfrac{\partial^2 v_3}{\partial x^2} & -\mathcal{A}_h\dfrac{\partial^2 v_3}{\partial y^2} & -\nu_E\dfrac{\partial^2 v_3}{\partial z^2} & +\dfrac{1}{\rho_0}\dfrac{\partial \widetilde{p}}{\partial z} = \dfrac{\widetilde{\rho}}{\rho_0}g \\
\dfrac{W}{T} & \dfrac{UW}{L} & \dfrac{UW}{L} & \dfrac{W^2}{H} & \mathcal{A}_h\dfrac{W}{L^2} & \mathcal{A}_h\dfrac{W}{L^2} & \nu_E\dfrac{W}{H^2} & \dfrac{P}{\rho_0 H}
\end{array}$$

with $\rho_0^{-1}\boldsymbol{\Theta} \times \boldsymbol{v} \approx \mathrm{f}(-v, u, 0)^\top$ and Coriolis parameter $\mathrm{f} = 2\Theta \sin\theta \approx 10^{-4} s^{-1}$, see e.g. [Ped86], with latitude θ and rotation of the earth Θ. Due to the order of W we deduce, that UW/H is of order U^2/L. Considering the horizontal momentum equations thus leads to

$$P = \rho_0 U \max\left\{\frac{L}{T},\, U,\, \mathcal{A}_h L^{-1}, \nu_E H^{-2} L, \mathrm{f}\,L\right\}$$

Anticipating, see also Section 2.6.3, we reformulate the terms $\mathcal{A}_h L^{-1}$ and $\nu_E H^{-2} L$ by use of the horizontal and vertical Ekman numbers, $Ek_h = \mathcal{A}_h(\mathrm{f}\,L^2)^{-1}$ and $Ek_v =$

$\nu_E(\mathrm{f}\, H^2)^{-1}$:

$$\mathcal{A}_h L^{-1} = Ek_h\, L\,\mathrm{f}, \qquad\qquad \nu_E H^{-2} L = Ek_v\, L\,\mathrm{f}\,.$$

In oceanic flows, i.e. for the presumed parameter setting of the Coriolis force the viscosities, the Ekman numbers are less than 1. I.e., the diffusive terms subordinate the Coriolis terms and we have

$$P = \rho_0 U \max\left\{\frac{L}{T},\, U,\, \mathrm{f}\, L\right\}\,.$$

Thus, the pressure dependent term in the vertical momentum equation is of order

$$\frac{P}{\rho_0 H} = \frac{U \max\left\{\frac{L}{T},\, U,\, \mathrm{f}\, L\right\}}{H} \quad = \quad \frac{UL}{H}\max\left\{\frac{1}{T},\, \frac{U}{L},\, \mathrm{f}\right\}\,.$$

The remaining terms on the left hand side of the vertical momentum equation are, in total, of order

$$W \max\left\{\frac{1}{T},\, \frac{U}{L},\, \frac{W}{H}, Ek_h\,\mathrm{f},\, Ek_v\,\mathrm{f}\right\}$$

and, due to the order of W, the ratio between the latter two terms is

$$\frac{W \max\left\{\frac{1}{T},\, \frac{U}{L},\, \frac{W}{H}, Ek_h\,\mathrm{f},\, Ek_v\,\mathrm{f}\right\}}{\frac{UL}{H}\max\left\{\frac{1}{T},\, \frac{U}{L},\, \mathrm{f}\right\}} \quad = \quad a^2 \frac{\max\left\{\frac{1}{T},\, \frac{U}{L},\, Ek_h\,\mathrm{f},\, Ek_v\,\mathrm{f}\right\}}{\max\left\{\frac{1}{T},\, \frac{U}{L},\, \mathrm{f}\right\}}\,,$$

which is of order a^2. As the aspect ratio a is small the vertical momentum equation finally can be approximated by the hydrostatic balance

$$\frac{\partial \widetilde{p}}{\partial z} = \widetilde{\rho} g\,.$$

2.5 Initial and boundary conditions

In this section we collect the still missing initial and boundary conditions. Note, that these conditions are attempts to model the behavior at initial time and on the boundaries, and are no physical principles. Moreover, if we assume, that the domain of interest is not surrounded by land, but by other flow regimes, different conditions have to be applied.

2.5.1 Initial conditions

State variables are the horizonal velocity components v_1, v_2, the temperature T and salinity S. The remaining variables are diagnostic, i.e. can be determined via the state variables. No initial data are necessary for those.

Initial values may be given by monthly mean values, based on a data record, which contains observational data, see e.g. [LBC+98].

Let $(v_{1,0}, v_{2,0}, T_0, S_0)$ be the given the initial data such that

$$\begin{aligned} v_1(x,y,z,0) &= v_{1,0}(x,y,z), & & v_2(x,y,z,0) = v_{2,0}(x,y,z), \\ T(x,y,z,0) &= T_0(x,y,z), & \text{and} \qquad & S(x,y,z,0) = S_0(x,y,z) \end{aligned}$$

apply for all $(x,y,z) \in \Omega$.

2.5.2 Boundary conditions

On the bottom of the domain Γ_b, and on the side walls Γ_s, no-slip boundary conditions are presumed for the horizontal velocity components v_1 and v_2, i.e.

$$v_1 = v_2 = 0 \qquad \text{on } (\Gamma_b \cup \Gamma_s) \times (0, \mathcal{T}) \,.$$

This approach has the disadvantage, that a boundary layer is imposed. Alternatively, slip boundary conditions can be imposed, i.e.

$$\partial_n (v_1, v_2) = 0 \qquad \text{on } (\Gamma_b \cup \Gamma_s) \times (0, \mathcal{T}) \,,$$

as well as suitable inflow or outflow conditions with transient boundaries. We restrict to homogeneous Dirichlet boundary conditions.
On the surface of the domain, the crucial impact, the wind stress, is modeled by

$$\partial_z (v_1, v_2) = (\rho_0 \nu_E)^{-1} \tau \qquad \text{on } \Gamma_u \times (0, \mathcal{T})$$

with wind stress τ. Due to the rigid lid approximation on the surface,

$$v_3 = 0 \qquad \text{on } \Gamma_u \times (0, \mathcal{T})$$

is indicated for the vertical velocity component v_3. Moreover, as the fluid is assumed to be incompressible, we have

$$v_3 = 0 \qquad \text{on } \Gamma_b \times (0, \mathcal{T}) \tag{2.13}$$

$$v_3 = - \int_{-d(x,y)}^{z} (\partial_x v_1 + \partial_y v_2) \, d\widehat{z} \qquad \text{on } \Gamma_s \times (0, \mathcal{T}) \,. \tag{2.14}$$

Similar to the horizontal velocity field, the boundary conditions for temperature and salinity are given by

$$\begin{aligned} -\kappa \partial_z T = \theta_T \qquad & -\kappa \partial_z S = \theta_S & & \text{on } \Gamma_u \times (0, \mathcal{T}) \\ T = 0 \qquad & S = 0 & & \text{on } (\Gamma_s \cup \Gamma_b) \times (0, \mathcal{T}) \end{aligned}$$

with functions θ_T and θ_S, which depend on the wind speed, the moisture, cloudiness etc.

2.6 Governing set of equations

The governing set of oceanic circulation models is called *primitive equations*. In this section we introduce this set, collecting all previous considerations. Moreover, we assume full incompressibility and end up in the hydrostatic Navier-Stokes equations, which are the central set of equations of this work. We finish the section with a consideration of relevant dimensionless numbers, which describe the characteristics of the considered fluid. Such are the Rossby, the Ekman and the Reynolds number.

2.6.1 Primitive Equations

Before assembling the set of *primitive equations*, we reformulate the continuity equation. Using the boundary conditions for the vertical velocity component (2.13) and (2.14), the equation of volume conservation can be reformulated as

$$\int_{-d(x,y)}^{0} (\partial_x v_1 + \partial_y v_2)\, d\widehat{z} = 0 \qquad \text{in } \overline{\omega} \times (0,T).$$

In the upcoming let $\boldsymbol{v} := (v_1, v_2)$. Applying the abbreviation $\mathbf{M}$ for the vertical integration as defined in (2.4) and the Leibniz integration rule, the continuity equation is given by

$$\operatorname{div}'(\mathbf{M}\,\boldsymbol{v}) \;=\; 0 \qquad \text{in } \Omega \times (0,\mathcal{T}).$$

Recall the approximation $\rho_0^{-1}\boldsymbol{\Theta}\times\boldsymbol{v} \approx \mathrm{f}\,\boldsymbol{v}^{\perp}$ with $\boldsymbol{v}^{\perp} = (-v_2, v_1)^{\top}$ and Coriolis parameter $\mathrm{f} = 10^{-4}s^{-1}$, see e.g. [Ped86]. Moreover, we set $\rho := \widetilde{\rho}/\rho_0$ and $p = \widetilde{p}/\rho_0$. The primitive

equations finally are given by:

$$
\begin{aligned}
\operatorname{div}'(\mathbf{M}\,\boldsymbol{v}) &= 0 && \text{in } \Omega\times(0,\mathcal{T}) && (2.15)\\
v_3(t,x,y,z) &= -\int_{-d(x,y)}^{z} \operatorname{div}'\boldsymbol{v}\,d\widehat{z} && \text{in } \Omega\times(0,\mathcal{T}) && (2.16)\\
D_t\,\boldsymbol{v} - \Delta_{\boldsymbol{\mathcal{A}}_\nu}\boldsymbol{v} + \mathrm{f}\,\boldsymbol{v}^{\perp} + \nabla' p &= \mathbf{0} && \text{in } \Omega\times(0,\mathcal{T}) && (2.17)\\
\partial_z p &= -\rho g && \text{in } \Omega\times(0,\mathcal{T}) && (2.18)\\
D_t T - \Delta_{\boldsymbol{\mathcal{A}}_\kappa} T &= 0 && \text{in } \Omega\times(0,\mathcal{T}) && (2.19)\\
D_t S - \Delta_{\boldsymbol{\mathcal{A}}_\kappa} S &= 0 && \text{in } \Omega\times(0,\mathcal{T}) && (2.20)\\
\rho &= \beta(S-S_0) - \alpha(T-T_0) && \text{in } \Omega\times(0,\mathcal{T}) && (2.21)\\
\boldsymbol{v}, T, S &= 0 && \text{on } (\Gamma_b\cup\Gamma_s)\times(0,\mathcal{T}) && (2.22)\\
\partial_z\boldsymbol{v} &= (\rho_0\nu_E)^{-1}\tau && \text{on } \Gamma_u\times(0,\mathcal{T}) && (2.23)\\
-\kappa\partial_z T &= \theta_T && \text{on } \Gamma_u\times(0,\mathcal{T}) && (2.24)\\
-\kappa\partial_z S &= \theta_S && \text{on } \Gamma_u\times(0,\mathcal{T}) && (2.25)\\
\boldsymbol{v}(x,y,z,0) &= \boldsymbol{v}_0(x,y,z) && \text{in } \Omega\times\{0\} && (2.26)\\
T(x,y,z,0) &= T_0(x,y,z) && \text{in } \Omega\times\{0\} && (2.27)\\
S(x,y,z,0) &= S_0(x,y,z) && \text{in } \Omega\times\{0\} && (2.28)
\end{aligned}
$$

2.6.2 Evolutionary 2.5D Navier-Stokes equations

In the following we apply a further simplification: Under the assumption of absent stratification, i.e. $\widetilde{\rho}=0$, [CRB11] conclude, that $\widetilde{p}$ can be considered to be z-independent and geophysical flows tend to be hydrostatic, even if significant movement is apparent. The only remnant of the primary vertical momentum balance is thus given by the *hydrostatic balance*, $p_0(z) = P_0 - \rho_0 g z$, which has already been retrieved in the context of the Boussinesq approximation. As the variations of the density completely vanish from the system, we can also neglect the equations for the temperature and salinity, as they are no longer dynamically relevant. Recalling, that we introduced the horizontal

velocity field $\boldsymbol{v} := (v_1, v_2)$ we end up in the problem set:

$$\begin{aligned}
\operatorname{div}'(\mathbf{M}\,\boldsymbol{v}) &= 0 && \text{in } \Omega \times (0,\mathcal{T}) && (2.29)\\
v_3(t,x,y,z) &= -\int_{-d(x,y)}^{z} \operatorname{div}'\boldsymbol{v}\, d\widehat{z} && \text{in } \Omega \times (0,\mathcal{T}) && (2.30)\\
\partial_t\,\boldsymbol{v} + ((\boldsymbol{v},v_3)\cdot\nabla)\,\boldsymbol{v} - \Delta_{\mathcal{A}_\nu}\boldsymbol{v} + \mathrm{f}\,\boldsymbol{v}^\perp + \nabla' p &= \mathbf{0} && \text{in } \Omega \times (0,\mathcal{T}) && (2.31)
\end{aligned}$$

$$\begin{aligned}
\boldsymbol{v} &= 0 && \text{on } \Gamma_w \times (0,\mathcal{T}) && (2.32)\\
\partial_z\boldsymbol{v} &= (\rho_0\nu_E)^{-1}\tau && \text{on } \Gamma_u \times (0,\mathcal{T}) && (2.33)
\end{aligned}$$

$$\boldsymbol{v}(x,y,z,0) = \boldsymbol{v}_0(x,y,z) \qquad \text{in } \Omega \times \{0\}\,. \quad (2.34)$$

Note, that the vertical variations of the pressure field has already been described in the hydrostatic balance equation. Thus, the dynamically relevant pressure p becomes 2D, but still is embedded in a 3D problem. Moreover, we emphasize, that the originally 3D divergence constraint is now vertically averaged and thus corresponds to the 2D pressure, and vice versa. Thirdly, we only consider the horizontal momentum equations. Due to these reasons, we call this set the set of *(incompressible) 2.5D Navier-Stokes equations*. In the upcoming, this set is also called *hydrostatic Navier-Stokes equations*.

2.6.3 Dimensionless quantities

In Section 2.2 we already sketched, that different scenarios lead to different behaviors of the considered fluid. Characteristics of such geophysical flows correlate with certain, typical dimensionless key quantities, such as the Ekman number or the Reynolds number. To retrieve these quantities, the hydrostatic Navier-Stokes equations are normalized.

Let L, H, T, U and W be the characteristic scales for horizontal length, vertical length, time, horizontal and vertical velocity, respectively. Note, that $T = L/U$. We consider the normalized quantities

$$t^* = \frac{t}{T}, \quad x^* = \frac{x}{L}, \quad y^* = \frac{y}{L}, \quad z^* = \frac{z}{H}, \quad \boldsymbol{v}^* = \frac{\boldsymbol{v}}{U}, \quad v_3^* = \frac{v_3}{W}, \quad p^* = \frac{1}{U^2}p\,.$$

For ease of clarity, we use the full 3D divergence constraint $\operatorname{div}(\boldsymbol{v}, v_3) = 0$ in the formulation of the normalized hydrostatic Navier-Stokes equations. Note, that this equation with the appropriate boundary conditions (which we assumed) is equivalent to (2.29) – (2.30).

The term $\operatorname{div}(\boldsymbol{v}, v_3) = 0$ and the terms occurring in (2.31) become

$$\begin{aligned}
\operatorname{div}^*(\boldsymbol{v}^*, v_3^*) &= \frac{L}{U}\operatorname{div}'\boldsymbol{v} + \frac{H}{W}\partial_z v_3\,,\\
\partial_{t^*}\boldsymbol{v}^* &= \frac{L}{U^2}\partial_t\boldsymbol{v},\\
((\boldsymbol{v}^*, v_3^*)\cdot\nabla^*)\boldsymbol{v}^* &= \left(\left(\frac{L}{U^2}\boldsymbol{v}, \frac{H}{UW}v_3\right)\cdot\nabla\right)\boldsymbol{v},\\
\nabla'^* p^* &= \frac{L}{U^2}\nabla' p\,,\\
\Delta^*_{\boldsymbol{\mathcal{A}},\nu}\boldsymbol{v}^* &= \frac{L^2}{U}\mathcal{A}_h\partial_{xx}\boldsymbol{v} + \frac{L^2}{U}\mathcal{A}_h\partial_{yy}\boldsymbol{v} + \frac{H^2}{U}\nu_E\partial_{zz}\boldsymbol{v}\,,
\end{aligned}$$

the maximal time is $\mathcal{T}^* = T^{-1}\mathcal{T}$ and the domain is given by

$$\Omega^* := \left\{\boldsymbol{x}^* \in \mathbb{R}^3 \mid (Lx^*,\, Ly^*) \in \omega \text{ and } z^* \in (-d^*(Lx^*,\, Ly^*),\, 0)\right\}$$

with depth function $d^*(Lx^*, Ly^*) = H^{-1}d(x,\, y)$. The normalized hydrostatic Navier-Stokes equations in $\Omega^* \times (0, \mathcal{T}^*)$ are given by

$$\begin{aligned}
\operatorname{div}'^*\boldsymbol{v}^* + \frac{WL}{UH}\partial_{z^*}v_3^* &= 0\\
\partial_{t^*}\boldsymbol{v}^* + \left(\left(\boldsymbol{v}^*, \frac{WL}{UH}v_3^*\right)\cdot\nabla^*\right)\boldsymbol{v}^* + \frac{\mathrm{f}\,L}{U}\boldsymbol{v}^{*\perp} + \nabla'^* p^*&\\
- \left(\frac{\mathcal{A}_h}{UL}\partial_{x^*x^*}\boldsymbol{v}^* + \frac{\mathcal{A}_h}{UL}\partial_{y^*y^*}\boldsymbol{v}^* + \frac{L\,\nu_E}{UH^2}\partial_{z^*z^*}\boldsymbol{v}^*\right) &= \mathbf{0}
\end{aligned}$$

The initial and boundary conditions are given appropriately. Following [CRB11], the ratio $WL(UH)^{-1}$, occurring twice in the normalized context, is on the order of the *Rossby number*

$$Ro := \frac{U}{\mathrm{f}\,L}\,.$$

It compares the advection to the Coriolis force and is a fundamental number in the context of geophysical fluid dynamics. Due to the scales of the underlying regime, $Ro \leq 1$ applies. Cushman-Roisin and Beckers emphasize, that the characteristics of oceanic flows are highly sensitively related to the Rossby number. The second important dimensionless number is the *Reynolds number*, which is defined as

$$Re := \frac{UL}{\nu_E}.$$

It is an important number for non rotating fluids and describes the relation between inertia forces and friction. Oceanic regimes show very large Reynolds numbers up to the order 10^{11}, if molecular viscosity has been used in the definition of the Reynolds number. Large values of Re are reflected in turbulent behavior.

Note, that for flows with large Reynolds number, special attention has to be payed near boundaries with a no slip condition, where strong gradients of the velocity might occur, as $\boldsymbol{v}$ is of order U in the inner part of the domain and zero on the boundary.

There is a relation between the Rossby and the Reynolds number, realized by an additional dimensionless number, the (vertical) *Ekman number* Ek (or Ek_v), which is defined as

$$Ek := \frac{\nu_E}{\mathrm{f}\, H^2}$$

and describes the relation between friction and Coriolis forces. The relation between these three numbers is

$$Re \;=\; \frac{U\,L}{\nu_E} \;=\; \frac{U}{\mathrm{f}\,L}\,\frac{\mathrm{f}\,H^2}{\nu_E}\,\frac{L^2}{H^2} \;=\; \frac{Ro}{Ek}\,\frac{L^2}{H^2}\,.$$

Note that in literature, see e.g. [Ped86], the horizontal counterpart of the (vertical) Ekman number is defined as $Ek_h := \mathcal{A}_h(\mathrm{f}\,H^2)^{-1}$. Due to the definition of the aspect ratio, $a := HL^{-1}$, and the suggested magnitudes for $\mathcal{A}_h$ and ν_E, the ratio $\nu_E L^2(\mathcal{A}_h H^2)^{-1}$ is of order 1. Thus, the friction term can be rewritten as $Re^{-1}\,\Delta^*(\boldsymbol{v}^*, v_3^*)$. Finally, we get the following expression for the dimensionless hydrostatic Navier-Stokes equations:

$$\begin{aligned} \mathrm{div}\,'^*\,\boldsymbol{v}^* \;+ Ro\,\partial_{z^*} v_3^* \;&=\; 0 \\ \partial_{t^*}\,\boldsymbol{v}^* + ((\boldsymbol{v}^*,\, Ro\,v_3^*)\cdot\nabla^*)\,\boldsymbol{v}^* + Ro^{-1}\,\boldsymbol{v}^{*\perp} + \nabla'^* p^* - Re^{-1}\,\Delta^*(\boldsymbol{v}^*, v_3^*) \;&=\; \mathbf{0}\,. \end{aligned}$$

Chapter 3

Variational Formulation of Hydrostatic Flow Problems

The variational framework on the one hand enables the discussions on existence, uniqueness and regularity of a solution of the underlying problem, especially in the context of complex flow problems, where a solution in the continuous framework is often not known (recall the seventh millennium problem of the Clay institute). On the other hand, it provides a suitable approach to the formulation and analysis of the discretized problems, which form the basis of numerical simulations.

Preliminary, we present basic notations in the variational context, which accompany us through the remaining of this work. We then introduce methods for the proofs of existence and uniqueness of solutions for classical, non hydrostatic problems. These techniques apply also in the hydrostatic framework in a similar fashion. The point of that survey is to recall the proving techniques and to get an impression, where the regularity results, collected later in this chapter, stem from.

After the presentation of these methods, we turn to the hydrostatic framework, particularly, analyze the variational averaging operator and the inf-sup constraint, formulated in Sobolev spaces of arbitrary regularity $p \in (1, \infty)$. In this context, we also examine the δ_{min}-dependence of the appropriate inf-sup constant and find out, that this inf-sup constant behaves as the classical counterpart. In [KB12], we developed these statements for the case $p = 2$.

In the Sections 3.2 and 3.2, we present the variational formulations of hydrostatic flow problems and give an overview over existence and uniqueness results, known from literature. We start from the less complex problem: the stationary hydrostatic Stokes problem, add advection to the system, i.e. consider the Oseen case, and turn to the appropriate nonlinear case. Afterwards we treat the evolutionary case, beginning with the linear problem and then turning to the nonlinear problem, i.e. the evolutionary hydrostatic Navier-Stokes equations (2.29) – (2.34). The collection of the regularity statements is not only interesting in the context of existence and uniqueness theory, but is also rather important for error estimates, in which the regularity of the solution determines the order of convergence. In the majority of the literature, the impact of

temperature and salinity is neglected. We also do not present regularity results for these variables, but refer to [Zia97] for the stationary hydrostatic Stokes system and to [LTW92, CT07] for the evolutionary hydrostatic Navier-Stokes problem.

In order to understand the regularity impact of the hydrostatic approximation with respect to existence and uniqueness theory, we close the chapter with a comparison of the regularity results of the non hydrostatic flow problems with their hydrostatic counterpart. Note, that the majority of the available analysis on the non hydrostatic part is settled in the framework of Dirichlet boundary conditions, whereas in most of the literature for the hydrostatic problems a mixture of Dirichlet and Neumann boundary conditions is imposed. As the main emphasis is not put on the topic of non hydrostatic problems, we present a rather rough collection of the main propositions. For more detailed informations, the reader is referred to the cited literature.

3.1 Fundamentals

We start this section with a presentation of basic notations, also broadening the Poincare–Friedrichs inequality to the case of Sobolev spaces with arbitrary regularity $p \in (1, \infty)$. Then, we consider the variational formulation of the averaging operator with respect to well-posedness, linearity, continuity and surjectivity in Sobolev spaces with arbitrary regularity $p \in (1, \infty)$. We finish the section with the consideration of the modified inf-sup constraint, formulated in the Sobolev framework with arbitrary regularity $p \in (1, \infty)$.

3.1.1 Domain and space definitions

Let $n \in \{2, 3\}$. Given an simply connected, open, bounded surface domain $\omega \subset \mathbb{R}^{n-1}$ and a positive depth function $d : \overline{\omega} \to \mathbb{R}_{\geq 0}$, the underlying domain $\Omega \subset \mathbb{R}^n$ is defined as

$$\Omega := \{ \boldsymbol{x} = (x, y, z) \in \mathbb{R}^n \mid (x, y) \in \omega \text{ and } z \in (-d(x, y),\, 0) \} ,$$

see also Section 2.1 for the 3D case. We take over the boundary notations, defined in that section.

Let $\delta_{min} > 0$, unless noted differently.
The domain Ω is a Lipschitz domain, if $\partial\Omega$ is partially Lipschitz, see also [Bra07]. For a given $p \geq 1$, we call Ω a $\mathcal{C}^p$– domain, if the boundary $\partial\Omega$ is a 2D manifold of class $\mathcal{C}^p$. Throughout this work, we consider Ω to be a Lipschitz domain. In particular, it is simply connected.

For any $p \in \mathbb{N}$, we denote the space of Lebesgue-integrable functions v with $\int_\Omega |v|^p \, d\boldsymbol{x} <$

∞ as $\mathrm{L}^p(\Omega)$. Equipped with the norm

$$\|v\|_{p,\Omega} := \begin{cases} \left(\int_\Omega |v|^p \, d\boldsymbol{x}\right)^{1/p}, & \text{if } p < \infty \\ \operatorname{ess\,sup}_{\boldsymbol{x}\in\Omega} \|v(\boldsymbol{x})\|, & \text{else,} \end{cases}$$

$\mathrm{L}^p(\Omega)$ forms a Banach space. We set

$$\mathrm{L}^p_0(\Omega) := \left\{ v \in \mathrm{L}^p(\Omega) \,\middle|\, \int_\Omega v \; d\boldsymbol{x} = 0 \right\}.$$

The Sobolev spaces $\mathrm{W}^{k,p}(\Omega)$consist of those functions $v \in \mathrm{L}^p(\Omega)$ with distributional derivatives $D^\alpha v \in \mathrm{L}^p(\Omega)^d$ for all $|\alpha| \le k$. Provided with the norm

$$\|v\|_{k,p,\Omega} := \begin{cases} \left(\sum_{|\alpha|\le k} \int_\Omega |D^\alpha v|^p \, d\boldsymbol{x} \right)^{1/p}, & \text{if } p < \infty \\ \max_{|\alpha|\le k} \|D^\alpha v\|_{0,\infty,\Omega} & \text{else,} \end{cases}$$

$\mathrm{W}^{k,p}(\Omega)$ is a Banach space. For $p < \infty$, $\mathrm{W}^{k,p}(\Omega)$ is separable. The appropriate semi norms are given by

$$|v|_{k,p,\Omega} := \begin{cases} \left(\sum_{|\alpha|=k} \int_\Omega |D^\alpha v|^p \, d\boldsymbol{x} \right)^{1/p}, & \text{if } p < \infty \\ \|D^\alpha v\|_{0,\infty,\Omega} & \text{else.} \end{cases}$$

For $p = 2$, the spaces $\mathrm{L}^2(\Omega)$ and $\mathrm{H}^k(\Omega) := \mathrm{W}^{k,2}(\Omega)$ are Hilbert spaces, if equipped with the norm-inducing scalar products

$$(u,v)_\Omega := \int_\Omega uv \; d\boldsymbol{x} \quad \text{and} \qquad (u,v)_{\Omega,k} := \sum_{|\alpha|\le k} (D^\alpha u, D^\alpha v)_\Omega,$$

respectively. We abbreviate $|\cdot|_{k,\Omega} := |\cdot|_{k,2,\Omega}$, $\|\cdot\|_\Omega := \|\cdot\|_{2,\Omega}$and $\|\cdot\|_{k,\Omega} := \|\cdot\|_{k,2,\Omega}$. Note, that there is an overlap in the definition of $\|\cdot\|_{k,\Omega}$ with the definition of the norm of $\mathrm{L}^p(\Omega)$. If the application of that expression is ambiguous, we will denote the underlying notion explicitely. Due to the existence of a continuous trace operator $\gamma : \mathrm{H}^1(\Omega) \to \mathrm{L}^2(\partial\Omega)$ with $\gamma(v) = v|_{\partial\Omega}$ and due to the Sobolev embedding theorem, the spaces

$$\begin{aligned} \mathrm{H}^1_0(\Omega) &:= \{v \in \mathrm{H}^1(\Omega) \,|\, v|_{\partial\Omega} = 0\} \quad \text{and} \quad \mathrm{H}^1_b(\Omega) := \{v \in \mathrm{H}^1(\Omega) \,|\, v|_{\Gamma_s\cup\Gamma_b} = 0\}, \\ \mathrm{W}^{1,p}_0(\Omega) &:= \{v \in \mathrm{W}^{1,p}(\Omega) \,|\, v|_{\partial\Omega} = 0\} \quad \text{and} \quad \mathrm{W}^{1,p}_b(\Omega) := \{v \in \mathrm{W}^{1,p}(\Omega) \,|\, v|_{\Gamma_s\cup\Gamma_b} = 0\} \end{aligned}$$

for $p \ge 2$ are well-defined. Considering the Poincaré – Friedrichs inequality, $\|v\|_\Omega \le c_\Omega |v|_{1,\Omega}$ for all $v \in \mathrm{H}^1_0(\Omega)$, the semi norm $|\cdot|_{1,\Omega}$ defines a norm on $\mathrm{H}^1_0(\Omega)$. Due to the structure of the appropriate proof, see e.g. [Bra07], this inequality also holds for $v \in \mathrm{H}^1_b(\Omega)$. The following lemma, which is a generalization of the Poincaré – Friedrichs inequality, states, that the semi norm $|\cdot|_{1,p,\Omega}$ also defines a norm on $\mathrm{W}^{1,p}_0(\Omega)$.

Lemma 3.1. *Let $\Omega \subset \mathbb{R}^n$, $n \in \mathbb{N}$, be contained in an n-dimensional cube of side length $s \in \mathbb{R}$. Then,*

$$\| \boldsymbol{v} \|_{0,p,\Omega} \quad \leq \quad s^{1/q} | \boldsymbol{v} |_{1,p,\Omega} \qquad\qquad \forall \boldsymbol{v} \in \mathrm{W}_0^{1,p}(\Omega)$$

applies for any $p \in (1,\infty)$ and q with $1/p + 1/q = 1$.

Proof. The proof is similar to the proof of the classical Poincare – Friedrichs inequality, see [Bra07]. As $\mathcal{C}_0^\infty(\Omega)$ is dense in $\mathbf{W}_0^{1,p}(\Omega)$, it suffices to prove the proposition for $\boldsymbol{v} \in \mathcal{C}_0^\infty(\Omega)$. Supposing $\Omega \subset C := \{(x_1,\dots,x_n) \mid 0 < x_i < s \; \forall i \in \{1,\dots,n\}\}$ and $\boldsymbol{v} = 0$ for $\boldsymbol{x} \in C \setminus \Omega$, we get

$$\boldsymbol{v}(x_1,\dots,x_n) = \boldsymbol{v}(0,x_2,\dots,x_n) + \int_0^{x_1} \partial_{x_1} \boldsymbol{v}(t,x_2,\dots,x_n)\, dt.$$

Application of the Hölder inequality and gives

$$| \boldsymbol{v}(\boldsymbol{x})|^p \;\leq\; s^{p/q} \int_0^s |\partial_{x_1} \boldsymbol{v}(t,x_2,\dots,x_n)|^p \; dt.$$

Integration along x_1 and along the remaining coordinates finally assures

$$\| \boldsymbol{v} \|_{0,p,\Omega}^p \leq s^{p/q} | \boldsymbol{v} |_{1,p,\Omega}^p .$$

Constant $c_\omega := s^{1/q}$ is called Poincare–Friedrichs constant. □

For a given Lebesgue space $\mathrm{L}^p(\Omega)$, the appropriate dual space $[\mathrm{L}^p(\Omega)]'$ is given by $\mathrm{L}^q(\Omega)$ with $1/p + 1/q = 1$ ($q = \infty$ if $p = 1$). For a given Sobolev space $\mathrm{W}_0^{k,p}(\Omega)$, the appropriate dual space is defined as $[\mathrm{W}_0^{k,p}(\Omega)]' := \mathrm{W}^{-k,q}(\Omega)$, for $p = 2$ we set $[\mathrm{H}_0^k(\Omega)]' = \mathrm{H}^{-k}(\Omega)$. Dependent on the underlying space $\mathrm{W}_0^{k,p}(\Omega)$, let $\langle \cdot, \cdot \rangle$ denote the duality between $\mathrm{W}^{-k,q}(\Omega)$ and $\mathrm{W}_0^{k,p}(\Omega)$. If we attempt to emphasize the underlying domain D, we write $\langle \cdot, \cdot \rangle_D$. Given a Hilbert space H, we can interprete each element $f \in \mathrm{H}'$ as a suitable element $y \in \mathrm{H}$, due to the following theorem.

Theorem 3.2 (Riesz representation Theorem)**.** *Let* H *be a Hilbert space, equipped with scalar product $(\cdot,\cdot)_\mathrm{H}$, norm $\| \cdot \|_\mathrm{H}$ and dual space* H′*. For any $f \in \mathrm{H}'$, there is a unique $y_f \in \mathrm{H}$ with $\|f\|_\mathrm{H} = \|y_f\|_\mathrm{H}$, s.t.*

$$f(x) = (x, y_f)_\mathrm{H} \qquad\qquad \forall x \in \mathrm{H} \; .$$

Conversely, for any $y \in \mathrm{H}$, there is a $f_y \in \mathrm{H}'$ with $\|f_y\|_\mathrm{H} = \|y\|_\mathrm{H}$ s. t.

$$f_y(x) = (x, y)_\mathrm{H} \qquad\qquad \forall x \in \mathrm{H} \; .$$

Proof. See [Yos80]. □

Note, that this theorem is applied when theoretical results concerning existence and uniqueness of a solution (see e.g. Theorem 3.3 of Lax-Milgram) are used to validate existence and uniqueness results of problems whose right hand sides are formulated as $(\boldsymbol{f}, \boldsymbol{\varphi})_\Omega$ instead of $\boldsymbol{f}(\boldsymbol{\varphi})$. A suitable interpretation is thus provided by the Riesz representation Theorem.

Vector-valued spaces are denoted bold-faced, e.g. $\mathbf{L}^2(\Omega), \mathbf{H}_0^1(\Omega)$, etc. The norms are interpreted appropriately.

For an interval $[0, \mathcal{T}]$, Banach space B and $1 \leq p \leq \infty$, $\mathrm{L}^p(0, \mathcal{T}; B)$ denotes the space of L^p-integrable functions mapping from $[0, \mathcal{T}]$ to B. Equipped with the norm

$$\|f\|_{\mathrm{L}^p(0,\mathcal{T};B)} := \begin{cases} \left(\int_0^{\mathcal{T}} \|f(t)\|_B^p \, dt \right)^{1/p}, & \text{if } p < \infty \\ \operatorname{ess\,sup}_{0 \leq t \leq \mathcal{T}} \|f(t)\|_B, & \text{else}, \end{cases}$$

it forms a Banach space, see e.g. [Tem79]. If B denotes a Hilbert space with scalar product $(\cdot, \cdot)_B$, then $\mathrm{L}^p(0, \mathcal{T}; B)$ also denotes a Hilbert space with norm-inducing scalar product $\int_0^{\mathcal{T}} (\cdot, \cdot)_B \, dt$.

3.1.2 Methods

We present fundamental theorems and methods for the existence and uniqueness analysis of incompressible flow problems and outline the proofs, in order to show basic concepts, which also find application in the hydrostatic context.

For sake of brevity we assume homogeneous Dirichlet boundary conditions on $\partial\Omega$. Moreover, let $\mathbf{V} := \mathbf{H}_0^1(\Omega)$ and $Q := \mathrm{L}_0^2(\Omega)$ be the variational spaces for the velocity and the pressure. Without loss of generality, we assume an isotropic viscosity, i.e. $\nu = \mathcal{A}_h = \nu_E > 0$.

Stationary linear problems

Incompressible flow problems show a saddle point structure, which reveals due to the divergence constraint and the pressure gradient. Given Hilbert spaces $\mathbf{V}$ and Q, equipped with the norms $\|\cdot\|_V$ and $\|\cdot\|_Q$, with dual spaces $\mathbf{V}'$ and Q', as well as continuous bilinear forms

$$\begin{aligned} \mathrm{a} : \mathbf{V} \times \mathbf{V} \to \mathbb{R}, \qquad \mathrm{a}(\boldsymbol{v}, \boldsymbol{\varphi}) &:= \nu(\nabla \boldsymbol{v}, \nabla \boldsymbol{\varphi})_\Omega + \mathrm{f}(\boldsymbol{v}^\perp, \boldsymbol{\varphi})_\Omega \qquad \text{and} \qquad (3.1) \\ \mathrm{b} : Q \times \mathbf{V} \to \mathbb{R}, \qquad \mathrm{b}(\xi, \boldsymbol{v}) &:= (\operatorname{div} \boldsymbol{v}, \xi)_\Omega, \qquad (3.2) \end{aligned}$$

with viscosity $\nu > 0$ and Coriolis force $\mathrm{f} \geq 0$, the saddle point problem is defined as

$$\begin{array}{c} \textit{Given } f \in \mathbf{V}', \textit{ find } (\boldsymbol{v}, q) \in \mathbf{V} \times Q \textit{ s. t.} \\ \begin{array}{rcll} \mathrm{a}(\boldsymbol{v}, \boldsymbol{\varphi}) - \mathrm{b}(q, \boldsymbol{\varphi}) &=& \langle \boldsymbol{f}, \boldsymbol{\varphi} \rangle & \forall \boldsymbol{\varphi} \in \mathbf{V} \\ \mathrm{b}(\xi, \boldsymbol{v}) &=& 0 & \forall \xi \in Q \end{array} \end{array} \qquad (3.3)$$

The element $q \in Q$, i.e. the pressure, plays the role of the Lagrangian multiplier of the second equation,

$$\mathrm{b}(\xi, \boldsymbol{v}) \quad = \quad 0 \qquad \forall \xi \in Q\,,$$

the divergence constraint. Incorporating this condition into the variational space $\mathbf{V}$, i.e. restricting $\mathbf{V}$ to $\mathbf{J}_1 := \{\boldsymbol{v} \in \mathbf{V} \mid \mathrm{b}(q, \boldsymbol{v}) = 0\ \forall q \in Q\}$, results in the elliptic problem

$$\textit{Given } \boldsymbol{f} \in \mathbf{V}', \textit{ find } \boldsymbol{v} \in \mathbf{J}_1 \textit{ s. t.} \quad \mathrm{a}(\boldsymbol{v}, \boldsymbol{\varphi}) = \langle \boldsymbol{f}, \boldsymbol{\varphi} \rangle \qquad \forall\, \boldsymbol{\varphi} \in \mathbf{J}_1\ . \tag{3.4}$$

For the present flow problem, the space $\mathbf{J}_1$ is defined as the space of divergence free functions, i.e.

$$\mathbf{J}_1 := \{\boldsymbol{v} \in \mathbf{V} \mid \operatorname{div} \boldsymbol{v} = 0\}\,. \tag{3.5}$$

Unique solvability of this problem can be validated due the following considerations.

Theorem 3.3 (Lax Milgram Lemma)**.** *Let $\mathbf{H}$ be a Hilbert space equipped with norm $\|\cdot\|$ and dual space $\mathbf{H}'$. If the bilinear form $\mathrm{a} : \mathbf{H} \times \mathbf{H} \to \mathbb{R}$ is continuous, i.e.*

$$\mathrm{a}(\boldsymbol{v}, \boldsymbol{\varphi}) \quad \leq \alpha_1 \| \boldsymbol{v} \| \, \| \boldsymbol{\varphi} \| \qquad \forall\ \boldsymbol{v}, \boldsymbol{\varphi} \in \mathbf{H}\,,$$

and coercive (or $\mathbf{H}$ – elliptic), i.e.

$$\mathrm{a}(\boldsymbol{v}, \boldsymbol{v}) \quad \geq \alpha_2 \| \boldsymbol{v} \|^2 \qquad \forall\ \boldsymbol{v} \in \mathbf{H}\,,$$

then for any $f \in \mathbf{H}'$ there is a unique solution $\boldsymbol{v} \in \mathbf{H}$ of

$$\mathrm{a}(\boldsymbol{v}, \boldsymbol{\varphi}) \quad = \boldsymbol{f}(\boldsymbol{\varphi}) \qquad \forall\, \boldsymbol{\varphi} \in \mathbf{H}\ .$$

Proof. See [Pet65]. □

Assuming a continuous and coercive bilinear form $\mathrm{a} : \mathbf{J}_1 \times \mathbf{J}_1 \to \mathbb{R}$, let $\boldsymbol{v} \in \mathbf{J}_1$ be the (unique) solution of problem (3.4). In order to assure a solution $(\boldsymbol{v}, q) \in \mathbf{V} \times Q$ of (3.3), the element $q \in Q$ has to fulfill

$$\mathrm{b}(q, \boldsymbol{\varphi}) \quad = \quad \mathrm{a}(\boldsymbol{v}, \boldsymbol{\varphi}) - \langle \boldsymbol{f}, \boldsymbol{\varphi} \rangle \qquad \forall\, \boldsymbol{\varphi} \in \mathbf{V}\ . \tag{3.6}$$

Let the operator $B : Q \to \mathbf{V}'$ and the linear operator $\boldsymbol{l} \in \mathbf{V}'$ be defined as

$$\langle Bq, \boldsymbol{\varphi} \rangle \quad := \quad \mathrm{b}(q, \boldsymbol{\varphi}) \quad \text{and} \quad \boldsymbol{l}(\boldsymbol{\varphi}) \quad := \quad \mathrm{a}(\boldsymbol{v}, \boldsymbol{\varphi}) - \langle \boldsymbol{f}, \boldsymbol{\varphi} \rangle \qquad \forall\, \boldsymbol{\varphi} \in \mathbf{V}\ .$$

Note, that the functional $\boldsymbol{l}$ is element of the annihilator of $\mathbf{J}_1$ in $\mathbf{V}'$, i.e. $\mathbf{J}_1^\circ := \{\boldsymbol{l} \in \mathbf{V}' \mid \boldsymbol{l}(\boldsymbol{\varphi}) = 0\ \forall\, \boldsymbol{\varphi} \in \mathbf{J}_1\}$. Thus, the question of existence and uniqueness of an element $q \in Q$ that satisfies (3.6) can be formulated as the search for a (unique) $q \in Q$, such that $Bq = \boldsymbol{l}$ applies for an arbitrarily given $\boldsymbol{l} \in \mathbf{J}_1^\circ$. For a suitably determined constant $\gamma > 0$, Braess proves the equivalence of the following two statements, [Bra07]:

(a) The operator $B : Q \to \mathbf{J}_1^\circ \subset V'$ is an isomorphism with $\|Bq\|_{\mathbf{V}'} \geq \gamma \|q\|_Q$ for any $q \in Q$.

(b) The inf-sup condition applies:

$$\inf_{q\in Q}\sup_{\boldsymbol{v}\in\mathbf{V}}\frac{\mathrm{b}(q,\boldsymbol{v})}{\|\boldsymbol{v}\|_{\mathbf{V}}\|q\|_{Q}}\geq\gamma\,. \tag{3.7}$$

In the context of non hydrostatic flow problems, the element $q \in Q$ represents the pressure, $\boldsymbol{v} \in \mathbf{V}$ the velocity field. The variational spaces are given by $Q := \mathrm{L}^2_0(\Omega)$ and $\mathbf{V} := \mathbf{H}^1_0(\Omega)$ (assuming homogeneous Dirichlet conditions on $\partial\Omega$). Bilinear form $\mathrm{b} : \mathbf{V} \times Q \to \mathbb{R}$ is defined as $\mathrm{b}(\boldsymbol{v}, q) := (\operatorname{div} \boldsymbol{v}, q)_\Omega$. The authors of [AG94] presented the validity of (3.7), proceeding on De Rham Lemma, i.e.

Theorem 3.4 (De Rham Lemma)**.** *Let $\Omega \subset \mathbb{R}^n$, $n \geq 2$ be an open set and $\mathcal{V} = \{\boldsymbol{v} \in \mathcal{D}(\Omega) \mid \operatorname{div} \boldsymbol{v} = 0\}$. If the distribution $\boldsymbol{l} \in \mathcal{D}(\Omega)$ satisfies $\langle \boldsymbol{l}, \boldsymbol{\varphi}\rangle = 0$ for any $\boldsymbol{\varphi} \in \mathcal{V}$, then there is a distribution $p \in \mathcal{D}'(\Omega)$ with $\boldsymbol{l} = \nabla p$.*

Proof. See [dR60]. □

Stationary nonlinear problems

The nonlinear case distinguishes oneself by the additional nonlinear advection term

$$\mathrm{c}(\widetilde{\boldsymbol{v}}, \boldsymbol{v}, \boldsymbol{\varphi}) \quad := \quad ((\widetilde{\boldsymbol{v}} \cdot \nabla)\, \boldsymbol{v}, \boldsymbol{\varphi})_\Omega\,. \tag{3.8}$$

We observe $\mathrm{c}(\boldsymbol{b}, \boldsymbol{v}, \boldsymbol{v}) = 0$ for any $\boldsymbol{b} \in \mathbf{J}_1$ and any $\boldsymbol{v} \in \mathbf{V}$. As in the linear case, the pressure can be decoupled from the governing system and be retrieved by the momentum equation and a velocity, which has been determined beforehand. Due to the nonlinearity of the problem, the previously introduced mechanisms can not be applied. Instead, the construction of a Galerkin approximation, as well as application of the Brouwer's fixed point Theorem and appropriate compactness results, provide a suitable handling of the problem.

Theorem 3.5 (Brouwer's fixed point Theorem)**.** *Let B be a closed n-dimensional unit ball, $n \in \mathbb{N}$, and $f : B \to B$ be continuous. Then there is a $x^* \in B$, such that $f(x^*) = x^*$*

Proof. See e.g. [Sca67]. □

Theorem 3.6 (Sobolev Embedding Theorem)**.** *Let $\Omega \subset \mathbb{R}^n$, $n \in \mathbb{N}$, be a Lipschitz domain, $m \geq 1$ and $p \in [1, \infty)$.*

(a) If $mp > n$ or $m = n$ and $p = 1$, then $\mathrm{W}^{m,p}(\Omega) \hookrightarrow \mathrm{L}^q(\Omega)$ for $p \leq q \leq \infty$.

(b) If $mp = n$, then $\mathrm{W}^{m,p}(\Omega) \hookrightarrow \mathrm{L}^q(\Omega)$ for $p \leq q < \infty$.

(c) If $mp < n$, then $\mathrm{W}^{m,p}(\Omega) \hookrightarrow \mathrm{L}^q(\Omega)$ for $p \leq q \leq np/(n - mp)$.

(d) Propositions (a) and (b) are valid for arbitrary domains Ω, if homogeneous Dirichlet boundary conditions are implied on $\partial\Omega$.

(e) If $mp > n$, then $\mathrm{W}^{m,p}(\Omega) \hookrightarrow \mathcal{C}(\overline{\Omega})$.

Proof. See e.g. [AF03, Wer05, Jos98]. □

Lemma 3.7 (Generalized Hölder Inequality)**.** *Let $p, q, r \in (1, \infty)$, and $f \in \mathrm{L}^p(\Omega)$, $g \in \mathrm{L}^q(\Omega)$, $h \in \mathrm{L}^r(\Omega)$, such that $1/p + 1/q + 1/r = 1$. Then $f\,g\,h \in \mathrm{L}^1(\Omega)$ and*

$$\|f\,g\,h\|_{0,1,\Omega} \quad \leq \quad \|f\|_{0,p,\Omega}\, \|g\|_{0,q,\Omega}\, \|h\|_{0,r,\Omega}\,.$$

Proof. The proof is an easy exercise, based on the common Hölder inequality:

$$\begin{aligned} &\textit{If } 1/s + 1/t = 1,\ f \in \mathrm{L}^s(\Omega) \textit{ and } g \in \mathrm{L}^t(\Omega), \\ &\qquad \textit{then } fg \in \mathrm{L}^1(\Omega) \textit{ with } \|fg\|_{0,1,\Omega} \quad \leq \quad \|f\|_{0,s,\Omega}\, \|g\|_{0,t,\Omega}\,. \end{aligned} \tag{3.9}$$

We first validate an altered version:

$$\begin{aligned} &\textit{If } 1/p + 1/q = 1/r',\ f \in \mathrm{L}^p(\Omega) \textit{ and } g \in \mathrm{L}^q(\Omega), \\ &\textit{then } fg \in \mathrm{L}^{r'}(\Omega) \textit{ with } \|fg\|_{r',0,\Omega} \leq \|f\|_{p,0,\Omega}\|g\|_{q,0,\Omega}\,. \end{aligned}$$

Defining $s = p/r'$ and $t = q/r'$, we can apply (3.9) and get

$$\|fg\|_{0,r',\Omega} \quad = \quad \left(\int_\Omega |f|^{r'}|g|^{r'}\,d\boldsymbol{x}\right)^{1/r'} \quad \leq \quad \left(\|f\|_{0,p,\Omega}^{p/s}\, \|g\|_{0,q,\Omega}^{q/t}\right)^{1/r'} \quad = \quad \|f\|_{0,p,\Omega}\, \|g\|_{0,q,\Omega}.$$

Let r' be chosen, such that $1/r' + 1/r = 1$. We thus get

$$\|f\,g\,h\|_{0,1,\Omega} \quad \leq \quad \|fg\|_{0,r',\Omega}\, \|h\|_{0,r,\Omega} \quad \leq \quad \|f\|_{0,p,\Omega}\, \|g\|_{0,q,\Omega}\, \|h\|_{0,r,\Omega}\,.$$

□

Theorem 3.8 (Rellich – Kondrachov)**.** *Let $\Omega \subset \mathbb{R}^n$, $n \in \mathbb{N}$, be an open, bounded Lipschitz domain. For $p \in [1, n)$ and $p^* := np/(n-p)$, $\mathrm{W}^{1,p}(\Omega)$ is*

(a) continuously embedded in $\mathrm{L}^q(\Omega)$ with $q \in [1, p^*]$ and

(b) compactly embedded in $\mathrm{L}^q(\Omega)$ with $q \in [1, p^*)$.

Proof. See [HK00]. □

The argumentation for existence of a solution is as follows, see also [Tem79]: As $\mathbf{V}_0$ is a subspace of $\mathbf{H}^1(\Omega)$, $\mathbf{J}_1$ is separable and we can assume finite-dimensional subsets $\mathbf{V}_m \subset \mathbf{J}_1$, such that $\cup_{m\in\mathbb{N}} \mathbf{V}_m$ is dense in $\mathbf{J}_1$. We denote $\mathbf{V}_m := span\{\boldsymbol{w}_1, \ldots, \boldsymbol{w}_m\}$ with basis functions $\boldsymbol{w}_1, \ldots, \boldsymbol{w}_m$. Thus, any $\boldsymbol{v} \in \mathbf{V}_0$ can be represented as $\boldsymbol{v} = \sum_{m=1}^{\infty} \alpha_m\, \boldsymbol{w}_m$ with suitable constants α_m.

In the Galerkin approximation of the nonlinear problem, $\mathbf{J}_1$ is approximated by $\mathbf{V}_m$, i.e. we get:

$$\textit{Find } \boldsymbol{v}_m \in \mathbf{V}_m \ \textit{ s. t. } \qquad \mathrm{a}(\boldsymbol{v}_m, \boldsymbol{\varphi}) + \mathrm{c}(\boldsymbol{v}_m, \boldsymbol{v}_m, \boldsymbol{\varphi}) = \langle \boldsymbol{f}, \boldsymbol{\varphi}\rangle \qquad \forall\, \boldsymbol{\varphi} \in \mathbf{V}_m\,. \tag{3.10}$$

In order to elaborate unique existence of (3.10), we linearize the problem by introduction of the mapping $Q_m : \mathbf{V}_m \to \mathbf{V}_m$, which, for a given $\boldsymbol{v}_m \in \mathbf{V}_m$, is defined as the solution of

$$\mathrm{a}(Q_m(\boldsymbol{v}_m), \boldsymbol{\varphi}) + \mathrm{c}(\boldsymbol{v}_m, Q_m(\boldsymbol{v}_m), \boldsymbol{\varphi}) \quad = \quad \langle \boldsymbol{f}, \boldsymbol{\varphi} \rangle \qquad \forall\, \boldsymbol{\varphi} \in \mathbf{V}_m \tag{3.11}$$

Lipschitz continuity of $\mathrm{a}(\cdot,\cdot)+\mathrm{c}(\boldsymbol{v}_m,\cdot,\cdot)$, and thus continuity, can be guaranteed by Theorem 3.6 and Lemma 3.7. Coercivity results from $\mathrm{a}(Q_m(\boldsymbol{v}_m), Q_m(\boldsymbol{v}_m)) = \nu |Q_m(\boldsymbol{v}_m)|^2_{1,\Omega}$ and $\mathrm{c}(\boldsymbol{v}_m, Q_m(\boldsymbol{v}_m), Q_m(\boldsymbol{v}_m)) = 0$. Application of Theorem 3.3 assures a unique solution, i.e. $Q_m(\boldsymbol{v}_m)$ is uniquely determined.
Obviously, $Q_m : B_m \to B_m$, whereas $B_m := \{\boldsymbol{v} \in \mathbf{V}_m \mid |\, \boldsymbol{v}\,|_{1,\Omega} \leq \nu^{-1} \|\boldsymbol{f}\|_{-1}\}$. Moreover, $Q_m : B_m \to B_m$ is continuous, which can be validated by diagonal testing (3.11) and recalling $\mathrm{c}(\boldsymbol{v}_m, Q_m(\boldsymbol{v}_m), Q_m(\boldsymbol{v}_m)) = 0$, which leads to $|Q_m(\boldsymbol{v}_m)|_{1,\Omega} \leq \nu^{-1}\|\boldsymbol{f}\|_{-1}$. The norm $\|\cdot\|_{-1}$ is defined with respect to $|\cdot|_{1,\Omega}$, i.e.

$$\|\boldsymbol{f}\|_{-1} \quad := \quad \sup_{\boldsymbol{\varphi}\in\mathbf{V}} \frac{\langle \boldsymbol{f}, \boldsymbol{\varphi}\rangle}{|\,\boldsymbol{\varphi}\,|_{1,\Omega}}\,.$$

Thus, we have

$$\|Q_m\| := \sup_{\boldsymbol{v}_m \in B_m} \frac{|Q_m(\boldsymbol{v}_m)|_{1,\Omega}}{|\,\boldsymbol{v}_m\,|_{1,\Omega}} \leq 1.$$

By means of a suitable transformation from the unit ball $B \subset \mathbf{J}_1$ to B_m, Brouwer's fixed point Theorem 3.5 assures existence of a solution of (3.10), see also [Ist01]. Thus, the solutions $\boldsymbol{v}_m$, $m \in \mathbb{N}$, define a bounded sequence in $\mathbf{J}_1$. Moreover, $\mathbf{J}_1$ is compactly embedded in

$$\mathbf{J_0} := \{\boldsymbol{v} \in \mathbf{L}^2(\Omega) \mid \text{div } \boldsymbol{v} = 0 \text{ and } \boldsymbol{v}\cdot\boldsymbol{n}|_{\partial\Omega} = 0\}\,, \tag{3.12}$$

whereas $\boldsymbol{v}\cdot\boldsymbol{n}|_{\partial\Omega}$ is meant in the $\mathbf{H}^{-1/2}(\partial\Omega)$-sense, see also Theorem 3.8. Thus, the sequence $(\boldsymbol{v}_m)_{m\in\mathbb{N}}$ is relatively compact, i.e. there is a subsequence $(\boldsymbol{v}_{m_k})_{k\in\mathbb{N}}$ which is convergent. I.e. existence of a solution of the nonlinear, infinite dimensional problem is assured. The pressure can be recovered as in the linear case.

For uniqueness, assume two solutions, $\boldsymbol{v}_1, \boldsymbol{v}_2 \in B := \{\boldsymbol{v} \in \mathbf{V} \mid |\,\boldsymbol{v}\,|_{1,\Omega} \leq \nu^{-1}\|\boldsymbol{f}\|_{-1}\}$. Application of Lemma 3.7 and the observation, that $\mathrm{c}(\boldsymbol{b},\boldsymbol{v},\boldsymbol{v}) = 0$ for any $\boldsymbol{b} \in \mathbf{J}_1$ and any $\boldsymbol{v} \in \mathbf{V}$, leads to the estimate $|\,\boldsymbol{v}_1 - \boldsymbol{v}_2\,|^2_{1,\Omega}\ (1 - c_\Omega^2\nu^{-2}\|\boldsymbol{f}\|_{-1}) \ \leq\ 0$. Thus, the solution is unique, if $c_\Omega^2\nu^{-2}\|\boldsymbol{f}\|_{-1} \ \leq\ 1$.

Evolutionary problems

We now expand the stationary (nonlinear) problem to the evolutionary case, i.e. we add the term $(\partial_t\,\boldsymbol{v}, \boldsymbol{\varphi})_\Omega$, demand suitable initial conditions $\boldsymbol{v}(0) = \boldsymbol{v}_0$ and consider the set of equations in a time interval $(0, \mathcal{T})$. The evolutionary problem is given by

$$\begin{aligned} &\textit{Find}\ \ \boldsymbol{v} \in \mathrm{L}^\infty(0,\mathcal{T};\mathbf{J_0}) \cap \mathrm{L}^2(0,\mathcal{T};\mathbf{J}_1) \\ &\textit{s. t.}\quad (\partial_t\,\boldsymbol{v},\boldsymbol{\varphi})_\Omega + \mathrm{a}(\boldsymbol{v},\boldsymbol{\varphi}) + \mathrm{c}(\boldsymbol{v},\boldsymbol{v},\boldsymbol{\varphi}) = \langle \boldsymbol{f},\boldsymbol{\varphi}\rangle \qquad \forall\,\boldsymbol{\varphi} \in \mathbf{J}_1\,. \end{aligned} \tag{3.13}$$

Solutions of (3.13) are subdivided with respect to their regularity properties:

Definition 3.9. *Let $\mathcal{T} > 0$ be given. A solution $\boldsymbol{v}$ of problem (3.13) is called*

(a) local weak *solution, if* $\boldsymbol{v} \in \mathrm{L}^\infty(0,\mathcal{T};\mathbf{J_0}) \cap \mathrm{L}^2(0,\mathcal{T};\mathbf{J}_1)$,

(b) local strong *solution, if* $\boldsymbol{v} \in \mathrm{L}^\infty(0,\mathcal{T}\,;\mathbf{J}_1) \cap \mathrm{L}^2(0,\mathcal{T}\,;\mathbf{J}_1 \cap \mathbf{H}^2(\Omega))$ *and*
$$\partial_t\, \boldsymbol{v} \in \mathrm{L}^2(0,\mathcal{T}\,;\mathbf{J_0}).$$

If (a) or (b) applies for arbitrary $\mathcal{T} > 0$, the solution is called (global) weak *or (global)* strong *solution, respectively.*

The analysis of existence and uniqueness of solutions is based on the ideas of the stationary case. The Galerkin approximation of the evolutionary set of equations can be considered as a finite dimensional system of ordinary differential equations (ODE). Therefore, we can use the techniques of the ODE framework. The most important theorems are presented in the following.

Theorem 3.10 (Picard - Lindelöf)**.** *Let $\boldsymbol{y}_0 \in \mathbb{R}^n$ and $B := \{\boldsymbol{y} \in \mathbb{R}^n \mid \|\boldsymbol{y} - \boldsymbol{y}_0\| \le \beta\}$, $\boldsymbol{f} : [t_0 - \alpha, t_0 + \alpha] \times B \to \mathbb{R}^n$ be continuous, bounded by M and Lipschitz continuous in its second component. Then, the ordinary differential equation (ODE)*

$$\boldsymbol{y}'(t) = \boldsymbol{f}(t, \boldsymbol{y}(t)), \quad \boldsymbol{y}(t_0) \;=\; \boldsymbol{y}_0$$

has a unique solution within $[t_0 - \varepsilon, t_0 + \varepsilon]$ for $\varepsilon = \min\{\alpha, \beta/M\}$.

Proof. See [Har02]. □

Theorem 3.11 (Gronwall)**.** *Let $I := [t_0, t_0 + \alpha]$ with $\alpha > 0$, such that $\boldsymbol{f}$ and $\boldsymbol{g}$ are continuous functions with $\boldsymbol{f}(t),\ \boldsymbol{g}(t) \ge 0$ in I and*

$$\boldsymbol{f}(t) \;\le\; c_1 \int_{t_0}^{t} \boldsymbol{g}(s)\boldsymbol{f}(s)\; ds + c_2 \qquad\qquad \forall t \in I$$

for constants $c_1, c_2 > 0$. Then,

$$\boldsymbol{f}(t) \;\le\; c_2 \exp\left(c_1 \int_{t_0}^{t} \boldsymbol{g}(s)\; ds\right) \qquad\qquad \forall t \in I\,.$$

Proof. See [Ver00]. □

We start with an outline of an existence analysis for local *weak* solutions. For any $t \in (0, \mathcal{T})$, the Galerkin approximated evolutionary problem is given by

$$\begin{aligned} &\textit{Find}\ \ \boldsymbol{v}_m(t) \in \mathbf{V}_m \\ &\textit{s. t.}\quad (\partial_t\, \boldsymbol{v}_m(t), \boldsymbol{\varphi})_\Omega + \mathrm{a}(\boldsymbol{v}_m(t), \boldsymbol{\varphi}) + \mathrm{c}(\boldsymbol{v}_m(t), \boldsymbol{v}_m(t), \boldsymbol{\varphi}) = \langle \boldsymbol{f}, \boldsymbol{\varphi}\rangle \quad \forall\, \boldsymbol{\varphi} \in \mathbf{V}_m\ . \end{aligned} \tag{3.14}$$

Application of Theorem 3.10 assures existence of local solutions of (3.14). For validation of the appropriate premises we refer to the stationary case and assume suitable

regularity of the forcing $\boldsymbol{f}$. If we diagonally test and temporally integrate problem (3.14), we result in a total energy budget, which is uniformly bounded in time, i.e.

$$\| \boldsymbol{v}_m(t)\|^2_{0,\Omega} + \nu \|\nabla \boldsymbol{v}_m \|^2_{\mathrm{L}^2(0,t,\mathbf{L}^2(\Omega))} \;\leq\; \| \boldsymbol{v}_0 \|^2_{0,\Omega} + \nu^{-1} \|\boldsymbol{f}\|^2_{\mathrm{L}^2(0,t,-1)}\,, \tag{3.15}$$

whereas the operator norm $\|\boldsymbol{f}\|_{\mathrm{L}^2(0,t,-1)}$ is defined as

$$\|\boldsymbol{f}\|_{\mathrm{L}^2(0,t,-1)} := (\int_0^t \|\boldsymbol{f}(s)\|^2_{-1} ds)^{1/2}\,.$$

Application of Theorem 3.11 then assures a global Lipschitz condition, such that the application of Theorem 3.10 assures (global) existence of solutions of (3.14). The inequality of Leray (3.15) applies for any $m \in \mathbb{N}$, such that $(\boldsymbol{v}_m)_{m\in\mathbb{N}}$ is bounded in $\mathrm{L}^\infty(0,\mathcal{T};\mathbf{J_0}) \cap \mathrm{L}^2(0,\mathcal{T};\mathbf{J}_1)$. Thus, $(\boldsymbol{v}_m)_{m\in\mathbb{N}}$ has a subsequence $(\boldsymbol{v}_{m'})_{m'\in\mathbb{N}}$, which is weakly convergent in $\mathrm{L}^2(0,\mathcal{T};\mathbf{J}_1)$ and which is weakly-* convergent in $\mathrm{L}^\infty(0,\mathcal{T};\mathbf{J_0})$. The limes is denoted as $\boldsymbol{v} \in \mathrm{L}^2(0,\mathcal{T};\mathbf{J}_1)$, which is the solution of (3.13).

Due to the missing regularity control of the solution, uniqueness of weak solutions is most difficult of access in concerns of regularity analysis of incompressible flow problems, see also [DG04]. An approach to assure the necessary regularity is provided by the increase of the regularity demands on the solution $\boldsymbol{v}$. This can be achieved by increased regularity of the data, i.e. the initial data and the forcing, and the underlying domain, see also Section 3.4.1, which also leads to increased regularity of the solution.

Given a solution $\boldsymbol{v}$, suppose sufficient regularity of $\boldsymbol{v}$. In particular, let $\|\nabla \boldsymbol{v}\|_{\infty,\Omega} < \infty$. Consider the estimate (3.15) formulated in $\mathbf{J}_1$, instead of $\mathbf{V}_m$. In order to prove uniqueness of $\boldsymbol{v}$, assume another solution $\widetilde{\boldsymbol{v}}$ of (3.13), take the difference of (3.13) formulated with $\boldsymbol{v}$ and with $\widetilde{\boldsymbol{v}}$ and test with $\boldsymbol{w} := \boldsymbol{v} - \widetilde{\boldsymbol{v}}$. Then, the resulting energy evolution equation for $\boldsymbol{w}$ is, see also [DG04],

$$\frac{1}{2}\partial_t \| \boldsymbol{w}\|^2_{0,\Omega} + ((\boldsymbol{w}\cdot\nabla)\,\boldsymbol{v}, \boldsymbol{w})_\Omega \quad = \quad -\nu \|\nabla \boldsymbol{w}\|^2_{0,\Omega}. \tag{3.16}$$

The authors of [DG04] further deduce, that if there is a sufficient estimate for the nonlinear term, such that

$$((\boldsymbol{w}\cdot\nabla)\,\boldsymbol{v}, \boldsymbol{w})_\Omega \;\leq\; \|\nabla \boldsymbol{v}\|_{\infty,\Omega} \| \boldsymbol{w}\|^2_{0,\Omega}$$

with finite expression $\|\nabla \boldsymbol{v}\|_{\infty,\Omega}$, then (3.16) can be recasted as an ODE. Applicating Theorem 3.11, we deduce

$$\| \boldsymbol{w}\|^2_{0,\Omega} \leq \| \boldsymbol{w}(0)\|^2_{0,\Omega} \exp\left(c + \int_0^t \|\nabla \boldsymbol{v}\|_{\infty,\Omega} ds \right)\,. \tag{3.17}$$

The term $\| \boldsymbol{w}(0)\|_{0,\Omega}$ is equal to zero, as we assumed $\boldsymbol{v}$ and $\widetilde{\boldsymbol{v}}$ to be solutions of the same problem, in particular $\boldsymbol{v}(0) = \widetilde{\boldsymbol{v}}(0) = \boldsymbol{v}_0$, which states uniqueness.

A similar approach is applied for the validation of existence of *strong* solutions. Here, the exponential term in (3.17) enforces smallness conditions on the data, unless suitable regularity constraints are presumed.

3.1.3 Hydrostatic issues

In [AG94], Amrouche and Girault developed an analysis for the stationary, linear, non hydrostatic problem in a broader frame, i.e. for $\mathbf{V} = \mathbf{W}_0^{1,p}(\Omega)$ and $Q := \mathrm{L}_0^q(\Omega)$, $p \in (1,\infty)$ and $1/p + 1/q = 1$, and thus deviated from the Hilbert space framework. Theorem 3.3 was circumvented by application of a Helmholtz-like decomposition and the isomorphism properties of $\nabla : \mathrm{W}^{-m,q}(\Omega)/\mathbb{R} \to \mathbf{V}_{m+1,p}^{\circ}$ and $\mathrm{div} : \mathbf{W}_0^{m+1,p}(\Omega)/\mathbf{V}_{m+1,p} \to \mathrm{W}_0^{m,p}(\Omega) \cap \mathrm{L}_0^p(\Omega)$. Here, constant m is an arbitrary nonnegative integer. The space $\mathbf{V}_{m+1,p}$ is defined as closure of $\mathcal{V}$, see Theorem 3.4, in $\mathrm{W}^{m,p}(\Omega)$ and $\mathbf{V}_{m+1,p}^{\circ}$ denotes the polar space of $\mathbf{V}_{m+1,p}$.

As it turns out in the upcoming, the analysis of hydrostatic problems involving suitable advection, necessitates a non Hilbertian approach. The article [AG94] supplies a basis for the discussions in that context. In particular, it assures, that a suitably modified hydrostatic inf-sup constraint leads to a unique hydrostatic pressure, if a suitable solution of the hydrostatic momentum equation, i.e. the horizontal velocity field, is determined in a $\mathrm{div}\,'(\mathbf{M}\,\cdot)$ - free variational horizontal velocity space. In the upcoming, we will validate this modified inf-sup condition for Sobolev spaces with arbitrary order $p \in (1,\infty)$. Beforehand, we collect some relevant properties of the averaging operator, which is part of the inf-sup constraint.

Averaging operator

The variational version of the averaging operator (2.4) is given by

$$\mathbf{M} : \mathbf{W}_b^{1,p}(\Omega) \to \mathbf{W}_0^{1,p}(\omega), \qquad \left(\mathbf{M}\,\boldsymbol{v} - \int_{-d(\cdot)}^{0} \boldsymbol{v}(\cdot,z)\,dz, \boldsymbol{\varphi} \right)_{\omega} = 0 \quad \forall\ \boldsymbol{\varphi} \in \mathbf{W}^{1,q}(\omega)\,. \tag{3.18}$$

We validated the following properties of the averaging operator in [KB12] for $p = 2$. In the upcoming subsections it turns out, that different kind of problems necessitate different choices of the variational spaces. In order to take that issue into account, we broaden the scope to the case $p \in (1,\infty)$.

Lemma 3.12. *Let $p \in (1,\infty)$, Ω be a flat domain and $\mathbf{V} = \mathbf{W}_0^{1,p}(\Omega)$ or $\mathbf{V} = \mathbf{W}_b^{1,p}(\Omega)$. The operator $\mathbf{M} : \mathbf{V} \to \mathbf{W}_0^{1,p}(\omega)$ is linear, continuous and surjective. Furthermore, for each $\boldsymbol{w} \in \mathbf{W}_0^{1,p}(\omega)$ there exists $\boldsymbol{v} \in \mathbf{V}$, so that $\mathbf{M}\,\boldsymbol{v} = \boldsymbol{w}$ and*

$$|\,\boldsymbol{v}\,|_{1,p,\Omega} \leq c_\omega \delta_{min}^{(1-2p)/p} |\,\boldsymbol{w}\,|_{1,p,\omega}\,.$$

c_ω is proportional to the Poincare-Friedrichs constant related to ω.

Proof. Operator $\mathbf{M} : \mathbf{V} \to \mathbf{W}_0^{1,p}(\omega)$ is defined by equation (3.18). Let $\boldsymbol{v} \in \mathbf{V}$ be chosen arbitrarily. Applicating Leibniz integration rule and the Hölder inequality leads to the bound

$$|\,\mathbf{M}\,\boldsymbol{v}\,|_{1,p,\omega} \;\leq\; \delta_{max}^{1/q} |\,\boldsymbol{v}\,|_{1,p,\Omega} \qquad \forall\,\boldsymbol{v} \in \mathbf{V}\,. \tag{3.19}$$

Thus, $\mathbf{M}$ is continuous. Let $\zeta \in \mathcal{C}(\mathbb{R})$ be defined by

$$\zeta(z) \;:=\; \begin{cases} -z & \text{if } -\delta_{min}/2 \le z \le 0, \\ z+\delta_{min} & \text{if } -\delta_{min} < z < -\delta_{min}/2, \\ 0 & \text{else.} \end{cases}$$

Due to this construction, we obtain $\int_{-d(x,y)}^{0} \zeta(z)\,dz = \delta_{min}^2/4$. Hence, for arbitrary $\boldsymbol{w} \in \mathbf{W}_0^{1,p}(\omega)$ the function $\boldsymbol{v}(x,y,z) := 4\delta_{min}^{-2}\,\boldsymbol{w}(x,y)\zeta(z)$ is element of $\mathbf{V}$ and $\mathbf{M}\,\boldsymbol{v} = \boldsymbol{w}$. In other words, $\mathbf{M}$ is surjective. By elementary calculus and Lemma 3.1 we obtain

$$\begin{aligned} |\,\boldsymbol{v}\,|_{1,p,\Omega} &= \frac{4}{\delta_{min}^2}(\|\zeta\|_{0,p,\mathbb{R}}|\,\boldsymbol{w}\,|_{1,p,\omega} + |\zeta|_{1,p,\mathbb{R}}\|\,\boldsymbol{w}\,\|_{0,p,\omega}) \\ &\le \frac{4}{\delta_{min}^2}(\|\zeta\|_{0,p,\mathbb{R}} + c_F|\zeta|_{1,p,\mathbb{R}})|\,\boldsymbol{w}\,|_{1,p,\omega}\,, \end{aligned}$$

with the Poincare-Friedrichs constant c_F. Finally, due to the estimates $\|\zeta\|_{0,p,\mathbb{R}} \le c\delta_{min}^{(p+1)/p}$ and $|\zeta|_{1,p,\mathbb{R}} \le c\delta_{min}^{1/p}$, the flatness of Ω, which leads to $2c_F \gg (p+1)^{-1/p}\delta_{min}$, we arrive at the desired estimate. □

Modified inf-sup constraint

In [KB12], we proved the following proposition for the case $p = 2$.

Proposition 3.13. *Let Ω be a flat domain and $p \in (1,\infty)$. Then*

$$\sup_{\boldsymbol{v}\in\mathbf{V}\setminus\{0\}} \frac{(div'\,\mathbf{M}\,\boldsymbol{v}, q)_\omega}{|\,\boldsymbol{v}\,|_{1,p,\Omega}} \;\ge\; \widetilde{\gamma}_{\Omega,\omega}\|q\|_{0,q,\omega} \qquad \forall q \in \mathrm{L}_0^q(\omega)$$

applies.

Proof. Based on the De Rham Lemma, see [dR60], the authors of [AG94] proved the modified inf-sup constraint, presented here for 2D domains,

$$\sup_{\boldsymbol{w}\in\mathbf{W}_0^{1,p}(\omega)\setminus\{0\}} \frac{(\mathrm{div}'\,\boldsymbol{w}, q)_\omega}{|\,\boldsymbol{w}\,|_{1,p,\omega}} \;\ge\; \widetilde{\gamma}_{\omega}\|q\|_{0,q,\omega} \qquad \forall q \in \mathrm{L}_0^q(\omega)\,.$$

Let $q \in \mathrm{L}_0^q(\omega)$ be given and $\boldsymbol{w} \in \mathbf{W}_0^{1,p}(\omega)$ a corresponding 2D velocity field with $|\,\boldsymbol{w}\,|_{1,p,\omega} = 1$ and

$$(\mathrm{div}'\,\boldsymbol{w}, q)_\omega \;\ge\; \widetilde{\gamma}_{\omega}\|q\|_{0,q,\omega}\,.$$

Due to Lemma 3.12 we find a $\boldsymbol{v} \in \mathbf{V}$ with $\mathbf{M}\,\boldsymbol{v} = \boldsymbol{w}$ and $|\,\boldsymbol{v}\,|_{1,p,\Omega} \le c_\omega\delta_{min}^{(1-2p)/p}|\,\boldsymbol{w}\,|_{1,p,\omega}$. By construction we obtain

$$(\mathrm{div}'\,\mathbf{M}\,\boldsymbol{v}, q)_\omega \;\ge\; \widetilde{\gamma}_{\omega}\|q\|_{0,q,\omega} \;\ge\; \widetilde{\gamma}_{\omega}\delta_{min}^{(2p-1)/p}c_\omega^{-1}\|q\|_{0,q,\omega}|\,\boldsymbol{v}\,|_{1,p,\Omega}\,.$$

The assertion follows with $\widetilde{\gamma}_{\Omega,\omega} := \widetilde{\gamma}_{\omega}\delta_{min}^{(2p-1)/p}c_\omega^{-1}$. □

Remark 3.14. *As already mentioned in [KB12] for the case $p = 2$, the δ_{min}-dependence of the previously defined inf-sup constant $\gamma_{\Omega,\omega}$ indicates a decrease of stability for flat domains Ω. In order to qualitatively understand this dependence, let us consider the surface $\omega := (0, d_1) \times (0, d_2)$. According to Dobrowolski [Dob03], the inf-sup constant for ω is to be found in the following range:*

$$\frac{\sin(\pi/8)}{\max(d_1/d_2, d_2/d_1)} \;\leq\; \gamma_\omega \;\leq\; \frac{\pi/\sqrt{12}}{\max(d_1/d_2, d_2/d_1)}\,.$$

Hence, if the directional diameters are similar, $d_1 \approx d_2$, we observe $\gamma_\omega \approx 1$. Further, for flat domains $\Omega := \omega \times (0, d_3)$, i.e. $a := d_1/d_3 > 1$, the inf-sup constant for the 3D Stokes problem in Ω is of order

$$\gamma_\Omega \;\sim\; a^{-1}.$$

On the other hand, let us consider the inf-sup constant of the discrete 2.5D problem. Since $\delta_{min} = d_3$ and $c_\omega \sim d_1$, we have

$$\widetilde{\gamma}_{\Omega,\omega} = \widetilde{\gamma}_\omega \delta_{min}^{(2p-1)/p} c_\omega^{-1} \;\sim\; d_3^{1/q} a^{-1}\,.$$

It seems reasonable to draw the conclusion, that the magnitude of the inf-sup constant of the hydrostatic problem can be adjusted to the depth of Ω, i.e. the scaling of $d_3^{1/q}$. But, this conclusion is misleading due to the fact, that the pressure and the bilinear term in the hydrostatic case are 2D, instead of 3D. The factor $d_3^{1/q}$ accounts for the different scaling of $\|p\|_{0,q,\omega}$ (hydrostatic pressure in the L^q-norm) and $\|q\|_{0,\Omega}$ (3D pressure in the L^2-norm). Thus, the anisotropic effects in the hydrostatic case and in the 3D case qualitatively match.

3.2 Variational stationary systems

In this section we consider stationary, hydrostatic problems. We start with the simplest case, the 2.5D Stokes problem, then add an advection term with fix advection to the problem, i.e. consider the 2.5D Oseen problem, which already shows some difficulties of the nonlinear case. More precisely, due to the construction of diagnostical vertical velocity component, the advection term shows less regularity than known from the full 3D problem. This results in a non symmetric choice of variational spaces and to a non standard regularity argumentation. We end with a treatment of the nonlinear case, i.e. we consider the 2.5D Navier-Stokes problem.

For each of the introduced problems we collect main regularity results, given in literature. Note, that the techniques to establish these regularity statements either are similar to the classical, non hydrostatic case as introduced in Section 3.1.2, or are retrieved in a limiting process by consideration of anisotropic versions of the classical problem in vertical anisotropic domains.

3.2.1 Hydrostatic Stokes problem

We neglect time derivatives, as well as the advection term in (2.31) and start with the appropriate stationary, linear problem, the *stationary hydrostatic Stokes problem*. As the vertical velocity v_3 thus has no further dynamical impact, we neglect this variable and skip equation (2.30) in this case.

Assuming low regularity on the data, i.e.

$$\boldsymbol{f} \in \mathrm{H}_b^{-1}(\Omega) \quad \text{and} \quad \boldsymbol{g} \in \mathrm{H}^{-1/2}(\Gamma_u)\,, \tag{3.20}$$

the stationary hydrostatic Stokes problem reads:

$$\begin{aligned} &\textit{Given (3.20), find } \boldsymbol{u} := (\boldsymbol{v}, p) \in \mathbf{H}_b^1(\Omega) \times \mathrm{L}_0^2(\omega) \textit{ s. t.} \\ &\qquad \mathrm{a}(\boldsymbol{v}, \boldsymbol{\varphi}) - \mathrm{b}(p, \boldsymbol{\varphi}) + \mathrm{b}(\xi, \boldsymbol{v}) = \boldsymbol{l}(\boldsymbol{\varphi}) \qquad \forall (\boldsymbol{\varphi}, \xi) \in \mathbf{H}_b^1(\Omega) \times \mathrm{L}_0^2(\omega) \end{aligned} \tag{3.21}$$

with

$$\mathrm{a}(\boldsymbol{v}, \boldsymbol{\varphi}) := (\nabla_{\boldsymbol{\mathcal{A}}_\nu} \boldsymbol{v}, \nabla_{\boldsymbol{\mathcal{A}}_\nu} \boldsymbol{\varphi})_\Omega + (\mathrm{f}\, \boldsymbol{v}^\perp, \boldsymbol{\varphi})_\Omega \tag{3.22}$$

$$\mathrm{b}(p, \boldsymbol{\varphi}) := (p, \mathrm{div}'\, \mathbf{M}\, \boldsymbol{\varphi})_\omega \tag{3.23}$$

$$\boldsymbol{l}(\boldsymbol{\varphi}) := \langle \boldsymbol{f}, \boldsymbol{\varphi} \rangle_\Omega + \langle \boldsymbol{g}, \boldsymbol{\varphi} \rangle_{\Gamma_u}\,. \tag{3.24}$$

The forcing term $\boldsymbol{f}$ denotes a suitable body force, whereas $\boldsymbol{g}$ describes the wind stress acting on Γ_u.

Similar to the full 3D Stokes problem, the Lagrangian multiplier of the nonlocal continuity constraint is given by the pressure, see e.g. [LTW92]. Recall the definitions (3.12) and (3.5) of $\mathbf{J_0}$ and $\mathbf{J}_1$, respectively. The hydrostatic analogon is given by

$$\mathbf{J_0} := \{\boldsymbol{v} \in \mathbf{L}^2(\Omega) \mid \mathrm{div}'(\mathbf{M}\, \boldsymbol{v}) = 0 \text{ and } \mathbf{M}\, \boldsymbol{v} \cdot \boldsymbol{n}|_{\partial\omega} = 0\} \tag{3.25}$$

$$\mathbf{J}_1 := \{\boldsymbol{v} \in \mathbf{H}_b^1(\Omega) \mid \mathrm{div}'(\mathbf{M}\, \boldsymbol{v}) = 0\}\,, \tag{3.26}$$

$\mathbf{M}\, \boldsymbol{v} \cdot \boldsymbol{n}|_{\partial\omega}$ is meant in the $\mathbf{H}^{-1/2}(\partial\omega)$-sense. The reformulated problem in $\mathrm{div}'(\mathbf{M}\,\cdot)$-free velocity spaces reads

$$\begin{aligned} &\textit{Given (3.20), find a (weak) solution } \boldsymbol{v} \in \mathbf{J}_1 \textit{ s. t.} \\ &\qquad \mathrm{a}(\boldsymbol{v}, \boldsymbol{\varphi}) = \boldsymbol{l}(\boldsymbol{\varphi}) \qquad \forall\, \boldsymbol{\varphi} \in \mathbf{J}_1 \end{aligned} \tag{3.27}$$

Given a solution $\boldsymbol{v} \in \mathbf{J}_1$ of (3.27), the pressure can be determined by

$$(p,\, \mathrm{div}'(\mathbf{M}\, \boldsymbol{\varphi}))_\omega = \boldsymbol{l}(\boldsymbol{\varphi}) - \mathrm{a}(\boldsymbol{v}, \boldsymbol{\varphi}) \qquad \forall\, \boldsymbol{\varphi} \in \mathbf{H}_b^1(\Omega)\,,$$

using a suitably adapted De Rham Lemma, see Theorem 3.4 and Section 3.1.3. This approach of $\mathrm{div}'(\mathbf{M}\,\cdot)$- free spaces can be applied in each of the following hydrostatic problems, leading to a pressure-free set of equations.

Regularity statements

Unique existence of a *weak* solution of problem (3.27) was proven by [BL92, CG00]. In [KB12], we similarly validated unique existence of *weak* solutions, imposing Dirichlet data on the entire boundary.

Ziane established unique existence of a *strong* solution $\boldsymbol{v} \in \mathbf{J}_1 \cap \mathbf{H}^2(\Omega)$ in domains with a $\mathcal{C}^3$– depth function $d \in \mathcal{C}^3(\overline{\omega})$, assuming additional regularity on the data, i.e.

$$\boldsymbol{f} \in \mathbf{L}^2(\Omega) \quad \text{and} \quad \boldsymbol{g} \in \mathbf{H}_0^{1/2+\varepsilon}(\Gamma_u)\,,\ \varepsilon > 0\,, \tag{3.28}$$

see [Zia97]. In [Zia95], the author also revealed unique existence of a *strong* solution in the case of homogeneous Dirichlet boundary conditions, as well as periodic Dirichlet boundary conditions in a domain with a $\mathcal{C}^3$– depth function, assuming $\mathrm{f} = 0$.

The pressure has L^2-regularity, see [CR04]. Assuming (3.28), Ziane proved H^1-regularity for the pressure in a domain with $\mathcal{C}^3$– depth function.

3.2.2 Hydrostatic Oseen problem

Turning to the stationary limit of (2.29) - (2.34), we are faced with the choice of the variational spaces:
For a given horizontal velocity field $\boldsymbol{v} \in \mathbf{H}_b^1(\Omega)$, the appropriate vertical velocity component v_3, determined by (2.30), generally has lower regularity than its horizontal counterpart, i.e. $v_3 \in \mathrm{L}^2(\Omega)$ and $\partial_z v_3 \in \mathrm{L}^2(\Omega)$. Thus, in general $v_3 \notin \mathrm{H}^1(\Omega)$ and the entire 3D velocity field (v_1, v_2, v_3) is element of the following set of $\mathrm{div}\,'(\mathbf{M}\,\cdot)$- free functions

$$\begin{aligned}\mathbf{H}_{\mathrm{a}} := \Big\{ \boldsymbol{b} = (b_1, b_2, b_3) \in \mathbf{H}_b^1(\Omega) \times \mathrm{L}^2(\Omega) \mid \\ b_3(x,y,z) = -\int_{-d(x,y)}^{z} (\partial_x b_1(x,y,\widehat{z}) + \partial_y b_2(x,y,\widehat{z}))\, d\widehat{z}\,,\ b_3|_{\Gamma_u} = 0 \Big\}\,,\end{aligned} \tag{3.29}$$

Thus, for any $\boldsymbol{b} \in \mathbf{H}_{\mathrm{a}}$ and $\boldsymbol{v} \in \mathbf{H}_b^1(\Omega)$, the advection term is given by

$$(\boldsymbol{b} \cdot \nabla)\, \boldsymbol{v} \in [\mathbf{W}^{1,3}(\Omega)]' \quad \text{with} \quad \langle (\boldsymbol{b} \cdot \nabla)\, \boldsymbol{v}, \boldsymbol{\varphi} \rangle := -((\boldsymbol{b} \cdot \nabla)\, \boldsymbol{\varphi}, \boldsymbol{v})_\Omega \quad \forall\, \boldsymbol{\varphi} \in \mathbf{W}_b^{1,3}(\Omega)\,, \tag{3.30}$$

see also [CG00]. This missing H^{-1}-regularity of the advection term effects the non Hilbertian choice of a suitable trial space, $\mathbf{X}$, and test space, $\mathbf{Y}$:

$$\mathbf{X} := \mathbf{V} \times Q \qquad \text{with } \mathbf{V} := \mathbf{H}_b^1(\Omega) \quad \text{and } Q := \mathrm{L}_0^{3/2}(\omega), \tag{3.31}$$

$$\mathbf{Y} := \widetilde{\mathbf{V}} \times \widetilde{Q} \qquad \text{with } \widetilde{\mathbf{V}} := \mathbf{W}_b^{1,3}(\Omega) \ \text{ and } \widetilde{Q} := \mathrm{L}_0^2(\omega). \tag{3.32}$$

The justification of these choices is the following: Due to (3.30), the test space of the velocity field has to be chosen as $\mathbf{W}^{1,3}(\Omega)$. Due to the pressure gradient term, this effects $\mathrm{W}^{1,3/2}(\omega)$-regularity for the pressure gradient, i.e. $\nabla' p \in \mathrm{W}^{1,3/2}(\omega)$, which in

turn means $p \in L_0^{3/2}(\omega)$. As the trial space of the velocity field is $\mathbf{H}_b^1(\Omega)$ and due to the divergence constraint, the test space for the pressure is $\mathrm{L}_0^2(\omega)$.
Given an advection $\boldsymbol{b} \in \mathbf{H}_\mathrm{a}$, the hydrostatic Oseen problem is:

$$\begin{aligned} &\textit{Given (3.20), find a (weak) solution } \mathbf{u} := (\boldsymbol{v}, p) \in \mathbf{X} \textit{ s. t.} \\ &\qquad A(\boldsymbol{b}; \mathbf{u}; \boldsymbol{\phi}) \quad = \quad \boldsymbol{l}(\boldsymbol{\varphi}) \qquad\qquad \forall\, \boldsymbol{\phi} := (\boldsymbol{\varphi}, \xi) \in \mathbf{Y} \end{aligned} \tag{3.33}$$

with

$$A(\boldsymbol{b}; \mathbf{u}; \boldsymbol{\phi}) := \quad \mathrm{a}(\boldsymbol{v}, \boldsymbol{\varphi}) + \mathrm{c}(\boldsymbol{b}, \boldsymbol{v}, \boldsymbol{\varphi}) - \mathrm{b}(p, \boldsymbol{\varphi}) + \mathrm{b}(\xi, \boldsymbol{v}) \tag{3.34}$$

$$\mathrm{c}(\boldsymbol{b}, \boldsymbol{v}, \boldsymbol{\varphi}) := \quad \langle (\boldsymbol{b} \cdot \nabla)\, \boldsymbol{v}, \boldsymbol{\varphi} \rangle\,. \tag{3.35}$$

Regularity statements

Due to the tight connection of the hydrostatic Oseen problem to the hydrostatic Navier-Stokes problem, we refer to the next section and note, that if existence of a solution is assured in the nonlinear context, existence of a solution accompanies uniqueness in the Oseen case, due to linearity of the problem.

3.2.3 Hydrostatic Navier-Stokes problem

Applying the considerations from the preceding section, the variational formulation of the hydrostatic Navier-Stokes problem (2.29) – (2.34) is given by:

$$\begin{aligned} &\textit{Given (3.20), find a (weak) solution } \mathbf{u} := (\boldsymbol{v}, p) \in \mathbf{X} \textit{ s. t.} \\ &\qquad A((\boldsymbol{v}, v_3); \mathbf{u}; \boldsymbol{\phi}) \quad = \quad \boldsymbol{l}(\boldsymbol{\varphi}) \qquad\qquad \forall\, \boldsymbol{\phi} := (\boldsymbol{\varphi}, \xi) \in \mathbf{Y} \end{aligned} \tag{3.36}$$

The operator A and the forcing $\boldsymbol{l}$ are given by (3.34) and (3.24), respectively. The vertical velocity component $v_3 \in \mathrm{L}_2(\Omega)$ is deduced by (2.30).

Regularity statements

Existence of a *weak* solution was validated in [BL92], presuming $\boldsymbol{f} = 0$ and $\boldsymbol{g} \in \mathbf{H}^{1/2}(\Gamma_u)$. Under the more extensive regularity assumption (3.20), the same results were obtained in [CG00, CLC00].

Uniqueness of *weak* solutions is still an open problem. The crux lies in the lack of regularity of the third velocity component v_3, given by (2.30), which is responsible for the lack of regularity of the advection term (3.30) and thus for the non standard non Hilbertian variational approach (3.36), see also [CLC00].

However, under smallness assumptions on $\boldsymbol{f}$ and $\boldsymbol{g}$ with respect to the norms $\mathbf{L}^2(\Omega)$ and $\mathbf{H}_0^{1/2+\varepsilon}(\Gamma_u)$, $\varepsilon > 0$, respectively, unique existence of a *strong* solution $\boldsymbol{v} \in \mathbf{J}_1 \cap \mathbf{H}^2(\Omega)$ of the nonlinear problem was proven in [GMR01].

Due to [CR04], the pressure has L^2-regularity, unless the domain definition is relaxed to the case $d(x,y) \geq 0$ for $(x,y) \in \partial\omega$. In this case, the pressure shows only $\mathrm{L}^{3/2}$-regularity. However, the authors of [CR04] point out, that the pressure converges in $\mathrm{L}^2(\omega')$ for any interior subdomain ω' of ω with $d(x,y) \geq \delta^*$ for all $(x,y) \in \omega'$ and some $\delta^* > 0$.

3.3 Variational evolutionary systems

In this section we turn to the time-dependent problems. We start with the linear Stokes case. As the main task of the Oseen problem, i.e. explaining the non symmetric choice of the variational spaces, has already been clarified in the stationary case, we do not consider the evolutionary counterpart, but immediately turn over to the nonlinear case, i.e. the Navier-Stokes problem. For both problems, we collect regularity statements, given in literature. The notions *weak* and *strong* solutions carry over from the classical framework as introduced in Section 3.1.2. As in the stationary case, the techniques to establish regularity statements either are similar to the classical, non hydrostatic case, see Section 3.1.2, or are retrieved in a limiting process by consideration of anisotropic versions of the classical problem.

3.3.1 Hydrostatic Stokes problem

We neglect the nonlinear advection term in (2.31) of the hydrostatic Navier-Stokes problem. Let $\mathcal{T} > 0$. Under the assumption of low regularity on the data, i.e.

$$\boldsymbol{v}_0 \in \mathbf{J_0}\,, \;\; \boldsymbol{f} \in \mathrm{L}^2(0,\mathcal{T};\mathbf{H}_b^{-1}(\Omega)) \;\; \text{and} \;\; \boldsymbol{g} \in \mathbf{L}^2(0,\mathcal{T};\mathbf{H}^{-1}(\Gamma_u)) \tag{3.37}$$

the variational formulation of the resulting evolutionary hydrostatic Stokes problem is given by

$$\begin{aligned} &\textit{Given (3.37), find a (weak) solution } \; \boldsymbol{v} \in \mathrm{L}^\infty(0,\mathcal{T};\mathbf{J_0}) \cap \mathrm{L}^2(0,\mathcal{T};\mathbf{J}_1) \; \textit{s. t.} \qquad (3.38)\\ &\int_0^{\mathcal{T}} -(\boldsymbol{v},\partial_t\boldsymbol{\varphi})_\Omega + \mathrm{a}(\boldsymbol{v};\boldsymbol{\varphi})\; dt = -(\boldsymbol{v}_0,\boldsymbol{\varphi}(0))_\Omega + \int_0^{\mathcal{T}} \boldsymbol{l}(\boldsymbol{\varphi})\; dt \\ &\qquad\qquad \forall\, \boldsymbol{\varphi} \in \left\{\boldsymbol{\xi} \in \mathrm{H}^1(0,\mathcal{T};\mathbf{J}_1) \mid \boldsymbol{\xi}(\mathcal{T}) = 0\right\}. \end{aligned}$$

Bilinear form a and forcing $\boldsymbol{l}$ are given by (3.22) and (3.24), respectively.

Regularity statements

Global unique existence of a *weak* solution with $\partial_t\,\boldsymbol{v} \in L^2(0,\mathcal{T},\mathbf{J}_1)$ was established in [CLC00] assuming

$$\begin{aligned} &\boldsymbol{v}_0 \in \mathbf{J}_1\,, \qquad \boldsymbol{f} \in \mathrm{L}^2(0,\mathcal{T},\mathbf{J_0}), \qquad (3.39)\\ &\boldsymbol{g} \in \mathrm{L}^2(0,\mathcal{T};\; \mathbf{H}^{-1/2}(\Gamma_u)) \qquad \text{and} \qquad \partial_t\boldsymbol{g} \in \mathrm{L}^2(0,\mathcal{T};\; \mathbf{H}^{-1/2}(\Gamma_u))\,. \end{aligned}$$

Based on the regularity assumptions

$$\begin{aligned} &\boldsymbol{v}_0 \in \mathbf{J}_1\,, \qquad \boldsymbol{f} \in \mathrm{L}^2(0,\mathcal{T};\ \mathbf{J_0})\,, \\ &\boldsymbol{g} \in \mathrm{L}^2(0,\mathcal{T};\ \mathbf{H}_0^{1/2+\varepsilon}(\Gamma_u))\,,\ \varepsilon>0 \qquad \text{and} \quad \partial_t \boldsymbol{g} \in \mathrm{L}^2(0,\mathcal{T};\ \mathbf{H}^{-1/2}(\Gamma_u))\,, \end{aligned} \tag{3.40}$$

global unique existence of a *strong* solution was deduced in [GR05a] for $\mathcal{C}^3$– domains $\Omega \subset \mathbb{R}^n$ with $n \in \{2,\,3\}$.

Unique existence of a pressure $p \in \mathrm{L}^2(0,\mathcal{T};\ \mathrm{L}_0^2(\Gamma_u))$ was established in [CLC00].

3.3.2 Hydrostatic Navier-Stokes problem

The variational formulation of the evolutionary nonlinear problem (2.29)–(2.34) is given by

Given (3.37), find a (weak) solution $\boldsymbol{v} \in \mathrm{L}^\infty(0,\mathcal{T};\mathbf{J_0}) \cap \mathrm{L}^2(0,\mathcal{T};\mathbf{J}_1)$ *s. t.* (3.41)

$$\int_0^{\mathcal{T}} -(\boldsymbol{v},\partial_t\,\boldsymbol{\varphi})_\Omega + \mathrm{a}(\boldsymbol{v};\boldsymbol{\varphi}) + \mathrm{c}((\boldsymbol{v},v_3),\boldsymbol{v};\boldsymbol{\varphi})\ dt = -(\boldsymbol{v}_0,\boldsymbol{\varphi}(0))_\Omega + \int_0^{\mathcal{T}} \boldsymbol{l}(\boldsymbol{\varphi})\ dt$$

$$\forall\,\boldsymbol{\varphi} \in \left\{\boldsymbol{\xi} \in \mathrm{H}^1(0,\mathcal{T};\mathbf{J}_1) \mid \boldsymbol{\xi}(\mathcal{T}) = 0 \text{ and } \partial_z\,\boldsymbol{\varphi} \in \mathrm{L}^\infty(0,\mathcal{T};\mathbf{L}^3(\Omega))\right\}\,.$$

The vertical velocity component $v_3 \in \mathrm{L}_2(\Omega)$ is deduced by (2.30). Bilinear forms a and c and the forcing $\boldsymbol{l}$ are given by (3.22), (3.35) and (3.24), respectively.

Regularity statements

Global existence of *weak* solutions was proven in [PTW04] for $\Omega \subset \mathbb{R}^2$, assuming $\boldsymbol{v}_0 \in \mathbf{J_0}$ and $\boldsymbol{f} \in \mathrm{L}^\infty(0,\mathcal{T};\mathbf{L}^2(\Omega))$. The authors also validated unique existence of solutions up to $\mathcal{C}^\infty$-regularity. On the premise of (3.37), global existence for *weak* solutions in $\Omega \subset \mathbb{R}^3$ was established in [LTW92]. Global existence of *weak* solutions in domains with $\delta_{min} \geq 0$ has been derived by [AG01].

Global uniqueness of *weak* solutions was proven in [GR04], demanding

$$\partial_z\,\boldsymbol{v} \in \mathrm{L}^\infty(0,\mathcal{T};\mathbf{L}^2(\Omega)) \cap \mathrm{L}^2(0,\mathcal{T};\mathbf{H}^1(\Omega))\,. \tag{3.42}$$

This proposition also holds for domains with $\delta_{min} \geq 0$. Note, that smallness conditions are negligible.

For the case of *strong* solutions let Ω be a $\mathcal{C}^3$-domain. Assuming (3.40) and sufficiently small data, global unique existence of *strong* solutions in $\Omega \subset \mathbb{R}^2$ have been established in [GR02]. The appropriate results for 3D domains were deduced in [GMR01] under the assumption of sufficiently small data, $\boldsymbol{v}_0 \in \mathbf{J}_1$, $\boldsymbol{f} = \boldsymbol{f}_1 + \boldsymbol{f}_2$ and $\boldsymbol{g} = \boldsymbol{g}_1 + \boldsymbol{g}_2$ with $(\boldsymbol{f}_1, \boldsymbol{g}_1)$ fulfilling the regularity (3.40), and

$$\begin{aligned} &\boldsymbol{f}_2 \in \mathrm{L}^\infty(0,\mathcal{T};\ \mathbf{L}^2(\Omega)), \\ &\boldsymbol{g}_2 \in \mathrm{L}^\infty(0,\mathcal{T};\ \mathbf{H}_0^{1/2+\varepsilon}(\Gamma_u))\,,\ \varepsilon>0 \qquad \text{and} \quad \partial_t \boldsymbol{g}_2 \in \mathrm{L}^\infty(0,\mathcal{T};\ \mathbf{H}^{-1/2}(\Gamma_u)) \end{aligned}$$

In [GR04], the authors were able to release the smallness assumption in the proof of uniqueness of *strong* solutions. Beside suitable regularity on the data, i.e.

$$\boldsymbol{f} \in \mathrm{L}^2(0,\mathcal{T};\mathbf{L}^2(\Omega))\,, \quad \boldsymbol{g} \in \mathrm{L}^2(0,\mathcal{T};\ \mathbf{H}_0^{1/2+\varepsilon}(\Gamma_u)) \cap L^\infty(0,\mathcal{T};\ \mathbf{H}^{-1/2}(\Gamma_u))\,,\ \varepsilon > 0,$$
$$\partial_t \boldsymbol{g} \in L^2(0,\mathcal{T};\mathbf{H}^{-3/2}(\Gamma_u)) \quad \text{and} \quad \boldsymbol{g}(0) \in \mathbf{H}^{-1/2}(\Gamma_u)\,,$$

the sufficient condition (3.42) was imposed. In [CT07], Cao and Titi proved global unique existence of a *strong* solution, for cylindric domains, assuming

$$\boldsymbol{v}_0 \in \mathbf{J}_1, \quad \boldsymbol{f} \in \mathrm{L}^\infty(0,\mathcal{T};\ \mathbf{H}^1(\Omega)), \quad \boldsymbol{g} = \mathbf{0}\,.$$

The authors note, that global unique existence of a *strong* solution also holds for inhomogeneous boundary conditions.

Applying a suitably adapted version of the lemma of De Rham, see Theorem 3.4, and recalling the regularity results of the stationary case, unique existence of a pressure $p \in \mathrm{W}^{-1,\infty}(0,\mathcal{T};\mathrm{L}^2(\omega))$ can be assured. If $\delta_{min} \geq 0$, the regularity of the pressure decreases to $\mathrm{W}^{-1,\infty}(0,\mathcal{T};\mathrm{L}^{3/2}(\omega))$, see [AG01].

3.4 Regularity effect of the hydrostatic approximation

This section devotes the regularity impact of the hydrostatic approximation. We start with a rough collection of regularity results for non hydrostatic flow problems and compare these to the regularity statements, we collected in the preceding sections.

3.4.1 Regularity statements of non hydrostatic flow problems

In [Tem79], Temam validated unique existence of a solution of the stationary Stokes problem. Literature on regularity of the solution is given by [Cat61, Sol68, JM86]. The latter of these articles states the relation between regularity of the solution and the regularity of the problem data and the domain, i.e. given a forcing term in $\mathbf{H}^m(\Omega)$, $m \geq -1$, and a $\mathcal{C}^r$-domain Ω with $r \geq m+2$, then the solution $\boldsymbol{v}$ has regularity $\mathbf{H}^{m+1}(\Omega)$.

Existence of weak solutions of the steady-state Navier-Stokes equations was established in [Ler33]. The author figured out, that uniqueness can only be assured for sufficiently small data or for an appropriate short time interval. As in the linear case, the relation between the regularity of the solution and the regularities of the problem data applies.

In [FS02], Serenikov validated global unique existence of *weak* and *strong* solutions of the evolutionary Stokes problem.

In 2D, global unique existence of *weak* and *strong* solutions of the evolutionary Navier-Stokes equations is validated, see [Soh01]. In [Tem00], Temam states, that the regularity of the solution increases with the increase of the regularity of the data. Global

existence of a 3D *weak* solution was assured in [LR02]. Uniqueness and regularity of *weak* solutions in 3D domains still are open problems, see e.g. [CT08].

Existence of 3D *strong* solutions is assured in a short time interval $(0, \mathcal{T})$, whereas $\mathcal{T} > 0$ depends on the problem data, see e.g. [FS02]. Cao and Titi elaborated existence of *strong* 3D solutions in $(0, \mathcal{T})$, imposing suitable regularity on the vertical velocity or on the pressure, respectively, whereas $\mathcal{T} > 0$ depends on the appropriate regularity constraint, see [CT08]. Due to [Ser63], there is no other weak solution in $(0, \mathcal{T})$.

Global existence of *strong* solutions in 3D is still an open problem, see [CT08]. Uniqueness of such a *strong* solution was established in [Lad69, Con95].

3.4.2 Comparison of the non hydrostatic and the hydrostatic results

Due to the relations between a given incompressible fluid problem and its hydrostatic approximation, the assumption of similar regularity results seems reasonable. We observe the following:

For the stationary, linear problems, unique existence applies in the non hydrostatic system and in its hydrostatic approximation. This adjusts due to the continuity and coercivity property of the bilinear form a and due to fact, that an altered version of the De Rham lemma also applies for the hydrostatic problem.

In the stationary nonlinear case, existence of *weak* solutions as well as unique existence of *strong* solutions could be proved for the non hydrostatic problem and for its hydrostatic approximation. Uniqueness of a *weak* solution of the non hydrostatic problem could be assured in $\Omega = \mathbb{R}^n$ for sufficiently small data. However, uniqueness of a *weak* solution for the hydrostatic problem is an open problem. The difficulty lies in the loss of regularity of the advection term.

Turning to the evolutionary Stokes case, unique existence of *weak* and *strong* solutions evolved for both, the non hydrostatic and the hydrostatic problem.

However, there is a gap between the evolutionary non hydrostatic Navier-Stokes problem and its hydrostatic approximation. Whereas unique existence of *weak* solutions of the 2D problem is assured, this proposition for the appropriate hydrostatic problem is missing. In 3D, existence of *weak* solutions is still an unresolved problem in both cases.

Note, that global uniqueness results for the *weak* and for the *strong* solutions of the evolutionary hydrostatic Navier-Stokes problem are known, where additional regularity on the solution or on the data, but *no* smallness assumptions on the data are imposed. A similar result for the appropriate non hydrostatic problem is not known to the author.

Concluding, there are a lot of similarities with respect to existence and uniqueness results. In the nonlinear case, the regularity loss in the advection term of the hydrostatic problem leads to still unresolved difficulties in the proof of uniqueness of *weak*

solutions. The appropriate non hydrostatic problems show less troublesome properties, especially in the evolutionary case.

However, the work [GR04] of Guillén González and Rodríguez Bellido, as well as [CT08] from Cao and Titi, show valuable results, as global uniqueness of *strong* solutions does not necessitate smallness conditions on the data. Note, that Cao and Titi even were able to release additional regularity on the solution. Comparable results for the non hydrostatic problem are not known to the author.

Chapter 4

Equal-Order Finite Element Discretization of Stationary Systems

Finite difference models enjoy frequent application in the context of ocean circulation, which is reasoned by their low costs. However, the finite element approach is also attractive due to its robustness with respect to the irregular and rough boundaries of the oceanic basins. While analysis of existence and uniqueness of a solution of the primitive equations ripened noticeably in the past decades, see e.g. [BL92, CT07, CRM03], the analysis of the discretized schemes of the primitive equations, particularly the finite element approach, however seems to be in its infancy. Note, that especially the possibility to use stabilized equal-order finite elements for this system is attractive in terms of higher-order schemes.
The publications concerning the finite element approach of hydrostatic flow problems known to the author are the following: In the context of inf-sup stable finite elements, Guillen and Rodriguez published [GR05b], where the authors designed and analyzed a consistent finite element method for the primitive equations of the ocean. Analysis of stabilized finite element schemes for the hydrostatic approximation of flow problems is done in [CGS12], where the authors considered the orthogonal sub-scales VMS method applied to the hydrostatic approximation of the Oseen problem. Moreover, in [KB12] we constructed several stabilization schemes for the hydrostatic Stokes system and studied them with respect to stability and error estimates. In [Kim12], we dealt the construction and analysis of symmetric stabilization schemes for the hydrostatic Oseen system, which are attractive as they do not exhibit surplus coupling like residual-based schemes.

Due to the structure of the problem we use a 2D trial space for the pressure and a 3D one for the velocity with suitable interaction between these two spaces. However, this necessitates a certain class of underlying meshes, such that the interaction between these problems of different dimensions are effective and enable sufficient stability and error estimates. Moreover, as we figured out in Chapter 2, the relation between the diameter of the surface ω and the depth of Ω is supposed to be very large in oceanic

flow regimes. In this case, the use of isotropic triangulations can not be recommended. Rather, anisotropic elements with large compression into the vertical coordinate direction are more appropriate. However, as anisotropic stabilization is not the focus of this chapter, we treat the case of isotropic meshes and give a glimpse on the treatment of the anisotropic case whenever necessary.

We observe the following stationary hydrostatic flow problems: First, we consider the problem with the lowest structure, which shows the crux of the hydrostatic approximation, i.e. the 2.5D Stokes problem. Second, we turn to the problems, which come into play, when dominant advection is entered into the problem. For ease of clarity, we do not consider the nonlinear problem, but restrict to its linearized version, the 2.5D Oseen problem.
Similar to the standard flow problems, equal-order interpolation for pressure and velocity suffer from the absence of a discrete (modified) inf-sup condition. Hence, existence and uniqueness of a discrete pressure are not given for the pure Galerkin formulation. However, a suitable pressure stabilization can be achieved by introducing additional terms in the corresponding bilinear form, which are based on stabilization terms of the 2D Stokes problem.
If the system additionally shows oscillations due to dominant advection, prevention is given by an adaptive use of stabilization schemes of the 3D Oseen problem. The introduction and analysis of these schemes is the subject of this chapter.

It is structured as follows: We start with fundamental definitions of the underlying meshes and spaces, and figure out their necessary properties. We then turn to the hydrostatic issues, where we determine relevant properties of the discrete averaging operator and the discrete modified inf-sup constraint. Subsequently, we recall well-known stabilization schemes for the equal-order finite element discretized 2D Stokes and 3D Oseen problem. For both problems, we review some stabilized finite element methods and provide some basic properties which are needed for transferring the different kinds of stability to the 2.5D case. The following two sections treat the hydrostatic Stokes and the hydrostatic Oseen problem, introducing and analyzing the discrete problem, and applying suitable stabilization schemes. In both problems, we face the numerical oscillations in the pressure field by application of pressure stabilization operators, stemming from the 2D Stokes problem. In the 2.5D Oseen case, the additional problem of dominant advection is treated by appropriate adaption of the stabilization schemes of the 3D Oseen problem.

Note, that the sections concerning the Stokes problem, i.e. Sections 4.2 and 4.4, as well as the basic definitions of the mesh (see Section 4.1.1) and, for $p = 2$, the properties of the discrete averaging operator and the discrete modified inf-sup constraint, see Section 4.1.3, are to be found in [KB12]. Moreover, the Oseen concerns, i.e. Section 4.5, as well as the generalizations in Section 4.1.3 to the Sobolev spaces of arbitrary regularity $p \in (1, \infty)$, are part of [Kim12].

4.1 Fundamentals

In this section we start with the description of triangulations of given domains $\Omega \subset \mathbb{R}^3$, and of appropriate surface domains $\omega \subset \mathbb{R}^2$. For ease of simplicity, we restrict to polyhedral domains. For domains with polygonal, not fitting in this framework, and non polygonal boundary we refer to [Bra07]. Special focus is set on the requirements for the 3D triangulation, in order to handle the different dimensions of the pressure and the velocity field. We then examine the discrete averaging operator and turn to the discrete counterpart of the modified inf-sup constraint, again elaborating a tight relation between the non hydrodynamic version and the hydrodynamic counterpart.

4.1.1 Triangulations and Finite Element spaces

Let $\mathcal{K}_h$ be a decomposition (triangulation) of the 2D surface ω into open quadrilaterals (cells) K. The set $\mathcal{K}_h = \{K\}$ is also denoted as *mesh*. Given a cell $K \in \mathcal{K}_h$, straight parts of ∂K are called *edges* and are indicated by e, nodes of a cell K are denoted as x. Constant ρ_K describes the radius of largest circle contained in K. The *diameter* of K is denoted by h_K and the *global mesh size* is defined as $h_\omega := \max\{h_K : K \in \mathcal{K}_h\}$.

Appropriately, let $\mathcal{T}_h$ be a decomposition of the 3D domain Ω into hexahedrals (cells) T. For a given cell $T \in \mathcal{T}_h$, the straight parts of the boundary ∂T are called *faces* and are denoted as f. As in the 2D case, edges of T are indicated by e. As well, nodes are represented by x. Constant ρ_T describes the diameter of the largest ball contained in T. The diameter of T is given by h_T and the *global mesh size* is defined as $h_\Omega := \max\{h_T : T \in \mathcal{T}_h\}$.

A given (2D or 3D) mesh $\mathcal{T}$ is called *admissible*, see [Bra07], if the following properties are satisfied:

(i) $\overline{\omega} = \cup_{T\in\mathcal{T}} \overline{T}$.

(ii) For any T_i, $T_j \in \mathcal{T}$, $T_i \cap T_j = \emptyset$ or $T_i = T_j$, applies.

(iii) Any edge/face of any T_i of a 2D/3D mesh $\mathcal{T}$, respectively, is either part of $\partial\Omega$, or edge/face of another cell $T_i \in \mathcal{T}$.

In order to enable local mesh refinement without application of additional, connecting elements, we weaken the last demand and allow for *hanging nodes*, i.e. we admit cells with nodes, that lie on midpoints of faces of neighboring cells. Each face is allowed to have at most one hanging node, see also Figure 4.1.

A family of meshes $\{\mathcal{T}\}$ is called *shape-regular*, see [Bra07], if there is a constant $c > 0$, such that for all meshes $\mathcal{T}$ of that family

$$\frac{h_T}{\rho_T} \leq c \qquad \forall T \in \mathcal{T} \tag{4.1}$$

applies. The notion *shape-regular* sometimes is abbreviated by *regular*, see e.g. [MS02].

Throughout this chapter we restrict to shape-regular families of admissible meshes. A mesh of such a family is denoted as shape-regular, admissible mesh. Note, that $h_\Omega \sim h_\omega$, i.e. $c_1 h_\Omega \leq h_\omega \leq c_2 h_\Omega$ with mesh- and problem-independent constants $c_1, c_2 > 0$. In the upcoming we assume $h_\Omega \leq 1$. In a similar fashion, $a \lesssim b$ denotes $a \leq cb$ for a constant $c \geq 0$, which is independent of the mesh size and the parameter of the underlying problem.
We denote shape-regular, admissible meshes $\mathcal{T}$ with constants $c_1, c_2 > 0$ of order one as *isotropic meshes*. In the isotropic framework and if the distinction between h_Ω and h_ω is negligible, we abbreviate h_Ω and h_ω by h. Throughout this chapter we restrict to isotropic meshes.

Anticipatory, in the framework of local projection stabilization we additionally restrict to such families of meshes, which are assembled in a patch-wise manner. I.e., a given mesh with global mesh size h results from a mesh with the coarser global mesh size $2h$ by one global refinement, see also Figure 4.1 for an example in 2D. The cells in the finer mesh, which are constructed of one cell in the coarser mesh are denoted as *patch*.

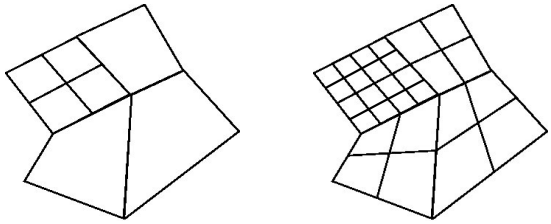

Figure 4.1: Coarse 2D mesh $\mathcal{K}_{2h}$ with hanging nodes (left) and the finer mesh $\mathcal{K}_{h_\Omega}$ (right), resulting from $\mathcal{K}_{2h}$ by one global refinement. Nonadmissible nodes are treated as hanging nodes.

Let $\mathbb{Q}_r(\widehat{K})$be the space of all polynomials on the reference quadrilateral $\widehat{K} = (-1,1)^2$ with maximal degree r in each coordinate direction. In the upcoming we use the finite element spaces resulting from linear transformations $B_K : \widehat{K} \to K$ from the reference quadrilateral $\widehat{K}$,

$$B_K \begin{pmatrix} \widehat{x} \\ \widehat{y} \end{pmatrix} = \begin{pmatrix} x_0 \\ y_0 \end{pmatrix} + \begin{pmatrix} \alpha_0 \widehat{x} + \alpha_1 \widehat{y} \\ \alpha_2 \widehat{x} + \alpha_3 \widehat{y} \end{pmatrix}. \tag{4.2}$$

The corresponding transformed polynomial space on K is

$$\mathbb{Q}_r(K) := \left\{ \phi \in \mathcal{C}(K) \;\middle|\; \phi = \widehat{\phi} \circ B_K^{-1} \text{ with } \widehat{\phi} \in \mathbb{Q}_r(\widehat{K}),\ B_K : \widehat{K} \to K \text{ linear} \right\}.$$

In order to treat the 2D – 3D interaction occurring in hydrostatic problems, we restrict to hexahedral elements $T \in \mathcal{T}_h$, which show the property that for the standard embedding $P : \mathbb{R}^3 \to \mathbb{R}^2$, $P(x,y,z) := (x,y)$,

$$\forall T \in \mathcal{T}_h : \ P(T) \in \mathcal{K}_h$$

applies. Hence, we consider 3D triangulations, which consist of cells obtained by linear transformations $B_T : \widehat{T} \to T$ from the reference cube $\widehat{T} = (-1,1)^3$ of the following type:

$$B_T \begin{pmatrix} \widehat{x} \\ \widehat{y} \\ \widehat{z} \end{pmatrix} = \begin{pmatrix} x_0 \\ y_0 \\ z_0 \end{pmatrix} + \begin{pmatrix} \alpha_0\widehat{x} + \alpha_1\widehat{y} \\ \alpha_2\widehat{x} + \alpha_3\widehat{y} \\ \alpha_4\widehat{x} + \alpha_5\widehat{y} + \alpha_6\widehat{z} \end{pmatrix}, \tag{4.3}$$

with $P(T)$– dependent parameters $x_0, y_0, z_0, \alpha_0, \ldots, \alpha_3$ according to (4.2) and additional parameters $\alpha_4, \alpha_5, \alpha_6$ for the transformation into vertical direction. Thus, the mesh $\mathcal{T}_h$ consists of vertical oriented prisms. Each of these prisms consists of a stack of elements $T \in \mathcal{T}_h$. For each element $K \in \mathcal{K}_h$ such a prism is denoted by

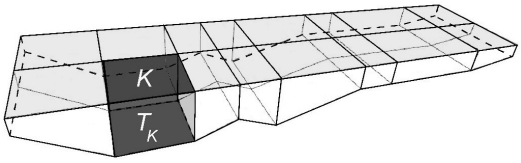

Figure 4.2: Sketch of patch $\mathcal{T}_K \subset \mathcal{T}_h$ for a given $K \in \mathcal{K}_h$.

$\mathcal{T}_K := \{T \in \mathcal{T}_h \,|\, P(T) = K\}$ with the standard 2D embedding $P : \mathcal{T}_h \to \mathcal{K}_h$, see also Figure 4.2. We observe, that the faces of hexahedrons on the top surface ω are flat, and that the faces on the bottom, $z = -d(x,y)$, may have a slope.

Let us make some remarks on the issue of hanging nodes. The additional (hanging) nodes cause no additional degrees of freedom. Instead, the values of the appropriate finite element functions are determined by suitable point-wise interpolation. Thus, we still have continuity and global conformity. Furthermore, we only permit local mesh-refinement on the surface mesh $\mathcal{K}_h$. Otherwise, the prismatic structure of the 3D mesh $\mathcal{T}_h$ would be violated.

Figure 4.3 also shows a permitted mesh (left) and an non admissible mesh (right). The highlighted faces indicate the violations of the "prism property", stemming from non admissible transformation $B_T : \widehat{T} \to T$ and from local mesh-refinement of the 3D mesh $\mathcal{T}_h$.

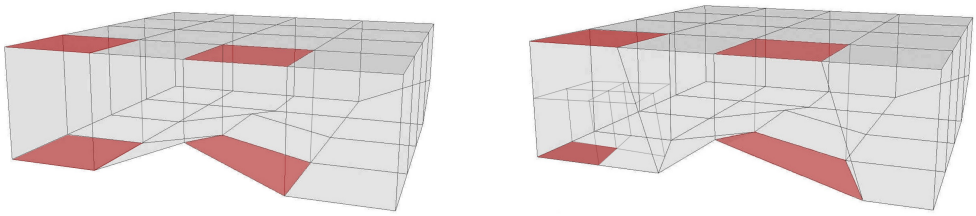

Figure 4.3: An admissible (left) and a non admissible mesh (right).

The considered transformed polynomials on $T \in \mathcal{T}_h$ form the space

$$\mathbb{Q}_r(T) \;:=\; \left\{ \phi \in \mathcal{C}(T) \;\middle|\; \phi = \widehat{\phi} \circ B_T^{-1} \;\text{ with }\; \widehat{\phi} \in \mathbb{Q}_r(\widehat{T}),\; B_T : \widehat{T} \to T \text{ as in (4.3)} \right\},$$

with polynomial space $\mathbb{Q}_r(\widehat{T})$ on the reference element $\widehat{T}$ of degree up to r in each variable.

Let Q, $\mathbf{W}$ and $\mathbf{V}$ be the variational spaces for the 2D pressure, the 2D velocity field and the 3D velocity field, respectively, and $r \geq 1$. The appropriate finite element spaces are given by

$$Q_h := \{q_h \in Q \cap \mathcal{C}(\overline{\omega}) \quad \big| \; q_h|_K \in \mathbb{Q}_r(K),\ \forall K \in \mathcal{K}_h\}\,, \tag{4.4}$$

$$\mathbf{W}_h := \{\boldsymbol{w}_h \in \mathbf{W} \cap \mathcal{C}(\overline{\omega})^2 \;\big|\; \boldsymbol{v}_{h,i}\,|_K \in \mathbb{Q}_r(K),\ i \in \{1,2\},\ \forall K \in \mathcal{K}_h\}\,, \tag{4.5}$$

$$\mathbf{V}_h := \{\boldsymbol{v}_h \in \mathbf{V} \cap \mathcal{C}(\overline{\Omega})^2 \quad \big|\; \boldsymbol{v}_{h,i}\,|_T \in \mathbb{Q}_r(T),\ i \in \{1,2\},\ \forall T \in \mathcal{T}_h\}\,. \tag{4.6}$$

4.1.2 Interpolation operators

Suppose a variational space $\mathrm{H}^m(\Omega)$. The quality of the finite element approximation of an element $v \in \mathrm{H}^m(\Omega)$ can be estimated due to approximation properties of a suitable interpolation operator. Let $V_h \subset \mathrm{H}^m(\Omega)$ be the space of finite elements of order r.

(a) Lagrangian interpolation operator

The Lagrangian interpolation operator $i_h : \mathcal{C}(\overline{\Omega}) \to V_h$ provides the following estimate for arbitrary $T \in \mathcal{T}_h$ on *isotropic meshes*, see e.g. [Bra07]:

$$|v - i_h v|_{k,2,T} \leq c h^{m-k} |v|_{m,2,T} \qquad \forall v \in \mathrm{H}^m(\Omega)\ \forall m \in [2, r+1]\ \forall\ k \in [0, m]$$

Stability is achieved by setting $k = m$.

(b) Clement interpolation operator

An operator, which assures similar estimates as the Lagrangian interpolation operator, but allows v to be less regular, is given by the Clement interpolation operator $c_h : \mathrm{L}^1(\Omega) \to V_h$ with $p \in [1, \infty)$, see e.g. [EG04]:

$$|v - c_h v|_{k,p,T} \leq c h^{m-k} |v|_{m,p,\tilde{\omega}_T} \qquad \forall v \in \mathrm{W}^{m,p}(\Omega)\ \forall m \in [0, r+1]\ \forall\ k \in [0, m]\,,$$

whereas $\tilde{\omega}_T$ denotes a suitable surrounding of $T \in \mathcal{T}_h$. The authors of [EG04] provide the following stability statement for $r \in [1, \infty)$ and $k \in [0, 1]$:

$$\|c_h v\|_{k,p,\Omega} \leq c \|v\|_{k,p,\Omega} \qquad\qquad \forall v \in \mathrm{W}^{k,p}(\Omega).$$

(c) Scott-Zhang interpolation operator

The disadvantages of the Clement interpolation operator are, that it does not preserve boundary conditions (which can be rectified by suitable modifications of the nodal values along the boundaries, see also [Bec95]), and second, that it is not a projection.

Let us therefore introduce the Scott-Zhang interpolation operator $z_h : \mathrm{W}^{m,p}(\Omega) \to V_h$, which does not show these undesired properties, see e.g. [EG04], and allows the following estimates:

$$|v - z_h v|_{k,p,T} \leq c h^{m-k} |v|_{m,p,\tilde{\omega}_T} \qquad \forall v \in \mathrm{W}^{m,p}(\Omega)\ \forall m \in [\widehat{m}, r+1]\ \forall\ k \in [0,m]\,,$$

whereas $\tilde{\omega}_T$ denotes a suitable surrounding of $T \in \mathcal{T}_h$. The lower bound for m is given by $\widehat{m} = 1$, if $p = 1$, and $\widehat{m} = p^{-1} + \varepsilon$ for arbitrary $\varepsilon > 0$, else. Assuming $k \in [0, \min\{1, m\}]$, the Scott-Zhang operator provides the stability property, see also [EG04]:

$$\|z_h v\|_{k,p,\Omega} \leq c \|v\|_{m,p,\Omega} \qquad\qquad \forall v \in \mathrm{W}^{k,p}(\Omega).$$

(d) L^2-orthogonal interpolation operator

In the case of local projection stabilization of the hydrostatic Oseen problem, a suitable orthogonality property is demanded in order to obtain optimal error estimates. This is assured by the interpolation operator $i_{h,3d} : \mathbf{V} \to \mathbf{V}_h$, which has been introduced in [BB06] and fulfills the following properties:

$$(\boldsymbol{v} - i_{h,3d}\,\boldsymbol{v}, \boldsymbol{\xi})_\Omega = 0 \qquad \forall\, \boldsymbol{v} \in \mathbf{V}\,, \forall \boldsymbol{\xi} \in [Q_{2h}^{r-1}(\Omega)]^2 \tag{4.7}$$

$$\|\,\boldsymbol{v} - i_{h,3d}\,\boldsymbol{v}\,\|_{0,\Omega} + h|\,\boldsymbol{v} - i_{h,3d}\,\boldsymbol{v}\,|_{1,\Omega} \lesssim h^{k+1} \|\,\boldsymbol{v}\,\|_{k+1,\Omega} \quad \forall\, \boldsymbol{v} \in \mathbf{H}^{k+1}(\Omega)\,,\ 0 \leq k \leq r \tag{4.8}$$

$$\|i_{h,3d}\,\boldsymbol{v}\,\|_{1,\Omega} \lesssim \|\,\boldsymbol{v}\,\|_{1,\Omega} \qquad \forall\, \boldsymbol{v} \in \mathbf{H}^1(\Omega)\,. \tag{4.9}$$

The appropriate operator $i_{h,2d} : Q \to Q_h$ for the 2D pressure field shows similar properties, i.e.

$$(p - i_{h,2d}p, \varphi)_\omega = 0 \qquad \forall p \in Q\,, \forall \varphi \in Q_{2h}^{r-1}(\omega) \tag{4.10}$$

$$\|p - i_{h,2d}p\|_{0,\omega} + h|p - i_{h,2d}p|_{1,\omega} \lesssim h^{k+1}\|p\|_{k+1,\omega} \quad \forall p \in \mathrm{H}^{k+1}(\omega)\,,\ 0 \leq k \leq r \tag{4.11}$$

$$\|i_{h,2d}p\|_{1,\omega} \lesssim \|p\|_{1,\omega} \qquad \forall p \in \mathrm{H}^1(\omega)\,. \tag{4.12}$$

4.1.3 Hydrostatic Issues

As in the infinite dimensional case, i.e. Chapter 3, the divergence constraint is the key issue in the analysis of existence and uniqueness. Due to that reasons, we examine the properties of the discrete modified inf-sup constraint. Necessary properties of the discrete version of the averaging operator are treated beforehand. The appropriate deductions are found in [KB12] for $p = 2$. An extension for arbitrary $p \in (1, \infty)$ is indicated in [Kim12] and is presented in the following.

Discrete averaging operator

The following statement figures out, that the discrete averaging operator can be identified by its counterpart as given in Chapter 3.

Lemma 4.1. *Let $p \in (1,\infty)$. Moreover, let $\mathbf{V} := \mathbf{W}_0^{1,p}(\Omega)$ or $\mathbf{V} := \mathbf{W}_b^{1,p}(\Omega)$, $p \geq 1$, and $\mathbf{V}_h \subset \mathbf{V}$ be given by (4.6). For any $\boldsymbol{v}_h \in \mathbf{V}_h$ the integration operator $\mathbf{M}$, given by (3.18), satisfies:*

$$\mathbf{M}\,\boldsymbol{v}_h \in \mathbf{W}_h \qquad \text{and} \qquad \mathbf{M}\,\boldsymbol{v}_h = \int_{-d(\cdot)}^{0} \boldsymbol{v}_h(\cdot,z)\,dz\,.$$

Proof. Given the definition of $\mathcal{T}_h$ recall that $\mathcal{T}_h$ consists of prismatic hexahedrons. Let $K \in \mathcal{K}_h$ be given. We denote $\mathcal{T}_K$ as the set of all $T \in \mathcal{T}_h$, that belong to such a prism with top surface K. Note that the (x,y)-parts of the transformations $B_T : \widehat{T} \to T$ are characterized by B_K as given by (4.2) and therefore identical for each $T \in \mathcal{T}_K$. Due to the construction of B_T, the determinant of the Jacobian of B_T is constant, $c_T := |\det J(B_T)| = \alpha_6(\alpha_0\alpha_3 - \alpha_1\alpha_2)$. Let $\widehat{\boldsymbol{v}}_T \in \mathbb{Q}_r(\widehat{T})^2$ such that $\boldsymbol{v}_h\,|_T = \widehat{\boldsymbol{v}}_T \circ B_T^{-1}$. As $\boldsymbol{v}_h$ is cell-wise polynomial, for each $(x,y) \in K$ we derive

$$\boldsymbol{w}_h(x,y) := \int_{-d(x,y)}^{0} \boldsymbol{v}_h(x,y,z)dz = \sum_{T\in\mathcal{T}_K} c_T \int_{-1}^{1} \widehat{\boldsymbol{v}}_T(\widehat{x},\widehat{y},\widehat{z})d\widehat{z}.$$

As $\widehat{\boldsymbol{v}}_T \in \mathbb{Q}_r(\widehat{T})^2$, the function $c_T \int_{-1}^{1} \widehat{\boldsymbol{v}}_T(\cdot,\cdot,\widehat{z})d\widehat{z}$ is an element of $\mathbb{Q}_r(\widehat{K})^2$. Hence, it follows $\boldsymbol{w}_h\,|_K \in \mathbb{Q}_r(K)^2$ and $\boldsymbol{w}_h \in \mathbf{W}_h$. Thus, we have

$$0 \;=\; \Big(\mathbf{M}\,\boldsymbol{v}_h - \int_{-d(\cdot)}^{0} \boldsymbol{v}_h(\cdot,z)dz, \boldsymbol{\varphi}\Big)_\omega = (\mathbf{M}\,\boldsymbol{v}_h - \boldsymbol{w}_h, \boldsymbol{\varphi})_\omega \qquad \forall\,\boldsymbol{\varphi} \in \mathbf{W}_0^q(\omega)$$

with $q \geq 1$ such that $1/p + 1/q = 1$. □

For upcoming proofs, among others, we need surjectivity of $\mathbf{M}$. This property is applied if the following assumption holds:

Assumption 4.2. *Let $p \in (1,\infty)$. Each $\mathcal{T}_h$ consists of cells obtained by a transformation of type (4.3) and there is an element $\widehat{\zeta}_h \in \mathrm{W}^{1,p}(\Omega) \cap \mathcal{C}(\Omega)$, which only depends on z, i.e. $\widehat{\zeta}_h(x,y,z) = \zeta_h(z)$, with $supp(\xi_h) \subset [-\delta_{min}, 0]$, $\widehat{\zeta}_h|_T \in \mathbb{Q}_r(T)$ for all $T \in \mathcal{T}_h$ and*

$$\int_{-\delta_{min}}^{0} \zeta_h\,dz \;=\; 1\,, \tag{4.13}$$

$$\|\zeta_h\|_{0,p,\mathbb{R}} \leq c\,\delta_{min}^{(1-p)/p} \quad \text{and} \quad |\zeta_h|_{1,\mathbb{R}} \leq c\,\delta_{min}^{(1-2p)/p}\,, \tag{4.14}$$

with h-independent constant $c \geq 0$.

Remark 4.3. *Let us briefly examine this assumption with respect to admissible meshes for Q_1-elements ($r = 1$). Beside the previously discussed prismatic structure of $\mathcal{T}_h$, let the mesh contain two straight layers of mesh points being parallel to the e_1, e_2-plane, at z-coordinates z_1, z_2 with $-\delta_{min} \leq z_1 < z_2 < 0$. The function ζ_h, occurring in Assumption 4.2, can be constructed as follows:*

$$\zeta_h(z) \;:=\; \begin{cases} \alpha(z - z_1) & \text{if } z_1 \leq z \leq z_2, \\ \alpha(1 - z_1/z_2)z & \text{if } z_2 \leq z \leq 0, \\ 0 & \text{else.} \end{cases}$$

Setting $\alpha = 2/[z_1(z_1 - z_2)]$ assures the mean value property (4.13). By elementary calculus we obtain $\|\zeta_h\|_{0,p,\mathbb{R}} = 2(p+1)^{-1/p}|z_1|^{(1-p)/p}$ and $|\zeta_h|_{1,p,\mathbb{R}} \leq 2|z_1|^{-1/p}(|z_2|(z_2 - z_1))^{(1-p)/p}$. This ensures the bounds (4.14) where the constant c depends on the regularity p of the underlying Sobolev space $\mathrm{W}^{1,p}(\Omega)$, and on the ratios $\delta_{min}/|z_1|$ and $\delta_{min}/|z_2 - z_1|$ (but independent of h). For $r \geq 2$ an even simpler construction is possible with only one straight line at z_1, with $-\delta_{min} \leq z_1 < 0$. Thus, Assumption 4.2 is less restrictive than an assumption to have a tensor mesh.

Lemma 4.4. *Let $\mathbf{V} := \mathbf{W}_0^{1,p}(\Omega)$ or $\mathbf{V} := \mathbf{W}_b^{1,p}(\Omega)$ and $\mathbf{W} := \mathbf{W}_0^{1,p}(\omega)$, $p \in (1, \infty)$. Moreover, consider $\mathbf{V}_h \subset \mathbf{V}$, $\mathbf{W}_h \subset \mathbf{W}$ given by (4.6), and (4.5), respectively. Let Ω be a flat domain.*
If Assumption 4.2 is valid, the operator $\mathbf{M}|_{\mathbf{V}_h} : \mathbf{V}_h \to \mathbf{W}_h$ is surjective. In particular, for each $\boldsymbol{w}_h \in \mathbf{W}_h$ there exists a $\boldsymbol{v}_h \in \mathbf{V}_h$, so that $\mathbf{M}\,\boldsymbol{v}_h = \boldsymbol{w}_h$,

$$\| \boldsymbol{v}_h \|_{0,p,\Omega} \leq c_\omega \delta_{min}^{(1-p)/p} \| \boldsymbol{w}_h \|_{0,p,\omega} \quad \text{and} \quad |\boldsymbol{v}_h|_{1,p,\Omega} \leq c_\omega \delta_{min}^{(1-2p)/p} |\boldsymbol{w}_h|_{1,p,\omega}\,. \tag{4.15}$$

Proof. Let $\boldsymbol{w}_h \in \mathbf{W}_h$ be given. The construction of $\boldsymbol{v}_h \in \mathbf{V}_h$ with $\mathbf{M}\,\boldsymbol{v}_h = \boldsymbol{w}_h$ is similar to the proof of the continuous version (Lemma 3.12) with the difference that we need the piecewise linear function $\zeta_h \in \mathcal{C}(\mathbb{R})$ from Assumption 4.2. Now, for $\boldsymbol{v}_h(x, y, z) := \boldsymbol{w}_h(x, y) \cdot \zeta_h(z)$ we obtain $\boldsymbol{v}_h \in \mathbf{V}_h$ by construction and

$$\int_{-d(x,y)}^{0} \boldsymbol{v}_h(x, y, z)\, dz \;=\; \boldsymbol{w}_h(x, y) \int_{-d(x,y)}^{0} \zeta_h(z)\, dz \;=\; \boldsymbol{w}_h(x, y)\,.$$

Hence, $\mathbf{M}$ is surjective. As $\mathbf{W}_h \subset \mathbf{W}$ and $\mathbf{V}_h \subset \mathbf{V}$, the bounds (4.15) are obtained similar to the bound in Lemma 3.12 by using the bounds of $\|\xi_h\|_{0,p,\mathbb{R}}$ and $|\xi_h|_{1,p,\mathbb{R}}$ in Assumption 4.2. □

Discrete modified inf-sup constraint

Dependent on the underlying problem we either consider $(\mathbf{V}, Q) := (\mathbf{H}_0^1(\Omega), \mathrm{L}_0^2(\omega))$ or $(\mathbf{V}, Q) := (\mathbf{W}_b^{1,p}(\Omega), \mathrm{L}_0^q(\omega))$, $p, q \in (1, \infty)$ such that $p^{-1} + q^{-1} = 1$. The 2D velocity space is given by $\mathbf{W} := \mathbf{H}_0^1(\omega)$ or $\mathbf{W} := \mathbf{W}_0^{1,p}(\omega)$, respectively. The appropriate discrete spaces $Q_h \subset Q$, $\mathbf{V}_h \subset \mathbf{V}$ and $\mathbf{W}_h \subset \mathbf{W}$ are given by (4.4) – (4.6). To assure existence of a solution of a finite element discretized hydrostatic problem, the *discrete modified*

inf-sup condition

$$\exists \gamma > 0 \qquad \sup_{\boldsymbol{v}_h \in \mathbf{V}_h \setminus \{\mathbf{0}\}} \frac{(\mathrm{div}'\, \mathbf{M}\, \boldsymbol{v}_h, q_h)_\Omega}{\| \boldsymbol{v}_h \|_{1,p,\Omega}} \geq \gamma \|q_h\|_{0,q,\omega} \qquad \forall q_h \in Q_h, \tag{4.16}$$

i.e. a sufficient upper bound for the pressure, has to apply. The following proposition states the tight connection between the hydrostatic issue and the classical, non hydrostatic case. Restricting this proposition to the Stokes case for a symmetric choice of variational spaces and to the Oseen problem, which necessitates a non symmetric choice of variational spaces, the appropriate Propositions can be found in [KB12] and [Kim12], respectively.

Proposition 4.5. *Let $p \in (1, \infty)$, Ω be a flat domain and $\mathcal{T}_h$ be a triangulation of Ω fulfilling Assumption 4.2. The lack as well as the validity of the inf-sup condition*

$$\exists \gamma_\omega > 0 \qquad \sup_{\boldsymbol{w}_h \in \mathbf{W}_h \setminus \{\mathbf{0}\}} \frac{(div'\, \boldsymbol{w}_h, q_h)_\omega}{\| \boldsymbol{w}_h \|_{1,p,\omega}} \geq \gamma_\omega \|q_h\|_{0,q,\omega} \qquad \forall q_h \in Q_h, \tag{4.17}$$

carries over to (4.16).

Proof. Throughout this proof, $c_\Omega > 0$ is a suitable, Ω – dependent constant. Let (4.17) be violated such that there is a pressure $p_h \in Q_h \setminus \{0\}$ with $(\mathrm{div}'\, \boldsymbol{w}_h, p_h)_\omega = 0$ for all $\boldsymbol{w}_h \in \mathbf{W}_h$. Due to the surjectivity of $\mathbf{M} : \mathbf{V}_h \to \mathbf{W}_h$, see Lemma 4.4, $(\mathrm{div}'\, \mathbf{M}\, \boldsymbol{v}_h, p_h)_\omega = 0$ applies for all $\boldsymbol{v}_h \in \mathbf{V}_h$. Moreover, we have $\| \mathbf{M}\, \boldsymbol{v}_h \|_{1,p,\omega} \leq c_\Omega \| \boldsymbol{v}_h \|_{1,p,\Omega}$. Repeated application of Lemma 4.4 leads to

$$0 = \sup_{\boldsymbol{w}_h \in \mathbf{W}_h} \frac{(\mathrm{div}'\, \boldsymbol{w}_h, q_h)_\omega}{\| \boldsymbol{w}_h \|_{1,p,\omega}} \geq c_\Omega \sup_{\boldsymbol{v}_h \in \mathbf{V}_h} \frac{(\mathrm{div}'\, \mathbf{M}\, \boldsymbol{v}_h, q_h)_\omega}{\| \boldsymbol{v}_h \|_{1,p,\Omega}} \geq 0.$$

The second kind of instability, i.e.

$$\exists q_h \in Q_h \setminus \{0\}\, \forall\, \boldsymbol{w}_h \in \mathbf{W}_h \setminus \{\mathbf{0}\} \qquad \frac{(\mathrm{div}'\, \boldsymbol{w}_h, q_h)_\omega}{\|q_h\|_{0,q,\omega} \| \boldsymbol{w}_h \|_{1,p,\omega}} \quad \geq \quad \gamma_h$$

with inf-sup constant $\gamma_h \to 0$ for $h \to 0$, transfers to the hydrostatic case by application of $\mathbf{M}(\mathbf{V}_h) = \mathbf{W}_h$ and the estimate of Lemma 4.4.

On the other hand, let (4.17) be fulfilled. Recall the relation $1/p + 1/q = 1$. Lemma 4.4 leads to (4.16) with constant

$$\gamma := \delta_{min}^{1/q} (1 + \delta_{min}^p)^{1/p} c_\omega^{-1} \gamma_\omega \,.$$

□

Remark 4.6. *The argumentation on the δ_{min}-dependence of the inf-sup constant $\widetilde{\gamma}_{\Omega,\omega}$, see Remark 3.14, also applies in the discrete case.*

4.2 2D Stokes problem

In this section we consider the discrete 2D Stokes problem. We start with the Galerkin formulation, indicating, that an equal-order finite element approach does not lead to a stable problem. We then introduce several stabilization techniques, known from literature and present and validate estimates, which are applicable in the hydrostatic frame. We close the section with the presentation of *a priori* estimates for the applied stabilization. The results and considerations of this sections can also be found in [KB12].

4.2.1 Galerkin formulation

Througout this section we consider velocity fields with imposed homogeneous Dirichlet data, i.e. the underlying variational spaces are $\mathbf{W} := \mathbf{H}_0^1(\omega)$ and $Q := \mathrm{L}_0^2(\omega)$ and the appropriate discrete spaces are given by (4.4) and (4.5). Without loss of generality we assume isotropic viscosities. In particular, we set $\nu = \boldsymbol{\mathcal{A}}_\nu = \nu_E = 1$. The equal-order finite element formulated 2D Stokes problem is given by

$$\textit{Find} \quad (\boldsymbol{w}_h, p_h) \in \mathbf{W}_h \times Q_h \quad \textit{s. t.} \; A^\omega(\boldsymbol{w}_h, p_h; \boldsymbol{\varphi}, \xi) = \langle \boldsymbol{f}, \boldsymbol{\varphi} \rangle \quad \forall (\boldsymbol{\varphi}, \xi) \in \mathbf{W}_h \times Q_h \tag{4.18}$$

with

$$A^\omega(\boldsymbol{w}_h, p_h; \boldsymbol{\varphi}, \xi) := (\nabla' \boldsymbol{w}_h, \nabla' \boldsymbol{\varphi})_\omega - (p_h, \operatorname{div}' \boldsymbol{\varphi})_\omega + (\operatorname{div}' \boldsymbol{w}_h, \xi)_\omega \,.$$

The validation of existence and uniqueness of a solution of this problem can be carried out as in the infinite dimensional case, see also Section 3.1.2. As we apply conform finite element spaces, i.e. $\mathbf{W}_h \subset \mathbf{W}$, continuity and coercivity of the Laplacian inherits from the infinite dimensional problem. However, the inf-sup constraint (3.7) does not apply in equal-order finite element spaces, see e.g. Braess [Bra07], and unique existence of a discrete pressure p_h cannot be assured. Introducing additional stabilization terms into this Galerkin formulation with maintainable error properties may circumvent this problem, i.e. the given problem is *stabilized*, which gives the method its name.

4.2.2 Stabilization of the problem

In the following we introduce and examine stabilization terms which are known from literature and stabilize the 2D Stokes problem. We first treat symmetric stabilization schemes, which only depent on Q_h, and then turn to residual based stabilizations, which also depend on the velocities.

Symmetric pressure dependent stabilized methods

The bilinear operator for the 2D Stokes problem with inherent symmetric pressure stabilization is given by

$$A_h^\omega(\boldsymbol{w}_h, p_h; \boldsymbol{\varphi}, \xi) \;:=\; A^\omega(\boldsymbol{w}_h, p_h; \boldsymbol{\varphi}, \xi) \;+\; s_h(p_h, \xi)\,.$$

The entire discrete problem is of the form

$$\textit{Find}\;\; (\boldsymbol{w}_h, p_h) \in \mathbf{W}_h \times Q_h \;\; \textit{s. t.}\; A_h^\omega(\boldsymbol{w}_h, p_h; \boldsymbol{\varphi}, \xi) = \langle \boldsymbol{f}, \boldsymbol{\varphi}\rangle \qquad \forall (\boldsymbol{\varphi}, \xi) \in \mathbf{W}_h \times Q_h\,. \tag{4.19}$$

In the upcoming we concentrate on the following established stabilization techniques, whose application results in an inf-sup stabilization of the problem (4.19):

(P-i) Brezzi and Pitkäranta [BP84] for linear elements $r = 1$:

$$s_h(p, \xi) \;:=\; \sum_{K \in \mathcal{K}_h} h_K^2 (\nabla' p,\, \nabla' \xi)_K.$$

(P-ii) Local projection stabilization (LPS) [BB01],

$$s_h(p_h, \xi) \;:=\; \sum_{K \in \mathcal{K}_h} h_K^2 (\kappa_h(\nabla' p_h), \kappa_h(\nabla' \xi))_K,$$

with $\kappa_h := id - \pi$ and L^2-projection $\pi : \mathrm{L}_0^2(\omega) \to Q_{2h}^{r-1}(\omega)$ onto the 'discontinuous' space

$$Q_{2h}^{r-1}(\omega) \;:=\; \{\phi \in \mathrm{L}^2(\omega) \big|\; \phi|_K \in \mathbb{Q}_{r-1}(K)\;\forall K \in \mathcal{K}_{2h}\}\,.$$

(P-iii) Continuous interior penalty stabilization (CIP) of Burman and Hansbo [BH06] for $r = 1$,

$$s_h(p_h, \xi) \;:=\; \sum_{e \in \mathcal{E}_h} h_e^3 \int_e [\nabla' p_h \cdot \boldsymbol{n}]_e \cdot [\nabla' \xi \cdot \boldsymbol{n}]_e ds,$$

where $\boldsymbol{n}$ denotes the outward normal to edge e and $[\boldsymbol{\phi}]_e$ the jump of $\boldsymbol{\phi}$ across e.

(P-iv) Pressure projection of Dohrmann & Bochev [DB04]:

$$s_h(p_h, \xi) \;:=\; -(p_h - P_{r-1} p_h,\, \xi - P_{r-1}\xi)_\omega,$$

with local L^2-projection $P_{r-1} : \mathrm{L}^2(\omega) \to Q_h^{r-1}(\omega)$.

More detailed informations on stability and error estimates of these techniques are to be found in the cited literature. In the upcoming we collect properties, which all of the schemes (P-i)-(P-iv) have in common. We start with a first, simple observation:

Lemma 4.7. *The stabilizations (P-i)–(P-iv) are bilinear forms and satisfy*

$$\begin{aligned} s_h(p,p) &\geq 0\,, && (4.20)\\ s_h(p,q) &\leq s_h(p,p)^{1/2} s_h(q,q)^{1/2} && (4.21) \end{aligned}$$

for any $p, q \in Q_h$.

Proof. Trivial to validate. □

Let us anticipate, that application of the introduced stabilization schemes in the hydrostatic framework leads to an appropriate stabilized hydrostatic problem. Preparatory for an appropriate proof we elaborate suitable propositions in the 2D non hydrostatic framework. Therefore, we define a norm $\|\!| \cdot |\!\|_\omega$ and validate, that the stabilized 2D Stokes problem is inf-sup stable with respect to that norm. As (4.20) applies and due to bilinearity of s_h,

$$\|\!|(\boldsymbol{w}_h, p_h)|\!\|_\omega := \left(\|\nabla \boldsymbol{w}_h\|_{0,\omega}^2 + \|p_h\|_{0,\omega}^2 + s_h(p_h,p_h)\right)^{1/2} \tag{4.22}$$

defines a norm on $\mathbf{W}_h \times Q_h$. Moreover, let

$$B_h^\omega := \{(\boldsymbol{w}_h, p_h) \in \mathbf{W}_h \times Q_h \,|\, \|\!|(\boldsymbol{w}_h, p_h)|\!\|_\omega = 1\}$$

be the unit sphere on $\mathbf{W}_h \times Q_h$ with respect to $\|\!| \cdot |\!\|_\omega$.

Application of the results in [BB01, BP84, BH06, DB04] we can easily prove, that application of each of the schemes (P-i)–(P-iv) to the 2D equal order finite element discretized Stokes problem leads to appropriate inf-sup stable schemes. I.e., there is an inf-sup constant $\gamma_\omega > 0$, indepenent on the mesh size h, such that

$$\inf_{(\boldsymbol{w}_h,p_h)\in B_h^\omega} \sup_{(\boldsymbol{\varphi},\xi)\in B_h^\omega} A_h^\omega(\boldsymbol{w}_h, p_h; \boldsymbol{\varphi}, \xi) \geq \gamma_\omega\,. \tag{4.23}$$

We reformulate this inf-sup constraint into the following property, which is more suitable in the hydrostatic framework:

Lemma 4.8. *Application of one of the schemes (P-i)–(P-iv) to the discrete 2D Stokes problem (4.18) leads to the following property: For any $p_h \in Q_h$ there is an element $\boldsymbol{\varphi} \in \mathbf{W}_h$ such that*

$$\|\nabla' \boldsymbol{\varphi}\|_{0,\omega} \leq \|p_h\|_{0,\omega} \qquad \textit{and} \qquad -(div'\,\boldsymbol{\varphi}, p_h)_\omega \geq \frac{\gamma_\omega}{4}\|p_h\|_{0,\omega}^2 - \frac{1}{\gamma_\omega} s_h(p_h,p_h).$$

Proof. Let $p_h \in Q_h$ be arbitrarily given, $\boldsymbol{w}_h := \mathbf{0} \in \mathbf{W}_h$ and an arbitrary stabilization from (P-i) – (P-iv) be applied. Due to the inf-sup stability of the stabilized 2D Stokes problem, there is a $(\boldsymbol{\psi}, \xi) \in B_h^\omega$ such that

$$A_h^\omega(\mathbf{0}, p_h; \boldsymbol{\psi}, \xi) = -(\mathrm{div}'\,\boldsymbol{\psi}, p_h)_\omega + s_h(p_h, \xi) \geq \gamma_\omega \|\!|(\mathbf{0}, p_h)|\!\|_\omega \|\!|(\boldsymbol{\psi}, \xi)|\!\|_\omega\,.$$

Due to the definition of the triple norm and $|\!|\!|(\boldsymbol{\psi},\xi)|\!|\!|_\omega = 1$ we can further deduce

$$-(\mathrm{div}'\,\boldsymbol{\psi}, p_h)_\omega \;\geq\; \frac{1}{2}\gamma_\omega \|p_h\|_{0,\omega} + \frac{1}{2}\gamma_\omega s_h(p_h,p_h)^{1/2} - s_h(p_h,\xi)\,.$$

Applying (4.21) and $s_h(\xi,\xi)^{1/2} \leq |\!|\!|(\boldsymbol{\psi},\xi)|\!|\!|_\omega = 1$ we get

$$\begin{aligned} -(\mathrm{div}'\,\boldsymbol{\psi}, p_h)_\omega &\geq \frac{1}{2}\gamma_\omega \|p_h\|_{0,\omega} - (1-\gamma_\omega/2) s_h(p_h,p_h)^{1/2} \\ &\geq \frac{1}{2}\gamma_\omega \|p_h\|_{0,\omega} - s_h(p_h,p_h)^{1/2}. \end{aligned}$$

Suitable scaling of $\boldsymbol{\psi}$, i.e. setting $\boldsymbol{\varphi} := \|p_h\|_{0,\omega}\,\boldsymbol{\psi}$, results in $\|\nabla'\boldsymbol{\varphi}\|_{0,\omega} \leq \|p_h\|_{0,\omega}$ such that we finish the proof with the following estimate, where we apply Young's inequality:

$$\begin{aligned} -(\mathrm{div}'\,\boldsymbol{\varphi}, p_h)_\omega &\geq \frac{\gamma_\omega}{2}\|p_h\|_{0,\omega}^2 - s_h(p_h,p_h)^{1/2}\|p_h\|_{0,\omega} \\ &\geq \frac{\gamma_\omega}{4}\|p_h\|_{0,\omega}^2 - \frac{1}{\gamma_\omega} s_h(p_h,p_h)\,. \end{aligned}$$

□

Remark 4.9. *We restrict our considerations on the stabilizations (P-i) – (P-iv). However, the preceding lemma only requires application of inf-sup stable pressure dependent stabilizations, which fulfill the estimates of Lemma 4.7. Thus, our considerations also apply for any other pressure dependent stabilization, which inherits these properties.*

Residual based stabilization

Literature also provides residual based stabilization schemes, which also depent on the velocity components. In these cases, the stabilization also enters the forcing and the entire stabilized problem is given as:

$$\textit{Find}\;\; (\boldsymbol{w}_h, p_h) \in \mathbf{W}_h \times Q_h \;\; \textit{s. t.}\;\; A_h^\omega(\boldsymbol{w}_h, p_h; \boldsymbol{\varphi}, \xi) = \langle \boldsymbol{f}_h, \boldsymbol{\varphi}\rangle \qquad \forall (\boldsymbol{\varphi},\xi) \in \mathbf{W}\times Q \tag{4.24}$$

with stabilized bilinear form

$$A_h^\omega(\boldsymbol{w}_h, p_h; \boldsymbol{\phi}, \xi) \;:=\; (\nabla'\,\boldsymbol{w}_h, \nabla'\,\boldsymbol{\phi})_\omega - (p_h, \mathrm{div}'\,\boldsymbol{\phi})_\omega + (\mathrm{div}'\,\boldsymbol{w}_h, \xi)_\omega + s_h^\omega(\boldsymbol{w}_h, p_h; \boldsymbol{\phi}, \xi)\,,$$

and suitably modified linear form $\boldsymbol{f}_h : \mathbf{W}_h \times Q_h \to \mathbb{R}$. Note, that we applied the subscript ω in the definition of the stablization. This is done, as we can not directly apply this stabilization in the hydrostatic context, but a slight modification of it. In the upcoming, we consider the following residual based schemes:

(P-v) Pressure Stabilization Petrov-Galerkin (PSPG) method [HFB86]:

$$\begin{aligned} s_h^\omega(\boldsymbol{w}, p; \xi) &:= \alpha_0 \sum_{K\in\mathcal{K}_h} h_K^2 (-\Delta'\,\boldsymbol{w} + \nabla' p, \nabla'\xi)_K\,, \\ \langle \boldsymbol{f}_h; \boldsymbol{\varphi}, \xi\rangle &:= (\boldsymbol{f}, \boldsymbol{\varphi})_\omega + \alpha_0 \sum_{K\in\mathcal{K}_h} h_K^2 (\boldsymbol{f}, \nabla'\xi)_K\,. \end{aligned}$$

(P-vi) Galerkin-Least-Squares (GLS) method for Stokes, introduced by Hughes, Franca and Stenberg [FHS93]:

$$\begin{aligned} s_h^\omega(\boldsymbol{w},p;\boldsymbol{\varphi},\xi) &:= \alpha_0 \sum_{K\in\mathcal{K}_h} h_K^2(-\Delta'\,\boldsymbol{w}+\nabla' p,-\Delta'\,\boldsymbol{\varphi}+\nabla'\xi)_K\,, \\ \langle \boldsymbol{f}_h;\boldsymbol{\varphi},\xi\rangle &:= (\boldsymbol{f},\boldsymbol{\varphi})_\omega + \alpha_0 \sum_{K\in\mathcal{K}_h} h_K^2(\boldsymbol{f},-\Delta'\,\boldsymbol{\varphi}+\nabla'\xi)_K\,. \end{aligned}$$

(P-vii) Combination of GLS and penalization of pressure jumps across cell edges for discontinuous discrete pressures, introduced by Douglas and Wang [DW89] :

$$\begin{aligned} s_h^\omega(\boldsymbol{w},p;\boldsymbol{\varphi},\xi) &:= \alpha_0 \sum_{K\in\mathcal{K}_h} h_K^2(-\Delta'\,\boldsymbol{w}+\nabla' p,-\Delta'\,\boldsymbol{\varphi}+\nabla'\xi)_K + \sum_{e\in\mathcal{E}_h} h_e \int_e [p][\xi]\,ds\,, \\ \langle \boldsymbol{f}_h;\boldsymbol{\varphi},\xi\rangle &:= (\boldsymbol{f},\boldsymbol{\varphi})_\omega + \alpha_0 \sum_{K\in\mathcal{K}_h} h_K^2(\boldsymbol{f},-\Delta'\,\boldsymbol{\varphi}+\nabla'\xi)_K\,. \end{aligned}$$

The stabilization coefficient $\alpha_0 > 0$, which occurs in the stabilization schemes (P-v) - (P-vii), is to be chosen in a suitable range. In particular, the coefficient has to be chosen suitably small in order to allow for the estimates in the upcoming lemma.

In the following section, we present a general stability proof for the appropriately stabilized hydrostatic Stokes problem, which is, most extensively, independent of the particular choice and structure of the stabilizations of avail. Further note, that the term s_h^ω, chosen from (P-v) – (P-vii), does not fulfill the (appropriately adapted) estimates of Lemma 4.10 and even may lead to negative expressions. Thus, the straightforward definition of the triple norm $|\!|\!| \cdot |\!|\!|_\omega$ in the residual based case may not lead to a norm. Thus, we introduce

$$s_h(p,\xi) := s_h^\omega(\mathbf{0},p_h;\mathbf{0},\xi)\,. \tag{4.25}$$

Lemma 4.10. *Let s_h^ω be arbitrarily chosen from (P-v)–(P-vii) and $\alpha_0 > 0$ be sufficiently small. Given the reduced form (4.25) and arbitrary $p,\xi \in Q_h$ and $\boldsymbol{w}_h,\boldsymbol{\varphi} \in \mathbf{W}_h$, the reduced term s_h satisfies*

$$s_h(p,p) \geq 0\,, \tag{4.26}$$

$$|s_h^\omega(\boldsymbol{w},p;\boldsymbol{\varphi},\xi)| \leq (|\,\boldsymbol{w}\,|_{1,\omega}^2 + s_h(p,p))^{1/2} |\!|\!|(\boldsymbol{\varphi},\xi)|\!|\!|_\omega\,. \tag{4.27}$$

The bilinear form A_h^ω is inf-sup stable and thus (4.23) applies.

Proof. The estimates are trivial to validate by an inverse estimate. For the proof of the inf-sup condition we refer to the cited literature. □

Lemma 4.11. *Let s_h^ω be arbitrarily chosen from (P-v) – (P-vii) and s_h be given by (4.25). For any $p_h \in Q_h$ there is an element $\boldsymbol{\psi} \in \mathbf{W}_h$ such that $\|\nabla\,\boldsymbol{\psi}\,\|_{0,\omega} \leq \|p_h\|_{0,\omega}$ and*

$$-(div'\,\boldsymbol{\psi},p_h)_\omega \geq \frac{\gamma_\omega}{4}\|p_h\|_{0,\omega}^2 - \frac{1}{2\gamma_\omega} s_h(p_h,p_h). \tag{4.28}$$

Proof. We chose an arbitrary $p_h \in Q_h$ and consider $(\mathbf{0}, p_h) \in \mathbf{W}_h \times Q_h$. Due to Lemma 4.10, the inf-sup constraint (4.23) applies and existence of an element $(\boldsymbol{\varphi}, \xi) \in B_h^\omega$ is assured, which fulfills

$$A_h^\omega(\mathbf{0}, p_h; \boldsymbol{\varphi}, \xi) \;=\; -(\operatorname{div}'\boldsymbol{\varphi}, p_h)_\omega + s_h^\omega(\mathbf{0}, p_h; \boldsymbol{\varphi}, \xi) \;\geq\; \gamma_\omega |\!|\!| (\mathbf{0}, p_h) |\!|\!|_\omega .$$

As well, application of Lemma 4.10 assures $s_h^\omega(\mathbf{0}, p_h; \boldsymbol{\varphi}, \xi) \leq s_h(p_h, p_h)^{1/2}$. Therefore and due to the definition of the triple norm $|\!|\!| \cdot |\!|\!|_\omega$,

$$-(\operatorname{div}'\boldsymbol{\varphi}, p_h)_\omega \;\geq\; \frac{1}{2}\gamma_\omega \|p_h\|_{0,\omega} - \frac{1}{2} s_h(p_h, p_h)^{1/2}$$

applies. Suitable scaling of $\boldsymbol{\varphi}$, i.e. setting $\boldsymbol{\psi} := \|p_h\|_{0,\omega}\, \boldsymbol{\varphi}$, results in the estimate $\|\nabla' \boldsymbol{\psi}\|_{0,\omega} \leq \|p_h\|_{0,\omega}$. Similarly to the symmetric pressure stabilization, application of the inequality of Young finishes the proof:

$$\begin{aligned} -(\operatorname{div}'\boldsymbol{\psi}, p_h)_\omega \;&\geq\; \frac{\gamma_\omega}{2}\|p_h\|_{0,\omega}^2 - \frac{1}{2} s_h(p_h, p_h)^{1/2} \|p_h\|_{0,\omega} \\ &\geq\; \frac{\gamma_\omega}{4}\|p_h\|_{0,\omega}^2 - \frac{1}{2\gamma_\omega} s_h(p_h, p_h)\,. \end{aligned}$$

□

4.2.3 *A priori* error estimates

Lemma 4.12. *The symmetric stabilizations schemes (P-i)–(P-iv) as well as the reduced terms (4.25) of the residual based stabilization schemes (P-v)–(P-vii) provide the following* a priori *bound for every* $1 \leq k \leq r$*:*

$$s_h(p, p)^{1/2} \;\leq\; c h_\omega^k \|p\|_{k,\omega} \qquad \forall p \in \mathrm{H}^k(\omega)\,.$$

Proof. The estimates for the schemes (P-i) – (P-iv) are to be found in [BP84, BB01, BH06, DB04]. For the schemes (P-v)–(P-vii) we refer to [HFB86, FHS93, DW89]. □

4.3 3D Oseen problem

In this section we introduce the discrete 3D Oseen problem. After mentioning the lack of the inf-sup constraint for equal-order finite elements, we collect some of symmetric stabilization techniques and present important bounds. We close the section with a presentation of suitable *a priori* error estimates, which find application in the hydrostatic framework.

4.3.1 Galerkin formulation

We consider the wind-driven 3D Oseen problem, neglecting Coriolis forces. Without loss of generality we assume isotropic viscosities and set $\nu = \boldsymbol{\mathcal{A}}_\nu = \nu_E$. I.e., let

$\mathbf{U} := \mathbf{H}^1_b(\Omega) \times \mathrm{H}^1_0(\Omega)$ and $P := \mathrm{L}^2_0(\Omega)$. The dual space of $\mathbf{U}$ is denoted as $\mathbf{U}^{-1}$. The appropriate finite dimensional spaces $\mathbf{U}_h$ and P_h are defined in a similar fashion as (4.4) and (4.6), respectively, on the spaces of piecewise polynomials of order r. The equal-order finite element formulation of the 3D Oseen problem is given by:

$$\begin{aligned} &\textit{Given } \boldsymbol{b}_h \in \mathbf{U}_h, \operatorname{div} \boldsymbol{b}_h = 0,\ \boldsymbol{f} \in \mathbf{U}^{-1},\ \boldsymbol{g} \in \mathbf{H}^{-1/2}(\Gamma_s) \times \{0\}, \\ &\quad \textit{find } \mathbf{y}_h = (\mathbf{u}_h, p_h) \in \mathbf{U}_h \times P_h \ \textit{ s.t.} \\ &\qquad\qquad A^\Omega(\boldsymbol{b}_h; \mathbf{y}_h; \boldsymbol{\phi}) = \ \boldsymbol{l}^\Omega(\boldsymbol{\varphi}) \qquad\qquad \forall\, \boldsymbol{\phi} = (\boldsymbol{\varphi}, \xi) \in \mathbf{U} \times P \end{aligned} \tag{4.29}$$

with

$$\begin{aligned} A^\Omega(\boldsymbol{b}_h; \mathbf{y}_h; \boldsymbol{\phi}) = \ & (\sigma\, \mathbf{u}_h, \boldsymbol{\varphi})_\Omega + ((\boldsymbol{b}_h \cdot \nabla)\, \mathbf{u}_h, \boldsymbol{\varphi})_\Omega \\ & + (\nu \nabla\, \mathbf{u}_h, \nabla\, \boldsymbol{\varphi})_\Omega - (p_h, \operatorname{div}\, \boldsymbol{\varphi})_\Omega + (\xi, \operatorname{div}\, \mathbf{u}_h)_\Omega\,, \\ \boldsymbol{l}^\Omega(\boldsymbol{\varphi}) = \ & (\boldsymbol{f}, \boldsymbol{\varphi})_\Omega + \ (\boldsymbol{g}, \boldsymbol{\varphi})_{\Gamma_u}. \end{aligned}$$

As in the 2D Stokes case, the inf-sup constraint (3.7) is not assured for the equal-order finite element approach and suitable stabilization of the pressure has to be applied. Moreover, the problem shows oscillations, that occur due to dominant advection, see also [RST08], which also have to be controlled.

4.3.2 Symmetric stabilization schemes

To circumvent the mentioned undesired properties, we add stabilizing terms to the system. Regarding suitable adaption of the stabilization for the appropriate hydrostatic problem, we restrict to the presentation of symmetric stabilizations:

$$s^\Omega_h(\mathbf{u}_h, p_h; \boldsymbol{\varphi}, \xi) := s^\Omega_{h,p}(p_h, \xi) + s^\Omega_{h,v}(\mathbf{u}_h, \boldsymbol{\varphi}) \qquad \forall (\mathbf{u}_h, p_h), (\boldsymbol{\varphi}, \xi) \in \mathbf{U}_h \times P_h\,,$$

whereas the term $s^\Omega_{h,p}(\cdot,\cdot)$ stabilizes the oscillations in the pressure and the term $s^\Omega_{h,v}(\cdot,\cdot)$ controls the undesired effect of the dominant advection. The stabilized problem then is given by:

$$\begin{aligned} &\textit{Given } \boldsymbol{b}_h \in \mathbf{U}_h, \operatorname{div} \boldsymbol{b}_h = 0,\ \boldsymbol{f} \in \mathbf{U}^{-1},\ \boldsymbol{g} \in \mathbf{H}^{-1/2}(\Gamma_s) \times \{0\}, \\ &\quad \textit{find } (\mathbf{u}_h, p_h) \in \mathbf{U}_h \times P_h \\ &\quad \textit{s.t.} \qquad A^\Omega(\boldsymbol{b}_h; \mathbf{u}_h, p_h; \boldsymbol{\varphi}, \xi) + s^\Omega_h(\boldsymbol{b}_h; \mathbf{u}_h, p_h; \boldsymbol{\varphi}, \xi) = \boldsymbol{l}^\Omega(\boldsymbol{\varphi}) \quad \forall (\boldsymbol{\varphi}, \xi) \in \mathbf{U}_h \times P_h\,. \end{aligned}$$

In the upcoming we consider the following schemes:

(V-i) LPS [BL09]:

$$s^\Omega_{h,p}(p_h, \xi) := \sum_{M \in \mathcal{T}_{2h}} h_M \big(\boldsymbol{\kappa}_{h,\Omega}(\nabla p_h\,), \boldsymbol{\kappa}_{h,\Omega}(\nabla \xi)\big)_M,$$

(a) with stabilization of the whole velocity gradient:

$$s_{h,v}^{\Omega}(\mathbf{u}_h, \boldsymbol{\varphi}) := \sum_{M \in \mathcal{T}_{2h}} h_M \|\boldsymbol{b}_h\|_{l,\infty,M} \big(\boldsymbol{\kappa}_{h,\Omega}(\nabla \mathbf{u}_h),\, \boldsymbol{\kappa}_{h,\Omega}(\nabla \boldsymbol{\varphi})\big)_M \,,$$

whereas $\boldsymbol{\kappa}_{h,\Omega} := id_\Omega - \pi_\Omega$ denotes the 3D fluctuation operator with identity $id_\Omega : \mathrm{L}^2(\Omega) \to \mathrm{L}^2(\Omega)$ and L^2-orthogonal projection operator $\pi_\Omega : \mathrm{L}^2(\Omega) \to Q_{2h}^{r-1}(\Omega)$.

(b) with stabilization in streamline direction:

$$\begin{aligned} s_{h,v}^{\Omega}(\mathbf{u}_h, \boldsymbol{\varphi}) := \sum_{M \in \mathcal{T}_{2h}} & \frac{h_M}{\|\boldsymbol{b}_h\|_{l,\infty,M}} \big(\boldsymbol{\kappa}_{h,\Omega}((\boldsymbol{b}_h \cdot \nabla)\, \mathbf{u}_h),\, \boldsymbol{\kappa}_{h,\Omega}((\boldsymbol{b}_h \cdot \nabla)\, \boldsymbol{\varphi})\big)_M \\ & + h_M (\boldsymbol{\kappa}_{h,\Omega}(\operatorname{div} \mathbf{u}_h), \boldsymbol{\kappa}_{h,\Omega}(\operatorname{div} \boldsymbol{\varphi}))_M \,, \end{aligned}$$

(V-ii) CIP [BFH06] for $r = 1$:

$$\begin{aligned} s_{h,p}^{\Omega}(p_h, \xi) &= \sum_{T \in \mathcal{T}_h} \lambda_T \frac{h_T^2}{\|\boldsymbol{b}_h\|_{0,\infty,T}} \int_{\partial T} [\nabla p_h]_{\partial T} \cdot [\nabla \xi]_{\partial T}\, d\,s \,, \\ s_{h,v}^{\Omega}(\mathbf{u}_h, \boldsymbol{\varphi}) &= \sum_{T \in \mathcal{T}_h} \lambda_T h_T^2 \int_{\partial T} \|\boldsymbol{b}_h \cdot \boldsymbol{n}\|_{0,\infty \partial T} [\boldsymbol{n} \cdot \nabla \mathbf{u}_h]_{\partial T} \cdot [\boldsymbol{n} \cdot \nabla \boldsymbol{\varphi}]_{\partial T}\, d\,s \\ &\quad + \lambda_T \|\boldsymbol{b}_h\|_{0,\infty,T} \int_{\partial T} [\operatorname{div} \mathbf{u}_h]_{\partial T} \cdot [\operatorname{div} \boldsymbol{\varphi}]_{\partial T}\, d\,s \,. \end{aligned}$$

These stabilization terms provide the following property:

Lemma 4.13. *The stabilization terms $s_{h,v}(\cdot,\cdot)$ given in* (V-i) – (V-ii) *satisfy*

$$s_{h,v}^{\Omega}(\mathbf{u}_h; \boldsymbol{\varphi}) \le s_{h,v}^{\Omega}(\mathbf{u}_h; \mathbf{u}_h)^{1/2} s_{h,v}^{\Omega}(\boldsymbol{\varphi}; \boldsymbol{\varphi})^{1/2} \qquad \forall\, \mathbf{u}_h,\, \boldsymbol{\varphi} \in \mathbf{U}_h \,. \tag{4.30}$$

Proof. See [BL09, BFH06] □

4.3.3 *A priori* estimates

Lemma 4.14. *The stabilization terms $s_{h,v}(\cdot,\cdot)$ given in* (V-i) – (V-ii) *provide the estimates*

$$0 \le s_{h,v}^{\Omega}(\mathbf{u}, \mathbf{u}) \lesssim h^{2k+1} \| \mathbf{u} \|_{k+1,\Omega}^2 \qquad \forall\, \mathbf{u} \in \mathbf{H}^{k+1}(\Omega) \cap \mathbf{U}_h \,, 0 \le k \le r \,. \tag{4.31}$$

Proof. We refer to the cited literature. □

4.4 Hydrostatic Stokes problem

This section aims to introduce the equal-order finite element discretization of hydrostatic flow problems, which has hardly been analyzed yet, see e.g. [CGS12, KB12, Kim12]. We restrict our view to the minimal system, which shows characteristic properties of hydrostatic flows: we consider the stationary, linear hydrostatic Stokes problem in a non rotating frame, i.e. we neglect Coriolis forces. Moreover, we impose Dirichlet data on the entire domain, assume isotropic viscosities, i.e. $\nu = \boldsymbol{\mathcal{A}}_\nu = \nu_E > 0$, and norm the problem, such that $\nu = 1$.

We start with the Galerkin formulation, validating the tight relation between the 2D and the 2.5D Stokes problem regarding inf-sup stability. Afterwards, we turn to stabilization methods, stemming from the already introduced stabilization techniques for the 2D Stokes problem. We validate stability and elaborate optimal *a priori* error estimates. The results of this section constitutes the heart of [KB12]. Note, that we furthermore have a closer look at the residual based stabilizations of the hydrostatic Stokes problem than has been done in [KB12] and elaborate some domain dependencies, which have been withhold in [KB12].

4.4.1 Galerkin formulation

Let $\mathbf{V} := \mathbf{H}_0^1(\Omega)$ and $Q := \mathrm{L}_0^2(\omega)$ be the underlying variational spaces. The dual space of $\mathbf{V}$ is denoted as $\mathbf{V}^{-1}$. The standard Galerkin formulation of the introduced hydrostatic Stokes problem by conforming finite elements in the finite dimensional space $\mathbf{X}_h := \mathbf{V}_h \times Q_h$ is given by:

$$\begin{aligned} &\textit{Given } \boldsymbol{f} \in \mathbf{V}^{-1}, \textit{ find } (\boldsymbol{v}_h, p_h) \in \mathbf{X}_h \\ &\quad \textit{s. t. } \mathrm{a}(\boldsymbol{v}_h, \boldsymbol{\varphi}) - \mathrm{b}(p_h, \boldsymbol{\varphi}) + \mathrm{b}(\xi, \boldsymbol{v}_h) \;=\; (\boldsymbol{f}, \boldsymbol{\varphi})_\Omega \qquad \forall (\boldsymbol{\varphi}, \xi) \in \mathbf{X}_h \end{aligned} \tag{4.32}$$

with bilinear forms $\mathrm{a}(\boldsymbol{v}_h, \boldsymbol{\varphi}) := (\nabla \boldsymbol{v}_h, \nabla \boldsymbol{\varphi})_\Omega$ and $\mathrm{b}(p_h, \boldsymbol{\varphi}) := (p_h, \mathrm{div}'\, \mathbf{M}\, \boldsymbol{\varphi})_\omega$. If we replace $\mathbf{X}_h$ by the space $\mathbf{X} := \mathbf{V} \times Q$ in problem (4.32), the system becomes the variational formulation of the underlying hydrostatic Stokes problem.

Note, that we restrict to the case of homogeneous Dirichlet data for the velocity field. However, each problem with inhomogenous Dirichlet data can be reformulated into a problem with homogeneous Dirichlet data by alteration of the right hand side into $\langle \boldsymbol{f}, \varphi \rangle := (\boldsymbol{f}, \varphi) - \mathrm{a}(\boldsymbol{v}_0, \varphi)$. The element $\boldsymbol{v}_0 \in \mathbf{H}^1(\Omega)$ is an extension of the appropriate boundary data to the entire domain Ω and is divergence-free in vertical mean.
The next proposition states the tight relation between the 2D and the 2.5D Stokes problem. Throughout this proposition we therefore broaden our attention to a wider range of possible discrete spaces:

Proposition 4.15. *Let Ω be a flat domain and $\mathcal{T}_h$ be a triangulation of Ω fulfilling Assumption 4.2. The hydrostatic Stokes problem (4.32) formulated on the finite element*

spaces $\mathbf{X}_h := \mathbf{V}_h \times Q_h$ *with*

$$\begin{aligned} Q_h &:= \{q_h \in Q \cap \mathcal{C}(\overline{\omega}) \quad \big| \, q_h|_K \in \mathbb{Q}_r(K),\ \forall K \in \mathcal{K}_h\}, \\ \mathbf{V}_h &:= \{\boldsymbol{v}_h \in \mathbf{V} \cap \mathcal{C}(\overline{\Omega})^2 \quad \big| \ \boldsymbol{v}_{h,i}\,|_T \in \mathbb{Q}_s(T),\ i \in \{1,2\},\ \forall T \in \mathcal{T}_h\} \end{aligned}$$

has a unique solution, if the 2D Stokes problem (4.18) formulated on the finite element spaces $\mathbf{W}_h \times Q_h$ *with*

$$\begin{aligned} Q_h &:= \{q_h \in Q \cap \mathcal{C}(\overline{\omega}) \quad \big| \, q_h|_K \in \mathbb{Q}_r(K),\ \forall K \in \mathcal{K}_h\}, \\ \mathbf{W}_h &:= \{\boldsymbol{w}_h \in \mathbf{W} \cap \mathcal{C}(\overline{\omega})^2 \quad \big| \ \boldsymbol{v}_{h,i}\,|_K \in \mathbb{Q}_s(K),\ i \in \{1,2\},\ \forall K \in \mathcal{K}_h\} \end{aligned}$$

has a unique solution. Moreover, if the 2D Stokes problem is not inf-sup stable, the same applies for the hydrostatic Stokes problem.

Proof. We apply the techniques, introduced in Section 3.1.2. First note, that the continuous bilinear form $a : \mathbf{V} \times \mathbf{V} \to \mathbb{R}$ is $\mathbf{V}$-elliptic and $\mathbf{V}_h \subset \mathbf{V}$. It thus suffices to assure, that the hydrostatic problem (4.32) satisfies the modified inf-sup condition (4.16), if the appropriate inf-sup condition (4.17) of the 2D Stokes problem is fulfilled. We already proved this statement in Proposition 4.5, restricting to $p = 2$. □

Thus, due to the relation $\mathbf{M}(\mathbf{V}_h) = \mathbf{W}_h$, see Lemma 4.4, and as equal-order finite elements do not lead to an inf-sup stable 2D Stokes problem, see e.g. [Bra07], the discrete hydrostatic Stokes problem (4.32) is not inf-sup stable. As introduced for the 2D case, we avoid this problem by adding suitable stabilization terms to the system.

4.4.2 Stabilization of the problem

We adapt the introduced stabilization schemes for the 2D Stokes problem to the hydrostatic case. As in the 2D case, the stabilized hydrostatic Stokes problem is given by

$$\textit{Find} \quad (\boldsymbol{v}_h, p_h) \in \mathbf{X}_h \ \ \textit{s. t.} \ \ A_h(\boldsymbol{v}_h, p_h; \boldsymbol{\varphi}, \xi) \ = \ (\boldsymbol{f}_h, \boldsymbol{\phi})_\Omega \quad \forall\, \boldsymbol{\phi} := (\boldsymbol{\varphi}, \xi) \in \mathbf{X}_h \tag{4.33}$$

with $\mathbf{X}_h = \mathbf{V}_h \times Q_h$. The bilinear form A_h is defined due to the chosen stabilization scheme. In the case of symmetric pressure stabilization, see Section 4.2.2, we set

$$A_h(\boldsymbol{v}_h, p_h; \boldsymbol{\varphi}, \xi) \ := \ a(\boldsymbol{v}_h, \boldsymbol{\varphi}) - b(p_h, \boldsymbol{\varphi}) + b(\xi, \boldsymbol{v}_h) + s_h(p_h, \xi) \tag{4.34}$$

and the forcing $\boldsymbol{f}_h$ equals $\boldsymbol{f}$. If a residual based stabilization term is applied, see Section 4.2.2, the bilinear form is given by

$$A_h(\boldsymbol{v}_h, p_h; \boldsymbol{\varphi}, \xi) \ := \ a(\boldsymbol{v}_h, \boldsymbol{\varphi}) - b(p_h, \boldsymbol{\varphi}) + b(\xi, \boldsymbol{v}_h) + s_h(\boldsymbol{v}_h, p_h; \boldsymbol{\varphi}, \xi)\,. \tag{4.35}$$

The stabilization term $s_h(\cdot, \cdot; \cdot, \cdot)$ and the forcing $\boldsymbol{f}_h$ are the hydrostatic 3D analogs of the 2D stabilization terms $s_h^\omega(\cdot, \cdot; \cdot, \cdot)$ and $\boldsymbol{f}_h$ as introduced in Section 4.2.2. E.g., in

the GLS case the stabilization is given by

$$\begin{aligned} s_h(\boldsymbol{v}_h, p_h; \xi) &:= \alpha_0 \sum_{K \in \mathcal{K}_h} h_K^2 (-\mathbf{M}(\Delta \boldsymbol{v}_h) + \nabla' p, -\mathbf{M}(\Delta \boldsymbol{\varphi}) + \nabla' \xi)_K \,, \\ \langle \boldsymbol{f}_h; \boldsymbol{\varphi}, \xi \rangle &:= (\boldsymbol{f}, \boldsymbol{\varphi})_\Omega + \alpha_0 \sum_{K \in \mathcal{K}_h} h_K^2 (\mathbf{M}\, \boldsymbol{f}, -\mathbf{M}(\Delta \boldsymbol{\varphi}) + \nabla' \xi)_K \,. \end{aligned}$$

Thus, in the case of residual based stabilization we observe global couplings of the velocity field and of the forcing, which in turn leads to a numerically more expensive scheme as in the case of symmetric pressure stabilization.

Remark 4.16. *Note, that it is also possible to adapt the 2D residual based stabilizations (P-v) – (P-vii) in a 3D manner. I.e. in the case of GLS we can also treat*

$$\begin{aligned} s_h(\boldsymbol{v}_h, p_h; \xi) &:= \alpha_0 \sum_{T \in \mathcal{T}_h} h_T^2 (-\Delta \boldsymbol{v}_h + \nabla' p, -\Delta \boldsymbol{\varphi} + \nabla' \xi)_T \,, \\ \langle \boldsymbol{f}_h; \boldsymbol{\varphi}, \xi \rangle &:= (\boldsymbol{f}, \boldsymbol{\varphi})_\Omega + \alpha_0 \sum_{T \in \mathcal{T}_h} h_T^2 (\boldsymbol{f}, -\Delta \boldsymbol{\varphi} + \nabla' \xi)_T \,. \end{aligned}$$

The upcoming considerations basically are the same. But, the constants may depend on the depth of the domain in a slightly different way. Anticipatory, such a difference occurs in Lemma 4.17, in the estimate of $s_h(\boldsymbol{v}_h, p_h, \widetilde{\boldsymbol{v}}_h, 0)$ of the proof of Proposition 4.18. The appropriate estimates are to be found in [KB12]. Moreover, the estimate of $s_h((\boldsymbol{z}_h \boldsymbol{v} - \boldsymbol{v}), z_h p - p; \boldsymbol{\varphi}, \xi)$ in Proposition 4.21 alters to

$$s_h((\boldsymbol{z}_h \boldsymbol{v} - \boldsymbol{v}), z_h p - p; \boldsymbol{\varphi}, \xi) \;\leq\; c(h^m \| \boldsymbol{v} \|_{m+1,\Omega} + h_\omega^m \delta_{max} \|p\|_{m,\omega}) \,,$$

whereas we applied the property $h_T \leq h_K$ for any element T whose projection onto ω is the 2D cell K.

Similar to the 2D case the triple norm on $\mathbf{X}_h$ is given by

$$|\!|\!| (\boldsymbol{v}, p) |\!|\!| := \left(\| \nabla \boldsymbol{v} \|_{0,\Omega}^2 + \|p\|_{0,\omega}^2 + s_h(p,p) \right)^{1/2} . \tag{4.36}$$

The term $s_h(\cdot,\cdot)$ coincides with the entire stabilization in the case of symmetric pressure stabilization. If a residual based scheme is applied, it is given similar to (4.25):

$$s_h(p, \xi) \;:=\; s_h(\mathbf{0}, p_h; \mathbf{0}, \xi) \,.$$

The residual based stabilization terms fulfill the following estimates, which are an adaption of Lemma 4.10:

Lemma 4.17. *The hydrostatically adapted versions of the stabilization schemes (P-v), (P-vi) and (P-vii), as defined in Section 4.2.2, fulfill*

$$\begin{aligned} s_h(\boldsymbol{v}_h, p_h; \boldsymbol{v}_h, p_h) &\geq \frac{1}{2} \left(s_h(p_h, p_h) - \delta_{max} | \boldsymbol{v}_h |_{1,\Omega}^2 \right) && \forall (\boldsymbol{v}_h, p_h) \in \mathbf{X}_h \,, \\ |s_h(\boldsymbol{v}_h, p_h; \boldsymbol{\varphi}, \xi)| &\leq c(\delta_{max} | \boldsymbol{v}_h |_{1,\Omega}^2 + s_h(p_h, p_h))^{1/2} |\!|\!| (\boldsymbol{\varphi}, \xi) |\!|\!| && \forall (\boldsymbol{v}_h, p_h), (\boldsymbol{\varphi}, \xi) \in \mathbf{X}_h \,. \end{aligned}$$

Proof. Under the constraint $0 < \alpha_0 < c_{inv}^{-2}$, with constant c_{inv} of the inverse estimate, the validation of the estimates can be easily done by application of an inverse estimate, see e.g. [Bra07], of Young's inequality as well as of the estimate (3.19). □

Given these preparatory estimates, we now turn to the proof of inf-sup stability of a suitably stabilized hydrostatic Stokes problem. Therefore, let

$$B_h \;:=\; \{(\boldsymbol{v}_h, p_h) \in \mathbf{X}_h \mid |\!|\!|(\boldsymbol{v}_h, p_h)|\!|\!| = 1\}\,.$$

Proposition 4.18. *The underlying domain Ω is assumed to be a flat basin. The triangulation of Ω is given by $\mathcal{T}_h$ and is presumed to fulfill Assumption 4.2. Let the hydrostatic Stokes problem be stabilized either by a symmetric pressure stabilization of (P-i)–(P-iv) or by a residual based stabilization chosen from the list (P-v)–(P-vii). Then, the stabilized 2.5D Stokes bilinear form (4.34) or (4.35), respectively, is inf-sup stable:*

$$\inf_{(\boldsymbol{v}_h,p_h)\in B_h} \sup_{(\boldsymbol{\varphi},\xi)\in B_h} A_h(\boldsymbol{v}_h, p_h; \boldsymbol{\varphi}, \xi) \;\geq\; \gamma_{\Omega,\omega}\,.$$

Proof. We assume an arbitrary $\boldsymbol{y}_h := (\boldsymbol{v}_h, p_h) \in \mathbf{X}_h$. The authors of [BS11] introduced an abstract criterion for the inf-sup condition. We also apply it here. I.e. we consider the following decomposition of the triple norm:

$$|\!|\!|\boldsymbol{y}_h|\!|\!|^2 = |\boldsymbol{y}_h|_a^2 + |\boldsymbol{y}_h|_b^2 \qquad \text{with}$$
$$|\boldsymbol{y}_h|_a^2 \;:=\; |\,\boldsymbol{v}_h\,|_{1,\Omega}^2 + s_h(p_h,p_h) \quad \text{and} \quad |\boldsymbol{y}_h|_b^2 \;:=\; \|p_h\|_{0,\omega}^2.$$

In the case of symmetric pressure stabilization, we get $A_h(\boldsymbol{y}_h;\boldsymbol{y}_h) = |\boldsymbol{y}_h|_a^2$. In the case of residual based stabilization, we apply Lemma 4.17, and estimate at least $A_h(\boldsymbol{y}_h;\boldsymbol{y}_h) \geq \frac{1}{2}|\boldsymbol{y}_h|_a^2$.
In order to prove the inf-sup condition, we construct an element $\widetilde{\boldsymbol{v}}_h \in \mathbf{V}_h$ with $|\!|\!|(\widetilde{\boldsymbol{v}}_h, 0)|\!|\!| \leq |\!|\!|\boldsymbol{y}_h|\!|\!|$ and

$$A_h(\boldsymbol{v}_h, p_h; \widetilde{\boldsymbol{v}}_h, 0) \;\geq\; c_1|\,\mathbf{u}_h\,|_b^2 - c_2|\,\mathbf{u}_h\,|_a^2\,.$$

Constant c_1 has to be strictly positive, i.e. $c_1 > 0$. Constant c_2 is no further restricted. For the construction, we chose a $\boldsymbol{\varphi} \in \mathbf{W}_h$, such that the element $(\boldsymbol{\varphi}, p_h)$ fulfills (4.28). As $\mathbf{M}$ is surjective, see also Lemma 4.4, an element $\widetilde{\boldsymbol{v}}_h \in \mathbf{V}_h$ is assured with $\boldsymbol{\varphi} = \mathbf{M}\,\widetilde{\boldsymbol{v}}_h$. Setting $\boldsymbol{w}_h := \mathbf{M}\,\boldsymbol{v}_h \in \mathbf{W}_h$ and applicating Lemma 4.8 leads to

$$\begin{aligned} A_h(\boldsymbol{y}_h; \widetilde{\boldsymbol{v}}_h, 0) &= (\nabla\,\boldsymbol{v}_h, \nabla\widetilde{\boldsymbol{v}}_h)_\Omega - (p_h, \mathrm{div}'\,\boldsymbol{w}_h)_\omega + s_h(\boldsymbol{v}_h, p_h; \widetilde{\boldsymbol{v}}_h, 0) \\ &\geq -|\,\boldsymbol{v}_h\,|_{1,\Omega}|\widetilde{\boldsymbol{v}}_h|_{1,\Omega} + \frac{\gamma_\omega}{4}\|p_h\|_{0,\omega}^2 - \frac{1}{\gamma_\omega}s_h(p_h,p_h) + s_h(\boldsymbol{v}_h, p_h; \widetilde{\boldsymbol{v}}_h, 0) \end{aligned}$$

in the case of residual based stabilization. If a symmetric pressure stabilization is applied, we can deduce the same estimate without the last term on the right hand side.

We further estimate the first term, $|\boldsymbol{v}_h|_{1,\Omega}|\widetilde{\boldsymbol{v}}_h|_{1,\Omega}$, on the right hand side:

$$\begin{aligned} |\boldsymbol{v}_h|_{1,\Omega}|\widetilde{\boldsymbol{v}}_h|_{1,\Omega} &\leq c_\omega \delta_{min}^{-3/2} |\boldsymbol{v}_h|_{1,\Omega} |\boldsymbol{\varphi}|_{1,\omega} \\ &\leq \frac{4}{\gamma_\omega} c_\omega^2 \delta_{min}^{-3} |\boldsymbol{v}_h|_{1,\Omega}^2 + \frac{\gamma_\omega}{16} |\boldsymbol{\varphi}|_{1,\omega}^2 \\ &\leq \frac{4}{\gamma_\omega} c_\omega^2 \delta_{min}^{-3} |\boldsymbol{v}_h|_{1,\Omega}^2 + \frac{\gamma_\omega}{16} \|p_h\|_{0,\omega}^2 . \end{aligned}$$

In the case of residual cased stabilization we apply the estimates (3.19) and (4.27):

$$\begin{aligned} |s_h(\boldsymbol{v}_h, p_h; \widetilde{\boldsymbol{v}}_h, 0)| &\leq c\delta_{max}(|\boldsymbol{v}_h|_{1,\Omega}^2 + s_h(p_h, p_h))^{1/2} |\widetilde{\boldsymbol{v}}_h|_{1,\Omega} \\ &\leq c\delta_{max}(|\boldsymbol{v}_h|_{1,\Omega}^2 + s_h(p_h, p_h))^{1/2} \delta_{max}^{-3/2} \|p_h\|_{0,\omega} \\ &\leq c c_\omega \delta_{max}^{-1/2} |\boldsymbol{y}_h|_a \|p_h\|_{0,\omega} \\ &\leq \frac{c c_\omega^2}{\gamma_\omega \delta_{max}} |\boldsymbol{y}_h|_a^2 + \frac{\gamma_\omega}{16} \|p_h\|_{0,\omega}^2 . \end{aligned}$$

Thus, we entirely get the following bound:

$$\begin{aligned} A_h(\boldsymbol{y}_h; \widetilde{\boldsymbol{v}}_h, 0) &\geq -\frac{c}{\gamma_\omega} c_\omega^2 \delta_{min}^{-1} |\boldsymbol{v}_h|_{1,\Omega}^2 + \frac{\gamma_\omega}{8} \|p_h\|_{0,\omega}^2 - \frac{1}{\gamma_\omega} s_h(p_h, p_h) \\ &\geq -\frac{1}{\gamma_\omega} \left(1 + c c_\omega^2 \delta_{min}^{-1}\right) |\boldsymbol{y}_h|_a^2 + \frac{\gamma_\omega}{8} |\boldsymbol{y}_h|_b^2 . \end{aligned}$$

□

4.4.3 *A priori* error estimates

In this section we analyze the *a priori* errors for the hydrostatic Stokes problem. In appropriate deductions we apply the estimates, which we already collected for the 2D Stokes problem. Moreover, we apply the following lemma, which states the strong consistency of residual based stabilization schemes.

Lemma 4.19. *Let s_h be chosen from (P-v)–(P-vii). The solution $(\boldsymbol{v}, p) \in \mathbf{X} := (\mathbf{V} \times Q)$ of (4.32) fulfills*

$$s_h(\boldsymbol{v}, p; \boldsymbol{\varphi}, \xi) = \langle \boldsymbol{f}_h; \boldsymbol{\varphi}, \xi \rangle - (\boldsymbol{f}, \boldsymbol{\varphi})_\Omega \qquad \forall (\boldsymbol{\varphi}, \xi) \in \mathbf{X}_h . \tag{4.37}$$

Proof. As we apply conforming finite elements, we can validate proposition (4.32) as follows. First, we insert the solution $(\boldsymbol{v}, p) \in \mathbf{X}$ into the stabilized hydrostatic Stokes problem (4.33), then test the variational problem with elements $(\boldsymbol{\varphi}, \xi)$ from the discrete space $\mathbf{X}_h$ and finally formulate the difference of these two equations. □

Before we turn to the main proposition of this section, we validate a simple estimate of the divergence constraint. We anticipatory add it here in order to accent the different demands on the estimate between the hydrostatic Stokes problem and the hydrostatic Oseen problem. These differences necessitate more endeavors in the hydrostatic Oseen case than for the present hydrostatic Stokes problem.

Lemma 4.20. *Let $\mathcal{T}_h$ be a triangulation of Ω fulfilling Assumption 4.2, $\boldsymbol{z}_h : \mathbf{V} \to \mathbf{V}_h$ be the Scott-Zhang interpolant, $\boldsymbol{v} \in \mathbf{H}^{k+1}(\Omega) \cap \mathbf{V}$, $0 \leq k \leq r$, and $\xi \in Q_h$. Then, the divergence constraint of the interpolation error $\boldsymbol{\eta}_v = \boldsymbol{v} - \boldsymbol{z}_h \boldsymbol{v}$ supplies the* a priori *error estimate:*

$$(div' \mathbf{M}\, \boldsymbol{\eta}_v, \xi)_\omega \quad \lesssim \quad h^m \| \boldsymbol{v} \|_{m+1,\Omega} \, |\!|\!| (\mathbf{0}, \xi) |\!|\!| \tag{4.38}$$

with $m = \min\{r, k\}$.

Proof. Partial integration of the divergence term in (4.38) leads to

$$|(\mathrm{div}' \mathbf{M}\, \boldsymbol{\eta}_v, \xi)_\omega| \;=\; |(\mathbf{M}\, \boldsymbol{\eta}_v, \nabla' \xi)_\omega| \;=\; |(\boldsymbol{\eta}_v, \nabla' \xi)_\Omega| \,.$$

When we go over to the 3D expression $|(\boldsymbol{\eta}_v, \nabla' \xi)_\Omega|$ we constantly continue $\nabla' \xi$ in vertical direction, i.e. use $\nabla' \xi(x, y, z) := \nabla' \xi(x, y)$ for any $(x, y, z) \in \Omega$. The latter term on the right hand side can be estimated as

$$|(\boldsymbol{\eta}_v, \nabla' \xi)_\Omega| \;\leq\; c_\omega \|\boldsymbol{\eta}_v\|_\Omega \|\nabla' \xi\|_\omega \,.$$

which finishes the proof due to the definition of the triple norm (4.36), application of an inverse estimate and the interpolation properties of the Scott-Zhang operator. □

Proposition 4.21. *Let Assumption 4.2 be valid and the continuous solution $(\boldsymbol{v}, p) \in \mathbf{X} := (\mathbf{V} \times Q)$ of (4.32) be sufficiently regular, $(\boldsymbol{v}, p) \in \mathbf{H}^{k+1}(\Omega) \times \mathrm{H}^k(\omega)$. The discrete solution $(\boldsymbol{v}_h, p_h)$ of (4.33), stabilized by any of the stabilization schemes (P-i)–(P-iv) and (P-v)–(P-vii) fulfills the* a priori *error estimate*

$$\| \boldsymbol{v} - \boldsymbol{v}_h \|_{1,\Omega} + \|p - p_h\|_{0,\omega} \leq c \left(h^m \| \boldsymbol{v} \|_{m+1,\Omega} + h_\omega^m \|p\|_{m,\omega} \right). \tag{4.39}$$

Value m is given by $m = \min\{r, k\}$ and c is a constant, which does not depend on h and h_ω.

Proof. We proceed as usual and partition the error into an interpolation and a projection part, applying the Scott-Zhang interpolants $\boldsymbol{z}_h \boldsymbol{v}$ and $z_h p$. Due to the interpolation properties of the Scott-Zhang interpolation operator, see also Section 4.1.2, it suffices to examine the projection errors $\|\boldsymbol{z}_h \boldsymbol{v} - \boldsymbol{v}_h\|_{1,\Omega}$ and $\|z_h p - p_h\|_{0,\omega}$. As we validated in Proposition 4.18, the stabilized discrete problem is inf-sup stable and thus an element $(\boldsymbol{\varphi}, \xi) \in \mathbf{X}_h$ with $|\!|\!| (\boldsymbol{\varphi}, \xi) |\!|\!| = 1$ is assured, such that

$$\gamma_{\Omega,\omega} |\!|\!| (\boldsymbol{z}_h \boldsymbol{v} - \boldsymbol{v}_h, z_h p - p_h) |\!|\!| \;\leq\; A_h(\boldsymbol{z}_h \boldsymbol{v} - \boldsymbol{v}_h, z_h p - p_h; \boldsymbol{\varphi}, \xi)$$

is fulfilled. In the case of symmetric pressure stabilization, i.e. for the schemes (P-i)–(P-iv), we argue by application of the perturbed Galerkin orthogonality:

$$\begin{aligned} \gamma_{\Omega,\omega} |\!|\!| (\boldsymbol{z}_h \boldsymbol{v} - \boldsymbol{v}_h, z_h p - p_h) |\!|\!| \;&\leq\; A_h(\boldsymbol{z}_h \boldsymbol{v} - \boldsymbol{v}, z_h p - p; \boldsymbol{\varphi}, \xi) + s_h(p, \xi) \\ &= \mathrm{a}(\boldsymbol{z}_h \boldsymbol{v} - \boldsymbol{v}, \boldsymbol{\varphi}) - \mathrm{b}(z_h p - p, \boldsymbol{\varphi}) + \mathrm{b}(\xi, \boldsymbol{z}_h \boldsymbol{v} - \boldsymbol{v}) - s_h(z_h p, \xi) \,. \end{aligned}$$

If one of the residual based stabilization schemes (P-v)-(P-vii) is applied we deduce

$$\begin{aligned}\gamma_{\Omega,\omega}|\!|\!|(\boldsymbol{z}_h\,\boldsymbol{v}-\boldsymbol{v}_h, z_hp-p_h)|\!|\!| &\leq A_h(\boldsymbol{z}_h\,\boldsymbol{v}-\boldsymbol{v}, z_hp-p;\boldsymbol{\varphi},\xi)\\ &= \mathrm{a}(\boldsymbol{z}_h\,\boldsymbol{v}-\boldsymbol{v},\boldsymbol{\varphi})-\mathrm{b}(z_hp-p,\boldsymbol{\varphi})+\mathrm{b}(\xi,\boldsymbol{z}_h\,\boldsymbol{v}-\boldsymbol{v})\\ &\quad -s_h(\boldsymbol{z}_h\,\boldsymbol{v}-\boldsymbol{v}, z_hp-p;\boldsymbol{\varphi},\xi)\,.\end{aligned}$$

The Galerkin terms can be estimated as, see also Lemma 4.20,

$$\begin{aligned}\mathrm{a}(\boldsymbol{z}_h\,\boldsymbol{v}-\boldsymbol{v},\boldsymbol{\varphi}) &\leq \|\boldsymbol{z}_h\,\boldsymbol{v}-\boldsymbol{v}\,\|_{1,\Omega}|\!|\!|(\boldsymbol{\varphi},0)|\!|\!| \leq ch^m\|\,\boldsymbol{v}\,\|_{m+1,\Omega}\\ -\mathrm{b}(z_hp-p,\boldsymbol{\varphi}) &\leq \|z_hp-p\|_{0,\omega}|\!|\!|(\boldsymbol{\varphi},0)|\!|\!| \leq ch_\omega^m\|p\|_{m,\omega}\\ \mathrm{b}(\xi,\boldsymbol{z}_h\,\boldsymbol{v}-\boldsymbol{v}) &\leq \|\mathrm{div}'\,\mathbf{M}(\boldsymbol{z}_h\,\boldsymbol{v}-\boldsymbol{v})\|_{\mathbf{0},\omega}|\!|\!|(0,\xi)|\!|\!| \leq ch^m\|\,\boldsymbol{v}\,\|_{m+1,\Omega}\,.\end{aligned}$$

The remaining stabilization terms for the schemes (P-i)–(P-iv) fulfill the following upper bound

$$\begin{aligned}s_h(z_hp,\xi) &= s_h(p,\xi)+s_h(z_hp-p,\xi)\\ &\leq (s_h(p,p)^{1/2}+s_h(z_hp-p,z_hp-p)^{1/2})s_h(\xi,\xi)^{1/2}\\ &\leq (s_h(p,p)^{1/2}+s_h(z_hp-p,z_hp-p)^{1/2})|\!|\!|(\mathbf{0},\xi)|\!|\!|\\ &\leq ch_\omega^m\|p\|_{m,\omega}+ch_\omega^m|z_hp-p|_{1,\omega}\\ &\leq ch_\omega^m\|p\|_{m,\omega}\,.\end{aligned}$$

The remaining estimate for the residual based schemes reads:

$$\begin{aligned}s_h((\boldsymbol{z}_h\,\boldsymbol{v}-\boldsymbol{v}), z_hp-p;\boldsymbol{\varphi},\xi) &\leq c(\delta_{max}|\boldsymbol{z}_h\,\boldsymbol{v}-\boldsymbol{v}\,|^2_{1,\Omega}+s_h(z_hp-p,z_hp-p))^{1/2}\\ &\leq c(h^m\delta_{max}\|\,\boldsymbol{v}\,\|_{m+1,\Omega}+h_\omega^m\|p\|_{m,\omega})\end{aligned}$$

The parts involving the pressure can be bounded as shown before. In sum, we arrive at the following estimate which implies the assertion:

$$\gamma_{\Omega,\omega}|\!|\!|(\boldsymbol{z}_h\,\boldsymbol{v}-\boldsymbol{v}_h, z_hp-p_h)|\!|\!| \leq c(h^m\|\,\boldsymbol{v}\,\|_{m+1,\Omega}+h_\omega^m\|p\|_{m,\omega})$$

with a constant c, which is independent of h and h_ω. □

4.5 Hydrostatic Oseen problem

In this section we broaden our attention to the discrete wind-driven hydrostatic Oseen problem (3.33), also considering the impact of Coriolis forces. We begin with the introduction of a suitable Galerkin formulation and recover regularity propositions. As in the preceeding hydrostatic Stokes case, additional stabilization of the pressure is necessary, and, additionally, suitable control over the advection has to be imposed. We realize the appropriate stabilizations by application of symmetric terms, which stem from appropriate classical, non hydrostatic problems and are adapted suitably. The performed analysis includes stability concerns and *a priori* error estimates.

The results of this section constitutes the crucial part of [Kim12].

4.5.1 Galerkin formulation

We approximate both, the variational spaces $\mathbf{X}$ and $\mathbf{Y}$ by $\mathbf{X}_h := \mathbf{V}_h \times Q_h$ as defined by (4.4) and (4.6). Similarly, we discretize the advection space $\mathbf{H}_{\mathrm{a}}$, see (3.29), as

$$\mathbf{H}_{a,h} := \left\{ \boldsymbol{b}_h \in \mathbf{H}_a \,\middle|\, b_{h,i}|_T \in \mathbb{Q}_r, i \in \{1,2,3\}, \forall T \in \mathcal{T}_h \right\}. \tag{4.40}$$

The space $\mathbf{H}_{a,h}$ is non trivial due to the following observations: Let $(u_{2d}, v_{2d}) \in \mathbf{W}$ be horizontal velocities, which are vertically invariant, i.e. $u_{2d} = u_{2d}(x,y)$ and $v_{2d} = v_{2d}(x,y)$. Moreover, let $c_u(x,y) := \partial_x u_{2d}(x,y)$ and $c_v(x,y) := \partial_v v_{2d}(x,y)$ for all $(x,y) \in \omega$. Due to Assumption 4.2 and Remark 4.3, the underlying 3D mesh $\mathcal{T}_h$ has at least one horizontally oriented inner node layer. Thus, we can define piecewise linear functions u_z and v_z, such that the velocities $u := u_{2d} \cdot u_z$ and $v := v_{2d} \cdot v_z$ vanish at the bottom of Ω and $\mathbf{M}(\partial_x u + \partial_y v) = 0$ applies. The appropriate vertical velocity w can be exactly determined by $w(x,y,z) := -\int_{-d(x,y)}^{z} (\partial_x u(x,y,\widehat{z}) + \partial_y v(x,y,\widehat{z})) d\,\widehat{z}$.

Note, that due to the regularity of the advection $(\widetilde{\boldsymbol{b}} \cdot \nabla)\, \boldsymbol{v} \in \mathbf{W}_b^{-1,3/2}(\Omega)$ with $\widetilde{\boldsymbol{b}} \in \mathbf{H}_a$, $\boldsymbol{v} \in \mathbf{V}$, and due to the embedding from $\mathrm{H}^1(\Omega)$ to $\mathrm{L}^6(\Omega)$, see Theorem 3.6, we have $((\widetilde{\boldsymbol{b}} \cdot \nabla)\, \boldsymbol{v}, \boldsymbol{\varphi}) \lesssim \|\widetilde{\boldsymbol{b}}\|_{0,3,\Omega} |\boldsymbol{v}|_{1,\Omega} |\boldsymbol{\varphi}|_{1,\Omega}$. In order to be able to suitably estimate the advection term we thus restrict to the following approximation of $\boldsymbol{b}$:

Assumption 4.22. *For $0 \leq k \leq r$ and any $\boldsymbol{b} \in \mathbf{H}_a \cap \mathbf{H}^{k+1}(\Omega)$ let $\boldsymbol{b}_h \in \mathbf{H}_{a,h}$ fulfill*

$$\|\boldsymbol{b} - \boldsymbol{b}_h\|_{0,3,\Omega} \;\lesssim\; h^k \, \|\boldsymbol{b}\|_{k+1,\Omega}.$$

The Galerkin formulation of the 2.5D Oseen problem is given by:

$$\begin{aligned} &\textit{Given } \boldsymbol{b}_h \in \mathbf{H}_{a,h},\ \boldsymbol{f} \in \mathbf{H}_b^{-1}(\Omega) \textit{ and } \boldsymbol{g} \in \mathbf{H}_b^{-1/2}(\Gamma_s), \quad && \textit{find } \boldsymbol{y}_h := (\boldsymbol{v}_h, p_h) \in \mathbf{X}_h \textit{ s. t.} \\ &\qquad A(\boldsymbol{b}_h; \boldsymbol{y}_h; \boldsymbol{\phi}) = \boldsymbol{l}(\boldsymbol{\varphi}) && \forall\, \boldsymbol{\phi} := (\boldsymbol{\varphi}, \xi) \in \mathbf{X}_h\,, \end{aligned} \tag{4.41}$$

whereas A is defined as in (3.34). Similar to the Stokes case we find a tight relation between the 2D and the 2.5D case. Again, we therefore broaden our attention to a wider range of possible discrete spaces throughout this proposition:

Proposition 4.23. *Let Ω be a flat domain and $\mathcal{T}_h$ be a triangulation of Ω fulfilling Assumption 4.2. The 2.5D Oseen problem (4.41) formulated on the finite element spaces $\mathbf{X}_h := \mathbf{V}_h \times Q_h$ with*

$$\begin{aligned} Q_h &:= \{q_h \in Q \cap \mathcal{C}(\overline{\omega}) \quad \big|\, q_h|_K \in \mathbb{Q}_r(K),\ \forall K \in \mathcal{K}_h\}\,, \\ \mathbf{V}_h &:= \{\boldsymbol{v}_h \in \mathbf{V} \cap \mathcal{C}(\overline{\Omega})^2 \quad \big|\, \boldsymbol{v}_{h,i}\,|_T \in \mathbb{Q}_s(T),\ i \in \{1,2\},\ \forall T \in \mathcal{T}_h\} \end{aligned}$$

fulfills the modified inf-sup condition and thus assures stability of the discrete pressure, if the appropriate discrete 2D non hydrostatic Oseen problem (4.29) formulated on the finite element spaces $\mathbf{W}_h \times Q_h$ with

$$\begin{aligned} Q_h &:= \{q_h \in Q \cap \mathcal{C}(\overline{\omega}) \quad \big|\, q_h|_K \in \mathbb{Q}_r(K),\ \forall K \in \mathcal{K}_h\}\,, \\ \mathbf{W}_h &:= \{\boldsymbol{w}_h \in \mathbf{H}_0^1(\omega) \cap \mathcal{C}(\overline{\omega})^2 \quad \big|\, \boldsymbol{v}_{h,i}\,|_K \in \mathbb{Q}_s(K),\ i \in \{1,2\},\ \forall K \in \mathcal{K}_h\} \end{aligned}$$

is inf-sup stable.

Proof. We already proved this statement in Proposition 4.5. □

Similar to the case of the full 3D Stokes problem an approach of equal order finite elements does not lead to an inf-sup stable discretization (4.41). As in the 2.5D Stokes case, we avoid this problem by adding suitable stabilization terms to the system. Moreover, as turns out later in this work, the advection term has to be bounded suitably. This is not realized in problem (4.41).

4.5.2 Stabilization of the problem

We circumvent the loss of stability by adding suitable terms to the system (4.41). First, we introduce suitable stabilization schemes, that stabilize the pressure, then turn to the stabilization of the velocity. We close this subsection with a stability analysis of the entire, stabilized problem.

Symmetric stabilization of the 2D pressure

In [KB12], the stabilization of the hydrodynamic 2D pressure has already been analyzed for the 2.5D Stokes case, i.e. $\boldsymbol{b}_h = \mathbf{0}$, $\sigma, \mathrm{f} = 0$ and $\nu = 1$. To account for the Stokes limit in the Oseen context we apply the 2D adapted local Peclet number $Pe_K := \max\{\|\boldsymbol{b}_h\|_{0,\infty,T} h_K/\nu \,|\, T \in \mathcal{T}_K\}$ for any cell $K \in \mathcal{K}_h$. Similarly, for each 2D cell $K \in \mathcal{K}_h$ we interprete $\|\boldsymbol{b}_h\|_{0,\infty,K}$ as $\|\boldsymbol{b}_h\|_{0,\infty,K} := \max\{\|\boldsymbol{b}_h\|_{0,\infty,T} \,|\, T \in \mathcal{K}_T\}$. For ease of presentation we set $\lambda_K := \min\{1, Pe_K\}$ and $\lambda := \max\{\lambda_K \,|\, K \in \mathcal{K}_h\}$.
We consider the solely pressure dependent, symmetric stabilization techniques (P-ii) and (P-iii), introduced in Section 4.2.2 for the Stokes limit. Here, we present the pressure stabilization schemes in a more common frame, which also covers the Oseen case. The differences concern the parameter choices.

(P'-ii) Local projection stabilization (LPS) [BL09]:

$$s_{h,p}(p_h, \xi) := \sum_{L \in \mathcal{K}_{2h}} \lambda_L h_L (\boldsymbol{\kappa}_{h,\omega}(\nabla' p_h),\, \boldsymbol{\kappa}_{h,\omega}(\nabla' \xi))_L \,,$$

with fluctuation operator $\boldsymbol{\kappa}_{h,\omega} := id_\omega - \pi_\omega$, the 2D identity operator $id_\omega : \mathrm{L}^2(\omega) \to \mathrm{L}^2(\omega)$ and the L^2-projection $\pi_\omega : \mathrm{L}^2_0(\omega) \to Q^{r-1}_{2h}(\omega)$ onto a 'discontinuous' space on the patch mesh $\mathcal{K}_{2h}$,

$$Q^{r-1}_{2h}(\omega) := \{\varphi \in \mathrm{L}^2(\omega) \mid \varphi|_L \in \mathbb{Q}_{r-1}(L)\ \forall L \in \mathcal{K}_{2h}\} \,,$$

(P'-iii) Continuous interior penalty stabilization (CIP) [BFH06] for $r = 1$:

$$s_{h,p}(p_h, \xi) = \sum_{K \in \mathcal{K}_h} \frac{\lambda_K h_K^2}{\|\boldsymbol{b}_h\|_{0,\infty,K}} \int_{\partial K} [\nabla' p_h]_{\partial K} \cdot [\nabla' \xi]_{\partial K} \, d\, s \,,$$

where $[\boldsymbol{\varphi}]_e$ denotes the jump of $\boldsymbol{\varphi}$ across the interior edge e and is set to zero if $e \subset \partial\omega$.

Due to [BB06, BFH06] and the choice of the stabilization parameter, the following bounds apply for the schemes (P'-iI) and (P'-iii):

$$s_{h,p}(p_h,\xi) \le s_{h,p}(p_h,p_h)^{1/2} s_{h,p}(\xi,\xi)^{1/2} \qquad \forall p_h,\xi \in Q_h\,, \quad (4.42)$$

$$0 \le s_{h,p}(p_h,p_h) \lesssim \lambda h^{2l+1} \|p_h\|^2_{l+1,\omega} \qquad \forall p_h \in Q_h \cap \mathrm{H}^{l+1}(\omega),\ 0 \le l \le r\,. \quad (4.43)$$

The propositions of the following lemma are crucial for the stability of the Oseen problem and are similar to Lemma 4.8, which we applied in the 2.5D Stokes case. However, due to the differing parameter choice, we have to examine these statements again for the Oseen case.

Lemma 4.24. *Let $s_{h,p}(\cdot,\cdot)$ be chosen from the list (P'-ii) and (P'-iii). There are constants $c_1, c_2 > 0$ such that for arbitrary $p_h \in Q_h$ there is a $\boldsymbol{\varphi} \in \mathbf{V}_h$ such that*

$$|\,\boldsymbol{\varphi}\,|_{1,\Omega} \le c\|p_h\|_{0,\omega} \text{ and } -(div'\,\mathbf{M}\,\boldsymbol{\varphi}, p_h)_\omega \ge c_1\|p_h\|^2_{0,\omega} - c_2 s_{h,p}(p_h,p_h)\,. \quad (4.44)$$

Proof. Due to [MST07, BFH06] we have unique existence of the discrete 2D Oseen problem for these cases (with different parameter settings than in the Stokes case). The proposition (4.44) thus can be proven as in the hydrostatic Stokes case. □

Symmetric stabilization of the 3D velocity dependent terms

As known from the 3D Oseen problem, the divergence constraint and, in the case $0 \le \nu \ll 1$, the advection term have to be controlled, [BBJL07]. We apply an adaption of known symmetric stabilizations for the 3D problem. The adaption is as follows: Starting from the 3D stabilizations and accounting for the reduction of dimension in the 2.5D case, the vertical components occurring in the 3D terms are set to zero. Moreover, the stabilization concerning the divergence constraint only treats the horizontal velocity components. Preventing numerical overhead, this divergence term is not considered as an average over the height, but controlled cellwise without vertical integration. In the context of error estimates it turns out, that the Coriolis force has to be controlled as well. Therefore we add a suitable stabilization of order zero to the discrete system.

In the upcoming we consider the following stabilizing terms $s_{h,v}(\cdot,\cdot)$:

(V'-i) LPS:

(a) with stabilization of the entire velocity gradient:

$$s_{h,v}(\boldsymbol{v}_h,\boldsymbol{\varphi}) := \sum_{M\in\mathcal{T}_{2h}} h_M\|\boldsymbol{b}_h\|_{l,\infty,M}\big(\boldsymbol{\kappa}_{h,\Omega}(\nabla\boldsymbol{v}_h),\,\boldsymbol{\kappa}_{h,\Omega}(\nabla\boldsymbol{\varphi})\big)_M + \mathrm{f}^2\,h_M\big(\boldsymbol{\kappa}_{h,\Omega}\,\boldsymbol{v}_h,\,\boldsymbol{\kappa}_{h,\Omega}\,\boldsymbol{\varphi}\,\big)_M\,,$$

(b) with stabilization in streamline direction:

$$s_{h,v}(\boldsymbol{v}_h,\boldsymbol{\varphi}) := \sum_{M\in\mathcal{T}_{2h}} \frac{h_M}{\|\boldsymbol{b}_h\|_{l,\infty,M}}\big(\boldsymbol{\kappa}_{h,\Omega}((\boldsymbol{b}_h\cdot\nabla)\,\boldsymbol{v}_h),\,\boldsymbol{\kappa}_{h,\Omega}((\boldsymbol{b}_h\cdot\nabla)\,\boldsymbol{\varphi})\big)_M + h_M(\boldsymbol{\kappa}_{h,\Omega}(\mathrm{div}'\,\boldsymbol{v}_h),\boldsymbol{\kappa}_{h,\Omega}(\mathrm{div}'\,\boldsymbol{\varphi})) + \mathrm{f}^2\,h_M\big(\boldsymbol{\kappa}_{h,\Omega}\,\boldsymbol{v}_h,\,\boldsymbol{\kappa}_{h,\Omega}\,\boldsymbol{\varphi}\,\big)_M\,,$$

(V'-ii) CIP for $r = 1$:

$$\begin{aligned} s_{h,v}(\boldsymbol{v}_h, \boldsymbol{\varphi}) := \sum_{T \in \mathcal{T}_h} \lambda_T h_T^2 \int_{\partial T} \|\boldsymbol{b}_h \cdot \boldsymbol{n}\|_{0,\infty \partial T} [\boldsymbol{n} \cdot \nabla \boldsymbol{v}_h]_{\partial T} \cdot [\boldsymbol{n} \cdot \nabla \boldsymbol{\varphi}]_{\partial T} \, d\, s \\ + \lambda_T \|\boldsymbol{b}_h\|_{0,\infty,T} \int_{\partial T} [\mathrm{div}' \, \boldsymbol{v}_h]_{\partial T} \cdot [\mathrm{div}' \, \boldsymbol{\varphi}]_{\partial T} \, d\, s \\ + \int_{\partial T} \mathrm{f}^2 [\boldsymbol{v}_h]_{\partial T} \cdot [\boldsymbol{\varphi}]_{\partial T} \, d\, s \, . \end{aligned}$$

We collect some estimates, which are used to validate stability and to prove error estimates.

Lemma 4.25. *The stabilization terms $s_{h,v}(\cdot,\cdot)$ given in* (V'-i) – (V'-ii) *provide the estimates*

$$s_{h,v}(\boldsymbol{v}_h; \boldsymbol{\varphi}) \leq s_{h,v}(\boldsymbol{v}_h; \boldsymbol{v}_h)^{1/2} s_{h,v}(\boldsymbol{\varphi}; \boldsymbol{\varphi})^{1/2} \qquad \forall \, \boldsymbol{v}_h, \, \boldsymbol{\varphi} \in \mathbf{V}_h \, , \tag{4.45}$$

$$0 \leq s_{h,v}(\boldsymbol{v}, \boldsymbol{v}) \lesssim \left(\mathrm{f}^2 \, h^2 + \|\boldsymbol{b}_h\|_{0,\infty,\Omega} \right) h^{2k+1} \| \, \boldsymbol{v} \, \|_{k+1,\Omega}^2 \quad \forall \, \boldsymbol{v} \in \mathbf{H}^{k+1}(\Omega) \cap \mathbf{V}_h \, , 0 \leq k \leq r \, . \tag{4.46}$$

Proof. Estimate (4.45) and the lower bound of (4.46) are trivial. The estimates of the advection stabilizing terms pass on from the 3D case, see Lemmata 4.13 and 4.14. The terms concerning the Coriolis force can be evaluated as follows: In the LPS case the estimate applies due to the approximation property of the fluctuation operator, see e.g. [BL09]:

$$\|\boldsymbol{\kappa}_{h,\Omega}(\boldsymbol{\varphi})\|_{0,M} \leq h_M^s |\, \boldsymbol{\varphi} \,|_{s,M} \qquad \forall \, \boldsymbol{\varphi} \in \mathrm{H}^s(M), \quad 0 \leq s \leq k+1 \, . \tag{4.47}$$

In the case of CIP stabilization, as is standard, the application of the trace inequality and of an inverse estimate results in the desired estimate, see e.g. [BFH06]. □

Stability analysis

Collecting the results from the preceeding sections, the stabilized hydrostatic Oseen problem reads:

$$\begin{aligned} &\textit{Given } \boldsymbol{b}_h \in \mathbf{H}_{a,h}, \; \boldsymbol{f} \in \mathbf{H}_b^{-1}(\Omega), \; \boldsymbol{g} \in \mathbf{H}_b^{-1/2}(\Gamma_u), \quad \textit{find } \boldsymbol{y}_h := (\boldsymbol{v}_h, p_h) \in \mathbf{X}_h \; \textit{s. t.} \\ &\qquad A_h(\boldsymbol{b}_h; \boldsymbol{y}_h; \boldsymbol{\phi}) = \boldsymbol{l}(\boldsymbol{\varphi}) \qquad\qquad \forall \, \boldsymbol{\phi} := (\boldsymbol{\varphi}, \xi) \in \mathbf{X}_h \end{aligned} \tag{4.48}$$

with

$$A_h(\boldsymbol{b}_h; \boldsymbol{y}_h; \boldsymbol{\phi}) := A(\boldsymbol{b}_h; \boldsymbol{y}_h; \boldsymbol{\phi}) + s_{h,p}(p_h, \xi) + s_{h,v}(\boldsymbol{v}_h, \boldsymbol{\varphi}) \, .$$

The stabilization terms $s_{h,p}$ and $s_{h,v}$ are chosen from (P'-i) – (P'-iii) and (V'-i) – (V'-ii). Note, that $\boldsymbol{b}_h \in \mathbf{H}_{a,h}$ is divergence free and thus $\langle (\boldsymbol{b}_h \cdot \nabla) \, \boldsymbol{v}_h, \boldsymbol{v}_h \rangle = 0$ applies for any $\boldsymbol{v}_h \in \mathbf{V}_h$. For ease of presentation we use the notations

$$A_h(\boldsymbol{b}_h; \boldsymbol{v}_h, p_h; \boldsymbol{\varphi}, \xi) := a(\boldsymbol{b}_h; \boldsymbol{v}_h, \boldsymbol{\varphi}) + b(p_h, \boldsymbol{\varphi}) - b(\xi, \boldsymbol{v}_h) + s_{h,v}(\boldsymbol{v}_h, \boldsymbol{\varphi}) + s_{h,p}(p_h, \xi)$$

with bilinear forms $a(\boldsymbol{b}_h;\boldsymbol{v}_h,\boldsymbol{\varphi}) := \nu(\nabla\boldsymbol{v}_h,\nabla\boldsymbol{\varphi})_\Omega + \sigma(\boldsymbol{v}_h,\boldsymbol{\varphi})_\Omega + ((\boldsymbol{b}_h\cdot\nabla)\boldsymbol{v}_h,\boldsymbol{\varphi})_\Omega + \mathrm{f}\,(\boldsymbol{v}_h^\perp,\boldsymbol{\varphi})_\Omega$ and $b(\boldsymbol{v}_h;\xi) := (\xi,\mathrm{div}'\,\mathbf{M}\,\boldsymbol{v}_h)_\omega$, whenever suitable.

We prove stability of problem (4.48) with respect to the mesh-dependent norm $|\!|\!|\cdot|\!|\!| : \mathbf{X}_h \to \mathbb{R}_+$,

$$|\!|\!|\boldsymbol{y}_h|\!|\!| := \big(A_h(\boldsymbol{b}_h;\boldsymbol{y}_h;\boldsymbol{y}_h) + (\nu+\sigma)\|q_h\|_{0,\Omega}^2\big)^{1/2} \qquad \forall \boldsymbol{y}_h := (\boldsymbol{v}_h,q_h)\in\mathbf{X}_h\ . \tag{4.49}$$

The unit sphere on $\mathbf{X}_h$ w.r.t. that norm is denoted by B_h.

Proposition 4.26. *Let Assumption 4.2 be valid and $\nu,\sigma,\mathrm{f},\|\boldsymbol{b}_h\|_{0,\infty,\Omega}\le C$. The stabilized 2.5D Oseen bilinear form (4.48) is inf-sup stable:*

$$\exists\ \gamma_{\Omega,\omega}>0: \qquad \inf_{\boldsymbol{y}_h\in B_h}\sup_{\boldsymbol{\phi}\in B_h} A_h(\boldsymbol{b}_h;\boldsymbol{y}_h;\boldsymbol{\phi}) \ \ge\ \gamma_{\Omega,\omega}\,.$$

Proof. Let $(\boldsymbol{v}_h,p_h)\in\boldsymbol{V}_h\times Q_h$. We use the criterion for inf-sup conditions proposed in [BS11]: We split the triple norm into two parts

$$|\!|\!|\boldsymbol{y}_h|\!|\!| := \big(|\boldsymbol{y}_h|_a^2+|\boldsymbol{y}_h|_b^2\big)^{1/2} \qquad \text{with}$$
$$|\boldsymbol{y}_h|_a^2 := A_h(\boldsymbol{b}_h;\boldsymbol{y}_h;\boldsymbol{y}_h) \qquad \text{and} \qquad |\boldsymbol{y}_h|_b^2 := (\nu+\sigma)\|q_h\|_{0,\Omega}^2\,.$$

Crucial of this proof is the existence of a $\boldsymbol{\varphi}\in\mathbf{V}_h$ fulfilling

$$|\,\boldsymbol{\varphi}\,|_{1,\Omega}\lesssim\|p_h\|_{0,\omega} \qquad \text{and} \qquad -(\mathrm{div}'\,\mathbf{M}\,\boldsymbol{\varphi},p_h)\ge c_1\|p_h\|_{0,\omega}^2 - c_2 s_{h,p}(p_h,p_h)$$

with h- and ν- independent constants c_1, $c_2>0$, see [KB12]. Given this $\boldsymbol{\varphi}\in\mathbf{V}_h$, we can estimate

$$\begin{aligned} A_h(\boldsymbol{b}_h;\boldsymbol{v}_h,p_h;\boldsymbol{\varphi},0)\ge\ & c_1\|p_h\|_{0,\omega}^2 - c_2 s_{h,p}(p_h,p_h)\\ & - C(\nu^{1/2}|\boldsymbol{v}_h|_{1,\Omega}+(1+c_F)\|\boldsymbol{v}_h\|_{0,\Omega})\|p_h\|_{0,\omega} + s_{h,v}(\boldsymbol{v}_h,\boldsymbol{\varphi})\,. \end{aligned}$$

Constant c_F denotes the constant of the inequality of Poincaré - Friedrichs. Due to Lemma 4.25 we get $s_{h,v}(\boldsymbol{v}_h,\boldsymbol{\varphi})\lesssim s_{h,v}(\boldsymbol{v}_h,\boldsymbol{v}_h)^{1/2}|\,\boldsymbol{\varphi}\,|_{1,\Omega}$. Scaling the element $(\boldsymbol{\varphi},0)$ produces

$$A_h(\boldsymbol{b}_h;\boldsymbol{v}_h,p_h;(\nu+\sigma)\,\boldsymbol{\varphi},0)\ge\ \widetilde{c_1}|(\boldsymbol{v}_h,p_h)|_b^2-\widetilde{c_2}|(\boldsymbol{v}_h,p_h)|_a^2\,.$$

Diagonal testing leads to $A_h(\boldsymbol{b}_h;\boldsymbol{v}_h,p_h;\boldsymbol{v}_h,p_h)=|\,\boldsymbol{v}_h,p_h|_a^2$, which finishes the proof. □

4.5.3 *A priori* error estimates

In this section we deduce error estimates of the symmetric stabilized 2.5D Oseen problem (4.48) with respect to a suitable mesh dependent triple norm. As already indicated in the Stokes case, the involved triple norm of the Stokes problem enables a comfortable approach to the divergence estimate, see Lemma 4.20. However, in the present case, the gradient of the pressure is multiplied by a factor of $(\nu+\sigma)^{-1/2}$, which disturbs the adaption of the proof of Lemma 4.20 to the Oseen case. Instead, we need appropriate relations between the 2D and the 3D fluctuation operator, in the case of LPS, and between the 2D and 3D jump terms across cell boundaries, in the case of CIP. In the upcoming we treat both stabilization techniques separately.

Estimates in the LPS framework

Lemma 4.27. *Let Assumption 4.2 be valid. The following estimate applies*

$$\sum_{M\in\mathcal{T}_{2h}} \|\boldsymbol{\kappa}_{h,\Omega}\,\boldsymbol{\varphi}\,\|_{0,M}^2 \quad \leq \quad c_\Omega \sum_{L\in\mathcal{K}_{2h}} \|\boldsymbol{\kappa}_{h,\omega}\,\boldsymbol{\varphi}\,\|_{0,L}^2 \qquad \forall\,\boldsymbol{\varphi}\in[\mathrm{L}^2(\omega)]^2\,.$$

The occurence of $\boldsymbol{\varphi}$ on the left hand side denotes the constant continuation of $\boldsymbol{\varphi}$ in vertical direction, i.e. we set $\boldsymbol{\varphi}(x,y,z) := \boldsymbol{\varphi}(x,y)$ for all $(x,y,z)\in\Omega$.

Proof. Let L be an element of the 2D patch mesh $\mathcal{K}_{2h}$ and $\mathcal{T}_L$ be given as defined in Section 4.2.2.

Note that the standard embedded $\boldsymbol{\pi}_{\boldsymbol{\omega}}\,\boldsymbol{\varphi}$ is element of $[Q_{2h}^{r-1}(\Omega)]^2$. Using the orthogonality property of $\boldsymbol{\pi}_{\boldsymbol{\Omega}}$ and applying the Hölder inequality as well as the weighted inequality of the geometric and arithmetic average, see e.g. [Bra07], we get:

$$\begin{aligned}
\sum_{M\in\mathcal{T}_{2h}} \|\boldsymbol{\kappa}_{h,\Omega}\,\boldsymbol{\varphi}\,\|_{0,M}^2 \;&=\; \sum_{M\in\mathcal{T}_{2h}} (\boldsymbol{\kappa}_{h,\Omega}\,\boldsymbol{\varphi}, \boldsymbol{\varphi}-\boldsymbol{\pi}_{\boldsymbol{\omega}}\,\boldsymbol{\varphi})_M \\
&=\; \sum_{M\in\mathcal{T}_{2h}} (\boldsymbol{\kappa}_{h,\Omega}\,\boldsymbol{\varphi}, \boldsymbol{\kappa}_{h,\omega}\,\boldsymbol{\varphi})_M \\
&\leq\; \left(\sum_{M\in\mathcal{T}_{2h}} \|\boldsymbol{\kappa}_{h,\Omega}\,\boldsymbol{\varphi}\|_{0,M}^2\right)^{1/2} \left(\sum_{L\in\mathcal{K}_{2h}}\sum_{M\in\mathcal{T}_L} \|\boldsymbol{\kappa}_{h,\omega}\,\boldsymbol{\varphi}\,\|_{0,M}^2\right)^{1/2}
\end{aligned}$$

For a given cell $M\in\mathcal{T}_L$ let $\delta_{min,M}$ and $\delta_{max,M}$ be the minimal and the maximal z-value of M, respectively. As $\boldsymbol{\kappa}_{h,\omega}\,\boldsymbol{\varphi}$ is vertically invariant, we can further estimate

$$\sum_{M\in\mathcal{T}_L} \|\boldsymbol{\kappa}_{h,\omega}\,\boldsymbol{\varphi}\,\|_{0,M}^2 \;\leq\; \sum_{M\in\mathcal{T}_L} (\delta_{max,M}-\delta_{min,M})\|\boldsymbol{\kappa}_{h,\omega}\,\boldsymbol{\varphi}\,\|_{0,L}^2 \;\leq\; c\,\delta_{max}\|\boldsymbol{\kappa}_{h,\omega}\,\boldsymbol{\varphi}\,\|_{0,L}^2\,,$$

whereas the constant c depends on the maximal vertical shearing of the cells $M\in\mathcal{T}_L$ and thus on the shape-regularity of the isotropic mesh, i.e. on $\max_{M\in\mathcal{T}_L}\{h_M/\rho_M\}$. Thus, we get

$$\sum_{M\in\mathcal{T}_{2h}} \|\boldsymbol{\kappa}_{h,\Omega}\,\boldsymbol{\varphi}\,\|_{0,M}^2 \;\leq\; \delta_{max}^{1/2}\left(\sum_{M\in\mathcal{T}_{2h}} \|\boldsymbol{\kappa}_{h,\Omega}\,\boldsymbol{\varphi}\|_{0,M}^2\right)^{1/2} \left(\sum_{L\in\mathcal{K}_{2h}} \|\boldsymbol{\kappa}_{h,\omega}\,\boldsymbol{\varphi}\,\|_{0,L}^2\right)^{1/2},$$

which finishes the proof. □

Lemma 4.28. *Let Assumption 4.2 be valid. The following estimate applies*

$$\sum_{L\in\mathcal{K}_{2h}} \|\kappa_{h,\omega}(\mathbf{M}\,\varphi)\|_{0,L}^2 \quad \leq \quad c_\Omega \sum_{M\in\mathcal{T}_{2h}} \|\kappa_{h,\Omega}\varphi\|_{0,M}^2 \quad \forall\,\boldsymbol{\varphi}\in[\mathrm{L}^2(\Omega)]^2\,,$$

Proof. Let L be an element of the 2D patch mesh $\mathcal{K}_{2h}$. Consider $\mathcal{T}_K$ as already defined in Section 4.2.2. Note that $\pi_\Omega\varphi\in Q_{2h}^{r-1}(\Omega)$ and $\mathbf{M}(\pi_\Omega\varphi)\in Q_{2h}^{r-1}(\omega)$. Using the

orthogonality properties of π_ω and π_Ω we get:

$$\begin{aligned}\|\kappa_{h,\omega}(\mathbf{M}\,\varphi)\|_{0,L}^2 &= (\kappa_{h,\omega}(\mathbf{M}\,\varphi),\mathbf{M}\,\varphi)_L \\ &= (\kappa_{h,\omega}(\mathbf{M}\,\varphi),\mathbf{M}\,\varphi-\mathbf{M}(\pi_\Omega\varphi))_L \\ &\leq \|\kappa_{h,\omega}(\mathbf{M}\,\varphi)\|_{0,L}\|\,\mathbf{M}(\kappa_{h,\Omega}\varphi)\|_{0,L}\,.\end{aligned}$$

Finally, the following estimate applies

$$\|\,\mathbf{M}(\kappa_{h,\Omega}\varphi)\|_{0,L}^2 \quad\leq\quad \delta_{max}\sum_{T\in\mathcal{T}_L}\|\kappa_{h,\Omega}\varphi\|_{0,T}^2\,.$$

□

Given the L^2-orthogonal interpolation operator $i_{h,3d}$, let $\boldsymbol{\eta}_v=\boldsymbol{v}-i_{h,3d}\,\boldsymbol{v}$ be the interpolation error of the velocity field. The following lemma aims to provide an optimal *a priori* error estimate for the divergence term $(\mathrm{div}'\,\mathbf{M}\,\boldsymbol{\eta}_v,\xi)_\omega$. We validated a similar proposition for the Stokes case, see Lemma 4.20. Recall, that the triple norms $|\!|\!|\cdot|\!|\!|$ applied in the Stokes case and in the present Oseen case differ. This effects a simple estimate in the Stokes case, as the pressure ξ simply enters the triple norm. In the present Oseen case, we would catch a factor of $(\nu+\sigma)^{-1/2}$, see (4.49). Thus the Oseen case necessitates a more elaborative approach in order to avoid this undesired factor.

Lemma 4.29. *Let $\mathcal{T}_h$ be a triangulation of Ω fulfilling Assumption 4.2, $i_{h,3d}:\mathbf{V}\to\mathbf{V}_h$ be the L^2-orthogonal interpolation operator of Section 4.1.2(d), $\boldsymbol{v}\in\mathbf{H}^{k+1}(\Omega)\cap\mathbf{V}$, $0\leq k\leq r$, and $\xi\in Q_h$.*

The local projection stabilization $s_{h,p}(\cdot,\cdot)$ of (P'-ii) supplies an optimal estimate of the divergence constraint:

$$(div'\,\mathbf{M}\,\boldsymbol{\eta}_v,\xi)_\omega \quad\lesssim\quad h^{k+1/2}\max_{K\in\mathcal{K}_h}\{\lambda_K^{-1/2}\}|\!|\!|\,\boldsymbol{v}\,|\!|\!|_{k+1,\Omega}\;s_{h,p}(\xi,\xi)^{1/2}\,. \tag{4.50}$$

Proof. Applying the orthogonality property of the interpolation operator as well as Lemma 4.27 we deduce

$$\begin{aligned}(\mathrm{div}'\,\mathbf{M}\,\boldsymbol{\eta}_v,\xi)_\omega &\leq |(\mathbf{M}\,\boldsymbol{\eta}_v,\nabla'\xi)_\omega| \\ &= |(\boldsymbol{\eta}_v,\nabla'\xi)_\Omega| \\ &= \left|\sum_{M\in\mathcal{T}_{2h}}(\boldsymbol{\eta}_v,\boldsymbol{\kappa}_{h,\Omega}\nabla'\xi)_M\right| \\ &\leq \|\boldsymbol{\eta}_v\|_{0,\Omega}\left(\sum_{M\in\mathcal{T}_{2h}}\|\boldsymbol{\kappa}_{h,\Omega}\nabla'\xi\|_{0,M}^2\right)^{1/2} \\ &\lesssim \|\boldsymbol{\eta}_v\|_{0,\Omega}\left(\sum_{L\in\mathcal{K}_{2h}}\|\boldsymbol{\kappa}_{h,\omega}\nabla'\xi\|_{0,L}^2\right)^{1/2} \\ &\leq h^{-1/2}\max_{K\in\mathcal{K}_h}\{\lambda_K^{-1/2}\}\|\boldsymbol{\eta}_v\|_{0,\Omega}\left(\sum_{L\in\mathcal{K}_{2h}}\lambda_L h_L\|\boldsymbol{\kappa}_{h,\omega}\nabla'\xi\|_{0,L}^2\right)^{1/2}.\end{aligned}$$

Due to the interpolation properties of the L^2-orthogonal interpolation operator the proof is finished. □

The following lemma considers the remaining problematic terms in the *a priori* error estimate.

Lemma 4.30. *Let Assumption 4.2 be valid, $i_{h,3d} : \mathbf{V} \to \mathbf{V}_h$ and $i_{h,2d} : Q \to Q_h$ be the L^2-orthogonal interpolation operators of Section 4.1.2(d). Assume $(\boldsymbol{v}, p) \in \mathbf{H}_b^{k+1}(\Omega) \times \mathrm{H}^{l+1}(\omega)$, $0 \leq k, l \leq r$, and $(\boldsymbol{\varphi}, \xi) \in \mathbf{V}_h \times Q_h$. The local projection stabilization terms $s_{h,v}(\cdot,\cdot)$ of (V'-i) allow the estimates:*

$$\langle (\boldsymbol{b}_h \cdot \nabla)(\boldsymbol{v} - i_{h,3d}\,\boldsymbol{v}), \boldsymbol{\varphi} \rangle + \mathrm{f}((\boldsymbol{v} - i_{h,3d}\,\boldsymbol{v})^{\perp}, \boldsymbol{\varphi})_{\Omega} \quad \lesssim \quad h^{k+1/2} \| \boldsymbol{v} \|_{k+1,\Omega} s_{h,v}(\boldsymbol{\varphi}, \boldsymbol{\varphi})^{1/2}\,, \tag{4.51}$$

$$(div'\,\mathbf{M}\,\boldsymbol{\varphi}, p - i_{h,2d}p)_{\omega} \quad \lesssim \quad h^{l+1/2} \|p\|_{l+1,\omega} s_{h,v}(\boldsymbol{\varphi}, \boldsymbol{\varphi})^{1/2}\,. \tag{4.52}$$

Proof. Estimate (4.51) applies via common LPS arguments. For the derivation of (4.52) we use Lemma 4.28:

$$\begin{aligned}
(\mathrm{div}'\,\mathbf{M}\,\boldsymbol{\varphi}, p - i_{h,2d}p)_{\omega} &= (\mathbf{M}(\mathrm{div}'\,\boldsymbol{\varphi}), p - i_{h,2d}p)_{\omega} \\
&= \sum_{L \in \mathcal{K}_{2h}} (\boldsymbol{\kappa}_{h,\omega}(\mathbf{M}(\mathrm{div}'\,\boldsymbol{\varphi})), p - i_{h,2d}p)_L \\
&\lesssim \left(\sum_{L \in \mathcal{K}_{2h}} \left(\sum_{M \in \mathcal{T}_L} \chi_M \|\boldsymbol{\kappa}_{h,\Omega}(\mathrm{div}'\,\boldsymbol{\varphi})\|_{0,M}^2 \right) h^{2l+1} \|p\|_{l+1,L}^2 \right)^{1/2} \\
&\lesssim s_{h,v}(\boldsymbol{\varphi}, \boldsymbol{\varphi})^{1/2} h^{l+1/2} \|p\|_{l+1,\omega}\,,
\end{aligned}$$

Constant χ_M is set to $\chi_M := h_M \|\boldsymbol{b}_h\|_{l,\infty,M}$ in the case (V-ia) and to $\chi_M := h_M$ in the case (V-ib). □

Proposition 4.31. *Let Assumptions 4.2 and 4.22 be valid. Moreover, let the stabilization terms be $s_{h,v}(\cdot,\cdot)$ and $s_{h,p}(\cdot,\cdot)$ be chosen from (V'-i) and (P'-ii), respectively. If the continuous solution of (3.33) is sufficiently regular, $\mathbf{u} := (\boldsymbol{v}, p) \in \mathbf{H}^{k+1}(\Omega) \times \mathrm{H}^{l+1}(\omega)$, $0 \leq k, l \leq r$, and if $\boldsymbol{b} \in \mathbf{H}_a \cap \mathbf{H}^{k+1}(\Omega)$, the following estimate for the discrete solution $\mathbf{u}_h := (\boldsymbol{v}_h, p_h)$ of (4.48) applies:*

$$|\!|\!| \mathbf{u} - \mathbf{u}_h |\!|\!| \;\lesssim C_v\, h^k \;\| \boldsymbol{v} \|_{k+1,\Omega} \;+\; C_p\, h^l \, \|p\|_{l+1,\Omega}$$

with

$$\begin{aligned}
C_v &:= \nu^{1/2} + (\sigma^{1/2} + \mathrm{f}\ h + \|\boldsymbol{b}_h\|_{0,\infty,\Omega}^{1/2}) h + h^{1/2} + \nu^{-1/2} \|\boldsymbol{b}\|_{k+1,\Omega} \\
C_p &:= (\nu + \sigma)^{1/2} h + h^{1/2}\,.
\end{aligned}$$

Proof. As usual, we split the triple norm into an interpolation and a projection part:

$$|\!|\!| \mathbf{u} - \mathbf{u}_h |\!|\!| \leq |\!|\!| \boldsymbol{\eta} |\!|\!| + |\!|\!| \boldsymbol{\varsigma} |\!|\!|\,.$$

with interpolation error $\boldsymbol{\eta} = \mathbf{u} - \boldsymbol{i}_h\,\mathbf{u}$ and projection error $\boldsymbol{\varsigma} = \boldsymbol{i}_h\,\mathbf{u} - \mathbf{u}_h$. The involved interpolation operators are given by the L^2-orthogonal ones as introduced in Section 4.1.2(d).

Considering estimates (4.7) - (4.9), (4.42), (4.43) and Lemma 4.25, $|\!|\!|\boldsymbol{\eta}|\!|\!|$ can be estimated as

$$\begin{aligned}|\!|\!|\boldsymbol{\eta}|\!|\!| \lesssim h^k \left(\nu^{1/2} + (\sigma^{1/2} + \mathrm{f}\ h + \|\boldsymbol{b}_h\|^{1/2}_{0,\infty,\Omega})\, h + h^{1/2}\right) \|\,\boldsymbol{v}\,\|_{k+1,\Omega} \\ +\ h^l \left((\nu+\sigma)^{1/2} h + h^{1/2}\right) \|p\|_{l+1,\omega}\,.\end{aligned}$$

For the estimate of $|\!|\!|\boldsymbol{\varsigma}|\!|\!|$ we apply the discrete stability result of Proposition 4.26. We chose a test function $\boldsymbol{\phi} := (\boldsymbol{\varphi}, \xi) \in B_h$, i.e. $\boldsymbol{\phi} \in \boldsymbol{X}_h$ and $|\!|\!|\,\boldsymbol{\phi}\,|\!|\!| = 1$, such that

$$A_h(\boldsymbol{b}_h; \boldsymbol{\varsigma}, \boldsymbol{\phi}) \geq \gamma_{\Omega,\omega} |\!|\!|\boldsymbol{\varsigma}|\!|\!|\,.$$

Note, that the solutions $\mathbf{u} \in \mathbf{X}$ of problem (3.33) and $\mathbf{u}_h \in \mathbf{X}_h$ of (4.48) fulfill the equality

$$A_h(\boldsymbol{b}_h; \mathbf{u}_h; \boldsymbol{\phi}) = \langle \boldsymbol{f}, \boldsymbol{\varphi}\rangle = A(\boldsymbol{b}; \mathbf{u}; \boldsymbol{\phi}) = A(\boldsymbol{b}_h; \mathbf{u}; \boldsymbol{\phi}) + \langle ((\boldsymbol{b} - \boldsymbol{b}_h)\cdot\nabla)\,\boldsymbol{v}; \boldsymbol{\varphi}\rangle\,.$$

Thus, it suffices to analyze the terms on the right hand side of

$$A_h(\boldsymbol{b}_h; \boldsymbol{\varsigma}; \boldsymbol{\phi}) = A(\boldsymbol{b}_h; \boldsymbol{\eta}; \boldsymbol{\phi}) + s_{h,v}(i_{h,3d}\,\boldsymbol{v}, \boldsymbol{\varphi}) + s_{h,p}(i_{h,2d}p, \xi) - \langle ((\boldsymbol{b} - \boldsymbol{b}_h)\cdot\nabla)\,\boldsymbol{v}; \boldsymbol{\varphi}\rangle\,.$$

For the estimate of bilinear form $A(\boldsymbol{b}_h; \boldsymbol{\eta}; \boldsymbol{\phi})$ we apply Lemmata 4.29 and 4.30 and bound the remaining terms as

$$\nu(\nabla(i_{h,3d}\,\boldsymbol{v} - \boldsymbol{v}), \nabla\,\boldsymbol{\varphi})_\Omega + \sigma(i_{h,3d}\,\boldsymbol{v} - \boldsymbol{v}, \boldsymbol{\varphi})_\Omega \quad \leq (\nu^{1/2} + \sigma^{1/2} h)\ h^k \|\,\boldsymbol{v}\,\|_{k+1,\Omega}\,.$$

Using the estimates (4.42) and (4.43), the results of Lemma 4.25 and H^1-regularity of the interpolation operators, the stabilization terms fulfill

$$s_{h,v}(\boldsymbol{i_{h,3d}}\,\boldsymbol{v}, \boldsymbol{\varphi}) + s_{h,p}(i_{h,2d}p, \xi) \lesssim \left(\mathrm{f}\ h + \|\boldsymbol{b}_h\|^{1/2}_{0,\infty,\Omega}\right) h^{k+1/2} \|\,\boldsymbol{v}\,\|_{k+1,\Omega} + h^{l+1/2}\|p\|_{l+1,\omega}\,.$$

The remaining term is the problematic one. Due to Assumption 4.22 we result in the estimate

$$\begin{aligned}\langle ((\boldsymbol{b} - \boldsymbol{b}_h)\cdot\nabla)\,\boldsymbol{v}, \boldsymbol{\varphi}\rangle &\leq \|\boldsymbol{b} - \boldsymbol{b}_h\|_{0,3,\Omega} |\,\boldsymbol{v}\,|_{1,\Omega} \|\,\boldsymbol{\varphi}\,\|_{0,6,\Omega} \\ &\lesssim h^k \|\boldsymbol{b}\|_{k+1,\Omega} |\,\boldsymbol{v}\,|_{1,\Omega} |\,\boldsymbol{\varphi}\,|_{1,\Omega} \\ &\leq h^k \nu^{-1/2} \|\boldsymbol{b}\|_{k+1,\Omega} \|\,\boldsymbol{v}\,\|_{k+1,\Omega}.\end{aligned} \tag{4.53}$$

□

Remark 4.32. *In the context of approximation theory, Assumption 4.22 is a suggestive assumption. However this premise leads to a suboptimal error estimate. Unfortunately, we can not apply the introduced stabilization terms to properly bound the problematic term. In the article [BL09], which treats the classical Oseen problem in the local projection stabilization context, there is no distinction between $\boldsymbol{b}$ and $\boldsymbol{b}_h$ and $\boldsymbol{b}_h \in \mathbf{W}^{1,\infty}(\Omega)$ is presumed. Thus, the suboptimal term vanishes. If we proceed similarly in the hydrostatic framework, the estimate is optimal as well.*

Estimates in the CIP framework

In order to derive error estimates for the CIP stabilized problem, we present a different approach, which follows the ideas of [BFH06]: we first present necessary tools and then elaborate estimates for the error in the velocity field and afterwards turn to the error concerning the pressure. As in [BFH06] we restrict to the case $\sigma > 0$, and assume $\boldsymbol{b}_h = \boldsymbol{b} \in \mathbf{W}^{1,\infty}(\Omega)$.

A crucial tool in the derivation of error estimates in the CIP case is the existence of a quasi-interpolant $\boldsymbol{\pi}^*_{h,r}$, which is given by

$$\boldsymbol{\pi}^*_{h,r}\,\boldsymbol{v}(x_i) := \frac{1}{n_i}\sum_{T:x_i\in T} \boldsymbol{v}\,|_T(x_i) \qquad\qquad \forall\,\boldsymbol{v}\in\mathbf{H}^2(\Omega)$$

for any node x_i and number n_i of elements, which contain x_i as a node. For the 2D pressure case it is defined appropriately. It allows the following estimates, see [BFH06]:

$$\|h^{1/2}((\boldsymbol{b}\cdot\nabla)\,\boldsymbol{v}_h - \boldsymbol{\pi}^*_{h,r}(\boldsymbol{b}\cdot\nabla)\,\boldsymbol{v}_h)\|^2_{0,\Omega} \;\lesssim\; \sum_{T\in\mathcal{T}_h}\int_{\partial T} h_T^2|\boldsymbol{b}\cdot\boldsymbol{n}|^2|\nabla\,\boldsymbol{v}_h\,\boldsymbol{n}|^2 d\,s \tag{4.54}$$

$$\|\phi^{1/2}(\mathrm{div}'\,\boldsymbol{v}_h - \pi^*_{h,r}\mathrm{div}'\,\boldsymbol{v}_h)\|^2_{0,\Omega} \;\lesssim\; \sum_{T\in\mathcal{T}_h}\int_{\partial_T} \phi h_T[\mathrm{div}'\,\boldsymbol{v}_h]^2\,d\,s \tag{4.55}$$

$$\|\phi^{1/2}(\nabla' p_h - \boldsymbol{\pi}^*_{h,r}\nabla' p_h)\|^2_{0,\Omega} \;\lesssim\; \sum_{T\in\mathcal{T}_h}\int_{\partial_T} \phi h_T|[\nabla p_h]|^2\,d\,s \tag{4.56}$$

for a function ϕ, constant per element.
We derive estimates for the velocity error with respect to the following mesh-dependent norm:

$$\|\,\boldsymbol{v}_h\,\|_{vel} := |\!|\!|(\boldsymbol{v}_h,0)|\!|\!|\,.$$

The error concerning the velocity field with respect to this norm can be estimated as:

Proposition 4.33. *Let Assumptions 4.2 and 4.22 be valid. Moreover, let the stabilization terms be $s_{h,v}(\cdot,\cdot)$ and $s_{h,p}(\cdot,\cdot)$ be given by (V'-ii) and (P'-iii).*
If the continuous solution of (3.33) is sufficiently regular, $\mathbf{u} := (\boldsymbol{v},p) \in \mathbf{H}^{k+1}(\Omega)\times \mathrm{H}^{l+1}(\omega)$, $1\le k\le r$ and $0\le l\le r$, the error of the velocity of the discrete solution $\mathbf{u}_h := (\boldsymbol{v}_h,p_h)$ of (4.48) can be estimated as:

$$\begin{aligned}\|\,\boldsymbol{v}-\boldsymbol{v}_h\,\|^2_{vel} \;\lesssim\; &\sum_{T\in\mathcal{T}_h}\Big((\sigma+\mathrm{f})h_T^{2(k+1)} + \max\{\nu,\|\boldsymbol{b}_h\|_{0,\infty,T}h_T\}h_T^{2k}\Big)\,\|\,\boldsymbol{v}\,\|^2_{k+1,T}\\ &+\max_{T\in\mathcal{T}_h}\{\sigma^{-1/2}|\boldsymbol{b}|_{1,\infty,T}h_T^{k+1}\}^2\|\,\boldsymbol{v}\,\|^2_{k+1,\Omega} + \sum_{K\in\mathcal{K}_k} h_K^{2l}\|p\|^2_{l+1,K}\sum_{T\in\mathcal{T}_K}\min\{\|\boldsymbol{b}\|^{-1}_{0,\infty,T}, h_T\nu^{-1}\}\end{aligned}$$

Proof. We follow the ideas of [BFH06] and decompose the velocity error as

$$\|\,\boldsymbol{v}-\boldsymbol{v}_h\,\|_{vel} \le \|\,\boldsymbol{v}-\boldsymbol{\pi}_{h,r}\,\boldsymbol{v}\,\|_{vel} + \|\boldsymbol{\pi}_{h,r}\,\boldsymbol{v}-\boldsymbol{v}_h\,\|_{vel}\,.$$

The operator $\boldsymbol{\pi}_{h,r}$ denotes the L^2-projection $\pi_{h,r} : L^2(\Omega) \to Q_h^r(\Omega)$ and supplies the estimates

$$\sum_{|\alpha|\leq l} \|\phi D^\alpha(v - \pi_{h,r}v)\|_{0,\Omega}^2 \;\leq\; \sum_{T\in\mathcal{T}_h} \|\phi\|_{0,\infty,T}^2 h^{2k} \|v\|_{k+1,\Omega}^2 \tag{4.57}$$

for any $v \in \mathrm{H}^{k+1}(\Omega)$, $0 \leq l \leq k+1$ and $\phi \in Q_h^r(\Omega)$ fulfilling $\phi > 0$ and $|\nabla\phi(\boldsymbol{x})| \leq ch_T^{-1}\phi(\boldsymbol{x})$ for all $\boldsymbol{x} \in T$ and $T \in \mathcal{T}_h$, see [BFH06].
A suitable estimate of $\| \boldsymbol{v} - \boldsymbol{\pi}_{h,r}\, \boldsymbol{v} \|_{vel}$ is assured by

$$\| \boldsymbol{v} - \pi_{h,r}\, \boldsymbol{v} \|_{vel}^2 \lesssim \sum_{T\in\mathcal{T}_h} \Big((\sigma + \mathrm{f}) h_T^{2(k+1)} + \max\{\nu, \|\boldsymbol{b}_h\|_{0,\infty,T} h_T\} h_T^{2k} \Big) \| \boldsymbol{v} \|_{k+1,T}^2$$

for any $\boldsymbol{v} \in \mathbf{H}^{k+1}(\Omega)$, see [BFH06]. Here, the Coriolis term is treated similar as the reaction term.

We set $\boldsymbol{\eta}_v := \boldsymbol{\pi}_{h,r}\, \boldsymbol{v} - \boldsymbol{v}_h$ and $\eta_p := \pi_{h,r} p - p_h$. The estimate of the term $\|\boldsymbol{\eta}_v\|_{vel}$ uses the coercivity property

$$A_h(\boldsymbol{b}; \boldsymbol{\varphi}, 0;\, \boldsymbol{v}_h, 0) \;\gtrsim\; \| \boldsymbol{\varphi} \|_{vel}^2 \qquad\qquad \forall\, \boldsymbol{\varphi} \in [Q_h^r(\Omega)]^2\,,$$

as well as the modified Galerkin orthogonality

$$A(\boldsymbol{b}; \boldsymbol{v} - \boldsymbol{v}_h, p - p_h; \boldsymbol{\varphi}, \xi) + s_{h,v}(\boldsymbol{v} - \boldsymbol{v}_h, \boldsymbol{\varphi}) - s_{h,p}(p_h, \xi) = 0 \tag{4.58}$$

for all $(\boldsymbol{\varphi}, \xi) \in [Q_h^r(\Omega)]^2 \times Q_h^r(\omega)$. Thus, the authors of [BFH06] get

$$\begin{aligned} \|\boldsymbol{\eta}_v\|_{vel}^2 + s_{h,p}(\eta_p, \eta_p) \;\lesssim\; & a(\boldsymbol{b}; \boldsymbol{v} - \boldsymbol{\pi}_{h,r}\, \boldsymbol{v}_h, \boldsymbol{\eta}_v) + b(p - \pi_{h,r}p, \boldsymbol{\eta}_v) - b(\eta_p, \boldsymbol{v} - \boldsymbol{\pi}_{h,r}\, \boldsymbol{v}) \\ & + s_{h,v}(\boldsymbol{v} - \boldsymbol{\pi}_{h,r}\, \boldsymbol{v}, \boldsymbol{\eta}_v) - s_{h,p}(\pi_{h,r}p, \eta_p) \end{aligned}$$

We estimate each of the terms on the right hand side separately. The estimate of the term $a(\boldsymbol{b}; \boldsymbol{v} - \boldsymbol{v}_h, \boldsymbol{\eta}_v)$ is standard, see [BFH06] and leads to

$$\begin{aligned} a(\boldsymbol{b}; \boldsymbol{v} - \boldsymbol{\pi}_{h,r}\, \boldsymbol{v}, \boldsymbol{\eta}_v) \;\lesssim\; & \| \boldsymbol{v} - \boldsymbol{\pi}_{h,r}\, \boldsymbol{v} \|_{vel} \|\boldsymbol{\eta}_v\|_{vel} + \max_{T\in\mathcal{T}_h} \{\sigma^{-1/2} |\boldsymbol{b}|_{1,\infty,T} h_T^{k+1}\} \| \boldsymbol{v} \|_{k+1,\Omega} \|\boldsymbol{\eta}_v\|_{vel} \\ & + \left(\sum_{T\in\mathcal{T}_h} \max\{\|\boldsymbol{b}\|_{0,\infty,T} h_T, \nu\} h_T^{2k} \| \boldsymbol{v} \|_{k+1,T}^2 \right)^{1/2} \|\boldsymbol{\eta}_v\|_{vel}\,. \end{aligned}$$

The estimate of the second term, i.e. $b(p - \pi_{h,r}p, \boldsymbol{\eta}_v)$, slightly differs from [BFH06] due to the different dimensions of the pressure and the velocity field:

$$\begin{aligned} b(p - \pi_{h,r}p, \boldsymbol{\eta}_v) &= (\nabla'(p - \pi_{h,r}p), \mathbf{M}\, \boldsymbol{\eta}_v)_\omega = (\nabla'(p - \pi_{h,r}p), \boldsymbol{\eta}_v)_\Omega \\ &= -(p - \pi_{h,r}p, \mathrm{div}'\, \boldsymbol{\eta}_v)_\Omega = -(p - \pi_{h,r}p, \mathrm{div}'\, \boldsymbol{\eta}_v - \pi_{h,r}^* \mathrm{div}'\, \boldsymbol{\eta}_v)_\Omega \\ &\lesssim \|\phi_1 (p - \pi_{h,r}p)\|_{0,\Omega} \|\phi_1^{-1} (\mathrm{div}'\, \boldsymbol{\eta}_v - \pi_{h,r}^* \mathrm{div}'\, \boldsymbol{\eta}_v)\|_{0,\Omega} \end{aligned}$$

with piecewise constant function $\phi_1 := \nu^{-1/2} \min\{Pe_T^{-1/2}, 1\}$. The latter one can be estimated as

$$\|\phi_1^{-1} (\mathrm{div}'\, \boldsymbol{\eta}_v - \boldsymbol{\pi}_{h,r}^* \mathrm{div}'\, \boldsymbol{\eta}_v)\|_{0,\Omega} \lesssim s_{h,v}(\boldsymbol{\eta}_v, \boldsymbol{\eta}_v)^{1/2}$$

using (4.55), see also [BFH06]. The former one can be cellwise estimated as $\|\phi_1\|_{0,\infty,T} \leq \min\{\|\boldsymbol{b}\|^{-1}_{0,\infty,T}, h_T\nu^{-1}\}^{1/2}$, such that

$$\|\phi_1(p - \pi_{h,r}p)\|^2_{0,\Omega} \lesssim \delta_{max} \sum_{K\in\mathcal{K}_h} h_K^{2l}\|p\|^2_{l+1,K} \sum_{T\in\mathcal{T}_K} \min\{\|\boldsymbol{b}\|^{-1}_{0,\infty,T}, h_T\nu^{-1}\}$$

applies. In the latter estimate we used the prism property of the underlying mesh.

For the estimate of the third term, i.e. $b(\eta_p, \boldsymbol{v} - \boldsymbol{\pi}_{h,r}\,\boldsymbol{v})$, we argue in the 3D framework, and follow [BFH06]. Therefore we use the orthogonality property of $\boldsymbol{\pi}_{h,r}$ and note, that $\boldsymbol{\pi}^*_{h,r}(\nabla'\eta_p) \in [Q^r_h(\Omega)]^2$ applies:

$$\begin{aligned} b(\eta_p, \boldsymbol{v} - \boldsymbol{\pi}_{h,r}\,\boldsymbol{v}) &= (\nabla'\eta_p, \boldsymbol{v} - \boldsymbol{\pi}_{h,r}\,\boldsymbol{v})_\Omega = (\nabla'\eta_p - \boldsymbol{\pi}^*_{h,r}(\nabla'\eta_p), \boldsymbol{v} - \boldsymbol{\pi}_{h,r}\,\boldsymbol{v})_\Omega \\ &\leq \|\phi_3^{-1}(\nabla'\eta_p - \boldsymbol{\pi}^*_{h,r}(\nabla'\eta_p))\|_{0,\Omega}\|\pi_{h,1}\phi_3(\boldsymbol{v} - \boldsymbol{\pi}_{h,r}\,\boldsymbol{v})\|_{0,\Omega} \end{aligned}$$

with $\phi_3 := h_T^{-1/2}\|\boldsymbol{b}\|^{1/2}_{0,\infty,T}\lambda_T^{-1/2}$ with $\lambda_T := \min\{Pe_T, 1\}$. Using (4.56) and (4.57), and recalling the definition of the coefficients of the 2D pressure stabilization term, we further get

$$\begin{aligned} &\|\phi_3^{-1}(\nabla'\eta_p - \boldsymbol{\pi}^*_{h,r}(\nabla'\eta_p))\|_{0,\Omega}\|\pi_{h,1}\phi_3(\boldsymbol{v} - \boldsymbol{\pi}_{h,r}\,\boldsymbol{v})\|_{0,\Omega} \\ &\leq c\,\delta_{max} s_{h,p}(\eta_p, \eta_p)^{1/2} \left(\sum_{T\in\mathcal{T}_h} \max\{\|\boldsymbol{b}\|_{0,\infty,T}h_T, \nu\} h_T^{2k} \|\,\boldsymbol{v}\,\|^2_{k+1,T} \right)^{1/2}, \end{aligned}$$

see also [BFH06].
The estimate of $s_{h,v}(\boldsymbol{v} - \boldsymbol{\pi}_{h,r}\,\boldsymbol{v}, \boldsymbol{\eta}_v)$ is straight forward:

$$\begin{aligned} s_{h,v}(\boldsymbol{v} - \boldsymbol{\pi}_{h,r}\,\boldsymbol{v}, \boldsymbol{\eta}_v) &\leq s_{h,v}(\boldsymbol{v} - \boldsymbol{\pi}_{h,r}\,\boldsymbol{v}, \boldsymbol{v} - \boldsymbol{\pi}_{h,r}\,\boldsymbol{v})^{1/2} s_{h,v}(\boldsymbol{\eta}_v, \boldsymbol{\eta}_v)^{1/2} \\ &\leq \|\,\boldsymbol{v} - \boldsymbol{\pi}_{h,r}\,\boldsymbol{v}\,\|_{vel}\|\boldsymbol{\eta}_v\|_{vel}\,. \end{aligned}$$

The estimate of the pressure stabilization term can be done in 2D and be directly taken from [BFH06] for dimension 2, noting the adapted choice of the pressure stabilization parameter:

$$s_{h,p}(\pi_{h,r}p, \eta_p) \lesssim s_{h,p}(\eta_p, \eta_p)^{1/2} \left(\sum_{K\in\mathcal{K}_h} h_k\|\boldsymbol{b}\|^{-1}_{0,\infty,K}\lambda_K h_K^{2l}\|p\|^2_{l+1,K} \right)^{1/2},$$

which finishes the proof. For more detailed information we refer to the cited literature. □

An estimate of the error of the pressure is given in the L^2-norm. Again, we follow [BFH06]:

Proposition 4.34. *Let Assumptions 4.2 and 4.22 be valid. Moreover, let the stabilization terms be $s_{h,v}(\cdot,\cdot)$ and $s_{h,p}(\cdot,\cdot)$ be given by (V'-ii) and (P'-iii).*
If the continuous solution of (3.33) is sufficiently regular, $\mathbf{u} := (\boldsymbol{v}, p) \in \mathbf{H}^{k+1}(\Omega) \times$

$\mathrm{H}^{l+1}(\omega)$, $1 \leq k \leq r$ *and* $0 \leq l \leq r$, *the error of the pressure of the discrete solution* $\mathbf{u}_h := (\boldsymbol{v}_h, p_h)$ *of (4.48) can be estimated as:*

$$\|p - p_h\|_{0,\omega} \lesssim C_u \left(\max_{T \in \mathcal{T}_h} \{ h_T \|\boldsymbol{b}\|_{0,\infty,T},\, \nu \}^{1/2} + \sigma^{1/2} + \sigma^{-1/2} \|\boldsymbol{b}\|_{0,\infty,\Omega} \right)$$

with

$$\begin{aligned} C_u := & \sum_{T \in \mathcal{T}_h} \left((\sigma + \mathrm{f}) h_T^{2(k+1)} + \max\{\nu, \|\boldsymbol{b}_h\|_{0,\infty,T} h_T\} h_T^{2k} \right) \| \boldsymbol{v} \|_{k+1,T}^2 \\ & + \max_{T \in \mathcal{T}_h} \{ \sigma^{-1/2} |\boldsymbol{b}|_{1,\infty,T} h_T^{k+1} \}^2 \| \boldsymbol{v} \|_{k+1,\Omega}^2 + \sum_{K \in \mathcal{K}_k} h_K^{2l} \|p\|_{l+1,K}^2 \sum_{T \in \mathcal{T}_K} \min\{ \|\boldsymbol{b}\|_{0,\infty,T}^{-1}, h_T \nu^{-1} \} . \end{aligned}$$

Proof. We follow the ideas given in [BFH06]. Therefore we present the mechanisms of the cited literature and present specifics of the hydrostatic case.
Given $p - p_h$, Burman et al. provide a $\boldsymbol{w}_p \in \mathbf{H}_0^1(\omega)$ such that

$$\operatorname{div}' \boldsymbol{w}_p = p - p_h, \quad \| \boldsymbol{w}_p \|_{0,\omega} + | \boldsymbol{w}_p |_{1,\omega} \lesssim \|p - p_h\|_{0,\omega}$$

apply, see [BFH06]. Taking advantage of the operator $\mathbf{M}$, see Section 4.1.3, an element $\boldsymbol{v}_p \in \mathbf{V}$ can be assured with $\mathbf{M}\, \boldsymbol{v}_p = \boldsymbol{w}_p$ and

$$\operatorname{div}' \mathbf{M}\, \boldsymbol{v}_p = p - p_h, \quad \| \boldsymbol{v}_p \|_{0,\Omega} + | \boldsymbol{v}_p |_{1,\Omega} \lesssim \|p - p_h\|_{0,\omega} . \tag{4.59}$$

Using the modified Galerkin orthogonality (4.58), applied with $(\boldsymbol{\varphi}, \xi) := (\boldsymbol{\pi}_{h,r}\, \boldsymbol{v}_p, 0)$, leads to

$$\begin{aligned} \|p - p_h\|_{0,\omega}^2 &= (p - p_h, \operatorname{div}' \mathbf{M}\, \boldsymbol{v}_p)_\omega \\ &= (p - p_h, \operatorname{div}' \mathbf{M}(\boldsymbol{v}_p - \boldsymbol{\pi}_{h,r}\, \boldsymbol{v}_p))_\omega + a(\boldsymbol{b}_h, \boldsymbol{v} - \boldsymbol{v}_h, \boldsymbol{\pi}_{h,r}\, \boldsymbol{v}_p) \\ &\quad + s_{h,v}(\boldsymbol{v} - \boldsymbol{v}_h, \boldsymbol{\pi}_{h,r}\, \boldsymbol{v}_p) , \end{aligned}$$

see also [BFH06]. We treat the first term on the right hand side in the 3D framework, noting, that $\pi_{h,r} \nabla' p, \pi_{h,r}^* \nabla' p \in Q_h^r(\Omega)$ and applying the orthogonality property of $\boldsymbol{\pi}_{h,r}$, as well as (4.57), (4.59) we derive:

$$\begin{aligned} (p - p_h, \operatorname{div}' \mathbf{M}(\boldsymbol{v}_p - \boldsymbol{\pi}_{h,r}\, \boldsymbol{v}_p))_\omega &\leq |((\nabla' p - \pi_{h,r} \nabla' p) + (\pi_{h,r}^* \nabla' p - \nabla' p_h), \boldsymbol{v}_p - \boldsymbol{\pi}_{h,r}\, \boldsymbol{v}_p)_\Omega| \\ &\leq |(\nabla' p - \pi_{h,r} \nabla' p, \boldsymbol{v}_p - \boldsymbol{\pi}_{h,r}\, \boldsymbol{v}_p)_\Omega + (\pi_{h,r}^* \nabla' p - \nabla' p_h, \boldsymbol{v}_p - \boldsymbol{\pi}_{h,r}\, \boldsymbol{v}_p)_\Omega| \\ &\lesssim \delta_{max}^{1/2} (h_\omega^{l-1/2} \|p\|_{l+1,\omega} + \max_{T \in \mathcal{T}_h} \{ h_T \|\boldsymbol{b}\|_{0,\infty,T}, \nu \}^{1/2} s_{h,p}(p_h, p_h)^{1/2}) \|p - p_h\|_{0,\omega} , \end{aligned}$$

see also [BFH06]. Note, that the estimate of the term $(\pi_{h,r}^* \nabla' p - \nabla' p_h, \boldsymbol{v}_p - \boldsymbol{\pi}_{h,r}\, \boldsymbol{v}_p)_\Omega$ differs from the deductions in [BFH06]. As $\pi_{h,r}^* \nabla' p$ is vertically invariant we deduce in the hydrostatic framework, using (4.56), (4.57) and (4.59):

$$\begin{aligned} (\pi_{h,r}^* \nabla' p - \nabla' p_h, \boldsymbol{v}_p - \boldsymbol{\pi}_{h,r}\, \boldsymbol{v}_p)_\Omega &= (\pi_{h,r}^* \nabla' p - \nabla' p_h, \mathbf{M}(\boldsymbol{v}_p - \boldsymbol{\pi}_{h,r}\, \boldsymbol{v}_p))_\omega \\ &\leq \|\phi^{-1} (\pi_{h,r}^* \nabla' p - \nabla' p_h)\|_{0,\omega} \|\phi\, \mathbf{M}(\boldsymbol{v}_p - \boldsymbol{\pi}_{h,r}\, \boldsymbol{v}_p)\|_{0,\omega} \\ &\lesssim \delta_{max}^{1/2}\, s_{h,p}(p_h, p_h)^{1/2} \max_{K \in \mathcal{K}_h} \{ h_K \|\boldsymbol{b}\|_{0,\infty,K} \max\{1, Pe_K^{-1}\} \}^{1/2} \|p - p_h\|_{0,\omega} \end{aligned}$$

with $\phi^2 := h_K^{-1}\lambda_K^{-1}\|\boldsymbol{b}\|_{0,\infty,K}$. Moreover note, that

$$\max_{K\in\mathcal{K}_h}\{h_K\|\boldsymbol{b}\|_{0,\infty,K}\max\{1,Pe_K^{-1}\}\}^{1/2} \;\leq\; \max_{T\in\mathcal{T}_h}\{h_T\|\boldsymbol{b}\|_{0,\infty,T},\nu\}^{1/2}$$

applies. The remaining terms can be estimated in a straight forward manner, using H^1-stability of $\boldsymbol{\pi}_{h,r}$, (4.59) and considering the definition of the norm $\|\cdot\|_{vel}$:

$$\begin{aligned} a(\boldsymbol{b},\boldsymbol{v}-\boldsymbol{v}_h,\boldsymbol{\pi}_{h,r}\,\boldsymbol{v}_p)+s_{h,v}(\boldsymbol{v}-\boldsymbol{v}_h,\boldsymbol{\pi}_{h,r}\,\boldsymbol{v}_p) \;&\leq\; \|\,\boldsymbol{v}-\boldsymbol{v}_h\,\|_{vel}\|\boldsymbol{\pi}_{h,r}\,\boldsymbol{v}_p\,\|_{vel} \\ &\quad + (\boldsymbol{v}-\boldsymbol{v}_h,\boldsymbol{b}_h\cdot\nabla\boldsymbol{\pi}_{h,r}\,\boldsymbol{v}_p) \\ \lesssim (\sigma^{1/2}+\max_{T\in\mathcal{T}_h}\{\|\boldsymbol{b}\|_{0,\infty,T}h_T,\nu\}^{1/2})\|p-p_h\|_{0,\omega} &+ \sigma^{-1/2}\|\boldsymbol{b}\|_{0,\infty,\Omega}\|\,\boldsymbol{v}-\boldsymbol{v}_h\,\|_{vel}\|p-p_h\|_{0,\Omega}\,. \end{aligned}$$

Collecting the estimates and recalling the velocity error estimate of Proposition 4.33 finishes the proof. □

Thus, we result in similar estimates for the CIP stabilization of the hydrostatic Oseen problem as given for the classical, 3D Oseen problem.

4.5.4 The vertical velocity component

Given the horizontal velocity field $\boldsymbol{v}\in\mathbf{V}$, the vertical velocity v_3 can be (uniquely) determined by (2.30). Assuming $\boldsymbol{v}$ to have $\mathrm{H}^{k+1}(\Omega)$- regularity, we only get $v_3\in\mathrm{H}^k(\Omega)$. Turning to the finite element formulation we observe for $v_{3,h}\in\{\varphi\in\mathcal{C}(\Omega)\,|\,\varphi|_{\Gamma_b}=0 \text{ and } \varphi|_T\in\mathbb{Q}_r,\ \forall T\in\mathcal{T}_h\}$:

$$\|v_3-v_{3,h}\|_{0,\Omega}^2 \quad=\quad \left|\left|\int_{-d(x,y)}^{z}\mathrm{div}\,'(\boldsymbol{v}-\boldsymbol{v}_h)\,d\widehat{z}\right|\right|_{0,\Omega}^2 \quad\leq\quad \delta_{max}^2|\,\boldsymbol{v}-\boldsymbol{v}_h\,|_{1,\Omega}^2\,.$$

Recalling Proposition 4.31 and the definition of $|||\cdot|||$ we thus get the L^2 estimate for the vertical velocity in the LPS framework:

$$\delta_{max}^{-1}\nu^{1/2}\|v_3-v_{3,h}\|_{0,\Omega} \quad\leq\quad \nu^{1/2}|\,\boldsymbol{v}-\boldsymbol{v}_h\,|_{1,\Omega} \quad\leq\quad C_v h^k\|\,\boldsymbol{v}\,\|_{k+1,\Omega}\,. \tag{4.60}$$

In the CIP framework, we get

$$\delta_{max}^{-1}\nu^{1/2}\|v_3-v_{3,h}\|_{0,\Omega} \quad\leq\quad \nu^{1/2}|\,\boldsymbol{v}-\boldsymbol{v}_h\,|_{1,\Omega} \quad\leq\quad C_u$$

with C_u being defined as in Proposition 4.34.
If we consider the *a priori* error estimates for $\boldsymbol{v}_h$, estimate (4.60) and recall, that we derived the Oseen problem from linearizing the nonlinear problem (3.36), the question of aptness of Assumption 4.22 arises. Unfortunately, due to the embedding theory, at this point we are not able to use the error estimates of Proposition 4.31 and (4.60) in the $\mathrm{W}^{1,2}$-context to get statements in the $\mathrm{W}^{1,3}$-frame, as Assumption 4.22 suggests. Also, the estimate in Assumption 4.22 could not be relaxed to the $\mathrm{W}^{1,2}$-frame due to the argumentation preceeding that Assumption.

If we consider the 2.5D Oseen problem as an independent problem, w.l.o.g. we can premise Assumption 4.22 and do not get into troublesome argumentation while deriving H^1- and L^2-errors for the solution $(\boldsymbol{v}_h,p_h)$ of the discrete problem and the appropriate vertical velocity $v_{3,h}$.

Chapter 5

Equal-Order Finite Element Discretization of Stationary Systems on Anisotropic Meshes

In the preceding we tacitly assumed a sufficiently small cellwise aspect ratio. Recall that we consider hydrostatic flow problems in *flat* and *horizontally stretched* domains. Application of isotropic meshes leads to similar resolutions in horizontal and vertical directions, which effects a too costly horizontal resolution at least in the case of ocean circulation models. Moreover, (comparative) strong vertical gradients are assumed to be apparent near the surface layer. In order to prevent numerical overhead it is advisable to apply triangulations whose cells are horizontally stretched. For an example of an applied grid we refer to [BMP+06], in which the global ORCA025 model is introduced with a resolution of 0.25° at the equator, i.e. 27 km, and a vertical resolution varying between 6 m near the surface and 250 m near the bottom. Such a grid for sure does not have small cellwise aspect ratios with strong anisotropy in vertical direction. Due to that reason, the notion of *anisotropic meshes* is used. In particular, we define the notion of *vertical anisotropic meshes*. Along coastlines a finer mesh resolution in one horizontal direction may be necessary, i.e. we thus not only have horizontally stretched cells, but anisotropic mesh structure may also be apparent in horizontal direction. Appropriately we introduce the notion of *horizontal anisotropic meshes*.

In the finite element context, application of equal-order finite elements still leads to a violation of the inf-sup constraint under the presumption of anisotropic meshes. Furthermore, depending on the finite element spaces, the inf-sup condition may suffer from small inf-sup constants due to the large aspect ratio, such that the entire discrete problem is numerically instable. Moreover, the application of the interpolation operator as introduced in the preceding chapter is questionable in the anisotropic context.
In the framework of anisotropic interpolation operators, let us mention the following publications: First, the work [Bec95] of Becker, in which the author introduces first examinations of interpolation operators and stabilizations in the anisotropic context in 2D and for bilinear finite elements. Further and more extensive analysison the issue of anisotropic interpolation operators in 2D and 3D has been done by Apel in

[Ape98, Ape99].
The issue of inf-sup stable finite elements has been treated in [AM08, AR01, AC00, SSS99, SS98]. The topic of anisotropic stabilization of the 2D Stokes problem has been treated in [AM08, AR01, AC00, Ric05, BT06a, MPP02] and of the 2D Oseen problem in [Bra08a], the authors of [LAK06] also treated the three dimensional case. Numerical validation of 2D Oseen problem is treated in [Bla08, Bra08b].

In this chapter we adapt and develop suitable results to the 2.5D, i.e. hydrostatic, case. We start with an introduction of anisotropic meshes and appropriate restrictions of those due to the requirements of the applied anisotropic interpolation operators. Afterwards, we present the interpolation operatorators, developped in [Ape98], which are the basis of our analysis. Anticipatory, we apply anisotropic local projection stabilization, which necessitates the application of projection operators with suitable properties. In [Bra08b], Braack develops an appropriate H^1-stable projection operator in 2D for bilinear finite elements with suitable interpolation properties. Based on this work, we use the derivations in [Ape98] to deduce an appropriate 3D H^1-stable projection operator for finite elements $Q_r(\Omega)$ on flat tensor product type meshes. We then turn to the issue of the discrete inf-sup constraint in the hydrostatic framework. It turns out, that isotroptic pressure stabilization may be applied as long as the surface mesh is isotropic. Presuming such meshes we then analyze the hydrostatic Stokes problem and the hydrostatic Oseen problem. The treatment of 3D meshes with anisotropy in the surface mesh is finally introduced. Unlike the former case we apply anisotropic pressure stabilization, which has been developped in [Bec95, Ric05, BT06a] for the 2D Stokes problem.

5.1 Preliminaries

5.1.1 Anisotropic meshes

We recall, that for *shape-regular* families of (admissible) meshes $\{\mathcal{T}\}$ the overall cellwise aspect ratio is bounded above by a suitable constant $c \in \mathbb{R}_{>0}$:

$$\frac{h_T}{\rho_T} =: c_T \leq c \qquad \forall T \in \mathcal{T} \tag{5.1}$$

with diameter h_T of the smallest ball containing T and diameter ρ_T of the largest ball contained in T, see constraint (4.1) Section 4.1.1.
If the smallest constant $c^* \in \mathbb{R}_{>0}$ satisfying (5.1) is small, i.e. of order $\mathcal{O}(1)$, then the cells of each mesh show a similar moderate aspect ratio (of order $\mathcal{O}(1)$) and we denote $\{\mathcal{T}\}$ as *isotropic*. Similar to the notion of a *shape-regular mesh*, a mesh of such a mesh family is denoted as *isotropic mesh*. Contrary, if c^* is large *or* if the family of meshes is *not* shape-regular, i.e.

$$\sup_{T \in \{\mathcal{T}\}} c_T = \infty, \tag{5.2}$$

then $\{\mathcal{T}\}$ is called *anisotropic*, see e.g. [Bla07], in which anisotropic meshes are characterized by apparency of a large c^*, or [Ape99], in which the author puts the main emphasis on (5.2).
Recall, that in Section 4.1.1 we introduced the local characteristic mesh sizes h_K and h_T for cells K and T of 2D and 3D mesh $\mathcal{K}_h$ and $\mathcal{T}_h$, respectively. However, these mesh sizes carry too little information in the framework of anisotropic meshes to characterize the partly highly distorted cells. We introduce the more adequate mesh sizes $h_{1,T}$, $h_{2,T}$, $h_{3,T}$:
For any quadrilateral E and any hexahedral T let

- $\text{meas}_2(E)$ be the surface area of E and
- $\text{meas}_3(T)$ be the volume of T.

Given a cell $T \in \mathcal{T}_h$, let E be one of the longest edges of T. Moreover, let Γ_E be the largest of the two faces of T such that $E \subseteq \overline{\Gamma_E}$. Then,

- $h_{1,T}$ denotes the length of E,
- $h_{2,T} := \text{meas}_2(\Gamma_E)/h_{1,T}$ and
- $h_{3,T} := \text{meas}_3(T)/(h_{1,T}h_{2,T})$,

see also [Ape98]. We abbreviate $\boldsymbol{h}_T := (h_{1,T}, h_{2,T}, h_{3,T})$. On *Cartesian meshes* $\mathcal{T}_h$, i.e. $\mathcal{T}_h$ consists of bricks T aligned with the coordinate axes, $h_{i,T}$, $i \in \{1,2,3\}$, simply are given by the different edge lengths of T. Note, that each Cartesian mesh with at least two subjacent vertical layers (which we presume) fulfill Assumption 4.2.

Vertical anisotropic meshes

In order to account for the crucial presumption of hydrostatic problems, i.e. a flat domain with large extents in horizontal directions, we introduce the notion of *vertical anisotropic* meshes:

Definition 5.1 (Vertical anisotropy)**.** *Let $\{\mathcal{T}_h\}$ be a family of anisotropic meshes $\mathcal{T}_h$ and let $\{\mathcal{K}_h\}$ be the appropriate family of surface meshes $\mathcal{K}_h$ of $\mathcal{T}_h$. Each mesh $\mathcal{T}_h$ is presumed to fulfill Assumption 4.2. If $\{\mathcal{K}_h\}$ is isotropic and $h_{1,T} = c_{2,T}\, h_{2,T} = c_{3,T} h_{3,T}$ for each $T \in \mathcal{T}_h$ with $1 \sim c_2 \ll c_3$, then $\{\mathcal{T}_h\}$ is denoted as* vertical anisotropic*.*

Horizontal anisotropic meshes

Moreover, in the case of strong currents, as e.g. are apparent in the Bering strait, the application of meshes which show also horizontal anisotropy may be useful.
Due to concerns of application we orient ourself towards to [BT06a], in which the authors discussed the local projection stabilization of the 2D Stokes problem on the following 2D anisotropic meshes:

Let $\mathcal{K}_h$ be a 2D mesh which can be representable via affine mappings G_K from $\widehat{K} := [0,1]^2$ onto K of the following type. For each $K \in \mathcal{K}_h$ we assume a cell wise shearing parameter $\sigma_K \in \mathbb{R}$, a cell wise angle of rotation $\theta_K \in [0, 2\pi)$ and stretching parameters $h_{1,K}$ and $h_{2,K}$ in x- and y-direction such that for all $(\widehat{x}, \widehat{y}) \in \widehat{K}$

$$G_K \begin{pmatrix} \widehat{x} \\ \widehat{y} \end{pmatrix} = \begin{pmatrix} x_{0,K} \\ y_{0,K} \end{pmatrix} + \begin{pmatrix} \cos\theta_K & -\sin\theta_K \\ \sin\theta_K & \cos\theta_K \end{pmatrix} \left[\begin{pmatrix} h_{1,K} & \sigma_K h_{2,K} \\ 0 & h_{2,K} \end{pmatrix} \begin{pmatrix} \widehat{x} \\ \widehat{y} \end{pmatrix} + \begin{pmatrix} \alpha_K \widehat{x}\widehat{y} \\ \beta_K \widehat{x}\widehat{y} \end{pmatrix} \right]$$

applies. Constant $|\sigma_K|$ is supposed to be bounded by a constant $\sigma_0 \geq 0$. Parameters α_K and β_K are assumed to satisfy

$$|\alpha_K| \leq \frac{h_{1,K}}{4} \quad \text{and} \quad |\beta_K| \leq \frac{1}{4} \min \left\{ h_{2,K}, \frac{h_{1,K}}{\sigma_0} \right\}.$$

Moreover neighboring cells are required to be of similar size. Without loss of generality we assume $h_{1,T} \geq h_{2,T}$. Restricting to these type of meshes we introduce the notion of *horizontal anisotropic* meshes:

Definition 5.2 (Horizontal anisotropy)**.** *Let $\{\mathcal{T}_h\}$ be a family of anisotropic meshes $\mathcal{T}_h$ and let $\{\mathcal{K}_h\}$ be the appropriate family of surface meshes $\mathcal{K}_h$ of $\mathcal{T}_h$. Each mesh $\mathcal{T}_h$ is presumed to fulfill Assumption 4.2.*

If each 2D surface mesh $\mathcal{K}_h$ fulfills the preceding demands and if each appropriate $\mathcal{T}_h$ has a global vertical mesh size h_3 and if

$$h_{1,T} \gtrsim h_3 \gtrsim h_{2,T} \qquad \forall T \in \mathcal{T}_h$$

with $h_{3,T} := c_T h_3$, $c_T = \mathcal{O}(1)$, then $\{\mathcal{T}_h\}$ is denoted as horizontal anisotropic*.*

(a) Mesh restrictions for the anisotropic Lagrangian interpolation operator

First of all, let us note, that each of the considered triangulation of Ω is assumed to have a prismatic structure, see Section 4.1.1.

Given an anisotropic mesh and a finite element space defined on this mesh, it is offhand *not* clear, which approximation properties apply for these discrete spaces. Usually, these properties are indicated by knowledge of the approximation properties of suitable interpolation operators. In [Ape98, Ape99] Apel examined the issue of interpolation operators defined on finite element spaces which are based on anisotropic meshes. In the upcoming we denote these operators as *anisotropic interpolation operators*. Apel's considerations in [Ape98, Ape99] are based on the following assumptions on the mesh (we present them for the 3D case):

Interior angle condition (iac) For any $T \in \mathcal{T}_h$ let

- γ_F be the maximal interior *angle of* the six *faces* of T,
- γ_T be the maximal *angle between* two *faces* of T.

There is a constant $0 < \gamma^* < \pi$ such that for any $T \in \mathcal{T}_h$: $\gamma^* \leq \gamma_F, \gamma_T \leq \pi - \gamma^*$.

Coordinate system condition (csc) For any $T \in \mathcal{T}_h$ let E and Γ_E be denoted as given above. Consider the origin Cartesian coordinate system (e_1, e_2, e_3) and the Cartesian coordinate system $(e_{1,T}, e_{2,T}, e_{3,T})$, which is constructed as follows:

- E is part of the $e_{1,T}$-axis,
- Γ_E is part of the $e_{1,T}, e_{2,T}$-plane,
- $(0,0,0)$ is a node of the reference element $\widehat{T}$.

The mapping from $(e_{1,T}, e_{2,T}, e_{3,T})$ into (e_1, e_2, e_3) consists of

- a translation,
- three rotations around $e_{i,T}$ by angles θ_i with

$$|\sin\theta_1| \leq Ch_{3,T}/h_{2,T}, \quad |\sin\theta_2| \leq Ch_{3,T}/h_{1,T}, \quad |\sin\theta_3| \leq Ch_{2,T}/h_{1,T}.$$

Remark 5.3. *We comment on these conditions in the hydrostatic framework and start with the examination of a (globally refined)* vertical anisotropic mesh $\mathcal{T}_h$. *I.e. the 2D surface mesh $\mathcal{K}_h$ of $\mathcal{T}_h$ is isotropic. Further note, that $\mathcal{K}_h$ is parallel to the e_1, e_2-plane, and that $\mathcal{T}_h$ fulfills the prism property, see Section 4.1.1, with vertical oriented edges being parallel to the e_3-axis. Thus, if the mesh is vertical anisotropic, the angle γ^* of the iac can be assumed to be fairly close to $\pi/2$ for horizontally stretched cells, see also the red highlighting in Figure 5.1. Else, γ^* is restricted by the depth of the domain and to the angles occurring in the coarsest mesh. If the considered $T \in \mathcal{T}_h$ has isotropic character, γ^* may decrease down to about $\pi/4$.*

Second, let us turn to the csc. For an isotropic cell this condition is not problematic due to $h_{1,T} \sim h_{3,T} \sim h_{3,T}$. For any stretched cell the longest edge E of T is almost horizontally oriented, whereas the degree of the skewness depends on the coarsest mesh. Due to the flatness of Ω and as ω is part of the e_1, e_2-plane, the angles of the rotations around $e_{1,T}$ and $e_{2,T}$ are small, see also Figure 5.1). The constraint on the remaining rotation is fairly unrestrictive as $h_{2,T}/h_{1,T} \approx 1$. Concluding, regular, vertical anisotropic meshes in the hydrostatic frame fulfill both requirements, the interior angle condition and the coordinate system condition.
If $\mathcal{T}_h$ is constructed by (partly) local mesh refinement in the sense that (some) vertical oriented edges and faces are halved, the same argumentation applies.

If the 2D surface mesh also is anisotropic, it is not clear offhand, which edge is the longest and thus the csc does not apply naturally. As well, the iap may be disturbed due to the 2D mesh and also due to the possible degeneration of γ_T, if stronger mesh refinement is applied on $\mathcal{K}_h$ than on the resolution of the depth. In this case, the iac and the csc have to be enforced explicitely.

Presuming that $\mathcal{T}_h$ provides the aic and the csc, Apel was able to derive suitable interpolation estimates for cells T, which are parallelepipeds with

$$\boldsymbol{F}_T(\widehat{\boldsymbol{x}}) = \boldsymbol{x}_0 + B_T\widehat{\boldsymbol{x}} \qquad \text{with } |\det B_T| = h_{1,T}h_{2,T}h_{3,T}\,,$$

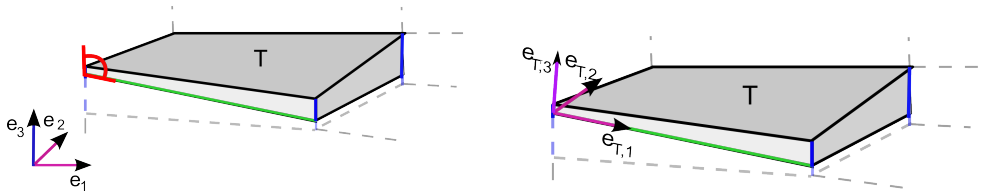

Figure 5.1: Extractive sketch of a vertical anisotropic mesh $\mathcal{T}_h$. The green colored edge denotes the longest edge in T. Left: The red highlighted angle indicates the non degeneration of the maximal possible angles occurring in $\mathcal{T}_h$. The blue edges are parallel to the e_3-axis, the green colored may be not parallel to e_1-axis. Right: After coordinate system transformation, the blue colored edges need not necessarily be parallel to the $e_{T,3}$-axis, but the green colored edge is part of the $e_{T,1}$-axis and the largest face adjacent to the green edge is part of the $e_{T,1}, e_{T,2}$-plane.

see [Ape99], or are subparametric, i.e. constructed by trilinear transformations

$$\boldsymbol{F}_T(\widehat{\boldsymbol{x}}) := \widetilde{\boldsymbol{F}}_T(\widehat{\boldsymbol{x}}) + \sum_{j=1}^{8} a^{(j)} \widehat{\varphi}_j(\widehat{\boldsymbol{x}}) \tag{5.3}$$

with

$$\widetilde{\boldsymbol{F}}_T(\widehat{\boldsymbol{x}}) \;:=\; \boldsymbol{x}_0 + B_T \widehat{\boldsymbol{x}}, \qquad B_T := diag(h_{1,T}, h_{2,T}, h_{3,T}) \tag{5.4}$$

$$|a_i^{(j)}| \;\leq\; a_i h_{3,T}, \qquad 0 \leq a_i \leq C \qquad \forall i \in \{1,2,3\}, j \in \{1,\ldots,8\} \tag{5.5}$$

$$\frac{1}{2} - \frac{h_{3,T}}{h_{1,T}} a_1 - \frac{h_{3,T}}{h_{2,T}} a_2 - a_3 \geq a_0 > 0 \tag{5.6}$$

and trilinear shape functions $\widehat{\varphi}_i$, see also [Ape98]. I.e. we are restricted to cells T, which are parallelepipeds or are slight deviations from a brick with side lengths $h_{i,T}$, $i \in \{1,2,3\}$. Note, that (5.6) assures $\boldsymbol{F}$ to be invertible. Moreover, for the affine case of parallelepipeds, we have

$$|\det B_T| = h_{1,T} h_{2,T} h_{3,T}, \quad |b_{ij}| \leq c \min\{h_{i,T}, h_{j,T}\} \;\text{ and }\; |b_{ij}^{-1}| \leq c \min\{h_{i,T}^{-1}, h_{j,T}^{-1}\}$$

for $i, j \in \{1, 2, 3\}$, see [Ape98]. For the subparametric approach (5.5) and (5.6) produce the appropriate estimates:

$$|\det D(\widehat{\boldsymbol{x}})| \sim h_{1,T} h_{2,T} h_{3,T}, \quad |d_{ij}| \leq c \min\{h_{i,T}, h_{j,T}\} \;\text{ and }\; |d_{ij}^{-1}| \leq c \min\{h_{i,T}^{-1}, h_{j,T}^{-1}\}$$

for all $\widehat{\boldsymbol{x}} \in \widehat{T}$, Jacobi matrix $D = (d_{ij})$ of $\boldsymbol{F}_T$ and $i, j \in \{1, 2, 3\}$, see [Ape98].

Remark 5.4. *If the given mesh $\mathcal{T}_h$ consists of parallelepipeds, then the underlying domain Ω has constant depth. This is due to the fact, that the surface ω is parallel to the e_1, e_2-plane and each vertical edge is parallel to the e_3-axis. Thus, the non rectangular angles can only occur horizontally. If $\mathcal{T}_h$ is a subparametric mesh, we are able to model the bottom structure to some extent.*

(b) Mesh restrictions for the anisotropic Scott-Zhang interpolation operator

In order to derive an interpolation operator, which is based on the Scott-Zhang operator for isotropic meshes and shows suitable interpolation estimates, Apel [Ape99] restricts to meshes of tensor product type. Supposing flat cells, i.e. $h_{1,T} \sim h_{2,T} \gg h_{3,T}$ the cellwise transformations are given as

$$\boldsymbol{F}_T(\widehat{\boldsymbol{x}}) = \boldsymbol{x}_0 + B\widehat{\boldsymbol{x}} \qquad \text{with } B = \begin{pmatrix} B_T & 0 \\ 0 & \pm h_{3,T} \end{pmatrix} \tag{5.7}$$

such that $|\det B_T| \sim h_{1,T}^2$, $\|B_T\| \sim h_{1,T}$, and $\|B_T^{-1}\| \sim h_{1,T}^{-1}$, see [Ape99]. Moreover, in order to treat the missing continuity of the underlying functions $\boldsymbol{v}$, abrupt changes in the element sizes are forbidden, i.e. $h_{i,T} \sim h_{i,T'}$ shall apply for all T, T' with $\overline{T} \cap \overline{T'} \neq \emptyset$. Speaking of which, the patch of T is denoted as

$$S_T \;=\; int\left(\bigcup_{T' \in \mathcal{T}_h} \left\{ \overline{T'} \mid \overline{T} \cap \overline{T'} \neq \emptyset \right\} \right).$$

Note, that the aip and the csc, as well as Assumption 4.2 obviously are fulfilled.

Lemma 5.5 (Inverse estimate)**.** *Let T be a cell of a vertical anisotropic tensor product type mesh $\mathcal{T}_h$, $\boldsymbol{v}_h \in \mathrm{H}^k(T) \cap \mathbb{Q}_r(T)$ and $0 \leq m \leq k \leq r$. Then, the following estimate applies:*

$$|\, \boldsymbol{v}_h \,|_{k,T} \;\leq\; h_{1,T}^m \, h_{3,T}^{-k} \, |\, \boldsymbol{v}_h \,|_{m,T}\,.$$

Proof. We collect some properties of the transformation $\boldsymbol{F}_T(\widehat{\boldsymbol{x}}) = \boldsymbol{x}_0 + B\widehat{\boldsymbol{x}}$ as given in (5.7). As $\mathcal{T}_h$ is vertical anisotropic we have $h_{3,T} \ll h_{1,T} \sim h_{2,T}$. Due to the construction of $\boldsymbol{F}$ we have $\|B\| \lesssim h_T \sim h_{1,T}$ and $\|B^{-1}\| \lesssim \rho_T^{-1} \sim h_{3,T}^{-1}$, see also Section 4.1.1 on page 49 for the notations h_T and ρ_T, and [Bra07]. Applicating the transformation theorem and suitable estimates on the reference element (both can be found in [Bra07]), we deduce for any $T \in \mathcal{T}_h$:

$$|\, \boldsymbol{v}_h \,|_{k,T} \;\lesssim\; \|B^{-1}\|^k \, |\det B^{-1}|^{-1/2} \, |\widehat{\boldsymbol{v}}_h|_{m,\widehat{T}} \;\lesssim\; \|B^{-1}\|^k \, \|B\|^m \, |\, \boldsymbol{v}_h \,|_{m,T}\,.$$

□

However, this estimate is too rough for the upcoming issues, as the scalings of the different directional derivates are not distinguished. On Cartesian meshes we observe the following improved estimate for first derivatives, which is expandable to tensor product type meshes:

Lemma 5.6 (Inverse estimate for brick elements)**.** *Given a brick cell T of a mesh $\mathcal{T}_h$ with side lengths $h_{1,T}, h_{2,T}, h_{3,T}$, for any $\boldsymbol{v}_h \in \mathrm{H}^1(T) \cap Q_r(T)$ and partial derivation ∂_{x_i}, $i \in \{1,2,3\}$, the following inverse estimate applies:*

$$\|\partial_{x_i} \boldsymbol{v}_h\|_{0,T} \lesssim h_{i,T}^{-1} \|\, \boldsymbol{v}_h \,\|_{0,T}\,.$$

Proof. We set $\widehat{x}_j := x_j h_{j,T}^{-1}$, $j \in \{1,2,3\}$ and consider the transformed brick element $\widehat{T}$ with side lengths 1, i.e. the transformation $F_T : \widehat{T} \to T$ is given by $F_T(\widehat{\boldsymbol{x}}) := B_T \widehat{\boldsymbol{x}}$ with $B_T = diag(h_1, h_2, h_3)$. We consider $\xi := \partial_{x_i} \boldsymbol{v}_h(\boldsymbol{x})$ and $\widehat{\xi} := \partial_{\widehat{x}_i} \widehat{\boldsymbol{v}}_h(\widehat{\boldsymbol{x}})$, and observe $\partial_{\widehat{x}_i}(F_T)_j(\widehat{\boldsymbol{x}}) = h_i \delta_{ij}$ as well as $\partial_{x_i}(F_T^{-1})_j(\boldsymbol{x}) = h_{i,T}^{-1}\delta_{ij}$. Thus the relation

$$|\partial_{\widehat{x}_i} \widehat{\boldsymbol{v}}_h(\widehat{\boldsymbol{x}})| \;=\; |\partial_{\widehat{x}_i}(\boldsymbol{v}_h \circ F_T)(\widehat{\boldsymbol{x}})| \;=\; \left| \sum_{j=1}^{3} \partial_{x_j} \boldsymbol{v}_h(\boldsymbol{x}) \cdot \partial_{\widehat{x}_i}(F_T)_j(\widehat{\boldsymbol{x}}) \right| \;=\; h_{i,T}\, |\partial_{x_i} \boldsymbol{v}_h(\boldsymbol{x})| \tag{5.8}$$

applies and, using the transformation formula, see also [Bra07], we get

$$\begin{aligned} \|\partial_{x_i} \boldsymbol{v}_h\|_{0,T}^2 \;&=\; \int_T |\partial_{x_i} \boldsymbol{v}_h(\boldsymbol{x})|^2 \, d\boldsymbol{x} \;=\; h_{i,T}^{-2} \int_T \left|\partial_{\widehat{x}_i} \widehat{\boldsymbol{v}}_h(F_T^{-1}(\boldsymbol{x}))\right|^2 d\boldsymbol{x} \\ &=\; h_{i,T}^{-2} |\det B_T^{-1}|^{-1} \int_{\widehat{T}} |\partial_{\widehat{x}_i} \widehat{\boldsymbol{v}}_h(\widehat{\boldsymbol{x}})|^2 \, d\widehat{\boldsymbol{x}} \;=\; h_{i,T}^{-2} |\det B_T^{-1}|^{-1} \|\partial_{\widehat{x}_i} \widehat{\boldsymbol{v}}_h\|_{0,\widehat{T}}^2 . \end{aligned}$$

On the cubic element $\widehat{T}$ we can apply the isotropic version of the inverse estimate of Lemma 5.5, see e.g. [Bra07],

$$\|\partial_{\widehat{x}_i} \widehat{\boldsymbol{v}}_h\|_{0,\widehat{T}}^2 \;\le\; |\widehat{\boldsymbol{v}}_h|_{1,\widehat{T}}^2 \;\lesssim\; \|\widehat{\boldsymbol{v}}_h\|_{0,\widehat{T}}^2 .$$

Again, applying the transformation formula we finally get

$$\|\partial_{x_i} \boldsymbol{v}_h\|_{0,T}^2 \;\lesssim\; h_{i,T}^{-2} |\det B_T^{-1}|^{-1} \|\widehat{\boldsymbol{v}}_h\|_{0,\widehat{T}}^2 \;\lesssim\; h_{i,T}^{-2} \|\boldsymbol{v}_h\|_{0,T}^2 .$$

□

Remark 5.7. *Consider a vertical anisotropic tensor product type mesh $\mathcal{T}_h$, i.e. we have $h_{\omega,T} := h_{1,T} \sim h_{2,T} \gg h_{3,T}$ and a cellwise transformation $\boldsymbol{F}_T$ as given in (5.7). The validation of the proposition of Lemma 5.6 for $\partial_{x_3} \boldsymbol{v}_h$ for any $T \in \mathcal{T}_h$ is completely the same. Considering either $\partial_{x_1} \boldsymbol{v}_h$ or $\partial_{x_2} \boldsymbol{v}_h$, the proof of Lemma 5.6 alters in (5.8) to*

$$\begin{aligned} |\partial_{\widehat{x}_i} \widehat{\boldsymbol{v}}_h(\widehat{\boldsymbol{x}})| \;&=\; |\partial_{\widehat{x}_i}(\boldsymbol{v}_h \circ F_T)(\widehat{\boldsymbol{x}})| \;=\; \left| \sum_{j=1}^{3} \partial_{x_j} \boldsymbol{v}_h(\boldsymbol{x}) \cdot \partial_{\widehat{x}_i}(F_T)_j(\widehat{\boldsymbol{x}}) \right| \\ &\lesssim\; h_{\omega,T} \sum_{j=1}^{2} \left|\partial_{x_j} \boldsymbol{v}_h(\boldsymbol{x})\right| . \end{aligned}$$

The remaining deductions remain. Thus we finally observe on vertical anisotropic, tensor product type meshes:

$$\begin{aligned} &\|\partial_{x_i} \boldsymbol{v}_h\|_{0,T} \lesssim h_{\omega,T}^{-1} \|\boldsymbol{v}_h\|_{0,T} && \forall i \in \{1,2\}, \forall T \in \mathcal{T}_h , \\ &\|\partial_{x_3} \boldsymbol{v}_h\|_{0,T} \lesssim h_{3,T}^{-1} \|\boldsymbol{v}_h\|_{0,T} . \end{aligned}$$

Remark 5.8. *The inverse estimates also apply for the 2D case with $h_{1,K} \gg h_{2,K}$ on tensor product meshes.*

5.1.2 Interpolation operators

We use the following notations: Given a multi index $\alpha := (\alpha_1, \alpha_2, \alpha_3)$, let $|\alpha| := \sum_i \alpha_i$, $c\alpha := (c\alpha_1, c\alpha_2, c\alpha_3)$, $\boldsymbol{x}^\alpha := x_1^{\alpha_1} x_2^{\alpha_2} x_3^{\alpha_3}$ and $D^\alpha := \partial^{|\alpha|}/(\partial x_1^{\alpha_1} \partial x_2^{\alpha_2} \partial x_3^{\alpha_3})$ for any $\alpha_1, \alpha_1, \alpha_2, \alpha_3 \in \mathbb{N}$ and $c \in \mathbb{R}_{>0}$. Moreover recall that we apply the space of polynomials of order r in each coordinate direction.

(a) Lagrangian interpolation operator

The operator $i^{(r)} : \mathcal{C}(\overline{\widehat{T}}) \to \mathbb{Q}_r(\widehat{T})$ denotes the Lagrangian interpolation operator. We set $(i^{(r)}\, \boldsymbol{v})(\boldsymbol{x}) = i^{(r)} \widehat{\boldsymbol{v}}(\widehat{\boldsymbol{x}})$ with $\widehat{\boldsymbol{v}}(\widehat{\boldsymbol{x}}) := \boldsymbol{v}(\boldsymbol{F}(\widehat{x}))$. Provided the considered mesh shows the aic and the csc, and T is a parallelepiped or the cellwise transformations are given by (5.3), Apel [Ape98, Ape99] elaborates the estimate

$$\| \boldsymbol{v} - i^{(r)}\, \boldsymbol{v} \|_{0,T}^2 \;\leq\; c \sum_{|\alpha|=r+1} \boldsymbol{h}_T^{2\alpha} \| D^\alpha \boldsymbol{v} \|_{0,T}^2 \qquad \forall\, \boldsymbol{v} \in \mathrm{H}^{r+1}(T) \cap \mathcal{C}(\overline{T})\ \forall T \in \mathcal{T}_h\,.$$

The estimates for $\boldsymbol{v} - i^{(r)}\, \boldsymbol{v}$ in the Sobolev spaces $\mathrm{H}^m(T)$ are as follows. Provided, $\mathcal{T}_h$ fulfills the aic and the csc, T is a *parallelepiped* and $m \in \{0, \ldots, r\}$, Apel [Ape99] further derives

$$| \boldsymbol{v} - i^{(r)}\, \boldsymbol{v} |_{m,T}^2 \;\leq\; c \sum_{r+1-m \leq |\alpha| \leq r+2-m} \boldsymbol{h}_T^{2\alpha} \| D^\alpha \boldsymbol{v} \|_{m,T}^2 \qquad \forall\, \boldsymbol{v} \in \mathrm{H}^{r+2}(T)\ \forall T \in \mathcal{T}_h\,.$$

For the *subparametric* case and $m = 1$ the same estimate is given in [Ape98].

(b) Scott-Zhang interpolation operator

In order to refrain from the high regularity demands of the Lagrangian interpolation operator on $\boldsymbol{v}$, a resort is given by application of the Scott-Zhang approach. Apel [Ape99] introduced Scott-Zhang operators for cells of different stretching, in particular for flat cells, which occur in the case of vertical anisotropic meshes. Apel restricts to (unions of) meshes of tensor product type. See also Subsection 5.1.1 (b) for appropriate notions and further restrictions.
Let $z^{(r)}$ denote this anisotropic Scott-Zhang interpolation operator, mapping on $\mathbb{Q}_r$. Given a cell $T \in \mathcal{T}_h$ with $h_{1,T}, h_{2,T} \geq h_{3,T}$ in S_T, Apel derived the following estimates

$$|z^{(r)}\, \boldsymbol{v}|_{m,T} \;\leq\; c |\, \boldsymbol{v}\, |_{m,S_T} \qquad \forall\, \boldsymbol{v} \in \mathrm{H}^l(S_T) \tag{5.9}$$

$$| \boldsymbol{v} - z^{(r)}\, \boldsymbol{v} |_{m,T} \;\leq\; c \sum_{|\alpha|=l-m} \boldsymbol{h}_T^\alpha |D^\alpha \boldsymbol{v}|_{m,S_T} \qquad \forall\, \boldsymbol{v} \in \mathrm{H}^l(S_T) \tag{5.10}$$

with $0 \leq m \leq l$ and $1 \leq l \leq r+1$, which are also valid for the 2D case.
For our purposes, the given estimates are not sufficient in order to get optimal *a priori* error estimates (in the vertical anisotropic hydrostatic Oseen case). Due to that reason, we examine the estimation properties a little further than has been done in [Ape99]:

Therefore, we have a look at some results given in [Bra06], in which Braack considered the 2D interpolation operator $i_{h,2d} : \mathrm{H}^1(\omega) \to \mathrm{W}_h$, introduced by [Bec95], on quadrilateral meshes with elements, whose transformations allow certain degrees of shearing and pure bilinearity. Braack defines the notion of *2D anisotropic* H^1*-stable* projections and substantially validates

$$\begin{aligned}
\|i_{h,2d}v\|_{0,K} &\lesssim \|v\|_{S_K} + (h_1 + s_0 h_2)\|\partial_x v\|_{0,S_K} + h_2\|\partial_y v\|_{0,S_K}\,, && (5.11)\\
\|\partial_x i_{h,2d}v\|_{0,K} &\lesssim (1 + s_0 h_1^{-1} h_2)\|\partial_x v\|_{0,S_K} + h_1^{-1} h_2\|\partial_y v\|_{0,S_K}\,, && (5.12)\\
\|\partial_y i_{h,2d}v\|_{0,K} &\lesssim s_1(s_0\|\partial_x v\|_{0,S_K} + \|\partial_y v\|_{0,K})\,, && (5.13)
\end{aligned}$$

$$\begin{aligned}
\|v - i_{h,2d}v\|_{0,K} &\lesssim s_1 h_1\|\partial_x v\|_{0,S_K} + h_2\|\partial_y v\|_{0,S_K}\,, && (5.14)\\
\|\partial_x(v - i_{h,2d}v)\|_{0,K} &\lesssim s_1^2 h_1\|\partial_x^2 v\|_{0,S_K} + s_1 h_2\|\partial_{xy} v\|_{0,S_K} + h_1^{-1} h_2^2\|\partial_y^2 v\|_{0,S_K}\,, && (5.15)\\
\|\partial_y(v - i_{h,2d}v)\|_{0,K} &\lesssim s_1^2 h_1\|\partial_x^2 v\|_{0,S_K} + s_1^2 h_1\|\partial_{xy} v\|_{0,S_K} + s_1 h_2\|\partial_y^2 v\|_{0,S_K}\,, && (5.16)
\end{aligned}$$

for any cell $K \in \mathcal{K}_h$ and appropriate patch S_K with upper shearing bound s_0, $s_1 = 1 + s_0$ and sufficiently regular v, see [Bra06].

Remark 5.9. *Note, that in the proof of (5.15) the author estimated*

$$\|\partial_y(v - i_{h,2d}v)\|_{0,K} \lesssim (s_0 h_1^{-1} + h_2^{-1}) s_1 h_1^2\|\partial_x^2 v\|_{0,S_K} + s_1^2 h_1\|\partial_{xy} v\|_{0,S_K} + s_1 h_2\|\partial_y^2 v\|_{0,S_K}\,,$$

such that the factor of the term $\|\partial_x^2 v\|_{0,S_K}$ in (5.16) should be enlarged to $h_1 h_2^{-1}$ due to the presumption $h_2 \le h_1$ made in that work [Bra06].

In the upcoming we derive appropriate estimates for the 3D anisotropic Scott-Zhang interpolator as introduced in [Ape99] for flat elements T for tensor product type meshes as introduced in Subsection 5.1.1(b). We start with the 3D analogies of (5.11) – (5.13):

Proposition 5.10. *Let $\mathcal{T}_h$ be a tensor product type mesh fulfilling the demands of Subsection 5.1.1(b) and $i_{h,3d} : \mathrm{H}^1(\Omega) \to \mathbb{Q}_r(\mathcal{T}_h)$ be the Scott-Zhang interpolation operator for flat cells as introduced in [Ape99]. Then, for any $T \in \mathcal{T}_h$ with $h_{1,T}, h_{2,T} \ge h_{3,T}$ the following estimates apply*

$$\begin{aligned}
\|z^{(r)}v\|_{0,T} &\lesssim \|v\|_{0,S_T} + \sum_{|\alpha|=1} \mathbf{h}_T^\alpha\|D^\alpha v\|_{0,S_T}\,, && (5.17)\\
h_{1,T}\|\partial_x z^{(r)}v\|_{0,T} &\lesssim \sum_{|\alpha|=1} \mathbf{h}_T^\alpha\|D^\alpha v\|_{0,S_T} && (5.18)\\
h_{2,T}\|\partial_y z^{(r)}v\|_{0,T} &\lesssim \sum_{|\alpha|=1} \mathbf{h}_T^\alpha\|D^\alpha v\|_{0,S_T} && (5.19)\\
\|\partial_z z^{(r)}v\|_{0,T} &\lesssim \|\partial_z v\|_{0,S_T}\,. && (5.20)
\end{aligned}$$

Proof. Let $T \in \mathcal{T}_h$ be arbitrarily chosen. For the proof of (5.17) we can use (5.10) with $m = 0$ and $l = 1$, and estimate

$$\|z^{(r)}v\|_{0,T} \le \|v\|_{0,T} + \|z^{(r)}v - v\|_{0,T} \lesssim \|v\|_{0,S_T} + \sum_{|\alpha|=1} \mathbf{h}^\alpha\|D^\alpha v\|_{0,S_T}\,.$$

For the proof of (5.18) we consider Lemma 3.5 (on p.117ff) and follow the deductions in the proof of Lemma 3.2 (on p. 109) of [Ape99]. Note that the latter Lemma treats the case of short edges, but Apel points out in the proof of Lemma 3.5, that the deductions are also valid for the present case for appropriately adapted indices. First we get

$$\begin{aligned}\|\partial_x z^{(r)} v\|_{0,T} &\lesssim h_{1,T}^{-1} \sum_{|\alpha|\le 1} \mathbf{h}_T^{\alpha} \|D^{\alpha}(v-w)\|_{0,S_T} \\ &= h_{1,T}^{-1} \left(\|v-w\|_{0,S_T} + \sum_{|\alpha|=1} \mathbf{h}^{\alpha} \|D^{\alpha}(v-w)\|_{0,S_T} \right)\end{aligned}$$

with a suitable polynomial w of order $r-1$. We treat the two cases $|\alpha| = 0$ and $|\alpha| = 1$, which arise due to the trace theorem, separately, and start with $|\alpha| = 1$. We argue further by transformation of T onto the cell $\widehat{T}$, which is created from $x_i = \widehat{x}_i h_{i,T}$, $i \in \{1,2,3\}$. I.e. we consider the transformation $F_T(\widehat{\boldsymbol{x}}) = B_T \widehat{\boldsymbol{x}}$ with $B_T := diag(h_{1,T}, h_{2,T}, h_{3,T})$. For any α with $|\alpha| = 1$ and using the derivations in the proof of Lemma 3.1 (p.100 in [Ape99]) with $m = 0$ and $l = 1$ we thus have

$$\|\widehat{D}^{\alpha}(\widehat{v} - \widehat{w})\|_{0,\widehat{S}_T} \lesssim \|\widehat{D}^{\alpha}\widehat{v}\|_{0,\widehat{S}_T} .$$

Transformation onto $\widehat{T}$, application of the latter estimate and transformation back to T we get

$$\|D^{\alpha}(v-w)\|_{0,S_T} \lesssim \|D^{\alpha} v\|_{0,S_T} .$$

Application of Lemma 3.1 of [Ape99] the term $\|v-w\|_{0,S_T}$ can be estimated as

$$\begin{aligned}\|v-w\|_{0,S_T} &= |\det(B_T^{-1})|^{-1/2} \|\widehat{v} - \widehat{w}\|_{0,\widehat{S}_T} \\ &\lesssim |\det(B_T^{-1})|^{-1/2} \sum_{|\alpha|=1} \|\widehat{D}^{\alpha}\widehat{v}\|_{0,\widehat{S}_T} .\end{aligned}$$

Similar as in the proof of Lemma 5.6, for any α with $|\alpha| = 1$ we can further deduce

$$\begin{aligned}\|\widehat{D}^{\alpha}\widehat{v}\|_{0,\widehat{S}_T}^2 &= \int_{\widehat{S}_T} |\widehat{D}^{\alpha}\widehat{v}(\widehat{\boldsymbol{x}})|^2 d\widehat{\boldsymbol{x}} = (\mathbf{h}_T^{\alpha})^2 |\det B_T|^{-1} \int_{S_T} |D^{\alpha} v(\boldsymbol{x})|^2 d\boldsymbol{x} \\ &= (\mathbf{h}_T^{\alpha})^2 |\det B_T|^{-1} \|D^{\alpha} v\|_{0,S_T}^2 .\end{aligned}$$

The estimate (5.19) can be proven in a similar fashion. The proof of the remaining estimate (5.20) can be directly taken from page 118 of the proof of Lemma 3.5 of [Ape99]. □

Remark 5.11. *Note, that the estimates (5.17) – (5.20) (for arbitrary degree r of the underlying polynomial space) correspond to the estimates (5.11) – (5.13) with $s_0 = 0$, which is justified due to the fact, that there is no shearing in vertical direction in tensor product type meshes.*

Let us turn to the remaining estimates (5.14) – (5.16).

Proposition 5.12. *Let $\mathcal{T}_h$ be a tensor product type mesh with cellwise transformations $\boldsymbol{F}_T$ fulfilling (5.7) and $h_{1,T} \geq h_{2,T} \geq h_{3,T}$ for arbitrary $T \in \mathcal{T}_h$. For any $T \in \mathcal{T}_h$ and $v \in \mathrm{H}^2(S_T)$ the following estimates apply:*

$$\|v - z^{(r)}v\|_{0,T} \lesssim \sum_{|\alpha|=i} \mathbf{h}_T^\alpha \|D^\alpha v\|_{0,S_T} \qquad i \in \{1,2\}, \quad (5.21)$$

$$\begin{aligned}\|\partial_x(v - z^{(r)}v)\|_{0,T} \lesssim\ & s_1^2 h_{1,T}\|\partial_x^2 v\|_{0,S_T} + s_1^2 h_{2,T}\|\partial_{xy} v\|_{0,S_T} + s_1^2 h_{1,T}^{-1} h_{2,T}^2 \|\partial_y^2 v\|_{0,S_T} \\ & + s_1^2\, h_{3,T}\, \left(\|\partial_{xz} v\|_{0,S_T} + h_{1,T}^{-1}\, h_{2,T}\, \|\partial_{yz} v\|_{0,S_T} + h_{1,T}^{-1}\, h_{3,T} \|\partial_z^2 v\|_{0,S_T}\right),\end{aligned} \quad (5.22)$$

$$\begin{aligned}\|\partial_y(v - z^{(r)}v)\|_{0,T} \lesssim\ & s_1^2 h_{1,T}^2 h_{2,T}^{-1}\|\partial_x^2 v\|_{0,S_T} + s_1^2 h_{1,T}\|\partial_{xy} v\|_{0,S_T} + s_1^2 h_{2,T} \|\partial_y^2 v\|_{0,S_T} \\ & + s_1^2\, h_{3,T}\, \left(h_{1,T}\, h_{2,T}^{-1}\, \|\partial_{xz} v\|_{0,S_T} + \|\partial_{yz} v\|_{0,S_T} + h_{2,T}^{-1} h_{3,T} \|\partial_z^2 v\|_{0,S_T}\right),\end{aligned} \quad (5.23)$$

$$\|\partial_z(v - z^{(r)}v)\|_{0,T} \lesssim (h_{1,T} + s_0 h_{2,T})\|\partial_{xz} v\|_{0,S_T} + h_{2,T}\, \|\partial_{yz} v\|_{0,S_T} + h_{3,T}\, \|\partial_z^2 v\|_{0,S_T}. \quad (5.24)$$

Constant s_1 is given by $s_1 := 1 + s_0$ with upper shearing bound s_0 of the appropriate surface mesh $\mathcal{K}_h$. In particular, for vertical anisotropic meshes the second rows in the estimates (5.22) and (5.23) reduce to

$$\begin{aligned} h_{3,T}(\|\partial_{xz} v\|_{0,S_T} &+ \|\partial_{yz} v\|_{0,S_T} + h_{1,T}^{-1} h_3 \|\partial_z^2 v\|_{0,S_T}) \qquad \text{and} \\ s_1\, h_{3,T}(\|\partial_{xz} v\|_{0,S_T} &+ \|\partial_{yz} v\|_{0,S_T} + h_1^{-1} h_{3,T} \|\partial_z^2 v\|_{0,S_T}), \end{aligned}$$

respectively.

Proof. Let $T \in \mathcal{T}_h$ be arbitrarily chosen. Estimate (5.21) is already given by (5.10). The proof of the remaining estimates are adaptions of the proof of Lemma 5 of [Bra06]. In this article, Braack considers bilinear transformations $\boldsymbol{F}_K : \widehat{K} \to K$, which can be represented as

$$\boldsymbol{F}_K \begin{pmatrix} \widehat{x} \\ \widehat{y} \end{pmatrix} = \begin{pmatrix} x_0 \\ y_0 \end{pmatrix} + \begin{pmatrix} \cos\theta & -\sin\theta \\ \sin\theta & \cos\theta \end{pmatrix} \left[\begin{pmatrix} 1 & s \\ 0 & 1 \end{pmatrix} \begin{pmatrix} h_1 & 0 \\ 0 & h_2 \end{pmatrix} \begin{pmatrix} \widehat{x} \\ \widehat{y} \end{pmatrix} + \begin{pmatrix} \alpha \widehat{x}\widehat{y} \\ \beta \widehat{x}\widehat{y} \end{pmatrix} \right] \quad (5.25)$$

with angle of rotation θ, shearing s bounded by $|s| \leq s_0$ and coefficients α, β of the pure bilinear parts fulfilling $|\alpha| \leq h_{1,T}/4$ and $|\beta| \leq \min\{h_{2,T}, h_{1,T}/s_0\}$. Note, that these upper bounds denote no serious restrictions in the case of isotropic meshes such as $\mathcal{K}_h$. Comparing this 2D transformation to the present tensor product type mesh cell transformations

$$\boldsymbol{F}_T(\widehat{\boldsymbol{x}}) = \boldsymbol{x}_0 + B\widehat{\boldsymbol{x}} \qquad \text{with } B = \begin{pmatrix} B_T & 0 \\ 0 & \pm h_3 \end{pmatrix},$$

see (5.7) we observe, that the transformation matrix B_T corresponds to the 2D mesh transformation as given by (5.25) but without considering the pure bilinear parts. In

the upcoming we adopt this representation for the horizontal transformation, noting that in our case $\alpha = \beta = 0$. Nevertheless we keep these constants in our considerations. Thus, the inverse of the entire transformation $\boldsymbol{F}_T$ is given by

$$\boldsymbol{F}_T^{-1}(\boldsymbol{x}) = -B^{-1}\boldsymbol{x}_0 + B^{-1}\boldsymbol{x} \qquad \text{with } B^{-1} = \begin{pmatrix} B_T^{-1} & 0 \\ 0 & \pm h_3^{-1} \end{pmatrix}$$

and

$$B_T^{-1} = \begin{pmatrix} \partial_{\widehat{x}}/\partial_x & \partial_{\widehat{x}}/\partial_y \\ \partial_{\widehat{y}}/\partial_x & \partial_{\widehat{y}}/\partial_y \end{pmatrix},$$

showing the following properties, collected from [Bra06]:

$$\begin{aligned} \partial_{\widehat{x}}/\partial_x &\sim h_{1,T}^{-1}, & \partial_{\widehat{y}}/\partial_y &\sim h_{2,T}^{-1}, \\ |\partial_{\widehat{y}}/\partial_x| &\leq h_{1,T}^{-1}, & |\partial_{\widehat{x}}/\partial_y| &\leq s_0 h_{1,T}^{-1} + h_{2,T}^{-1}. \end{aligned}$$

These relations and $|\partial_{\widehat{z}}/\partial_z| \sim h_3^{-1}$ can be used to deduce further for any $\varphi \in \mathrm{H}^1(S_T)$:

$$\begin{aligned} \|\partial_x\varphi\|_{0,S_T} &\lesssim |\det B^{-1}|^{-1/2} h_{1,T}^{-1} \left(\|\partial_{\widehat{x}}\widehat{\varphi}\|_{0,S_{\widehat{T}}} + \|\partial_{\widehat{y}}\widehat{\varphi}\|_{0,S_{\widehat{T}}}\right), \\ \|\partial_y\varphi\|_{0,S_T} &\lesssim |\det B^{-1}|^{-1/2} \left((s_0\, h_{1,T}^{-1} + h_{2,T}^{-1})\|\partial_{\widehat{x}}\widehat{\varphi}\|_{0,S_{\widehat{T}}} + h_{2,T}^{-1}\|\partial_{\widehat{y}}\widehat{\varphi}\|_{0,S_{\widehat{T}}}\right), \\ \|\partial_z\varphi\|_{0,S_T} &\lesssim |\det B^{-1}|^{-1/2} h_{3,T}^{-1}\|\partial_{\widehat{z}}\widehat{\varphi}\|_{0,S_{\widehat{T}}}, \end{aligned}$$

such that we can elaborate first upper bounds for the left hand sides of (5.22) – (5.24):

$$\|\partial_x(v - z^{(r)}v)\|_{0,S_T}^2 \lesssim |\det B|\, h_{1,T}^{-2} \left(\|\partial_{\widehat{x}}(\widehat{v} - \widehat{z^{(r)}v})\|_{0,S_{\widehat{T}}}^2 + \|\partial_{\widehat{y}}(\widehat{v} - \widehat{z^{(r)}v})\|_{0,S_{\widehat{T}}}^2\right), \quad (5.26)$$

$$\begin{aligned} \|\partial_y(v - z^{(r)}v)\|_{0,S_T}^2 \lesssim |\det B| \Big((s_0\, h_{1,T}^{-1} + h_{2,T}^{-1})^2\|\partial_{\widehat{x}}(\widehat{v} - \widehat{z^{(r)}v})\|_{0,S_{\widehat{T}}}^2 + \\ h_{2,T}^{-2}\|\partial_{\widehat{y}}(\widehat{v} - \widehat{z^{(r)}v})\|_{0,S_{\widehat{T}}}^2\Big), \end{aligned} \quad (5.27)$$

$$\|\partial_z(v - z^{(r)}v)\|_{0,S_T}^2 \lesssim |\det B|\, h_{3,T}^{-2}\|\partial_{\widehat{z}}(\widehat{v} - \widehat{z^{(r)}v})\|_{0,S_{\widehat{T}}}^2. \quad (5.28)$$

The resulting terms on the reference patch $\widehat{S}_T$ can be estimated by application of (5.10) on page 95:

$$\|\partial_{\widehat{x}}(\widehat{v} - \widehat{z^{(r)}v})\|_{0,S_{\widehat{T}}} \lesssim \|\partial_{\widehat{x}}\widehat{\nabla}\widehat{v}\|_{0,S_{\widehat{T}}} + \|\partial_{\widehat{y}}\widehat{\nabla}\widehat{v}\|_{0,S_{\widehat{T}}} + \|\partial_{\widehat{z}}\widehat{\nabla}\widehat{v}\|_{0,S_{\widehat{T}}}, \quad (5.29)$$

$$\|\partial_{\widehat{y}}(\widehat{v} - \widehat{z^{(r)}v})\|_{0,S_{\widehat{T}}} \lesssim \|\partial_{\widehat{x}}\widehat{\nabla}\widehat{v}\|_{0,S_{\widehat{T}}} + \|\partial_{\widehat{y}}\widehat{\nabla}\widehat{v}\|_{0,S_{\widehat{T}}} + \|\partial_{\widehat{z}}\widehat{\nabla}\widehat{v}\|_{0,S_{\widehat{T}}}, \quad (5.30)$$

$$\|\partial_{\widehat{z}}(\widehat{v} - \widehat{z^{(r)}v})\|_{0,S_{\widehat{T}}} \lesssim \|\partial_{\widehat{x}}\widehat{\nabla}\widehat{v}\|_{0,S_{\widehat{T}}} + \|\partial_{\widehat{y}}\widehat{\nabla}\widehat{v}\|_{0,S_{\widehat{T}}} + \|\partial_{\widehat{z}}\widehat{\nabla}\widehat{v}\|_{0,S_{\widehat{T}}}. \quad (5.31)$$

The latter estimate (5.31) can be improved, i.e. some terms on the right hand side of (5.31) are superfluous.

To validate this statement and to figure out, which terms can be deleted, we enter the proof (p. 110ff) of Theorem 3.2. in [Ape99], which again treats the case of the interpolation operator S_h choosing small sides and can be carried out for the present

operator, see also the proof of Theorem 3.3 in [Ape99]. For a given γ with $|\gamma| = 1$ and $v \in \mathrm{H}^2(S_{\widehat{T}})$ we thus have

$$\|\widehat{D}^\gamma(\widehat{v} - \widehat{z^{(r)}}\widehat{v})\|_{0,S_{\widehat{T}}} \;\leq\; \|\widehat{D}^\gamma(\widehat{v} - w)\|_{0,S_{\widehat{T}}} + \|\widehat{D}^\gamma \widehat{z^{(r)}}(w - \widehat{v})\|_{0,S_{\widehat{T}}}$$

for any constant w. Due to the argumentation (on the reference element) in p.118 in [Ape99] for the estimate (5.20), as well as for the horizontal cases, this estimate becomes

$$\begin{aligned}
\|\widehat{D}^\gamma(\widehat{v} - \widehat{z^{(r)}}\widehat{v})\|_{0,S_{\widehat{T}}} &\lesssim \|\widehat{D}^\gamma(\widehat{v} - w)\|_{0,S_{\widehat{T}}}\,, && \text{if } D^\gamma = \partial_z\,,\\
\|\widehat{D}^\gamma(\widehat{v} - \widehat{z^{(r)}}\widehat{v})\|_{0,S_{\widehat{T}}} &\lesssim \|\widehat{D}^\gamma(\widehat{v} - w)\|_{0,S_{\widehat{T}}} + \|\widehat{\nabla}(\widehat{v} - w)\|_{0,S_{\widehat{T}}}\,,\\
&\lesssim \|\widehat{\nabla}(\widehat{v} - w)\|_{0,S_{\widehat{T}}} && \text{else.}
\end{aligned}$$

The last term in the latter estimate can not be neglected due to the application of the trace theorem (3.21) of [Ape99] in the deduction of the appropriate estimates (see Lemma 3.2 on page 109 in [Ape99]).

Using the proof (see p.101) of Lemma 3.1 on page of [Ape99] we deduce further

$$\|\widehat{D}^\gamma(\widehat{v} - w)\|_{0,S_{\widehat{T}}} \;\lesssim\; \sum_{|\beta|=1} \|\widehat{D}^{\gamma+\beta}\widehat{v}\|_{0,S_{\widehat{T}}}\,.$$

Thus, we do not end up in an improvement of (5.29) – (5.30), but estimate (5.31) can be replaced by

$$\|\partial_{\widehat{z}}(\widehat{v} - \widehat{z^{(r)}}\widehat{v})\|_{0,\widehat{S}_T} \;\lesssim\; \|\partial_{\widehat{z}}\widehat{\nabla}\widehat{v}\|_{0,\widehat{S}_T}\,. \tag{5.32}$$

Now, it essentially remains to estimate the terms on the right hand sides of (5.29), (5.30) and (5.32), and to assemble the entire informations elaborated above. Therefore we collect the following estimates of the second derivatives. As also figured out in [Bra06] for the horizontal parts we observe the estimates:

$$\begin{aligned}
|\partial^2_{\widehat{x}}\widehat{v}| &\lesssim h^2_{1,T}\,|\partial^2_x v| \;+\; h_{1,T}\,h_{2,T}\,|\partial_{xy} v| \;+\; h^2_{2,T}\,|\partial^2_y v|\,,\\
|\partial_{\widehat{y}}\partial_{\widehat{x}}\widehat{v}| &= |\partial_{\widehat{y}}\partial_{\widehat{x}}\widehat{v}| \lesssim (s_0\,h_{2,T} + \alpha)\,h_{1,T}\,|\partial^2_x v| \;+\; (s_0\,h_{2,T} + \alpha)\,h_{2,T}\,|\partial_{xy} v| \;+\; h^2_{2,T}\,|\partial^2_y v|\,,\\
|\partial_{\widehat{z}}\partial_{\widehat{x}}\widehat{v}| &= |\partial_{\widehat{x}}\partial_{\widehat{z}}\widehat{v}| \lesssim h_{3,T}\,h_{1,T}\,|\partial_{xz} v| \;+\; h_{3,T}\,h_{2,T}\,|\partial_{yz} v|\,,\\
|\partial^2_{\widehat{y}}\widehat{v}| &\lesssim (s_0\,h_{2,T} + \alpha)^2\,|\partial^2_x v| \;+\; (s_0\,h_{2,T} + \alpha)\,h_{2,T}\,|\partial_{xy} v| \;+\; h^2_{2,T}\,|\partial^2_y v|\,,\\
|\partial_{\widehat{z}}\partial_{\widehat{y}}\widehat{v}| &= |\partial_{\widehat{y}}\partial_{\widehat{z}}\widehat{v}| \lesssim h_{3,T}\,(s_0\,h_{2,T} + \alpha)\,|\partial_{xz} v| \;+\; h_{3,T}\,h_{2,T}\,|\partial_{yz} v|\,,\\
|\partial^2_{\widehat{z}}\widehat{v}| &\lesssim h^2_{3,T}\,|\partial^2_z v|\,.
\end{aligned}$$

Assembling these estimates as well as using the limitations for α and $h_{2,T} \leq h_{1,T}$ we

get

$$\|\partial_{\widehat{x}}\widehat{\nabla}\widehat{v}\|_{0,\widehat{S}_T} \lesssim |\det B|^{-1/2}\left(h_{1,T}^2\,\|\partial_x^2 v\|_{0,S_T} + h_{1,T}\,h_{2,T}\,\|\partial_{xy}v\|_{0,S_T} + h_{2,T}^2\,\|\partial_y^2 v\|_{0,S_T} + h_{1,T}\,h_{3,T}\,\|\partial_{xz}v\|_{0,S_T} + h_{2,T}\,h_{3,T}\,\|\partial_{yz}v\|_{0,S_T}\right), \tag{5.33}$$

$$\|\partial_{\widehat{y}}\widehat{\nabla}\widehat{v}\|_{0,\widehat{S}_T} \lesssim |\det B|^{-1/2}\left(s_1\,h_{1,T}^2\,\|\partial_x^2 v\|_{0,S_T} + s_1\,h_{1,T}\,h_{2,T}\,\|\partial_{xy}v\|_{0,S_T} + h_{2,T}^2\,\|\partial_y^2 v\|_{0,S_T} + s_1\,h_{1,T}\,h_{3,T}\,\|\partial_{xz}v\|_{0,S_T} + h_{2,T}\,h_{3,T}\,\|\partial_{yz}v\|_{0,S_T}\right), \tag{5.34}$$

$$\|\partial_{\widehat{z}}\widehat{\nabla}\widehat{v}\|_{0,\widehat{S}_T} \lesssim |\det B|^{-1/2} h_{3,T}\left((h_{1,T} + s_0 h_{2,T})\|\partial_{xz}v\|_{0,S_T} + h_{2,T}\,\|\partial_{yz}v\|_{0,S_T} + h_{3,T}\,\|\partial_z^2 v\|_{0,S_T}\right). \tag{5.35}$$

Combining (5.26) – (5.35) and suitable upper bounding finally lead to the desired estimates. □

Corollary 5.13. *Let $\gamma = (\gamma_1, \gamma_2, \gamma_3)$ and $\widehat{\gamma} = (\gamma_1, \gamma_2, 0)$ be multi-indices. For vertical anisotropic meshes the results of Proposition 5.12 can also be described as*

$$\|\partial_x(v - z^{(r)}v)\|_{0,T} \lesssim h_\omega \sum_{|\widehat{\gamma}|=2} \|D^{\widehat{\gamma}}v\|_{0,S_T} + h_\omega^{-1}\,h_{3,T} \sum_{|\gamma|=1} \mathbf{h}_T^\gamma \|\partial_z D^\gamma v\|_{0,S_T}, \tag{5.36}$$

$$\|\partial_y(v - z^{(r)}v)\|_{0,T} \lesssim h_\omega \sum_{|\widehat{\gamma}|=2} \|D^{\widehat{\gamma}}v\|_{0,S_T} + h_\omega^{-1}\,h_{3,T} \sum_{|\gamma|=1} \mathbf{h}_T^\gamma \|\partial_z D^\gamma v\|_{0,S_T}, \tag{5.37}$$

$$\|\partial_z(v - z^{(r)}v)\|_{0,T} \lesssim \sum_{|\gamma|=1} \mathbf{h}_T^\gamma \|\partial_z D^\gamma v\|_{0,S_T}. \tag{5.38}$$

Remark 5.14. *Comparing the results of Proposition 5.12 we see, that the 3D Scott-Zhang interpolation operator maintains the results as introduced in [Bra06] as well in three dimensions.*

However, some further studies on the proofs of the propositions in [Ape99] reveal, that the estimates of Proposition 5.12 can be extended to the more common case of arbitrary polynomial order r of the underlying finite element space on tensor product type meshes. Due to our field of examination we restrict to the case of vertical anisotropic meshes.

Proposition 5.15. *Let $\mathcal{T}_h$ be a vertical anisotropic tensor product type mesh with cellwise transformations $\boldsymbol{F}_T$ fulfilling (5.7) and $h_{1,T} \geq h_{2,T} \geq h_{3,T}$. For any $T \in \mathcal{T}_h$, $v \in \mathrm{H}^{k+1}(S_T)$, $k \leq r$ and γ with $|\gamma| = 1$ the following estimates apply:*

$$\|D^\gamma(v - z^{(r)}v)\|_{0,T} \lesssim \mathbf{h}_T^{-\gamma} \sum_{|\alpha|\leq k+1} \mathbf{h}_T^\alpha \|D^\alpha\, \boldsymbol{v}\,\|_{0,S_T} \tag{5.39}$$

Proof. The proof uses the deductions of Lemma 3.5 in [Ape99], which are explicitely formulated in Lemmata 3.1 and 3.2 in [Ape99]. We first observe for any polynomial w of order $r-1$:

$$\|D^\gamma(v - z^{(r)}v)\|_{0,T} \leq \|D^\gamma(v - w)\|_{0,T} + \|D^\gamma z^{(r)}(v - w)\|_{0,T}.$$

Lemma 3.1 [Ape99] with $m = 0$ and $l = k + 1$ gives

$$\mathbf{h}_T^{\gamma} \|D^{\gamma}(v - w)\|_{0,T} \;\leq\; \sum_{|\alpha|=k+1} \mathbf{h}_T^{\alpha} |D^{\alpha} v|_{0,S_T}$$

for a suitably chosen w. Existence of such a polynomial is assured due to Lemma 3.1. Let $\gamma = (1, 0, 0)$ or $\gamma = (0, 1, 0)$. Then, the term $\|D^{\gamma} z^{(r)}(v - w)\|_{0,T}$ can be suitably estimated as in the proof of Lemma 3.2, which supplies the estimate

$$\|D^{\gamma} z^{(r)}(v - w)\|_{0,T} \;\leq\; \mathbf{h}_T^{-\gamma} \left(\|v - w\|_{0,S_T} + \sum_{|\alpha|=1} \mathbf{h}^{\alpha} \|D^{\alpha}(v - w)\|_{0,S_T} \right) .$$

Again, applicating the estimates of Lemma 3.1 [Ape99] and noting, that $\mathbf{h}^{\alpha} \leq \mathbf{h}^{\gamma}$ for any multi index α with $|\alpha| = 1$ we get

$$\|D^{\gamma} z^{(r)}(v - w)\|_{0,T} \;\lesssim\; \mathbf{h}_T^{-\gamma} \sum_{|\alpha|=k+1} \mathbf{h}_T^{\alpha} \|v\|_{0,S_T} .$$

For the first order vertical derivative it suffices to consider the estimate (5.10) for $l = k + 1$ and $m = 1$:

$$\|\partial_z(\boldsymbol{v} - z^{(r)}\, \boldsymbol{v})\|_{0,T} \;\lesssim\; \sum_{|\alpha|=k} \boldsymbol{h}_T^{\alpha} |D^{\alpha}\, \boldsymbol{v}\,|_{1,S_T} \;\lesssim\; h_{3,T}^{-1} \sum_{|\alpha|=k+1} \boldsymbol{h}_T^{\alpha} \|D^{\alpha}\, \boldsymbol{v}\,\|_{0,S_T} .$$

□

(c) L^2-orthogonal interpolation operator

In the case of local projection stabilization of the hydrostatic Oseen problem in the anisotropic framework, it pays to have an interpolation operator, which not only exhibits suitable interpolation error estimates and stability properties, but also is L^2-orthogonal with respect to a certain discrete space. Recall also Section 4.5.

Proposition 5.16. *Assuming a vertical anisotropic tensor product type triangulation $\mathcal{T}_h$ of Ω, such that the requirements of Subsection 5.1.1(b) for the Scott-Zhang interpolation operator are fulfilled. Let $0 \leq k \leq r$. Then, there is an interpolation operator $i_{h,3d} : \mathbf{V} \to \mathbf{V}_h$ such that*

$$(\boldsymbol{v} - i_{h,3d}\, \boldsymbol{v}, \xi)_{\Omega} \;=\; 0 \qquad\qquad \forall\, \boldsymbol{v} \in \mathbf{V}\,, \forall \xi \in Q_{2h}^{r-1}(\Omega)\,, \tag{5.40}$$

Moreover, for any $\boldsymbol{v} \in \mathbf{V}$ and arbitrary $T \in \mathcal{T}_h$ the following estimates apply:

$$\|\partial_x i_{h,3d}\, \boldsymbol{v}\,\|_{0,T} + \|\partial_y i_{h,3d}\, \boldsymbol{v}\,\|_{0,T} \;\lesssim\; h_{\omega}^{-1} \sum_{|\alpha|=1} \mathbf{h}_T^{\alpha} \|D^{\alpha}\, \boldsymbol{v}\,\|_{0,S_T} \tag{5.41}$$

$$\|\partial_z i_{h,3d}\, \boldsymbol{v}\,\|_{0,T} \;\lesssim\; h_{3,T}^{-1} \sum_{|\alpha|=1} \mathbf{h}_T^{\alpha} \|D^{\alpha}\, \boldsymbol{v}\,\|_{0,S_T} . \tag{5.42}$$

The horizontal mesh size of the isotropic mesh $\mathcal{K}_h$ is given globally, i.e. by h_ω. For any $\boldsymbol{v} \in \mathbf{H}^{k+1}(\Omega)$ and $T \in \mathcal{T}_h$ the interpolation operator $i_{h,3d}$ fulfills

$$\| \boldsymbol{v} - i_{h,3d}\, \boldsymbol{v} \|_{0,T} + \sum_{|\gamma|=1} \mathbf{h}_T^{\gamma} \| D^{\gamma}(\boldsymbol{v} - i_{h,3d}\, \boldsymbol{v}) \|_{0,T} \lesssim \sum_{|\alpha|=k+1} \mathbf{h}_T^{\alpha} \| D^{\alpha}\, \boldsymbol{v} \|_{0,S_T} . \tag{5.43}$$

Proof. The proof is an adaption the proof of the isotropic version as given in Lemma 4.5 of [BB06] to the vertical anisotropic case. The operator $i_{h,3d} : \mathbf{V} \to \mathbf{V}_h$ is constructed as $i_{h,3d} = z^{(r)} + m_h$, with the anisotropic Scott-Zhang interpolant $z^{(r)}$ as introduced in Section 5.1.2(b). Due to (5.10), the operator $z^{(r)}$ fulfills the estimate (5.43). Moreover (5.41) and (5.42) apply for $z^{(r)}$, due to (5.18) –(5.20).

But the orthogonality property (5.40) is not assured, which has to be realized by the involvement of m_h. Operator m_h denotes the local projection from $\mathbf{V}$ onto $\mathbf{V}_h$ and is uniquely defined via

$$(m_h\, \boldsymbol{v}, \xi)_M \quad = \quad (\boldsymbol{v} - z^{(r)}\, \boldsymbol{v}, \xi)_M \qquad \forall \xi \in Q_{2h}^{r-1}(M) \,, \forall M \in \mathcal{T}_{2h} \,. \tag{5.44}$$

Thus, $i_{h,3d}$ fulfills the orthogonality property (5.40). To reassure properties (5.41) – (5.43) note that due to (5.44) and the inverse estimate $\| D^{\gamma}\, \boldsymbol{v}_h \|_{0,T} \leq \mathbf{h}_T^{-\gamma} \| \boldsymbol{v}_h \|_{0,T}$ for any $T \in \mathcal{T}_h$ and multi index γ with $|\gamma| = 1$, see Lemma 5.6 and Remark 5.7, the estimates

$$\begin{aligned} \| m_h\, \boldsymbol{v} \|_{0,T}^2 \quad &= \quad \int_T (\boldsymbol{v} - z^{(r)}\, \boldsymbol{v}) m_h\, \boldsymbol{v}\; dx \qquad \lesssim \quad \| \boldsymbol{v} - z^{(r)}\, \boldsymbol{v} \|_{0,T} \| m_h\, \boldsymbol{v} \|_{0,T} \,, \\ \| D^{\gamma} m_h\, \boldsymbol{v} \|_{0,T}^2 \quad &\leq \quad \mathbf{h}_T^{-2\gamma} \| m_h\, \boldsymbol{v} \|_{0,T}^2 \qquad \lesssim \quad \mathbf{h}_T^{-2\gamma} \| \boldsymbol{v} - z^{(r)}\, \boldsymbol{v} \|_{0,T} \| m_h\, \boldsymbol{v} \|_{0,T} \end{aligned}$$

apply. Using the estimate of $\| m_h\, \boldsymbol{v} \|_{0,T}$, the term $\| D^{\gamma} m_h\, \boldsymbol{v} \|_{0,T}$ can be further estimated as

$$\| D^{\gamma} m_h\, \boldsymbol{v} \|_{0,T} \quad \leq \quad \mathbf{h}_T^{-\gamma} \| \boldsymbol{v} - z^{(r)}\, \boldsymbol{v} \|_{0,T} \quad \leq \quad \mathbf{h}_T^{-\gamma} \sum_{|\alpha|=k+1} h_{\omega}^{\alpha_1+\alpha_2}\, h_{3,T}^{\alpha_3} \| D^{\alpha}\, \boldsymbol{v} \|_{0,T} \,.$$

Due to (5.10) and Proposition 5.15, $z^{(r)}$ provides property (5.43), and this estimate is fulfilled for the entire interpolation operator. The remaining estimates (5.41) and (5.42) for the common case are assured due to the improved inverse estimate, see Remark 5.7, the estimate

$$\| D^{\gamma} m_h\, \boldsymbol{v} \|_{0,T}^2 \;\lesssim\; \mathbf{h}_T^{-2\gamma} \| m_h\, \boldsymbol{v} \|_{0,T}^2 \;\lesssim\; \mathbf{h}_T^{-2\gamma} \| \boldsymbol{v} - z^{(r)}\, \boldsymbol{v} \|_{0,T}^2$$

for any $T \in \mathcal{T}_h$ and multi-index γ with $|\gamma| = 1$, as well as the observation

$$\| D^{\gamma}(i_{h,3d}\, \boldsymbol{v}) \|_{0,T} \leq \| D^{\gamma}(z^{(r)}\, \boldsymbol{v}) \|_{0,T} + \| D^{\gamma}(m_h\, \boldsymbol{v}) \|_{0,T} \,.$$

□

Remark 5.17. *Note, that the estimates (5.41) and (5.42) (for arbitrary r on vertical anisotropic tensor product type meshes) correspond to the results of the* L^2*-orthogonal*

2D interpolation operator of [Bra08a] on Cartesian meshes for $r = 1$. The L^2-estimate in (5.43) can be coarsened to

$$\| \boldsymbol{v} - i_{h,3d}\, \boldsymbol{v} \|_{0,T} \lesssim h_\omega^2 \left(\| \partial_x \nabla \boldsymbol{v} \|_{0,S_T} + \| \partial_y \nabla \boldsymbol{v} \|_{0,S_T} \right) + h_{3,T}^2 \| \partial_z \nabla \boldsymbol{v} \|_{0,S_T} ,$$

which corresponds to the appropriate L^2-estimate of [Bra08a] on 2D Cartesian meshes for $r = 1$. The same argumentation applies for the estimate of the first order derivatives.

5.1.3 Hydrostatic Issues

Discrete averaging operator on anisotropic meshes

The deductions and results of Subsection 4.1.3 on the discrete averaging operator are unaffected by the application of anisotropic meshes.

Discrete modified inf-sup constraint on anisotropic meshes

Let us recall the considerations of Section 4.1.3 on the discrete modified inf-sup constraint. Given the discrete 3D velocity space $\mathbf{V}_h \subset \mathbf{V}$ with $\mathbf{V} := \mathbf{H}_0^1(\Omega)$ or $\mathbf{V} := \mathbf{W}_b^{1,p}(\Omega)$, chosen with respect to the underlying problem, and the discrete 2D pressure space $Q_h \subset Q$ with $Q := \mathrm{L}_0^2(\omega)$ or $Q := \mathrm{L}_0^q(\omega)$, respectively, the discrete modified inf-sup constraint is given by

$$\exists \gamma > 0 \qquad \sup_{\boldsymbol{v}_h \in \mathbf{V}_h \setminus \{\mathbf{0}\}} \frac{(\mathrm{div}'\, \mathbf{M}\, \boldsymbol{v}_h, q_h)_\Omega}{\| \boldsymbol{v}_h \|_{1,p,\Omega}} \geq \gamma \| q_h \|_{0,q,\omega} \qquad \forall q_h \in Q_h \,. \tag{5.45}$$

Proposition 5.18. *The statements in Proposition 4.5 carry over to the case, when* vertical anisotropic *or* horizontal anisotropic *meshes are applied.*

Proof. As the results of the discrete averaging operator $\mathbf{M} : \mathbf{V}_h \to \mathbf{W}_h$ are unaffected when anisotropic meshes are applied, the proof can directly be adapted from the isotropic case to the cases of vertical and horizontal anisotropic meshes. □

Recalling the notions *vertical anisotropic* and *horizontal anisotropic meshes*, as well as Proposition 5.18, we observe the following:

(a) If the underlying 3D mesh $\mathcal{T}_h$ is *vertical anisotropic*, then the appropriate 2D problem is defined on a 2D *isotropic* mesh $\mathcal{K}_h$. For those meshes we already know that e.g. equal-order finite elements are not suggestible without any further stabilization on the pressure.

(b) If the underlying 3D mesh is *horizontal anisotropic*, i.e. the 2D surface mesh is *anisotropic*, we have to fall back on hydrostatic finite element spaces $\mathbf{V}_h$ and Q_h, such that $\mathbf{W}_h := \mathbf{M}(\mathbf{V}_h)$ and Q_h are 2D inf-sup stable on *anisotropic* meshes.

In the framework of conforming finite elements, the authors of [AR01] presented an overview of inf-sup stable pairs in the anisotropic context. We give some notes on the inf-sup stability results of [Bec95] and give an account of the survey in [AR01]:

Becker in [Bec95] validated inf-sup stability for stabilized elements $Q_1 - Q_0$ and $Q_1 - Q_1$, where he added suitably anisotropically adapted pressure stabilization terms of continuous interior penalty type (see also (P-iii) on page 58 for the isotropic case) and of type (P-i) to the 2D Stokes problem. Moreover note, that Becker paves the way for the LPS approach in an anisotropic framework on Q_1 elements using L^2 projection on the constants. The LPS approach for bilinear elements on 2D finally was proposed in [Ric05]. In [SS98, SSS99], Schötzau, Schwab and Stenberg examined the elements $Q_r - Q_{r-2}$ and $P_r - P_{r-2}$, $r \geq 2$. It turned out, that that this approach is aspect ratio independent inf-sup stable on 2D Cartesian meshes with thin layers along 2 opposite sides. Problems are supposed to arise near corners. The authors of [AC00] validated for the 2D case for the finite element space choice $Q_{r+\max\{\mu r,1\},r} - P_{r-1}$ for arbitrary but fix μ, that the inf-sup constant is bounded away from zero and independent on the aspect ratio. In this case, the inf-sup constant depends on μ. Aspect ratio independent inf-sup stability for the 3D case for $Q_r - Q_{r-2}$ elements on meshes with refinements towards faces has been proven by [TS01]. Apel and Randrianarivony figure out, that $Q_r - Q_{r-2}$ and the Taylor–Hood pair $P_2 - P_1$ is (experimentally) inf-sup stable on layered meshes, which is not the rule for arbitrary anisotropic meshes. Moreover, the mini element is observed to be not inf-sup stable.

5.2 Hydrostatic Stokes problem on vertical anisotropic meshes

In this section we consider the hydrostatic Stokes problem in the vertical anisotropic framework. We start with a stability analysis of the Galerkin formulation of the problem on vertical anisotropic meshes. As in the isotropic case it turns out, that the equal-order finite element approach we use does not lead to an inf-sup stable problem. Motivated by this lack, we consider the symmetric stabilization schemes (P-i) – (P-iv) of the isotropic hydrostatic Stokes problem in the vertical anisotropic framework. We elaborate stability and optimal error estimates of the stabilized problem. Finally we compare the results with the results of the appropriate isotropic problem and with some results given in literature for the anisotropic 2D Stokes problem.

5.2.1 Galerkin formulation

Let $\mathcal{T}_h$ be a vertical anisotropic triangulation fulfilling Assumption 4.2. Based on this mesh we define the discrete velocity space $\mathbf{V}_h \subset \mathbf{V} := \mathbf{H}_0^1(\Omega)$ and the pressure space $Q_h \subset Q := \mathrm{L}_0^2(\omega)$ as given in (4.6) and (4.4), and set $\mathbf{X}_h := \mathbf{V}_h \times Q_h$. As in the case of

isotropic meshes the hydrostatic Stokes problem reads

$$\begin{aligned} &\textit{Given } \boldsymbol{f} \in \mathbf{V}^{-1}, \textit{ find } (\boldsymbol{v}_h, p_h) \in \mathbf{X}_h \\ &\quad \textit{s. t. } \mathrm{a}(\boldsymbol{v}_h, \boldsymbol{\varphi}) - \mathrm{b}(p_h, \boldsymbol{\varphi}) + \mathrm{b}(\xi, \boldsymbol{v}_h) \;=\; (\boldsymbol{f}, \boldsymbol{\varphi})_\Omega \qquad \forall (\boldsymbol{\varphi}, \xi) \in \mathbf{X}_h \end{aligned} \tag{5.46}$$

with bilinear forms $\mathrm{a}(\boldsymbol{v}_h, \boldsymbol{\varphi}) \;:=\; (\nabla \boldsymbol{v}_h, \nabla \boldsymbol{\varphi})_\Omega$ and $\mathrm{b}(p_h, \boldsymbol{\varphi}) \;:=\; (p_h, \operatorname{div}' \mathbf{M} \boldsymbol{\varphi})_\omega$.

As indicated in the preceding subsection (see note (a) on page 104) the elaborated properties for the hydrostatic Stokes problem on isotropic meshes are recovered in the case of vertical anisotropic meshes:

Proposition 5.19. *Let Ω be a flat domain and $\mathcal{T}_h$ be a vertical anisotropic triangulation of Ω fulfilling Assumption 4.2. The 2.5D Stokes problem (5.46) has a unique solution, if the 2D Stokes problem (4.18) has a unique solution.*

Proof. We argue as in the proof of Proposition 4.15. First, the continuous bilinear form $\mathrm{a} : \mathbf{V} \times \mathbf{V} \to \mathbb{R}$ is still $\mathbf{V}$-elliptic, and we still have conforming finite elements, i.e. $\mathbf{V}_h \subset \mathbf{V}$. Moreover, due to Proposition 5.18, the 2.5D problem (5.46) fulfills the discrete modified inf-sup condition (5.45), if the appropriate inf-sup condition (4.17) of the 2D Stokes problem is fulfilled. □

Due to consideration (a) on page 104, the equal-order finite element discretized hydrostatic Stokes problem (5.46) on vertical anisotropic meshes is not inf-sup stable. As introduced for the case of isotropic meshes we avoid this problem by adding suitable stabilization terms to the system.

Remark 5.20. *Anticipatory we note, that the discrete hydrostatic Stokes problem in the vertical anisotropic context, i.e. problem (5.46), is formulated for a large class of triangulations (and domains).*
In order to derive suitable error estimates we split the entire error into an interpolation and a projection error. Restrictively, suitable interpolation results, see also Section 5.1.2, are only known (to the author) for a quite small class of triangulations (and thus of Ω).

5.2.2 Stabilization of the problem

As the inf-sup stability is a 2D concern, the solely pressure dependent stabilization schemes for the hydrostatic Stokes case on isotropic meshes are expected to be easily adaptable. The deductions and estimates *concerning the pressure* are anticipated to be transferable in a straightforward matter. The *velocity field concerning* parts however are expected to need some altered treatment as this field is defined on an anisotropic mesh, unlike the 2D pressure.
The appropriately stabilized 2.5D Stokes problem is given as in the isotropic case:

$$\begin{aligned} &\textit{Find } (\boldsymbol{v}_h, p_h) \in \mathbf{X}_h \textit{ s. t.} \\ &\qquad A_h(\boldsymbol{v}_h, p_h; \boldsymbol{\varphi}, \xi) \;=\; (\boldsymbol{f}, \boldsymbol{\phi})_\Omega \qquad \forall\, \boldsymbol{\phi} := (\boldsymbol{\varphi}, \xi) \in \mathbf{X}_h \end{aligned} \tag{5.47}$$

$$\textit{with } A_h(\boldsymbol{v}_h, p_h; \boldsymbol{\varphi}, \xi) \;:=\; a(\boldsymbol{v}_h, \boldsymbol{\varphi}) - b(p_h, \boldsymbol{\varphi}) + b(\xi, \boldsymbol{v}_h) + s_h(p_h, \xi)\,. \tag{5.48}$$

The applied stability term is chosen from the list (P-i) – (P-iv) of Section 4.2.2.

We define the triple norm on $\mathbf{X}_h$ as in (4.36),

$$|\!|\!|(\boldsymbol{v},p)|\!|\!| := \left(\|\nabla\,\boldsymbol{v}\,\|_{0,\Omega}^2 + \|p\|_{0,\omega}^2 + s_h(p,p)\right)^{1/2}\,, \tag{5.49}$$

as well as B_h:

$$B_h \;:=\; \{(\boldsymbol{v}_h,p_h)\in\mathbf{X}_h \mid |\!|\!|(\boldsymbol{v}_h,p_h)|\!|\!| = 1\}\,.$$

The following proposition shows that adding an arbitrary stabilization term of the methods (P-i)–(P-iv) leads to an inf-sup stable discretization of the 2.5D Stokes problem on vertical anisotropic meshes.

Proposition 5.21. *Let Ω be a flat basin and $\mathcal{T}_h$ be a vertical anisotropic triangulation of Ω fulfilling Assumption 4.2. We consider the symmetric stabilizations (P-i)–(P-iv) of Section 4.2.2. The resulting 2.5D Stokes bilinear form (5.48) is also inf-sup stable:*

$$\inf_{(\boldsymbol{v}_h,p_h)\in B_h}\;\sup_{(\boldsymbol{\varphi},\xi)\in B_h} A_h(\boldsymbol{v}_h,p_h;\boldsymbol{\varphi},\xi) \;\geq\; \gamma_{\Omega,\omega}\,.$$

Proof. The proof can be accomplished as the proof of Proposition 4.18. We collect the corner stones of that proof which are relevant for the present class of stabilizations:
Let $\boldsymbol{y}_h := (\boldsymbol{v}_h,p_h)\in\mathbf{X}_h$ be arbitrarily chosen. Splitting the triple norm into two parts

$$\begin{aligned} |\!|\!|\boldsymbol{y}_h|\!|\!|^2 &= |\boldsymbol{y}_h|_a^2 + |\boldsymbol{y}_h|_b^2\,,\\ |\boldsymbol{y}_h|_a^2 &:= |\,\boldsymbol{v}_h\,|_{1,\Omega}^2 + s_h(p_h,p_h)\,,\\ |\boldsymbol{y}_h|_b^2 &:= \|p_h\|_{0,\omega}^2\,, \end{aligned}$$

and diagonal testing of the bilinear form (5.48) gives $A_h(\boldsymbol{y}_h;\boldsymbol{y}_h) = |\boldsymbol{y}_h|_a^2$. The inf-sup condition follows if a $\widetilde{\boldsymbol{v}}_h\in\mathbf{V}_h$ exists such that $|\!|\!|(\widetilde{\boldsymbol{v}}_h,0)|\!|\!| \leq |\!|\!|\boldsymbol{y}_h|\!|\!|$ and

$$A_h(\boldsymbol{v}_h,p_h;\widetilde{\boldsymbol{v}}_h,0) \;\geq\; c_1|\,\mathbf{u}_h\,|_b^2 - c_2|\,\mathbf{u}_h\,|_a^2\,,$$

with suitable constants $c_1>0$ and c_2. In order to find such $\widetilde{\boldsymbol{v}}_h\in\mathbf{V}_h$ let $\boldsymbol{\varphi}\in\mathbf{W}_h$ be chosen, so that $(\boldsymbol{\varphi},p_h)$ satisfies estimate (4.28). Using the surjectivity of $\mathbf{M}$ (Lemma 4.4) we choose a $\widetilde{\boldsymbol{v}}_h\in\mathbf{V}_h$ with $\boldsymbol{\varphi} = \mathbf{M}\,\widetilde{\boldsymbol{v}}_h$, such that we can apply Lemma 4.8.
Thus, the crucial argumentation passes on to a 2D argumentation on an *isotropic* mesh and we can further argue as in the proof of Proposition 4.18: With $\boldsymbol{w}_h := \mathbf{M}\,\boldsymbol{v}_h\in\mathbf{W}_h$ and due to Lemma 4.8 we obtain

$$\begin{aligned} A_h(\boldsymbol{y}_h;\widetilde{\boldsymbol{v}}_h,0) =\;& (\nabla\,\boldsymbol{v}_h,\nabla\widetilde{\boldsymbol{v}}_h)_\Omega - (p_h,\mathrm{div}'\,\boldsymbol{w}_h)_\omega + s_h(p_h;0)\\ \geq\;& -|\,\boldsymbol{v}_h\,|_{1,\Omega}|\widetilde{\boldsymbol{v}}_h|_{1,\Omega} + \frac{\gamma_\omega}{4}\|p_h\|_{0,\omega}^2 - \frac{1}{\gamma_\omega}s_h(p_h,p_h)\\ \geq\;& -\left(\frac{4}{\gamma_\omega}c_\omega^2\delta_{min}^{-3}|\,\boldsymbol{v}_h\,|_{1,\Omega}^2 + \frac{\gamma_\omega}{16}\|p_h\|_{0,\omega}^2\right) + \frac{\gamma_\omega}{4}\|p_h\|_{0,\omega}^2 - \frac{1}{\gamma_\omega}s_h(p_h,p_h)\\ \geq\;& -\frac{c}{\gamma_\omega}c_\omega^2\delta_{min}^{-3}|\,\boldsymbol{v}_h\,|_{1,\Omega}^2 + \frac{\gamma_\omega}{8}\|p_h\|_{0,\omega}^2 - \frac{1}{\gamma_\omega}s_h(p_h,p_h)\\ \geq\;& -\frac{1}{\gamma_\omega}\left(1+cc_\omega^2\delta_{min}^{-3}\right)|\boldsymbol{y}_h|_a^2 + \frac{\gamma_\omega}{8}|\boldsymbol{y}_h|_b^2\,. \end{aligned}$$

□

5.2.3 *A priori* error estimates

The deduction of *a priori* error estimates for the stabilized 2.5D Stokes problem is based on the estimates of the stabilization terms for the 2D Stokes problem. As in the isotropic case, the (perturbed) 2D Galerkin orthogonality,

$$A_h^\omega(\boldsymbol{w}-\boldsymbol{w}_h, p-p_h; \boldsymbol{\varphi}, \xi) \;=\; s_h(p,\xi) \qquad \forall (\boldsymbol{\varphi},\xi) \in \mathbf{W}_h \times Q_h\,,$$

plays a crucial role in the derivation of suitable error estimates.

Proposition 5.22. *Let Ω be chosen such that there is a vertical anisotropic triangulation $\mathcal{T}_h$ of Ω, fulfilling the restrictions of Subsection 5.1.1(b). If the continuous solution of (4.32) formulated in $\mathbf{X} := (\mathbf{V} \times Q)$ is sufficiently regular, $(\boldsymbol{v}, p) \in \mathbf{H}^{r+1}(\Omega) \times \mathrm{H}^r(\omega)$, we obtain the following estimate for the discrete solutions $(\boldsymbol{v}_h, p_h)$ of (5.47) for the methods (P-i)–(P-iv):*

$$|\!|\!|(\boldsymbol{v}-\boldsymbol{v}_h, p-p_h)|\!|\!| \;\lesssim\; \sum_{T\in\mathcal{T}_h} \sum_{|\alpha|=r} \mathbf{h}_T^\alpha \; |D^\alpha \boldsymbol{v}\,|_{1,S_T} + \sum_{K\in\mathcal{K}_h} h_K^r \, \|p\|_{r,S_K} \tag{5.50}$$

with patches S_T and S_K for any $T \in \mathcal{T}_h$ and $K \in \mathcal{K}_h$.

Proof. As usual we split the error into an interpolation error and a projection error. Note that the pressure is defined on an isotropic mesh. Let $z_h p$ be the Scott-Zhang interpolant as given in the isotropic case, and $\boldsymbol{z}_h\,\boldsymbol{v}$ be the Scott-Zhang interpolant for anisotropic meshes of tensor product type as introduced in Subsection 5.1.2. (Note that the latter interpolation operator is responsible for the restrictive choice of $\mathcal{T}_h$.) With these interpolants and Lemma 4.12 we already get estimate (5.50) for $|\!|\!|(\boldsymbol{v}-\boldsymbol{z}_h\,\boldsymbol{v}_h, p - z_h p_h)|\!|\!|$.

Thus it remains to bound the projection errors $\|\boldsymbol{z}_h\,\boldsymbol{v}-\boldsymbol{v}_h\,\|_{1,\Omega}$ and $\|z_h p - p_h\|_{0,\omega}$ by the right hand side of (5.50). Due to the discrete inf-sup condition there is a test function $(\boldsymbol{\varphi},\xi) \in \mathbf{X}_h$ with $|\!|\!|(\boldsymbol{\varphi},\xi)|\!|\!| = 1$ and

$$\gamma_{\Omega,\omega}|\!|\!|(\boldsymbol{z}_h\,\boldsymbol{v}-\boldsymbol{v}_h, z_h p - p_h)|\!|\!| \;\le\; A_h(\boldsymbol{z}_h\,\boldsymbol{v}-\boldsymbol{v}_h, z_h p - p_h; \boldsymbol{\varphi},\xi)\,.$$

Using the (perturbed) Galerkin orthogonality we obtain

$$\begin{aligned}\gamma_{\Omega,\omega}|\!|\!|(\boldsymbol{z}_h\,\boldsymbol{v}-\boldsymbol{v}_h, z_h p - p_h)|\!|\!| \;&\le\; A_h(\boldsymbol{z}_h\,\boldsymbol{v}-\boldsymbol{v}, z_h p - p; \boldsymbol{\varphi},\xi) + s_h(p,\xi)\\ &=\; \mathrm{a}(\boldsymbol{z}_h\,\boldsymbol{v}-\boldsymbol{v}, \boldsymbol{\varphi}) - \mathrm{b}(z_h p - p, \boldsymbol{\varphi})\\ &\qquad + \mathrm{b}(\xi, \boldsymbol{z}_h\,\boldsymbol{v}-\boldsymbol{v}) - s_h(z_h p, \xi)\,.\end{aligned}$$

The Galerkin terms on the right hand side can be bounded by

$$\begin{aligned}\mathrm{a}(\boldsymbol{z}_h\,\boldsymbol{v}-\boldsymbol{v}, \boldsymbol{\varphi}) \;&\le\; |\boldsymbol{z}_h\,\boldsymbol{v}-\boldsymbol{v}\,|_{1,\Omega}|\!|\!|(\boldsymbol{\varphi},0)|\!|\!| \;\le\; c\sum_{T\in\mathcal{T}_h}\sum_{|\alpha|=r} \mathbf{h}_T^\alpha |D^\alpha \boldsymbol{v}\,|_{1,S_T}\\ -\mathrm{b}(z_h p - p, \boldsymbol{\varphi}) \;&\le\; \|z_h p - p\|_{0,\omega}|\!|\!|(\boldsymbol{\varphi},0)|\!|\!| \;\le\; c h_\omega^r \|p\|_{r,\omega}\\ \mathrm{b}(\xi, \boldsymbol{z}_h\,\boldsymbol{v}-\boldsymbol{v}) \;&\le\; \|\mathrm{div}'\,\mathbf{M}(\boldsymbol{z}_h\,\boldsymbol{v}-\boldsymbol{v})\|_{\mathbf{0},\omega}|\!|\!|(0,\xi)|\!|\!| \;\le\; c_\omega \sum_{T\in\mathcal{T}_h}\sum_{|\alpha|=r} \mathbf{h}_T^\alpha |D^\alpha \boldsymbol{v}\,|_{1,S_T}\,.\end{aligned}$$

The stabilization term is 2D. Particularly it is defined on an isotropic mesh, and can be bounded as in the proof of Proposition 4.21 by

$$s_h(z_h p, \xi) \quad \leq \quad c h_\omega^r \|p\|_{r,\omega} \,,$$

see page 71. In sum we arrive at the following estimate which implies the assertion:

$$\gamma_{\Omega,\omega} |\!|\!| (\boldsymbol{z}_h \boldsymbol{v} - \boldsymbol{v}_h, z_h p - p_h) |\!|\!| \quad \lesssim \quad h_\omega^r \|p\|_{r,\omega} + \sum_{|\alpha|=r} \mathbf{h}_T^\alpha |D^\alpha \boldsymbol{v}|_{1,S_T} \,.$$

□

In the proof of Proposition 5.22 we used the anisotropic Scott-Zhang interpolation operator for the velocity, which forced us to restrict to tensor product type meshes. A relaxation of this constraint is given by the anisotropic Lagrangian interpolation operator, which has the lack of higher regularity demands on the solution of the problem:

Proposition 5.23. *Let $\mathcal{T}_h$ be a vertical anisotropic triangulation of Ω fulfilling Assumption 4.2 and the demands of Subsection 5.1.1(a). If the continuous solution of (4.32) formulated in $\mathbf{X} := (\mathbf{V} \times Q)$ is sufficiently regular, $(\boldsymbol{v}, p) \in \mathbf{H}^{r+2}(\Omega) \times \mathrm{H}^r(\omega)$, we obtain the following estimate for the discrete solutions $(\boldsymbol{v}_h, p_h)$ of (5.47) with stabilization scheme chosen from (P-i)–(P-iv):*

$$|\!|\!| (\boldsymbol{v} - \boldsymbol{v}_h, p - p_h) |\!|\!| \lesssim \sum_{T \in \mathcal{T}_h} \sum_{|\alpha|=r} \mathbf{h}_T^\alpha \, |D^\alpha \boldsymbol{v}|_{1,S_T} + h_\omega^r \, \|p\|_{r,\omega} \,, \tag{5.51}$$

with meshsize independent constant c.

Proof. The proof is the same as the proof of Proposition 5.22 with the difference, that we now apply the anisotropic Lagrangian interpolation operator. For the appropriate regularity constraints and differing estimates see Subsection 5.1.2(a). □

Remark 5.24. *Let $r \geq 1$. For ease of an upcoming comparison with appropriate results given in literature, the estimates of Propositions 5.22 and 5.23 can easily be reformulated as*

$$\begin{aligned} |\!|\!| (\boldsymbol{v} - \boldsymbol{v}_h, p - p_h) |\!|\!| \lesssim \quad \sum_{T \in \mathcal{T}_h} \Bigg(& h_{1,T} \sum_{|\alpha|=r-1} \mathbf{h}_T^\alpha \, |\partial_x D^\alpha \boldsymbol{v}|_{1,S_T} + h_{2,T} \sum_{|\alpha|=r-1} \mathbf{h}_T^\alpha \, |\partial_y D^\alpha \boldsymbol{v}|_{1,S_T} \\ & + h_{3,T} \sum_{|\alpha|=r-1} \mathbf{h}_T^\alpha \, |\partial_z D^\alpha \boldsymbol{v}|_{1,S_T} \Bigg) + h_\omega^r \, \|p\|_{r,\omega} \,. \end{aligned}$$

5.2.4 Conclusions

Application of the symmetric pressure stabilization applied in the isotropic case also leads to stabilization of the hydrostatic Stokes problem in the vertical anisotropic framework. The reason is the isotropic structure of $\mathcal{K}_h$ and the fact, that the pressure

is defined on that 2D mesh.
Comparing the present results to the isotropic case we end up in similar *a priori* error estimates. But, in the anisotropic framework we are able to account for the anisotropy of the mesh and get suitably weighted results. However, the price to be paid is either the restriction on the mesh and on the underlying domain, or weaker restrictions on the mesh than in the former (Scott-Zhang) case but higher regularity demands for the solution of the variational problem.

Comparing the present results to the results of the anisotropic 2D Stokes problem, see e.g. [Bec95, MPP02, BT06a, AM08, Bla08], we observe the following: The most conspicuous difference to the anisotropic 2D Stokes problem is, that we do *not* have to alter the stabilization of the scheme, neither the scheme itself nor the stabilization parameters, although the mesh shows (certain) anisotropic behavior. This is owed to the fact, that the (hydrostatic) pressure is only 2D and lives on an isotropic mesh. This enables the successful application of appropriate symmetric stabilizations in the vertical anisotropic framework, and a choice of the polynomial degree r as in the isotropic framework.
Comparing the present results with the results of the non conforming approach the authors of [AM08] (for the 2D Stokes problem) we get similar estimates but without catching an additional term due to the non conformity. Moreover, the results in [AM08] apply for suitably constructed, inf-sup stable finite element spaces of order $r \geq 3$ for the velocity and pressure finite element spaces of order $r-1$ on rectangular triangulations. I.e. the authors do not have to apply an extra stabilization to the scheme, but have rather costly finite elements.
The authors of [MPP02, Bla08] apply the residual-based approach of GLS stabilization, in which the overall shape of the stabilization does not alter from its isotropic counterpart, but the stabilization parameters are set in order to account for the anisotropy. The results (for $\mathrm{H}^2 - \mathrm{H}^1$ regularity of the solution) are comparable to the results we derived above.
Similar results for $\mathrm{H}^2 - \mathrm{H}^1$ regular solutions of the Stokes problem in 2D were elaborated in [Bec95] for symmetric pressure stabilization on meshes with rectangular elements and [BT06a] for local projection stabilization on parallelograms.

Concluding, we elaborated *a priori* error estimates of similar quality as to be found in literature for the 2D Stokes problem. However, the structure of the hydrostatic problem on vertical anisotropic meshes enables the application of the Lagrangian interpolation operator for which approximation properties are available not only on parallelograms and rectangular elements, but also on quadrilaterals and hexahedrals, which are (slight) deviances from rectangular and brick elements. Moreover, the analytical approach of the hydrostatic Stokes problem for different choices of finite element spaces is quite comfortable as argumentation ascribes either to the isotropic 2D case or can be directly done by application of a suitable anisotropic 3D interpolation operator.

5.3 Hydrostatic Oseen problem on vertical anisotropic meshes

In this section we analyze the hydrostatic Oseen problem in the vertical anisotropic framework. We proceed as before by analyzing the Galerkin formulation of the problem on vertical anisotropic meshes, but restrict to meshes of tensor product type. The latter restriction is due to the availability of an appropriate L^2-orthogonal interpolation operator, being defined on such meshes. As expected it turns out to be not inf-sup stable for equal-order finite elements. The canonical treatment follows: application of suitable stabilization schemes. We restrict our considerations to the case of local projection stabilization. For the stabilization of the velocity in the anisotopic framework we adapt the local projection stabilization of the entire velocity gradient on anisotropic meshes as introduced and analyzed in [Bra08a]. We validate stability of the appropriately stabilized hydrostatic Oseen problem and elaborate *a priori* error estimates. We finish the section with conclusive words, collecting the main results of this section and comparing these with results known from literature and sketching the treatment for the non hydrostatic 3D Stokes and Oseen problem, which (to the authors knowledge) has not been analyzed yet.

5.3.1 Galerkin formulation

We recall and adapt the notions and propositions from Section 4.5.1. We approximate both, the variational spaces $\mathbf{X}$ and $\mathbf{Y}$ by $\mathbf{X}_h := \mathbf{V}_h \times Q_h$ as defined by (4.4) and (4.6). Recall the definitions (3.29) and (4.40) of the advection space $\mathbf{H}_{\mathrm{a}}$ and its discrete counterpart $\mathbf{H}_{a,h}$.

In order to be able to suitably estimate the advection term we restrict to approximations of $\boldsymbol{b}$, which fulfill the following anisotropic version of Assumption 4.22:

Assumption 5.25. *For $0 \leq k \leq r$ and any $\boldsymbol{b} \in \mathbf{H}_a \cap \mathbf{H}^{k+1}(\Omega)$ let $\boldsymbol{b}_h \in \mathbf{H}_{a,h}$ fulfill*

$$\|\boldsymbol{b} - \boldsymbol{b}_h\|_{0,3,\Omega} \lesssim \sum_{T \in \mathcal{T}_h} h_{3,T}^{-1} \sum_{|\alpha|=k+1} \mathbf{h}_T^{\alpha} \|D^{\alpha} \boldsymbol{b}\|_{0,T} \,.$$

Recall the Galerkin formulation of the 2.5D Oseen problem:

$$\begin{aligned} &\textit{Given } \boldsymbol{b}_h \in \mathbf{H}_{a,h},\ \boldsymbol{f} \in \mathbf{H}_b^{-1}(\Omega) \textit{ and } \boldsymbol{g} \in \mathbf{H}_b^{-1/2}(\Gamma_s), \qquad \textit{find } \boldsymbol{y}_h := (\boldsymbol{v}_h, p_h) \in \mathbf{X}_h \textit{ s. t.} \\ &A(\boldsymbol{b}_h; \boldsymbol{y}_h; \boldsymbol{\phi}) = \boldsymbol{l}(\boldsymbol{\varphi}) \qquad\qquad \forall\, \boldsymbol{\phi} := (\boldsymbol{\varphi}, \xi) \in \mathbf{X}_h \,, \end{aligned} \tag{5.52}$$

whereas A is defined as in (3.34). Similar to the Stokes case we find a tight relation between the 2D and the 2.5D case:

Proposition 5.26. *Let Ω be a flat domain and $\mathcal{T}_h$ be a triangulation of Ω fulfilling Assumption 4.2. The 2.5D Oseen problem (5.52) fulfills the modified inf-sup condition*

and thus assures stability of the discrete pressure, if the appropriate discrete non hydrostatic Oseen problem (4.29) in 2D with homogeneous Dirichlet boundary conditions on $\partial\omega$ is inf-sup stable.

Proof. We already proved this statement in Proposition (5.18). □

Due to consideration (a) on page 104, the equal-order finite element discretized hydrostatic Oseen problem (5.52) on vertical anisotropic meshes is not inf-sup stable. We avoid this problem by adding suitable stabilization terms to the system. As in the isotropic case we suitably stabilize the advection term in order to derive appropriate bounds for that term.

5.3.2 Stabilization of the 2D pressure

We apply the local projection pressure stabilization scheme (P'-ii) as presented in Section 4.5.2, which acts on the isotropic surface mesh $\mathcal{K}_h$:

(P'-ii) Local projection stabilization (LPS) [BL09]:

$$s_{h,p}(p_h,\xi) := \sum_{L\in\mathcal{K}_{2h}} \frac{\sigma_L h_L}{\|\boldsymbol{b}_h\|_{0,\infty,L}} (\boldsymbol{\kappa}_{h,\omega}(\nabla' p_h),\, \boldsymbol{\kappa}_{h,\omega}(\nabla'\xi))_L\,,$$

with fluctuation operator $\boldsymbol{\kappa}_{h,\omega} := id_\omega - \pi_\omega$, the 2D identity operator $id_\omega : \mathrm{L}^2(\omega) \to \mathrm{L}^2(\omega)$ and the L^2-projection $\pi_\omega : \mathrm{L}^2_0(\omega) \to Q^{r-1}_{2h}(\omega)$ onto a 'discontinuous' space on the patch mesh $\mathcal{K}_{2h}$,

$$Q^{r-1}_{2h}(\omega) := \{\varphi \in \mathrm{L}^2(\omega) \mid \varphi|_L \in \mathbb{Q}_{r-1}(L)\ \forall L \in \mathcal{K}_{2h}\}\,,$$

For any $L \in \mathcal{K}_{2h}$ constant σ_L is given as $\sigma_L := \min\{1, Pe_L\}$ with 2D, hydrostatically adapted local Peclet number

$$Pe_L := \max_{L\in\mathcal{K}_{2h}} \{\|\boldsymbol{b}_h\|_{0,\infty,L} h_L/\nu\} \qquad \text{with} \quad \|\boldsymbol{b}_h\|_{0,\infty,L} := \max_{M\in\mathcal{T}_L} \{\|\boldsymbol{b}_h\|_{0,\infty,M}\}\,.$$

Note, that due to the definition of vertical anisotropic meshes we have $h_L \sim h_{1,L} \sim h_{2,L}$.

Let us recall the properties of these stabilization schemes and suitably adapt them for the vertical anisotropic case whenever necessary: The stabilization scheme (P'-ii) fulfills the estimates :

$$s_{h,p}(p_h,\xi) \le s_{h,p}(p_h,p_h)^{1/2} s_{h,p}(\xi,\xi)^{1/2} \qquad \forall p_h,\xi \in Q_h\,, \tag{5.53}$$

$$0 \le s_{h,p}(p_h,p_h) \lesssim \sum_{L\in\mathcal{K}_{2h}} \sigma_L \,\|\boldsymbol{b}_h\|^{-1}_{0,\infty,L}\, h_\omega^{2l+1} \|p_h\|^2_{l+1,L} \qquad \forall p_h \in Q_h \cap \mathrm{H}^{l+1}(\omega) \tag{5.54}$$

for $0 \le l \le r$. Moreover, for the purpose of stability we need the result of Lemma 4.24: For arbitrary $p_h \in Q_h$ there is a $\boldsymbol{\varphi} \in \mathbf{V}_h$ such that

$$|\,\boldsymbol{\varphi}\,|_{1,\Omega} \le c\|p_h\|_{0,\omega} \text{ and } -(\mathrm{div}'\,\mathbf{M}\,\boldsymbol{\varphi}, p_h)_\omega \ge c_1\|p_h\|^2_{0,\omega} - c_2 s_{h,p}(p_h,p_h) \tag{5.55}$$

with suitable constants $c_1, c_2 > 0$.

In order to treat the anisotropy and the properties of local projection stabilization appropriately we apply the interpolation operator introduced in Section 5.1.2(c).

Similar to the isotropic case the demands on the estimate of the modified divergence term $(\mathrm{div}'\,\mathbf{M}(\boldsymbol{v} - i_{h,3d}\,\boldsymbol{v}), \xi)_\omega$ are stronger for the Oseen case than for the Stokes problem. The following lemma aims to provide suitable *a priori* error estimates for this divergence term, see also the discussion on page 78.

Lemma 5.27. *Let $\mathcal{T}_h$ be a vertical anisotropic tensor product type triangulation of Ω, such that the requirements of Subsection 5.1.1(b) are fulfilled. Moreover, let $i_{h,3d} : \mathbf{V} \to \mathbf{V}_h$ be taken from Lemma 5.16, $\boldsymbol{v} \in \mathbf{H}^{k+1}(\Omega) \cap \mathbf{V}$, $0 \le k \le r$, and $\xi \in Q_h$.*
Abbreviating the interpolation error as $\boldsymbol{\eta}_v = \boldsymbol{v} - i_{h,3d}\,\boldsymbol{v}$, the stabilization $s_{h,p}(\cdot,\cdot)$ supplies the following estimate:

$$(\mathbf{M}\,\boldsymbol{\eta}_v, \nabla'\xi)_L \lesssim \delta_{max}^{1/2}(h_\omega\,\sigma_L)^{-1/2}\,\|\boldsymbol{b}_h\|_{0,\infty,L}^{1/2} \sum_{|\alpha|=k+1} \sum_{M\in\mathcal{T}_L} \mathbf{h}_M^\alpha \|D^\alpha\,\boldsymbol{v}\,\|_{0,M}\; s_{h,p}(\xi,\xi)^{1/2}. \tag{5.56}$$

with $\sigma_L := \min\{1, Pe_L\}$, any $L \in \mathcal{K}_{2h}$ and $\mathcal{T}_L := \{M \in \mathcal{T}_{2h} \,|\, P(M) = L\}$ as defined on page 51.

Proof. The proof is similar to the proof of Lemma 4.29. Given an element $L \in \mathcal{K}_{2h}$ and applying the orthogonality property of the interpolation operator, we deduce

$$\begin{aligned}(\mathbf{M}(\boldsymbol{v} - \boldsymbol{i_{h,3d}}\,\boldsymbol{v}), \nabla'\xi)_L &\lesssim \|\,\mathbf{M}(\boldsymbol{v} - \boldsymbol{i_{h,3d}}\,\boldsymbol{v})\|_{0,L}\|\boldsymbol{\kappa}_{h,\omega}\nabla'\xi\|_{0,L}\,. \\ &\le \alpha_L^{-1/2}\|\,\mathbf{M}\,\boldsymbol{\eta}_v\|_{0,L}\,\alpha_L^{1/2}\|\boldsymbol{\kappa_{h,\omega}}\nabla'\xi\|_{0,L} \\ &\lesssim \delta_{max}^{1/2}(h_\omega\sigma_L)^{-1/2}\|\boldsymbol{b}_h\|_{0,\infty,L}^{1/2} \sum_{T\in\mathcal{T}_L}\sum_{|\alpha|=k+1} \mathbf{h}_T^\alpha\|D^\alpha\,\boldsymbol{v}\,\|_{0,T}\,s_{h,p}(\xi,\xi)^{1/2}\end{aligned}$$

with $\alpha_L := \sigma_L h_L \|\boldsymbol{b}_h\|_{0,\infty,L}^{-1}$, $L \in \mathcal{K}_{2h}$. □

5.3.3 Stabilization of 3D velocity dependent terms

Recall, that a suitable stabilization of the 3D velocity field should control the divergence constraint and, in the case $0 \le \nu \ll 1$, the advection term. In Section 4.5 we already obtained (inter alia) that the local projection stabilization of the entire velocity gradient performs that task satisfactorily. A slightly altered version of this stabilization accompanies us in the vertical anisotropic framework.
An analysis of a local projection stabilized 2D Oseen problem for $r = 1$ and primarily on anisotropic Cartesian meshes has been done in [Bra08a]. We take a bearing on that local projection stabilization (of the entire velocity gradient) introduced in that work in order to find a suitable stabilization for the hydrostatic Oseen problem.

To account for the mesh anisotropy we define the local minimal Peclet number, see also [Bra08a] for the 2D case:

$$Pe_{min,T} := \frac{\min\{h_{1,T}, h_{2,T}, h_{3,T}\}\|\boldsymbol{b}\|_{0,\infty,T}}{\nu}\,.$$

As we consider the case of vertical anisotropic meshes, $Pe_{min,T} := h_{3,T}\|\boldsymbol{b}\|_{0,\infty,T}\nu^{-1}$ applies. Moreover, we use stabilization parameters, which depend on the direction of the appropriate derivative. Therfore, we introduce the following stabilization matrix:

$$S_\delta := diag(\delta_1^{1/2}, \delta_2^{1/2}, \delta_3^{1/2})$$

with suitable directional stabilization parameters $\delta_1, \delta_2, \delta_3$.

Noting the construction in [Bra08a] and using the ideas of Section 3.4 of [Ric05], we consider the following local projection stabilization of the 3D velocity field:

(V") LPS with stabilization of the entire velocity gradient:

$$s_{h,v}(\boldsymbol{v}_h, \boldsymbol{\varphi}) := \sum_{M\in\mathcal{T}_{2h}} \big(S_{\delta_M}\nabla(\boldsymbol{\kappa}_{h,\Omega}\,\boldsymbol{v}_h),\, S_{\delta_M}\nabla(\boldsymbol{\kappa}_{h,\Omega}\,\boldsymbol{\varphi})\big)_M \quad + \gamma_M\big(\boldsymbol{\kappa}_{h,\Omega}\,\boldsymbol{v}_h,\, \boldsymbol{\kappa}_{h,\Omega}\,\boldsymbol{\varphi}\big)_M$$

with coefficients

$$\delta_{i,M} := h_{i,M}^2\lambda_M, \qquad i\in\{1,2,3\}\,,\ \lambda_M := \min\{1, Pe_{min,M}^{-1}\}\,\nu^{-1}\,\|\boldsymbol{b}_h\|_{0,\infty,M}^2\,,$$
$$\gamma_M := \mathrm{f}^2\,\lambda_M\|\boldsymbol{b}_h\|_{0,\infty,M}^{-2}h_{1,M}^2\,.$$

The fluctuation operator is given by $\boldsymbol{\kappa}_{h,\Omega} := id_\Omega - \pi_\Omega$ with $\pi_\Omega := i_{2h,3d}$, as defined in Lemma 5.16 but on the coarser mesh $\mathcal{T}_{2h}$. In particular, we have

$$(\boldsymbol{v}_h - i_{2h,3d}\,\boldsymbol{v}_h, \xi)_\Omega \;=\; 0 \qquad\qquad \forall\,\boldsymbol{v}_h\in\mathbf{V}_h\,, \forall\xi\in Q_{2h}^r(\Omega)\,.$$

Compared to the stabilization as presented and analyzed in [Bra08a] we switched the order of gradient and fluctuation operator. I.e. we directly apply the fluctuation operator to the element $\boldsymbol{v}_h$ and then treat the gradient of this element $\boldsymbol{\kappa}_{h,\Omega}\,\boldsymbol{v}_h$.
We collect some estimates, which are used to validate stability and to prove error estimates.

Lemma 5.28. *Let $i_{h,3d}$ be the interpolation operator of Lemma 5.16, the vertical anisotropic tensor product type mesh $\mathcal{T}_h$ fulfill the demands of Lemma 5.16 and $k\in\mathbb{N}$ with $0\le k\le r$. Then, for any $\boldsymbol{v}\in\mathbf{V}\cap\mathbf{H}^{k+1}(\Omega)$ the following estimate applies:*

$$s_{h,v}(i_{h,3d}\,\boldsymbol{v}-\boldsymbol{v}, i_{h,3d}\,\boldsymbol{v}-\boldsymbol{v}) \;\lesssim\; \sum_{M\in\mathcal{T}_{2h}}[\lambda_M+\gamma_M]\sum_{|\alpha|=k+1}\mathbf{h}_T^{2\alpha}\|D^\alpha\,\boldsymbol{v}\,\|_{0,S_M}^2\,.$$

Proof. Abbreviating $\eta_v := \boldsymbol{v} - i_{h,3d}\,\boldsymbol{v}$, recalling the definition of $\boldsymbol{\kappa}_{h,\Omega} := id_\Omega - i_{2h,3d}$ and using the estimate (5.43) and we observe for any $M\in\mathcal{T}_{2h}$ and multi index γ with $|\gamma|=1$

$$\|D^\gamma\boldsymbol{\kappa}_{h,\Omega}\eta_v\|_{0,M} \;=\; \|D^\gamma(\eta_v - i_{2h,3d}\eta_v)\|_{0,M} \;\lesssim\; \mathbf{h}_M^{-\gamma}\sum_{|\alpha|=1}\mathbf{h}_M^\alpha\|D^\alpha\eta_v\|_{0,S_M}\,.$$

Thus, we observe

$$\|S_{\delta_M}\nabla(\boldsymbol{\kappa}_{h,\Omega}\eta_v)\|_{0,M} \lesssim \lambda_M^{1/2}\sum_{|\alpha|=1}\mathbf{h}_M^{\alpha}\|D^{\alpha}\eta_v\|_{0,S_M},$$

recalling the definition of $S_{\delta,M} := diag(\delta_{1,M}^{1/2}, \delta_{2,M}^{1/2}, \delta_{3,M}^{1/2})$ with $\delta_{i,M} := h_{i,M}^2\lambda_M$. Restricting $s_{h,v}(\eta_v,\eta_v)$ to a patch cell $M \in \mathcal{T}_{2h}$ and applying the estimate (5.43), we get

$$\begin{aligned} s_{h,v}(\eta_v,\eta_v)|_M &= \|S_{\delta_M}\nabla(\boldsymbol{\kappa}_{h,\Omega}\eta_v)\|_{0,M}^2 + \gamma_M\|\boldsymbol{\kappa}_{h,\Omega}\eta_v\|_{0,M}^2 \\ &\lesssim \lambda_M\sum_{|\gamma|=1}\mathbf{h}_M^{2\gamma}\|D^{\gamma}\eta_v\|_{0,S_M}^2 + \gamma_M\sum_{|\alpha|=k+1}\mathbf{h}_M^{2\alpha}\|D^{\alpha}\,\boldsymbol{v}\,\|_{0,S_M}^2 \\ &\lesssim (\lambda_M + \gamma_M)\sum_{|\alpha|=k+1}\mathbf{h}_M^{2\alpha}\|D^{\alpha}\,\boldsymbol{v}\,\|_{0,S_M}^2. \end{aligned}$$

□

Lemma 5.29. *Let $i_{h,3d}$ be the interpolation operator of Lemma 5.16, the vertical anisotropic tensor product type mesh $\mathcal{T}_h$ fulfill the demands of Lemma 5.16 and $k \in \mathbb{N}$ with $0 \le k \le r$.*
For any $\boldsymbol{v}_h$, $\boldsymbol{\varphi} \in \mathbf{V}_h$ and any $\boldsymbol{v} \in \mathbf{H}^{k+1}(\Omega)$ the stabilization term $s_{h,v}(\cdot,\cdot)$ given in (V") provides

$$0 \le s_{h,v}(\boldsymbol{v}_h;\boldsymbol{v}_h) \tag{5.57}$$

$$s_{h,v}(\boldsymbol{v}_h;\boldsymbol{\varphi}) \le s_{h,v}(\boldsymbol{v}_h;\boldsymbol{v}_h)^{1/2}s_{h,v}(\boldsymbol{\varphi};\boldsymbol{\varphi})^{1/2} \tag{5.58}$$

$$s_{h,v}(i_{h,3d}\,\boldsymbol{v},\boldsymbol{\varphi}) \lesssim \sum_{M\in\mathcal{T}_{2h}}(\lambda_M^{1/2}+\gamma_M^{1/2})\sum_{|\alpha|=k+1}\mathbf{h}_M^{\alpha}\|D^{\alpha}\,\boldsymbol{v}\,\|_{0,M}\,s_{h,v}(\boldsymbol{\varphi},\boldsymbol{\varphi})^{1/2}. \tag{5.59}$$

Proof. Estimates (5.57) and (5.58) are trivial. We deduce estimate (5.59) following the argumentation in Section 3.4. of [Ric05]:

$$\begin{aligned} s_{h,v}(i_{h,3d}\,\boldsymbol{v},\boldsymbol{\varphi}) &\le s_{h,v}(i_{h,3d}\,\boldsymbol{v},i_{h,3d}\,\boldsymbol{v})^{1/2}\,s_{h,v}(\boldsymbol{\varphi},\boldsymbol{\varphi})^{1/2} \\ &\le \left(\sum_{M\in\mathcal{T}_{2h}}\gamma_M\|\boldsymbol{\kappa}_{h,\Omega}(i_{h,3d}\,\boldsymbol{v})\|_{0,M}^2 + \sum_{i\in\{1,2,3\}}\delta_{i,M}\|\nabla(\boldsymbol{\kappa}_{h,\Omega}i_{h,3d}\,\boldsymbol{v})\|_{0,M}^2\right)^{1/2} s_{h,v}(\boldsymbol{\varphi},\boldsymbol{\varphi})^{1/2}. \end{aligned}$$

Recalling $\boldsymbol{\kappa}_{h,\Omega} := id_\Omega - i_{2h,3d}$ and the properties of $i_{2h,3d}$ as given in Lemma 5.16 on $Q_{2h}^r(\Omega)$ instead of $Q_h^r(\Omega)$ we deduce further for any $M \in \mathcal{T}_{2h}$

$$\begin{aligned} \|S_{\delta,M}\nabla(\boldsymbol{\kappa}_{h,\Omega}i_{h,3d}\,\boldsymbol{v})\|_{0,M}^2 &\le \|S_{\delta,M}\nabla(\boldsymbol{v}-i_{h,3d}\,\boldsymbol{v})\|_{0,M}^2 + \|S_{\delta,M}\nabla(\boldsymbol{\kappa}_{h,\Omega}\,\boldsymbol{v})\|_{0,M}^2 \\ &\lesssim \|S_{\delta,M}\nabla(\boldsymbol{v}-i_{2h,3d}\,\boldsymbol{v})\|_{0,M}^2. \end{aligned}$$

Let γ be a multi index with $|\gamma| = 1$. Application of (5.43), see Lemma 5.16, and the definition of $\delta_{i,M}$ then results in

$$\|\mathbf{h}_M^{\gamma}\lambda_M^{1/2}D^{\gamma}(\boldsymbol{v}-i_{2h,3d}\,\boldsymbol{v})\|_{0,M} \lesssim \lambda_M^{1/2}\sum_{|\alpha|=k+1}\mathbf{h}_M^{\alpha}\|D^{\alpha}\,\boldsymbol{v}\,\|_{0,S_M},$$

which in turn leads to

$$\|S_{\delta_M}\nabla(\boldsymbol{v}-i_{2h,3d}\,\boldsymbol{v})\|_{0,M} \;\lesssim\; \lambda_M^{1/2}\sum_{|\alpha|=k+1}\mathbf{h}_M^{\alpha}\|D^{\alpha}\,\boldsymbol{v}\,\|_{0,S_M}\,.$$

The estimate of the Coriolis term results in a similar fashion:

$$\gamma_M\|\boldsymbol{\kappa}_{h,\Omega}(i_{h,3d}\,\boldsymbol{v})\|_{0,M}^2 \lesssim \gamma_M\|\,\boldsymbol{v}-i_{2h,3d}\,\boldsymbol{v}\,\|_{0,M}^2 \lesssim \gamma_M\sum_{|\alpha|=k+1}\mathbf{h}_M^{2\alpha}\|D^{\alpha}\,\boldsymbol{v}\,\|_{0,M}^2\,.$$

□

5.3.4 Stability analysis

The stabilized version of the (not inf-sup stable) discrete problem (5.52) is given by:

$$\begin{aligned} &\textit{Given } \boldsymbol{b}_h\in\mathbf{H}_{a,h},\ \boldsymbol{f}\in\mathbf{H}_b^{-1}(\Omega),\ \boldsymbol{g}\in\mathbf{H}_b^{-1/2}(\Gamma_u), \quad \textit{find } \boldsymbol{y}_h:=(\boldsymbol{v}_h,p_h)\in\mathbf{X}_h \textit{ s. t.}\\ &\qquad A_h(\boldsymbol{b}_h;\boldsymbol{y}_h;\boldsymbol{\phi})=\boldsymbol{l}(\boldsymbol{\varphi}) \qquad\qquad \forall\,\boldsymbol{\phi}:=(\boldsymbol{\varphi},\xi)\in\mathbf{X}_h \end{aligned} \tag{5.60}$$

with

$$A_h(\boldsymbol{b}_h;\boldsymbol{y}_h;\boldsymbol{\phi}) := A(\boldsymbol{b}_h;\boldsymbol{y}_h;\boldsymbol{\phi}) + s_{h,p}(p_h,\xi)+s_{h,v}(\boldsymbol{v}_h,\boldsymbol{\varphi})\,.$$

Recall, that $\boldsymbol{b}_h\in\mathbf{H}_{a,h}$ is divergence free and thus $\langle(\boldsymbol{b}_h\cdot\nabla)\,\boldsymbol{v}_h,\boldsymbol{v}_h\rangle=0$ applies for any $\boldsymbol{v}_h\in\mathbf{V}_h$.

We prove stability of problem (5.60) with respect to the mesh-dependent norm $|\!|\!|\cdot|\!|\!|:\mathbf{X}_h\to\mathbb{R}_+$,

$$|\!|\!|\boldsymbol{y}_h|\!|\!| := \big(A_h(\boldsymbol{b}_h;\boldsymbol{y}_h;\boldsymbol{y}_h)+(\nu+\sigma)\|q_h\|_{0,\Omega}^2\big)^{1/2} \qquad \forall\boldsymbol{y}_h:=(\boldsymbol{v}_h,q_h)\in\mathbf{X}_h\,. \tag{5.61}$$

The unit sphere on $\mathbf{X}_h$ w.r.t. that norm is denoted by B_h.

Proposition 5.30. *Let $\mathcal{T}_h$ be a vertical anisotropic tensor product type mesh fulfilling the demands of Lemma 5.16, and $\nu,\sigma,\mathrm{f},\|\boldsymbol{b}_h\|_{0,\infty,\Omega}\le C$. The stabilized 2.5D Oseen bilinear form (5.60) is inf-sup stable:*

$$\exists\ \gamma_{\Omega,\omega}>0: \qquad \inf_{\boldsymbol{y}_h\in B_h}\sup_{\boldsymbol{\phi}\in B_h} A_h(\boldsymbol{b}_h;\boldsymbol{y}_h;\boldsymbol{\phi}) \;\ge\; \gamma_{\Omega,\omega}\,.$$

Proof. The proof is similar to the proof of Proposition 4.26. Let $(\boldsymbol{v}_h,p_h)\in\boldsymbol{V}_h\times Q_h$. We use the criterion for inf-sup conditions proposed in [BS11]: We split the triple norm into two parts

$$|\!|\!|\boldsymbol{y}_h|\!|\!| := \big(|\boldsymbol{y}_h|_a^2+|\boldsymbol{y}_h|_b^2\big)^{1/2} \qquad \text{with}$$
$$|\boldsymbol{y}_h|_a^2 := A_h(\boldsymbol{b}_h;\boldsymbol{y}_h;\boldsymbol{y}_h) \qquad \text{and} \qquad |\boldsymbol{y}_h|_b^2 := (\nu+\sigma)\|q_h\|_{0,\Omega}^2\,.$$

Crucial of this proof is the existence of a $\boldsymbol{\varphi} \in \mathbf{V}_h$ fulfilling

$$|\,\boldsymbol{\varphi}\,|_{1,\Omega} \lesssim \|p_h\|_{0,\omega} \qquad \text{and} \qquad -(\mathrm{div}'\,\mathbf{M}\,\boldsymbol{\varphi}, p_h) \geq c_1\|p_h\|_{0,\omega}^2 - c_2 s_{h,p}(p_h,p_h)$$

with h- and ν- independent constants c_1, $c_2 > 0$, see [KB12]. Given this $\boldsymbol{\varphi} \in \mathbf{V}_h$, we can estimate

$$\begin{aligned} A_h(\boldsymbol{b}_h; \boldsymbol{v}_h, p_h; \boldsymbol{\varphi}, 0) \geq \quad & c_1\|p_h\|_{0,\omega}^2 - c_2 s_{h,p}(p_h,p_h) \\ & - C(\nu^{1/2}|\boldsymbol{v}_h|_{1,\Omega} + (1+c_F)\|\boldsymbol{v}_h\|_{0,\Omega})\|p_h\|_{0,\omega} + s_{h,v}(\boldsymbol{v}_h, \boldsymbol{\varphi})\,. \end{aligned}$$

Constant c_F denotes the constant of the inequality of Poincaré - Friedrichs. Moreover we have $s_{h,v}(\boldsymbol{v}_h, \boldsymbol{\varphi}) \lesssim s_{h,v}(\boldsymbol{v}_h, \boldsymbol{v}_h)^{1/2} s_{h,v}(\boldsymbol{\varphi}, \boldsymbol{\varphi})^{1/2}$. Applying the estimate (5.43), as well as bounding the stabilization parameter and the Poincare-Friedrichs inequality with constant c_F we get

$$\begin{aligned} s_{h,v}(\boldsymbol{\varphi}, \boldsymbol{\varphi}) &= \sum_{M \in \mathcal{T}_{2h}} \| S_{\delta_M} \nabla(\boldsymbol{\kappa}_{h,\Omega}\,\boldsymbol{\varphi})\|_{0,M}^2 \quad + \gamma_M \|\boldsymbol{\kappa}_{h,\Omega}\,\boldsymbol{\varphi}\,\|_{0,M}^2 \\ &\lesssim |\,\boldsymbol{\varphi} - i_{2h,3d}\,\boldsymbol{\varphi}\,|_{1,\Omega}^2 + \|\,\boldsymbol{\varphi} - i_{2h,3d}\,\boldsymbol{\varphi}\,\|_{0,\Omega}^2 \\ &\lesssim |\,\boldsymbol{\varphi}\,|_{1,\Omega}^2 + |i_{2h,3d}\,\boldsymbol{\varphi}\,|_{1,\Omega}^2 + |\,\boldsymbol{\varphi}\,|_{1,\Omega}^2 \\ &\leq \ (2 + c_F)\|p_h\|_{0,\omega}^2\,. \end{aligned}$$

Scaling the element $(\boldsymbol{\varphi}, 0)$ with the factor $\nu + \sigma$ produces

$$A_h(\boldsymbol{b}_h; \boldsymbol{v}_h, p_h; (\nu+\sigma)\,\boldsymbol{\varphi}, 0) \geq \quad \widetilde{c_1}|(\boldsymbol{v}_h, p_h)|_b^2 - \widetilde{c_2}|(\boldsymbol{v}_h, p_h)|_a^2\,.$$

Diagonal testing leads to $A_h(\boldsymbol{b}_h; \boldsymbol{v}_h, p_h; \boldsymbol{v}_h, p_h) = |\,\boldsymbol{v}_h, p_h|_a^2$, which finishes the proof. □

5.3.5 *A priori* error estimates

In this section we deduce error estimates of the symmetric stabilized 2.5D Oseen problem (4.48). We start with some preparatory considerations.

Lemma 5.31. *Let $\mathcal{T}_h$ be a vertical anisotropic tensor product type mesh. The operator $i_{h,3d}$ is chosen from Lemma 5.16 and $i_{h,2d} : Q \to Q_h$ denotes the isotropic 2D version concerning the pressure space. Moreover, let $\|\boldsymbol{b}_h\|_{0,\infty,\Omega} \leq C$. Assume $(\boldsymbol{v}, p) \in \mathbf{H}_b^{k+1}(\Omega) \times \mathrm{H}^{l+1}(\omega)$, $0 \leq k, l \leq r$, and let $(\boldsymbol{\varphi}, \xi) \in \mathbf{V}_h \times Q_h$ arbitrarily be chosen. The term $s_{h,v}(\cdot,\cdot)$ defined by (V") permits the estimates:*

$$\langle(\boldsymbol{b}_h \cdot \nabla)(\boldsymbol{v} - i_{h,3d}\,\boldsymbol{v}), \boldsymbol{\varphi}\rangle_M \lesssim \|\boldsymbol{b}_h\|_{0,\infty,M}\,\rho_M^{1/2} \sum_{|\alpha|=k+1} \mathbf{h}_M^{\alpha} \|D^{\alpha}\,\boldsymbol{v}\,\|_{0,M} |\!|\!|(\boldsymbol{\varphi}, \xi)|\!|\!|\,, \tag{5.62}$$

$$\mathrm{f}((\boldsymbol{v} - i_{h,3d}\,\boldsymbol{v})^{\perp}, \boldsymbol{\varphi})_M \lesssim \gamma_M^{-1/2}\,\mathrm{f} \sum_{|\alpha|=k+1} \mathbf{h}_M^{\alpha} \|D^{\alpha}\,\boldsymbol{v}\,\|_{0,M} s_{h,v}(\boldsymbol{\varphi}, \boldsymbol{\varphi})^{1/2} \tag{5.63}$$

$$(div'\,\mathbf{M}\,\boldsymbol{\varphi}, p - i_{h,2d}p)_L \ \lesssim \ \delta_{max}^{1/2}\,\rho_{\mathcal{T}_L}^{1/2}\,h_{\omega}^{l+1} \|p\|_{l+1,L} |\!|\!|(\boldsymbol{\varphi}, \xi)|\!|\!|\,, \tag{5.64}$$

for any $M \in \mathcal{T}_{2h}$, arbitrary $L \in \mathcal{K}_{2h}$, with $\rho_{\mathcal{T}_L} := \min\{\max_{M \in \mathcal{T}_L}\{\delta_{3,M}^{-1}\}, \nu^{-1}\}$, $\rho_M := \min\{\delta_{3,M}^{-1}, \nu^{-1}\}$.

Proof. We start with the validation of estimate (5.62). Let $\boldsymbol{v} \in \mathbf{H}_b^{k+1}(\Omega)$ and $\boldsymbol{\varphi} \in \mathbf{V}_h$ be arbitrarily given. Using the L^2-orthogonality of $i_{h,3d}$ on $Q_h^r(\Omega)$, see (5.40), and the observation that $\nabla(i_{2h,3d}\,\boldsymbol{\varphi}) \in \boldsymbol{Q}_h^r(\Omega)$, the advection term then can be estimated as:

$$\begin{aligned}
|\langle(\boldsymbol{b}_h \cdot \nabla)(\boldsymbol{v} - i_{h,3d}\,\boldsymbol{v}), \boldsymbol{\varphi}\rangle_M| &\leq \|\boldsymbol{b}_h\|_{0,\infty,M} |(\boldsymbol{v} - i_{h,3d}\,\boldsymbol{v}, \nabla\,\boldsymbol{\varphi})_{0,M}| \\
&\leq \|\boldsymbol{b}_h\|_{0,\infty,T} |(\boldsymbol{v} - i_{h,3d}\,\boldsymbol{v}, \nabla(\boldsymbol{\kappa}_{h,\Omega}\,\boldsymbol{\varphi}))_{0,M}| \\
&\leq \|\boldsymbol{b}_h\|_{0,\infty,T} \delta_{3,M}^{-1/2} \|\,\boldsymbol{v} - i_{h,3d}\,\boldsymbol{v}\,\|_{0,M} \|S_{\delta_M} \nabla(\boldsymbol{\kappa}_{h,\Omega}\,\boldsymbol{\varphi})\|_{0,M} \\
&\lesssim \|\boldsymbol{b}_h\|_{0,\infty,T} \delta_{3,M}^{-1/2} \sum_{|\alpha|=k+1} \boldsymbol{h}^\alpha \|D^\alpha\,\boldsymbol{v}\,\|_{0,M} s_{h,v}(\boldsymbol{\varphi},\boldsymbol{\varphi})^{1/2}\,.
\end{aligned}$$

Moreover, we have

$$\begin{aligned}
|\langle(\boldsymbol{b}_h \cdot \nabla)(\boldsymbol{v} - i_{h,3d}\,\boldsymbol{v}), \boldsymbol{\varphi}\rangle_M| &\leq \|\boldsymbol{b}_h\|_{0,\infty,M} \|\,\boldsymbol{v} - i_{h,3d}\,\boldsymbol{v}\,\|_{0,M} |\,\boldsymbol{\varphi}\,|_{1,M} \\
&\leq \|\boldsymbol{b}_h\|_{0,\infty,M}\, \nu^{-1/2} \sum_{|\alpha|=k+1} \mathbf{h}_M^\alpha \|D^\alpha\,\boldsymbol{v}\,\|_{0,M} (\nu^{1/2} |\,\boldsymbol{\varphi}\,|_{1,M})\,.
\end{aligned}$$

In a similar fashion, the Coriolis term can be estimated as

$$\begin{aligned}
|\,\mathrm{f}((\boldsymbol{v} - i_{h,3d}\,\boldsymbol{v})^\perp, \boldsymbol{\varphi})_M| &\leq \|\,\boldsymbol{v} - i_{h,3d}\,\boldsymbol{v}\,\|_{0,M}\, \mathrm{f}\, \|\boldsymbol{\kappa}_{h,\Omega}\,\boldsymbol{\varphi}\,\|_{0,M} \\
&\lesssim \gamma_M^{-1/2}\, \mathrm{f} \sum_{|\alpha|=k+1} \mathbf{h}_M^\alpha \|D^\alpha\,\boldsymbol{v}\,\|_{0,M} s_{h,v}(\boldsymbol{\varphi},\boldsymbol{\varphi})^{1/2}\,.
\end{aligned}$$

For the derivation of (5.64) we observe for any $\boldsymbol{\varphi} \in \mathbf{V}_h$ and any $p \in \mathrm{H}^{l+1}(\omega)$:

$$|(\mathrm{div}'\,\mathbf{M}(i_{2h,3d}\,\boldsymbol{\varphi}), p - i_{h,2d}p)_L| \;=\; 0\,,$$

due to $i_{2h,3d}\,\boldsymbol{\varphi} \in Q_{2h}^r(\Omega)$ and $\mathbf{M} : Q_{2h}^r(\Omega) \to Q_{2h}^r(\omega)$ (see Lemma 4.4), and due to the L^2-orthogonality of $i_{h,2d}$. Denoting e_i, $i \in \{1,2,3\}$, as the unit vectors aligned to the coordinate axes we thus deduce further

$$\begin{aligned}
(\mathrm{div}'\,\mathbf{M}\,\boldsymbol{\varphi}, p - i_{h,2d}p)_L &= (\mathbf{M}\,\mathrm{div}'(\boldsymbol{\kappa}_{h,\Omega}\,\boldsymbol{\varphi}), p - i_{h,2d}p)_L \\
&\lesssim \|\,\mathbf{M}\,\mathrm{div}'(\boldsymbol{\kappa}_{h,\Omega}\,\boldsymbol{\varphi})\|_{0,L}\, h_\omega^{l+1}\, \|p\|_{l+1,L} \\
&\lesssim \delta_{max}^{1/2} \left(\sum_{M \in \mathcal{T}_L} \|\mathrm{div}'(\boldsymbol{\kappa}_{h,\Omega}\,\boldsymbol{\varphi})\|_{0,M}^2 \right)^{1/2} h_\omega^{l+1} \|p\|_{l+1,L} \\
&\lesssim \delta_{max}^{1/2} \left(\sum_{M \in \mathcal{T}_L} \delta_{3,M}^{-1} \sum_{i \in \{1,2,3\}} \delta_{i,M} \|\partial_{e_i}(\boldsymbol{\kappa}_{h,\Omega}\,\boldsymbol{\varphi})\|_{0,M}^2 \right)^{1/2} h_\omega^{l+1} \|p\|_{l+1,L} \\
&\leq \delta_{max}^{1/2} \max_{M \in \mathcal{T}_L} \{\delta_{3,M}^{-1/2}\} s_{h,v}(\boldsymbol{\varphi},\boldsymbol{\varphi})^{1/2} h_\omega^{l+1} \|p\|_{l+1,L}\,.
\end{aligned}$$

Moreover, we can estimate

$$\begin{aligned}
(\mathrm{div}'\,\mathbf{M}\,\boldsymbol{\varphi}, p - i_{h,2d}p)_L &\leq \|\mathrm{div}'\,\mathbf{M}\,\boldsymbol{\varphi}\,\|_{0,L} \|p - i_{h,2d}p\|_{0,L} \\
&\leq \delta_{max}^{1/2} \nu^{-1/2} (\nu^{1/2} \|\nabla\,\boldsymbol{\varphi}\,\|_{0,L}) h_\omega^{l+1} \|p\|_{l+1,L}\,.
\end{aligned}$$

□

Before we turn to the *a priori* error estimates of the stabilized hydrostatic Oseen problem on vertical anisotropic tensor product type grids, we consider the coefficients of the relevant estimates, i.e. (5.54), Lemmata 5.27, 5.28, 5.29 and 5.31:

Lemma 5.32. *For any $M \in \mathcal{T}_{2h}$ and any $L \in \mathcal{K}_{2h}$ the following estimates apply:*

$$\min\{1, Pe_L\} \min_{M\in\mathcal{T}_L} \|\boldsymbol{b}_h\|^{-1}_{0,\infty,M} \lesssim \max_{M\in\mathcal{T}_L} \left\{\sigma_M \|\boldsymbol{b}_h\|^{-1}_{0,\infty,M}\right\} h_\omega h^{-1}_{3,M} \tag{5.65}$$

$$\delta^{1/2}_{max}(\sigma_L h_\omega)^{-1/2} \max_{M\in\mathcal{T}_L} \|\boldsymbol{b}_h\|^{1/2}_{0,\infty,M} \lesssim \delta^{1/2}_{max} h_\omega^{-1/2} \min_{M\in\mathcal{T}_L} \left\{\max\{\nu\, h^{-1}_{3,M},\, \|\boldsymbol{b}_h\|_{0,\infty,M}\, \sigma_M\}\right\}^{1/2} \tag{5.66}$$

$$\lambda_M + \gamma_M \sim \sigma_M h^{-1}_{3,M} h^2_\omega \left(\|\boldsymbol{b}_h\|_{0,\infty,M} + h^2_\omega\, \mathrm{f}^2\, \|\boldsymbol{b}_h\|^{-1}_{0,\infty,M}\right) \tag{5.67}$$

$$\lambda^{1/2}_M + \gamma^{1/2}_M \sim \sigma^{1/2}_M h^{-1/2}_{3,M} (\|\boldsymbol{b}_h\|^{1/2}_{0,\infty,M} + h_\omega\, \mathrm{f}\, \|\boldsymbol{b}_h\|^{-1/2}_{0,\infty,M}) \tag{5.68}$$

$$\min\left\{\delta^{-1}_{3,M}, \nu^{-1}\right\}^{1/2} \|\boldsymbol{b}_h\|_{0,\infty,M} \sim (\sigma_M \|\boldsymbol{b}_h\|_{0,\infty,M} h^{-1}_{3,M})^{1/2} \tag{5.69}$$

$$\delta^{1/2}_{max} \min\left\{\max_{M\in\mathcal{T}_L}\{\delta^{-1}_{3,M}\}, \nu^{-1}\right\}^{1/2} \sim \delta^{1/2}_{max} \max_{M\in\mathcal{T}_L}\{\sigma_M \|\boldsymbol{b}_h\|^{-1}_{0,\infty,M} h^{-1}_{3,M}\}^{1/2} \tag{5.70}$$

$$\gamma^{-1/2}_M\, \mathrm{f} \sim \max\{\nu h_3^{-1},\, \sigma_M \|\boldsymbol{b}_h\|_{0,\infty,M}\}^{1/2} h^{1/2}_{3,M} \tag{5.71}$$

with 2D parameters $Pe_L := \max\{\|\boldsymbol{b}_h\|_{0,\infty,L} h_L \nu^{-1}\}$ and $\sigma_L := \max\{\sigma_M \,|\, M \in \mathcal{T}_L\}$, and 3D parameters $\lambda_M = \sigma_M h^{-1}_{3,M} \|\boldsymbol{b}_h\|_{0,\infty,M}$, $\sigma_M := \min\{Pe_{min,M}, 1\}$, and $\gamma_M := \mathrm{f}^2\, \lambda_M \|\boldsymbol{b}_h\|^{-2}_{0,\infty,M} h^2_{1,M}$.

Proof. The estimates (5.67) and (5.68) are obvious.
For the derivation of estimate (5.69) we use the deductions in the proof of Lemma 4.6 in [Bra08a]: We define $\chi := \nu^{-1} \min\{1, Pe^{-1}_{min,M}\} h^2_{M,1} = \min\{\nu^{-1}, h^{-1}_{3,M} \|\boldsymbol{b}_h\|^{-1}_{0,\infty,M}\} h^2_{1,M}$. According to $\delta_{3,M} = h_{3,M} \|\boldsymbol{b}_h\|_{0,\infty,M} \sigma_M$, we can further deduce

$$\begin{aligned} \chi &= \min\{\nu^{-1}, \delta^{-1}_{3,M}\sigma_M\} h^2_{1,M} \\ &= \min\{\nu^{-1}, \delta^{-1}_{3,M}, Pe_{min,M}\delta^{-1}_{3,M}\} h^2_{1,M} \\ &= \min\{\nu^{-1}, \delta^{-1}_{3,M}\} h^2_{1,M} \end{aligned} \tag{5.72}$$

and get

$$\begin{aligned} \min\left\{\delta^{-1}_{3,M}, \nu^{-1}\right\}^{1/2} \|\boldsymbol{b}_h\|_{0,\infty,M} &= \nu^{-1/2} \min\{1, Pe^{-1/2}_{min,M}\} \|\boldsymbol{b}_h\|_{0,\infty,M} \\ &= (\sigma_M \|\boldsymbol{b}_h\|_{0,\infty,M} h^{-1}_{3,M})^{1/2}\,. \end{aligned}$$

In order to estimate the left hand side of 5.70 we observe the following:

$$\min\left\{\max_{M\in\mathcal{T}_L}\{\delta^{-1}_{3,M}\}, \nu^{-1}\right\}^{1/2} = \max_{M\in\mathcal{T}_L}\left\{\min\{\delta^{-1/2}_{3,M}, \nu^{-1/2}\}\right\}.$$

Applicating (5.72), see also [Bra08a], we get

$$\min\{\delta^{-1/2}_{3,M}, \nu^{-1/2}\} = \chi^{1/2} h^{-1}_{1,M} = \min\{\nu^{-1/2}, h^{-1/2}_{3,M} \|\boldsymbol{b}_h\|^{-1/2}_{0,\infty,M}\} = (\sigma_M \|\boldsymbol{b}_h\|^{-1}_{0,\infty,M} h^{-1}_{3,M})^{1/2},$$

which finishes the proof of (5.70). The estimate (5.66) can be validated in a similar fashion. We deduce

$$\begin{aligned}
(\sigma_L h_\omega)^{-1/2} \max_{\widetilde{M}\in\mathcal{T}_L} \left\{ \|\boldsymbol{b}_h\|^{1/2}_{0,\infty,\widetilde{M}} \right\} &= h_\omega^{-1/2} \left[\max_{M\in\mathcal{T}_L} \{\sigma_M\} \right]^{-1/2} \max_{\widetilde{M}\in\mathcal{T}_L} \left\{ \|\boldsymbol{b}_h\|^{1/2}_{0,\infty,\widetilde{M}} \right\} \\
&= h_\omega^{-1/2} \left[\min_{M\in\mathcal{T}_L} \left\{ \max\{\nu h_{3,M}^{-1} \|\boldsymbol{b}_h\|^{-1}_{0,\infty,M},\, 1\} \right\} \right]^{1/2} \max_{\widetilde{M}\in\mathcal{T}_L} \left\{ \|\boldsymbol{b}_h\|^{1/2}_{0,\infty,\widetilde{M}} \right\} \\
&= h_\omega^{-1/2} \left[\min_{M\in\mathcal{T}_L} \left\{ \|\boldsymbol{b}_h\|^{-1}_{0,\infty,M} \max\{\nu h_{3,M}^{-1},\, \|\boldsymbol{b}_h\|_{0,\infty,M}\} \max_{\widetilde{M}\in\mathcal{T}_L} \left\{ \|\boldsymbol{b}_h\|_{0,\infty,\widetilde{M}} \right\} \right\} \right]^{1/2} \\
&\leq h_\omega^{-1/2} \left[\min_{M\in\mathcal{T}_L} \left\{ \max\{\nu h_{3,M}^{-1},\, \|\boldsymbol{b}_h\|_{0,\infty,M}\} \right\} \right]^{1/2} \\
&= h_\omega^{-1/2} \left[\min_{M\in\mathcal{T}_L} \left\{ h_{3,M}^{-1} \max\{\nu,\, \|\boldsymbol{b}_h\|_{0,\infty,M} h_{3,M}\} \right\} \right]^{1/2} \\
&= h_\omega^{-1/2} \left[\max_{M\in\mathcal{T}_L} \left\{ h_{3,M} \min\{\nu^{-1},\, \|\boldsymbol{b}_h\|^{-1}_{0,\infty,M} h_{3,M}^{-1}\} \right\} \right]^{-1/2} .
\end{aligned}$$

Using the definition of χ and (5.72), the equality

$$\min\{\nu^{-1},\, \|\boldsymbol{b}_h\|^{-1}_{0,\infty,M} h_{3,M}^{-1}\} = \min\{\nu^{-1},\, \delta_{3,M}^{-1}\}$$

applies, such that we get

$$\begin{aligned}
(\sigma_L h_\omega)^{-1/2} \max_{\widetilde{M}\in\mathcal{T}_L} \left\{ \|\boldsymbol{b}_h\|^{1/2}_{0,\infty,\widetilde{M}} \right\} &\leq h_\omega^{-1/2} \left[\max_{M\in\mathcal{T}_L} \left\{ h_{3,M} \min\{\nu^{-1},\, \delta_{3,M}^{-1}\} \right\} \right]^{-1/2} \\
&= h_\omega^{-1/2} \left[\min_{M\in\mathcal{T}_L} \left\{ \max\{\nu\, h_{3,M}^{-1},\, \delta_{3,M}\, h_{3,M}^{-1}\} \right\} \right]^{1/2} \\
&= h_\omega^{-1/2} \left[\min_{M\in\mathcal{T}_L} \left\{ \max\{\nu\, h_{3,M}^{-1},\, \|\boldsymbol{b}_h\|_{0,\infty,M}\, \sigma_M\} \right\} \right]^{1/2} .
\end{aligned}$$

Similar to the preceding case, the estimate (5.65) results due to the following deduction:

$$\begin{aligned}
\min\{1, Pe_L\} \min_{\widetilde{M}\in\mathcal{T}_L} \{\|\boldsymbol{b}_h\|^{-1}_{0,\infty,\widetilde{M}}\} &= \min\left\{ 1, \max_{M\in\mathcal{T}_L} \{\nu^{-1} h_\omega \|\boldsymbol{b}_h\|_{0,\infty,M}\} \right\} \min_{\widetilde{M}\in\mathcal{T}_L} \{\|\boldsymbol{b}_h\|^{-1}_{0,\infty,\widetilde{M}}\} \\
&= \max_{M\in\mathcal{T}_L} \left\{ \min\{1, \nu^{-1} h_\omega \|\boldsymbol{b}_h\|_{0,\infty,M}\} \right\} \min_{\widetilde{M}\in\mathcal{T}_L} \{\|\boldsymbol{b}_h\|^{-1}_{0,\infty,\widetilde{M}}\} \\
&\leq \max_{M\in\mathcal{T}_L} \left\{ \min\{\|\boldsymbol{b}_h\|^{-1}_{0,\infty,M}, \nu^{-1} h_\omega\} \right\} \\
&\leq \max_{M\in\mathcal{T}_L} \left\{ h_\omega \nu^{-1} \min\{\|\boldsymbol{b}_h\|^{-1}_{0,\infty,M} h_{3,M}^{-1} \nu, 1\} \right\} \\
&\sim \max_{M\in\mathcal{T}_L} \left\{ \chi h_\omega^{-1} \right\} \\
&\sim \max_{M\in\mathcal{T}_L} \left\{ \sigma_M \|\boldsymbol{b}_h\|^{-1}_{0,\infty,M} h_\omega h_3^{-1} \right\} .
\end{aligned}$$

The remaining estimate (5.71) can be deduced by $\gamma_M^{-1/2}\,\mathrm{f} = (\sigma_M^{-1} h_{3,M} \|\boldsymbol{b}_h\|_{0,\infty,M})^{1/2}$ and the application of (5.72):

$$\begin{aligned}
\sigma_M^{-1} h_{3,M} \|\boldsymbol{b}_h\|_{0,\infty,M} &= \max\{h_{3,M}\|\boldsymbol{b}_h\|_{0,\infty,M},\, \nu\} \\
&= \left[\min\{h_{3,M}^{-1}\|\boldsymbol{b}_h\|_{0,\infty,M}^{-1},\, \nu^{-1}\}\right]^{-1} \\
&= \left[\min\{\nu^{-1},\, \delta_{3,M}^{-1}\}\right]^{-1} \\
&= \max\{\nu,\, \delta_{3,M}\} \\
&= \max\{\nu,\, \sigma_M h_{3,M}\|\boldsymbol{b}_h\|_{0,\infty,M}\} \\
&= \max\{\nu\, h_{3,M}^{-1},\, \sigma_M\|\boldsymbol{b}_h\|_{0,\infty,M}\}\, h_{3,M}\,,
\end{aligned}$$

which finishes the entire proof. □

Proposition 5.33. *Let $\mathcal{T}_h$ be a vertical anisotropic tensor product type mesh fulfilling the demands of Subsection 5.1.1(b). Moreover, let Assumption 5.25 be valid.*
If the continuous solution of (3.33) is sufficiently regular, $\mathbf{u} := (\boldsymbol{v}, p) \in \mathbf{H}^{k+1}(\Omega) \times \mathrm{H}^{l+1}(\omega)$, $0 \le k, l \le r$, the following estimate for the discrete solution $\mathbf{u}_h := (\boldsymbol{v}_h, p_h)$ of (5.60) applies:

$$\|\!|\, \mathbf{u} - \mathbf{u}_h \,|\!\| \lesssim \sum_{M\in\mathcal{T}_{2h}} C_{v,M}\, h_{3,M}^{-1/2} \sum_{|\alpha|=k+1} \mathbf{h}_M^{\alpha} \|D^{\alpha}\,\boldsymbol{v}\,\|_{0,M} + \sum_{L\in\mathcal{K}_{2h}} C_{p,L} h_{3,*}^{-1/2} h_L^{l+1} \|p\|_{l+1,L}$$

with
$$C_{v,M}^2 := \nu\, h_{3,M}^{-1} + \sigma\, h_{3,M} + \|\boldsymbol{b}_h\|_{0,\infty,M} + h_\omega^2\,\mathrm{f}^2\,\sigma_M \|\boldsymbol{b}_h\|_{0,\infty,M}^{-1}$$
$$C_{p,L}^2 := \nu + \sigma + \max_{M\in\mathcal{T}_L} \left\{\sigma_M \|\boldsymbol{b}_h\|_{0,\infty,M}^{-1}\right\}$$

and $h_{3,*} := \min\{h_{3,T} \,|\, T \in \mathcal{T}_h\}$.

Proof. We split the triple norm of $\mathbf{u} - \mathbf{u}_h := (\boldsymbol{v} - \boldsymbol{v}_h, p - p_h)$ into an interpolation and a projection part:

$$\|\!|\, \mathbf{u} - \mathbf{u}_h \,|\!\| \le \|\!|\boldsymbol{\eta}|\!\| + \|\!|\boldsymbol{\varsigma}|\!\|\,.$$

with interpolation error $\boldsymbol{\eta} = \mathbf{u} - \boldsymbol{i}_h\,\mathbf{u}$ and projection error $\boldsymbol{\varsigma} = \boldsymbol{i}_h\,\mathbf{u} - \mathbf{u}_h$. The interpolation operator $\boldsymbol{i}_h$ consists of velocity interpolation operator $i_{h,3d} : \mathbf{V} \to \mathbf{V}_h$, which is taken from Proposition 5.16, and of the 2D pressure interpolation operator $i_{h,2d} : Q \to Q_h$, which is taken from the isotropic 2D case. I.e. the latter one denotes the 2D version of the L^2-orthogonal interpolation operator as defined in Subsection 4.1.2(d). Considering (5.54), Proposition 5.16 as well as Lemmata 5.28 and 5.32, $|\!|\!|\boldsymbol{\eta}|\!|\!|$ can thus be estimated as

$$\begin{aligned}
|\!|\!|\boldsymbol{\eta}|\!|\!|^2 &:= \nu\|\nabla(\boldsymbol{v} - i_{h,3d}\,\boldsymbol{v})\|_{0,\Omega}^2 + \sigma\|\,\boldsymbol{v} - i_{h,3d}\,\boldsymbol{v}\,\|_{0,\Omega}^2 + s_{h,v}(\boldsymbol{v} - i_{h,3d}\,\boldsymbol{v}, \boldsymbol{v} - i_{h,3d}\,\boldsymbol{v}) \\
&\quad + (\nu+\sigma)\|p - i_{h,2d}p\|_{0,\Omega}^2 + s_{h,p}(p - i_{h,2d}p, p - i_{h,2d}p) \\
&\lesssim \sum_{M\in\mathcal{T}_{2h}} (\nu h_{3,M}^{-2} + \sigma + \sigma_M h_{3,M}^{-1}(\|\boldsymbol{b}_h\|_{0,\infty,M} + h_\omega^2\,\mathrm{f}^2\,\|\boldsymbol{b}_h\|_{0,\infty,M}^{-1})) \sum_{|\alpha|=k+1} \mathbf{h}_M^{2\alpha} \|D^{\alpha}\,\boldsymbol{v}\,\|_{0,M}^2 \\
&\quad + \sum_{L\in\mathcal{K}_{2h}} h_L^{2l+1}((\nu+\sigma)h_L + \max_{M\in\mathcal{T}_L}\left\{\sigma_M\|\boldsymbol{b}_h\|_{0,\infty,M}^{-1}\right\}\, h_L h_{3,*}^{-1})\|p\|_{l+1,L}^2\,.
\end{aligned}$$

For the estimate of $\|\!|\boldsymbol{\varsigma}|\!\|$ we apply the discrete stability result of Proposition 5.30. We chose a test function $\boldsymbol{\phi} := (\boldsymbol{\varphi}, \xi) \in B_h$, i.e. $\boldsymbol{\phi} \in \boldsymbol{X}_h$ and $\|\!|\, \boldsymbol{\phi} \,|\!\| = 1$, such that

$$A_h(\boldsymbol{b}_h; \boldsymbol{\varsigma}, \boldsymbol{\phi}) \geq \gamma_{\Omega,\omega} \|\!|\boldsymbol{\varsigma}|\!\| \,.$$

Note, that the solutions $\mathbf{u} \in \mathbf{X}$ of problem (3.33) and $\mathbf{u}_h \in \mathbf{X}_h$ of (5.60) fulfill

$$A_h(\boldsymbol{b}_h; \mathbf{u}_h; \boldsymbol{\phi}) = \langle \boldsymbol{f}, \boldsymbol{\varphi} \rangle = A(\boldsymbol{b}; \mathbf{u}; \boldsymbol{\phi}) = A(\boldsymbol{b}_h; \mathbf{u}; \boldsymbol{\phi}) + \langle ((\boldsymbol{b} - \boldsymbol{b}_h) \cdot \nabla)\, \boldsymbol{v}; \boldsymbol{\varphi} \rangle \,.$$

Thus, it suffices to analyze the terms on the right hand side of

$$A_h(\boldsymbol{b}_h; \boldsymbol{\varsigma}; \boldsymbol{\phi}) = A(\boldsymbol{b}_h; \boldsymbol{\eta}; \boldsymbol{\phi}) + s_{h,v}(i_{h,3d}\, \boldsymbol{v}, \boldsymbol{\varphi}) + s_{h,p}(i_{h,2d} p, \xi) - \langle ((\boldsymbol{b} - \boldsymbol{b}_h) \cdot \nabla)\, \boldsymbol{v}; \boldsymbol{\varphi} \rangle \,.$$

In order to estimate of the bilinear form $A(\boldsymbol{b}_h; \boldsymbol{\eta}; \boldsymbol{\phi})$ we apply Lemmata 5.27 and 5.31, as well as 5.32 and the property $\sigma_M \leq 1$ for any $M \in \mathcal{T}_L$:

$$\begin{aligned}
(\mathrm{div}'\, \mathbf{M}\, \boldsymbol{\eta}_v, \xi)_\omega \;&\leq |(\mathbf{M}\, \boldsymbol{\eta}_v, \nabla' \xi)_\omega| \\
&\lesssim \delta_{max}^{1/2} \sum_{L \in \mathcal{K}_{2h}} (h_L \sigma_L)^{-1/2} \|\boldsymbol{b}_h\|_{0,\infty,L}^{1/2} \sum_{|\alpha|=k+1} \sum_{M \in \mathcal{T}_L} \mathbf{h}_M^\alpha \, \| D^\alpha \boldsymbol{v} \|_{0,M} \\
\lesssim\; \delta_{max}^{1/2} \sum_{L \in \mathcal{K}_{2h}} \min_{M \in \mathcal{T}_L} \{ \max\{ \nu h_{3,M}^{-1}, \sigma_M \|\boldsymbol{b}_h\|_{0,\infty,M} \} \}^{1/2} h_\omega^{-1/2} \sum_{|\alpha|=k+1} \sum_{M \in \mathcal{T}_L} \mathbf{h}_M^\alpha \, \| D^\alpha \boldsymbol{v} \|_{0,M} \\
\lesssim\; \delta_{max}^{1/2} \sum_{M \in \mathcal{T}_{2h}} \max\{ \nu h_{3,M}^{-1}, \|\boldsymbol{b}_h\|_{0,\infty,M} \}^{1/2} h_\omega^{-1/2} \sum_{|\alpha|=k+1} \mathbf{h}_M^\alpha \, \| D^\alpha \boldsymbol{v} \|_{0,M} \\
\langle (\boldsymbol{b}_h \cdot \nabla) \boldsymbol{\eta}_v, \boldsymbol{\varphi} \rangle \;&\lesssim \sum_{M \in \mathcal{T}_{2h}} \|\boldsymbol{b}_h\|_{0,\infty,M} \min\{ \delta_{3,M}^{-1/2}, \nu^{-1/2} \} \sum_{|\alpha|=k+1} \mathbf{h}_M^\alpha \| D^\alpha \boldsymbol{v} \|_{0,M} \\
&\lesssim \sum_{M \in \mathcal{T}_{2h}} (\|\boldsymbol{b}_h\|_{0,\infty,M} h_{3,M}^{-1})^{1/2} \sum_{|\alpha|=k+1} \mathbf{h}_M^\alpha \| D^\alpha \boldsymbol{v} \|_{0,M} \\
\mathrm{f}(\boldsymbol{\eta}_v^\perp, \boldsymbol{\varphi})_\Omega \;&\lesssim \sum_{M \in \mathcal{T}_{2h}} \gamma_M^{-1/2}\, \mathrm{f} \sum_{|\alpha|=k+1} \mathbf{h}_M^\alpha \| D^\alpha \boldsymbol{v} \|_{0,M} \\
&\lesssim \sum_{M \in \mathcal{T}_{2h}} \max\{ \nu h_{3,M}^{-1}, \, \|\boldsymbol{b}_h\|_{0,\infty,M} \}^{1/2} h_{3,M}^{1/2} \sum_{|\alpha|=k+1} \mathbf{h}_M^\alpha \| D^\alpha \boldsymbol{v} \|_{0,M} \,, \\
(\mathrm{div}'\, \mathbf{M}\, \boldsymbol{\varphi}, \eta_p)_\omega \;&\lesssim \delta_{max}^{1/2} \sum_{L \in \mathcal{K}_{2h}} \min\{ \max_{M \in \mathcal{T}_L} \{ \delta_{3,M}^{-1/2} \}, \nu^{-1/2} \}\, h_\omega^{l+1} \, \|p\|_{l+1,L} \\
&\lesssim \delta_{max}^{1/2} \sum_{L \in \mathcal{K}_{2h}} \max_{M \in \mathcal{T}_L} \{ \sigma_M \|\boldsymbol{b}_h\|_{0,\infty,M}^{-1} h_{3,M}^{-1} \}^{1/2} h_\omega^{l+1} \, \|p\|_{l+1,L}
\end{aligned}$$

and bound the remaining terms canonically as

$$\nu(\nabla \boldsymbol{\eta}_v, \nabla\, \boldsymbol{\varphi})_\Omega + \sigma(\boldsymbol{\eta}_v, \boldsymbol{\varphi})_\Omega \quad \leq \sum_{T \in \mathcal{T}_h} (\nu^{1/2} (h_\omega^{-1} + h_{3,T}^{-1}) + \sigma^{1/2}) \sum_{|\alpha|=k+1} \mathbf{h}_T^\alpha \| D^\alpha \boldsymbol{v} \|_{0,T} \,.$$

Using the estimates (5.53) and (5.54), and applying the results of Lemmata 5.29 and

5.32 we get

$$\begin{aligned} s_{h,p}(i_{h,2d}p,\xi) &\lesssim \sum_{L\in\mathcal{K}_{2h}} \sigma_L^{1/2}\|\boldsymbol{b}_h\|_{0,\infty,L}^{-1/2} h_L^{l+1/2}\|p\|_{l+1,L}\,, \\ s_{h,v}(i_{h,3d}\,\boldsymbol{v},\boldsymbol{\varphi}) &\lesssim \sum_{M\in\mathcal{T}_{2h}} (\lambda_M^{1/2}+\gamma_M^{1/2}) \sum_{|\alpha|=k+1} \mathbf{h}_M^{\alpha}\|D^{\alpha}\,\boldsymbol{v}\,\|_{0,M} \\ &\lesssim \sum_{M\in\mathcal{T}_{2h}} \sigma_M^{1/2}(\|\boldsymbol{b}_h\|_{0,\infty,M}^{1/2} + h_\omega\,\mathrm{f}\,\|\boldsymbol{b}_h\|_{0,\infty,M}^{-1/2})\, h_{3,M}^{-1/2} \sum_{|\alpha|=k+1} \mathbf{h}_M^{\alpha}\|D^{\alpha}\,\boldsymbol{v}\,\|_{0,M}\,. \end{aligned}$$

Due to Assumption 5.25 the remaining term can be estimated as

$$\begin{aligned} \langle((\boldsymbol{b}-\boldsymbol{b}_h)\cdot\nabla)\,\boldsymbol{v},\boldsymbol{\varphi}\rangle &\leq \sum_{T\in\mathcal{T}_h} \|\boldsymbol{b}-\boldsymbol{b}_h\|_{0,3,T}|\,\boldsymbol{v}\,|_{1,T}\|\,\boldsymbol{\varphi}\,\|_{0,6,T} \\ &\lesssim \sum_{T\in\mathcal{T}_h} h_{3,T}^{-1} \sum_{|\alpha|=k+1} \mathbf{h}_T^{\alpha}|\,\boldsymbol{v}\,|_{1,T}|\,\boldsymbol{\varphi}\,|_{1,T} \qquad (5.73) \\ &\leq \nu^{-1/2} \sum_{T\in\mathcal{T}_h} h_{3,T}^{-1} \sum_{|\alpha|=k+1} \mathbf{h}^{\alpha}\|\,\boldsymbol{v}\,\|_{k+1,T}\,. \end{aligned}$$

Combining the resulting estimates finishes the proof. □

5.3.6 The vertical velocity component

As in the isotropic case we examine the *a priori* error estimates of the vertical velocity component. Recall, that the vertical velocity v_3 can be (uniquely) determined by (2.30) for a given horizontal velocity field $\boldsymbol{v}\in\mathbf{V}$. The finite element discretized vertical velocity $v_{3,h}\in\{\varphi\in\mathcal{C}(\Omega)\,|\,v_{3,h}|_{\Gamma_b}=0 \text{ and } v_{3,h}|_T\in\mathbb{Q}_r,\ \forall T\in\mathcal{T}_h\}$ thus fulfills:

$$\|v_3-v_{3,h}\|_{0,\Omega}^2 \quad = \quad \left|\left|\int_{-d(x,y)}^{z} \mathrm{div}\,'(\boldsymbol{v}-\boldsymbol{v}_h)\,d\widehat{z}\right|\right|_{0,\Omega}^2 \quad \leq \quad \delta_{max}^2|\,\boldsymbol{v}-\boldsymbol{v}_h\,|_{1,\Omega}^2\,.$$

Assuming sufficient regularity of $\boldsymbol{v}$ and recalling the results of Proposition 5.33, as well as the definition of $|||\cdot|||$ we get:

$$\begin{aligned} \delta_{max}^{-1}\nu^{1/2}\|v_3-v_{3,h}\|_{0,\Omega} &\leq \nu^{1/2}|\,\boldsymbol{v}-\boldsymbol{v}_h\,|_{1,\Omega} \\ &\lesssim \sum_{M\in\mathcal{T}_{2h}} \nu^{1/2}C_{v,M}h_{3,M}^{-1/2} \sum_{|\alpha|=k+1} \mathbf{h}_M^{\alpha}\|D^{\alpha}\,\boldsymbol{v}\,\|_{0,M}\,. \end{aligned}$$

For further argumentation we refer to the isotropic case.

5.3.7 Conclusions

We concentrated on the case of local projection stabilization for the velocity stabilization and developed a stabilization scheme, which assures inf-sup stability of the problem, as well as derived suitable *a priori* error estimates.

Note, that the estimate of the divergence constraint (5.64) evokes a nonlocal dependence on the vertical mesh sizes $h_{3,M}$ for all elements M of a prism $\mathcal{T}_K$, which enters in the *a priori* estimate of Proposition 5.33 of the pressure as $h_{3,*} := \min\{h_{3,T} \,|\, T \in \mathcal{T}_h\}$. Thus, if non regular meshes $\mathcal{T}_h$ are apparent, these estimates may become large and effect the entire prism with surface cell $L \in \mathcal{K}_h$. However note, that such a term is also part of the estimate of the non hydrostatic case, see e.g. [Bra08a] for the 2D Oseen problem. Entirely, we qualitatively resulted in the same results for the 2.5D problem as derived in [Bra08a] for the 2D case.

If we would aim to transfer the present results to the 3D non hydrostatic case, we need to assure existence of a suitable 3D anisotopic pressure stabilization, such that inf-sup stability is guaranteed, independent on the aspect ratio. In the case of local projection stabilization, this means, that we need an inf-sup stable finite element pair in 3D as projected space. Recalling the considerations of Section 5.1.3 the choice $Q_r - Q_{r-2}$ is an option for layered meshes and the 3D pressure stabilization then reads

$$s_{h,p}(p,\xi) := \sum_{T\in\mathcal{T}_h} \alpha_T(\kappa_h^\Omega(\nabla p), \kappa_h^\Omega(\nabla\xi))_T$$

with $\kappa_h^\Omega = id^\Omega - \pi$ and L^2-projection $\pi : \mathrm{L}_0^2(\Omega) \to Q_{2h}^{r-2}(\Omega)$, constructed as in Section 5.1.1(d). The stabilization of the velocity field in the Oseen case is the adaption of $s_{h,v}$ presented beforehand. The error estimates for the pressure and the velocity part then are similar to the hydrostatic case, but a little simpler, as the vertical integration is not apparent in the divergence constraint.

5.4 Hydrostatic Stokes problem on horizontal anisotropic meshes

In this section we examine the hydrostatic Stokes problem on horizontal anisotropic Cartesian meshes. We proceed as in the previous cases by introducing the discrete problem, analysis of its stability property. We then introduce suitable stabilization schemes, validate the desired stability property and turn to the estimates of the *a priori* error.

5.4.1 Galerkin formulation

Let $\mathcal{T}_h$ be a horizontal anisotropic mesh fulfilling Assumption 4.2. The appropriate discrete spaces are given by $\mathbf{V}_h \subset \mathbf{V} := \mathbf{H}_0^1(\Omega)$ and $Q_h \subset Q := \mathrm{L}_0^2(\omega)$ as defined in (4.6) and (4.4) for $r = 1$. We set $\mathbf{X}_h := \mathbf{V}_h \times Q_h$. As in the case of vertical anisotropic meshes the hydrostatic Stokes problem reads

$$\begin{aligned} &\textit{Given } \boldsymbol{f} \in \mathbf{V}^{-1}, \textit{ find } (\boldsymbol{v}_h, p_h) \in \mathbf{X}_h \\ &\quad \textit{s. t. } \mathrm{a}(\boldsymbol{v}_h, \boldsymbol{\varphi}) - \mathrm{b}(p_h, \boldsymbol{\varphi}) + \mathrm{b}(\xi, \boldsymbol{v}_h) \;=\; (\boldsymbol{f}, \boldsymbol{\varphi})_\Omega \qquad \forall (\boldsymbol{\varphi}, \xi) \in \mathbf{X}_h \end{aligned} \tag{5.74}$$

with bilinear forms $\mathrm{a}(\boldsymbol{v}_h, \boldsymbol{\varphi}) := (\nabla \boldsymbol{v}_h, \nabla \boldsymbol{\varphi})_\Omega$ and $\mathrm{b}(p_h, \boldsymbol{\varphi}) := (p_h, \mathrm{div}' \mathbf{M} \boldsymbol{\varphi})_\omega$.

Similar to the vertical anisotropic case we recover the following stability result:

Proposition 5.34. *Let Ω be a flat domain and $\mathcal{T}_h$ be a horizontal anisotropic triangulation of Ω fulfilling Assumption 4.2. The 2.5D Stokes problem (5.46) has a unique solution, if the 2D Stokes problem (4.18) has a unique solution.*

Proof. The proof coincides with the vertical anisotropic analogue. □

Referring to the discussions in Section 5.1.3, stabilization of the problem (5.74) is necessary in order to result in an inf-sup stable scheme. In the upcoming we restrict to the case of bilinear finite elements.

5.4.2 Stabilization of the problem

For sake of brevity we restrict to Cartesian meshes and refer to the cited literature. We consider the stabilization schemes of the equal-order finite element discretized 2D Stokes problem on anisotropic meshes as introduced and analyzed in [Bec95, Ric05, BT06a]:

($\mathbf{P}_{aniso}$-i) Becker [Bec95] for linear elements $r = 1$:

$$s_h(p, \xi) := \sum_{K \in \mathcal{K}_h} h_{1,K}^2 (\partial_x p,\, \partial_x \xi)_K + h_{2,K}^2 (\partial_y p,\, \partial_y \xi)_K.$$

($\mathbf{P}_{aniso}$-ii) Local projection stabilization (LPS) [Ric05],

$$s_h(p_h, \xi) := \delta_0 \sum_{K \in \mathcal{K}_h} h_{1,K}^2 (\partial_x(\kappa_h p_h), \partial_x(\kappa_h p_h))_K + h_{2,K}^2 (\partial_y(\kappa_h p_h), \partial_y(\kappa_h p_h))_K$$

with $\kappa_h := id - \pi$ and L^2-projection $\pi : \mathrm{L}_0^2(\omega) \to Q_{2h}^1(\omega)$ onto the 'discontinuous' space $Q_{2h}^1(\omega)$.

($\mathbf{P}_{aniso}$-iii) Local projection stabilization (LPS) [BT06a],

$$s_h(p_h, \xi) := \delta_0 \sum_{K \in \mathcal{K}_h} (\kappa_h(\partial_x p_h), \kappa_h(\partial_x p_h))_K + h_{2,K}^2 (\kappa_h(\partial_y p_h), \kappa_h(\partial_y p_h))_K,$$

with $\kappa_h := id - \pi$, L^2-projection $\pi : \mathrm{L}_0^2(\omega) \to Q_{2h}^1(\omega)$ onto the 'discontinuous' space $Q_{2h}^1(\omega)$.

Using one of these stabilization schemes, the stabilized problem is given by

$$\begin{aligned} &\textit{Find } (\boldsymbol{v}_h, p_h) \in \mathbf{X}_h \textit{ s. t.} \\ &\qquad A_h(\boldsymbol{v}_h, p_h; \boldsymbol{\varphi}, \xi) = (\boldsymbol{f}, \boldsymbol{\phi})_\Omega \qquad \forall\, \boldsymbol{\phi} := (\boldsymbol{\varphi}, \xi) \in \mathbf{X}_h \qquad (5.75) \\ &\textit{with } A_h(\boldsymbol{v}_h, p_h; \boldsymbol{\varphi}, \xi) := a(\boldsymbol{v}_h, \boldsymbol{\varphi}) - b(p_h, \boldsymbol{\varphi}) + b(\xi, \boldsymbol{v}_h) + s_h(p_h, \xi)\,. \qquad (5.76) \end{aligned}$$

For the upcoming proofs we apply the triple norm $|\!|\!| \cdot |\!|\!|$ as given in (5.49) and the appropriate sphere B_h.

The inf-sup stability property,

$$\inf_{(\boldsymbol{v}_h,p_h)\in B_h} \sup_{(\boldsymbol{\varphi},\xi)\in B_h} A_h(\boldsymbol{v}_h,p_h;\boldsymbol{\varphi},\xi) \;\geq\; \gamma_{\Omega,\omega}\,.$$

can be validated in the same way as in the case of vertical anisotropic meshes, i.e. Proposition 5.21, applying the inf-sup stability results on anisotropic meshes $\mathcal{K}_h$ as proven in [Bec95, Ric05, BT06a]. We omit an additional proposition and proof here and refer to Proposition 5.21.

5.4.3 *A priori* error estimates

In order to suitable establish *a priori* error estimates, we collect some estimates of the introduced stabilization schemes.

Lemma 5.35. *The Cartesian mesh $\mathcal{K}_h$ is assumed to fulfill the demands of Section 5.1.1 for the surface mesh of a horizontal anisotropic mesh. Let $i_{h,2d}$ be the modified Scott-Zhang interpolation operator as constructed in [BT06a]. The stabilization schemes (P_{aniso}-i) – (P_{aniso}-iii) allow the estimates*

$$s_{h,p}(i_{h,2d}p, i_{h,2d}p) \lesssim \sum_{L\in\mathcal{K}_{2h}} h_{1,L}^2\|\partial_x p\|_{0,L}^2 + h_{2,L}^2\|\partial_y p\|_{0,L}^2 \quad \forall p\in H^1(\omega)\,, \tag{5.77}$$

$$s_{h,p}(i_{h,2d}p - p, i_{h,2d}p - p) \lesssim \sum_{L\in\mathcal{K}_{2h}} h_{1,L}^2\|\partial_x p\|_{0,L}^2 + h_{2,L}^2\|\partial_y p\|_{0,L}^2 \quad \forall p\in H^1(\omega)\,. \tag{5.78}$$

Proof. The estimates are to be found in [Bec95, Ric05, BT06a] or simple consequences of the estimates in the cited literature. □

Note, that in the case of Cartesian meshes fulfilling Assumption 4.2 we have $h_{i,K} = h_{i,T}$, $i = 1, 2$ for any $T \in \mathcal{T}_h$ whose 2D projection onto the surface mesh $\mathcal{K}_h$ is K.
Applying the above estimates of the stabilization schemes we can prove the following *a priori* error estimates:

Proposition 5.36. *Let Ω be chosen such that there is a horizontal anisotropic Cartesian triangulation $\mathcal{T}_h$ of Ω. If the continuous solution of (4.32) formulated in $\mathbf{X} := (\mathbf{V}\times Q)$ is sufficiently regular, $(\boldsymbol{v},p)\in\mathbf{H}^2(\Omega)\times\mathrm{H}^1(\omega)$, we obtain the following estimate for the discrete solutions $(\boldsymbol{v}_h,p_h)$ of (5.75) for the methods (P_{aniso}-i)–(P_{aniso}-iii):*

$$\begin{aligned}|\!|\!|(\boldsymbol{v}-\boldsymbol{v}_h, p-p_h)|\!|\!| \;\lesssim\; & \sum_{T\in\mathcal{T}_h}\sum_{|\alpha|=1} \mathbf{h}_T^{\alpha}\;|D^{\alpha}\,\boldsymbol{v}\,|_{1,S_T} \\ & + \sum_{K\in\mathcal{K}_h} h_{1,K}\,\|\partial_x p\|_{0,S_K} + h_{2,K}\,\|\partial_y p\|_{0,S_K}\end{aligned} \tag{5.79}$$

with patches S_T and S_K for any $T\in\mathcal{T}_h$ and $K\in\mathcal{K}_h$.

Proof. We split the error into an interpolation and a projection part. As in the case of vertical anisotropic meshes, we apply different interpolation operators for the velocity and the pressure. The interpolation operator for the pressure, $i_{h,2d}$, is given by the modified Scott-Zhang interpolation operator as introduced in [BT06a], see also Section 5.1.2. The interpolation operator for the velocity, $i_{h,3d}$, is given by the Scott-Zhang interpolant for anisotropic meshes of tensor product type as introduced in [Ape99] for needle cells (see p.123f in [Ape99]), which also has the desired interpolation properties, see Section 5.1.2.
Due to the interpolation properties of these operators, it remains to examine the projection error. This estimate can be done as in the proof of Proposition 5.50 using the estimates of Lemma 5.35. □

5.4.4 Prospects for the hydrostatic Oseen problem

The introduced anisotropic pressure stabilization schemes can be used in order to construct suitable stabilizations for the hydrostatic Oseen problem on horizontal anisotropic meshes. The argumentation remains as in the vertical anisotropic case with a suitably altered anisotropic stabilization, as e.g. is introduced in [Bra08a] for the 2D case. But note, that the stabilization parameters differ as $h_{3,T}$ generally is not the smallest mesh size characteristic. Thus, the local Peclet number has to be altered, see e.g. [Bra08a], not only in the velocity stabilization but also in the pressure stabilization. However, due to the modified inf-sup constraint, the coupling within a (vertical oriented) prism of the considered mesh still remains.

Chapter 6

Discretization of Evolutionary Hydrostatic Systems

Based on the results of the discretization of stationary problems we now broaden our attention to the discretization of the *evolutionary* problems, i.e. beside the space discretization we also have to treat time dependencies.
In [CR02], Chacón Rebollo and Rodriguez Gomez treat the Rothe approach for hydrostatic flow problems and solve the problem. However in the context of ocean circulation modeling this approach is far too expensive. The reason is, that due to the incompressibility constraint coupled numerical solution of ocean circulation problems show a coupling of the velocity and pressure field.
In the context of nonhydrostatic flow problems, a popular resort is provided by the class of *pressure segregation* (or *splitting*) *schemes*, which have been invented in the late 1960's by Chorin [Cho68] and Temam [Tem68]. Several splitting schemes have been invented and analyzed since then, see e.g. [BC08, GMS06, Pro97, Ran92, NP05]. These schemes commonly consist of two subproblems, one for the pressure and one for the velocity, such that standard solvers for the appropriate subproblems can be applied. Analysis of splitting schemes in the context of stabilized flow problems has been studied in [BC08]. The authors treated the case of OSS stabilization. For a couple of schemes they observed improved stability properties, which do not break down when the time step goes to zero.
The tight relation between hydrostatic and nonhydrostatic problems suggests the application of these splitting schemes in the hydrostatic framework. Moreover, one might suspect a further computing time advantage, as the pressure problem has to be solved solely in 2D, whereas the horizontal velocity problem remains a 3D problem. Recall, that this was the original impetus for the application of the hydrostatic approximation. Due to that reason, we restrict our attention to the field of splitting schemes. Note that due to the authors knowledge application of splitting schemes to hydrostatic problems is a widely undealt field and appropriate analysis is still missing.

The chapter is structured as follows: In Section 6.1 we present the basic ideas of splitting schemes. Due to the suitability of pressure correction schemes for hydrostatic issues we restrict to this class of splitting schemes in Section 6.2. We also present im-

portant examples of this class. For further interest note, that in Appendix A.2 we give a survey of further common schemes and consider the treatment for stabilized problems. In Section 6.3 we turn to the application of pressure correction schemes to hydrostatic problems. We start this section with notes on the interaction between the 2D pressure and the 3D velocity field. Justifying the applicability of pressure correction schemes to hydrostatic problems we draw observations of the transferability of properties in the nonhydrostatic framework to the hydrostatic case. Such are the projection property, which is crucial in this context, the restriction on velocity boundary conditions and the possibility of improving the artificial boundary conditions on the pressure. We finally present a pressure correction algorithm for hydrostatic flow problems. As we apply equal order finite elements, we consider stabilized problems.

6.1 Principles of splitting schemes

In this section we collect main aspects of splitting schemes as given in literature, such as [GMS06, BC08, Pro08, Pro97]. The majority of publications in this field focuses on nonhydrostatic flow problems with *homogeneous Dirichlet data on the whole boundary of* Ω. Recall, that we assume Ω to be a bounded, simply connected Lipschitz domain, see Section 3.1.1. Corresponding to these boundary conditions, the L^2-orthogonal Helmholtz decomposition

$$\mathbf{L}^2(\Omega) = \mathbf{J_0} \oplus \mathbf{J_0}^\perp ,$$

see also [GR86], plays a crucial role in the analysis of the class of *projection methods*, such as the henceforth introduced pressure correction and velocity correction schemes. For the definition of $\mathbf{J_0}$ see (3.12) on page 33. The space $\mathbf{J_0}^\perp$ can be identified by

$$\mathbf{J_0}^\perp := \{\nabla p \mid p \in \mathrm{H}^1(\Omega)\} ,$$

which, anticipating, indicates the role of the pressure. In the case of open boundary conditions on parts $\Gamma_1 \neq \emptyset$ of $\partial\Omega$, the decomposition of $\mathrm{L}^2(\Omega)$ differs, i.e. we have a Hodge decomposition,

$$\begin{aligned} \mathbf{L}^2(\Omega) &= \mathbf{J} \oplus \widetilde{\mathbf{J}} && \text{with} \\ \mathbf{J} &:= \{\boldsymbol{v} \in \mathbf{L}^2(\Omega) \mid \operatorname{div} \boldsymbol{v} = 0 \text{ and } \boldsymbol{v} \cdot \boldsymbol{n}|_{\Gamma_1} = 0\} && \text{and} \\ \widetilde{\mathbf{J}} &:= \{\nabla p \in \mathbf{L}^2(\Omega) \mid p \in \mathrm{H}^1(\Omega) \text{ and } p|_{\partial\Omega\setminus\Gamma_1} = 0\} . \end{aligned} \tag{6.1}$$

This effects a different boundary setting for the pressure in the occurring pressure Poisson problem, see [GMS06]. This case as well as the case of differing velocity boundary conditions but homogeneous Dirichlet data on $\partial\Omega$ have been rarely discussed in literature.

Provided a Helmholtz decomposition of $\mathbf{L}^2(\Omega)$, the appropriate L^2-orthogonal projection operator P maps a given element $\widetilde{\boldsymbol{v}} \in \mathbf{L}^2(\Omega)$ onto $\boldsymbol{v} = \widetilde{\boldsymbol{v}} + \nabla q$ with $\nabla q \in \mathbf{J_0}^\perp$ and $\boldsymbol{v} \in \mathbf{J_0}$, or $\nabla q \in \mathbf{J}^\perp$ and $\boldsymbol{v} \in \mathbf{J}$, respectively. This projection plays an essential

role in the context of pressure and velocity correction schemes and justifies the notion *projection schemes*, which is occasionally used. Under the presumption that Ω is a $\mathcal{C}^{r+1}$-domain, $r \geq 1$, this projection operator is $\mathrm{H}^r(\Omega)$-stable, see [Tem68], i.e.

$$\|Pv\|_{0,\Omega} \leq C_{r,\Omega}\|v\|_{r,\Omega}\,.$$

This projection is embedded in a time discretization process, using established time-discretization schemes, see e.g. Section A.1. In order to announce accuracy statements of the splitting schemes, we denote the following: For a given time step $\Delta t > 0$ and $t^i = i\Delta t$ with $i \in \{0, \ldots, i_{max} = \mathcal{T}/\Delta t\}$, let

$$\varphi_{\Delta t} := (\varphi_i)_{i=0}^{i_{max}}$$

be a sequence in a Hilbert space V. We use the discrete norms

$$\|\varphi_{\Delta t}\|_{l^2(V)} := \left(\Delta t \sum_{i=0}^{i_{max}} \|\varphi_i\|_V^2\right)^{1/2}, \quad \|\varphi_{\Delta t}\|_{l^\infty(V)} := \max_{i\in\{0,\ldots,i_{max}\}} \|\varphi_i\|_V\,.$$

In the upcoming we distinguish and introduce the classes of *pressure-correction schemes*, *velocity-correction schemes* and *consistent splitting schemes*.

As the nonlinearity of the Navier-Stokes equations does not effect the splitting error, see [GMS06], we restrict to the 3D Stokes equations (3.3). Moreover we set $\mathrm{f} = 0$, apply isotropic viscosity, i.e. consider only *one* viscosity $\nu > 0$ for all space dimensions, and, being guided by the literature at hand, demand homogeneous Dirichlet boundary conditions on $\partial\Omega$. I.e. given a sufficiently smooth forcing $\boldsymbol{f}$ and initial condition $\boldsymbol{v}_0 \in \mathbf{J}_1 \cap \mathbf{H}_0^1(\Omega)$ we consider the problem

$$\begin{array}{lrcll} \textit{Find } (\boldsymbol{v}, p) \textit{ s. t.} & \partial_t \boldsymbol{v} - \nu\Delta\boldsymbol{v} + \nabla p &=& \boldsymbol{f} & \text{in } \Omega\times[0,\mathcal{T}] \\ & \operatorname{div}\boldsymbol{v} &=& 0 & \text{in } \Omega\times[0,\mathcal{T}] \\ & \boldsymbol{v}|_{\partial\Omega} &=& 0 & \text{in } [0,\mathcal{T}] \\ & \boldsymbol{v}|_{t=0} &=& \boldsymbol{v}_0 & \text{in } \Omega\,. \end{array} \tag{6.2}$$

6.2 Pressure correction methods for non hydrostatic problems

The idea of pressure correction schemes is to apply established time-discretizations, see e.g. Section A.1, to use an explicite, extrapolated pressure in the momentum equation, and to treat the momentum and the continuity equation separately.
Let $p^{i-(l-1)}, \ldots, p^i$, $i \geq l-1$, be the approximations of the pressure at time steps $(i-l+1)\Delta t, \ldots, i\Delta t$. The l-th order extrapolation of the pressure at time $(i+1)\Delta t$ is given by

$$p^{i+1,*} := \sum_{n=0}^{l-1} \gamma_n p^{i-n} \tag{6.3}$$

with constant $\gamma_0, \ldots, \gamma_{l-1} \in \mathbb{R}$. For $n = 0, 1, 2$, appropriate parameter settings are given on the right hand side of Table A.1. Moreover, we apply the following approximation for a given time derivative, see (A.1):

$$D_k y^{i+1} \quad = \quad \alpha_0 y^{i+1} + D_{k,1} y^{i+1} \quad := \quad \alpha_0 y^{i+1} + \sum_{j=1}^{k} \alpha_j y^{i-j+1} \,. \tag{6.4}$$

Thus, the class of pressure correction schemes is given by

Algorithm 6.1 (Pressure correction scheme)**.** *Let $\chi \in \{0, 1\}$, $k, l \in \mathbb{N}$, and, for any $i \geq \max\{k, l\} - 1$, initial values $\boldsymbol{v}^{i-k+1}, \ldots, \boldsymbol{v}^i$ and $p^{i-l+1}, \ldots, p^i$ be given.*

The i-th step of the scheme is given by:

(i) Velocity predictor step *Find the velocity predictor $\widetilde{\boldsymbol{v}}^{i+1}$ s.t.*

$$\Delta t^{-1}(\alpha_0 \widetilde{\boldsymbol{v}}^{i+1} + D_{k,1}\, \boldsymbol{v}^{i+1}) - \nu \Delta \widetilde{\boldsymbol{v}}^{i+1} + \nabla p^{i+1,*} = \boldsymbol{f}(t^{i+1}) \qquad \text{in } \Omega, \tag{6.5}$$

$$\widetilde{\boldsymbol{v}}^{i+1} = 0 \qquad \text{on } \partial\Omega \tag{6.6}$$

(ii) Velocity corrector and pressure predictor step

Determine a pressure q_{i+1} and the appropriate corrected (divergence free) velocity $\boldsymbol{v}^{i+1}$, s. t.

$$\Delta t^{-1} \alpha_0 (\boldsymbol{v}^{i+1} - \widetilde{\boldsymbol{v}}^{i+1}) + \nabla q^{i+1} = 0 \qquad \text{in } \Omega \tag{6.7}$$

$$div\, \boldsymbol{v}^{i+1} = 0 \qquad \text{in } \Omega \tag{6.8}$$

$$\boldsymbol{v}^{i+1} \cdot \boldsymbol{n} = 0 \qquad \text{on } \partial\Omega \tag{6.9}$$

(iii) Pressure corrector step *Update the pressure due to*

$$p^{i+1} = q^{i+1} + p^{i+1,*} - \chi \nu\, div\, \widetilde{\boldsymbol{v}}^{i+1} \qquad \text{in } \Omega \tag{6.10}$$

In step (i) of the algorithm, an established time discretization, see Section A.1, is applied, whereas the yet undetermined velocity with (consistent) boundary conditions is denoted by $\widetilde{\boldsymbol{v}}^{i+1}$. This velocity is not divergence free. As well, the pressure is treated explicitely by the extrapolation $p^{i+1,*}$. In step (ii), the swap of $\boldsymbol{v}^{i+1}$ by $\widetilde{\boldsymbol{v}}^{i+1}$ in step (i) is corrected with the help of a predictive pressure q^{i+1}, demanding correct boundary conditions on $\boldsymbol{v}^{i+1}$ only in normal direction. Step (iii) of the pressure correction algorithm gathers the remaining "inconsistencies" evoked in steps (i) and (ii), i.e. the introductions of the pressure extrapolation in step (i) and the artificial pressure of step (ii) are corrected. The additional term $\chi\nu \mathrm{div}\, \widetilde{\boldsymbol{v}}^{i+1}$ in step (iii) accounts for the accuracy of the pressure boundary conditions. If $\chi = 0$, the schemes are called *standard pressure correction schemes* , if $\chi = 1$ they are denoted as *rotational pressure correction schemes*.

The *numerical realization* of step (ii) draws on the following: Applying the divergence operator on (6.7) and noting (6.8) as well as the appropriate boundary condition (6.9) produces the Poisson equation

$$-\Delta q^{i+1} = -\frac{\alpha_0}{\Delta t}\operatorname{div}\widetilde{\boldsymbol{v}}^{i+1} \qquad \text{in } \Omega\,, \tag{6.11}$$

$$\partial_n q^{i+1} = 0 \qquad \text{on } \partial\Omega\,. \tag{6.12}$$

Note, that in the case of open boundaries on a part $\Gamma_1 \neq \emptyset$ of the boundary, the condition $q^{i+1}|_{\partial\Omega\setminus\Gamma_1} = 0$ has to be imposed and boundary condition (6.12) only applies on Γ_1, recall also the Hodge decomposition (6.1), the appropriate projection operator and see [GMS06].
Given this artificial pressure q^{i+1}, the projection of $\widetilde{\boldsymbol{v}}^{i+1}$ onto the space of divergence free velocity functions can be realized by making use of relation (6.7):

$$\boldsymbol{v}^{i+1} = \widetilde{\boldsymbol{v}}^{i+1} - \frac{\Delta t}{\alpha_0}\nabla q^{i+1} \qquad \text{in } \Omega\,. \tag{6.13}$$

Thus, this second step can be understood as the application of the projection operator P, $P(\widetilde{\boldsymbol{v}}^{i+1}) = \boldsymbol{v}^{i+1}$, whereas the (weighted) gradient of the artificial pressure acts as the projector. Note, that $P^2(\widetilde{\boldsymbol{v}}^{i+1}) = P(\widetilde{\boldsymbol{v}}^{i+1})$, as there is no update for $P(\widetilde{\boldsymbol{v}})$ with $\operatorname{div} P(\widetilde{\boldsymbol{v}}) = 0$.

The effect of the additional term $\chi\nu\operatorname{div}\widetilde{\boldsymbol{v}}^{i+1}$ in step (iii) is the following: Note, that the relation

$$\nabla\times\nabla\times\widetilde{\boldsymbol{v}}^{i+1} = \nabla\times\nabla\times\boldsymbol{v}^{i+1} \quad (= \nabla\times\nabla\times\boldsymbol{v}^{i+1} - \nabla\operatorname{div}\boldsymbol{v}^{i+1} = -\Delta\boldsymbol{v}^{i+1}) \tag{6.14}$$

applies. Supposing the *rotational* case, i.e. $\chi = 1$, we thus observe the following (for the Stokes problem *consistent*) boundary condition for the pressure

$$\partial_n p^{i+1}|_{\partial\Omega} = (\boldsymbol{f}(t^{i+1}) - \nu\nabla\times\nabla\times\boldsymbol{v}^{i+1})\cdot\boldsymbol{n}|_{\partial\Omega}\,. \tag{6.15}$$

This can be understood by adding steps (i) and (ii), as well as considering step (iii) and the relation (6.14). Instead, if $\chi = 0$, the pressure correction step (iii) can be inserted in step (ii), yielding the altered version of (6.7):

$$\Delta t^{-1}\alpha_0(\boldsymbol{v}^{i+1} - \widetilde{\boldsymbol{v}}^{i+1}) + \nabla(p^{i+1} - p^{i+1,*}) = 0 \qquad \text{in } \Omega\,,$$

which in turn implies $\nabla(p^{i+1} - p^{i+1,*})\cdot\boldsymbol{n}|_{\partial\Omega} = 0$ and thus gives

$$\nabla p^{i+1}\cdot\boldsymbol{n}|_{\partial\Omega} = \nabla p^{i+1,*}\cdot\boldsymbol{n}|_{\partial\Omega}\,.$$

For the frequently used pressure extrapolations of orders 0 and 1 we observe: Considering the 0-th order pressure extrapolation we get

$$\nabla p^{i}\cdot\boldsymbol{n}|_{\partial\Omega} = 0$$

for any $i \in \mathbb{N}$. Using the 1-st order extrapolation of the pressure causes

$$\nabla p^i \cdot \boldsymbol{n}|_{\partial\Omega} = \nabla p_0 \cdot \boldsymbol{n}|_{\partial\Omega}$$

for any $i \in \mathbb{N}$, with initially given pressure p_0. These artificial boundary conditions enforce numerical boundary layers, which spoil the order of the splitting error.

Implementations of Algorithm 6.1 commonly use the velocity predictor step as given in step (i). Step (ii) however is realized by first determining the predictive pressure as the solution of the Poisson equation (6.11), and second projecting the predicted velocity $\widetilde{\boldsymbol{v}}^{i+1}$ onto the space of divergence free functions, which is represented in equation (6.13). We postpone the determination of the initial values to the appropriate schemes.

Frequent discussions are held on the question which velocity is the right one. Whereas $\widetilde{\boldsymbol{v}}^i$ shows correct boundary conditions but is not divergence free, the updated velocity $\boldsymbol{v}^i$ has incorrect boundary conditions but is divergence free. Error analysis shows, that both velocities show similar accuracies, such that both can be used.

Let us consider the *extention to the nonlinear* case by adding the nonlinear advection term to the Stokes problem. In [GMS06] it is stated that application of the unconditionally stable semi-implicit skew-symmetric, $\frac{1}{2}(\boldsymbol{v} \cdot \nabla \boldsymbol{v} + (\operatorname{div} \boldsymbol{v})\, \boldsymbol{v})$, divergence, $\operatorname{div}(\boldsymbol{v} \otimes \boldsymbol{v})$, and rotational, $(\nabla \times \boldsymbol{v}) \times \boldsymbol{v}$, forms of the convections term enables the application of non divergence free velocities as (approximate) advection, i.e. $\widetilde{\boldsymbol{v}}$ can be applied as advection. In [BC08], Badia and Codina follow this approach and use a skew symmetric form of the advection term. In [Pro97], Prohl applies the divergence free velocity, $\boldsymbol{v}^n$, in the standard form of the advection term at time iteration step $n+1$.

For stability aspects and the treatment of stabilized problems we refer to Section A.2.4.

6.2.1 Chorin-Temam scheme

The pioneering splitting scheme is also known as the *Chorin scheme*. As this scheme has contemporaneously been invented by Chorin [Cho68] and Temam [Tem69], we denote this scheme *Chorin-Temam scheme*. It uses backward Euler (i.e. BDF1) and neglects the pressure in the momentum equation , as well as the additional term $\nu \operatorname{div} \widetilde{\boldsymbol{v}}^{i+1}$, i.e. $\chi = 0$. The equation in the velocity predictor step is given by

$$\Delta t^{-1}(\widetilde{\boldsymbol{v}}^{i+1} - \boldsymbol{v}_i^h) - \nu \Delta \widetilde{\boldsymbol{v}}^{i+1} = \boldsymbol{f}(t^{i+1}) \qquad \text{in } \Omega, \tag{6.16}$$

with boundary conditions (6.6), see also Table A.1. Equation (6.7) of the velocity corrector step reads

$$\Delta t^{-1}(\boldsymbol{v}^{i+1} - \widetilde{\boldsymbol{v}}^{i+1}) + \nabla p^{i+1} = 0 \qquad \text{in } \Omega\,. \tag{6.17}$$

As the extrapolation is of order 0 and $\chi = 0$, step (iii) is neglected. The already mentioned loss of accuracy due to the artificial boundary conditions can be found in the error estimates:

Let $(\mathbf{v}, \mathrm{p})$ be the (sufficiently smooth) solution of problem (6.2) and $\boldsymbol{v}^i$, $\widetilde{\boldsymbol{v}}^i$ and p^i, $i \in \{0, \ldots, i_{max}\}$, be the solution of the Chorin-Temam scheme. Shen [She92] and Rannacher [Ran92] proposed the following estimates:

$$\|\mathbf{v}_{\Delta t} - \boldsymbol{v}_{\Delta t}\|_{l^\infty(\mathbf{L}^2(\Omega))} + \|\mathbf{v}_{\Delta t} - \widetilde{\boldsymbol{v}}_{\Delta t}\|_{l^\infty(\mathbf{L}^2(\Omega))} \leq c\Delta t \tag{6.18}$$

$$\|\mathrm{p}_{\Delta t} - p_{\Delta t}\|_{l^\infty(\mathbf{L}^2(\Omega))} + \|\mathbf{v}_{\Delta t} - \widetilde{\boldsymbol{v}}_{\Delta t}\|_{l^\infty(\mathbf{H}^1(\Omega))} \leq c\Delta t^{1/2}\,, \tag{6.19}$$

whereas constant $c > 0$ depends on $\boldsymbol{v}, p$ and on the upper bound of the considered time interval $\mathcal{T}$. Thus, the Chorin-Temam scheme has an irreducible splitting error of order $\mathcal{O}(\Delta t)$. Moreover, the scheme does not assure first order convergence for the velocity with respect to the H^1-norm and for the pressure in the L^2-norm. Further, Rannacher [Ran92] conjectures, that the artificial boundary condition enforces a numerical boundary layer of width $\mathcal{O}(\sqrt{\nu\Delta t})$.

Finally, let us comment, that higher order time stepping schemes do not improve the overall convergence and 1-st order time stepping schemes are sufficient, such as the applied Euler backward scheme. Badia and Codina [BC08] also denote this scheme as *BDF1-SE1*, pointing out the orders of the underlying BDF scheme and of the splitting error.

Characteristics for the Chorin-Temam scheme are, that (a) even for smooth initial data the algorithm breaks down for $\mathcal{T} \to 0$, see [HR82, Pro08], and (b) due to the neglection of the pressure in the momentum equation, the pressure undergoes a stabilization, such that this scheme is applicable also for finite element spaces which are not inf-sup stable without any further stabilizing modifications, see also [Pro08].

6.2.2 Van Kan scheme

One option to improve the Chorin-Temam scheme is the application of an improved extrapolation of the pressure and (to account for the improved splitting error) the use of a higher order time discretization scheme. Goda in [God79] suggested the use of a formerly determined pressure in the momentum equation followed by a suitably adapted velocity update. In [vK86] Van Kan finally introduced the appropriate second order (standard) pressure correction scheme, the *Van Kan scheme*, using a second order time discretization and a first order pressure extrapolation. When a BDF2 scheme is applied, the splitting scheme is also denoted as *BDF2-SE2* in terms of Badia and Codina [BC08]. The appropriate shape of the momentum equation (6.5) in the velocity predictor step (i) is given by

$$\Delta t^{-1}\left(\frac{3}{2}\widetilde{\boldsymbol{v}}^{i+1} - 2\,\boldsymbol{v}^i + \boldsymbol{v}^{i-1}\right) - \nu\Delta\widetilde{\boldsymbol{v}}^{i+1} + \nabla p_i^h = \boldsymbol{f}(t^{i+1}) \qquad \text{in } \Omega, \tag{6.20}$$

imposing the homogenous Dirichlet boundary conditions (6.6) on $\widetilde{\boldsymbol{v}}^{i+1}$. As we do not consider the rotational form, i.e. $\chi = 0$, we can simplify the algorithm by incorporation the pressure corrector step (iii) into step (ii) and get

$$\frac{3}{2\Delta t}\left(\boldsymbol{v}^{i+1} - \widetilde{\boldsymbol{v}}^{i+1}\right) + \nabla(p^{i+1} - p^i) = 0 \qquad \text{in } \Omega$$

Suppose a (sufficiently smooth) solution $\mathbf{v}$ and p of problem (6.2). Under the assumption of suitable estimates of the initially given iterates $\boldsymbol{v}^1, \widetilde{\boldsymbol{v}}^1$ and p^1, i.e.

$$\|\mathbf{v}(\Delta t) - \widetilde{\boldsymbol{v}}^1\|_{0,\Omega} \leq c\Delta t^2\,, \qquad \|\mathbf{v}(\Delta t) - \widetilde{\boldsymbol{v}}^1\|_{1,\Omega} \leq c\Delta t^{3/2}\,, \qquad \|\mathrm{p}(\Delta t) - p^1\|_{1,\Omega} \leq c\Delta t\,, \tag{6.21}$$

the Van Kan scheme fulfills the following error estimate, see also [GMS06]:

$$\|\mathbf{v}_{\Delta t} - \boldsymbol{v}_{\Delta t}\|_{l^2(\mathbf{L}^2(\Omega))} + \|\mathbf{v}_{\Delta t} - \widetilde{\boldsymbol{v}}_{\Delta t}\|_{l^2(\mathbf{L}^2(\Omega))} \leq c\Delta t^2\,, \tag{6.22}$$

$$\|\mathrm{p}_{\Delta t} - p_{\Delta t}\|_{l^\infty(\mathbf{L}^2(\Omega))} + \|\mathbf{v}_{\Delta t} - \widetilde{\boldsymbol{v}}_{\Delta t}\|_{l^\infty(\mathbf{H}^1(\Omega))} \leq c\Delta t \tag{6.23}$$

with constant c being dependent on $\mathbf{v}, \mathrm{p}$ and $\mathcal{T}$. An appropriate proof has been given in [She96] for the Crank-Nicolson time-discretization scheme, and in [Gue99] for the BDF2 scheme. The authors in [GMS06] also note, that the error estimates hold for any A-stable second order time discretization scheme.

Thus the Van Kan scheme has a splitting error of $\mathcal{O}(\Delta t^2)$, but the L^2-error of the pressure as well as the H^1-error of the velocity is not second order. The induced numerical boundary layer has a width of $\mathcal{O}(\sqrt{\nu}\Delta t)$.

The requirements (6.21) are fulfilled, if $\boldsymbol{v}^0$ is set to the initial value $\mathbf{v}_0$ and p^0 is determined by setting $t = 0$ and determining $\mathrm{p}(0)$ in (6.2). The values $\boldsymbol{v}^1, \widetilde{\boldsymbol{v}}^1$ and p^1 are then determined by a BDF1-SE1 scheme, i.e. using the Euler backward scheme and applicate the same extrapolation of the pressure as in the Van Kan scheme, see also [GMS06].

6.2.3 Rotational Van Kan scheme

As indicated several times, the application of the rotational form aims to improve the error estimates by improving the boundary conditions for the pressure. The idea to use the term $\nu \mathrm{div}\, \widetilde{\boldsymbol{v}}^{i+1}$ in step (iii) of Algorithm 6.1 stems from Timmermans, Minev and Van der Vosse [TMV96]. Using BDF2 for time discretization and first order pressure extrapolation, the algorithm is given as in the Van Kan scheme: the momentum equation of step (i) of the algorithm is given by (6.20). Due to the differing pressure update, steps (ii) and (iii) can not be assembled, i.e. the velocity corrector equation of step (ii) of the algorithm by

$$\frac{3}{2\Delta t}\left(\boldsymbol{v}^{i+1} - \widetilde{\boldsymbol{v}}^{i+1}\right) + \nabla q_{i+1} = 0 \qquad \text{in } \Omega$$

and the pressure update reads

$$p^{i+1} = q_{i+1} + p^i - \nu \mathrm{div}\, \widetilde{\boldsymbol{v}}^{i+1} \qquad \text{in } \Omega$$

At the beginning of this subsection we already explained, that this equation imposes the improved boundary condition (6.15) on the pressure. However, due to the boundary condition (6.9) in step (ii) of the algorithm (which is also imposed here), the splitting

causes an inexact velocity boundary condition. This finds expression in the error estimates, see also [GS04, GMS06]:
Given a (sufficiently smooth) solution $\boldsymbol{v}$ and p of problem (6.2) and first iterates $\boldsymbol{v}^1, \widetilde{\boldsymbol{v}}^1, p^1$ fulfilling Assumption (6.21), the iterates of the BDF2-SE1 scheme in rotational form show the following estimates:

$$\|\mathbf{v}_{\Delta t} - \boldsymbol{v}_{\Delta t}\|_{l^2(\mathbf{L}^2(\Omega))} + \|\mathbf{v}_{\Delta t} - \widetilde{\boldsymbol{v}}_{\Delta t}\|_{l^2(\mathbf{L}^2(\Omega))} \leq c\Delta t^2 \tag{6.24}$$

$$\|\mathbf{v}_{\Delta t} - \boldsymbol{v}_{\Delta t}\|_{l^2(\mathbf{H}^1(\Omega))} + \|\mathbf{v}_{\Delta t} - \widetilde{\boldsymbol{v}}_{\Delta t}\|_{l^2(\mathbf{H}^1(\Omega))} + \|\mathrm{p}_{\Delta t} - p_{\Delta t}\|_{l^2(\mathbf{L}^2(\Omega))} \leq c\Delta t^{3/2}\,, \tag{6.25}$$

again constant $c > 0$ depends on $\mathbf{v}, \mathrm{p}$ and on $\mathcal{T}$. We observe a splitting error of $\mathcal{O}(\Delta t^2)$, as well as improved H^1-errors of the velocities and an L^2-error of the pressure.
Recall, that the determination of the initial values as presented for the Van Kan scheme leads to the estimates (6.21) and thus can also be applied here.

6.2.4 Applicability of different BDFk-SEr schemes

Let the pressure correction schemes be constructed with a BDFk scheme and a pressure extrapolation of r-th order in rotational form, i.e. $\chi = 1$. Anticipating, the authors in [GMS06] propose, that inf-sup stability of the space discretized problem has to be assured for each of the following schemes.

We first consider applications to problem (6.2), see also [GMS06]. The appropriate case including open boundary is considered afterwards. The authors of [GMS06] indicate that choosing $r = k - 1$ leads to a *consistency error of the velocity* with respect to the H^1-norm of order k and to a *consistency error of the pressure* with respect to the L^2-norm of order r.
However, *stability* and *convergence* could only be validated for $(k, r) = (1, 0)$ and $(k, r) = (2, 1)$. In nonrotational form, these are the already introduced *Chorin-Temam scheme* and the *Van Kan scheme*, respectively.
The case $(k, r) = (3, 2)$ is also discussed in [GMS06]. The authors claim, that the velocity is third order accurate for Δt being *not too small*. The scheme is supposed to become unstable if $\Delta t < ch^2$ using the finite element approach. This is troublesome, if the scheme is applied to nonlinear problems, due to the CFL criterion. The appropriate (numerically validated) orders of the errors are: third order for the L^2-velocity error and 5/2-th order for the H^1-velocity error and the L^2-pressure error.

If $k = r$, the appropriate consistency errors have the same order, but *stability* and *convergence* could only be validated for $k = r = 1$. The velocity error in the L^2-norm, as well as in the H^1-norm, and the L^2-error of the pressure could be proven to be of first order. Considering the scheme with $k = r = 2$, numerical experiments suggest second order accuracies for these errors. Applying finite element approximations, $ch^2 \leq \Delta t$ seems to be necessary for stability of the scheme. An appropriate proof is missing.

In the case of open boundaries, the authors of [GMS06] considered the cases $k = r = 1$ and $k = 2$ and $r = 1$. For the first case they depict convergence order better than 3/4 for the L^2-error of the velocity and the pressure as well as for the H^1-error of the velocity. For the second case the same estimates apply, except for the L^2-error of the velocity,

where better than 5/4 order of convergence could be proven. The improvements of these 3/4 and 5/4 convergence orders are determined by the properties of the Stokes operator. Moreover, considering finite element discretizations, the authors numerically observe stability for the case $k = r = 2$ only if $h^2 \sim \Delta t$, which is impracticable.

In [BC08] Badia and Codina conjecture, that pressure correction schemes of order three and higher are unstable. The reason behind however is still unclear.

6.3 Pressure correction methods for hydrostatic problems

In this section we turn to the hydrostatic framework. We start with the operators, which enable the combination of the 2D pressure and the 3D velocity problems. Afterwards we face the questions which arise, if we aim to adopt the schemes to hydrostatic problems. The section closes with the representation of a splitting scheme for the LPS stabilized hydrostatic Navier-Stokes problem.

Hydrostatic flow problems show the characteristics, that the velocity field and the pressure live in spaces of different dimensions. Moreover, the divergence constraint is also 2D instead of 3D. In the context of *pressure correction schemes*, the divergence constraint is part of the pressure Poisson problem, which would also be 2D in the hydrostatic case. In a (3D) velocity prediction step the pressure is treated explicitely and thus does not have to be solved coupled with the velocity. Thus, the class of pressure correction methods suits well in the hydrostatic context.
The characteristics of hydrostatic problems do not benefit in the context of *velocity correction schemes*. Moreover, the class of *consistent splitting schemes* could be applied in the hydrostatic context. As the analysis of *pressure correction schemes* is more substantial than the latter one, we concentrate on the idea of pressure correction schemes. Note that due to the author's knowledge, at present no analysis of the splitting schemes applied to hydrostatic flow problems is available.

6.3.1 Interaction between 2D and 3D

To account for the interaction between the occurring 2D and 3D subproblems we denote the operator P_{3D}. It embeds a 2D pressure $p_h \in Q_h$, which is defined on the surface mesh $\mathcal{K}_h$, into the appropriate 3D discrete pressure space P_h, see also Section 4.3.1. Due to the prismatic structure of the 3D mesh $\mathcal{T}_h$, see definition (4.3) and Figure 4.3, each node in $\mathcal{T}_h$ with 3D coordinates (x, y, z) can be assigned to a node in the surface mesh $\mathcal{K}_h$ with 2D coordinates (x, y). Thus, the embedding passes on each pressure value of a given node to its spatial subjacent nodes of $\mathcal{T}_h$.

Another aspect is the implementation of the vertical integration operator. If we aim to adapt Algorithm 6.1 to the hydrostatic case, we have to algorithmically realize the

vertical integration operator in step (ii) of the Algorithm, i.e. we have to discretize

$$\mathbf{M}\,\boldsymbol{w}_h \;:=\; \int_{-d(x,y)}^{0} \boldsymbol{w}_h \;dz \qquad \forall (x,y)\in\omega \tag{6.26}$$

for a given scalar element $\boldsymbol{w}_h$ of an appropriate finite element space. The transformation (4.3) shows the following property: Consider the reference element $\widehat{T}$ and the vertically oriented line with end points $(x,y,0)$ and $(x,y,1)$. Under the transformation $B_T : \widehat{T} \to T$, see (4.3), these line remains vertically oriented. This implicates, that all degrees of freedom, which lie on top of each other, remain lieing on top of each other after the transformation. Due to the spatial ordering of the degrees of freedom (dofs) it suffices to evaluate (6.26) only for each dof, with coordinates (x,y), on the surface mesh. Assuming $\boldsymbol{w}_h = 0$ on the bottom of the domain, we can reformulate the determination of (6.26) as a set of ODEs by

$$\partial_z \phi(x,y,z) = \partial_z \left(\int_{-d(x,y)}^{z} \boldsymbol{w}_h(x,y,t)\; dt \right) \;=\; \boldsymbol{w}_h(x,y,z) \quad \forall \text{ dofs } (x,y)\in\omega\,. \tag{6.27}$$

Thus, determining $\phi(x,y,0)$ corresponds the evaluation of $\mathbf{M}\,\boldsymbol{w}_h$, which can be discretized by one of the established time discretization schemes, see Section A.1.
In the upcoming algorithm $\boldsymbol{w}_h$ will be $\mathrm{div}'\widetilde{\boldsymbol{v}}_h^{n+1}$. Thus, solving (6.27) corresponds to the determination of the appropriate vertical velocity component, recall (2.30).

Note, that these considerations also apply for stabilized pressure correction schemes, see Algorithm A.4.

6.3.2 Hydrostatic issues

As motivated in the introductory words of this section we consider the class of pressure correction schemes and apply the ideas to the time discretization of the evolutionary hydrostatic Navier-Stokes problem (3.36). Due to the properties of pressure correction schemes and available analysis, several questions arise in the context of hydrostatic problems:

(a) "Do the mechanisms of the pressure correction schemes transfer to the hydrostatic case? In particular, based on the ideas of pressure correction schemes and a hydrostatic flow problem, is it possible to construct a suitable projection scheme?"

(b) "Does the application of rotational pressure correction schemes lead to superior pressure boundary conditions compared to the standard form? "

(c) "Do we have to restrict to homogeneous velocity boundary conditions on the *entire* boundary in order to make (fairly) sure to apply correct boundary conditions on the pressure Poisson problem?"

In the henceforth subsections we discuss on these points. For ease of simplicity we restrict to the hydrostatic Stokes problem (3.21) with f = 0 and add some notes on the nonlinear case, where suitable.

Projection property of pressure correction schemes

Consider Algorithm 6.1. In step (ii) of the algorithm the non divergence free velocity is Helmholtz projected onto the space of divergence free velocities by determination of a suitable pressure. This is the crucial step in projection schemes.
Adapting the ideas of pressure correction schemes to the treatment of problem (3.21) a suitable algorithm should guarantee, that the predicted velocity $\widetilde{\boldsymbol{v}}$ is projected onto the space of velocities, which fulfill the modified divergence constraint

$$\operatorname{div}'\mathbf{M}\,\boldsymbol{v} = 0\,. \tag{6.28}$$

Due to the construction of pressure correction schemes, this projection should be realized by application of the gradient of a suitable pressure to the predictor velocity $\widetilde{\boldsymbol{v}}$. Thus, question (a) is related to the question whether $\mathbf{L}^2(\Omega)$ has a Helmholtz-like decomposition in the sense:

$$\begin{aligned}
\mathbf{L}^2(\Omega)\ (=[\mathrm{L}^2(\Omega)]^2) \ &= \boldsymbol{J}\oplus\boldsymbol{G} && \text{with} \\
\boldsymbol{J} &:= \left\{\boldsymbol{v}\in\mathbf{L}^2(\Omega)\ \middle|\ \boldsymbol{v}\,|_{\Gamma_s}=0 \text{ and } \operatorname{div}'\mathbf{M}\,\boldsymbol{v}=0\right\} && \text{and} \qquad (6.29)\\
\boldsymbol{G} &:= \{P_{3D}(d^{-1}\nabla' q)\in\mathbf{L}^2(\Omega)\mid q\in\mathrm{L}^2_0(\omega)\}\,. && (6.30)
\end{aligned}$$

Function $d:\omega\to\mathbb{R}_{>0}$ denotes the bounded depth function of the domain.

Lemma 6.2 (Helmholtz-like decomposition of $\mathbf{L}^2(\Omega)$)**.** *Let Ω be simply connected and bounded with depth function $d>0$ in $\overline{\omega}$, and $\boldsymbol{J}$ and $\boldsymbol{G}$ be as given in (6.29) and (6.30), respectively. Then $\boldsymbol{J}\cup\boldsymbol{G}$ denotes an orthogonal decomposition of $\mathbf{L}^2(\Omega)$, i.e.*

$$\mathbf{L}^2(\Omega)=\boldsymbol{J}\oplus\boldsymbol{G}\,,$$

whereas the orthogonality property applies with respect to the scalar product $\langle\cdot,\cdot\rangle_d := (d\cdot,\cdot)_\Omega$

Proof. First note that $\boldsymbol{J}$ is a closed subset $\mathbf{L}^2(\Omega)$. Let $\boldsymbol{v}\in\mathbf{L}^2(\Omega)$ be arbitrarily given. Due to Lemma 3.12 we get an element $\boldsymbol{w}\in\mathbf{L}^2(\omega)$ with $\mathbf{M}\,\boldsymbol{v}=\boldsymbol{w}$. The space $\mathbf{L}^2(\omega)$ has a Helmholtz decomposition,

$$\begin{aligned}
&\mathbf{L}^2(\omega)=\boldsymbol{J}_\omega\oplus\boldsymbol{G}_\omega && \text{with}\\
&\quad\boldsymbol{J}_\omega := \{\boldsymbol{w}\in\mathbf{L}^2(\omega)\mid \boldsymbol{w}\,|_{\partial\omega}=0 \text{ and } \operatorname{div}'\boldsymbol{w}=0\}\\
&\quad\boldsymbol{G}_\omega := \{\nabla' p\in\mathrm{L}^2(\omega)\,|\,p\in\mathrm{L}^2_0(\omega)\}\,,
\end{aligned}$$

see e.g. [AG94]. Thus, there are uniquely determined $\boldsymbol{w}_1\in\boldsymbol{J}_\omega$ and $\nabla' p\in\boldsymbol{G}_\omega$ such that $\mathbf{M}\,\boldsymbol{v}=\boldsymbol{w}=\boldsymbol{w}_1+\nabla' p$. We set $\boldsymbol{v}_2=P_{3D}(d^{-1}\nabla' p)$ and $\boldsymbol{v}_1=\boldsymbol{v}-\boldsymbol{v}_2$. Thus, we have $\boldsymbol{v}=\boldsymbol{v}_1+\boldsymbol{v}_2$. Obviously, $\boldsymbol{v}_2\in\boldsymbol{G}$, and $\boldsymbol{v}_1\in\boldsymbol{J}$ due to

$$\begin{aligned}
\operatorname{div}'\mathbf{M}\,\boldsymbol{v}_1 &= \operatorname{div}'\mathbf{M}(\boldsymbol{v}-P_{3D}\left(d^{-1}\nabla' p\right))\\
&= \operatorname{div}'(\boldsymbol{w}_1+\nabla' p)-\operatorname{div}'(\nabla' p)\\
&= 0\,.
\end{aligned}$$

Moreover, for any $\boldsymbol{v}_1 \in \boldsymbol{J}$ and $\boldsymbol{v}_2 = P_{3D}(d^{-1}\nabla' p) \in \boldsymbol{G}$, we observe

$$(d\ \boldsymbol{v}_1, P_{3D}(d^{-1}\nabla' p))_\Omega \quad = \quad (\mathbf{M}\,\boldsymbol{v}_1, \nabla' p)_\omega \quad = \quad -(\mathrm{div}\,'(\mathbf{M}\,\boldsymbol{v}_1), p)_\omega \quad = \quad 0\,,$$

i.e. $\boldsymbol{J}$ and $\boldsymbol{G}$ are orthogonal with respect to the scalar product $\langle\cdot,\cdot\rangle_d := (d\cdot,\cdot)_\Omega$. □

As $\boldsymbol{G}_\omega$ can also be considered as a rotation free vector field, see e.g. [Wan10], the space $\mathbf{L}^2(\Omega)$ is decomposable into a height-averaged divergence free field and a 3D projected and height weighted 2D rotational free field.
The choice of this decomposition wises up due to the following considerations: Let $\widetilde{\boldsymbol{v}}$ be a velocity, which does not fulfill the constraint (6.28) and let the (2D) artificial pressure q be solution of the Poisson equation

$$\begin{array}{rcll} -\Delta q & = & -\alpha_0\,\Delta t^{-1}\,\mathrm{div}\,'\,\mathbf{M}\,\widetilde{\boldsymbol{v}} & \text{in } \omega\,, \\ \partial_n q & = & 0 & \text{on } \partial\omega\,. \end{array} \tag{6.31}$$

Then, $\boldsymbol{v} := \widetilde{\boldsymbol{v}} + \Delta t\,\alpha_0^{-1} P_{3D}(d^{-1}\nabla' q)$ fulfills the condition (6.28):

$$\begin{array}{rcl} \mathrm{div}\,'\,\mathbf{M}\,\boldsymbol{v} & = & \mathrm{div}\,'\,\mathbf{M}\,\widetilde{\boldsymbol{v}} + \mathrm{div}\,'\left(\Delta t\,\alpha_0^{-1}\,\mathbf{M}(1)\,d^{-1}\nabla' q\right) \\ & = & \mathrm{div}\,'\,\mathbf{M}\,\widetilde{\boldsymbol{v}} + \Delta t\,\alpha_0^{-1}\Delta' q\,, \end{array}$$

which equals zero due to (6.31).

Concluding, we answer question (a) as follows: As we assumed the underlying domain to fulfill $\delta_{min} > 0$, there *is* a Helmholtz-like decomposition of $\mathbf{L}^2(\Omega)$ which enables the application of the projection in step (ii) of Algorithm 6.1 to the hydrostatic case. I.e., for any given velocity $\widetilde{\boldsymbol{v}}$, there is a (unique) pressure p and a (unique) velocity $\boldsymbol{v}$, which fulfills (6.28), such that $\boldsymbol{v} = \widetilde{\boldsymbol{v}} + d^{-1}\nabla p$. Thus, the projection property applies also in the hydrostatic context, even though in a modified fashion. However, the involvement of the scalar product $\langle\cdot,\cdot\rangle_d$ effects the pressure and thus entire system. We discuss that issue in the following subsection.

Remark 6.3. *This Helmholtz-like decomposition of the* $\mathbf{L}^2(\Omega)$ *suggests an appropriate adaption of pressure correction schemes in the hydrostatic framework with domains showing the property* $\delta_{min} > 0$*. However it is not clear how to proceed in the case when the minimal depth of the domain is allowed to be zero, i.e.* $\delta_{min} \geq 0$*.*

For appropriate discussions on the Oseen and on the Navier-Stokes case recall Chapter 3: As we assumed the minimal depth of the domain to be strictly positive, $\delta_{min} > 0$, the pressure part of the appropriate solution belongs to $\mathrm{L}^2_0(\omega)$. As the velocity spaces of the Stokes, the Oseen and the Navier-Stokes problems coincide, the preceding argumentation also applies for the Oseen and the Navier-Stokes case.

Pressure Update

In the preceding subsection we elaborated a projection of a velocity, which does not satisfy the modified divergence constraint, onto the space $\boldsymbol{J}$ by a depth weighted horizontal gradient of a 2D artificial pressure. Let us figure out this effect on the pressure,

updated in step (iii) of Algorithm 6.1. We consider the standard case, i.e. $\chi = 0$, and adapt the equations of Algorithm 6.1 to the hydrostatic Stokes problem. We incorporate the considerations of the preceding subsection. Equation (6.5) then is given by

$$\Delta t^{-1}(\alpha_0 \widetilde{\boldsymbol{v}}^{i+1} + D_{k,1}\, \boldsymbol{v}^{i+1}) - \nu \Delta \widetilde{\boldsymbol{v}}^{i+1} + P_{3D}(\nabla' p^{i+1,*}) = \boldsymbol{f}(t^{i+1}) \qquad \text{in } \Omega\,. \tag{6.32}$$

Considering the precedingly considered, altered projection properties for hydrostatic problems, the equations in step (ii) then turns out to be

$$\Delta t^{-1}\alpha_0(\boldsymbol{v}^{i+1} - \widetilde{\boldsymbol{v}}^{i+1}) + P_{3D}(d^{-1}\nabla' q^{i+1}) = 0 \qquad \text{in } \Omega \tag{6.33}$$

$$\operatorname{div}' \mathbf{M}\, \boldsymbol{v}^{i+1} = 0 \qquad \text{in } \omega \tag{6.34}$$

$$\boldsymbol{v}^{i+1} \cdot \boldsymbol{n} = 0 \qquad \text{on } \Gamma_s \tag{6.35}$$

Inserting equation (6.33) into (6.32) leads to

$$\Delta t^{-1} D_k\, \boldsymbol{v}^{i+1} - \nu \Delta \widetilde{\boldsymbol{v}}^{i+1} + P_{3D}(d^{-1}\nabla' q^{i+1} + \nabla' p^{i+1,*}) = \boldsymbol{f}(t^{i+1}) \qquad \text{in } \Omega\,. \tag{6.36}$$

Thus the updated pressure p^{i+1} shall

$$\nabla' p^{i+1} = d^{-1}\nabla' q^{i+1} + \nabla' p^{i+1,*}\,.$$

For constant depth, $d \equiv c_d > 0$, the update is similar as in the nonhydrostatic case:

$$p^{i+1} = d^{-1}\, q^{i+1} + p^{i+1,*}\,. \tag{6.37}$$

However, in the case of nonconstant depth, the task to find an appropriate pressure update is not that obvious. Due to $\nabla'(d^{-1}q^{i+1}) = d^{-1}\nabla' q^{i+1} + q^{i+1}\nabla' d^{-1}$, applicating an update of kind (6.37) leads to the relation

$$\begin{aligned} \nabla' p^{i+1} &= d^{-1}\nabla' q^{i+1} + \nabla' p^{i+1,*} + (\nabla' d^{-1})\, q^{i+1} \\ &= d^{-1}\nabla' q^{i+1} + \nabla' p^{i+1,*} + d\,(\nabla' d^{-1})\,(p^{i+1} - p^{i+1,*})\,, \end{aligned}$$

and thus (6.36) becomes

$$\Delta t^{-1} D_k\, \boldsymbol{v}^{i+1} - \nu \Delta \widetilde{\boldsymbol{v}}^{i+1} + P_{3D}\left(\nabla' p^{i+1} - d\,(\nabla' d^{-1})\,(p^{i+1} - p^{i+1,*})\right) = \boldsymbol{f}(t^{i+1}) \quad \text{in } \Omega\,,$$

i.e. beside the disturbance due to the viscous term of the predictor velocity we have to face the additional error due to the term

$$(\nabla' d^{-1})\, q^{n+1} = (\nabla' d^{-1})\, d(p^{i+1} - p^{i+1,*})\,. \tag{6.38}$$

Obviously, its contribution decreases with the increase of the order of pressure extrapolation. As this additional term does not occur in the nonhydrostatic case, the overall impact of this term is not known. But, as (6.38) is an additional term of 0-th order with unknown sign, it is suggestive that the imposed additional term has no additional stability but rather disturbing impact on the system. Therfore, we aim to correct it by extrapolating q^{n+1} by $q^{i+1,*}$, and adding the term $P_{3D}\,((\nabla' d^{-1}) q^{i+1,*})$ to the left hand side of (6.32).

Pressure correction schemes - in standard or in rotational form?

Let us now ponder on the use of the rotational variant of a pressure correction scheme. For ease of simplicity we restrict on the case of constant depth function d with $d \equiv 1$. Thus, no additional impact due to the artificial pressure in step (i) has to be considered. Due to the preceding discussions we consider the modified pressure update (6.37) and add an adapted variant of $\nu \mathrm{div}\, \widetilde{\boldsymbol{v}}^{n+1}$, which is responsible for an improvement of the pressure boundary conditions in the nonhydrostatic case. I.e., we consider the update

$$p^{n+1} = d^{-1}\, q^{n+1} + p^{n+1,*} - \nu \mathrm{div}'\, \mathbf{M}\, \widetilde{\boldsymbol{v}}^{n+1}\,. \tag{6.39}$$

As in the preceding subsection the momentum equation can be reformulated as

$$\Delta t^{-1} D_k\, \boldsymbol{v}^{i+1} - \nu \Delta \widetilde{\boldsymbol{v}}^{i+1} + P_{3D}\left(\nabla' p^{i+1} - \nu \nabla' \mathrm{div}'\, \mathbf{M}\, \widetilde{\boldsymbol{v}}^{n+1}\right) = \boldsymbol{f}(t^{i+1}) \qquad \text{in } \Omega\,,$$

which leads to the following boundary condition for the pressure:

$$\begin{aligned} \nabla'(P_3 p^{n+1}) \cdot \boldsymbol{n} = {} & \boldsymbol{f}(t^{n+1}) \cdot \boldsymbol{n} + \nu \left(\Delta \widetilde{\boldsymbol{v}}^{n+1} + P_3(\nabla' \mathrm{div}'\, \mathbf{M}\, \widetilde{\boldsymbol{v}}^{n+1})\right) \cdot \boldsymbol{n} \\ & - \delta_{\Gamma_u} \Delta t^{-1} D_k\, \boldsymbol{v}^{i+1} \cdot \boldsymbol{n} \qquad \text{on } \partial\Omega\,, \end{aligned}$$

whereas δ_{Γ_u} equals 1 on Γ_u and is zero else.
The first conspicuousness is that *Neumann boundary conditions* are only imposed on the side walls Γ_s (due to the verticality of those boundary parts), which coincides with the domain of definition of the pressure. Attempting to analyze this boundary condition we note, that the rotation operator is not defined for our 3D two-componential horizontal velocity field. Thus, we evade this lack by application of the approach done with the Coriolis term, see (2.31), which resulted by neglecting the vertical component of the vector field (which indeed is not apparent) as well as the third component of the rotation operator (which could be determined). Instead of $\nabla \times \nabla \times (\boldsymbol{v}, v_3)$ we now have $-(\partial_{zz} v_1, \partial_{zz} v_2)$. Moreover,

$$\nabla' \mathrm{div}'\, \mathbf{M}\, \boldsymbol{v} \quad = \quad (\partial_{xx}\, \mathbf{M}\, v_1 + \partial_{xy}\, \mathbf{M}\, v_2\,,\ \partial_{yx}\, \mathbf{M}\, v_1 + \partial_{yy}\, \mathbf{M}\, v_2)$$

applies, such that

$$\begin{aligned} \partial_{zz} v_1 + P_3(\nabla' \mathrm{div}'\, \mathbf{M}\, \boldsymbol{v})_1 &= \partial_{zz} v_1 + \partial_{xx}\, \mathbf{M}\, v_1 + \partial_{xy}\, \mathbf{M}\, v_2\,, \\ \partial_{zz} v_2 + P_3(\nabla' \mathrm{div}'\, \mathbf{M}\, \boldsymbol{v})_2 &= \partial_{zz} v_2 + \partial_{yx}\, \mathbf{M}\, v_1 + \partial_{yy}\, \mathbf{M}\, v_2\,. \end{aligned}$$

Contrary to (6.14) we do *not* observe the relation $(\partial_{zz} v_1, \partial_{zz} v_2) + P_3(\nabla' \mathrm{div}'\, \mathbf{M}\, \boldsymbol{v}) = \Delta \boldsymbol{v}$. Thus and to answer question (b), it is not clear, whether the rotational approach leads to an improved approximation of the pressure boundary condition or if it worsens it, which is the more likely suggestion. In order to avoid these uncertainties, and likely sources of errors, it is suggestible to rather apply the pressure correction scheme in *standard* form.

Restrictions on the choice of velocity boundary conditions

Analysis on the pressure correction schemes essentially is available only for homogeneous Dirichlet data. The question arises, whether we should also impose homogeneous Dirichlet data for the horizontal velocity field on the *entire* domain. For example, note that imposing natural boundary conditions evokes a Hodge decomposition (6.1), which leads to a different boundary setting for the artificial pressure, see [GMS06].

As discussed above, the modified divergence constraint (6.28) effects a Helmholtz-like decomposition, if homogeneous Dirichlet data are imposed on the side walls Γ_s of Ω. This perfectly applies to our framework, see e.g. Chapter 3.

If one attempts to partly impose *natural boundary conditions*, as might occur when channel outflows our surrounding water masses are considered, one has to examine whether a Hodge decomposition applies. This seems to be likely due to the tight connection with the 2D case, see also Lemma 6.2.

The algorithm

As we apply equal order finite element spaces, we directly move on to the consideration of the stabilized problem. An appropriate analysis on this issue for the OSS stabilization has been done by Badia and Codina in [BC08], see also Section A.2.4. The vertical integration, which is realized by (6.27), is discretized with the Crank-Nicolson scheme. Based on a suitable adaption of Algorithm 6.1 to the stabilized problem, i.e. we consider Algorithm A.4, its shaping (in standard form, i.e. $\chi = 0$) in the hydrostatic framework is as follows:

Algorithm 6.4 (Pressure correction scheme for the stabilized 2.5D Navier-Stokes problem)**.** *Let $k, l, m \in \mathbb{N}$, and, for any $n \geq \min\{k, l\} - 1$, and $0 \leq m < l$, initial values $\boldsymbol{v}_h^{n-k+1}, \ldots, \boldsymbol{v}_h^n$, $p_h^{n-l+1}, \ldots, p_h^n$, and $q_h^{n-m+1}, \ldots, q_h^n$ be given.*

The n-th time step of the scheme is given by:

(i) Velocity predictor step *Find the velocity predictor $\widetilde{\boldsymbol{v}}_h^{n+1}$ s.t.*

$$\begin{aligned} \Delta t^{-1} \left(\alpha_0 \widetilde{\boldsymbol{v}}_h^{n+1} + D_{k,1}\, \boldsymbol{v}_h^{n+1}, \boldsymbol{\varphi}\right)_\Omega + \nu \left(\nabla \widetilde{\boldsymbol{v}}_h^{n+1}, \nabla\, \boldsymbol{\varphi}\right)_\Omega \\ + \left(((\widetilde{\boldsymbol{v}}_h^{n+\rho}, \widetilde{\boldsymbol{v}}_{3h}^{\,n+\rho_3}) \cdot \nabla) \widetilde{\boldsymbol{v}}_h^{n+1}, \boldsymbol{\varphi}\right)_\Omega + s_{h,v}^\Omega(\widetilde{\boldsymbol{v}}_h^{n+\rho}, \boldsymbol{\varphi}) \\ + \left(P_{3D}(\nabla p_h^{n+1,*} + (\nabla' d^{-1}) q_h^{n+1,*}), \boldsymbol{\varphi}\right)_\Omega = \left\langle \boldsymbol{f}(t^{n+1}), \boldsymbol{\varphi}\right\rangle \quad \forall\, \boldsymbol{\varphi} \in \mathbf{V}_h \end{aligned} \tag{6.40}$$

(ii) Divergence integration step

(a) *Solve*

$$\begin{aligned} \partial_z \widetilde{\boldsymbol{v}}_{3h}^{\,n+1} &= div' \widetilde{\boldsymbol{v}}_h^{n+1} && \text{in } \Omega\,, \\ \widetilde{\boldsymbol{v}}_{3h}^{\,n+1} &= 0 && \text{on } \Gamma_b\,. \end{aligned}$$

(b) *Set* $\boldsymbol{g}_h^{n+1}(x,y) = \widetilde{\boldsymbol{v}}_{3h}^{n+1}(x,y,0) \quad \forall$ *dofs of* $\mathcal{K}_h$.

(iii) Pressure predictor step *Determine the pressure* q_h^{n+1}*, s. t.*

$$\Delta t\ {\alpha_0}^{-1} \left(\nabla q_h^{n+1}, \xi\right)_\omega + s_{h,p}(q_h^{n+1}, \xi) = (\boldsymbol{g}_h^{n+1}, \xi)_\omega - s_{h,p}(p_h^{n+1,*}, \xi) \quad \forall \xi \in Q_h\,. \tag{6.41}$$

(iv) Velocity update step *Determine the updated velocity* $\boldsymbol{v}_h^{n+1}$*, s.t.*

$$\Delta t^{-1}\ \alpha_0 \left(\boldsymbol{v}_h^{n+1} - \widetilde{\boldsymbol{v}}_h^{n+1}, \boldsymbol{\varphi}\right)_\Omega + \left(P_{3D}(d^{-1}\nabla q_h^{n+1}), \boldsymbol{\varphi}\right)_\Omega = 0 \quad \forall\, \boldsymbol{\varphi} \in \mathbf{V}_h\ . \tag{6.42}$$

(v) Pressure update step *Determine the updated pressure* p_h^{n+1}*, s.t.*

$$p_h^{n+1} = d^{-1}\, q_h^{n+1} + p_h^{n+1,*}\,. \tag{6.43}$$

Note, that in step (i) of the algorithm, the vertical velocity component $\widetilde{\boldsymbol{v}}_{3h}^{n+1}$ of the predictive velocity has to be used for the advection. However, this is only determined in step (ii), such that the entire advection may be approximated by former iteratives of an iterative loop or by a time extrapolation, either only for the vertical component or for the entire advection. This is indicated by ρ and ρ_3. Step (ii) is solved by application of the Crank-Nicolson scheme. For sake of brevity we refrained tidying it up in detail.

For the algorithmic realization, the subproblems occurring in the above algorithm commonly still are too complex to apply direct solvers. Instead, Krylov subspace methods, as well as multigrid schemes can be applied, see also Appendix B.4 and [KR11].

Chapter 7

Algorithmic Issues

In the preceding chapters we derived the set of governing equations, considered existence, uniqueness and regularity properties of possible solutions, and analyzed its equal-order finite element discretization. But, unless we are not able to derive solutions of these discretized problems, the preceding considerations are practically futile.

The main observation we make is, that in hydrostatic problems the velocity field and the pressure are defined in domains of different dimensions. Thus, common approaches to solve such problems, such as direct iterative methods, see also Appendix B, can not be adapted offhand. The task of this chapter is to show possible accesses to algorithmically treat hydrostatic problems.

In the context of evolutionary hydrostatic flow problems, we already treated one possibility to deal with the different dimensions for the evolutionary case. For the algorithmic treatment of the resulting subproblems we refer to the Appendix B. Thus it remains to consider stationary hydrostatic flow problems.
We consider two possibilities to algorithmically treat the stationary hydrostatic problems. On the one hand, this is the idea of pressure correction schemes. On the other hand, we can apply the idea of Uzawa algorithms. These two issues are content of Sections 7.1 and 7.2. After having dealt these two approaches we turn to the issue of parallelization in Section 7.3. For a closer look into this topic we refer to [KR11], in which we introduced issues on parallelization in detail, particularly in the context of multigrid schemes.

7.1 Uzawa approach

We figured out in Chapter 3 and frequently applied in Chapters 4 and 5 the saddle point structure of hydrostatic flow problems. When we attempt to solve such problems, we again can make use of this property.

We consider the discretized stationary problem

$$A(\boldsymbol{u}_h)(\boldsymbol{\phi}) = \boldsymbol{f}(\boldsymbol{\phi}) \qquad \forall\, \boldsymbol{\phi} \in \mathbf{X}_h\,,$$

whereas $\boldsymbol{u}_h$ denotes the discrete solution of the problem, $A : \boldsymbol{X}_h \times \boldsymbol{X}_h \to \mathbb{R}$ denotes the bilinear form and $\boldsymbol{f}$ the forcing. Let

$$\Phi_h := \{\varphi_h^i, i = 1, \ldots, m\} \quad \text{and} \quad \Xi_h := \{\xi_h^i, i = 1, \ldots, n\}$$

be the common Lagrange basis systems of $\mathbf{V}_h$ and Q_h with $\varphi_i(x_j) = \delta_{ij}$ and $\xi_i(y_j) = \delta_{ij}$, where x_j are the m dofs of the velocity field and y_j the n dofs of the pressure field. Thus, we end up in the following algebraic system

$$M\boldsymbol{z} \;:=\; \begin{pmatrix} A & B^T \\ -B & D \end{pmatrix} \begin{pmatrix} \boldsymbol{x} \\ \boldsymbol{y} \end{pmatrix} = \begin{pmatrix} \boldsymbol{f} \\ 0 \end{pmatrix}$$

with nonsingular matrix $A \in \mathbb{R}^{m\times m}$, matrix $D \in \mathbb{R}^{n\times n}$ of the pressure stabilization and matrix $B \in \mathbb{R}^{m\times n}$, accounting for the modified inf-sup constraint. The expression $\boldsymbol{f}$ on the right hand side is to be interpreted elementwisely.

If we apply the idea of the Schur complement and apply the (simple) Richardson iteration to the resulting pressure problem, see also Sections B.1.2 and B.2.3, we get the following algorithm:

Algorithm 7.1. *Let $\boldsymbol{y}^{(0)} \in \mathbb{R}^n$ and θ be a sufficiently small damping parameter. The i-th step, $i \geq 1$, of the algorithm is given by:*

(i) $A\boldsymbol{x}^{(i)} \;=\; \boldsymbol{f} - P(B^T\boldsymbol{y}^{(i)})$,

(ii) $\boldsymbol{y}^{(i+1)} \;=\; y^{(i)} + \theta(B\boldsymbol{x}^{(i)} + D\boldsymbol{y}^{(i)})\,,$

whereas P denotes the embedding from 2D to 3D. Thus, once we have determined the 2D pressure gradient $B^T\boldsymbol{y}^{(i)}$, we can embed it to 3D and are thus able to determine the next velocity iterative, $\boldsymbol{x}^{(i)}$, in step (i) of the algorithm. Given this $\boldsymbol{x}^{(i)}$, the modified divergence constraint, $B\boldsymbol{x}^{(i)}$, can be determined, see also Section 6.3, which enable to solve the 2D subproblem (ii).
For a suitable preconditioning for the non hydrostatic case we refer to B.3.4. For an appropriate argumentation in the hydrostatic case, let us assume $D = 0$. Then, the task of the preconditioning of the hydrostatic Schur complement is to find a suitable approximation of $S^{-1} = (BA^{-1}B^T)^{-1}$. Given the hydrostatic Stokes problem we have $B = \operatorname{div}'\mathbf{M}$, $A = \Delta$, $B^T = P\nabla'$ and thus

$$S \;=\; \operatorname{div}'\mathbf{M} \circ \Delta^{-1} \circ P\nabla' \sim id\,,$$

such that the inverse mass matrix of the pressure space, i.e. M_p^{-1}, can be applied as preconditioner for the pressure problem.

In order to accelerate the iterative process, the search directions can be chosen more sophisticatedly. For symmetric problems, such as evolve for the hydrostatic Stokes problem, we can apply the conjugate gradient approach, see also Section B.4.3. The realization can be done in a similar fashion as described above. For non symmetric problems, such as the hydrostatic Oseen problem, suitable schemes, such as biconjugate gradient schemes have to be applied. However, numerical tests for the hydrostatic

Oseen problem revealed, that a good performance is only observed for problems with small magnitudes of the advection field. For the case of stronger advection, suitable preconditioners have to be applied.

The resulting subproblems commonly still are too complex to apply a direct solver. Instead, Krylov subspace methods, as well as multigrid schemes can be applied, see also Appendix B.4 and [KR11].

7.2 Application of pressure correction schemes

Another approach to solve a stationary hydrostatic flow problem is the application of a pressure correction scheme. We already introduced this issue in Chapter 6. In this chapter we also noted, that an appropriate convergence analysis is still missing. Given a hydrostatic flow problem, which is assumed to have a stationary solution, i.e.

$$\begin{gathered} \textit{Find } (\boldsymbol{v}_h, p_h) \in \mathbf{X}_h \quad s.\ t. \\ \mathrm{a}(\boldsymbol{v}_h, \boldsymbol{\varphi}) - \mathrm{b}(p_h, \boldsymbol{\varphi}) + \mathrm{b}(\xi, \boldsymbol{v}_h) \ = \ (\boldsymbol{f}, \boldsymbol{\varphi})_\Omega \forall (\boldsymbol{\varphi}, \xi) \in \mathbf{X}_h \,, \end{gathered}$$

we add the time derivative terms $(\partial_t \boldsymbol{v}_h, \boldsymbol{\varphi})_\Omega$ to the system and proceed as in the evolutionary case. If two consecutive solutions only differ in a negligible manner, we stop the iterative process.
This approach may be quite expensive, as the evolution to the steady state may take some time. Thus, if suitable and efficient Uzawa methods are at hand, this approach should be preferred, such as the Uzawa-CG-scheme in the case of the hydrostatic Stokes problem.
A different possibility was applied in [CGS12], where the authors used a coupled solver implemented with the finite element solver FreeFem++, see also [DHP03].

7.3 Parallelization

Given complex hydrostatic fluid problems, a feasible approach to handle the appropriate immense algebraic system is the parallelization of the problem. In the former chapter, as well as in the two preceding sections we followed an approach, in which subproblems of different dimensions are to be solved. Whereas the pressure problem is 2D, the (altered) momentum equation still is 3D, which causes the main effort. Moreover, the vertical integration has to be realized in order to determine the vertical velocity on the one hand, and the modified divergence constraint on the other hand.

The benefit of parallelizing the 2D pressure Poisson problem is marginal, see also [KR11], and it suffices to parallelize the 3D subproblems. For the parallelization of the 3D momentum equation we refer to Section 3 of [KR11]. In order to efficiently parallelize the vertical integration, the mesh distribution should be done in such way, that as less communication as possible takes places. Indeed it can be done without

communication, if the mesh distribution takes care of the prismatic structure of the 3D mesh, i.e. only the x y plane is decomposed, see also Figure 8 in [KR11].

Chapter 8

Numerical Examples

This chapter aims to illustrate and validate the analytical results and deductions of the preceding chapters. We start with the case of the stationary hydrostatic Stokes problem on isotropic meshes, demonstrating the proven convergence results and illustrating the effect of the hydrostatic approximation. We then turn to the stationary hydrostatic Oseen problem on isotropic meshes, showing numerical results for the linear case as well as the nonlinear case. The numerical results for the hydrostatic Stokes case are also to be found in [KB12]. The results for the hydrostatic Oseen problem are also presented in [Kim12]. Afterwards, we turn to the case of vertical anisotropic meshes in the framework of the hydrostatic Stokes problem. Further, we examine the evolutionary case, more precise, we consider physical phenomena, which are apparent in oceanic regimes.
Another topic is the issue of parallelization. This has been numerically treated in [KR11] and is given in Appendix C. In order to avoid redundancy we skip the representation of those tests and results, and refer to to appended article.

For the implementation of the hydrostatic problems we use different splitting schemes, as presented in the respective sections, see also Chapter 6. We apply the finite element space $Q_1 - Q_1$. For the stabilization of the schemes we use local projection stabilization schemes.

8.1 Stationary hydrostatic Stokes problem on isotropic meshes

In this section we numerically validate the results of Section 4.4 for the local projection stabilization method as one choice of the presented stabilization methods. Moreover, we give an intuition of the quality of the hydrostatic approximation for domains with different aspect ratios.

8.1.1 Algorithm

The Algorithm we apply here is based on the ideas of Chapter 6 for pressure correction schemes. We apply the extrapolation $p^{m+1,*} := p^m$ of the pressure in iteration step $m+1$. As suggested in Section 6.3.2, the update of the pressure is in standard form, i.e. no divergence term enters the update step of the pressure. Moreover, we apply a relaxation of the velocity by a factor of λ_v and "neglect" the time derivatives. I.e. we algorithmically treat the hydrostatic Stokes problem by a kind of mixture of a pressure correction scheme and an Uzawa algorithm. Still, convergence analysis for the upcoming algorithm is missing, as it is also the case for the splitting schemes of Chapter 6. However, it can be easily seen, that a fixed point of the following Algorithm is the solution of the local projection stabilized 2.5D Stokes problem.
At the m-th iteration, the solution is denoted by $(\boldsymbol{v}^m, p^m) \in \mathbf{X}_h$. We start with $m = 0$, initial pressure $p^m = 0$ and a velocity $\boldsymbol{v}^m$ satisfying the boundary condition.

Algorithm 8.1 (Splitting scheme for LPS stabilized 2.5D Stokes problems)**.**

(i) Find $\boldsymbol{w}^{m+1}$ *such that*

$$\begin{aligned} -\Delta \boldsymbol{w}^{m+1} + \nabla' p^m &= \boldsymbol{f} + \Delta\, \boldsymbol{v}^m, \\ \boldsymbol{w}^{m+1} &= 0 \qquad \text{on } \partial\Omega\,. \end{aligned}$$

(ii) Update velocity: $\boldsymbol{v}^{m+1} = \boldsymbol{v}^m + \lambda_v \boldsymbol{w}^{m+1}\,.$

(iii) Determine the divergence in vertical mean

$$\mathbf{g}^{m+1} \;=\; \int_{-d(x,y)}^{0} div'\, \boldsymbol{v}^{m+1}\; dz\,.$$

If $\|\mathbf{g}^{m+1}\| + \|\boldsymbol{w}^{m+1}\| < tol$ *stop iteration.*

(iv) Find pressure correction q^{m+1}*:*

$$\begin{aligned} (\nabla q^{m+1}, \nabla\, \boldsymbol{\phi}) &= -(\alpha^{-1/2}\mathbf{g}^{m+1}, \alpha^{-1/2}\, \boldsymbol{\phi}) - (\kappa_h \nabla p^m, \kappa_h \nabla\, \boldsymbol{\phi}) \\ p^{m+1} &= p^m + \lambda_p q^{m+1}\,. \end{aligned}$$

(v) Set $m := m+1$ *and go to (i).*

Reasonable values for the damping parameters λ_v and λ_p are about 0.1. However, the converged solutions are independent of these parameters.

8.1.2 Example 1: Convergence rates

We demonstrate the proven convergence results by application of the Q_1 finite elements. The domain is the unit cube $\Omega := (0,1)^3$ and the (smooth) solution is given by

$$\begin{aligned} &v_1(x,y,z) = x(x-1)\,(2y-1)\,z(1-z), \qquad p(x,y) = \sin(2\pi x)\sin(2\pi y), \\ &v_2(x,y,z) = (1-2x)\,y(y-1)\,/6. \end{aligned}$$

The forcing term is set to $\boldsymbol{f} = (-\Delta v_1 + \partial_x p, -\Delta v_2 + \partial_y p)$. The boundary conditions are given by $\boldsymbol{v}_0(x, y, z) := \boldsymbol{v}(x, y, z)$ on $\partial\Omega$. Note that this problem can be reformulated as a 2.5D Stokes problem with homogeneous Dirichlet data. We use equidistant triangulations of the mesh with mesh size h (for $\mathcal{T}_h$ and $\mathcal{K}_h$ as well) and set $\alpha_0 = 1$.

The errors of the solution according to the mesh size h are shown in Figure 8.1. The L^2-error of pressure and velocity obviously converge as $\mathcal{O}(h^2)$. The error in the gradient of $\boldsymbol{v}$, i.e. $\|\nabla(\boldsymbol{v} - \boldsymbol{v}_h)\|$ behaves as expected, $\mathcal{O}(h)$. The h^2-convergence of the pressure in L^2 is a super-convergence effect due to the applied equidistant mesh. This effect does not occur on locally refined meshes.

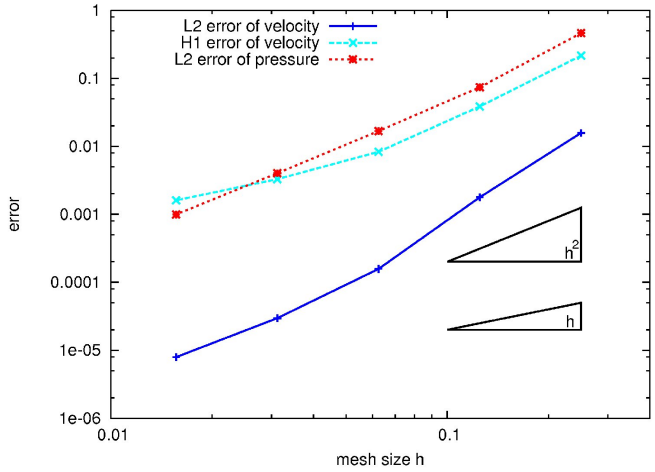

Figure 8.1: Error development for Example 1 depending on the mesh size h. The upper triangle denotes a quadratic decrease rate, the lower one a linear rate.

8.1.3 Example 2: Effect of the hydrostatic approximation

We compare the full 3D Stokes problem with the hydrostatic approximation in three dimensional domains in the form of bins with different aspect ratios. The horizontal size is $L = 100$, the maximal depth is ranging from $D = 100$ down to $D = 1$. In order to have a changing topography, the bottom has an elevation (see Figure 8.2):

$$\begin{aligned} \Omega &= \left\{(x, y, z) \in \mathbb{R}^3 \,|\, (x, y) \in (0, L)^2 \text{ and } z \in (-d(x, y), 0)\right\} \\ d(x, y) &= \begin{cases} -1 + 0.2 \cdot \cos(2\pi x/L) \cdot \cos(2\pi y/L) & \text{if } (x, y) \in [L/4, L \cdot 3/4] \\ -1 & \text{else.} \end{cases} \end{aligned}$$

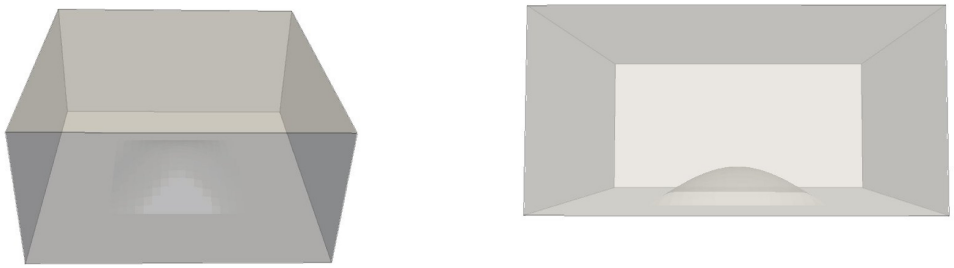

Figure 8.2: Domain Ω for Example 2 of Section 8.1.3 sketched in profile (left) and front view (right) for $L = 100$ and $D = 50$.

The forcing $\boldsymbol{f}$ is set to zero, noting, that the gravity impact, i.e. the hydrostatic balance, can be subtracted from the system. The boundary data for the horizontal velocity components is given by

$$\begin{aligned} u_1 &= \begin{cases} 0 & \text{on } \partial\Omega \setminus (\omega \times \{0\}), \\ -1 & \text{on } \omega \times \{0\}, \end{cases} \\ u_2 &= 0 \quad \text{on } \partial\Omega\,. \end{aligned}$$

In the case of the 2.5D system, Dirichlet conditions for the vertical velocity component can not be enforced at the vertical part of the boundaries, $\Gamma_{vert} := \{(x, y, z) \in \partial\Omega \mid -d(x, y) < z < 0\}$. Setting the normal derivative of the vertical component to zero seams to be an appropriate approximation:

$$\begin{aligned} u_3 &= 0 \quad \text{on } \partial\Omega \setminus \Gamma_{vert}, \\ \partial_n u_3 &= 0 \quad \text{on } \Gamma_{vert}\,. \end{aligned}$$

In Figures 8.3 we show streamlines and in Figure 8.4 we show isolines of the (hydrodynamic) pressure of the solution of the Stokes 3D problem and its hydrostatic approximation for a bin of maximal depth $D = 10$. The pressure is two-dimensional for 2.5 Stokes (lower right) by definition and nearly two-dimensional in the case of 3D Stokes (lower left). Only a small impact of the hydrostatic approximation on the path of fluid particles (streamlines) can be observed.

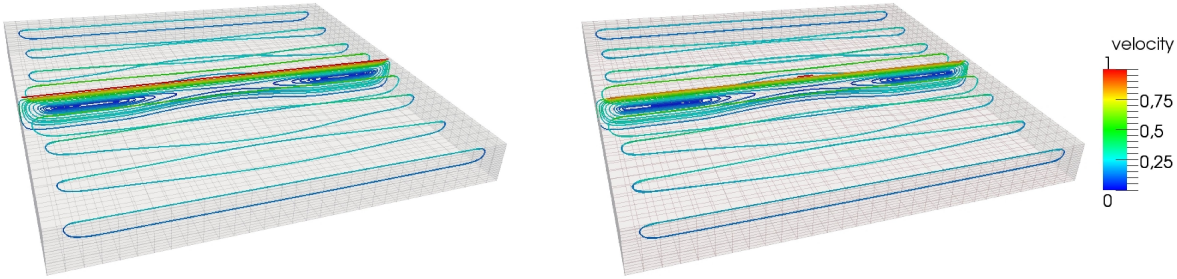

Figure 8.3: Streamlines of the velocity field of the 3D Stokes problem (left) and its (2.5D) hydrostatic approximation (right) in a domain with aspect ratio of $L/D = 10$ of Example 2 in Section 8.1.3.

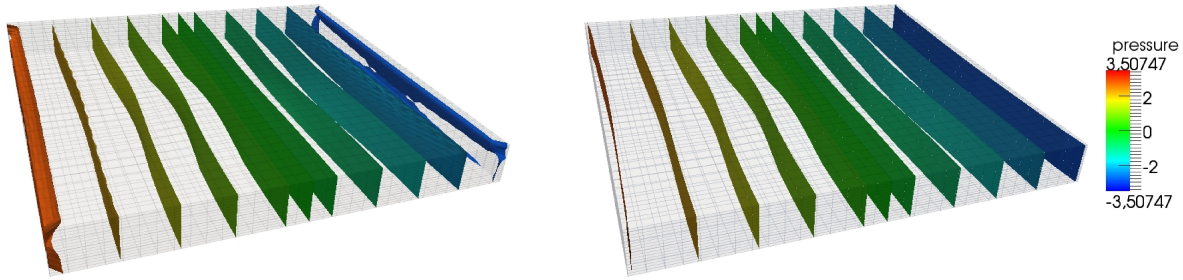

Figure 8.4: Isolines of the pressure field of the 3D Stokes problem (left) and its (2.5D) hydrostatic approximation (right) in a domain with aspect ratio of $L/D = 10$ of Example 2 in Section 8.1.3.

In order to analyze the differences (model errors) more accurately, we compare the differences in dependence of the aspect ratio L/D in Figure 8.5. Because the domain changes with varying D, relative differences of the 3D solution $(\mathbf{u}, p)$ and the 2.5D solution $(\boldsymbol{v}, q)$ are more reasonable quantities than absolute values. The green line shows the relative difference in the norm $\left(\|\mathbf{u}\|_{1,\Omega}^2 + \|p\|_{0,\Omega}^2\right)^{1/2}$. It behaves as $\mathcal{O}((D/L)^2)$. The individual parts $\|p-q\|_{0,\Omega}/\|p\|_{0,\Omega}$ (red line), the L^2-norm of the velocities (deep blue), and the H^1-semi norm of the velocities (light blue) behave very similar.

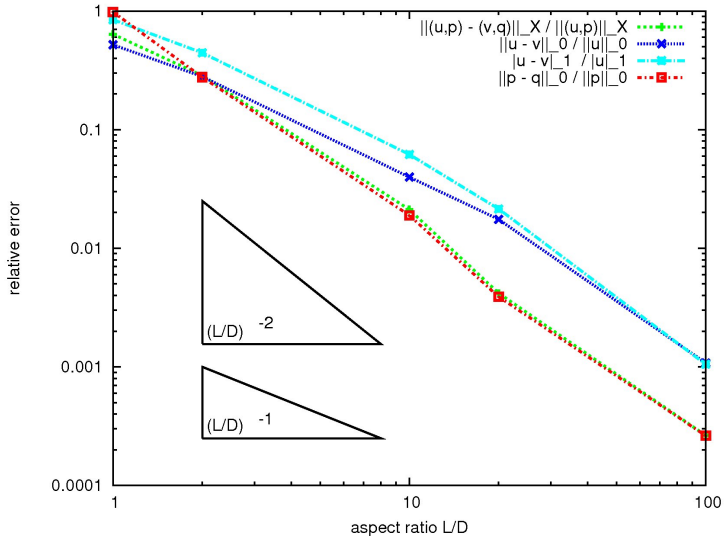

Figure 8.5: Relative differences between the hydrostatic approximation and the full 3D problem in the L^2-, H^1-seminorm and in $\|(\mathbf{u}, p)\|_X := \left(\|\mathbf{u}\|_{1,\Omega}^2 + \|p\|_{0,\Omega}^2\right)^{1/2}$ for $(\mathbf{u}, p) \in \boldsymbol{X}$ with respect to the aspect ratio L/D of Example 2 in Section 8.1.3.

Figure 8.6 shows the error development of the horizontal and vertical velocity components separately. Whereas the relative modeling error of the horizontal velocities converge as expected (red and orange line of left plot), the vertical velocities do not show convergence when the relative error is considered (deep blue and magenta line of left plot). The reason is that the vertical velocity components itself decrease for $D \to 0$.

This agrees with the scaling arguments in the deduction of the 2.5D problem that the impact of the vertical component of the 3D velocity field decreases when flattening the domain. The absolute model errors of the vertical velocities still converge (see right plot of Figure 8.6).

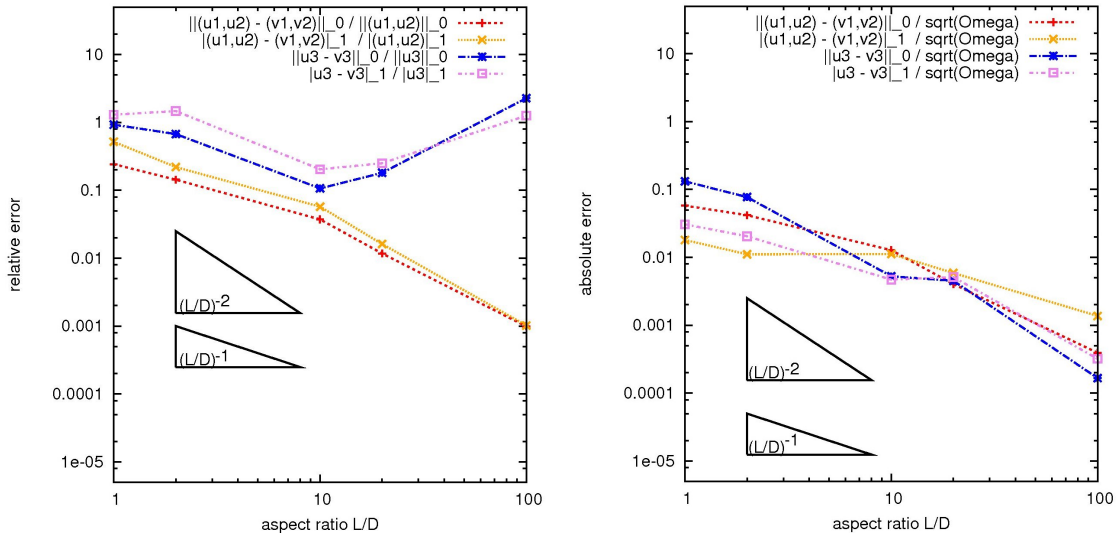

Figure 8.6: Relative (left) and absolute (right) differences between the hydrostatic approximation and the full 3D problem for the velocities, split into the horizontal and vertical components with respect to the aspect ratio L/D of Example 2 in Section 8.1.3.

8.2 Stationary hydrostatic Oseen problem on isotropic meshes

In this section we numerically validate the results of Section 4.5. We treat the linear hydrostatic Oseen problem, as well as the nonlinear hydrostatic Navier-Stokes problem, whose determination is based on the hydrostatic Oseen problem.
Basis of our numerical tests is the stabilized $Q_1 - Q_1$ formulation of problem (4.48). The applied stabilization are the local projection stabilizations (P-ii) and (V-i b).

8.2.1 Algorithm

The algorithm we apply is based on the 2nd order BDF scheme and initialized by one application of the Chorin scheme, see also Chapter 6. For the evaluation of our numerical results we consider the stationary limit of the time integration process.

The solution of the m-th iteration is denoted by $(\boldsymbol{v}^m, p^m) \in \boldsymbol{X}_h$. For ease of presenta-

tion let

$$\boldsymbol{a}_s(\boldsymbol{b}_h;\boldsymbol{v};\boldsymbol{\varphi}) := (\nu\nabla\boldsymbol{v},\nabla\boldsymbol{\varphi})_\Omega + (\sigma\boldsymbol{v},\boldsymbol{\varphi})_\Omega + \big((\boldsymbol{b}_h\cdot\nabla)\,\boldsymbol{v} + \mathrm{f}\ \boldsymbol{v}^\perp,\boldsymbol{\varphi}\big)_\Omega + s_{h,v}(\boldsymbol{v};\boldsymbol{\varphi}).$$

We use an Oseen linearization of the advection term. For a presumed $\boldsymbol{v}^0 = \boldsymbol{v}_0$, the algorithm is thus given by:

Algorithm 8.2 (Pressure correction scheme based on BDF2 for the local projection stabilized hydrostatic Navier-Stokes problem)**.** *Let $m = 1$.*

(i) *If $m = 1$* *set $\lambda = (\delta t)^{-1}$,* $\chi = 0$ *and* $\widehat{\boldsymbol{v}}^m = \boldsymbol{v}^m$,
else *set $\lambda = 3\,(2\delta t)^{-1}$,* $\chi = 1$ *and* $\widehat{\boldsymbol{v}}^m = (2\boldsymbol{v}^m - \frac{1}{2}\boldsymbol{v}^{m-1})$.

(ii) *Find $\boldsymbol{w}^{m+1}$ such that*

$$\big(\lambda\boldsymbol{w}^{m+1},\boldsymbol{\varphi}\big)_\Omega + \boldsymbol{a}_s(\boldsymbol{v}^m;\boldsymbol{w}^{m+1};\boldsymbol{\varphi}) - \chi(p^m, div'\,\boldsymbol{\varphi})_\Omega \;=\; \boldsymbol{l}^{m+1}(\boldsymbol{\varphi}) + (\delta t)^{-1}\,(\widehat{\boldsymbol{v}}^m,\boldsymbol{\varphi})_\Omega$$

(ii) *Determine the divergence in vertical mean*

$$\boldsymbol{g}^{m+1} \;=\; \int_{-d(x,y)}^{0} div'\boldsymbol{w}^{m+1}\,dz\,.$$

(iii) *Find pressure correction q^{m+1}:*

$$\lambda^{-1}(\nabla' q^{m+1},\nabla'\xi)_\omega + \ s_{h,p}(q^{m+1},\xi) \;=\; -(\boldsymbol{g}^{m+1},\xi)_\omega - s_{h,p}(p^m;\xi)$$

If $\|q\|_{0,\omega} < tol$ stop iteration.

(iv) *Update pressure:* $p^{m+1} = \chi\,p^m + \ d^{-1}\,q^{m+1}\,.$

(v) *Update velocity:* $\boldsymbol{v}^{m+1} = \boldsymbol{w}^{m+1} - \lambda^{-1}\nabla' q^{m+1}$ *and* $v_3{}^{m+1} = \int_{-d(x,y)}^{z} div'\boldsymbol{v}^{m+1}\,d\widehat{z}\,.$

(vi) *Set $m := m+1$ and go to (i).*

It is claimed in[GMS06], that the splitting error of the introduced scheme affects the rate of timal convergence and pointed out, that spatial convergence tests with fixed time steps δt may lead to false results. Due to that we set $\delta t = h$ in our computations.

8.2.2 Example 1: Convergence rates in the linear case

We start with the examination of the linear problem. For bilinear elements and $\sigma,\nu \sim 1$, Proposition 4.31 anticipates a decrease of $\|\nu^{1/2}\nabla(\boldsymbol{v}-\boldsymbol{v}_h)\|_{0,\Omega}$ and $\|(\nu+\sigma)^{1/2}(p-p_h)\|_{0,\Omega}$ of orders $\mathcal{O}(h)$ and $\mathcal{O}(h^{3/2})$, respectively. We thus expect linear convergence of $\|\nabla(\boldsymbol{v}-\boldsymbol{v}_h)\|_{0,\Omega}$ and convergence of order $\mathcal{O}(h^{3/2})$ for $\|p-p_h\|_{0,\Omega}$. Applying standard duality arguments, the observed convergence of the velocity error in the L^2-norm shall be of order $\mathcal{O}(h^2)$.

In the case $\nu \ll h$ and $\sigma \sim 1$, Proposition 4.31 suggests a decrease of $\|\nu^{1/2}\nabla(\boldsymbol{v}-\boldsymbol{v}_h)\|_{0,\Omega}$ and $\|(\nu+\sigma)^{1/2}(p-p_h)\|_{0,\Omega}$ both of order $\mathcal{O}(h^{3/2})$. Thus we shall observe convergence rates for $\|\nabla(\boldsymbol{v}-\boldsymbol{v}_h)\|_{0,\Omega}$, $\|p-p_h\|_{0,\Omega}$ and $\|\boldsymbol{v}-\boldsymbol{v}_h\|_{0,\Omega}$ as in the former case. If $\nu, \sigma \ll h$, the convergence of $\|p-p_h\|_{0,\Omega}$ is supposed to be at least of order $\mathcal{O}(h)$. Note, that due to Section 4.5.4, the L^2-error of the vertical velocity component is supposed to converge linearly.

The underlying domain for all test cases is the unit cube $\Omega := (0,\,1)^3$. We use equidistant triangulations of Ω and ω with mesh size h for both. In each case we set the right hand side $\boldsymbol{f}$ and the forcing $\boldsymbol{g}$ according to the solution

$$\begin{aligned} \boldsymbol{v}(x,y,z) &= \begin{pmatrix} e^{-x}\sin(\pi x)^2\partial_y\left(\sin(\pi y)^2\right)\sin(z) \\ -\partial_x\left(e^{-x}\sin(\pi x)^2\right)\sin(\pi y)^2\, 2(1-\cos(1))z \end{pmatrix} \\ p(x,y) &= e^x - (e^1-1)\,. \end{aligned}$$

Moreover, the advection term $\boldsymbol{b}$ is set to $(1,1,0)$ in each of these three tests. To account for the mentioned, different cases, we examine three scenarios. The according parameter setting is to be found in Table 8.1.

	ν	σ	f
Test case 1	1	1	1
Test case 2	10^{-4}	1	10^{-1}
Test case 3	10^{-4}	0	10^{-1}

Table 8.1: Parameter settings for the test cases of the linear problem.

The errors of the solution w.r.t. the H^1-semi- and L^2-norm according to the mesh size h are shown in Fig. 8.7, on the top left for the first test case, on the top right for the second. The results for the third test case are presented in the lower left figure.

Considering the depicted graphs we see, that in each of the test cases 1 – 3, the H^1-errors of the velocity are of order 1. The L^2-errors of the velocity converge quadratically, as expected. Moreover, the L^2-errors of the pressure converge at least with order $\mathcal{O}(h^{1.5})$. As well, the L^2-error of the vertical velocity component subordinates a linear convergence behavior.

8.2.3 Example 2: Convergence rates in the nonlinear case

We consider the solution of Example 1. The advection term $\boldsymbol{b}$ is set to the velocity determined in the former iteration step. For ease of stationarity of the solution we set $\nu = 1$. The remaining parameters are set to $\sigma = \mathrm{f} = 1$. We pass on the considerations from Example 1 to the present example. The observed convergence rates are depicted in the lower right graph of Fig. 8.7. As in Example 1 we recover the theoretical results in the numerical computations.

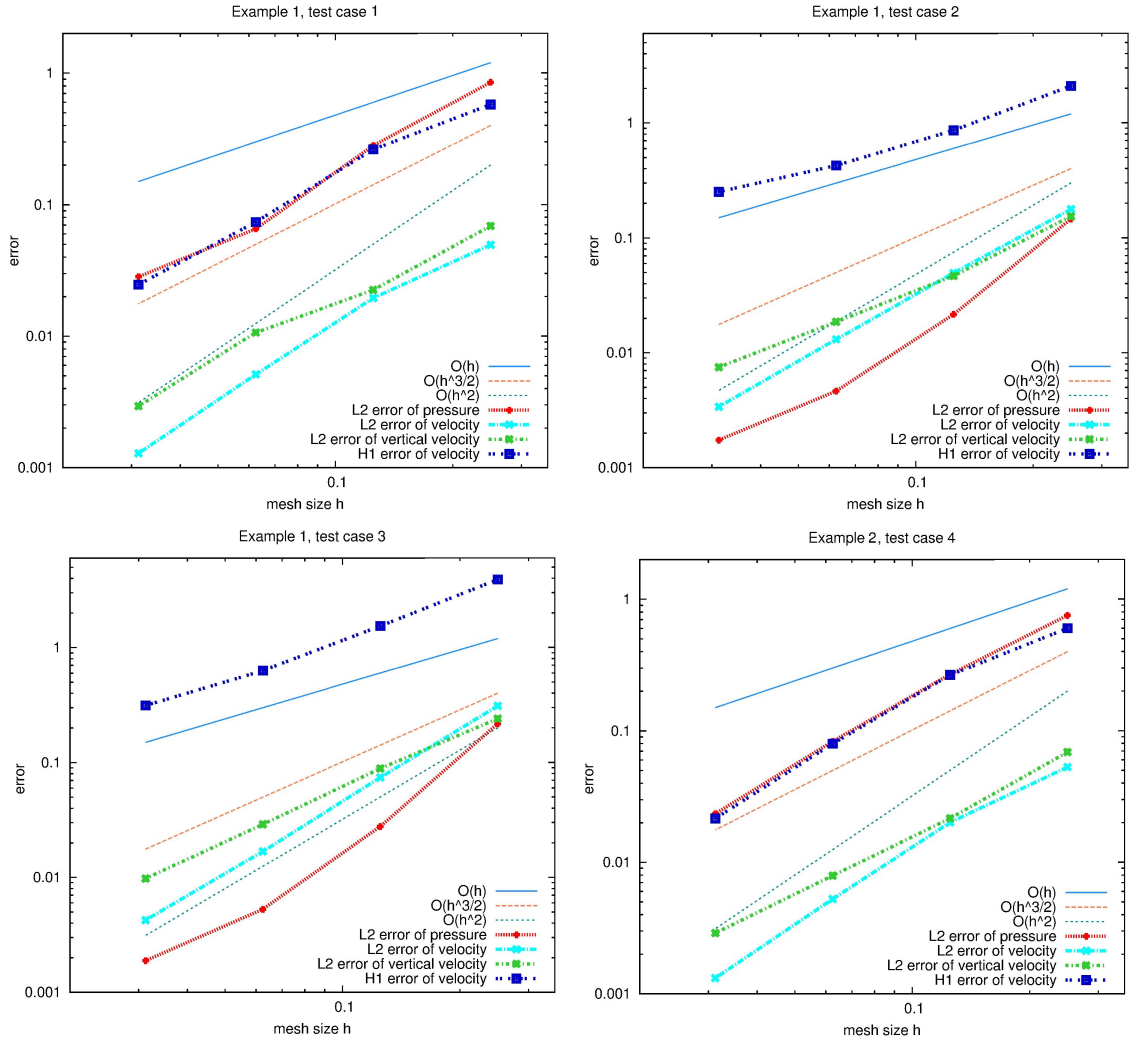

Figure 8.7: Error developments depending on the mesh size.

8.3 Stationary hydrostatic Stokes problem on vertical anisotropic meshes

In this section we turn to anisotropic meshes. We restrict to the case of vertical anisotropy. The numerical tests apply the isotropically stabilized $Q_1 - Q_1$ formulation of the hydrostatic Stokes problem.

8.3.1 Algorithm

For the evaluation of our numerical results we apply the BiCG Uzawa scheme, which is also applicable to non symmetric problems such as the hydrostatic Oseen problem. Note that in its unpreconditioned form the advection has to have moderate magnitudes in order to assure applicability.
For the stabilization of the pressure we apply the local projection stabilization (P-ii). The solution of the m-th iteration is denoted by $(\boldsymbol{v}^m, p^m) \in \boldsymbol{X}_h$. For a presumed $\boldsymbol{v}^0 = \boldsymbol{v}_0$, the algorithm is given by:

Algorithm 8.3 (Uzawa BiCG algorithm for the stabilized 2.5D Stokes problem)**.**

(i) Initialization.

(a) Given $p^{(0)}$ find $\boldsymbol{v}^{(0)}$ such that

$$(\nabla \boldsymbol{v}^{(0)}, \nabla \boldsymbol{\varphi})_\Omega \;=\; (\boldsymbol{f}, \boldsymbol{\varphi})_\Omega - (\nabla' P_{3d} p^{(0)}, \boldsymbol{\varphi})_\Omega \,.$$

The forcing $\boldsymbol{f}$ incorporates the boundary conditions imposed on the velocity field.

(b) Set $\widehat{q}^{(0)} = -\boldsymbol{v}^{(0)}$, $r^{(0)} = -div'\,\mathbf{M}\,\widehat{q}^{(0)}$, $r_{init} = r^{(0)}$, $q^{(0)} = r^{(0)}$, $\beta = 0$, $\rho^{(0)} = \langle r^{(0)}, r_{init}\rangle$, $i = 0$.

(ii) While $\|r^{(i)}\| > TOL$ do

(a) Set $p^{(i)} = q^{(i)}$.

(b) Find $q^{(i)}$ such that $(\nabla \widehat{q}^{(i)}, \nabla \boldsymbol{\varphi})_\Omega \;=\; (\nabla' P_{3d} p^{(i)}, \boldsymbol{\varphi})_\Omega \,.$

(c) Find $s^{(i)}$ such that $(s^{(i)}, \xi)_\omega \;=\; s_{h,p}(q^{(i)}, \xi) - (div'\,\mathbf{M}\,\widehat{q}^{(i)}, \xi)_\omega \,.$

(d) If $\sigma := \langle s^{(i)}, r_{init}\rangle = 0$, then stop.

(e) Set $\alpha := \rho^{(i)}/\sigma$, $w^{(i+1)} = r^{(i)} + \beta q_2^{(i)}$, $q_2^{(i+1)} = w^{(i+1)} - \alpha s^{(i)}$, $u^{(i+1)} = q_2^{(i+1)} + w^{(i+1)}$.

(f) Solve $(\nabla \widehat{w}^{(i+1)}, \nabla \boldsymbol{\varphi})_\Omega \;=\; (\nabla' P_{3d} u^{(i+1)}, \boldsymbol{\varphi})_\Omega \,.$

(g) Solve $(\widehat{s}^{(i+1)}, \xi)_\omega = \; s_{h,p}(u^{(i+1)}, \xi) - (div'\,\mathbf{M}\,\widehat{w}^{(i+1)}, \xi)_\omega \,.$

(h) Update $p^{(i+1)} = p^{(i)} - \alpha u^{(i+1)}$, $r^{(i+1)} = r^{(i)} - \alpha \widehat{s}^{(i+1)}$, $\boldsymbol{v}^{(i+1)} = \boldsymbol{v}^{(i)} + \alpha \widehat{w}^{(i+1)}$.

(i) Set $\rho^{(i+1)} = \langle r^{(i+1)}, r_{init}\rangle$, $\beta = \rho^{(i+1)}/\rho^{(i)}$, $i = i + 1$.

The scalar product is given by $\langle \cdot, \cdot \rangle$. P_{3d} denotes the 3D embedding of the 2D terms.

8.3.2 Example: Convergence rates

The domain is given by $\Omega := (0,1)^3$. We consider different meshes which show cellwise aspect ratios ranging from 1/2 to 1/100, see also Figure 8.8, in which we depicted the underlying coarse meshes for different aspect ratios.

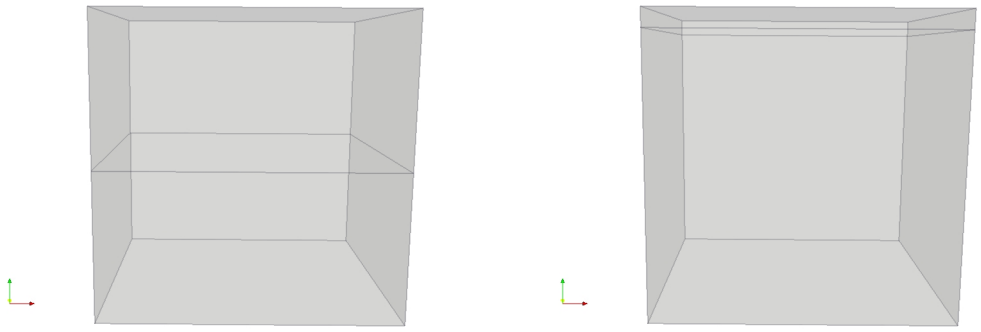

Figure 8.8: Basis meshes of Section 8.3.2. Left: Both cells have the same aspect ratio 1/2. Right: The upper cell has the aspect ratio 1/16, the lower cell shows the aspect ratio 15/16.

Each cell in the mesh on the left hand side has an aspect ratio of 1/2. The upper cell in the mesh on the right hand side has an aspect ratio of 1/16, the lower cell of 15/16, i.e. is almost cubic. Thus, we consider meshes, in which the vertical anisotropy (which here means a large aspect ratio) only occurs in the upper part of the domain. We yield the applied meshes by global refinement of such basis meshes, which retains the cellwise aspect ratios.

We consider two problems. The appropriate (smooth) solutions are given by

$$\begin{cases} v_1(x,y,z) &= x(x-1)\,(2y-1)\,f_1(z), \qquad p(x,y) = \sin(2\pi x)\sin(2\pi y), \\ v_2(x,y,z) &= (1-2x)\,y(y-1)\,f_2. \end{cases} \tag{8.1}$$

and

$$\begin{cases} v_1(x,y,z) &= y\,(y-1)\,f_1(z), \qquad p(x,y) = \sin(2\pi x)\sin(2\pi y), \\ v_2(x,y,z) &= 0.001 \cdot f_2 \cdot x \end{cases} \tag{8.2}$$

with

$$f_1(z) = 1 - \frac{1}{2}\frac{e^d - e^{dz}}{e^d - 1} \quad \text{and} \quad f_2 = 1 + \frac{1}{2(e^d-1)}\left(\frac{e^d}{d} - e^d - 1\right), \quad d = 100\,.$$

The function $f_1(z)$ effects v_1 to be vertically almost invariant up to the upper region of the domain. It it depicted in Figure 8.9.

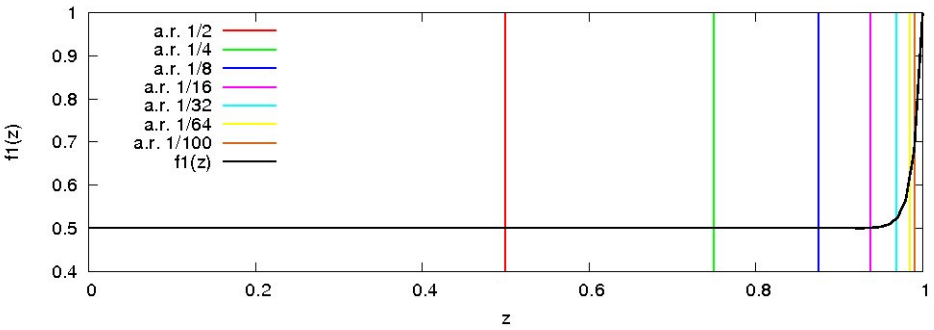

Figure 8.9: Function $f_1(z)$ and marks, where the change in the cellwise aspect ratios (a.r.) of the considered domains takes place.

The definition of f_2 provides for the modified divergence constraint. In both cases, the forcing term is set to $\boldsymbol{f} = (-\Delta v_1 + \partial_x p, -\Delta v_2 + \partial_y p)$. The boundary conditions are given by $\boldsymbol{v}_0(x, y, z) := \boldsymbol{v}(x, y, z)$ on $\partial\Omega$.

For clarity of the representation we refrain from depicting the convergence results via graphs and illustrate the numerical results in tables. The L^2-errors of the pressure and the velocity field, as well as the H^1-error of the velocity field of both problems are collected in Table 8.10. We observe as in the isotropic case, that the elaborated *a priori* error estimates are represented in the convergence results. Moreover we observe, that the convergence of the pressure is independent on the aspect ratio of the underlying domain to a great extent. This is also expected from the analysis. However, the quality of the velocity error estimates is affected by the cellwise aspect ratio. We observe a slight improvement from the results for the aspect ratio 1/2 towards the results for the aspect ratio 1/16 and a slight worsening of the results for further increasing cellwise aspect ratios. The reason for that can be found in Figure 8.9, where we observe, that for larger aspect ratios than 1/16 parts of the strong increasing of $f_1(z)$ is treated within cells of larger mesh sizes. Thus, higher resolution in the upper domain part of depths "1 minus aspect ratio" accompanies a coarser treatment of also relevant parts of the velocity field.

h	$\|\eta_p\|_{0,\omega}$	$\|\boldsymbol{\eta}_v\|_{0,\Omega}$	$\|\nabla\boldsymbol{\eta}_v\|_{0,\Omega}$	$\|\eta_p\|_{0,\omega}$	$\|\boldsymbol{\eta}_v\|_{0,\Omega}$	$\|\nabla\boldsymbol{\eta}_v\|_{0,\Omega}$
a.r. 1/2						
1/4	2.91e-01	1.26e-02	1.70e-01	3.32e-01	1.29e-02	1.75e-01
1/8	8.04e-02	2.34e-03	4.41e-02	8.92e-02	4.86e-03	7.32e-02
1/16	1.98e-02	5.13e-04	1.18e-02	2.19e-02	1.01e-03	2.01e-02
1/32	4.99e-03	9.80e-05	1.92e-03	5.13e-03	1.08e-04	2.59e-03
a.r. 1/4						
1/4	3.26e-01	1.25e-02	1.73e-01	3.35e-01	1.35e-02	1.87e-01
1/8	7.68e-02	1.18e-03	2.68e-02	7.70e-02	1.54e-03	3.27e-02
1/16	1.99e-02	1.79e-04	5.45e-03	1.99e-02	1.84e-04	5.76e-03
1/32	5.11e-03	4.08e-05	1.19e-03	5.05e-03	2.73e-05	9.34e-04
a.r. 1/8						
1/4	3.31e-01	1.24e-02	1.71e-01	3.31e-01	1.25e-02	1.74e-01
1/8	7.70e-02	1.07e-03	2.43e-02	7.83e-02	1.13e-03	2.66e-02
1/16	2.02e-02	1.55e-04	5.13e-03	1.99e-02	1.19e-04	4.80e-03
1/32	5.20e-03	3.35e-05	1.15e-03	5.12e-03	2.13e-05	8.47e-04
a.r. 1/16						
1/4	3.33e-01	1.23e-02	1.70e-01	3.31e-01	1.24e-02	1.72e-01
1/8	7.72e-02	1.07e-03	2.41e-02	7.83e-02	1.08e-03	2.60e-02
1/16	2.03e-02	1.53e-04	5.10e-03	1.99e-02	1.01e-04	4.68e-03
1/32	5.22e-03	3.27e-05	1.14e-03	5.12e-03	1.94e-05	8.32e-04
a.r. 1/32						
1/4	3.22e-01	1.23e-02	1.69e-01	3.33e-01	1.24e-02	1.73e-01
1/8	7.65e-02	1.31e-03	2.95e-02	7.90e-02	1.66e-03	3.75e-02
1/16	1.97e-02	1.98e-04	6.65e-03	1.99e-02	2.45e-04	9.16e-03
1/32	5.13e-03	3.71e-05	1.28e-03	5.12e-03	1.90e-05	1.29e-03
a.r. 1/64						
1/4	2.87e-01	1.27e-02	1.83e-01	3.41e-01	1.41e-02	2.35e-01
1/8	7.31e-02	2.16e-03	6.43e-02	8.31e-02	3.81e-03	1.16e-01
1/16	1.92e-02	4.10e-04	1.93e-02	1.99e-02	5.88e-04	3.42e-02
1/32	5.00e-03	8.81e-05	4.52e-03	5.18e-03	9.73e-05	5.79e-03
a.r. 1/100						
1/4	2.63e-01	1.30e-02	2.00e-01	3.48e-01	1.51e-02	2.97e-01
1/8	7.32e-02	2.51e-03	9.09e-02	8.14e-02	4.18e-03	1.67e-01
1/16	1.93e-02	5.72e-04	2.91e-02	2.06e-02	8.76e-04	5.21e-02
1/32	5.01e-03	1.61e-04	1.06e-02	5.51e-03	2.22e-04	1.18e-02

Figure 8.10: Convergence results for problem (8.1) (columns 2-4) and (8.2) (columns 5-7) for different aspect ratios. The mesh size h denotes the global mesh size of the surface mesh $\mathcal{K}_h$, $\boldsymbol{\eta}_v := \boldsymbol{v} - \boldsymbol{v}_h$ and $\eta_p := p - p_h$ denote the errors. The abbreviation a.r. denotes aspect ratio.

8.4 Evolutionary hydrostatic flow problems

In this section we treat the evolutionary case and consider physical phenomena, which apparent in oceanic regimes. We start with the impact of the Coriolis force on its own, where we observe an oscillation of the solution, which is imposed due to the rotation of the earth. We then turn to the Ekman transport, which occurs due to the Coriolis force when wind stress is imposed on the surface of the domain. We observe, that the thus induced surface velocity field is turned southwards by 45° from the direction of the wind stress. Moreover we observe the Ekman layer, which adjusts near the upper surface and where the so called Ekman spirals of the velocity field can be observed. Further, we consider the case of a sheared wind stress, which effects the Ekman pumping, which is an important mechanism of the ocean, as it transports the water masses and nutrients from deeper regions to the surface. For this examples we took our cue from [Ped86, CR02, Cha, CRB11]. We close this section with an flow example, where we imposed a sheared wind stress, induced an inflow region and opened a part of the wall, such that an outflow is possible.

8.4.1 Considered set of equations

We consider the evolutionary hydrostatic Navier Stokes equations. I.e. we consider the system (2.29) – (2.34). To account for the unresolved scales, we assume (constant) turbulent viscosity, $\boldsymbol{\mathcal{A}}_\nu$. For ease of presentation we denote the entire velocity field as $\boldsymbol{u}$ and the horizontal velocity field as $\boldsymbol{v}$. The vertical velocity field is given by v_3.

The entire set of equations thus becomes

$$\begin{aligned}
\operatorname{div}'(\mathbf{M}\,\boldsymbol{v}) &= 0 \\
v_3 &= -\int_{-d(x,y)}^{z} \operatorname{div}'\boldsymbol{v}\; d\widehat{z} \\
\partial_t\,\boldsymbol{v} + \boldsymbol{u}\cdot\nabla\,\boldsymbol{v} - \Delta_{\boldsymbol{\mathcal{A}}_\nu}\,\boldsymbol{v} + \mathrm{f}\,\boldsymbol{v}^\perp + \nabla' p &= 0 \\
\boldsymbol{v}\,|_{t=0} &= \boldsymbol{v}_0\,, \\
\boldsymbol{v}\,|_{\Gamma_b\cup\Gamma_s} = \mathbf{0}\,, \quad \nu_E\partial_z\,\boldsymbol{v}\,|_{\Gamma_u} &= \boldsymbol{\tau}\,,
\end{aligned}$$

Proper initial and boundary conditions, as well as domain and time interval specifications are given in the appropriate examples.

8.4.2 Algorithm

We apply a similar algorithm as in Section 8.2 for the stationary hydrostatic Oseen problem. The solution of the m-th iteration is denoted by $(\boldsymbol{v}^m, p^m) \in \boldsymbol{X}_h$. Again, we abbreviate

$$\boldsymbol{a}_s(\boldsymbol{b}_h;\boldsymbol{v};\boldsymbol{\varphi}) := (\boldsymbol{\mathcal{A}}_\nu\nabla\boldsymbol{v},\nabla\,\boldsymbol{\varphi})_\Omega + (\sigma\boldsymbol{v},\boldsymbol{\varphi})_\Omega + \big((\boldsymbol{b}_h\cdot\nabla)\,\boldsymbol{v} + \mathrm{f}\;\boldsymbol{v}^\perp,\boldsymbol{\varphi}\big)_\Omega + s_{h,v}(\boldsymbol{v};\boldsymbol{\varphi})$$

with anisotropic velocity stabilization (V") as examined in Section 5.3. The applied pressure stabilization $s_{h,p}$ is chosen as (P'-ii), see also Section 5.3. We use an Oseen linearization of the advection term. For a presumed $\boldsymbol{v}^0 = \boldsymbol{v}_0$, the algorithm is thus given by:

Algorithm 8.4 (Pressure correction scheme based on BDF2 for the evolutionary local projection stabilized hydrostatic Navier-Stokes problem)**.** *Let $m = 1$.*

(i) *If $m = 1$* *set $\lambda = (\delta t)^{-1}$,* $\chi = 0$ *and* $\widehat{\boldsymbol{v}}^m = \boldsymbol{v}^m$,
else *set $\lambda = 3\,(2\delta t)^{-1}$,* $\chi = 1$ *and* $\widehat{\boldsymbol{v}}^m = (2\boldsymbol{v}^m - \frac{1}{2}\boldsymbol{v}^{m-1})$.

(ii) *Find $\boldsymbol{w}^{m+1}$ such that*

$$\begin{aligned}\left(\lambda \boldsymbol{w}^{m+1}, \boldsymbol{\varphi}\right)_\Omega + \boldsymbol{a}_s(\boldsymbol{v}^m; \boldsymbol{w}^{m+1}; \boldsymbol{\varphi}) - \chi(p^m, div'\,\boldsymbol{\varphi})_\Omega \;&= \boldsymbol{l}^{m+1}(\boldsymbol{\varphi}) \\ &\quad + (\delta t)^{-1}\,(\widehat{\boldsymbol{v}}^m, \boldsymbol{\varphi})_\Omega\end{aligned}$$

(iii) *Determine the divergence in vertical mean*

$$\boldsymbol{g}^{m+1} \;=\; \int_{-d(x,y)}^{0} div'\boldsymbol{w}^{m+1}\,dz\,.$$

(iv) *Find pressure correction q^{m+1}:*

$$\lambda^{-1}(\nabla' q^{m+1}, \nabla'\xi)_\omega + \; s_{h,p}(q^{m+1}, \xi) \;\;=\;\; -(\boldsymbol{g}^{m+1}, \xi)_\omega - s_{h,p}(p^m; \xi)$$

If $\|q\|_{0,\omega} < tol$ stop iteration.

(v) *Update pressure:* $p^{m+1} = \chi\, p^m + d^{-1}\, q^{m+1}\,.$

(vi) *Update velocity:* $\boldsymbol{v}^{m+1} = \boldsymbol{w}^{m+1} - \lambda^{-1}\nabla' q^{m+1}$ *and*
$v_3{}^{m+1} = \int_{-d(x,y)}^{z} div'\boldsymbol{v}^{m+1}\,d\widehat{z}\,.$

(vii) *Set $m := m + 1$ and go to (i).*

8.4.3 Example 1: Inertial oscillations

Phenomenom of interest: Inertial frequency

We start with a phenomenom, which is caused by the Coriolis force. (For the deductions we refer to [CRB11].) Therefore we consider the set of equations, in which no additional forces and no viscous terms are apparent, as well pressure variations are neglected, i.e. we consider the system

$$\partial_t u - \mathrm{f}\, v = 0\,, \qquad\qquad \partial_t v + \mathrm{f}\, u = 0\,.$$

The general solution of this set of equations is given by

$$u = V \sin(\mathrm{f}\, t + \phi), \qquad v = V \cos(\mathrm{f}\, t + \phi)$$

with suitable constants $V \geq 0$ and ϕ of integration. Thus, on the one hand the magnitude of the entire velocity remains unchanged but the velocity components oscillate with frequency $2\pi/\mathrm{f}$.

Problem set

In order to reproduce these oscillations we induce a non trivial velocity field by adding a wind stress to the system. Moreover we treat the hydrostatic approximation of the 3D Navier-Stokes equations as introduced in Subsection 8.4.1. The underlying domain is given by $\Omega := (0, 10^6)^2 \times (-500, 0) m^3$ the considered time interval is $I := [0, 4\, d]$. The parameter set reads

$$\begin{aligned} \boldsymbol{\tau} &= (2.2 \cdot 10^{-3},\, 0)\, m\, s^{-1} \\ \mathcal{A}_{hx} &= 500\, m^2\, s^{-1} \qquad & \mathcal{A}_{hy} &= 500\, m^2\, s^{-1} \qquad & \nu_E &= 0.05\, m^2\, s^{-1} \\ \mathrm{f} &= 2\theta \sin\Phi \ (= \sqrt{2}\, \theta\, s^{-1}) \qquad & \Phi &= 45^\circ N \qquad & \theta &= 7.3 \cdot 10^{-5}\, s^{-1}\,. \end{aligned}$$

The applied mesh is depicted in Figure 8.11. Its grid size is $31250m$ in horizontal extend and $7.9375m$ in vertical direction. For the horizontal velocity field we have 141570 dofs, for the pressure 1089 dofs. The time step size is $\delta t = 250s$.

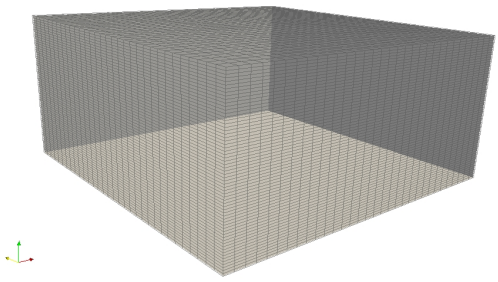

Figure 8.11: Domain Ω and mesh $\mathcal{T}_h$ of Section 8.4.3. Due to visibility, the depth is scaled by a factor of 900.

Numerical observation

In Figure 8.12 we depict the solution of the velocity field (left) and of the pressure (right) after 4 days. We see, that the surface velocity turned southwards. Moreover, the main mass flow occurs in that surface region and rapidly decreases with depth. This concern is issue of the following example. Further, we observe little impact of the Coriolis force on the pressure field.

Let us turn to the phenomenom of interest, which is depicted in the graphs in Figure 8.13. In these graphs we consider the velocity and pressure values at the points

$N1 := (2.5 \cdot 10^5, 2.5 \cdot 10^5, 0)$, $N2 := (7.5 \cdot 10^5, 2.5 \cdot 10^5, 0)$, $N3 := (2.5 \cdot 10^5, 7.5 \cdot 10^5, 0)$, $N4 := (7.5 \cdot 10^5, 7.5 \cdot 10^5, 0)$, $N5 := (2.5 \cdot 10^5, 5 \cdot 10^5, 0)$, $N6 := (7.5 \cdot 10^5, 5 \cdot 10^5, 0)$, $N7 := (2.5 \cdot 10^5, 5 \cdot 10^5, -250)$ and $N8 := (7.5 \cdot 10^5, 5 \cdot 10^5, -250)$. The upper most graph in this Figure shows the development of the velocity components at each of those points. Due to visibility aspects we split the pressure evaluation into the negative and positive values.

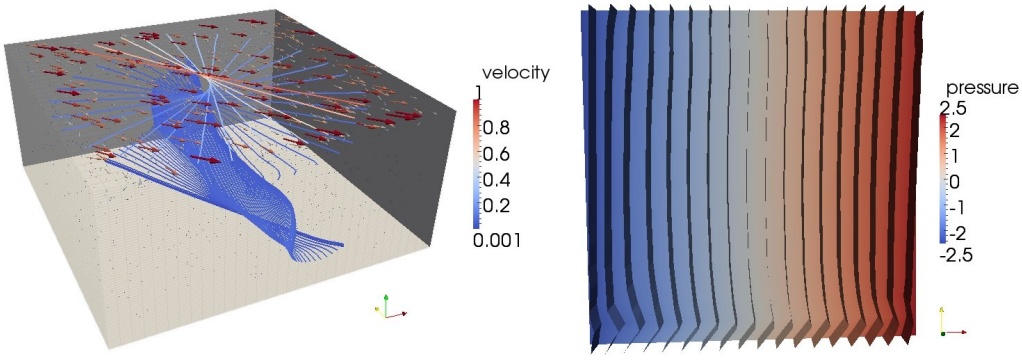

Figure 8.12: Velocity field (left) and pressure (right) of Section 8.4.3 at time $t = 4d\,s$. Due to visibility, the depth of the domain is scaled by a factor of 900.

First of all we observe the expected oscillations in the velocity as well as in the pressure field. As expected we observe a frequency of about $2\pi/\mathrm{f}$, which is approximately $61500\,s$. Moreover the oscillations undergo a damping, which occurs due to the added viscosity terms. Further note, that the vertical velocity components have negligible magnitudes compared to the horizontal ones. Last we observe, that the magnitudes of the velocity components in the inner of the domain are of lower magnitude than those at the surface, which also could be observed in Figure 8.12.

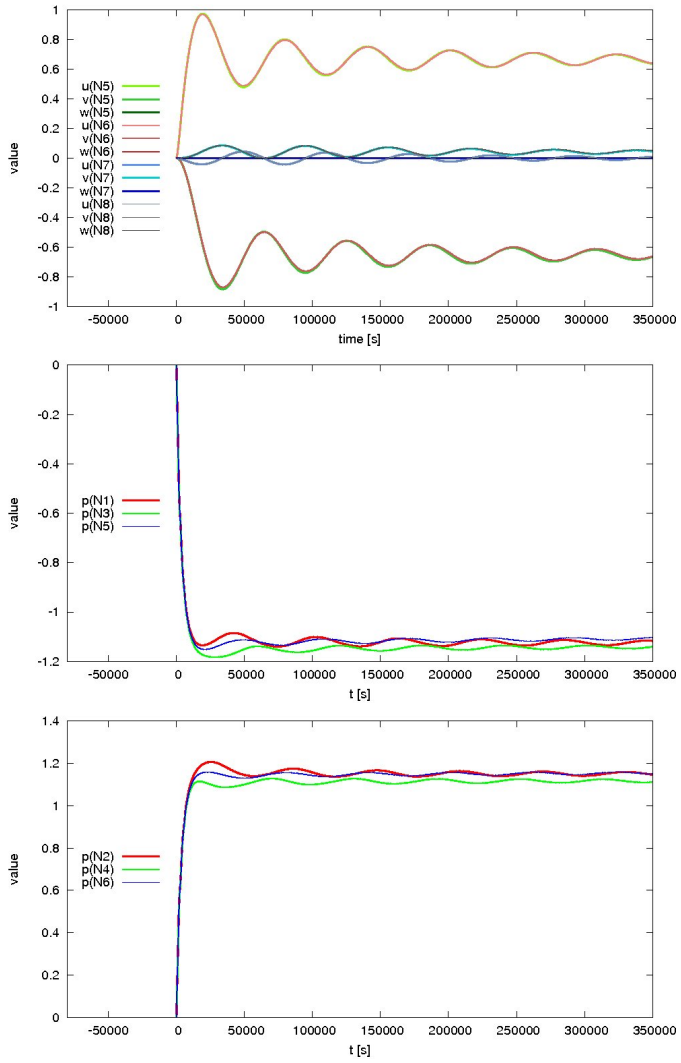

Figure 8.13: Time development of the magnitudes of the velocity components u, v and w of Section 8.4.3 at points $N5$ – $N6$ (top) and appropriate values of the pressure at points $N1$, $N3$, $N5$ (center) and $N2$, $N4$ and $N6$ (bottom).

8.4.4 Example 2: Ekman transport

Phenomenom of interest - Ekman transport

The upcoming considerations can also be found in [CRB11, CR02, Cha] and aim to throw light on the effect of the interacting forces friction and Coriolis forces on the entire basin flow.
In [CRB11] Cushman-Roisin and Beckers figure out, that near the bottom and side walls, where no-slip conditions are imposed, friction acts to reduce the velocity components towards the walls. This induces a shear flow along the walls. In non rotating frames, the appropriate boundary layers grow by downstreaming processes or by time.

Adding Coriolis forces to the system, i.e. presuming a rotating frame, changes the scenario noticeably. The appropriate boundary layer now has a fixed thickness, i.e. rotation imposes a characteristic length scale along the boundaries. Moreover, in this boundary layer the velocities are diverted, which leads to transverse currents.

More precise, in geophysical flows Coriolis forces typically superior friction forces, i.e. these flows show very small Ekman numbers, $Ek = \nu_E \,\mathrm{f}^{-1}\, H^{-2} \sim 10^{-4}$, whereas $\mathrm{f} \sim 10^{-4} s^{-1}$ and $\nu_E \sim 10^{-2} m^2 s^{-1}$ in basins of depth of about $1\,000\, m$. However, in the boundary layer, also called *Ekman layer*, friction is the dominant force, i.e. $Ek = \nu_E \,\mathrm{f}^{-1}\, d_{Ek}^{-2} \sim 1$ with thickness $d_{Ek} \sim (\nu_E \,\mathrm{f}^{-1})^{1/2} \ll H$ of the boundary layer.

For further explanation assume a uniform (i.e. absence of horizontal gradients), geostrophic (i.e. Coriolis forces and pressure gradient forces are balanced) flow in a homogeneous fluid with (interior) velocity field $(\overline{u}, \overline{v})$. Imposing wind stress (τ_x, τ_y) along the surface we obtain the following set of equations in the Ekman layer, see also [CRB11]:

$$\begin{aligned} -\mathrm{f}(v-\overline{v}) &= \mathcal{A}_h \partial_z^2 u\,, & \mathrm{f}(u-\overline{u}) &= \mathcal{A}_h \partial_z^2 v\,,\\ \rho_0 \mathcal{A}_h \partial_n u|_{\Gamma_u} &= \tau_x\,, & \rho_0 \mathcal{A}_h \partial_n v|_{\Gamma_u} &= \tau_y\,,\\ u|_{z=-d_{Ek}} &= \overline{u}\,, & v|_{z=-d_{Ek}} &= \overline{v} \end{aligned}$$

with (approximate) solution (*Ekman spiral*)

$$\begin{aligned} u &\sim \overline{u} + \frac{\sqrt{2}}{\rho_0 \,\mathrm{f}\, d_{Ek}} \exp\left(\frac{z}{d_{Ek}}\right)\left[\tau_x \cos\left(\frac{z}{d_{Ek}} - \frac{\pi}{4}\right) - \tau_y \sin\left(\frac{z}{d_{Ek}} - \frac{\pi}{4}\right)\right]\,,\\ v &\sim \overline{v} + \frac{\sqrt{2}}{\rho_0 \,\mathrm{f}\, d_{Ek}} \exp\left(\frac{z}{d_{Ek}}\right)\left[\tau_x \sin\left(\frac{z}{d_{Ek}} - \frac{\pi}{4}\right) + \tau_y \cos\left(\frac{z}{d_{Ek}} - \frac{\pi}{4}\right)\right]\,. \end{aligned}$$

We observe the following:
(a) The deviation from the interior flow, i.e. the drift velocity, occurs solely due to the wind stress.
(b) As the magnitude of this drift velocity depends inversely proportional on the thickness of the Ekman layer, this deviation from $(\overline{u}, \overline{v})$ decreases exponentially towards the inner flow and, for small viscosities and moderate wind stress the drift velocity can be quite large.
(c) At the surface, the angle between the drift velocity and the wind stress is 45°.
(d) The horizontal transport due to the wind stress in the surface Ekman layer is (approximately) given by

$$U \sim \int_{-d_{Ek}}^{0} (u-\overline{u}) dz = (\rho_0 \,\mathrm{f})^{-1} \tau_y\,, \qquad V \sim \int_{-d_{Ek}}^{0} (v-\overline{v}) dz = -(\rho_0 \,\mathrm{f})^{-1} \tau_x\,,$$

which is oriented perpendicular to the wind stress, to the east in the northern hemisphere and to the west in the southern hemisphere due to the sign of the Coriolis force.

Problem set

We consider the domain $\Omega := \{(x,y,z) \in \mathbb{R}^3 \,|\, (x,y) \in \omega \text{ and } z \in (-d(x,y), 0)\ \forall (x,y) \in \omega\}$ as (suitably scaled) given in Figure 8.14 with surface ω and depth function $d : \omega \to$

$\mathbb{R}_+$ being defined by

$$\omega := [0,\, 10^4] \times [0,\, 5 \cdot 10^3]$$

$$d(x,y) := \begin{cases} 50 & \text{if } 0 \le x \le 4\,375 \\ 50 \cdot \frac{5\,000-x}{10^3} + 100 \cdot \frac{x-4\,375}{10^3} & \text{if } 4\,375 \le x \le 5\,000 \\ 100 & \text{if } 5\,000 \le x \le 10\,000\,. \end{cases}$$

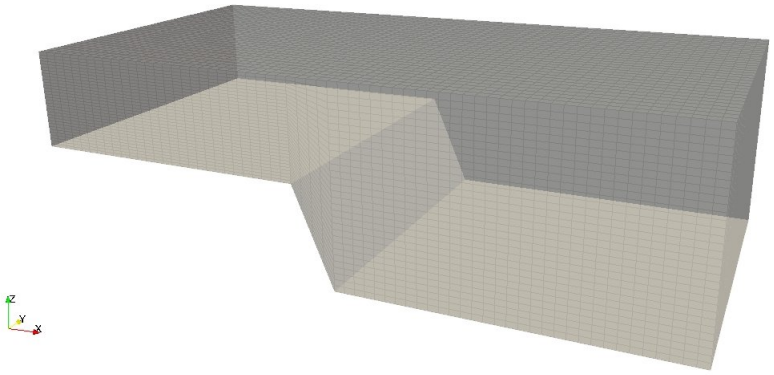

Figure 8.14: Domain Ω and mesh $\mathcal{T}_h$ of Section 8.4. Due to visibility, the depth is scaled by a factor of 30.

The spatial resolution of the considered mesh $\mathcal{T}_h$ is $156.25\,m$ is horizontal directions and $1.5625 - 3.125\,m$ in vertical extent. Thus the horizontal 3D velocity field has 141570 dofs and the 2D pressure field 1089 dofs. The vertical velocity component has 70785 dofs. The time interval is given by $I := [0,\, \mathcal{T}]$ with $\mathcal{T} = 10^5\,s = 1d\,3h\,46min\,40s$. We use equidistant time steps of size $\delta t = 50\,s$.

We assume no body forcing. The remaining problem parameter are set to

$$\begin{aligned} \boldsymbol{\tau} &= \epsilon(t)\,\mathbf{v} & \mathbf{v} &= (7.5 \cdot 10^{-5},\, 0)\,m\,s^{-1} & & \\ & & \epsilon(t) &= 1 - \exp(-t/\mathcal{T}_0) & \mathcal{T}_0 &= 3600\,s \\ \mathcal{A}_{hx} &= 100\,m^2\,s^{-1} & \mathcal{A}_{hy} &= 10\,m^2\,s^{-1} & \nu_E &= 10^{-2} m^2\,s^{-1} \\ \mathrm{f} &= 2\theta \sin\Phi \;(= \sqrt{2}\,\theta\,s^{-1}) & \Phi &= 45^\circ N & \theta &= 7.3 \cdot 10^{-5}\,s^{-1} \end{aligned}$$

Note, that we apply different horizontal diffusivity constants $\mathcal{A}_{hx}$ and $\mathcal{A}_{hy}$ to account for the different horizontal extentions of the domain. Considering this parameter set and the physical introduction of the preceding subsection the Ekman number is of order 10^{-2} and the supposed thickness of the Ekman layer is $d_{Ek} = 10m$.

Numerical observations

Considering the snapshots in Figures 8.15 and 8.16 of the surface velocity and the hydrodynamic pressure at times $t = 10^3 s$, $t = 15 \cdot 10^3 s$, $t = 45 \cdot 10^3 s$ and $t = 10^5 s$, we recognize the rotational impact of the Coriolis force. At the beginning of the flow,

the rotation of the earth hardly impacts the flow field, as the flow only slightly deviates from equilibrium state and the Coriolis force has hardly any velocity field to act on. Letting the wind stress the fluid surface over time, a drift of the surface velocity field and of the pressure field can be observed. As well, the expected angle of 45° between the velocity field and the direction of the wind stress is distinctibly brought out.

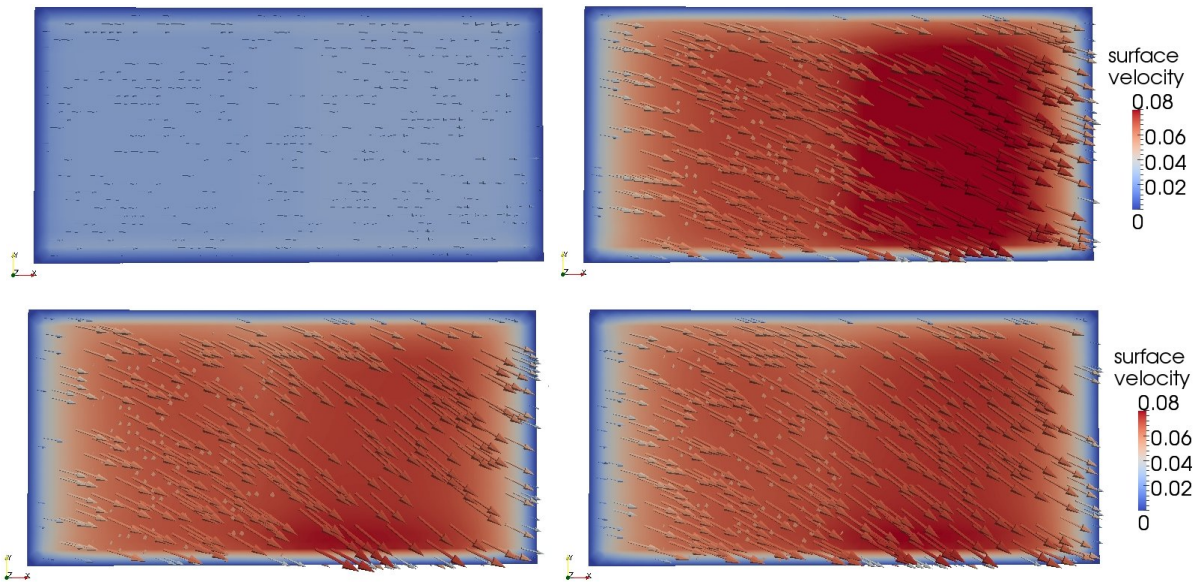

Figure 8.15: Surface velocity field of Section 8.4.4 at times $t = 10^3 s$ (top left), $t = 15 \cdot 10^3 s$ (top right), $t = 45 \cdot 10^3 s$ (bottom left), $t = 10^5 s$ (bottom right).

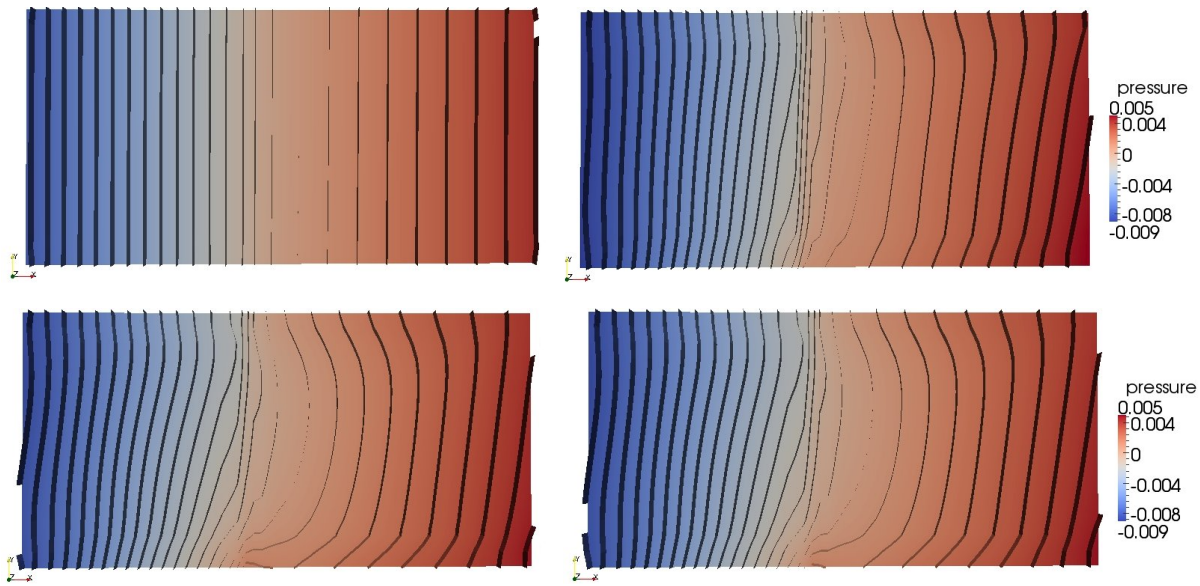

Figure 8.16: Isolines of the hydrodynamic pressure of Section 8.4.4 at times $t = 10^3 s$ (top left), $t = 15 \cdot 10^3 s$ (top right), $t = 45 \cdot 10^3 s$ (bottom left), $t = 10^5 s$ (bottom right).

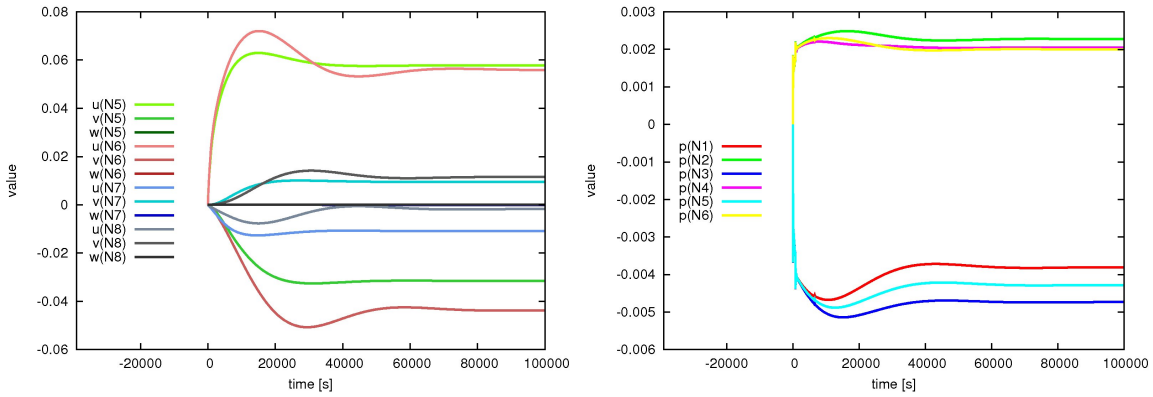

Figure 8.17: Time development of the magnitudes of the velocity components u, v and w of Section 8.4.4 at points $N5$ – $N6$ (left) and appropriate values of the pressure at points $N1$ – $N6$ (right).

Furthermore, the similarities of the latter two snapshots of Figure 8.16 and 8.15 indicate, that the flow runs into steady state. This observation can also be made in the graphs of Figure 8.17, where we consider the values of the single velocity components and of the pressure at the surface points $N1 := (2500, 625, 0)$, $N2 := (7500, 625, 0)$, $N3 := (2500, 4375, 0)$, $N4 := (7500, 4375, 0)$, $N5 := (2500, 2500, 0)$ and $N6 := (7500, 2500, 0)$, as well as at the inner points $N7 := (2500, 2500, -25)$ and $N8 := (7500, 2500, -50)$. We observe, that each of the values tends to a constant value, whereas the vertical velocities each comparatively are of negligible value. Moreover, we see, that the velocities on the surface are of larger magnitude than those in the inner part of the domain, which may be an indication for the Ekman transport in the Ekman layer. Moreover, the pressure shows the expected behavior: being negative at the points where mass is removed by the flow and being positive at the points near the boundaries, where the fluid transports the water masses to.

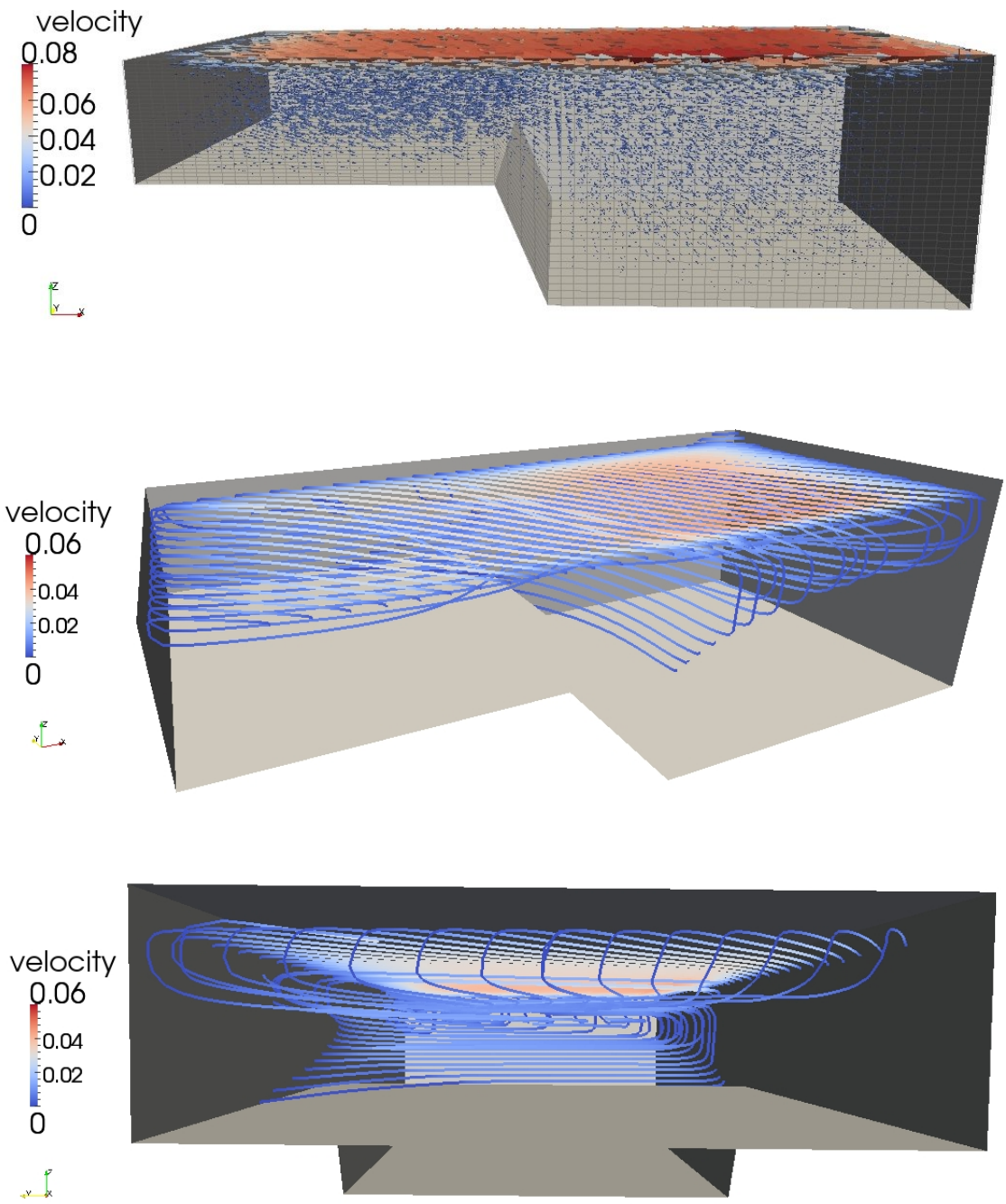

Figure 8.18: Velocity field of Section 8.4.4 at time $t = 10^5\,s$ in side view (top), zenit view (center) and front view (bottom). Due to visibility, the depth of the domain is scaled by a factor of 30.

The snapshots in Figure 8.18 of the velocity field at time $t = 10^5 s$ reveals that the major current takes place in an upper part of the domain, i.e. in the Ekman layer. As presumed, we find a depth of the Ekman layer of about $10\,m$, see center and bottom

snapshot in Figure 8.18. Moreover, the velocity field shows a recirculation of the Ekman transported water masses. An upwelling takes place at the northern part of the domain and an appropriate downwelling occurs along the southern boundary, which is justified due to locating of the domain is in the northern hemisphere (see the choice of the Coriolis parameter).

Last, consider the sector of the velocity field at time $t = 10^5\,s$ in Figure 8.19. In that snapshot we observe an Ekman spiral in the Ekman layer, which exponentially decreases its magnitude, indicated by the different shades. The velocity field in the lower regions of the domain occur due to the recirculation.

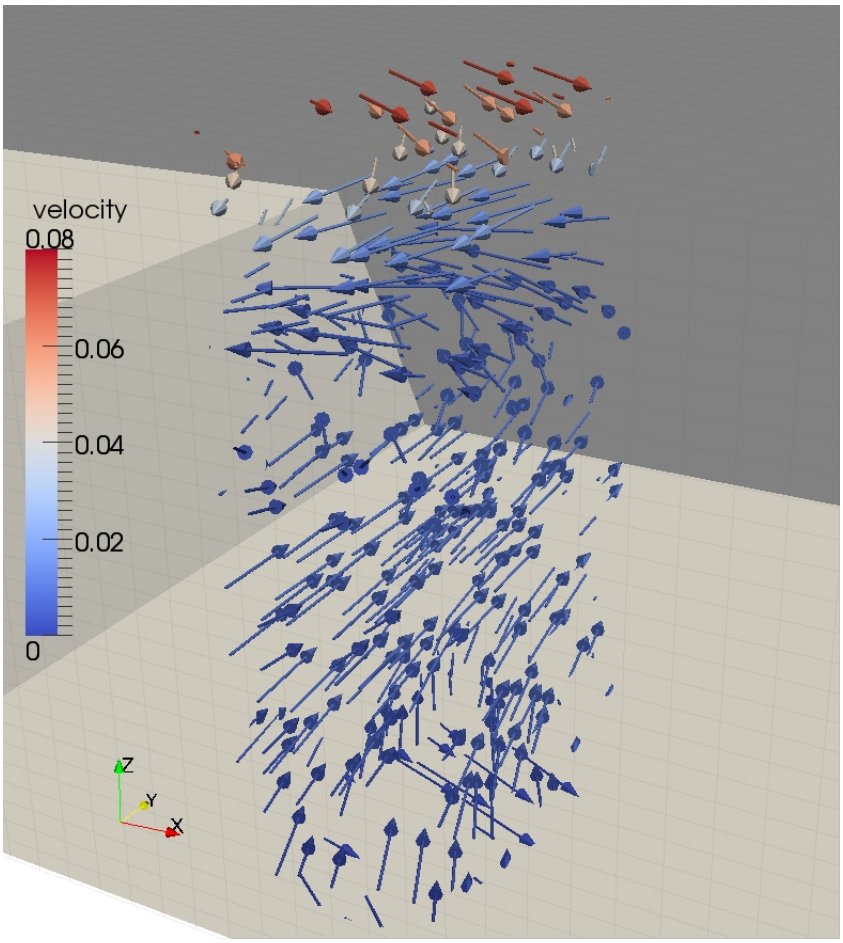

Figure 8.19: Sector of the velocity field of Section 8.4.4 at time $t = 10^5\,s$ indicating the Ekman spiral occurring in the Ekman layer near the surface. Due to visibility, the depth of the domain is scaled by a factor of 30.

8.4.5 Example 3: Ekman pumping

Phenomenom of interest: Ekman pumping

We resume to the considerations of Example 1 and start our argumentation from the Ekman transport in the surface Ekman layer. As figured out in the former section, the eastwards directed wind stress and the Coriolis forces, acting on the moving fluid, imposes a south–easternwards water mass transport in the Ekman layer (in the northern hemisphere). The numerical test of Example 1 reveals, that the Ekman transport invokes circulation with an upwelling at the northern boundary and a downwelling at the southern boundary. However, this resulting circulation in the upper flow region occurs due to the imposed Dirichlet boundary conditions along the side and bottom walls of the velocity field.
In oceanic flows, wind stress induced water mass exchanges from *deeper* regions, which are abundant in nutrients, is an important mechanism and takes place, when the wind stress is not rotation free, see also [CRB11].
Let us explain this more involved up- and downwelling, also called *Ekman pumping* and *Ekman suction*, respectively.

Therefore, let $\overline{w}$ be the vertical velocity in the interior, defined by the divergence constraint

$$\overline{w} \;=\; \int_0^\infty \left(\partial_x u + \partial_y v\right) dz \;=\; \left(\rho_0\, \mathrm{f}\right)^{-1} \left(\partial_x \tau_y - \partial_y \tau_x\right) \,.$$

I.e. if the curl of the imposed wind stress does not vanish, the appropriate spatial variations in the wind drive vertical currents, which in turn drive the *interior* circulation of the ocean.
Moreover, the drift velocities in the Ekman layer *along the bottom wall* are (approximately) given by

$$\begin{aligned} u &\approx \overline{u} - \exp\left(\frac{-(d+z)}{d_{Ek}}\right)\left[\overline{u}\cos\left(\frac{z+d}{d_{Ek}}\right) + \overline{v}\sin\left(\frac{z+d}{d_{Ek}}\right)\right] \,, \\ v &\approx \overline{v} + \exp\left(\frac{-(d+z)}{d_{Ek}}\right)\left[\overline{u}\sin\left(\frac{z+d}{d_{Ek}}\right) - \overline{v}\cos\left(\frac{z+d}{d_{Ek}}\right)\right] \,, \end{aligned}$$

with depth function d and resulting vertical drift velocity $w = w_d + w_{pump}$ with $w_d = -\overline{u}\partial_x d - \overline{v}\partial_y d$, accounting for the bottom structure, and an Ekman pumping or suction contribution $w_{pump} = d_{Ek}(\partial_x \overline{v} - \partial_y \overline{u})/2$, see also [CRB11]. I.e. at the lower Ekman boundary an upwelling/downwelling takes place due to the vorticity of the interior velocity field, which has been imposed by the wind stress.

Problem set

We consider the same problem set as in Example 1, except for the wind stress, which now is assumed to have a non zero curl, i.e. we set

$$\begin{aligned}
\boldsymbol{\tau} &= 7.5 \cdot 10^{-5}\, \epsilon(t)\, \mathbf{v} & \mathbf{v} &= (\cos(\pi\, y/5000),\, 0)\, m\, s^{-1} & & \\
& & \epsilon(t) &= 1 - \exp(-t/\mathcal{T}_0) & \mathcal{T}_0 &= 3600\, s \\
\mathcal{A}_{hx} &= 100\, m^2\, s^{-1} & \mathcal{A}_{hy} &= 10\, m^2\, s^{-1} & \nu_E &= 10^{-2} m^2\, s^{-1} \\
\mathrm{f} &= 2\theta \sin\Phi\ (= \sqrt{2}\,\theta\, s^{-1})\,. & & & &
\end{aligned}$$

Numerical observations

We imposed a wind stress which is directed eastwards at the northern surface part and directed westwards at the southern surface. Due to that reason we expect, that the surface velocity aligns in north-west direction in the northern part of the surface and in south-east direction in the southern part of the surface. This is exactly what we observe in the bottom right sketch of Figure 8.20. The former sketches in that figure depict the adjustment to this state.

Matching to the surface water mass transports and having in mind the Ekman transport mechanisms we suppose a negative pressure in the center of the domain and along the north-eastern and south-western boundary, and a positive one in the north-western and the south-eastern boundary regions. This is also to be observed, see the bottom right sketch of the hydrodynamic pressure in Figure 8.21. Again, the remaining sketches in that figure show the adjustment to the latter state. These observations describe the Ekman transport. The upper sketch of Figure 8.22 also reveals, that again the main transport takes place in the near surface regions.
Recalling the considerations of the Ekman pumping an Ekman pumping, i.e. an upwelling, is supposed to take place in the center of the domain. Considering the aligned velocity field of Figure 8.20 and the streamlines presented in Figure 8.22 we observe this Ekman pumping from the deeper regions of the domain to the surface regions in the (east-west) center region of the domain. At the surface, these water masses are then transported southwards and northwards. At the northern and southern walls we observe a downwelling, i.e. Ekman suction.

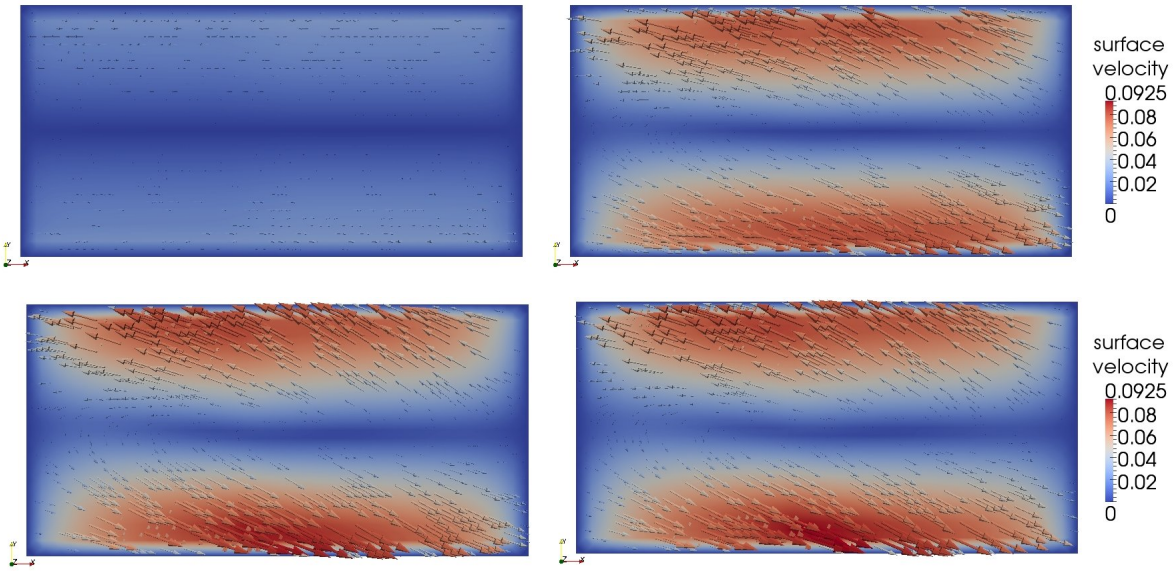

Figure 8.20: Surface velocity field of Section 8.4.5 at times $t = 10^3 s$ (top left), $t = 15 \cdot 10^3 s$ (top right), $t = 45 \cdot 10^3 s$ (bottom left), $t = 10^5 s$ (bottom right).

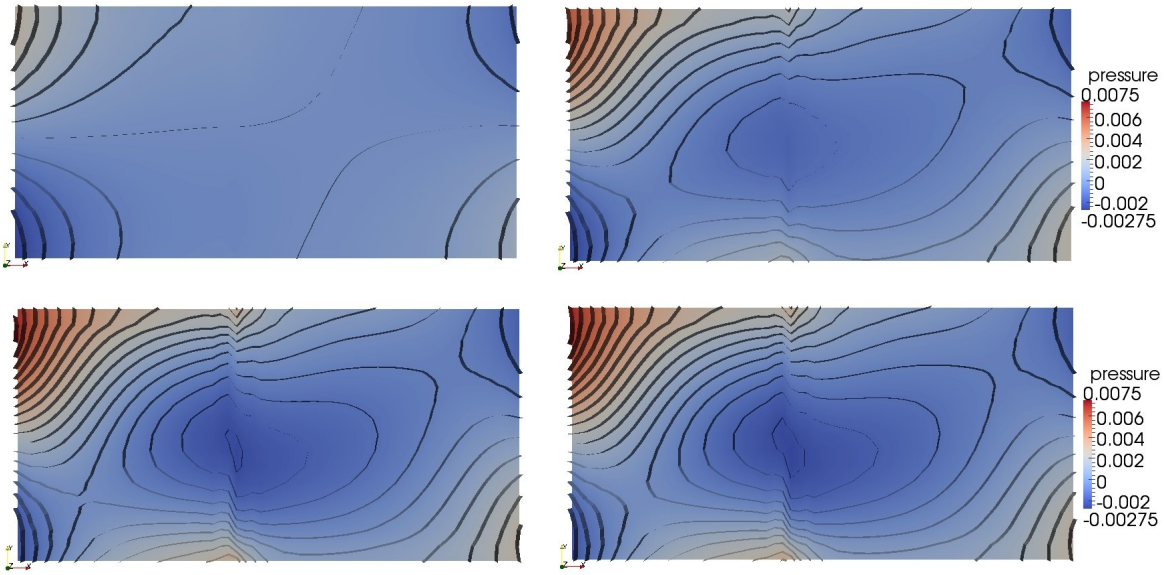

Figure 8.21: Isolines of the hydrodynamic pressure of Section 8.4.5 at times $t = 10^3 s$ (top left), $t = 15 \cdot 10^3 s$ (top right), $t = 45 \cdot 10^3 s$ (bottom left), $t = 10^5 s$ (bottom right).

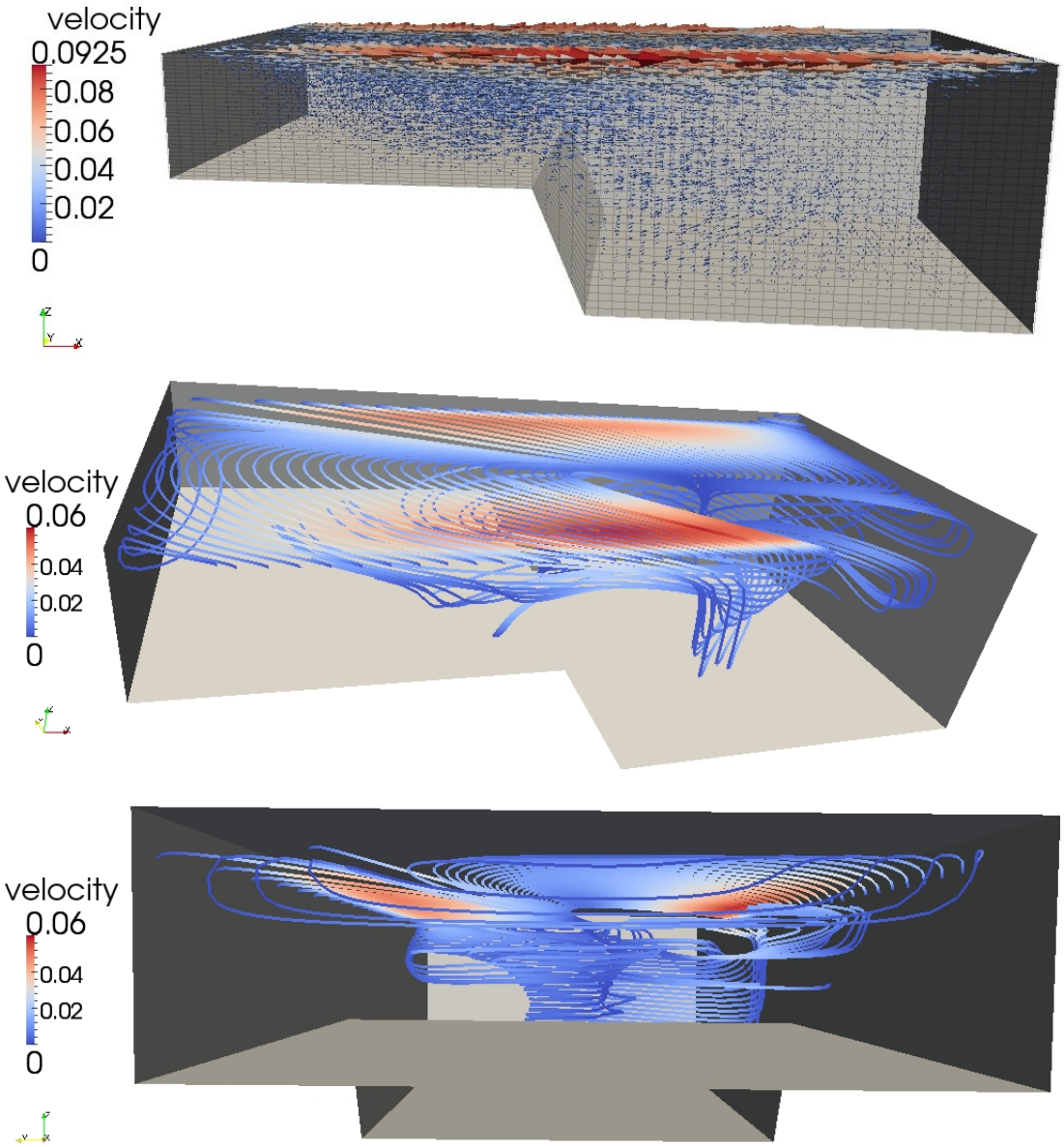

Figure 8.22: Velocity field of Section 8.4.5 at time $t = 10^5\,s$ in side view (top), zenit view (center) and front view (bottom). Due to visibility, the depth of the domain is scaled by a factor of 30.

Note, that the role of the upwelling and the downwelling in the center of the domain would swap, if the sign of the wind stress changes. The crooked upwelling region, which is shown in Figure 8.22, occurs due to the Dirichlet boundary conditions along the walls.
In Figure 8.23 the starting points in both sketches for the streamlines are chosen along the same lines. We observe, that in the present case a more active vertical mass exchange (also in the center of the domain) takes place than in the former case and does

not only occur along the sidewalls. Thus, the upwelling concerns a larger region, i.e. also water masses in the inner part of the domain are transported to upper regions and not only in horizontal directions.

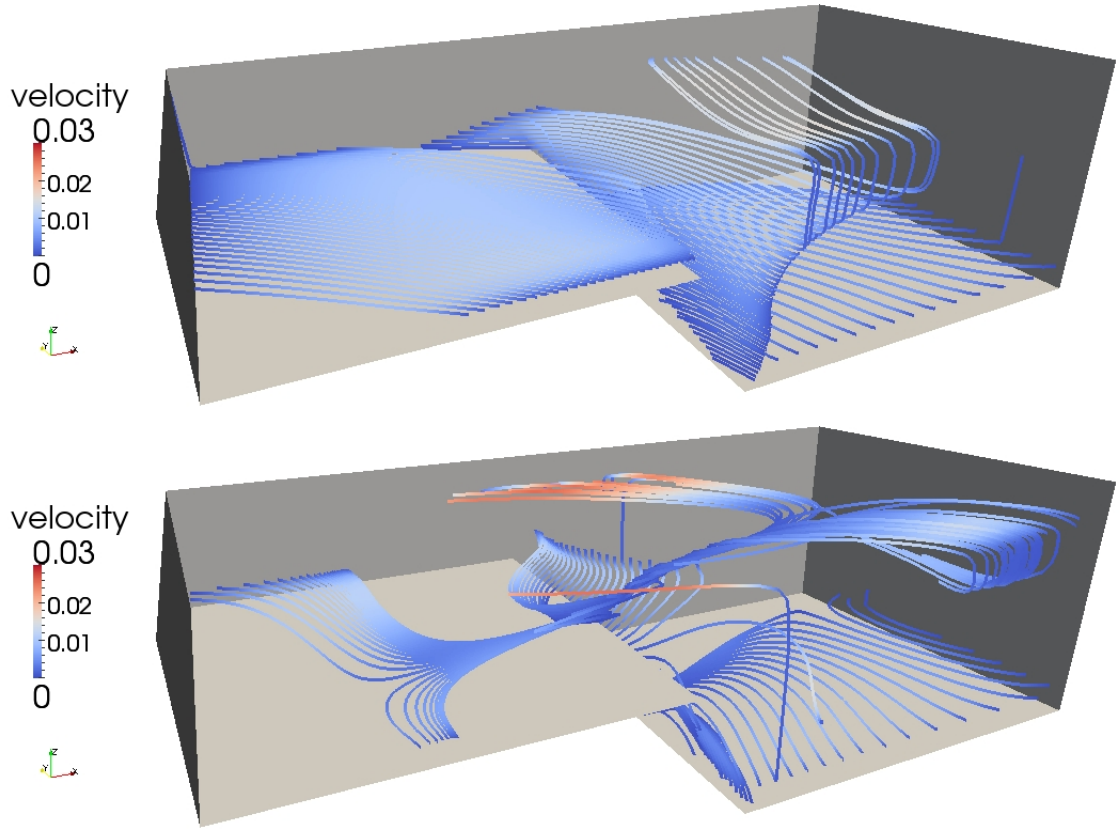

Figure 8.23: Streamlines of the velocity field of Section 8.4.4 (top) and of Section 8.4.5 (bottom), starting along three lines near the bottom at time $t = 10^5\,s$. Due to visibility, the depth of the domain is scaled by a factor of 30.

8.4.6 Example 4: Inflow and wind stress induced flow

Problem set

In this section we keep the the domain of Section 8.4.5. In a first subexample we take over the parameter set of the previous section. In an upcoming subexample we lower the viscosities by a factor of 10 in the parameter set of the previous section, i.e. we then consider

$$\boldsymbol{\tau} = 7.5 \cdot 10^{-5}\,\epsilon(t)\,\mathbf{v} \qquad \mathbf{v} = (\cos(\pi\, y/5000),\, 0)\, m\, s^{-1}$$

$$\epsilon(t) = 1 - \exp(-t/\mathcal{T}_0) \qquad \mathcal{T}_0 = 3600\, s$$

$$\mathcal{A}_{hx} = 10\, m^2\, s^{-1} \qquad \mathcal{A}_{hy} = 1\, m^2\, s^{-1} \qquad \nu_E = 10^{-3} m^2\, s^{-1}$$

$$\mathrm{f} = 2\theta \sin\Phi \;\; (= \sqrt{2}\,\theta\, s^{-1})$$

In each case we add an inflow at the western boundary, Γ_{in}. Here, we impose the inflow

$$(u, v)|_{\Gamma_{in}} = ((50 + z)/50\, m s^{-1}, 0\, m s^{-1})\,.$$

Moreover, we open a part $\Gamma_{out} := \{(x, y, z) \in \partial\Omega \,|x = 10000\, m \text{ and } y \in (625\, m,\, 1875\, m)\,\}$ of the eastern boundary and impose a *do nothing* outflow condition on Γ_{out}.

Numerical observations

For the first case, i.e. the viscosities are chosen as $\mathcal{A}_{hx} = 100\, m^2\, s^{-1}$, $\mathcal{A}_{hy} = 10\, m^2\, s^{-1}$ and $\nu_E = 10^{-2} m^2\, s^{-1}$ we observe a steady behavior, see Figures 8.24, 8.25 and 8.26, in which we depicted the pressure and the velocity field at times $t = 6\, h\ 50\, min$, $t = 13\, h\ 40\, min$ and $t = 16\, h$.

We observe a pressure field, which has higher values in the southern part of the domain and higher values in the northern regions, which is justified by the observed velocity field. The velocity field itself show a south-eastwards streaming, which is justified on the one hand due to the inflow and on the other hand due to the impact of the Coriolis force. Moreover, we observe a comparatively large scale current in the north-eastern region, which is initiated due to the main stream and the boundary conditions.

Last we observe, that the flow runs into steady state.

Let us turn to the second case, i.e. the viscosities are altered to $\mathcal{A}_{hx} = 10\, m^2\, s^{-1}$, $\mathcal{A}_{hy} = 1\, m^2\, s^{-1}$ and $\nu_E = 10^{-3} m^2\, s^{-1}$. In Figures 8.27, 8.28 and 8.29 we collect snapshots of the velocities and the pressure at times $dt = 6\, h\ 15\, min$, $dt = 8\, h\ 20\, min$ and $dt = 11\, h\ 40\, min$.

For the pressure field we observe higher pressures along the southern boundaries and at the boundaries of the outflow region. In the north-eastern part of the domain a large area with lower pressure can be observed, see Figure 8.27. This is the region, in which noticeable currents in the velocity fields reveal, see Figures 8.28 and 8.29.

For the velocity field we observe that, beside the main stream, currents develop. After $6\, h\ 15\, min$, they act on a comparatively large scale. By time, this structure becomes finer and processes of smaller scales develop.

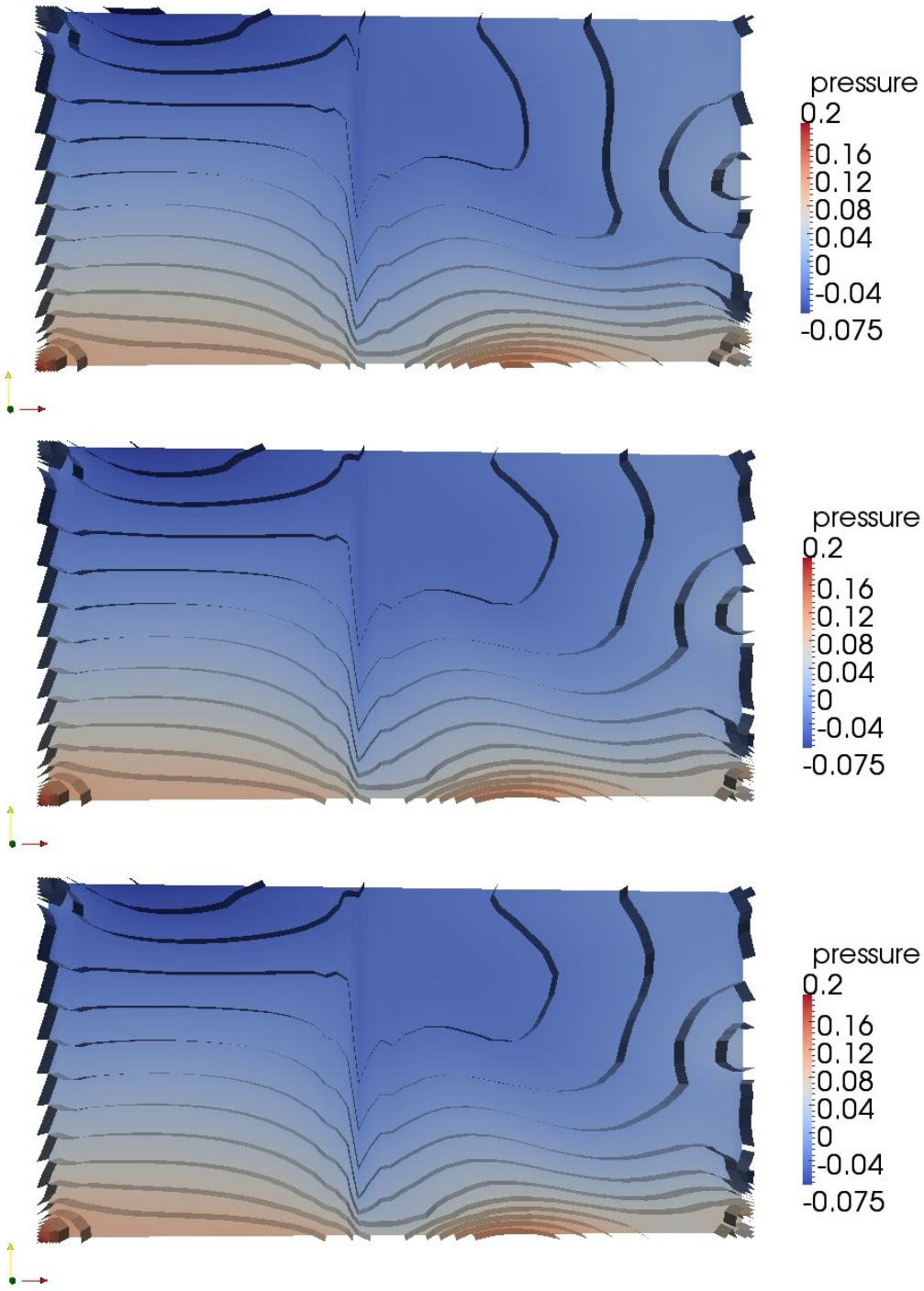

Figure 8.24: Pressure field of Section 8.4.6 for the more viscous case at times $t = 6\,h\ 50\,min$ (top), $t = 13\,h\ 40\,min$ (center) and $t = 16\,h$ (bottom) in top view.

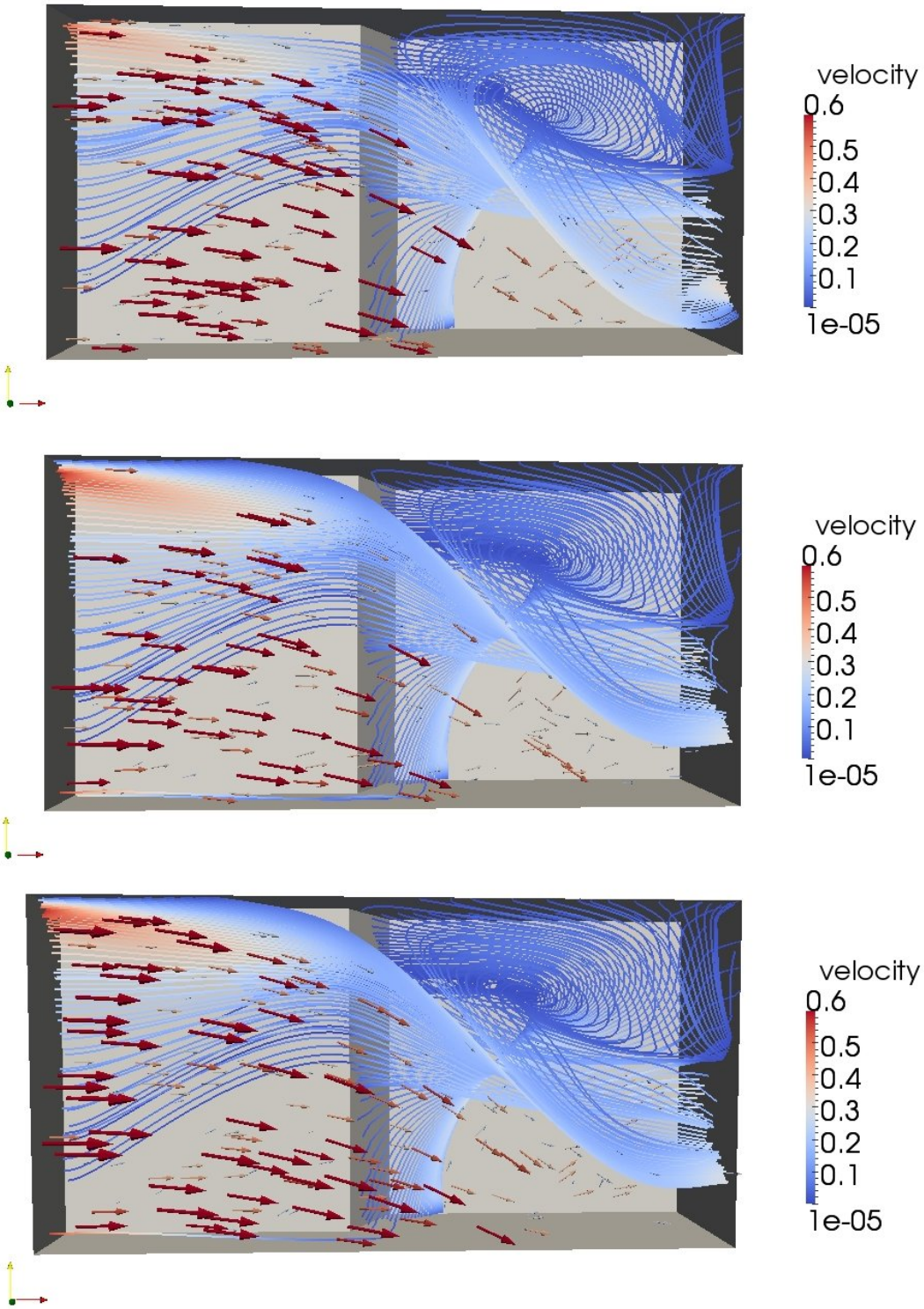

Figure 8.25: Velocity field of Section 8.4.6 for the more viscous case at times $t = 6\,h\ 50\,min$ (top), $t = 13\,h\ 40\,min$ (center) and $t = 16\,h$ (bottom) in zenit view. Due to visibility, the depth of the domain is scaled by a factor of 30.

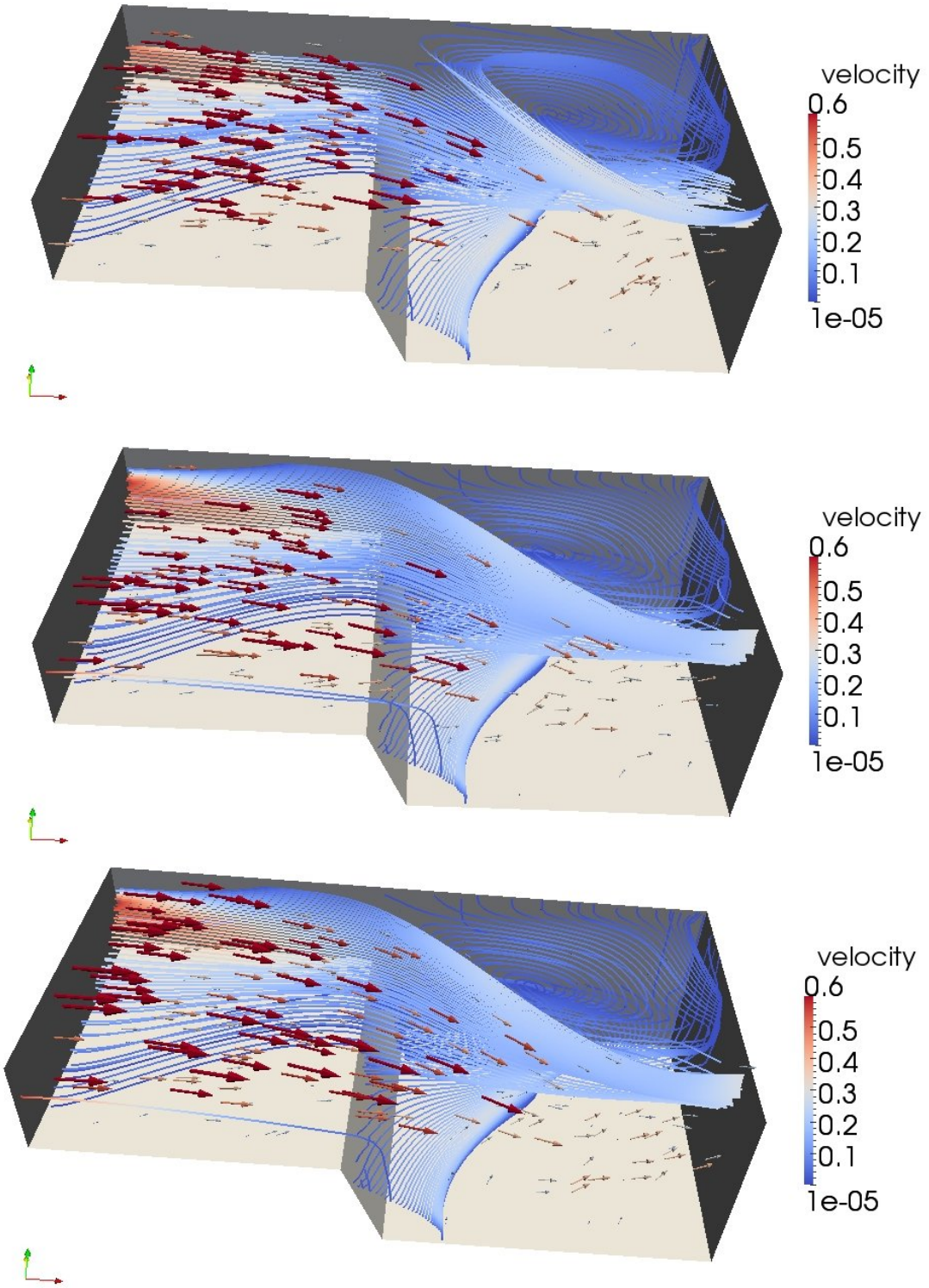

Figure 8.26: Velocity field of Section 8.4.6 for the more viscous case at times $t = 6\,h\ 50\,min$ (top), $t = 13\,h\ 40\,min$ (center) and $t = 16\,h$ (bottom) in zenit view. Due to visibility, the depth of the domain is scaled by a factor of 30.

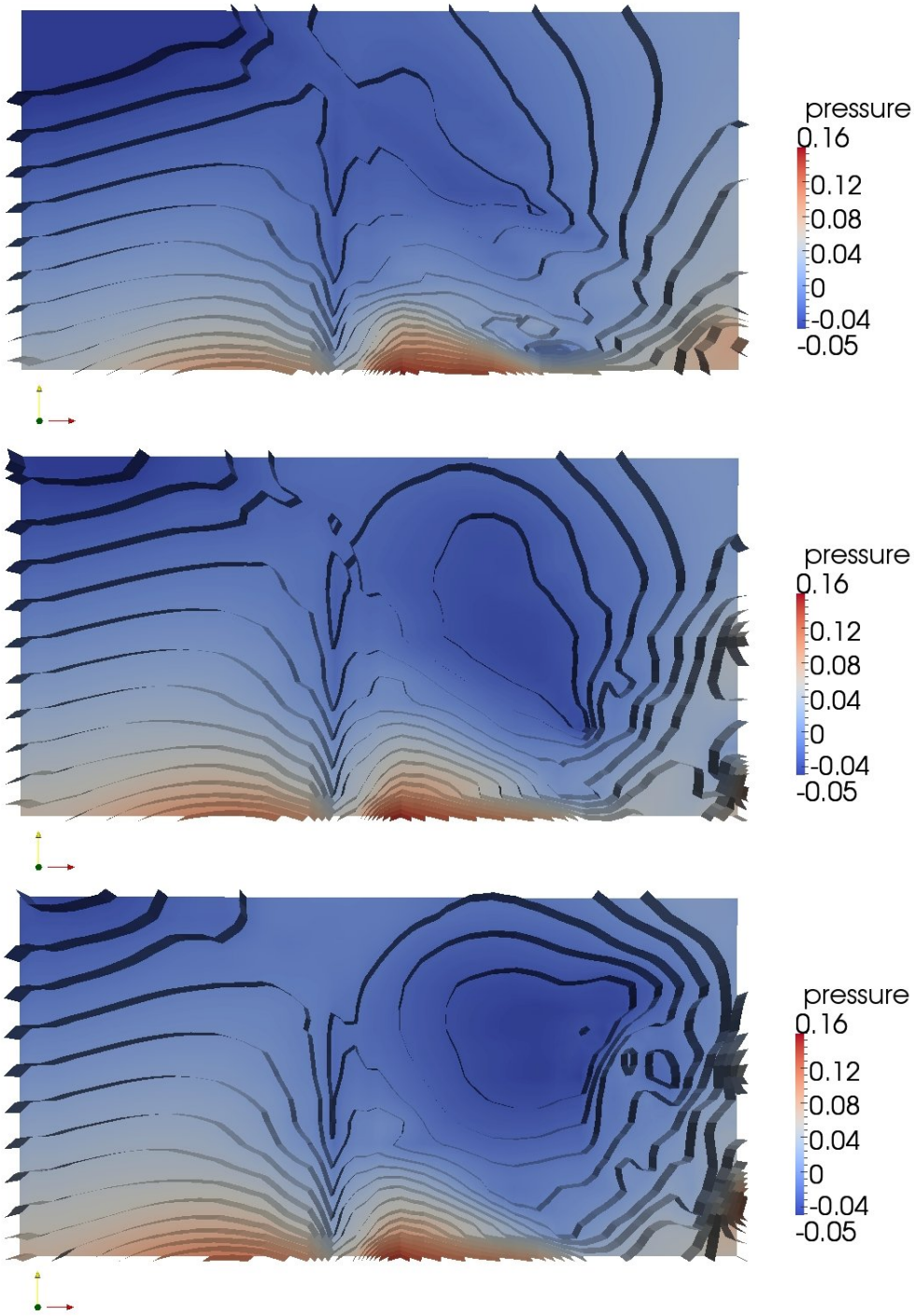

Figure 8.27: Pressure field of Section 8.4.6 for the less viscous case at times $t = 6\,h\ 15\,min$ (top), $t = 8\,h\ 20\,min$ (center) and $t = 11\,h\ 40\,min$ (bottom).

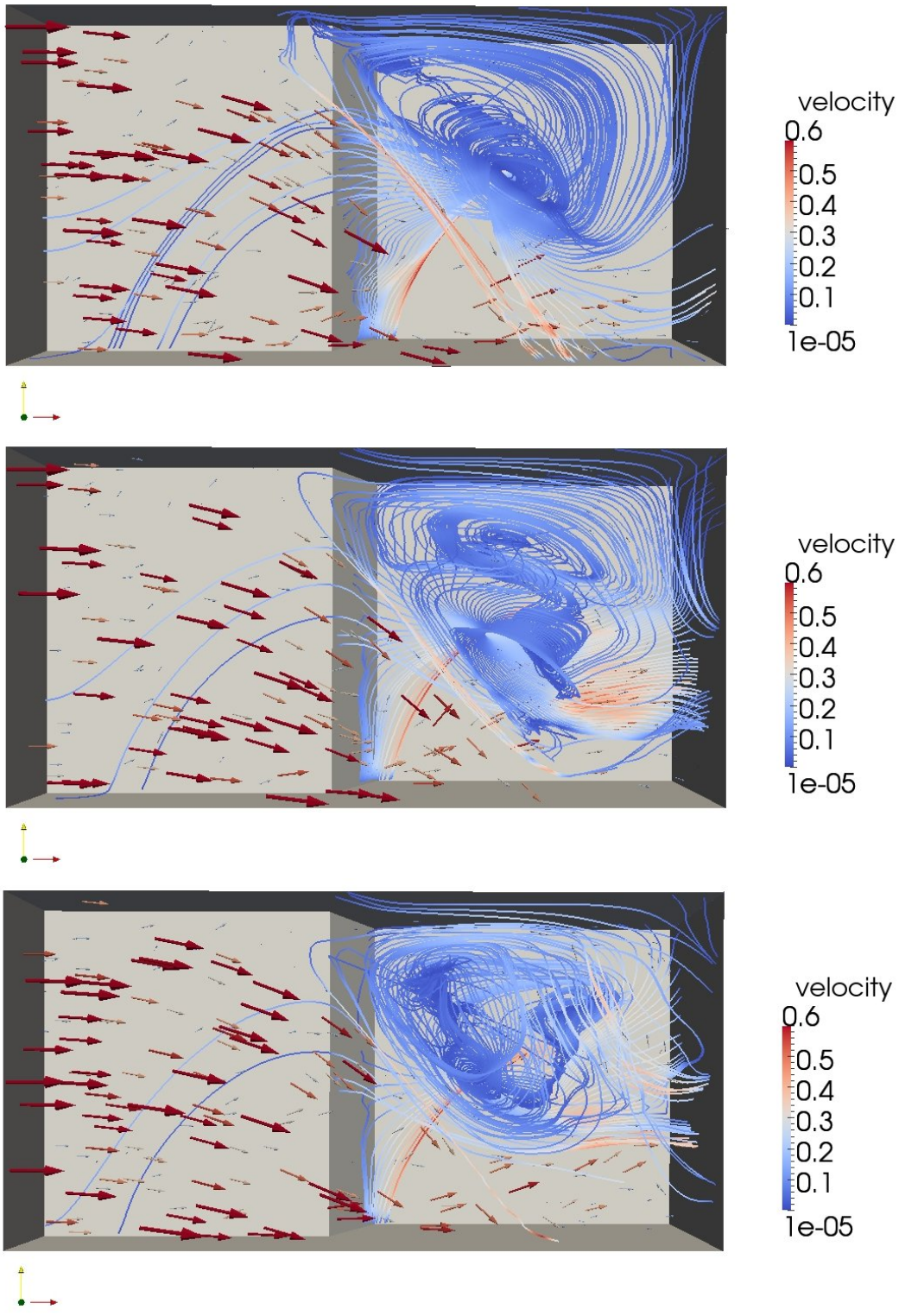

Figure 8.28: Velocity field of Section 8.4.6 for the less viscous case at times $t = 6\,h\ 15\,min$ (top), $t = 8\,h\ 20\,min$ (center) and $t = 11\,h\ 40\,min$ (bottom) in top view. Due to visibility, the depth of the domain is scaled by a factor of 30.

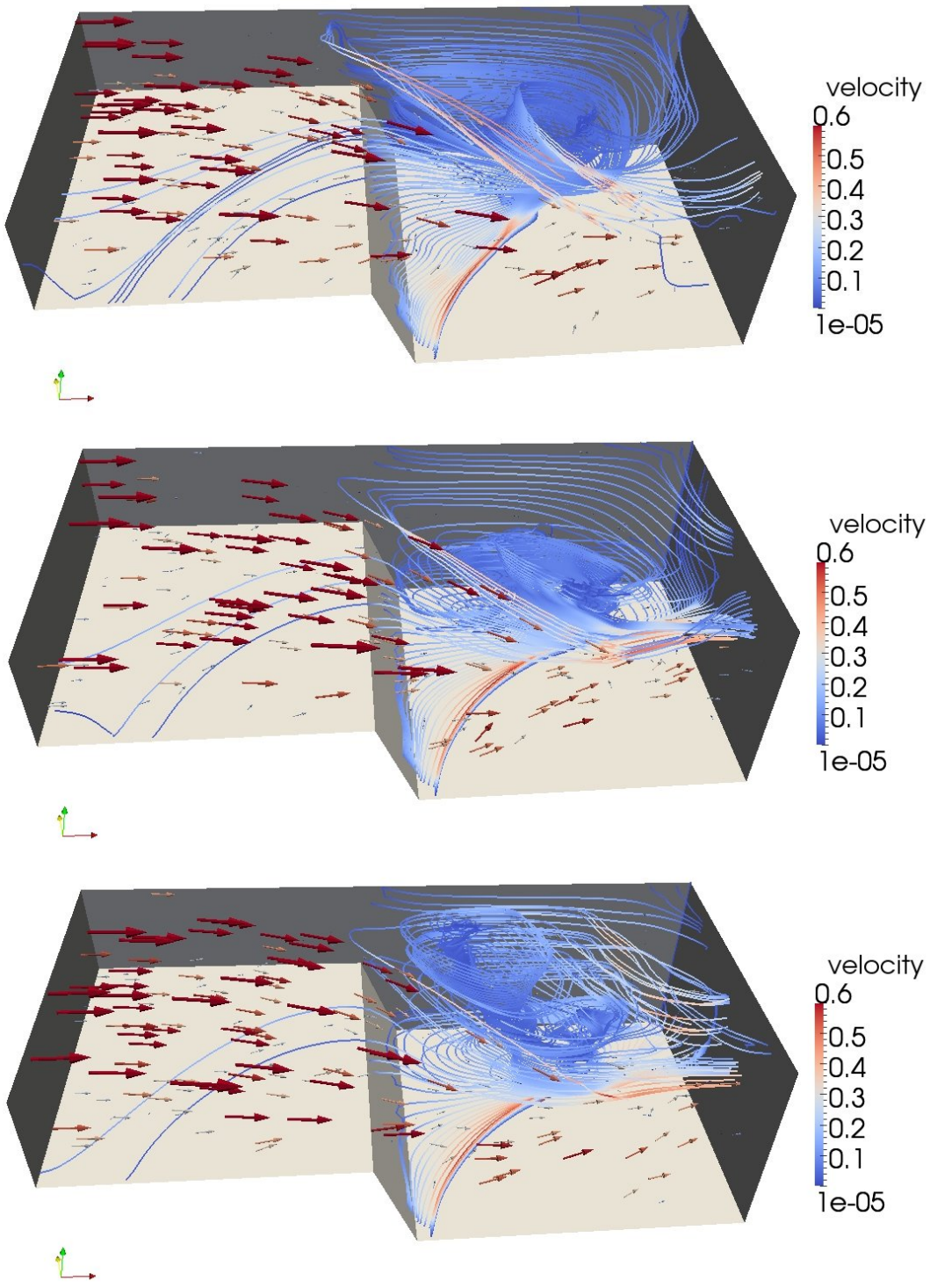

Figure 8.29: Velocity field of Section 8.4.6 for the less viscous case at times $t = 6\,h\ 15\,min$ (top), $t = 8\,h\ 20\,min$ (center) and $t = 11\,h\ 40\,min$ (bottom) in zenit view. Due to visibility, the depth of the domain is scaled by a factor of 30.

Chapter 9

Conclusions and Perspectives

We started this thesis with an introduction of the topic of hydrostatic flow problems ranging from the physical background to the variational context. The main issue of this work was the analysis of equal-order finite element discretized hydrostatic flow problems. We analyzed the equal-order finite element discretization of the hydrostatic Stokes and the hydrostatic Oseen problem on isotropic and on vertical anisotropic meshes. Within this context we developed suitable stabilization schemes, which ensure the modified inf-sup constraint and, in the Oseen case, also stabilizes the oscillations occurring due to dominant advection. These stabilization schemes are based on established schemes for the classical, i.e. non hydrostatic, case. We elaborated, that these stabilization schemes lead to optimal *a priori* error estimates. Within the anisotropic framework we elaborated suitable error estimates, which are based on [Ape98] and [Bra06]. As well, we developed a suitable H^1-stable, 3D projection operator, which opened the possibility of anisotropic local projection stabilization of the 3D velocity field. Closing the chapter on anisotropy we treated the hydrostatic Stokes problem on meshes, where anisotropy also is allowed to occur on the surface mesh. We examined the stability property of the unstabilized scheme. As in the former cases, suitable stabilization turned out to be necessary. Unlike the former cases, we had to apply anisotropic pressure stabilization schemes. We applied anisotropic stabilization schemes, which are given by [Bec95, Ric05, BT06a], and elaborated inf-sup stability as well as optimal *a priori* error estimates, which are comparable with the results known for the 2D standard problem.

Turning to the evolutionary problems, we introduced splitting schemes, which are established in the classical framework. Due to their structure, i.e. splitting the entire problem into a pressure and a velocity problem, these schemes seemed to be a good choice for the algorithmic treatment of the evolutionary, but also for the *stationary* hydrostatic problems. Within this context we explained how to adapt these schemes to the hydrostatic case. This is not straightforward due to the modified inf-sup constraint. In particular we dedicated to the questions, whether the hydrostatically adapted schemes in turn are projection schemes, whether to use the rotational or the standard approach and we shortly discussed on the choice of boundary conditions.

The quality of the stabilization schemes on isotropic meshes has been numerically tested in Chapter 8. In this chapter we also numerically portrayed different phenomena found

in oceanic regimes, which are primarily induced by the rotation of the earth, i.e. the Coriolis force. Further, we presented parallel efficiency of a partly parallelized problem. Here, the parallelization was applied to the numerically expensive 3D momentum equation and to the 3D equation for salinity and temperature, whereas the 2D pressure problem remained unchanged.

Throughout the entire work we presumed the domain to have a depth, which is strictly bounded away from zero. However, there is analysis for the variational problem in a domain with $\delta_{min} = 0$, see e.g.[BL92]. The extention to the discretized problem, as well to the issue of splitting schemes is still missing.

The issue of pressure correction schemes itself in the hydrostatic framework also seems to be undealt to the most extent. We gave an intention in the present work, but a proper convergence analysis is still missing in the hydrostatic framework, quite apart from appropriately stabilized schemes. Moreover, the authors of [BC08] examined stabilized version of pressure correction schemes in the classical context for *symmetric* stabilization schemes. How to apply splitting schemes to *non symmetric* stabilized problems is also an open question.

In the present work we did not deal with the topic of non conforming finite elements in the hydrostatic framework. As well, we did not treat the issue of local mesh refinement and adaptivity, being accompanied with that topic, the field of *a posteriori* error estimates for hydrostatic flow problems is still missing. Moreover, the treatment of corners and edges in the anisotropic, hydrostatic case is still undone.

With respect to the numerical realization of the given hydrostatic problem it has to be noted, that the splitting approach is suitable in the context of evolutionary problem. However, it revealed to be numerically too expensive in the context of stationary problems. A coupled solver, such as applied in [CGS12] in the toolbox FreeFem++, see [DHP03], is more suggestible.

Broadening the attention also to the energy equations, which effects a varying density and thus dynamically couples to the hydrostatic Navier-Stokes equations, a suitable analysis of the discrete problem still is missing. Within this context, the authors of [BB02] already considered this issue in the classical, compressible framework. Moreover in the context of constant density in the classical framework, the authors of [AL94] considered the case of convection-diffusion problems.

Finally let us mention, that we presumed a fixed set of equations, including all the simplifications and approximations, see also Chapter 2. Within this context, parameterizations were applied in order to present unresolved but important processes in the resolved range. Within this context, huge uncertainties are apparent, e.g. in the context of turbulent parameterization. We applied a quite simple parameterization, the Smagorinsky approach. However, the suitability of this approach is doubtful and improved parameterizations are eagerly desired.

Appendix A

Discretization Schemes for Evolutionary Systems

We start with the introduction of classical time stepping schemes, which form a basis element in the construction of splitting schemes. The presented schemes and their properties are a taken from classical textbooks, e.g. [Her01]. Considering nonhydrostatic flow problems, we then turn to the field of splitting schemes. Note, that the basic ideas of splitting schemes have already been introduced in Section 6.1. As well we already treated the class of pressure correction schemes in Section 6.2. We neglect both topics here and refer to the appropriate sections whenever necessary. Instead, we introduce further established approaches to suitably split flow problems: penalty projection schemes, velocity correction schemes and consistent splitting schemes. We deal with convergence and stability aspects and present the application of splitting schemes in the context of stabilized problems at the example of pressure correction schemes. This sections is a summary of [GMS06, GS04, Pro97, Pro08, BC08]. It introduces the main aspects, stressing on the topics which may profit in the deduction of the hydrostatic case.

A.1 Time discretization schemes

In this section we shortly collect common time discretization schemes, focusing on A-stable schemes as given in textbooks, such as [Her01]. We do not consider the case of step size control and thus restrict to the case of one step size for the entire time discretization. For further informations we refer to the cited literature.

Given a time interval $I := [0, \mathcal{T}]$ we consider the ODE

$$y'(t) = f(t, y), \quad y(0) = y_0 \qquad \forall t \in I$$

with sufficiently regular function f. There are a couple of commonly used methods, such as Runge-Kutta schemes, Adams-Bashforth formulas, Adams-Moulton schemes or backward differentiation formulas (BDF schemes). In the following we use the *generalized θ-scheme* and the *BDFk scheme*.

Let $\theta \in (0,1]$ be the parameter for the generalized θ-scheme, $i \in \mathbb{N}$ denote the iteration step, $\Delta t > 0$ be the (*equidistant*) time step and y^i be the approximation of $y(t^i)$, $t^i := i\Delta t$, on the time discrete level with respect to the underlying time discretization scheme. The same applies for f^i. Denoting

$$f^{i+\theta} := \theta f^{i+1} + (1-\theta) f^i \qquad \text{and} \qquad D_k y^{i+1} := \sum_{j=0}^{k} \alpha_j y^{i-j+1} \tag{A.1}$$

with suitably given constants $\alpha_j \in \mathbb{R}$, see Table A.1 for $k = 1, 2, 3$, the applied schemes are:

Generalized θ-scheme

$$D_1 y^{i+1} = \Delta t f^{i+\theta}\,,$$

whereas $\theta = 1$ gives the (1st order) Euler backward scheme and $\theta = 0.5$ results in the (2nd order) Crank-Nicolson scheme,

BDFk schemes

$$D_k y^{i+1} = \Delta t f(t^{i+1}, y^{i+1}),$$

whereas zero-stability and thus convergence can only be assured for $k \leq 6$.

In the context of ocean circulation the occurring problems commonly are stiff, such that it is suggestible to use A-stable methods, or to revert $A(\alpha)$-stable methods for $\alpha \in (0, \pi/2)$ being sufficiently large. The notions *A-stability* and *$A(\alpha)$-stability* are linked with the *Dahlquist equation*:

$$y'(t) = \lambda y(t), \quad y(0) = 1$$

with $\lambda \in \mathbb{C}$. The interesting case is $\lambda \in \mathbb{C}^- := \{z \in \mathbb{C} \mid \Re(z) \leq 0\}$, as then we have $|y(t)| \leq |y(0)|$. A suitable, i.e. *A-stable*, discretization of the Dahlquist equation shall show a decaying behavior for any $\Delta t > 0$, i.e.

$$|\, y^{i+1} \,| \leq |\, y^i \,| \qquad\qquad \forall i \in \mathbb{N}\,.$$

k	α_0	α_1	α_2	α_3
1	1	-1		
2	3/2	-2	1/2	
3	11/6	-3	3/2	$-1/3$

l	γ_0	γ_1
0		
1	1	
2	2	-1

Table A.1: *Left:* Coefficients of $D_k y^{i+1}$ for $k = 1, 2, 3$, chosen such that the appropriate BDF schemes are consistent. *Right:* Coefficients of the pressure extrapolation of order $l = 0, 1, 2$.

If this decay does not apply for all $\lambda \in \mathbb{C}^-$, but for all $\lambda \in \mathbb{C}^-$ with

$$\left|\arctan\left(\frac{\Re(\lambda)}{\Im(\lambda)}\right)\right| \leq \alpha$$

for a fixed $\alpha \in (0, \pi/2)$, the numerical scheme is called $A(\alpha)$-*stable*. For some applications it is sufficient to apply (convergent) $A(\alpha)$-stable schemes, provided α to be suitably large.

The Euler backward scheme is A-stable. Due to the *2nd Dahlquist barrier*, see also [Her01], the BDF1 scheme and the BDF2 schemes are A-stable and the (A-stable and implicit) trapezoidal formula (θ-scheme with $\theta = 1/2$) has convergence order of 2. Moreover, the BDF3 scheme is $A(\alpha)$-stable with $\alpha = 86°$.

A.2 Splitting schemes for nonhydrostatic problems

This section provides a summary of different classes of splitting schemes, besides the already introduced class of pressure correction schemes, see Section 6.2. The deductions are collected from [GMS06, BC08, Pro08, Pro97].

A.2.1 Penalty projection schemes

Based on the Chorin-Temam scheme as introduced in Section 6.3, Prohl [Pro08] chooses the following approach: Consider the parameter setting of the Chorin-Temam scheme, which reflects in $D_{k,1}\,\boldsymbol{v}^{i+1} = \boldsymbol{v}^i$ and $p^{i+1,*} = 0$. Prohl adds (6.16) at time $(i+1)\Delta t$ to (6.17) at time $i\Delta t$, exploiting the reformulation (6.11) of the latter equation. The resulting set of equations is given by

$$\begin{aligned} \Delta t^{-1}(\widetilde{\boldsymbol{v}}^{i+1} - \widetilde{\boldsymbol{v}}^{i}) - \nu\Delta\widetilde{\boldsymbol{v}}^{i+1} + \nabla p^i &= \boldsymbol{f}(t^{i+1}) && \text{in } \Omega \\ \operatorname{div}\widetilde{\boldsymbol{v}}^{i+1} - \Delta t\Delta p^{i+1} &= 0 && \text{in } \Omega \\ \partial_n p^{i+1} &= 0 && \text{on } \partial\Omega\,. \end{aligned}$$

Prohl postulates the following drawbacks, which we partly already have faced: (a) the apparent velocity $\widetilde{\boldsymbol{v}}^{i+1}$ satisfies the divergence constraint only up to a penalty term, (b) artificial pressure boundary conditions are imposed, (c) due to the explicit treatment of the pressure in the momentum equation the discrete energy law is violated. In order to tackle the artificial boundary layer, he suggests the introduction of a modified pressure extrapolation and a divergence concerning term in the momentum equation as well as application of a pressure update, which calls the pressure updates of the preceding rotational schemes to mind, see also [Pro08]:

Algorithm A.1 (Chorin-penalty scheme)**.** *Let $\beta \geq 0$. The i-th step of the scheme is given by:*

(i) Velocity predictor step *Find the velocity predictor $\widetilde{\boldsymbol{v}}^{i+1}$ s.t.*

$$\Delta t^{-1}(\widetilde{\boldsymbol{v}}^{i+1} - \boldsymbol{v}^i) - \beta \nabla div\left(\Delta t^{-1}(\widetilde{\boldsymbol{v}}^{i+1} - \widetilde{\boldsymbol{v}}^i)\right) \tag{A.2}$$

$$-\nu\Delta\widetilde{\boldsymbol{v}}^{i+1} + \nabla\left(p^i - q^i\right) = \boldsymbol{f}(t^{i+1}) \qquad in\ \Omega,$$

$$\widetilde{\boldsymbol{v}}^{i+1} = 0 \qquad on\ \partial\Omega \tag{A.3}$$

(ii) Velocity corrector and pressure predictor step

Determine a pressure q^{i+1} and a corrected (divergence free) velocity $\boldsymbol{v}^{i+1}$, s. t.

$$\Delta t^{-1}(\boldsymbol{v}^{i+1} - \widetilde{\boldsymbol{v}}^{i+1}) + \nabla q^{i+1} = 0 \qquad in\ \Omega \tag{A.4}$$

$$div\ \boldsymbol{v}^{i+1} = 0 \qquad in\ \Omega \tag{A.5}$$

$$\boldsymbol{v}^{i+1}\cdot\boldsymbol{n} = 0 \qquad on\ \partial\Omega \tag{A.6}$$

(iii) Pressure corrector step *Update the pressure due to*

$$p^{i+1} = p^{i+1} - \alpha\, div\,\widetilde{\boldsymbol{v}}^{i+1} \qquad in\ \Omega, \quad 0 < \alpha < 1 \tag{A.7}$$

Similar to the precedingly introduced schemes, step (ii) can be reformulated as a pressure Poisson problem. For $\beta = 0$, the scheme is denoted as *Chorin-Uzawa scheme*. A suitable reformulation of the resulting set of equations reads, see [Pro08]:

$$\Delta t^{-1}(\widetilde{\boldsymbol{v}}^{i+1} - \widetilde{\boldsymbol{v}}^i) - \beta\nabla\mathrm{div}\left(\Delta t^{-1}(\widetilde{\boldsymbol{v}}^{i+1} - \widetilde{\boldsymbol{v}}^i)\right)$$

$$-\nu\Delta\widetilde{\boldsymbol{v}}^{i+1} + \nabla p^i = \boldsymbol{f}(t^{i+1}) \qquad \text{in } \Omega$$

$$\mathrm{div}\,\widetilde{\boldsymbol{v}}^{i+1} + \alpha^{-1}(p^{i+1} - p^i) = 0 \qquad \text{in } \Omega$$

$$\widetilde{\boldsymbol{v}}^{i+1} = 0 \qquad \text{on } \partial\Omega\,,$$

i.e. no artificial boundary conditions on the pressure are imposed, but the divergence constraint and, for $\beta > 0$, the momentum equation are still disturbed.

Under the assumption of a strong solution of problem (6.2) and initial data $q_{\tilde{i}} = 0$, $(\boldsymbol{v}^{\tilde{i}}, \widetilde{\boldsymbol{v}}^{\tilde{i}}, p^{\tilde{i}}) \in \mathbf{J_0} \times \mathbf{H}^1_0(\Omega) \times \mathrm{L}^2_0(\Omega)$ with $0 < \tilde{i}\Delta t \in \mathcal{O}(1)$ and

$$\|\mathbf{v}(\tilde{i}\Delta t) - \boldsymbol{v}^{\tilde{i}}\|_{2,\Omega} + \|\mathbf{v}(\tilde{i}\Delta t) - \widetilde{\boldsymbol{v}}^{\tilde{i}}\|_{2,\Omega} + \sqrt{\Delta t}\|\mathrm{p}(\tilde{i}\Delta t) - p^{\tilde{i}}\|_{2,\Omega} \leq c\Delta t\,,$$

the accuracy of the Chorin-Uzawa scheme ($\beta = 0$) in the time interval $[\tilde{i}\Delta t, \mathcal{T}]$ is, see [Pro08]:

$$\|\mathbf{v}_{\Delta t} - \widetilde{\boldsymbol{v}}_{\Delta t}\|_{l^\infty(\mathrm{L}^2(\Omega))} \ + \ \sqrt{\Delta t}\|\mathrm{p}_{\Delta t} - p_{\Delta t}\|_{l^\infty(\mathrm{L}^2(\Omega))} \ +$$

$$\sqrt{\Delta t}\|\mathbf{v}_{\Delta t} - \widetilde{\boldsymbol{v}}_{\Delta t}\|_{l^2(\mathrm{L}^2(\Omega))} \quad \leq \quad c(1 + \log(\Delta t^{-1}))\Delta t\,.$$

The crux of this scheme is to assure sufficient regularity of the strong solution and the accuracy of the initial data. To shrink from that difficulties, Prohl alters the pressure update (step (iii) in Algorithm A.1) to

$$p^{i+1} = -\Delta t^{-1} \mathrm{div}\, \widetilde{\boldsymbol{v}}^{i+1}\,.$$

The resulting schemes are called *Chorin-penalty schemes*. The naming of this class of schemes is owed to this *penalty constraint*. Under the (less restrictive) assumptions

$$\|\mathbf{v}(0) - \boldsymbol{v}^0\,\|_{2,\Omega} + \|\mathbf{v}(0) - \widetilde{\boldsymbol{v}}^0\|_{2,\Omega} + \leq c\Delta t$$

on the initial data and presuming $\beta > 1$, Prohl proposes the following error estimates

$$\begin{aligned} \|\mathbf{v}_{\Delta t} - \widetilde{\boldsymbol{v}}_{\Delta t}\|_{l^\infty(\mathrm{L}^2(\Omega))} \;+\; & \|\min\{1, i\Delta t\}(\mathrm{p}_{\Delta t} - p_{\Delta t})\|_{l^\infty(\mathrm{L}^2(\Omega))} + \\ & \|\sqrt{\min\{1, i\Delta t\}}(\mathbf{v}_{\Delta t} - \widetilde{\boldsymbol{v}}_{\Delta t})\|_{l^\infty(\mathrm{H}^1(\Omega))} \quad \leq \quad c\Delta t\,. \end{aligned}$$

A.2.2 Velocity correction methods

The class of *velocity correction methods* stems back to Karniadakis, Israeli and Orszag [KOI91]. In rotational form they have been introduced by Guermond and Shen in [GS03b]. Similar to the class of *pressure correction methods*, the construction of *velocity correction methods* is based on a suitable time discretization scheme and an extrapolation. Contrary to the formerly discussed case, the velocity in the momentum equation is extrapolated and the pressure is taken implicitly. I.e. keeping the notations of Section 6.2 *velocity correction methods* are given by

Algorithm A.2 (Velocity correction scheme)**.** *Let $\chi \in \{0, 1\}$, $k, l \in \mathbb{N}$, and, for any $i \geq \min\{k, l\} - 1$, initial values $\boldsymbol{v}^{i-k+1}, \ldots, \boldsymbol{v}^i$ be given.*

The i-th step of the scheme is given by:

(i) Velocity projection step *Find the velocity $\boldsymbol{v}^{i+1}$ s.t.*

$$\begin{aligned} \Delta t^{-1}(\alpha_0 \widetilde{\boldsymbol{v}}^{i+1} + D_{k,1}\,\boldsymbol{v}^{i+1}) - \nu\Delta\widetilde{\boldsymbol{v}}^{i+1,*} + \chi\nu\nabla\, div\,\widetilde{\boldsymbol{v}}^{i+1,*} + \nabla p^{i+1} &= \boldsymbol{f}(t^{i+1}) \qquad \text{in } \Omega, \\ div\;\boldsymbol{v}^{i+1} &= 0 \qquad \text{in } \Omega, \\ \boldsymbol{v}^{i+1}\cdot\boldsymbol{n} &= 0 \qquad \text{on } \partial\Omega \end{aligned}$$

(ii) Determine velocity corrector *Determine $\widetilde{\boldsymbol{v}}^{i+1}$ s. t.*

$$\begin{aligned} \Delta t^{-1}\alpha_0(\widetilde{\boldsymbol{v}}^{i+1} - \boldsymbol{v}^{i+1}) - \nu\Delta(\widetilde{\boldsymbol{v}}^{i+1} - \widetilde{\boldsymbol{v}}^{i+1,*}) - \chi\nu\nabla\, div\,\widetilde{\boldsymbol{v}}^{h,*}_{i+1} &= 0 \qquad \text{in } \Omega \\ \widetilde{\boldsymbol{v}}^{i+1} &= 0 \qquad \text{on } \partial\Omega \end{aligned}$$

Step (i) of Algorithm A.2 denotes the projection of

$$\widehat{\boldsymbol{v}}^{i+1} \;:=\; \frac{1}{\alpha_0}\left(D_{k,1}\,\boldsymbol{v}^{i+1} + \nu\Delta\widetilde{\boldsymbol{v}}^{i+1,*} - \chi\nabla\mathrm{div}\,\widetilde{\boldsymbol{v}}^{i+1,*} + \Delta t\boldsymbol{f}(t^{i+1})\right)$$

onto the space of divergence free velocities, i.e. $\boldsymbol{v}^{i+1} = P(\widehat{\boldsymbol{v}}^{i+1})$. Note the task of the pressure as the Lagrangian multiplier, which effects the projection. Step (ii) compensates the additionally introduced extrapolations and the applied splitting occurring in the approximation of the time derivative. As in the case of pressure correction methods, the schemes with $\chi = 1$ are denoted as *rotational*, whereas schemes with $\chi = 0$, are denoted as in *standard* form.
Let $\chi = 0$. Considering step (ii) of Algorithm A.2 gives

$$\Delta\widetilde{\boldsymbol{v}}^{i+1} \cdot \boldsymbol{n} = \Delta\widetilde{\boldsymbol{v}}^{i+1,*} \cdot \boldsymbol{n} \qquad \text{on } \partial\Omega\,.$$

Applying this to step (i) results in

$$\partial_n p^{i+1} = \left(\boldsymbol{f}(t^{i+1}) + \nu\Delta\widetilde{\boldsymbol{v}}^{i+1,*}\right) \cdot \boldsymbol{n} \qquad \text{on } \partial\Omega\,.$$

For $r = 0$ and $r = 1$, which is frequently applied, this pressure boundary condition becomes

$$\partial_n p^{i+1} = \begin{cases} \boldsymbol{f}(t^{i+1}) \cdot \boldsymbol{n} & \text{if } r = 0\,, \\ (\boldsymbol{f}(t^{i+1}) + \nu\Delta\widetilde{\boldsymbol{v}}_0) \cdot \boldsymbol{n} & \text{if } r = 1\,, \end{cases}$$

which constitutes an artificial boundary layer. Using $\chi = 1$, the hope is to improve these errors, as in the case of pressure correction schemes.

The following error estimates are validated, see also [GMS06]:
For the case of $k = 1$ and $r = 0$, i.e. Euler backward time discretization and no extrapolation, the same results as in the appropriate pressure correction scheme, i.e. the Chorin-Temam scheme, (6.18) – (6.19) apply. Numerical tests suggest a pressure stabilizing effect of this scheme, such that for a suitably chosen time step Δt finite elements can be applied, which are not inf-sup stable.

For the Van Kan equivalent, i.e. using BDF2 and first order extrapolation $\widetilde{\boldsymbol{v}}^{i+1,*} = \widetilde{\boldsymbol{v}}^{i}$, similar assumptions have to be presumed on the initial data. Note, that instead of the demand on the pressure in (6.21) we propose

$$\|\mathbf{v}(\Delta t) - \widetilde{\boldsymbol{v}}^1\|_{2,\Omega} \leq c\Delta t.$$

The two remaining presumptions in (6.21) remind. Similar to the Van Kan scheme, the initial iterates can be determined by application of an Euler backward time step instead of BDF2 in Algorithm A.2. The established error estimates then coincide with (6.22) – (6.23), see [GMS06].

The rotational variant of this velocity correction scheme also shows similar error estimates as the rotational Van Kan scheme (6.24) – (6.25), see [GMS06].

As well, the case $k = r = 1$ shows first order convergence, as it is also observed for the pressure correction schemes. The remaining error estimates of Section 6.2 are supposed to apply in this framework as well, although these propositions are not analytically proven, but only *numerically evidenced*.

A.2.3 Consistent splitting schemes

These schemes have been introduced by Guermond and Shen in [GS03a]. The basic idea of this scheme is the variational testing of (6.2) with ∇q for arbitrary $\xi \in \mathrm{H}^1(\Omega)$, which can be reformulated as an equation for the pressure at time t^{i+1}. The divergence constraint has been incorporated into the appropriate pressure equation by application of

$$(\partial_t \boldsymbol{v}, \nabla\xi)_\Omega = -(\operatorname{div}(\partial_t \boldsymbol{v}), \xi)_\Omega = 0 \qquad \forall \xi \in \mathrm{H}^1(\Omega).$$

The time discretization and splitting of the momentum equation then uses a BDF scheme and an extrapolation for the pressure. After suitable adaption in order to avoid third order derivatives, consistent splitting schemes are given by

Algorithm A.3. *Let $\chi \in \{0,1\}$, $k,l \in \mathbb{N}$, and, for any $i \geq k-1$, initial values $\boldsymbol{v}^{i-k+1}, \ldots, \boldsymbol{v}^i$ and $p^{i-k+1}, \ldots, p^i$ be given.*

The i-th step of the scheme is given by:

(i) Velocity predictor step *Find the velocity $\boldsymbol{v}^{i+1}$ s.t.*

$$\begin{aligned} \Delta t^{-1} D_k \boldsymbol{v}^{i+1} - \nu\Delta \boldsymbol{v}^{i+1} + \nabla p^{i+1,*} &= \boldsymbol{f}(t^{i+1}) && \text{in } \Omega, \\ \boldsymbol{v}^{i+1} \cdot \boldsymbol{n} &= 0 && \text{on } \partial\Omega \end{aligned}$$

(ii) Pressure predictor step *Determine q^{i+1} s. t.*

$$(\nabla q^{i+1}, \nabla\xi)_\Omega = \Delta t^{-1}(D_k \boldsymbol{v}^{i+1}, \nabla\xi)_\Omega \qquad \forall \xi \in \mathrm{H}^1(\Omega)$$

(iii) Pressure update step *Determine p^{i+1} s. t.*

$$p^{i+1} = q^{i+1} + p^{i+1,*} - \chi\nu \operatorname{div} \boldsymbol{v}^{i+1}$$

Note, that this is neither a projection scheme nor the velocity is divergence free. However, these schemes produce results with similar estimates as known from the previously introduced pressure correction and velocity correction schemes.

Again, the *standard* case shows artificial boundary conditions, but in the *rotational* case for $k = 1$ and $k = 2$, numerical results indicate, see [GS03a, GMS06], that the pressure no longer suffers from artificial boundary conditions. For $k = 1$, optimal convergence results have been validated in [GS03a]. For $k = 2$, numerical experiments indicate second order convergence, appropriate analytical proofs however are missing. The application of inf-sup stable finite elements is necessary for the given formulation of the schemes, see also [GMS06].

A.2.4 Stability aspects

As indicated in Section 6.2 for the Chorin-Temam scheme, some of the introduced schemes (for certain time steps Δt) allow the application of finite element spaces, which are not inf-sup stable. However it is stated in [GMS06], that this is *not* the rule. On the contrary, the authors suggest that, generally, the inf-sup condition is necessary and sufficient for the well-posedness of the fully discretized problem. Thus, either inf-sup stable finite elements are to be chosen, or an appropriate stabilization has to be incorporated into the splitting scheme. In [BC08] Badia and Codina collected known stability results for the unstabilized problems, and introduced and analyzed the application of splitting schemes to stabilized finite element approximations of nonhydrostatic flow problems, i.e. the fully discretized problem is analyzed. Due to applicability for hydrostatic problems we restrict our attention to the results concerning *pressure correction schemes*, given in [BC08]. For further informations we refer to the cited literature.

Beforehand, we introduce some notations, see also [BC08]. Let $d \in \mathbb{N}$ denote the dimension of the problem. Considering the finite element spaces $\mathbf{V}_h$ and Q_h based on polynomials of order r_v and r_q, respectively, let

$$\{\phi_{i,j}\}_{i\in\mathcal{N}_v, j\in\{1,\dots,d\}} \oplus \{\phi_{i,j}\}_{i\in\mathcal{N}_d, j\in\{1,\dots,d\}} \quad \text{and} \quad \{\xi_i\}_{i\in\mathcal{N}_p}$$

be Lagrangian bases of $\mathbf{V}_h$ and Q_h, respectively. The set $\mathcal{N}_d$ denotes the fixed nodal velocity values due to the boundary conditions. The remaining nodes of the velocity space are given by $\mathcal{N}_v$, the nodes of the pressure space are represented by $\mathcal{N}_p$. Based on the evolutionary 3D Navier-Stokes problem

$$\begin{aligned} \textit{Find } (\boldsymbol{v}, p) \textit{ s. t.} \quad \partial_t \boldsymbol{v} + (\boldsymbol{v}\cdot\nabla)\,\boldsymbol{v} - \nu\Delta\,\boldsymbol{v} + \nabla p &= \boldsymbol{f} && \text{in } \Omega\times[0,\mathcal{T}] \\ \operatorname{div} \boldsymbol{v} &= 0 && \text{in } \Omega\times[0,\mathcal{T}] \\ \boldsymbol{v}\,|_{\partial\Omega} &= 0 && \text{in } [0,\mathcal{T}] \\ \boldsymbol{v}\,|_{t=0} &= \boldsymbol{v}_0 && \text{in } \Omega\,, \end{aligned} \tag{A.8}$$

let $(\boldsymbol{v}_h^{n+1}, p_h^{n+1})$ be the solution of the discretized problem at time $(n+1)\Delta t$. The solution is determined using one of the introduced splitting schemes with an appropriate time discretization scheme, and applying the introduced finite element spaces for the spatial discretization. Thus, $\boldsymbol{v}_h^{i+1}$ and p_h^{i+1} can be represented by

$$\begin{aligned} \boldsymbol{v}_h^{n+1}(\boldsymbol{x}) &= \sum_{i\in\mathcal{N}_v} (\mathbf{U}^{n+1})_i \phi_i(\boldsymbol{x}) + \sum_{i\in\mathcal{N}_d} (\mathbf{U}_d^{n+1})_i \phi_i(\boldsymbol{x}) && \forall \boldsymbol{x}\in\Omega \\ p_h^{n+1}(\boldsymbol{x}) &= \sum_{i\in\mathcal{N}_q} (\mathbf{P}^{n+1})_i \xi_i(\boldsymbol{x}) && \forall \boldsymbol{x}\in\Omega \end{aligned}$$

with vectors $\mathbf{U}^{n+1}$ and $\mathbf{P}^{n+1}$ containing the nodal values of $\boldsymbol{v}_h^{n+1}$ and p_h^{n+1}. Vector $\mathbf{U}_d^{n+1}$ contains the fixed data of the velocity.
Recall the definitions (3.1), (3.2) and (3.8) of the forms a, b and c, and set f = 0.

Moreover we define

$$\begin{aligned} K_{ij}^{ab}(\mathbf{U}) &:= \mathrm{a}(\phi_{a,i},\phi_{b,j}) + c(\boldsymbol{v}_h,\phi_{a,i},\phi_{b,j}) && \forall a,b \in \mathcal{N}_v \\ M_{ij}^{ab} &:= (\phi_{a,i},\phi_{b,j})_\Omega && \forall a,b \in \mathcal{N}_v \\ G_i^{ab} &:= \mathrm{b}(\xi_b,\phi_{a,i}) && \forall a \in \mathcal{N}_v, b \in \mathcal{N}_p \end{aligned}$$

and denote the appropriate matrices as K, M, G and $D := -G^T$ by grouping space and nodal indices.

Unstabilized problems

The unstabilized discretization of problem (A.8) is given by

$$\Delta t^{-1} M \left(\alpha_0 \widetilde{\mathbf{U}}^{n+1} + D_{k,1}\,\mathbf{U}^{n+1}\right) + K(\widetilde{\mathbf{U}}^{n+1})\widetilde{\mathbf{U}}^{n+1} + G\,\mathbf{P}^{n+1,*} = \boldsymbol{f}^{n+1}\,, \tag{A.9}$$

$$\Delta t\,\alpha_0^{-1} D M^{-1} G(\mathbf{P}^{n+1} - \mathbf{P}^{n+1,*}) = D\widetilde{\mathbf{U}}^{n+1}\,, \tag{A.10}$$

$$\Delta t^{-1}\alpha_0 M \left(\mathbf{U}^{n+1} - \widetilde{\mathbf{U}}^{n+1}\right) + G(\mathbf{P}^{n+1} - \mathbf{P}^{n+1,*}) = 0\,, \tag{A.11}$$

where the finite element spaces $\mathbf{V}_h$ and Q_h, as well as a standard pressure correction scheme, see Algorithm 6.1, with BDFk time discretization and r-th order pressure extrapolation, represented by $\mathbf{P}^{n+1,*}$, are applied. The boundary conditions are incorporated in the forcing term $\boldsymbol{f}^{n+1}$. For the application of the θ-scheme, the term $D_{k,1}\,\mathbf{U}^{n+1}$ is neglected, and the terms $K(\widetilde{\mathbf{U}}^{n+1})\widetilde{\mathbf{U}}^{n+1}$ and $\boldsymbol{f}^{n+1}$ are replaced by $K(\mathbf{U}^{n+\theta})\,\mathbf{U}^{n+\theta}$ and $\boldsymbol{f}^{n+\theta}$, respectively. Note, that we applied the pressure correction scheme in standard form. The appropriate artificial pressure boundary conditions still are apparent, but are imposed in a weak sense. For a more extensive discussion on this topic we refer to [GMS06].

The authors of [BC08] suggest the application of the approximation:

$$DM^{-1}G \sim L \text{ with } L := -(\nabla\xi_a, \nabla\xi_b) \quad \forall \xi_a, \xi_b \in \mathcal{N}_p\,. \tag{A.12}$$

In order to identify the perturbations due to the splitting, the scheme (A.9) – (A.11) can be reformulated as

$$\begin{aligned} \Delta t^{-1} M D_k\,\mathbf{U}^{n+1} + K(\mathbf{U}^{n+1})\,\mathbf{U}^{n+1} + E(\mathbf{U}^{n+1}) + G\,\mathbf{P}^{n+1} &= \boldsymbol{f}^{n+1}\,, \\ D\,\mathbf{U}^{n+1} - \beta\Delta t\,(DM^{-1}G - L)(\mathbf{P}^{n+1} - \mathbf{P}^{n+1,*}) &= 0\,, \end{aligned}$$

with

$$\begin{aligned} E(\mathbf{U}^{n+1}) &:= K(\mathbf{S}^{n+1})\,\mathbf{U}^{n+1} + K(\mathbf{U}^{n+1})\mathbf{S}^{n+1} \\ \mathbf{S}^{n+1} &:= \Delta t M^{-1} G(\mathbf{P}^{n+1} - \mathbf{P}^{n+1,*})\,, \end{aligned}$$

and setting $\beta = 1$, if the approximation (A.12) has been applied, and $\beta = 0$, else.
We observe two sources of perturbations: the terms $\beta\Delta t\,(DM^{-1}G - L)(\mathbf{P}^{n+1} - \mathbf{P}^{n+1,*})$

and $E(\mathbf{U}^{n+1})$, both being of order $\mathcal{O}(\Delta t^{r+1})$. For BDF1 schemes, the authors of [BC08] claim the former term, i.e. application of (A.12), to be responsible for the stability of pressure correction methods and emphasize the application of an appropriate Laplacian pressure stabilization term, such as the Orthogonal Subscale Stabilization (OSS). Moreover, Badia and Codina state, that for BDFk schemes with $k > 1$ the stabilization due to (A.12) is too weak.

For ease of presentation we set the following notations: For any symmetric positive semidefinite matrix A, vectors $\mathbf{X}, \mathbf{Y}$ and any sequence $\{\mathbf{Y}^n\}_{n\in\{0,\dots,N\}}$ let

$$
\begin{aligned}
(\mathbf{X},\mathbf{Y})_A &:= \mathbf{X}\cdot A\,\mathbf{Y}, \qquad & \|\,\mathbf{X}\,\|_A &:= (\mathbf{X}\cdot A\,\mathbf{X})^{1/2}\,,\\
\{\mathbf{Y}^n\} \;\in\; l^p(A) \;&\leftrightarrow\; \sum_{n=0}^{N} \Delta t \|\,\mathbf{Y}^n\,\|_A^p \le c < \infty \qquad & \forall n \in \{0,\dots,N\}\,,\; 1 \le p < \infty\\
\{\mathbf{Y}^n\} \;\in\; l^\infty(A) \;&\leftrightarrow\; \|\,\mathbf{Y}^n\,\|_A \le c < \infty \qquad & \forall n \in \{0,\dots,N\}
\end{aligned}
$$

In the case of matrix K note $\mathbf{U}\cdot K(\mathbf{U})\,\mathbf{U} = \mathbf{U}\cdot K_{visc}(\mathbf{U})\,\mathbf{U} =: \|\,\mathbf{U}\,\|_K^2$ due to the skew-symmetry of the advection term. Matrix K_{visc} denotes the viscous part. Moreover, we set $L_+ := -L$, which is positive semidefinite. Given these notations, the following stability results are stated in [BC08]:

Chorin-Temam $\{\mathbf{U}^n\} \in l^\infty(M)$, $\{\widetilde{\mathbf{U}}^n\} \in l^\infty(M) \cap l^2(K)$, $\{\sqrt{\Delta t}\,\mathbf{P}^n\} \in l^2(L_+)$,

Van Kan with CN $\{\widetilde{\mathbf{U}}^n\}$, $\{\mathbf{U}^n\} \in l^\infty(M)$, $\{\widetilde{\mathbf{U}}^{n+1/2}\} \in l^2(K)$, $\{\Delta t\,\mathbf{P}^n\} \in l^\infty(L_+)$, $\{\sqrt{\Delta t}\,\delta\,\mathbf{P}^n\} \in l^2(L_+)$,

BDF2-SE2 $\{\mathbf{U}^n\} \in l^\infty(M)$, $\{\widetilde{\mathbf{U}}^n\} \in l^2(K)$, $\{\Delta t\,\mathbf{P}^n\} \in l^\infty(L_+)$, $\{\sqrt{\Delta t}\,\delta\,\mathbf{P}^n\} \in l^2(L_+)$.

From those results we can infer the following: The stability of the pressure is strongest in the Chorin-Temam scheme. Due to [BC08] an optimal choice for Δt is of order $\mathcal{O}(h^2)$. Instead of $\sqrt{\Delta t}$, the factor Δt determines the weaker stability of the pressure in the remaining schemes. Badia and Codina state, that application of a suitable inf-sup condition could improve these stability results. This can be achieved either by application of inf-sup stable finite elements of by the use of suitable stabilization terms.

Stabilized problems

In [BC08], Badia and Codina state the following results for the OSS stabilization with velocity stabilization $s^\Omega_{h,v}$ and pressure stabilization $s^\Omega_{h,p}$. We consider the problem

$$
\begin{aligned}
&\textit{Find } (\boldsymbol{v}_h^{n+1}, p_h^{n+1}) \in \mathbf{V}_h \times Q_h \textit{ s.t.}\\
&\quad (\partial_t\,\boldsymbol{v}_h^{n+1}, \boldsymbol{\varphi})_\Omega + ((\boldsymbol{v}_h^{n+1}\cdot\nabla)\,\boldsymbol{v}_h^{n+1}, \boldsymbol{\varphi})_\Omega + (\nu\nabla\,\boldsymbol{v}_h^{n+1}, \nabla\,\boldsymbol{\varphi})_\Omega\\
&\qquad\qquad - (p_h^{n+1}, \operatorname{div}\,\boldsymbol{\varphi})_\Omega + s^\Omega_{h,v}(\boldsymbol{v}_h^{n+1}, \boldsymbol{\varphi}) \qquad = \langle \boldsymbol{f}, \boldsymbol{\varphi}\rangle \quad \forall\,\boldsymbol{\varphi} \in \mathbf{V}_h\,,\\
&\quad (\xi, \operatorname{div}\,\mathbf{u}_h)_\Omega\,, + s^\Omega_{h,p}(p_h^{n+1}, \xi) \qquad = 0 \qquad \forall \xi \in Q_h\,.
\end{aligned}
$$

The advection occurring in the definition of $s_{h,v}$ can be set to the velocity determined in a former iteration step of an iterative loop, or may be given as a suitable extrapolation of the retrieved velocities of former time steps. The appropriate algorithm is originated from Algorithm 6.1 and is given (in standard form, i.e. $\chi = 0$) by

Algorithm A.4 (Pressure correction scheme for the stabilized Navier-Stokes problem)**.** *Let $k, l \in \mathbb{N}$, and, for any $n \geq \min\{k, l\} - 1$, initial values $\boldsymbol{v}_h^{n-k+1}, \ldots, \boldsymbol{v}_h^n$ and $p_h^{n-l+1}, \ldots, p_h^n$ be given.*

The n-th time step of the scheme is given by:

(i) Velocity predictor step *Find the velocity predictor $\widetilde{\boldsymbol{v}}_h^{n+1}$ s.t.*

$$\begin{aligned} \Delta t^{-1}(\alpha_0 \widetilde{\boldsymbol{v}}_h^{n+1} + D_{k,1}\, \boldsymbol{v}_h^{n+1}, \boldsymbol{\varphi})_\Omega + \ & ((\widetilde{\boldsymbol{v}}_h^{n+1} \cdot \nabla)\widetilde{\boldsymbol{v}}_h^{n+1}, \boldsymbol{\varphi})_\Omega \\ +\nu(\nabla \widetilde{\boldsymbol{v}}_h^{n+1}, \nabla\, \boldsymbol{\varphi})_\Omega + s_{h,v}^\Omega(\widetilde{\boldsymbol{v}}_h^{n+\rho}, \boldsymbol{\varphi}) + (\nabla p_h^{n+1,*}, \boldsymbol{\varphi})_\Omega \ &= \ \langle \boldsymbol{f}(t^{n+1}), \boldsymbol{\varphi} \rangle \quad \forall\, \boldsymbol{\varphi} \in \mathbf{V}_h \end{aligned} \tag{A.13}$$

(ii) Pressure update step *Determine the pressure p_h^{n+1}, s. t.*

$$\Delta t\ {\alpha_0}^{-1} \left(\nabla(p_h^{n+1} - p_h^{n+1,*}), \nabla\xi\right)_\Omega + s_{h,p}^\Omega(p_h^{n+1}, \xi) = (div\, \widetilde{\boldsymbol{v}}_h^{n+1}, \xi)_\Omega \quad \forall \xi \in Q_h \tag{A.14}$$

(iii) Velocity update step *Determine the updated velocity $\boldsymbol{v}_h^{n+1}$, s.t.*

$$\Delta t^{-1}\ \alpha_0 \left(\boldsymbol{v}_h^{n+1} - \widetilde{\boldsymbol{v}}_h^{n+1}, \boldsymbol{\varphi}\right)_\Omega + \left(\nabla(p_h^{n+1} - p_h^{n+1,*}), \boldsymbol{\varphi}\right)_\Omega = 0 \quad \forall\, \boldsymbol{\varphi} \in \mathbf{V}_h\ . \tag{A.15}$$

The constant ρ occurring in step (i) is either set to 0, if the velocity stabilization is treated explicitely, or set to 1 for the implicit treatment. Moreover, note, that in step (ii) of the algorithm, the Laplacian approximation of $DM^{-1}G$, written in matrix form, took place.

For implementational issues we replace $p_h^{n+1} - p_h^{n+1,*}$ by q_h^{n+1} in (A.14). With slight modifications and using the linearity of $s_{h,p}$ this equation then reads

$$\Delta t\ {\alpha_0}^{-1} \left(\nabla q_h^{n+1}, \xi\right)_\Omega + s_{h,p}^\Omega(q_h^{n+1}, \xi) = (\mathrm{div}\, \widetilde{\boldsymbol{v}}_h^{n+1}, \xi)_\Omega - s_{h,p}^\Omega(p_h^{n+1,*}, \xi) \quad \forall \xi \in Q_h\,.$$

Moreover, equation (A.15) then can be written as

$$\Delta t^{-1}\ \alpha_0 \left(\boldsymbol{v}_h^{n+1} - \widetilde{\boldsymbol{v}}_h^{n+1}, \boldsymbol{\varphi}\right)_\Omega + \left(\nabla q_h^{n+1}, \boldsymbol{\varphi}\right)_\Omega = 0 \qquad \forall\, \boldsymbol{\varphi} \in \mathbf{V}_h\,,$$

and a postponed pressure update,

$$p_h^{n+1} = q_h^{n+1} + p_h^{n+1,*}$$

has to be added. Badia and Codina [BC08] state, that the Chorin-Temam scheme, the Van Kan scheme using the Crank Nicolson scheme, as well as the BDF2-SE2 scheme applied to the *OSS stabilized* Navier-Stokes problem leads to the improved pressure stability result

$$\{\sqrt{\tau}\, \mathbf{P}^n\} \in l^1(L_+)\,,$$

whereas τ denotes the parameter occurring in the pressure stabilization. Thus, the results are independent of the time step, i.e. the stability of the scheme is not affected when $\Delta t \to 0$.

Appendix B

Algorithmic Principles

The field of discrete mathematics shows a large variety of methods to algorithmically treat flow problems, such as Newton iteration, direct methods, linear iterative schemes, Krylov subspace methods, multigrid methods, or the idea of preconditioning, which aims to increase the performance of the iteration by solving an equivalent problem with improved matrix properties.

For large systems, direct methods and linear iterative schemes are far too expensive. However, they are often used as a preconditioner in iterative methods or as smoothing operators in multigrid schemes in an incomplete form, and find application as solvers for small subproblems.
With the Krylov subspace methods a class of efficient methods is given, which assures the determination of the exact solution of a linear problem after maximal n iteration steps for underlying (nonsingular) matrices of dimension $n \times n$.
The computational costs of each of the previously mentioned schemes depend on the condition number of the underlying matrix. Due to the computational costs of solving one iterative and due to the amount of sufficient iterations, these procedures are impracticable for large linear systems. Multigrid schemes are efficient schemes, which are independent on the condition number, and still have a simple structure.
A large variety of scales inheres ocean circulation. A major difficulty is the strong stiffness. Without implicit and very robust solution methods it is a difficult task to solve such systems at all. To sufficiently reduce the complexity of the problems different techniques can be combined: adaptive local mesh refinement [BR01] to resolve reaction fronts and singularities, special storage techniques [BT06b], implicit methods to allow for large time steps, splitting and approximation of equations [Pro97] for a reduction of the dimension. Still, the remaining systems may be so large that parallelization is necessary.

Following these considerations the chapter is structured as follows: We start with an introduction of essential notations and short derivation of a suitable linear system, which can be treated by appropriate schemes for linear problems, such as linear iterative methods or Krylov subspace methods. Moreover, we have a glimpse on the treatment of problems showing a saddle point structure. We then present an overview over simple algorithms, such as direct and linear iterative schemes, to solve linear systems.

Due to the dimensions of the underlying problems, they are not used as solvers for these problems on their own, but serve as preconditioners, smoothers or as solver for suitably small subproblems. The following section, Section B.3, introduces the field of preconditioning and presents a few preconditioners. For a closer look into that topic the reader is referred to [BBC+94, Hac93]. Section B.4 considers the class of Krylov subspace methods, which assure convergence of the iteration after a fixed, but (for our applications) commonly large amount of iterations. Similar to the formerly introduced methods, they are solely applied for subproblems occurring in the multigrid framework when direct and linear iterative methods are not applicable. The topic of multigrid methods is already treated in Appendix C. We skip an additional treatment here.

The topics can be found in textbooks such as [Mei11, Hac93, BBC+94, Saa03].

B.1 Preliminaries

In this section we present basic notations used in this chapter. Moreover, we account for the special structure of the present problems, i.e. the saddle point structure, which allows us to draw on algorithms for linear algebraic problems and split the given problem in order to reduce the computational costs. Each of the reducing subproblems can be solved with the methods introduced in the upcoming sections.

B.1.1 Basic notations

We relax the definition of the underlying domain, see Section 3.1.1, and consider open domains $\Omega \subset \mathbb{R}^3$. In particular we do not consider the 2D case here. Let $\mathbf{u} \in \mathbf{V}$ be the solution of a system of partial differential equations (not necessarily a flow problem) given in the weak formulation on Ω:

$$\mathbf{u} \in \mathbf{V}: \quad \mathrm{a}(\mathbf{u})(\boldsymbol{\phi}) = 0 \qquad \forall\, \boldsymbol{\phi} \in \mathbf{V}, \tag{B.1}$$

where $\mathrm{a}(\cdot)(\cdot)$ is a semi-linear form, linear in the second argument. Let $\mathrm{a}(\cdot)(\cdot)$ describe a system of $\mathcal{N}_c$ equations and $\mathbf{u} : \Omega \to \mathbb{R}^{\mathcal{N}_c}$ have $\mathcal{N}_c$ solution components. E.g., for 3D (nonhydrostatic) Navier-Stokes flows we have $\mathcal{N}_c = 4$ with three velocity and one pressure component.

Recall the notions of Section 4.1.1 on triangulations and finite element spaces. I.e. note, that a triangulation $\mathcal{T}_h$ of the domain Ω is assumed to be regular, and that we apply the concept of hanging nodes in order to allow for locally refined meshes. Nodes, faces and edges of $\mathcal{T}_h$ are denoted as x, f and e, respectively.
The argumentations in this chapter are not only valid for finite element spaces, which are based on linear transformations $B_T : \widehat{T} \to T$ of type (4.3), but also apply for arbitrary affine mappings from the reference element $\widehat{T}$ to the computational element T. We denote the appropriate conforming finite element space as $\mathbf{V}_h \subset \mathbf{V}$. Let

$$\Psi_h := \{\phi_h^i, i = 1, \ldots, \mathcal{N}_h\},$$

be the common Lagrange basis system of V_h with $\phi_i(x_j) = \delta_{ij}$, where x_j are the $\mathcal{N}_h$ degrees of freedom. With $\mathcal{N}_h$ we identify the size of the problem to be solved.

To approximate the partial differential equation in this discrete space V_h we associate the finite element function $\mathbf{u}_h \in [\mathrm{V}_h]^{\mathcal{N}_c}$ with a coefficient vector $\mathbf{u}_h \in \mathbb{R}^{\mathcal{N}_h \times \mathcal{N}_c}$ given by

$$(\mathbf{u}_h)_j = u_h(x_j) \in \mathbb{R}^{\mathcal{N}_c}, \quad u_h = \sum_{j=1}^{\mathcal{N}_h} (\mathbf{u}_h)_j \phi_h^j(x). \tag{B.2}$$

We solve the partial differential equation (B.1) with a Newton method yielding iterates u_h^t by:

$$a'(u_h^t)(u_h^{t+1} - u_h^t, \phi_h) = -a(u_h^t)(\phi_h) \quad \forall \phi_h \in [\mathrm{V}_h]^{\mathcal{N}_c},$$

where $a'(u_h)(w_h, \phi_h)$ is the directional derivative of the form $a(\cdot)(\cdot)$ in direction of the update w_h evaluated in the last approximation u_h. The discrete solution of the partial differential is then characterized by the solution of the linear equations

$$\mathbf{A}_h \mathbf{u}_h = \mathbf{b}_h,$$

where the system matrix $\mathbf{A}_h$ and the load vector $\mathbf{b}_h$ are given by:

$$(\mathbf{A}_h)_{ij} = a'(u_h^t)(\phi_h^j, \phi_h^i), \ i, j = 1, \ldots, \mathcal{N}_h,$$
$$(\mathbf{b}_h)_j = -a(u_h^t)(\phi_h^j), \ j = 1, \ldots, \mathcal{N}_h.$$

Remark B.1. *We store the matrix and the vectors in a block-wise sense: every entry of the matrix $(\mathbf{A}_h)_{ij} \in \mathbb{R}^{\mathcal{N}_c \times \mathcal{N}_c}$ is a matrix itself, gathering all couplings between the $\mathcal{N}_c$ equation components and every entry of the vectors $(\mathbf{b}_h)_i \in \mathbb{R}^{\mathcal{N}_c}$ is a vector. Thus, all algebraic algorithms can be presented independent of the number of solution components $\mathcal{N}_c$.*
Anticipating, the block-wise storage technique clusters local dependencies of the different solution components and is crucial to obtain an efficient parallel method.

B.1.2 Saddle point problems

The following considerations are based on [Car86, LQ86, Bra07]. As already discussed in Chapter 3, hydrostatic flow problems show a saddle point structure, which, in steady state, is also apparent in their appropriate (conforming) finite element discretization, see also Chapter 4. This can be explored in order to reduce computational costs by a suitable splitting of the fully discrete problem. The commonly applied *Uzawa algorithm* originates from the framework of linear algebraic problems and finds its appropriate algorithmical realization due to the properties of the underlying problem matrix.
As examined in Chapter 6, evolutionary flow problems are also numerically tackled with splitting schemes. These schemes may also show the structure of an Uzawa algorithm, which moved some authors to suitably name the appropriate splitting schemes.

We consider the linear algebraic system

$$M\boldsymbol{x} := \begin{pmatrix} A & B^T \\ B & D \end{pmatrix} \begin{pmatrix} \boldsymbol{v} \\ p \end{pmatrix} = \begin{pmatrix} \boldsymbol{f} \\ \boldsymbol{g} \end{pmatrix} \tag{B.3}$$

with nonsingular matrix $A \in \mathbb{R}^{m\times m}$, matrix $D \in \mathbb{R}^{n\times n}$ and matrix $B \in \mathbb{R}^{m\times n}$. Applying blockwise Gauss elimination leads to

$$(BA^{-1}B^T - D)p = BA^{-1}\boldsymbol{f} - \boldsymbol{g}\,, \tag{B.4}$$

$$\boldsymbol{v} = A^{-1}\boldsymbol{f} - A^{-1}B^T p \tag{B.5}$$

with *Schur complement* $S := BA^{-1}B^T - D$. [Oue81, Car86] provide the following regularity statements:

(i) Let $\rho(M)$ be the rank of M. $\rho(M) = \rho(A) + \rho(S)$. I.e. if M is nonsingular, so is S.

(ii) Let M be symmetric and A be nonsingular and positive definite.

(ii-a) M is positive definite if and only if S is positive definite,

(ii-b) M is positive semidefinite if and only if S is positive semidefinite.

(iii) If M is nonsingular and Hermitean, then S is nonsingular and Hermitean.

Thus, the nonsingularity property of the entire matrix M carries over to its Schur complement S. If problem (B.3) has a uniqie solution, the same applies for (B.4) – (B.5). In particular, some properties of the underlying entire problem inherit to the reduced problem (B.4) – (B.5).

The basic idea of an Uzawa algorithm is to solve equation (B.4) for p iteratively and contemporeaneously update $\boldsymbol{v}$ due to (B.5), at best in an efficient way.
Dependent on the properties of S, different schemes offer, such as the motivative *Richardson iteration* or the (faster) *BiConjugate Gradient scheme* for nonsymmetric problems, or the *Conjugate Gradient Scheme* for symmetric matrices.

B.2 Direct and linear iterative methods

In this section we present an overview over simple algorithms for linear systems, starting with the class of direct methods. These methods assure, that at the end of the (expensive) procedure, the solution x of the linear system $Ax = b$ is known (up to errors due to machine inaccuracy). Due to their high costs this approach is not manageable for large systems, but can be used to handle subproblems of suitable size. Henceforth we introduce the still expensive linear iterative methods . Schemes of these classes can be used - in an inexact manner - in the construction of preconditioners. We treat this issue in Section B.3. Throughout this section we consider the linear problem

$$Ax = b \tag{B.6}$$

with nonsingular matrix $A \in \mathbb{R}^{n\times n}$.

B.2.1 Direct methods

The simplest approach to determine the solution x of the linear problem (B.6) is the application of a suitable factorization of matrix A, i.e. $A = A_1 A_2$, such that the resulting subproblem are to be solved easily.

LU factorization

The procedure of LU factorization decomposes matrix A into an upper triangular matrix L and a lower triangular matrix U. Conveniently, in order to assure existence of such a decomposition, partial pivoting is applied. Based on the Gaussian algorithm, the factorization with partial pivoting can be described with suitable permutation matrices P_k, concentrated in the matrix P, and Gaussian transformations, given by Frobenius matrices L_k. The LU scheme with partial pivoting is as follows:

1. Determine $PA = LU$.
2. Solve $Lz = Pb$.
3. Solve $Ux = z$.

In order to solve the linear problem with this approach, $\mathcal{O}(n^3)$ floating point operations (flops) are necessary, i.e. this approach is quite expensive. The approach for symmetric, positive-definite matrices, i.e. the Cholesky scheme, does not lead to a considerable improvement, even if a more economical storage is possible exploiting symmetry. However, the effort of the LU decomposition (step 1) and solving the forward and backward substitution (steps 2 and 3) for tridiagonal matrices A becomes linear.

QR factorization

The QR decomposition of matrix A consists of a unitary matrix Q and an upper triangular matrix R, which has the same norm and condition number as A. As the columns of Q denote an orthonormal basis of $\mathbb{R}^n$, it is suggestible to apply known orthogonalization strategies for the construction of the factorization $A = QR$, such as the Gram-Schmidt scheme, the Givens scheme or the Householder scheme. Due to the numerical instability of the Gram-Schmidt method, it is customary to apply either the Givens, the Householder scheme, or a modified Gram-Schmidt scheme. Using $Q^* = Q^{-1}$, the QR factorization for solving the problem (B.6) is given by

1. Determine $A = QR$.
2. Solve $Rx = Q^* b$.

The algorithmic complexity is as large as in the LU factorization, $\mathcal{O}(n^3)$.

B.2.2 Linear iterative methods

Linear iterative methods to solve the linear problem (B.6) can be expressed (in 1st normal form) as

$$x^k \;=\; \Phi(x^{k-1}, b) \;:=\; Mx^{k-1} + Nb \tag{B.7}$$

with matrices M and N. Such an iterative method is consistent, if (and only if) the iteration matrix M takes the shape $M = I - NA$ with identity matrix I. If (and only if) the spectral radius of M satisfies $\rho(M) < 1$, the method is convergent. Due to the relation $\rho(M) \leq \|M\|$, a (sharper) criterion for convergence is $\|M\| < 1$ for any natural matrix norm $\|\cdot\|$.

In this section we shortly recall the most common linear iterative schemes, i.e. the Jacobi method (J), the Gauss-Seidel scheme (GS), successive over-relaxation (SOR) and the Richardson iteration (RI).

Let $A = D - L - U$ whereas $-L$ denotes the strictly lower triangular part of A, $-U$ the strictly upper part and D the diagonal of A. A characterization of the introduced schemes is listed in Table B.1. The appropriate iteration matrices of these consistent

scheme	$\boldsymbol{\Phi}$	$\boldsymbol{N}$
J	$D^{-1}((L+U)x + b)$	D^{-1}
GS	$(D-L)^{-1}(Ux + b)$	$(D-L)^{-1}$
SOR	$(D-\theta L)^{-1}\left((\theta U + (1-\theta)D)x + \theta b\right)$	$(\theta^{-1}D - L)^{-1}$
RI	$(I - \theta A)x + \theta b$	θI

Table B.1: Iteration function Φ and matrix N of the introduced linear iterative methods. Parameter $\theta > 0$ is denoted as relaxation parameter.

schemes are given by $M = I - NA$.

Convergence of the Jacobi scheme, i.e. $\rho(M) < 1$, is assured for positive definite, strictly diagonal dominant matrices. The requirement of strict diagonal dominance can be released, if a relaxed version of the Jacobian scheme is applied, see e.g. [Mei11, Hac93]. If the nonsingular matrix A is strictly diagonal dominant, convergence of the Gauss-Seidel scheme can be assured. For self-adjoint and positive definite matrices A, a relaxed version of the Gauss-Seidel scheme converges, if the relaxation parameter θ fulfills $\theta \in (0, 2)$. The theorem of Ostrowsky-Reich assures convergence of the SOR scheme, if the nonsingular matrix A is symmetric and if the relaxation parameter θ lies in the interval $(0, 2)$. In order to assure convergence of the Richardson iteration, the eigenvalues of A have to be on the positive side of the real axis, e.g. if A is positive definite, and the relaxation parameter has to satisfy $\theta \in (0, 2/\lambda_{max})$, whereas λ_{max} denotes the largest eigenvalue of A.

B.2.3 Example: Uzawa algorithm

Let us now treat the Schur complement problem introduced in the preliminary Subsection B.1.2. Recall problem (B.4) – (B.5) and assume the Schur complement S to be nonsingular.

Algorithm B.2 (Richardson based Uzawa algorithm)**.** *Let $p_0 \in \mathbb{R}^m$ and θ be a sufficiently small damping parameter. The i-th step, $i \geq 1$, of the algorithm is given by:*

$$\textit{(i)}\ A\,\boldsymbol{v}_i \;=\; \boldsymbol{f} - B^T p_i,$$

$$\textit{(ii)}\ p_{i+1} \;=\; p_i + \theta B\,\boldsymbol{v}_i + \theta(Dp_i - \boldsymbol{g})$$

Thus, although the Schur complement has a structure, which suggests large algorithmical effort, the overall algorithm is quite clear. Due to the preceeding argumentation, this algorithm converges, if $\rho(S) < 1$.

B.3 Preconditioning

In this section we shortly introduce the topic of preconditioning and sketch three common preconditioning techniques, which are based on the already introduced Jacobi, SOR and on the ILU method.

Presume a linear problem $Ax = b$ with nonsingular matrix A. As indicated for the linear iterative schemes, the convergence of a process to solve the linear problem iteratively depends on the spectral properties of the matrix A. The task of *preconditioning* is to find a suitable matrix P, such that the solution of transformed problem

$$PAx = Pb$$

is also the solution of the original one, whereas the spectral radius $\rho(PA)$ and the condition number $\kappa(PA)$ are small enough. In order to assure a small condition number, P shall be a sufficiently good approximation of A^{-1}.

Let us note, that convergence of some iterative schemes is only assured for symmetric matrices. However, the product PA is commonly not symmetric, even if P and A are symmetric. One attempt is the suitable adaption of the iterative schemes. E.g. for the CG scheme, the P-inner product can be applied for the determination of the residuals. Alternatively, P can be split into a left and a right preconditioner, i.e. $P = P_1P_2$, such that the altered problem

$$P_1AP_2(P_2^{-1}x) \;=\; P_1b \tag{B.8}$$

is to be solved. In practice, a suitable reformulation of (B.8) assures, that the explicit splitting is not needed, see e.g. [BBC+94].

B.3.1 Jacobi preconditioner

We recall the fixed point scheme (B.7) and reformulate the Jacobi iteration as

$$x^{k+1} \;=\; x^k - D^{-1}(Ax - b)$$

with D as a simple approximation of A. The Jacobi preconditioner uses the same approximation, i.e. $P = D^{-1}$. This simple approach is easy to implement and does not lead to particular problems in the context of parallel computing. However, more sophisticated preconditioners lead to larger improvements of the convergence behavior, see [BBC+94].

B.3.2 Symmetric SOR preconditioner

Assuming a symmetric matrix A with $A = D - L - L^\top$, the preconditioner, which is based on a symmetric version of the SOR scheme is given by $P^{-1} = (2-\theta)^{-1}(\theta^{-1}D - L)(\theta^{-1}D)^{-1}(\theta^{-1}D - L)^\top$ with a similar approach as in the Jacobian case. An optimal choice of the relaxation parameter leads to an improved decrease of the iteration steps. Note, that the application of this preconditioner in parallelized computations necessitates a suitable ordering of the variables. Again, we refer to [BBC+94] for further informations.

B.3.3 ILU preconditioners

ILU preconditioners are based on incomplete LU factorization. A common approach is to consider the set S of nontrivial matrix positions (i, j), i.e. $a_{ij} \neq 0$. Let B be a matrix of same dimensions as A. The positions $(\hat{i}, \hat{j}) \notin S$ with $b_{\hat{i}\hat{j}} \neq 0$ are called *fill-ins*. The idea of ILU factorization is to ignore (certain) fill-ins in the matrices occurring in the LU factorization process of A, such that the matrices occurring in the factorization process are almost as sparse as the problem matrix A and $P \approx A^{-1}$.

Such a preconditioner P may be given by $P^{-1} = L_P U_P$ with nonsingular, lower and upper triangular matrices L_P and U_P, or, more frequently, by $P^{-1} = (D_P + L_P)D_P^{-1}(D_P + U_P) = (D_P + L_P)(I + D_P^{-1}U_P)$. In the latter case D_P denotes a diagonal matrix, and L_P and U_P are strictly lower and upper triangular matrices. For further information on the construction of preconditioners we refer to [BBC+94, Hac93].

Due to the incompleteness of the factorization of a given matrix, zero pivots or indefinite matrices (due to occurrences of negative pivot elements) may lead to a break down in the creating step of the preconditioner. However, there are mechanisms, e.g. suitable replacing of the pivot elements, such that the break down is intercepted. Moreover we observe higher construction costs compared to the formerly introduced preconditioners. These costs can be amortized, if the same preconditioner is used repeatedly, e.g. in time or Newton iterations. The authors of [BBC+94] note a poor efficiency in the parallel context.

B.3.4 Example: Preconditioned Uzawa algorithm

Again, we consider the reformulated saddle point problem (B.4) – (B.5). [Bra07] indicates, that the condition number of the Schur complement (at least for $D = 0$) is unevenly. Thus, it offers to apply a suitable preconditioning of the Schur complement. We build up our argumentation on the Richardson based Uzawa algorithm B.2 and on a stable finite element discretization of the nonhydrostatic Stokes problem formulated on shape regular meshes.

Given the Schur complement $S = B^T A^{-1} B$ (with $D = 0$), the task is to find a suitable approximation of S^{-1}. Given the nonhydrostatic Stokes problem we have $B^T = \operatorname{div}$, $A = \Delta$, $B = \nabla$ and thus

$$S \;=\; \operatorname{div} \circ \Delta^{-1} \circ \nabla \;\sim\; id\,,$$

see also [BC08]. As the Schur complement is defined on the pressure space, we thus can apply the inverse of the mass matrix on the pressure space, M_p^{-1}. The resulting scheme is given by:

Algorithm B.3 (Preconditioned Richardson based Uzawa algorithm)**.** *Let $p_0 \in \mathbb{R}^m$ and θ be a sufficiently small damping parameter. The i-th step, $i \geq 1$, of the algorithm is given by:*

(i) $A\,\boldsymbol{v}_i \;=\; \boldsymbol{f} - B^T p_i,$

(ii) $M_p p_{i+1} \;=\; M_p p_i + \theta B\,\boldsymbol{v}_i$

Step (i) of the origin Uzawa algorithm B.2 remains unchanged, as it is the update of the velocity, which also can be determined at the end of the overall Richardson iteration of the Schur complement problem. However, in step (ii), the preconditioner M_p^{-1} was applied to S, which is incorporated in the iteration function Φ.

B.4 Krylov subspace methods

In this section we introduce the idea of Krylov subspace methods. Corresponding on the type of the underlying matrices, different optimizations can be applied, which leads to different classes of methods. We present one method for symmetric matrices, the CG method, and one for common nonsingular matrices, the method of generalized minimal residuals (GMRES).

Again, we consider the linear problem

$$Ax \;=\; b \tag{B.9}$$

with nonsingular matrix $A \in \mathbb{R}^{n\times n}$, and a suitable initial element $y \in \mathbb{R}^n$. Krylov subspace methods are based on the spaces

$$\begin{aligned}\mathcal{K}_m(A, y) :=\; & \operatorname{span}\{y,\, Ay,\, A^2y, \ldots,\, A^{m-1}y\} \\ & = \{v \in \mathbb{R}^n \mid v = p(A)y\,, p \text{ is polynomial of degree } \deg p \leq m-1\}\,,\end{aligned}$$

the *Krylov subspaces*. Obviously, $\mathcal{K}_{m-1}(A,y) \subseteq \mathcal{K}_m(A,y)$, $m \geq 1$. The number grade(y) denotes the degree of the polynomial p with minimal degree, such that $p(A)y = 0$. Due to the Cayley-Hamilton theorem, we have grade$(y) \leq n$. The set $\{y, Ay, \ldots, A^{m-1}y\}$ denotes a basis of $\mathcal{K}_m(A,y)$, if the only polynomial p of degree $\deg p \leq m-1$ with $p(A)y = 0$ is the trivial polynom $p \equiv 0$, which leads to

$$\dim(\mathcal{K}_m(A,y)) = \min\{m, \text{grade}(y)\} \;\leq\; n\,.$$

For a given initial guess $x^{(0)}$ we set $y = r^{(0)} := b - Ax^{(0)}$. The preceding assures existence of a polynom p of (minimal) degree $\deg p := \hat{n} \leq n-1$, such that

$$p(A)r^{(0)} \;=\; \sum_{i=0}^{\hat{n}} \alpha_i A^i r^{(0)} \;=\; 0 \tag{B.10}$$

applies with suitable constants $\alpha_i \in \mathbb{R}$. As $r^{(0)}, Ar^{(0)}, \ldots, A^{\hat{n}}r^{(0)}$ are linearly independent, at least α_0 and $\alpha_{\hat{n}}$ are non-trivial, i.e. $\alpha_0,\, \alpha_{\hat{n}} \neq 0$. Thus, we get

$$A^{-1}r^{(0)} \;=\; -\sum_{i=1}^{\hat{n}} \frac{\alpha_i}{\alpha_0} A^{i-1} r^{(0)} \in \mathcal{K}_{\hat{n}-1}(A, r^{(0)})\,. \tag{B.11}$$

Recalling the underlying problem (B.9) and the definition of the initial residual, $r^{(0)} := b - Ax^{(0)}$, we thus get

$$x = A^{-1}b = x^{(0)} + A^{-1}r^{(0)}\,, \tag{B.12}$$

whereas $x^{(0)}$ is initially given and $A^{-1}r^{(0)}$ has to be determined in an iterative but finite process.

Considering the representations (B.11) and (B.12), the successive approximation of $A^{-1}r^{(0)}$ by suitable elements of $\mathcal{K}_m(A, r^{(0)})$ in order to construct an approximation $x^{(m)} \in x^{(0)} + \mathcal{K}_m(A, r^{(0)})$ for $0 \leq m \leq \hat{n}$, suggests itself. Indeed, the approach in the Krylov subspace methods is to construct a sequence of elements $x^{(m)} \in x^{(0)} + \mathcal{K}_m(A, r^{(0)})$, such that

(a) $x^{(m)}$ is the best approximation of x in $x^{(0)} + \mathcal{K}_m(A, r^{(0)})$ and

(b) the sequence $(x^{(m)})_{0 \leq m \leq \hat{n}}$ converges sufficiently fast to the solution $x = A^{-1}b$.

Note, that due to $\mathcal{K}_i(A, r^{(0)}) \subset \mathcal{K}_j(A, r^{(0)})$ for $i < j \leq \hat{n}$ and $\mathcal{K}_{\hat{n}}(A, r^{(0)}) = \mathcal{K}_{\hat{n}+k}(A, r^{(0)})$ for any $k \in \mathbb{N}$, requirement (a) assures convergence of the sequence $(x^{(i)})_{i \in \mathbb{N}}$. In order to assure (a) and (b), it is useful to glance at the theory of projection methods, see e.g. [Saa03]:

Let $\mathcal{K}$ and $\mathcal{L}$ be two m-dimensional subspaces of $\mathbb{R}^n$. We set the space $\mathcal{K}$ as $\mathcal{K}_m(A, r^{(0)})$. The definition of $\mathcal{L}$ is postponed. The appropriate projection method with respect to our linear problem (B.9) and due to these m-dimensional spaces is given by

$$\textit{Find } x^{(m)} \in x^{(0)} + \mathcal{K}_m(A, r^{(0)})\,, \textit{ such that } b - Ax^{(m)} \perp \mathcal{L}\,. \tag{B.13}$$

Denoting $x^{(m)} = x^{(0)} + \delta^{(m)}$, problem (B.13) can be reformulated as

$$\textit{Find } \delta^{(m)} \in \mathcal{K}_m(A, r^{(0)}) \,, \textit{ such that } (r^{(0)} - A\delta^{(m)}, \varphi) = 0 \qquad \forall \varphi \in \mathcal{L} \,, \tag{B.14}$$

whereas $(\cdot, \cdot)$ denotes the Euclidean scalar product. Let $B_k := [b_1, \ldots, b_m]$ and $B_l := [\hat{b}_1, \ldots, \hat{b}_m]$ be the $n \times m$- matrices, whose column vectors are the basis elements of $\mathcal{K}_m(A, r^{(0)})$ and $\mathcal{L}$, respectively. Problem (B.14) then can be formulated as

$$\textit{Find } C^{(m)} \in \mathbb{R}^n, \textit{ such that } B_l^\top A B_k C^{(m)} = B_l^\top r^{(0)} \,. \tag{B.15}$$

I.e. $x^{(m)} = x^{(0)} + B_k (B_l^\top A B_k)^{-1} B_l^\top r^{(0)}$. Now, to justify the latter deductions, note that the matrix $B_l^\top A B_k$ is nonsingular, if (see also [Saa03]):

(a1) A is positive definite and $\mathcal{L} = \mathcal{K}_m(A, r^{(0)})$, or

(b1) A is nonsingular and $\mathcal{L} = A\mathcal{K}_m(A, r^{(0)})$.

In particular, assuming (a1) or (b1), respectively, the solution $x^{(m)}$ of (B.13) fulfills one of the following best approximations:

(a2) if A is symmetric and positive definite, and $\mathcal{L} = \mathcal{K}_m(A, r^{(0)})$, then

$$(A(x - x^{(m)}), (x - x^{(m)})) = \min_{y \in x^{(0)} + \mathcal{K}_m(A, r^{(0)})} (A(x - y), (x - y)) \,, \qquad \text{or}$$

(b2) if A is nonsingular and $\mathcal{L} = A\mathcal{K}_m(A, r^{(0)})$, then

$$\|b - Ax^{(m)}\|_2 = \min_{y \in x^{(0)} + \mathcal{K}_m(A, r^{(0)})} \|b - Ay\|_2 \,,$$

whereas $\|\cdot\|_2$ denotes the Euclidean norm.

Thus, depending on the choice of $\mathcal{L}$, we end up in two different classes of Krylov subspace schemes, one class for symmetric positive definite matrices, such as the CG method, and one class for nonsingular matrices. Members of that class are the GMRES scheme or the BiCG iteration.

Concluding, Krylov subspace methods consist in the determination of successive approximations $x^{(m)} \in x^{(0)} + \mathcal{K}_m(A, r^{(0)})$, which are the best approximations of x in $x^{(0)} + \mathcal{K}_m(A, r^{(0)})$, see (a2) and (b2), and are orthogonal to an m-dimensional space $\mathcal{L}$, which either is the space $\mathcal{K}_m(A, r^{(0)})$ itself or $A\mathcal{K}_m(A, r^{(0)})$. For large n, the orthogonalization process is quite expensive. In practice, n is large. Commonly, the solution x is only determined approximately, i.e. the iterative process is stopped after $m \ll n$ iterations, and a restarting of the algorithm with $x'^{(0)} = x^{(m)}$ takes place.

In the upcoming we present one method of each class, the CG scheme for symmetric positive definite matrices A, and the GMRES scheme of nonsingular matrices A. We start with the GMRES scheme, as the CG scheme can be introduced via simplification of some sub-algorithms occurring in the GMRES scheme.

B.4.1 Generalized Minimal Residuals (GMRES)

The following algorithm is based on the Arnoldi-Gram-Schmidt algorithm, which constructs an orthonormal basis via the Gram-Schmidt orthogonalization, and then uses the properties of the resulting Hessenberg matrix in order to define a simplification of the minimizing problem (b2) and thus constructs the approximation $x^{(m)}$ of x. Note, that the orthonormalization process also can take place with other methods, such as the Householder-Arnoldi scheme.

Algorithm B.4 (Arnoldi-Gram-Schmidt based GMRES scheme)**.**

(i) Initialization.

1. *Set* $r^{(0)} := b - Ax^{(0)}, \quad \beta := \|r^{(0)}\|_2, \quad v_1 := r^{(0)}/\beta.$
2. *Initialize* $\overline{H}_m = \{h_{ij}\}_{1\leq i\leq m+1, 1\leq j\leq m}$. *Set* $\overline{H}_m = 0$.

(ii) Arnoldi scheme.

For $j = 1, 2, \ldots, m$ *do:*

1. $w_j := Av_j$
2. *For* $i = 1, 2, \ldots, j$ *do:*
   (a) $h_{ij} := (w_j, v_i)$
   (b) $w_j := w_j - h_{ij}v_i$
3. $h_{j+1,j} := \|w_j\|_2$
4. *If* $h_{j+1,j} = 0$ *set* $m := j$ *and go to* **(iii)**.
5. $v_{j+1} := w_j/h_{j+1,j}$

(iii) Minimization.

1. *Determine* y_m *such that* $\|\beta e_1 - \overline{H}_m y\| = \min_{\hat{y}\in\mathbb{R}^{m+1}} \|\beta e_1 - \overline{H}_m \hat{y}\|$.
2. $x^{(m)} := x^{(0)} + V_m y$

B.4.2 Conjugate Gradient Method (CG)

Basically, the CG algorithm does the same as Algorithm B.4, suitably adapting the symmetry of A and the differing minimizing property (a2). Applying the observation, that the Hessenberg matrix $H_m = V_m^\top A V_m$ is symmetric and tridiagonal, the Arnoldi-scheme and the (a2) minimization can be suitably simplified to the Lanczos method (which we do not introduce here, but refer to [Saa03]). A reformulation of this scheme and application of different orthogonality properties lead to the following scheme:

Algorithm B.5 (CG iteration)**.**

(i) Initialization. *Set* $r^{(0)} := b - Ax^{(0)}, \quad p^{(0)} := r^{(0)}$.

(ii) Orthogonalization and minimization.

For $j = 1, 2, \ldots,$ *until convergence do:*

1. $\alpha_j := \|r^{(j)}\|_2^2 / (Ap^{(j)}, p^{(j)})$
2. $x^{(j+1)} := x^{(j)} + \alpha_j p^{(j)}$
3. $r^{(j+1)} := r^{(j)} - \alpha_j A p^{(j)}$
4. $\beta_j := \|r^{(j+1)}\|_2^2 / \|r^{(j)}\|_2^2$
5. $p^{(j+1)} := r^{(j+1)} + \beta_j p^{(j)}$

Note, that the CG scheme can also be retrieved starting from the gradient scheme with steepest descent $d^{(m)}$ and assuring, that not only two neighboring residuals are orthogonal, i.e. $(r^{(m)}, r^{(m+1)}) = 0$, $m \geq 0$, but each, i.e. $(r^{(i)}, r^{(j)}) = 0$ for $i \neq j$. This, again leads to a Galerkin system of kind (a2).

B.4.3 Example: CG-Uzawa algorithm

Considering the Schur complement problem (B.4)–(B.5), we solve equation (B.5) by application of the *conjugate gradient method*. As already mentioned before, this scheme is only applicable to problems with symmetric matrices, such as the symmetric stabilized finite element discretized Stokes problem.

Algorithm B.6 (CG Uzawa iteration)**.**

(i) Initialization.

1. *Determine* $h^{(0)}$ *due to* $Ah^{(0)} = \boldsymbol{f} - B^T p^{(0)}$.
2. *Set* $r^{(0)} := Bh^{(0)} + Dp^{(0)} - \boldsymbol{g}, \quad q^{(0)} := r^{(0)}$.

(ii) Orthogonalization and minimization.

For $j = 1, 2, \ldots,$ *until convergence do:*

1. *Solve* $Ah^{(k)} = (B^T q^{(j)})$
2. $\alpha_j := \|r^{(j)}\|_2^2 / (Bh^{(j)} - Dq^{(j)}, q^{(j)})$
3. $p^{(j+1)} := p^{(j)} + \alpha_j q^{(j)}$
4. $\boldsymbol{v}^{(j+1)} := \boldsymbol{v}^{(j)} - \alpha_j h^{(j)}$
5. $r^{(j+1)} := r^{(j)} - \alpha_j (Bh^{(j)} - Dq^{(j)})$
6. $\beta_j := \|r^{(j+1)}\|_2^2 / \|r^{(j)}\|_2^2$
7. $q^{(j+1)} := r^{(j+1)} + \beta_j q^{(j)}$

The structure of the Schur complement comes into effect repeatedly in (ii) step 4, where the velocity is updated by use of the already determined variable $h^{(j)}$.

Note, that in the case of the (stabilized) Stokes problem, the main effort of this algorithm consists in solving Poisson problems in the initialization step and in (ii) step 1. For unsymmetric problems, a Krylov subspace method for problems with unsymmetric matrices can be applied. However, inverting matrix A is much more expensive. Thus it is suggestable to solve the entire, coupled problem, e.g. with a multigrid scheme.

Appendix C

Published and Submitted Articles

Abstract of the Article "Equal-order finite elements for the hydrostatic Stokes problem"

Simulation of flow phenomena in the ocean and in other large but relatively flat basins are typically based on the so-called primitive equations, which, among oth- ers, result from application of the hydrostatic approximation. The crucial premise for this approximation is the dominance of the hydrostatic balance over remaining vertical flow phenomena in large but flat domains, which leads to a decomposition of the three-dimensional (3D) pressure field into a hydrostatic part and an only two-dimensional (2D) hydrodynamic part. The former pressure can be obtained by solving Ordinary Differential Equations. The latter one is determined by a 2D elliptic problem which can be solved quite efficiently. The velocity field remains three dimensional. However, its vertical component can be eliminated from the dynamic system. In this work, we analyze such 2.5-dimensional (2.5D) Stokes systems and formulate stabilized finite element schemes with equal-order interpolation. The absence of a discrete inf-sup condition is compensated by introducing additional terms into the discrete variational form. We show stability and give an a priori error estimate for several established stabilized equal-order schemes, as pressure-stabilized Petrov-Galerkin (PSPG), Galerkin least squares (GLS) and local projection schemes (LPS) which are extended here to the hydrostatic approximation. The basic assumption we need is a certain property of the underlying 3D mesh. We illustrate the order of convergence of the 2.5D problem by numerical examples and demonstrate the effect of the hydrostatic approximation in comparison to the full 3D problem.

Abstract of the Article "Symmetric Stabilization of Equal-order Finite Element Discretized Hydrostatic Flow Problems"

Simulation of flow phenomena in the ocean and in other large but relatively flat basins are typically based on the so-called primitive equations, which, among others, result from application of the hydrostatic approximation. The crucial premise for this approximation is the dominance of the hydrostatic balance over remaining vertical flow phenomena in large but flat domains, which leads to a decomposition of the three-dimensional (3D) pressure field into a hydrostatic part and an only two-dimensional (2D) hydrodynamic part. The former pressure can be obtained by solving Ordinary Differential Equations. The latter one is determined by a 2D elliptic problem which can be solved quite efficiently. The velocity field remains 3D. However, its vertical component can be eliminated from the dynamic system. In this work, we analyze such "2.5-dimensional" (2.5D) Oseen systems and formulate symmetric stabilized finite element schemes with equal-order interpolation. The absence of a discrete inf-sup condition as well as problems due to dominating advection are compensated by introducing suitable stabilizing terms into the discrete variational form. We show stability, give an a priori error estimate for several established symmetric stabilization schemes and illustrate the order of convergence of the 2.5D problem by numerical examples.

Parallel multigrid method for finite element simulations of complex flow problems on locally refined meshes

Madlen Kimmritz[1], Thomas Richter[2,*]

[1] *University of Kiel*
[2] *University of Heidelberg*

SUMMARY

We present a parallel multigrid solver on locally refined meshes for solving very complex three dimensional flow problems. Besides describing the parallel implementation in detail, we proof the smoothing property of the suggested iteration for a simple model problem. For demonstration of the efficiency and feasibility of the solver, we show a chemically reactive flow simulation for a Methane burner using detailed chemical reaction modeling. Further, we give results of a ocean flow simulation. All described methods are implemented in the finite element toolbox *Gascoigne*.

KEY WORDS: adaptive finite elements, multigrid, parallelization, flow simulation, reactive flows, computation hydrodynamics

1. Introduction

In this paper we describe a parallel solution method for very complex three dimensional flow problems given as large systems of partial differential equations. We present two diverse applications: first the simulation of a Methane burner using detailed modeling of the chemical reactions. Second, the simulation of ocean flows. Both problems are described by very large systems of partial differential equations based on the Navier-Stokes equations. For the simulation of the Methane burner besides the four flow variables velocity and pressure, the temperature as well as the concentrations of all chemical species have to be considered. Here we use a chemical reaction system involving 39 chemical species leading to a coupled system of 43 solution components. For modeling ocean flows we at least have to consider the velocity, the pressure, the temperature, and the salinary saturation. Further solution components are required, if chemical reactions are to be modeled.

The complexity of the numerical problem grows quadratically with the number of solution components, thus the resulting algebraic systems are immense. Further, both problems are

*Correspondence to: Institute of Applied Mathematics, INF 294, 69120 Heidelberg, Germany `richter@uni-hd.de`)

naturally three dimensional problems and have to deal with a large variety of scales. Fine computational meshes are necessary. Major difficulty besides the shear size of the resulting systems is the strong stiffness. Without implicit and very robust solution methods it is not possible to solve these systems at all.

To sufficiently reduce the complexity of the problems different techniques need to be combined: adaptive local mesh refinement [3] to resolve reaction fronts and singularities, special storage techniques [7], implicit methods to allow for large time steps, splitting and approximation of equations [15] for a reduction of the dimension. Still, the remaining systems are so large that parallelization is necessary. Here, we describe the parallelization of a geometric multigrid method with optimal computational complexity to solve the arising algebraic equations.

The implementation of the parallel multigrid method will use and will benefit from the properties of the problems under consideration: the large amount of local work will keep the computational overhead due to parallelization small.

In the next section we will shortly present the finite element discretization of complex systems of partial differential equations and we give details on the multigrid method. It's parallelization is topic of Section 3. We will discuss the parallel multigrid smoother in Section 4. Here we will proof the smoothing property of the parallel iteration for a simple model example. In the final fifth section the two applications are presented. Here we also emphasize on the parallel efficiency of the implemented multigrid method.

2. Finite elements and the hierarchical multigrid method

In this section we shortly recapitulate the adaptive finite element method and describe the hierarchical multigrid method used and implemented in the software library *Gascoigne* [10]. Let $u \in V$ be the solution of a system of partial differential equations given in the weak formulation on the open domain $\Omega \subset \mathbb{R}^3$:

$$u \in V : \quad a(u)(\phi) = 0 \; \forall \phi \in V, \tag{1}$$

where $a(\cdot)(\cdot)$ is a semi-linear form, linear in the second argument. Let $a(\cdot)(\cdot)$ describe a system of $\mathcal{N}_c$ equations and $u : \Omega \to \mathbb{R}^{\mathcal{N}_c}$ have $\mathcal{N}_c$ solution components. For Navier-Stokes flows we have $\mathcal{N}_c = 4$ with three velocity and one pressure component. Let $\mathcal{T}_h$ be a regular triangulation (see [9] for a detailed discussion on finite element meshes) of the domain Ω into open hexahedrals K, nodes x, faces f and edges e (we do not discuss the two-dimensional case here). To allow for locally refined meshes we use the concept of *hanging nodes*: a corner node $x \in \bar{K}$ can reside in the middle of an edge or face of a neighboring element $\bar{K}' \cap \bar{K} \neq \emptyset$. Every edge or face can have at most one such hanging node. See Figure 1 for locally refined meshes with hanging nodes.

On the triangulation $\mathcal{T}_h$ we assemble the discrete finite element subspace $V_h \subset V$ as follows: for $r \in \mathbb{N}$ let

$$\hat{Q}^r = \text{span}\{x^\alpha y^\beta z^\gamma, \; \alpha, \beta, \gamma = 0, \dots r\},$$

be the polynomial space of degree up to r in both variables. Further for every $K \in \mathcal{T}_h$ let $T_K : \hat{K} \to K$ be the affine mapping from the *reference element* $\hat{K} = (0,1)^3$ to the

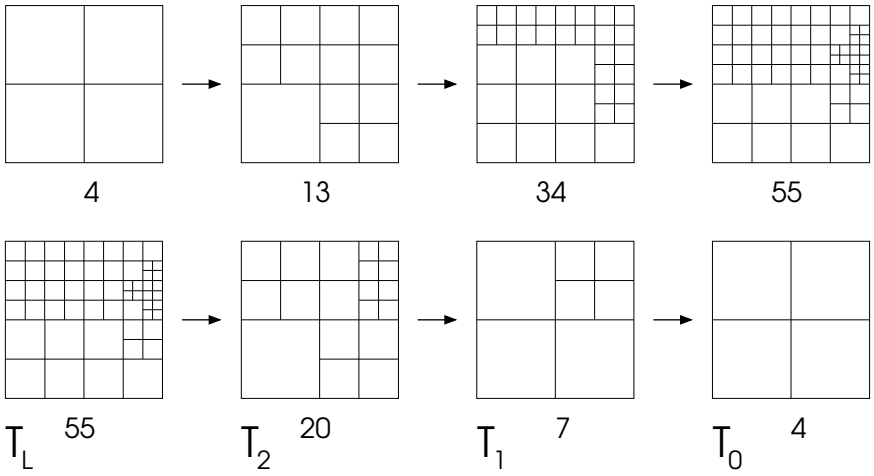

Figure 1. Top row: adaptive refinement of meshes. Bottom row: global coarsening for the generation of a multigrid hierarchy. The numbers indicate the number of elements in every mesh.

computational element K. Then, we define the finite element space:

$$V_h := \{\phi \in V : \phi\Big|_K = \phi_h \circ T_K^{-1},\ \phi_h \in \hat{Q}^r\}.$$

Let

$$\Psi_h := \{\phi_h^i, i = 1, \ldots, \mathcal{N}_h\},$$

be the common Lagrange basis system of the finite element space V_h with $\phi_i(x_j) = \delta_{ij}$, where x_j are the $\mathcal{N}_h$ degrees of freedom. With $\mathcal{N}_h$ we will identify the size of the problem to be solved.

To approximate the partial differential equation in this discrete space V_h we associate the finite element function $u_h \in [V_h]^{\mathcal{N}_c}$ with a coefficient vector $\mathbf{u}_h \in \mathbb{R}^{\mathcal{N}_h \times \mathcal{N}_c}$ given by

$$(\mathbf{u}_h)_j = u_h(x_j) \in \mathbb{R}^{\mathcal{N}_c}, \quad u_h = \sum_{j=1}^{\mathcal{N}_h} (\mathbf{u}_h)_j \phi_h^j(x). \tag{2}$$

We solve the partial differential equation (1) with a Newton method yielding iterates u_h^t by:

$$a'(u_h^t)(u_h^{t+1} - u_h^t, \phi_h) = -a(u_h^t)(\phi_h) \quad \forall \phi_h \in [V_h]^{\mathcal{N}_c},$$

where $a'(u_h)(w_h, \phi_h)$ is the directional derivative of the form $a(\cdot)(\cdot)$ in direction of the update w_h evaluated in the last approximation u_h. The discrete solution of the partial differential is then characterized by the solution of the linear equations

$$\mathbf{A}_h \mathbf{u}_h = \mathbf{b}_h,$$

where the system matrix $\mathbf{A}_h$ and the load vector $\mathbf{b}_h$ are given by:

$$(\mathbf{A}_h)_{ij} = a'(u_h^t)(\phi_h^j, \phi_h^i),\ i, j = 1, \ldots, \mathcal{N}_h,$$
$$(\mathbf{b}_h)_j = -a(u_h^t)(\phi_h^j),\ j = 1, \ldots, \mathcal{N}_h.$$

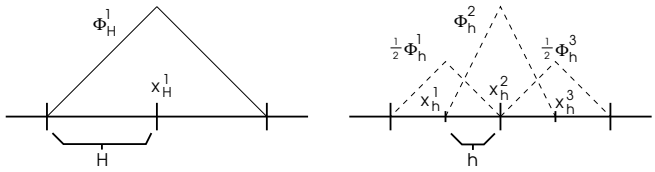

Figure 2. Nested function spaces between refined meshes: $\Phi_H^1 = \frac{1}{2}\Phi_h^1 + \Phi_h^2 + \frac{1}{2}\Phi_h^3$.

We store the matrix and the vectors in a block-wise sense: every entry of the matrix $(\mathbf{A}_h)_{ij} \in \mathbb{R}^{\mathcal{N}_c \times \mathcal{N}_c}$ is a matrix itself, gathering all couplings between the $\mathcal{N}_c$ equation components and every entry of the vectors $(\mathbf{b}_h)_i \in \mathbb{R}^{\mathcal{N}_c}$ is a vector. This storage technique clusters local dependencies of the different solution components and will be crucial to obtain an efficient parallel method. Further, all algebraic algorithms can be presented independent of the number of solution components $\mathcal{N}_c$. We use an *adaptive algorithm* for obtaining a good approximation u_h to u:

Algorithm 1. *Adaptive finite element algorithm*
Let TOL be a prescribed error tolerance, $\mathcal{T}_h$ an initial triangulation of the domain Ω.

1. *On the triangulation $\mathcal{T}_h$ define the finite element space V_h.*
2. *Solve the partial differential equation*
$$a(u_h)(\phi_h) = 0 \quad \forall \phi_h \in V_h.$$
3. *Estimate the error $\eta_h(u_h)$*
4. *If $|\eta_h(u_h)| < TOL$ break*
5. *Refine the mesh using the estimate: $\mathcal{T}_h \to \mathcal{T}_{h'}$. Restart at* 1. *using $\mathcal{T}_{h'}$.*

By this algorithm a sequence of locally refined meshes $\mathcal{T}_1, \ldots, \mathcal{T}_L = \mathcal{T}_h$ is generated. (See the top row of Figure 1). In step 5. of the algorithm, certain elements K of $\mathcal{T}_h$ are split into eight new hexahedrals. For a review of advanced error estimation and mesh refinement techniques used in these calculations see [3] or [6].

This hierarchy of finite element meshes calls for geometric multigrid methods as solver for the linear systems. Here we briefly describe the *multiplicative multigrid method*. Let $\mathcal{T}_l$, $l = 0, \ldots, L$ be a hierarchy of finite element meshes with $\mathcal{T}_L = \mathcal{T}_h$ being the finest mesh. The coarser meshes are generated by the process of *global coarsening* (see [2]). Instead of using the mesh sequence as produced in the adaptive algorithm 1, we start with the finest mesh $\mathcal{T}_L := \mathcal{T}_h$ and produce coarse meshes by successively coarsening the mesh as much as possible. This way we have $\mathcal{N}_l \gg \mathcal{N}_{l-1}$ for large l and obtain optimal complexity for the multigrid method for most meshes $\mathcal{T}_h$. See [2] for details and the lower row of Figure 1 for an example. Here, in this simple example, the ratios are $\mathcal{N}_L/\mathcal{N}_2 \approx 2.9$ and $\mathcal{N}_2/\mathcal{N}_1 \approx 2.9$ instead of 1.6 and 2.6 if one would use the meshes produced by the adaptive algorithm in reverse order. In [2] the mesh nesting is studied in detail. Opposed to most multigrid methods on locally refined meshes, every mesh level $\mathcal{T}_l$ covers the whole domain Ω. This will simplify the construction of an efficient parallel multigrid method.

By this construction the function spaces V_l on $\mathcal{T}_l$ are nested $V_{l-1} \subset V_l$ and every basis function $\phi_{l-1}^i \in \Psi_{l-1}$ can be linearly combined by adequate basis functions of Ψ_l. By

$\mathcal{P}_l \in \mathbb{R}^{\mathcal{N}_l \times \mathcal{N}_{l-1}}$ we denote the prolongation of the coefficient vector $\mathbf{u}_{l-1}$ to $\mathbf{u}_l$ so that

$$\mathbf{u}_l = \mathcal{P}_l \mathbf{u}_{l-1}, \quad \sum_{j=1}^{\mathcal{N}_l} (\mathbf{u}_l)_j \phi_l^j(x) = \sum_{j=1}^{\mathcal{N}_{l-1}} (\mathbf{u}_{l-1})_j \phi_{l-1}^j(x) \quad \forall x \in \mathcal{T}_l.$$

See Figure 2 for a one-dimensional example. By $\mathcal{R}_l := \mathcal{P}_l^T$ we denote the restriction operator. These two operators will also be used as restriction and prolongation operators between the function spaces V_l and V_{l-1}.

On the sequence of meshes $\mathcal{T}_l$ and spaces V_l for $l = 0, \ldots, L$ we can now give the hierarchical multigrid method to solve $\mathbf{A}_h \mathbf{u}_h = \mathbf{b}_h$:

Algorithm 2. *Hierarchical Multigrid Method on level l*
If $l = 0$ solve $\mathbf{A}_0 \mathbf{u}_0 = \mathbf{b}_0$. Otherwise,

1. *Pre-smooth:* $\mathbf{u}_l' = S_l^{pre}(\mathbf{A}_l, \mathbf{b}_l, \mathbf{u}_l)$
2. *Compute the residual* $\mathbf{r}_l = \mathbf{b}_l - \mathbf{A}_l \mathbf{u}_l'$
3. *Restrict the residual* $\mathbf{r}_{l-1} = \mathcal{R}_l \mathbf{r}_l$
4. *Solve* $\mathbf{A}_{l-1} \mathbf{w}_{l-1} = \mathbf{r}_{l-1}$ *with the multigrid algorithm on level* $l-1$.
5. *Prolongate the coarse mesh solution:* $\mathbf{w}_l = \mathcal{P}_l \mathbf{w}_{l-1}$.
6. *Update:* $\mathbf{u}_l'' = \mathbf{u}_l' + \mathbf{w}_l$
7. *Post-smooth:* $\mathbf{u}_l = S_l^{post}(\mathbf{A}_l, \mathbf{b}_l, \mathbf{u}_l'')$.

In step 4. the algorithm itself is called in a recursive way. The multigrid method consists of 3 parts: first, solution of the coarse mesh problem. second, the prolongation and restriction operation and third, the smoothing. The smoothing process is an approximate solution process with the goal of reducing the high frequent error contributions. Usually very easy iterative schemes like Jacobi, Gauss-Seidel or SOR are used. Having flow applications in mind we use a Richardson iteration (with approximately 5 steps) preconditioned by an ILU as smoother:

$$\mathbf{u}_l' = S_l(\mathbf{A}_l, \mathbf{b}_l, \mathbf{u}_l) = \mathbf{u}_l + (\mathbf{L}_l \mathbf{U}_l)^{-1}(\mathbf{b}_l - \mathbf{A}_l \mathbf{u}_l),$$

where $\mathbf{L}_l \mathbf{U}_l \approx \mathbf{A}_l$ is an incomplete decomposition of $\mathbf{A}_l$ with zero fill in.

The prolongation and restriction operators are as described before. For the coarse mesh solution we use a direct solver if the size of the coarse mesh $\mathcal{T}_0$ permits it. Otherwise we use a GMRES iteration, preconditioned with an ILU.

3. Parallel multigrid on locally refined meshes

Parallel multigrid methods for the solution of linear systems are well established, see [8]. The basic outline is as follows. Let $\mathcal{M}_{\text{cpu}}$ be the number of subdomains to be used for splitting the problem. This can be the number of cpu's on a cluster system or the number of cores on a shared memory system. The *vertical hierarchy* of multigrid meshes $\mathcal{T}_l$ for $l = 0, \ldots, L$ is *horizontally partitioned* into subdomains

$$\mathcal{T}_l = \cup_{p=1,\ldots,\mathcal{M}_l} \mathcal{T}_l^p, \quad \mathcal{M}_l \leq \mathcal{M}_{\text{cpu}},$$

in the following non-overlapping sense: every element $K \in \mathcal{T}_l$ is uniquely allotted to one subdomain $K \in \mathcal{T}_l^p$. Nodes $x \in \mathcal{T}_l$, edges $e \in \mathcal{T}_l$ and faces $f \in \mathcal{T}_l$ can belong to more than one

subdomain. The set of nodes $x \in \mathcal{T}_l^p$ also belonging to other subdomains is called the *interface* $\mathcal{I}_l^p$ of $\mathcal{T}_l^p$:

$$\mathcal{I}_l^p := \{x \in \mathcal{T}_l^p : \exists q \neq p : x \in \mathcal{T}_l^q\}.$$

On every $\mathcal{T}_l^p$ we define the finite element space V_l^p in the usual way.

Let $\mathcal{R}_l^p \in \mathbb{R}^{\mathcal{N}_l^p \times \mathcal{N}_l}$ be the restriction of $\mathcal{T}_l$ to $\mathcal{T}_l^p$. It holds $(\mathcal{R}_l^p)_{ij} = 1$ if ϕ_j^p corresponds to the same basis function in V_l^p as ϕ_i in V_l. All other entries of $\mathcal{R}_l^p$ are zero. By $\mathcal{P}_l^p := (\mathcal{R}_l^p)^T$ we denote the prolongation from $\mathcal{T}_l^p$ to $\mathcal{T}_l$. Then, for a coefficient vector (2) $\mathbf{x}_l \in \mathbb{R}^{\mathcal{N}_l}$ we define the local distributed vector $\mathbf{x}_l^p \in \mathbb{R}^{\mathcal{N}_l^p}$ by

$$\mathbf{x}_l^p := \mathcal{R}_l^p \mathbf{x}_l.$$

The system matrix $\mathbf{A}_l$ is assembled locally by

$$(\mathbf{A}_l^p)_{ij} = a'(u_h^t)(\phi_l^j, \phi_l^i), \quad i,j = 0, \ldots, \mathcal{N}_l^p.$$

This results in an additive distribution. The local matrices $\mathbf{A}_l^p$ are not point-wise restrictions of $\mathbf{A}_l$ but given by

$$\mathbf{A}_l = \sum_{p=1}^{\mathcal{M}_l} \mathcal{P}_l^p \mathbf{A}_l^p \mathcal{R}_l^p.$$

The matrix-vector product $\mathbf{y}_l = \mathbf{A}_l \mathbf{x}_l$ can be split into two steps:

Algorithm 3. *Parallel matrix vector product* $\mathbf{y}_l = \mathbf{A}_l \mathbf{x}_l$

1. *On* $p = \{1, \ldots, \mathcal{M}_l\}$ *compute* $\bar{\mathbf{y}}_l^p = \mathbf{A}_l \mathbf{x}_l^p$
2. *Balance values on the interface* $\mathbf{y}_l^p = \mathcal{R}_l^p \sum_{q=1}^{\mathcal{M}_l} \mathcal{P}_l^q \bar{\mathbf{y}}_l^q$

While the first step can be done in parallel, the second step requires communication on the interface nodes. This *interface balancing operator* will be used again and is indeed the most important ingredient to the parallel multilevel method.

Parallel multigrid can now be regarded as a subspace correction method with a two dimensional splitting, vertically into mesh levels $\mathcal{T}_0, \ldots, \mathcal{T}_L$ and horizontally into subdomains $\mathcal{T}_l^1, \ldots, \mathcal{T}_l^{\mathcal{M}_l}$, see [21] for this concept. Parallelization aims at implementing the existing algorithm in a most efficient way on a distributed memory machine. As far as possible, the algorithm itself shall not be changed. In the following paragraphs we will discuss the different steps of Algorithm 2 with respect to the parallelization.

3.1. The parallel multigrid smoother

In Steps 1. and 7. of Algorithm 2, the multigrid smoother is applied as a Richardson iteration. Every step $t = 0, 1, \ldots$ of this iteration yields an update:

$$\mathbf{L}_l \mathbf{U}_l \mathbf{y}_l^t = \mathbf{r}_l^t := \mathbf{b}_l - \mathbf{A_l} \mathbf{u}_l^t, \quad \mathbf{u}_l^{t+1} = \mathbf{u}_l^t + \mathbf{y}_l^t.$$

The assembly of the ILU decomposition is a globally coupled process and not easy to parallelize. We alter the smoothing process in order to get an algorithm better suitable for parallelization. Instead of computing the global ILU of $\mathbf{A}_l$ we simply construct local ILU's on every subdomain:

$$\mathbf{L}_l^p \mathbf{U}_l^p \approx \overline{\mathbf{A}}_l^p, \tag{3}$$

and replace the smoothing operation by local updates:

$$\mathbf{L}_l^p \mathbf{U}_l^p \bar{\mathbf{y}}_l^{p,(t)} = \mathbf{r}_l^{p,(t)}, \quad \mathbf{y}_l^{p,(t)} = \mathcal{R}_l^p \sum_{q=1}^{\mathcal{M}_l} \mathcal{P}_l^q \bar{\mathbf{y}}_l^q.$$

The first step can be done in parallel while in second step the application of the *interface balancing operator* is necessary.

Since the matrix $\mathbf{A}_l$ is distributed in an additive sense to the subdomains, the local matrices $\mathbf{A}_l^p$ correspond to Neumann problems which in general are not regular. For the ILU-construction in (3) we construct local Dirichlet versions $\overline{\mathbf{A}}_l^p$ of $\mathbf{A}_l^p$ by summing up all values on the interface:

$$\overline{\mathbf{A}}_l^p := \mathcal{R}_l^p \mathbf{A}_l \mathcal{P}_l^p = \mathcal{R}_l^p \left(\sum_q \mathcal{P}_l^q \mathbf{A}_l^q \mathcal{R}_l^q \right) \mathcal{P}_l^p.$$

Here, we need to exchange all matrix rows belonging to interface nodes. This procedure does not represent the original smoothing process from the sequential algorithm, but it yields a robust smoothing operator. Solving the local problems exactly

$$\overline{\mathbf{A}}_l^p \mathbf{y}_l^p = \mathbf{r}_l^p,$$

the parallel smoother would correspond to an additive Schwarz iteration with overlap h (one layer of cells) with homogeneous Dirichlet values. In Section 4 we will show, that this minimal overlap is sufficient to obtain a fixed reduction rate for high frequent error parts in a multigrid context applied to the Laplace equation.

Algorithm 4. *Parallel Smoothing Iteration*
On $p \in \{1, \ldots, \mathcal{M}_l\}$, *given* $\mathbf{u}_l^{p,(0)}$ *for* $t = 0, 1, \ldots$

1. *Local residual:* $\bar{\mathbf{r}}_l^{p,(t)} = \mathbf{b}_l^p - \mathbf{A}_l^p \mathbf{u}_l^{p,(t)}$
2. *Exchange on interface:* $\mathbf{r}_l^{p,(t)} = \mathcal{R}_l^p \sum \mathcal{P}_l^q \bar{\mathbf{r}}_l^{q,(t)}$
3. *Local update:* $\mathbf{L}_l^p \mathbf{U}_l^p \bar{\mathbf{y}}_l^{p,(t)} = \mathbf{r}_l^{p,(t)}$
4. *Update:* $\mathbf{u}_l^{p,(t+1)} = \mathbf{u}_l^{p,(t)} + \mathcal{R}_l^p \sum \mathcal{P}_l^q \bar{\mathbf{y}}_l^{q,(t)}$

Steps 2. and 4. require communication along the interface, all other steps can be done in parallel. To get an efficient algorithm all domains have to be of the same size and the interfaces have to be as small as possible:

(M1) Create balanced partitionings

$$\mathcal{N}_l^p \approx \mathcal{N}_l^q, \quad \forall p, q \in \{1, \ldots, \mathcal{M}_l\}, \ \forall l \in \{0, \ldots, L\} \tag{4}$$

(M2) Minimize the size of the interfaces

$$\max_{1 \le p \le P} \# \mathcal{I}_l^p \to \min! \tag{5}$$

3.2. Mesh transfer operators

The second important ingredient to geometric multigrid methods is the mesh transfer operator: the restriction in step 3. of Algorithm 2 and the prolongation in step 5. Here, both hierarchies get involved. To process the prolongation to node x_H^1 of the coarse mesh $\mathcal{T}_H$ in Figure 2, nodes x_h^1, x_h^2 and x_h^3 from the fine mesh $\mathcal{T}_h$ are necessary. In the parallel version all four involved nodes can rest in different subdomains making communication necessary. We split the mesh transfer into two parts: first we process the vector to be prolongated on the fine mesh $\mathcal{T}_h$. Then, we carry the contributions of $\mathcal{T}_h$ to the corresponding nodes on the coarse mesh $\mathcal{T}_H$. With respect to the situation in Figure 2, for a vector $\mathbf{u}_h$ to be prolongated to $\mathbf{u}_H$ the algorithm is as follows:

1. Collect the contributions on $\mathcal{T}_h$:
$$\bar{\mathbf{u}}_h(x_h^2) = \frac{1}{2}\mathbf{u}_h(x_h^1) + \mathbf{u}_h(x_h^2) + \frac{1}{2}\mathbf{u}_h(x_h^3).$$
2. Copy the entries to the corresponding nodes on $\mathcal{T}_H$
$$\mathbf{u}_H(x_H^1) = \bar{\mathbf{u}}_h(x_h^2).$$

The communication pattern for the first step is the same as the usual exchange of values on the interfaces. In the second step there is no communication required, if the distribution of the meshes is nested and the nodes $x_H^1 = x_h^2$ are distributed to the same subdomain p. For the parallel mesh transfer to be efficient we demand the mesh distribution to be as nested as possible:

(M3) Create nested partitionings of the triangulations:
$$x \in \mathcal{T}_{l-1}^p \quad \Rightarrow \quad x \in \mathcal{T}_l^p. \tag{6}$$

This demand is usually not feasible: The efficiency of multigrid methods relies on small coarse meshes. Often, the number of elements in the coarse mesh is smaller than the number of subdomains $\mathcal{M}_{\text{cpu}}$. Furthermore, using locally refined meshes the claim for a nested partitioning contravenes the claim for a balanced partitioning of every level. In Section 3.4 we will explain our approach to fulfill the three mesh demands **(M1)**, **(M2)** and **(M3)** as good as possible.

3.3. The interface exchange operator

One of the basic operators in the parallel multigrid method is the exchange of node values across the interfaces. E.g. to guarantee the overlapping partitioning of vectors after the matrix-vector product:
$$\mathbf{y}_l^p = \mathcal{R}_l^p \sum_{q=1}^{\mathcal{M}_l} \mathcal{P}_l^q \bar{\mathbf{y}}_l^q.$$

For a node x_l^i on the interface $\mathcal{I}_l^p$, this operator adds all the values $\mathbf{u}_l^q(x_l^i)$ from adjacent subdomains q with $x_l^i \in \mathcal{T}_l^q$:
$$(\mathbf{u}_l^p)_i = \sum_{x_j^q \in \mathcal{T}_l^q:\ x_j^q = x_i^p} (\mathbf{u}_l^q)_j.$$

In the worst case, if every subdomain touches every other subdomain, this is an all-to-all communication. Usually however every subdomain has a common interface only with a small number of neighboring domains. For every node x_l^i on the interface between at least two subdomains, let $\mathcal{M}_l(x_l^i) \subset \{1, \dots, \mathcal{M}_l\}$ be the set of subdomains containing the node and let $\#M_l(x)$ be bounded by:

$$\#M_l(x) \leq C_{\text{nei}}, \quad \forall x \in \mathcal{T}_l,\ \forall l = 0, \dots, L.$$

In [17] an algorithm is described which creates a communication network to process as many interface in parallel as possible. The overall communication effort depends on

$$W_{\text{int}}(\mathcal{T}_l) = O(C_{\text{nei}} \cdot \max_{q \in \{1,\dots,\mathcal{M}_l\}} (\#I_l^q)),$$

the product of the maximum interface size and the maximum number of neighbors a subdomain can have.

3.4. Partitioning of the meshes

This section is devoted to the partitioning of the mesh hierarchy. In the previous discussion we have collected the three objectives **(M1)**-**(M3)**, see (4), (5), (6) for the mesh partitioning to yield an efficient parallel algorithm. The first two objectives **(M1)** and **(M2)** can be transformed into a standard graph partitioning problem: *create a balanced partitioning with minimal edge-cut*. The third task, the generation of a nested partitioning is harder to accomplish. On structured meshes, one could just partition the coarse mesh $\mathcal{T}_0$ and carry over this partitioning to all the finer meshes $\mathcal{T}_l$ in the following way: If the element $K \in \mathcal{T}_{l-1}$ belongs to subdomain $p \in \{1, \dots, \mathcal{M}_{l-1}\}$, all the children $K^i \in \mathcal{T}_l$ are assigned to subdomain $\mathcal{T}_l^p$. All the partitionings would be nested and **(M3)** would be fulfilled perfectly.

This easy algorithm does not work, if the coarse mesh is too coarse to make a balanced partitioning possible, e.g. if $\mathcal{N}_0 < \mathcal{M}_{\text{cpu}}$. With respect to locally refined meshes this algorithm is not optimal, since it is possible, that the finer meshes $\mathcal{T}_L$ are mostly refined in certain regions all belonging to the same subdomain in the coarse mesh. A non-balanced partitioning of the fine meshes, where most of the work happens would be the result.

In Bastian [1] a dynamic load balancing scheme for local multigrid methods on adaptively refined meshes is described. Prior to distributing the multigrid meshes, elements are gathered in clusters combining neighboring elements in both directions, neighbors on one level as well as neighbors across the mesh levels. If all elements in one cluster stay together on the same cpu, no communication will be necessary, neither for the mesh transfer nor for balancing on any interface. Schupp [18] used a similar setting for a parallel multigrid solver with dynamic load balancing. The main problem of this partitioning procedure is the setup of the clusters. These clusters can be considered as cones $\mathcal{K}$ with some element $K \in \mathcal{T}_l$ as the cone end. The cones then widen up with all descendents of K in finer meshes $\mathcal{T}_{l+1}, \dots, \mathcal{T}_L$.

The method of global coarsening simplifies the generation of a balanced, yet nested partitioning. For every fixed mesh level $k \in \{0, \dots, L\}$ we can build a set of cones $\mathcal{C}(k)$ which consists of all cones $\mathcal{K} \in \mathcal{C}(k)$ with the elements $K \in \mathcal{T}_k$ as ends and widening up to the finest mesh $\mathcal{T}_L$. If we partition these cones to $\mathcal{M}_{\text{cpu}}$ parts, we get a nested partitioning of all fine meshes $\mathcal{T}_k, \dots, \mathcal{T}_L$. On locally refined meshes we introduce weighted cones. The cone-weight of $\mathcal{K}$ is the number of elements $K \in \mathcal{K}$ that are fine-mesh elements in $\mathcal{T}_L$. A balanced partitioning of the weighted cones then results in balanced fine meshes. The mesh level k has to be chosen

large enough to get a sufficient number of cones to produce a balanced partition. The lower the mesh level k is chosen, the more meshes are distributed in a nested way:

Algorithm 5. *Distribution of the fine meshes*

1. *Get smallest number* $k \in \{0, \dots, L\}$ *with* $\#\mathcal{T}_k \geq C_{minpart} \cdot \mathcal{M}_{cpu}$.
2. *Construct set of cones* $\mathcal{C}(k)$.
3. *Construct weighted graph* $\mathcal{G}(k)$ *with nodes* $\mathcal{K} \in \mathcal{C}(k)$, *node-weights* $\omega(\mathcal{K}) = \#\mathcal{K}$ *and edges* $(\mathcal{K}, \mathcal{K}') \in \mathcal{G}(k)$ *if elements* K *and* K' *in* $\mathcal{T}_k$ *are adjacent. The edge-weight* $\omega(\mathcal{K}, \mathcal{K}')$ *is the number of contacts between elements* $K \in \mathcal{K}$ *and* $K' \in \mathcal{K}'$.
4. *Partition the graph* $\mathcal{G}(k) \rightarrow \mathcal{G}(k)^1, \dots, \mathcal{G}(k)^{\mathcal{M}_{cpu}}$ *to yield a partitioning with balanced node-weights and minimal edge-cut.*
5. *Carry the partitioning to* $\mathcal{T}_k, \dots, \mathcal{T}_L$*: for* $l = k, \dots, L$ *assign element* $K \in \mathcal{T}_l$ *to subdomain* $\mathcal{T}_l^q$, *if* $K \in \mathcal{K} \in \mathcal{G}(k)^q$.

Once the set of cones $\mathcal{C}(k)$ is distributed, we get a distribution of the meshes $\mathcal{T}_k, \dots, \mathcal{T}_L$. In a second step, this distribution has to be carried over to all coarse meshes $\mathcal{T}_0, \dots, \mathcal{T}_{k-1}$:

Algorithm 6. *Distribution of the coarse meshes*
For $l = k-1, \dots, 0$*:*

1. *For* $K \in \mathcal{T}_l$, *let* $K^i \in \mathcal{T}_{l+1}$ *be the children. Assign* K *to* $\mathcal{T}_l^p$, *where* p *is the subdomain* $\mathcal{T}_{l+1}^p$ *containing the most children* K^i.
2. *If* $\#\mathcal{T}_l^q < C_{minpart}$, *combine* $\mathcal{T}_l^q$ *and* $\mathcal{T}_l^{q'}$, *where* q' *is the index of the next-smallest subdomain.*

The first step assures that the partitioning is as nested as possible. The second step is called the *coarse mesh agglomeration* and assures that the meshes are not too small.

The process of mesh partitioning is not implemented in parallel. Further, we do not use *dynamic load balancing* and redistribution of partitionings. The mesh partitioning is carried out sequentially and the partitioned meshes are afterwards transferred to the different cpu's. For the simulation of small pde systems, this procedure will not result in a scalable parallel algorithm. Since we only consider complex multi-component flow problems, this approach is justifiable, see the numerical examples.

3.5. Distribution of locally refined meshes

To correctly and efficiently deal with hanging nodes some small variations of the mesh partitioning algorithms from the preceding sections are necessary. In the finite element simulation, hanging nodes are no real degrees of freedom. Instead the values are interpolated using neighboring degrees of freedom. To avoid additional communication here, we change the assemble of cones in Algorithm 5 in a way, that all information needed to handle hanging nodes are clustered in the cones. In [17] we explain details on this modification.

In Figure 3 we show the partitioning process in detail for the mesh hierarchy given in Figure 1. Let $\mathcal{M}_{\text{cpu}} = 2$ and $C_{\text{minpart}} = 8$ for this example. The mesh $\mathcal{T}_2$ is the smallest mesh still large enough to satisfy $\mathcal{M}_{\text{cpu}} C_{\text{minpart}} \geq \mathcal{N}_2$. These cones then need to be clustered to combine hanging nodes information. The weighted graph has four nodes and six edges. Finally this graph is distributed into two subdomains with weights 28 and 24. This describes steps 1. to 4. of Algorithm 5. It remains to carry this partitioning to the meshes of the hierarchy. This is demonstrated in Figure 4: The two fine meshes $\mathcal{T}_L$ and $\mathcal{T}_2$ are large enough to satisfy

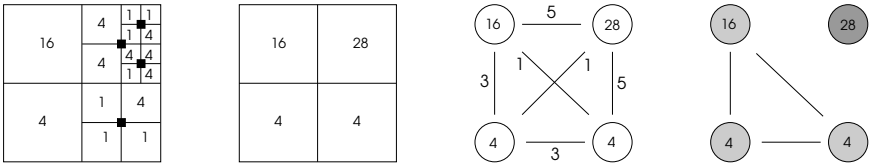

Figure 3. From left to right: the smallest mesh $\mathcal{T}_2$ with $\mathcal{N}_2 \geq C_{\text{minpart}}\mathcal{M}_{\text{cpu}}$, clustering of hanging nodes constraints, transformation to a corresponding weighted graph, partitioning of the graph.

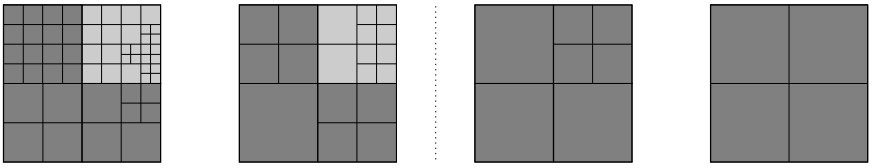

Figure 4. Partitioning of the complete mesh hierarchy. The partitioning of the left two meshes is carried over from Figure 3, the right two meshes are to small to satisfy $\mathcal{N}_l \geq C_{\text{minpart}}\mathcal{M}_{\text{cpu}}$.

$\mathcal{N}_l^p \geq C_{\text{minpart}}$ and the partitioning can be directly carried over. The two coarse meshes are too small and coarse mesh agglomeration is applied: just one subdomain is used.

3.6. Parallel efficiency

Losses in efficiency are either due to non-optimality of the parallelized algorithm or due to work and communication overhead produced by the parallelization. The used parallel algorithm only differs in the choice of the multigrid smoother, having a Schwarz type decomposition as basis.

Overhead is mainly communication overhead for exchange of values across the interface and for communication during the mesh transfer. In the following, we assume, that $N := \mathcal{N}_L = \mathcal{N}_h$ is the problem-size and that $N \gg \mathcal{M}_{\text{cpu}} \cdot C_{\text{minpart}}$. Then let $\mathcal{T}_k$ with $\mathcal{N}_k \geq M_{\text{cpu}} \cdot C_{\text{minpart}}$ be the set of cones used for the decomposition and C_{minpart} large enough to produce a balanced partitioning with local problem sizes:

$$\mathcal{N}_l^p \approx \frac{\mathcal{N}_l}{\mathcal{M}_{\text{cpu}}}, \quad l \geq k,\ p = 1, \ldots, \mathcal{M}_l.$$

First we discuss the parallel overhead on the fine meshes $l = k, \ldots, L$ where the partitioning is balanced and $P = \mathcal{M}_{\text{cpu}}$ cpu's are used. The overhead emerges from communication in the interface exchange operator (Section 3.3) and in the mesh-transfer (Section 3.2). For fine meshes with a nested partitioning $l \geq k$, all additional work is due to exchange of values along the interface. The set of nodes on the interface of a subdomain $\mathcal{T}_l^p$ is a lower-dimensional entity,

$$\#\mathcal{I}_l^p = O\left((\mathcal{N}_l^p)^{\frac{d-1}{d}}\right),$$

where d is the spatial dimension. Considering systems of $\mathcal{N}_c$ coupled partial differential equations, every subdomain has to exchange $O(\mathcal{N}_c \cdot \#\mathcal{I}_l^p)$ values with adjacent subdomains. Using the distributed communication network mentioned in Section 3.3 this communication is

done in at most C_{nei} steps leading to an overall communication work for the interface exchange operator of

$$W_{\text{int}}^{\text{comm}}(\mathcal{T}_l, P) = c_{\text{comm}} O\left(\mathcal{N}_c \cdot C_{\text{nei}} \left(\frac{\mathcal{N}_l}{P}\right)^{\frac{d-1}{d}}\right)$$

3.6.1. Parallel efficiency of the matrix-vector product For a system of $\mathcal{N}_c$ partial differential equations, the block-matrix on mesh level $\mathcal{T}_l$ has $\mathcal{N}_l$ rows, each with C_{row} entries (depending on the finite element space). The matrix entries are matrices of size $\mathbf{A}_{ij} \in \mathbb{R}^{\mathcal{N}_c \times \mathcal{N}_c}$. Usually we have $C_{\text{row}} \approx (2r+1)^d$, where d is the spatial dimension and r is the polynomial degree. The numerical work for a matrix-vector product is $O(C_{\text{row}}^2 \mathcal{N}_c^2 \mathcal{N}_l)$. In the parallel version, the numerical work is equally split to P cpu's and the overall effort is given by:

$$W_{\text{m-v}}(\mathcal{T}_l, P) = O\left(c_{\text{num}} C_{\text{row}}^2 \mathcal{N}_c^2 \frac{\mathcal{N}_l}{P} + c_{\text{comm}} \mathcal{N}_c \cdot C_{\text{nei}} \left(\frac{\mathcal{N}_l}{P}\right)^{\frac{d-1}{d}}\right).$$

and the parallel efficiency by:

$$E_{\text{m-v}}(\mathcal{T}_l, P) = \frac{1}{1 + \frac{c_{\text{comm}}}{c_{\text{num}}} \cdot \frac{C_{\text{nei}}}{C_{\text{row}}^2 \mathcal{N}_c} \left(\frac{P}{\mathcal{N}_l}\right)^{\frac{1}{d}}}.$$

Usually – depending on the architecture of the computer system – we have $c_{\text{comm}} \gg c_{\text{num}}$. All the other constants however are in favor of efficiency for complex systems. For three dimensional problems using quadratic finite elements, we have $C_{\text{nei}} \approx 6$ and $C_{\text{row}} \approx 125$. For the Navier-Stokes equations it is $N_{\text{comp}} = 4$ and for the chemical reactive flow example in Section 5.1, we have $\mathcal{N}_c = 43$. Thus, we have for Navier-Stokes equations (NS) and for the reactive flow equations (RF)

$$C_{\text{m-v}}^{\text{NS}} = \frac{C_{\text{nei}}}{C_{\text{row}}^2 \mathcal{N}_c} = \frac{6}{125^2 4} \approx 10^{-4}, \quad C_{\text{m-v}}^{\text{RF}} = \frac{C_{\text{nei}}}{C_{\text{row}}^2 \mathcal{N}_c} = \frac{6}{125^2 43} \approx 10^{-5},$$

and we get a good scalability if the ratio of problem size and number of CPU's is constant.

3.6.2. Parallel efficiency of matrix and residual assembly Besides the linear algebra part, finite element applications spend a large share of time for the assembly of the system matrix and for the integration of nonlinear residuals. Here we only analyze the integration of residuals, which is the harder task in terms of parallelization since the amount of sequential numerical work to be done is less. On a mesh $\mathcal{T}_l$ we have to compute

$$(\mathbf{r}_l)_j = a(u_h)(\phi_l^j), \quad \forall j = 1, \ldots, N_l.$$

The numerical integration is done locally on every element $K \in \mathcal{T}_l$ by a Gauss-rule. For finite elements of degree r in d space dimensions, Gauss-rules with

$$C_{\text{gauss}} = (2r)^d$$

integration points per element are used. The evaluation of the bi-linear form $a(\cdot)(\cdot)$ in every Gauss-point takes C_{form} operations, where C_{form} can vary between 5 for the simple Laplace-equation and $\gg 1000$ for complicated nonlinear equations (like the reactive flow equation in

Section 5.1). For a coupled system of $\mathcal{N}_c$ equations, the sequential work for the assemble of the residual is given by

$$W_{\text{residual}}(\mathcal{T}_l) = O\left(c_{\text{num}} C_{\text{gauss}} C_{\text{form}} \mathcal{N}_c^2 \mathcal{N}_l\right).$$

In the parallel version the local numerical work is again distributed in an optimal sense. The communication overhead is due to exchange of interface values. We thus get as parallel efficiency:

$$E_{\text{residual}}(\mathcal{T}_l, P) = \frac{1}{1 + \frac{c_{\text{comm}}}{c_{\text{num}}} \frac{C_{\text{nei}}}{C_{\text{gauss}} C_{\text{form}} \mathcal{N}_c} \left(\frac{P}{\mathcal{N}_l}\right)^{\frac{1}{d}}}.$$

For quadratic finite elements in three dimensions we have $C_{\text{gauss}} = 64$. For the Navier-Stokes equations it is $C_{\text{form}} \approx 20$ for the reactive flow system (RF) $C_{\text{form}} \approx 5\,000$:

$$C_{\text{residual}}^{\text{NS}} = \frac{C_{\text{nei}}}{C_{\text{gauss}} C_{\text{form}} \mathcal{N}_c} \approx 10^{-3}, \quad C_{\text{residual}}^{\text{RF}} = \frac{C_{\text{nei}}}{C_{\text{gauss}} C_{\text{form}} \mathcal{N}_c} \approx 10^{-7}.$$

3.6.3. Parallel efficiency on the coarse meshes and the full multigrid method In the case of balanced partitioning, all numerical algorithms based on local calculations followed by an exchange of interface values show a parallel efficiency of

$$E(\mathcal{T}_l, P) = \frac{1}{1 + c\left(\frac{P}{\mathcal{N}_l}\right)^{\frac{1}{d}}},$$

with a small constant c. On coarse meshes $\mathcal{T}_l$ with $l < k$ we use a lower number of cpu's than on the fine meshes, thus $P_l < P = \mathcal{M}_{\text{cpu}}$, and the parallel efficiency is limited by:

$$E(\mathcal{T}_l, P_l, P) = \frac{1}{\frac{P}{P_l}\left(1 + c\left(\frac{P}{\mathcal{N}_l}\right)^{\frac{1}{d}}\right)} \leq \frac{P_l}{P}$$

The overall sequential work for the multigrid method on L levels is given by

$$W_{\text{mg}}(\mathcal{T}_0, \ldots, \mathcal{T}_L) = c \sum_{l=0}^{L} \mathcal{N}_l \approx C_{\text{mg}} \mathcal{N}_L.$$

where C_{mg} is a constant depending on the growth ratio between two consecutive meshes $\mathcal{N}_l$ and $\mathcal{N}_{l+1}$. In the parallel version we get

$$W_{\text{mg}}(P_0, \ldots, P_L, \mathcal{T}_0, \ldots \mathcal{T}_L) = \sum_{l=0}^{L} \left(\frac{\mathcal{N}_l}{P_l} + c\left(\frac{\mathcal{N}_l}{P_l}\right)^{\frac{d-1}{d}}\right)$$

and by using $\mathcal{N}_l / P_l = C_{\text{minpart}}$ for all coarse meshes $l < k$ we get

$$W_{\text{mg}}(P, \mathcal{T}_0, \ldots, \mathcal{T}_L) \approx C_\alpha C_{\text{minpart}} + C_\alpha \left(\frac{N}{P} + C_\alpha \left(\frac{N}{P}\right)^{\frac{d-1}{d}}\right),$$

to get the overall parallel efficiency

$$E_{\text{mg}}(P, \mathcal{T}_0, \ldots, \mathcal{T}_L) \approx \frac{1}{1 + C_{\text{minpart}} \frac{P}{N} + c\left(\frac{P}{N}\right)^{\frac{1}{d}}}.$$

For $N/P \gg C_{\text{minpart}}$ we get a good parallel efficiency of the overall multigrid scheme.

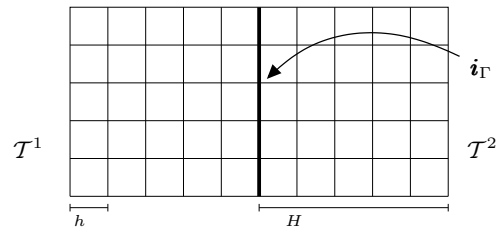

Figure 5. Uniform mesh and uniform mesh-distribution

4. Analysis of the parallel multigrid-smoother

In this section we analyze the convergence of the parallel multigrid-smoother, Algorithm 4, for the Laplace equation. Let $\boldsymbol{b}$ be the right hand side and $\boldsymbol{u}$ the solution before smoothing. Then, we can write the residual $\boldsymbol{r}$ before smoothing, the update $\boldsymbol{w}$ and the residual $\bar{\boldsymbol{r}}$ after smoothing as follows:

$$\boldsymbol{r} = \boldsymbol{b} - \sum_q \mathcal{P}^q \boldsymbol{A}^q \boldsymbol{u}^q, \quad p = 1, \dots, P: \ \overline{\boldsymbol{A}}^p \boldsymbol{w}^p = \boldsymbol{r}^p, \quad \bar{\boldsymbol{r}} = \boldsymbol{b} - \sum_q \mathcal{P}^q \boldsymbol{A}^q (\boldsymbol{u}^q + \boldsymbol{w}^q). \tag{7}$$

Here, as a first step, we have replaced the incomplete LU-decomposition of $\overline{\boldsymbol{A}}^p$ by the real inverse of the matrix. We remind, that $\overline{\boldsymbol{A}}^p$ is the node-wise restriction of $\boldsymbol{A}$ to the subdomain $\mathcal{T}^p$ and corresponds to a Dirichlet-matrix (see Section 3.1). By $\widehat{\boldsymbol{A}}^p := \overline{\boldsymbol{A}}^p - \boldsymbol{A}^p$ we denote the difference. This matrix $\widehat{\boldsymbol{A}}^q$ only acts on the interface-nodes.

We want to relate the residuals $\boldsymbol{r}$ and $\bar{\boldsymbol{r}}$ before and after the smoothing step. From (7) we derive

$$\bar{\boldsymbol{r}} = \boldsymbol{r} - \sum_q \mathcal{P}^q \boldsymbol{A}^q \boldsymbol{w}^q. \tag{8}$$

We split the local matrices via $\boldsymbol{A}^q = \overline{\boldsymbol{A}}^q - \widehat{\boldsymbol{A}}^q$ and using the relation $\overline{\boldsymbol{A}}^q \boldsymbol{w}^q = \boldsymbol{r}^q$ we get

$$\bar{\boldsymbol{r}} = \boldsymbol{r} - \sum_q \mathcal{P}^q (\boldsymbol{r}^q - \widehat{\boldsymbol{A}}^q [\overline{\boldsymbol{A}}^q]^{-1} \boldsymbol{r}^q). \tag{9}$$

The old residual $\boldsymbol{r}$ is distributed by $\boldsymbol{r}^p = \mathcal{R}^p \boldsymbol{r}$ and the sum $\boldsymbol{r} \neq \sum_q \mathcal{P}^q \boldsymbol{r}^q$ includes the interface values multiple times. By $\mathcal{I}^p : \mathcal{T}^q \to \mathcal{T}^p$ we denote the operator which restricts a grid-vector to the interface nodes and scales every value by the number of neighbors in such a way that holds:

$$\sum_p \mathcal{P}^p \boldsymbol{x}^p = \boldsymbol{x} + \sum_p \mathcal{P}^p \mathcal{I}^p \boldsymbol{x}.$$

If for example every boundary value of a domain touches one other domain, $\mathcal{I}^p$ is given by

$$\mathcal{I}^p \boldsymbol{x}^p = \frac{1}{2} \boldsymbol{x}^p \Big|_{\partial \mathcal{T}^q}.$$

Using this interface operator, we can transform (9) to get

$$\bar{\boldsymbol{r}} = (1-1)\boldsymbol{r} - \sum_q \mathcal{P}^q \Big\{ \mathcal{I}^q \boldsymbol{r}^q - \widehat{\boldsymbol{A}}^q [\overline{\boldsymbol{A}}^q]^{-1} \boldsymbol{r}^q \Big\}. \tag{10}$$

The first term in $\overline{\boldsymbol{r}}$ is zero. The second term only contains values in interface-nodes, since the matrices $\widehat{\boldsymbol{A}}^q$ and the interface operator $\mathcal{I}^q$ only act here and are zero elsewhere.

To analyze these remaining terms, we introduce a discrete Fourier basis of the subdomains $\mathcal{T}^p$. We assume, that $\mathcal{T}^p = (0,H)^2$ has N_p^2 nodes with local mesh-size $h = H/(N_p-1)$. See Figure 5 for an easy example with only two subdomains. For $\boldsymbol{\theta} = (\theta_x, \theta_y) \in \{1,\dots,N_p\}^2$ we define the discrete Fourier grid-functions:

$$\Phi^p(\boldsymbol{\theta})(\boldsymbol{i}) = \sin\left(\frac{\pi\theta_x(i_x-1)}{N_p+1}\right)\sin\left(\frac{\pi\theta_y(i_y-1)}{N_p+1}\right), \quad \boldsymbol{i} = (i_x,i_y) \in \{0,\dots,N_p+1\}^2.$$

These functions are zero for $i_x, i_y \in \{0, N_p+1\}$ which corresponds to the boundary of the domain $\partial[-h,H+h]^2$, one layer of elements across the interface to the neighboring subdomain. Using this notation, a finite element vector $\boldsymbol{v}^p$ on $\mathcal{T}^p$ can be written as

$$\boldsymbol{v}^p = \sum_{\boldsymbol{\theta}} v^p_{\boldsymbol{\theta}} \Phi^p(\boldsymbol{\theta}), \quad v^p_{\boldsymbol{\theta}} \in \mathbb{R} \text{ with } \boldsymbol{\theta} \in \{1,\dots,N_p\}^2. \tag{11}$$

On these uniform meshes, the matrix $\overline{\boldsymbol{A}}^p$ for the Laplace equation discretized with piecewise bilinear finite elements in stencil notation reads:

$$\overline{\boldsymbol{A}}^p = \frac{1}{3}\begin{bmatrix} -1 & -1 & -1 \\ -1 & 8 & -1 \\ -1 & -1 & -1 \end{bmatrix}.$$

Using the basic principles of trigonometric functions, the action of $\overline{\boldsymbol{A}}^p$ on a Fourier grid-function $\Phi^p(\boldsymbol{\theta})$ can by calculated as

$$\begin{aligned} &\overline{\boldsymbol{A}}^p\Phi^p(\boldsymbol{\theta}) = \lambda(\boldsymbol{\theta})\Phi^p(\boldsymbol{\theta}), \\ &\lambda(\boldsymbol{\theta}) := \frac{1}{3}\left\{8 - 2\cos\left(\frac{\pi\theta_x}{N_p+1}\right) - 2\cos\left(\frac{\pi\theta_y}{N_p+1}\right) - 4\cos\left(\frac{\pi\theta_x}{N_p+1}\right)\cos\left(\frac{\pi\theta_y}{N_p+1}\right)\right\} \end{aligned} \tag{12}$$

Writing the residual $\boldsymbol{r}$ before smoothing like (11) in the Fourier basis and by using (12) we get an explicit presentation of the local update $\widetilde{\boldsymbol{w}}^p$:

$$\boldsymbol{r}^p = \sum_{\boldsymbol{\theta}} r_{\boldsymbol{\theta}}\Phi^p(\boldsymbol{\theta}) \quad \Rightarrow \quad \widetilde{\boldsymbol{w}}^p = \sum_{\boldsymbol{\theta}} \frac{r_{\boldsymbol{\theta}}}{\lambda(\boldsymbol{\theta})}\Phi^p(\boldsymbol{\theta}). \tag{13}$$

To estimate the remaining term in (10) we need to describe the action of the difference-matrix $\widehat{\boldsymbol{A}}^p = \overline{\boldsymbol{A}}^p - \boldsymbol{A}^p$. Let $\boldsymbol{i}_\Gamma \in \mathcal{T}^p$ be a point on a vertical interface touching one neighbor (see Figure 5). Here, the matrix $\widehat{\boldsymbol{A}}^p$ in stencil notation is given by (as seen from the left subdomain):

$$\widehat{\boldsymbol{A}}^p(\boldsymbol{i}_\Gamma) = \frac{1}{3}\left[\begin{array}{cc} 0 & -\frac{1}{2} \\ 0 & 4 \\ 0 & -\frac{1}{2} \end{array}\right],$$

Like (12) we get for each Fourier component $\Phi^p(\boldsymbol{\theta})$:

$$\widehat{\boldsymbol{A}}^p(\boldsymbol{i}_\Gamma)\Phi^p(\boldsymbol{\theta}) = \mu(\boldsymbol{\theta})\Phi^p(\boldsymbol{\theta}), \quad \mu(\boldsymbol{\theta}) := \frac{1}{3}\left\{4 - \cos\left(\frac{\pi\theta_y}{N_p+1}\right)\right\}. \tag{14}$$

Hence, we can combine (11), (12), (13) and (14) to get for the Fourier components $\bar{r}_{\boldsymbol{\theta}}$ of the new residual (assuming the interface is touched by two subdomains)

$$\mathcal{I}^q \boldsymbol{r}^q - \widehat{\boldsymbol{A}}^q [\overline{\boldsymbol{A}}^q]^{-1} \boldsymbol{r}^q = \sum_{\boldsymbol{\theta}} \left(\frac{1}{2} - \frac{\mu(\boldsymbol{\theta})}{\lambda(\boldsymbol{\theta})} \right) r^q_{\boldsymbol{\theta}} \Phi^q(\boldsymbol{\theta}).$$

For all high frequencies we get by simple estimation:

$$\left| \frac{1}{2} - \frac{\mu(\boldsymbol{\theta})}{\lambda(\boldsymbol{\theta})} \right| \leq \frac{1}{8} \text{ for } \boldsymbol{\theta} \in \{N_p/2, \ldots, N_p\}^2.$$

Finally, for the overall residual combining both sides of the interface, the residual is reduced by the factor 4

$$|\bar{r}^p_{\boldsymbol{\theta}}| \leq \frac{1}{4} |r^p_{\boldsymbol{\theta}}|, \tag{15}$$

which yields a fixed convergence rate for all high frequencies. This estimate does not depend on the mesh-size h or the size of the subdomains H and is always valid for this minimal-overlap configuration.

At last, we discuss the case, where the local update $\boldsymbol{w}^q$ is not computed exactly, but by an incomplete LU-iteration:

$$\boldsymbol{w}^{q,(\nu)} = \mathcal{S}^\nu(\overline{\boldsymbol{A}}^q) \boldsymbol{r}^q.$$

Then, we introduce the additional error term

$$\boldsymbol{w}^{q,(\nu)} = \boldsymbol{w}^q + (\mathcal{S}^\nu(\overline{\boldsymbol{A}}^q) - [\overline{\boldsymbol{A}}^q]^{-1}) \boldsymbol{r}^q.$$

This local ILU-iteration does not depend on the partitioning of the domain, or the overlap, and thus there exists a $\nu_0 \in \mathbb{N}$, such that:

$$\|(\mathcal{S}^\nu(\overline{\boldsymbol{A}}^q) - [\overline{\boldsymbol{A}}^q]^{-1}) \boldsymbol{r}^q\| \leq \frac{1}{4} \|\boldsymbol{r}^q\| \text{ for } \nu \geq \nu_0.$$

Combining this estimate with (15), the parallel multigrid smoother applied to the Laplace equation exhibits a reduction rate smaller than $\frac{1}{2}$ for all high frequent error contributions.

5. Numerical examples

5.1. Simulation of chemically reactive flows

In this section we present the simulation of a Methane burner under consideration of a detailed chemical reaction system involving $N_{\mathrm{CS}} = 39$ chemical species and 302 elementary chemical reactions. The equations for modeling reactive flows are the Navier-Stokes equations with an energy equation for the temperature and one diffusion-reaction-transport equation for every chemical species. Since the flow is comparatively slow, and changes in the density are mainly due to temperature changes, the equations are written in the Low-Mach-Number limit splitting the pressure into a hydrodynamical p_{hyd} and into a thermodynamical p_{th} part $p = p_{\mathrm{th}} + p_{\mathrm{hyd}}$,

see [5]:

$$\begin{aligned}
\nabla \cdot \mathbf{v} + \frac{1}{\bar{m}}\mathbf{v} \cdot \nabla \bar{m} - \frac{1}{T}\mathbf{v} \cdot \nabla T &= 0, \\
\rho \partial_t \mathbf{v} + \rho v \cdot \nabla \mathbf{v} - \nabla \cdot (\mu \nabla \mathbf{v}) + \nabla p_{\mathrm{hyd}} &= \rho g, \\
\rho c_p \partial_t T + \rho c_p \mathbf{v} \cdot \nabla T - \nabla \cdot \lambda \nabla T &= f_T(T, w), \\
\rho \partial_t w_k + \rho \mathbf{v} \cdot \nabla w_k + \nabla \cdot \mathcal{F}_k &= f_k(T, w),\ k = 1 \ldots, N_{CS} - 1, \\
\rho &= \frac{p\bar{m}}{RT}.
\end{aligned}$$

Here, $\mathbf{v}$ is the velocity, T the temperature, w_k, $k = 1, \ldots, N_{CS}$ are the mass fractions of the species mixture, $\bar{m}$ the mean molecular weight of the mixture and ρ the mixtures density. All together the system includes $\mathcal{N}_c = 43$ coupled solution components. The chemical production terms f_k are given by

$$f_K(T, w) := m_k \sum_{r=1}^{N_{CR}} \left\{ (\nu_{rk} - \tilde{\nu}_{rk}) k_r(T) \prod_{j=1}^{N_{CS}} c_j^{\nu_{rj}(w)} \right\},$$

where for every reaction $r = 1, \ldots, N_{CR}$, ν_{rk} are the stoichiometric indices of species k and c_j is the concentration and m_j the molecular weight of species j. The reaction rate is given by an Arrhenius law

$$k_r(T) = A_r T^{\beta_r} \exp\left\{ \frac{-E_{ar}}{RT} \right\}.$$

The values A_r, E_{ar} and β_r are read from tables. For evaluating the residual of the equations in one point, for every of the N_{CS} species every of the N_{CR} reactions has to be evaluated where all species can couple. Reactive flow calculations thus show an enormous local computational effort. Our example uses a 39 species reaction model considering 302 chemical reactions. The reaction system is usually very sparse (not all species appear in every reaction, usually only 4). Here, the average numerical effort to evaluate the complete reaction system in every Gauss-point is $39 \cdot 302 \cdot 4 \approx 50\,000$.

In Figure 6 we show the model of the Methane burner under consideration. On the right side of the figure the reduced three dimensional computational domain is shown. With the three different lamella, the cooling pipe it features the characteristic properties of the geometry.

In [17, 7] a numerical study of this Methane burner has been performed. In particular it has been found out, that considering the full three dimensional geometry is compulsive. For obtaining results with an estimated error tolerance of $\leq 5\%$ locally refined meshes with about 300 000 mesh elements where necessary. For storing the system matrix more than $30GB$ of memory was used. The calculations have been done in 2005 on a Linux-Cluster with 32 nodes, running at 2.4 GHz each and connected with a standard Gigabit Ethernet network.

In Table I results from the calculations are given. Due to the very large memory consumption systematical studies on the parallel efficiency are not possible. We thus show results from the progress of the adaptive algorithm, using different numbers of cpu's. In the last column we give an index for the parallel efficiency which measures the efficiency compared to the first row of the table:

$$E_{\mathrm{i}}(P) := \frac{P_S \frac{T_S}{N_S}}{P \frac{T_P}{N_P}},$$

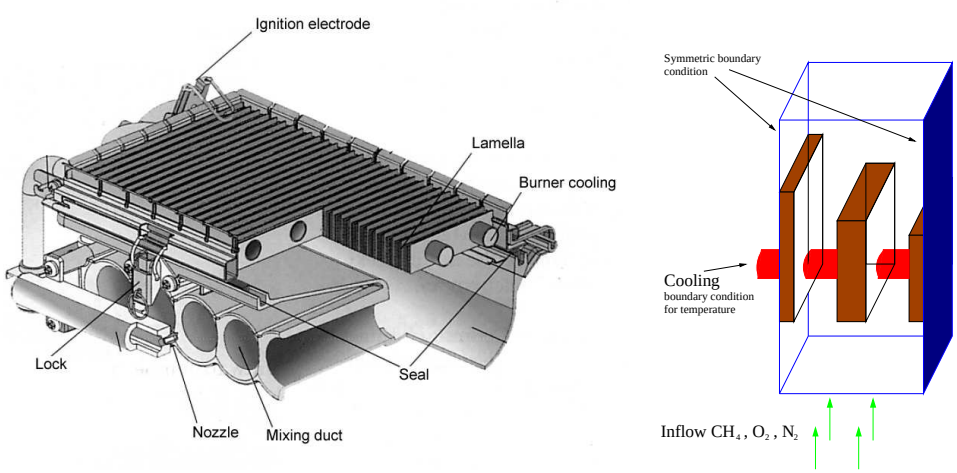

Figure 6. Sketch of the methane burner configuration and plot of the simplified computational domain.

Table I. Running times and memory consumption for the reactive flow simulation on locally refined meshes.

elements	unknowns	time (sec)	#CPU	memory	E_{i}
15 872	825 084	1 772	3	1 132 MB	1.00
29 648	1 505 946	1 583	5	2 286 MB	1.23
60 784	3 136 248	2 248	10	5 379 MB	0.90
197 816	9 863 082	6 096	10	17 328 MB	1.04
197 816	9 863 082	2 106	32	19 111 MB	0.94
291 102	14 299 478	4 681	18	25 858 MB	1.09
291 102	14 299 478	2 572	37	29 152 MB	0.97
291 102	14 299 478	1 581	64	34 512 MB	0.91

where $P_s = 3$, $T_S = 1772$ and $N_s = 825\,084$ and P_P, N_P and T_P are the number of cpu's used, the number of unknowns and the time spent in the parallel computations. The value $E_{\mathrm{i}} = 1$ indicates optimal iso-efficiency for $N/P = \mathrm{const}$. Here, the resulting values show nearly optimal efficiency. This is mainly due to the huge local effort connected with complex reactive flow simulations.

In Figure 7 we show some solution components of the simulation on adaptively refined meshes.

5.2. Simulation of ocean flows

In this section we will consider the primitive equations, see also [14]. They form the background of ocean simulation models like MOM3 [11], or ocean models as part of coupled atmosphere-ocean models, e.g. SPEEDO [19]. Basis of the primitive equations are the incompressible 3D

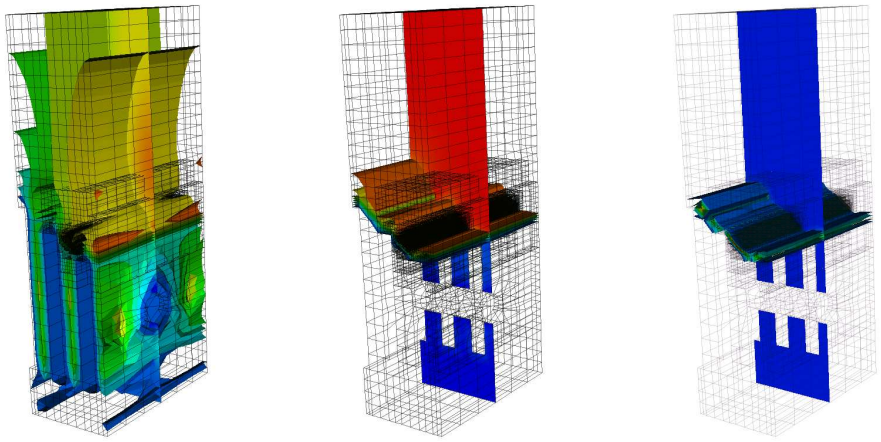

Figure 7. Velocity (left), temperature (middle) and concentration for Formaldehyde (right) for the Methane burner simulation.

Navier-Stokes equations in a rotating frame:

$$\begin{aligned} \nabla \cdot \mathbf{v} &= 0 \\ \rho_c \partial_t \mathbf{v} + \rho_c \mathbf{v} \cdot \nabla \mathbf{v} - \nabla \cdot (\mu \nabla \mathbf{v}) - f \mathbf{i}_3 \times \mathbf{v} + \nabla p &= \rho \mathbf{g} + \mathbf{\Phi} \\ \rho &= G(p). \end{aligned}$$

State variables are velocity $\mathbf{v}$, pressure p and density ρ. Model parameters are viscosity μ, mean density ρ_c, Coriolis parameter f and gravity $\mathbf{g}$, given as $\mathbf{g} := (0, 0, -g)^\top$ with gravity constant g. The vector $\mathbf{i}_3$ denotes the vertical unit vector. We will neglect large scale effects like tidal and centrifugal forces $\mathbf{\Phi}$ and Coriolis forces, i.e. we set $\mathbf{\Phi} = \mathbf{0}$ and disregard the term $f\mathbf{i}_3 \times \mathbf{v}$. Density ρ is determined in an equation of state. In ocean modeling lots of different approximate formulae for this equation are applied [14]. We will employ a polynomial approach.
An observed feature of large-scale motions in the ocean is its small aspect ratio. This means, that the characteristic vertical length scale D is much smaller than the horizontal, L, one, i.e. $\delta := D/L \ll 1$. Scaling arguments lead to a neglection of vertical acceleration, see [13]. Thus the third momentum equation becomes

$$\partial_z p = -\rho g,$$

the hydrostatic balance. We denote the pressure occurring due to gravitational acceleration as hydrostatic pressure p_{hs}.
Furthermore we enrich the given set of equations by conservation equations for potential temperature θ and salinity S, both being important for the (thermo-) dynamic behavior of oceanic systems.
As we are not able to resolve motions of all appearing scales, we have to parameterize the smallest ones, which have an important impact on larger, resolvable scales. For parameterization of this turbulent behavior we use a simplified Smagorinsky model, see [4].

I.e. we add the diffusive term $\nabla \cdot (\nu_{turb} \nabla \tilde{\mathbf{v}})$ to the horizontal momentum equations. The value ν_{turb} is the parameter of turbulent viscosity and $\tilde{\mathbf{v}} := (v_1, v_2)^\top$ denotes the horizontal velocity field. The vertical velocity field is given by v_3. As kinematic viscosity is much smaller than the turbulent one, we neglect the former. Analogously we proceed with equations of potential temperature and salinity. The entire set of equations thus becomes

$$\begin{aligned} \nabla \cdot \mathbf{v} &= 0 \\ \rho_c \partial_t \tilde{\mathbf{v}} + \rho_c \mathbf{v} \cdot \nabla \tilde{\mathbf{v}} - \nabla \cdot (\mu_{turb} \nabla \tilde{\mathbf{v}}) + \widetilde{\nabla} p &= 0 \\ \partial_z p_{hs} &= -\rho g \\ \rho_c \partial_t \theta + \rho_c \mathbf{v} \cdot \nabla \theta - \nabla \cdot (\kappa_{turb} \nabla \theta) &= 0 \\ \rho_c \partial_t S + \rho_c \mathbf{v} \cdot \nabla S - \nabla \cdot (\zeta_{turb} \nabla S) &= 0 \\ \rho &= G(p, \theta, S). \end{aligned} \tag{16}$$

Here, $\widetilde{\nabla}$ is defined as $\widetilde{\nabla}\phi := (\partial_x \phi, \partial_y \phi)^\top$ for scalar field $\phi : \Omega \subset \mathbb{R}^3 \to \mathbb{R}$. The equation of state will be given by a linearized equation for buoyancy:

$$\rho = \alpha(\theta - \theta_c) - \beta(S - S_c)$$

with positive constant coefficients α and β of thermal and haline expansion and reference values for potential temperature, θ_c, and salinity, S_c. We consider domains $\Omega \subset \mathbb{R}^3$, that can be formulated as

$$\Omega := \{\mathbf{x} \in \mathbb{R}^3 \,|(x, y) \in \widetilde{\Omega} \text{ and } z \in (-D(x, y), 0)\},$$

for 2D domains $\widetilde{\Omega}$ and functions $D : \widetilde{\Omega} \to \mathbb{R}^+$. Due to the small aspect ratio, $\delta \ll 1$, domain $\widetilde{\Omega}$ and function D have to satisfy $\max_{(x,y)\in\widetilde{\Omega}} D(x, y) \ll diam(\widetilde{\Omega})$. In particular we neglect variations from plain sea surface due to wave formation (rigid lid approximation). We result in a natural boundary condition for v_3:

$$v_3 = 0 \quad \text{ on } \{\mathbf{x} \in \partial\Omega \,|\, z \in \{-D(x, y),\, 0\}\ \}.$$

Together with the incompressibility constraint and the assumption of continuous differentiability in z-direction of v_3 we have

$$\int_{z=-D(x,y)}^{0} \widetilde{\nabla} \cdot \tilde{\mathbf{v}}\, dz = 0, \quad \forall (x, y) \in \widetilde{\Omega}.$$

This demand is an auxiliary tool for development of an efficient algorithm for the given problem.

To solve the introduced problem, a standard incremental pressure-correction projection scheme has been implemented. Projection schemes, as invented in the late 1960's, see also [12], [15], [16], aim to overcome the computational difficulties and decouple the pressure from the velocity field, which are interdependent due to the incompressibility constraint. The resulting set of decoupled elliptic problems is supposed to be very efficient for large scale problems, see [12].

We suppose an equidistant decomposition of the given time interval $[0, T]$ with time steps of size k. The $(m + 1)$-rst iteration of the implemented algorithm is as follows: Let $(\mathbf{v}^m, p^m, \theta^m, S^m, \rho^m)$ be solution of the m-th iteration. Then

Algorithm 7. *Splitting scheme for the hydrostatic approximation*

(i) find $\widetilde{\mathbf{w}}^{m+1} := (\widetilde{w}_1^{m+1}, \widetilde{w}_2^{m+1})^\top$ *such that*

$$k^{-1}(\widetilde{\mathbf{w}}^{m+1} - \tilde{\mathbf{v}}^m) + (\mathbf{v}^m \cdot \nabla)\widetilde{\mathbf{w}}^{m+1} - \nabla \cdot (\frac{\mu_{turb}}{\rho_c}\nabla\widetilde{\mathbf{w}}^{m+1}) + \frac{1}{\rho_c}\widetilde{\nabla}\, p^m = 0,$$

with appropriate boundary conditions for $\widetilde{\mathbf{w}}^{m+1}$,

(ii) determine f_q^{m+1} *such that*

$$f_q^{m+1} = \int_{z=-D(x,y)}^{0} \nabla \cdot \widetilde{\mathbf{w}}^{m+1}\, dz$$

(iii) update horizontal velocities

$$\begin{aligned} -\Delta q^{m+1} &= f_q^{m+1}, & \partial_{\mathbf{n}} q^{m+1}|_{\partial\widetilde{\Omega}} &= 0 \\ \tilde{\mathbf{v}}^{m+1} &= \widetilde{\mathbf{w}}^{m+1} - \widetilde{\nabla}\pi_{3d}(q^{m+1}) \end{aligned}$$

(iv) find v_3^{m+1} *such that*

$$-\partial_z v_3^{m+1} = \widetilde{\nabla} \cdot \tilde{\mathbf{v}}^{m+1}, \qquad v_3^{m+1}|_{\partial\Omega_{bot}} = 0$$

(v) identify θ^{m+1} *and* S^{m+1} *such that*

$$\begin{aligned} k^{-1}(\theta^{m+1} - \theta^m) + (\mathbf{v}^{m+1} \cdot \nabla)\theta^{m+1} - \frac{\kappa_{turb}}{\rho_c}\Delta\theta^{m+1} &= 0, \\ k^{-1}(S^{m+1} - S^m) + (\mathbf{v}^{m+1} \cdot \nabla)S^{m+1} - \frac{\zeta_{turb}}{\rho_c}\Delta S^{m+1} &= 0, \end{aligned}$$

with appropriate boundary conditions for θ^{m+1} *and* S^{m+1},

(vi) u pdate pressure

$$\begin{aligned} \rho^{m+1} &= \alpha(\theta^{m+1} - \theta_c) - \beta(S^{m+1} - S_c), \\ \partial_z p_{hs}^{m+1} &= -g\rho^{m+1}, & p_{hs}^{m+1}|_{\partial\Omega_{top}} &= 0, \\ p^{m+1} &= p_{hs}^{m+1} + \pi_{3d}(q^{m+1}). \end{aligned}$$

The operator π_{3d}, used in steps *(iii)* and *(vi)* of algorithm, is given by

$$\pi_{3d}(\phi)(\mathbf{x}) := D^{-1}(x,y)\phi(x,y), \quad \forall\phi : \widetilde{\Omega} \to \mathbb{R} \quad \forall\mathbf{x} \in \Omega.$$

In *(i)* we compute vertical velocities, which are not divergence-free in vertical mean. In the second step we determine the right hand side f_q^{m+1} of the equation for the artificial pressure q^{m+1}. This pressure is used to update the horizontal velocities $\tilde{\mathbf{v}}^{m+1}$ in *(iii)*. In step *(iv)* the vertical velocity v_3^{m+1} is determined, such that the entire velocity field $\mathbf{v}^{m+1}$ is divergence free. Potential temperature and salinity are computed in *(v)*, which are used in *(vi)* to determine the density ρ^{m+1} and to update the pressure p^{m+1}.

Standard schemes for the instationary, incompressible three dimensional Navier-Stokes equations including equations for potential temperature and salinity use one system of three dimensional equations with six unknowns. Instead, the presented algorithm solves problems in three dimensions with two components each, one scalar three dimensional ode and two dimensional scalar Poisson-equations.

5.2.1. Example. The domain Ω is given by $\Omega := (0, 10\,000)^2 \times (-1\,000, 0)$. We denote $\Gamma_{top} := (0, 10\,000)^2 \times \{0\}$ and $\Gamma_{bot} := (0, 10\,000)^2 \times \{-1.000\}$. Model parameters are set to

$$\begin{aligned} &\rho_c = 1000 \qquad g = 9.81 \qquad \kappa_{turb} = 0.1 \qquad \zeta_{turb} = 0.1 \qquad \mu_{turb} = 0.1 \\ &\theta_c = 283 \qquad S_c = 0.035 \qquad \alpha = 0.2 \qquad \beta = 400, \end{aligned}$$

using SI units. Boundary conditions are set to

$$\begin{aligned} &\tilde{\mathbf{v}}|_{\Gamma_{top}} = (1,\, 0.1)^\top, \qquad \tilde{\mathbf{v}}|_{\Gamma_{bot}} = 0, \qquad v_3|_{\Gamma_{top}\cup\Gamma_{bot}} = 0, \qquad p_{hs}|_{\Gamma_{top}} = 0, \\ &\theta|_{\Gamma_{top}\cup\Gamma_{bot}} = 278, \qquad S|_{\Gamma_{top}} = 0.035, \quad S|_{\Gamma_{bot}} = 0.033. \end{aligned}$$

The remaining boundary conditions are *do-nothing* boundary conditions. Initial values are set to

$$\tilde{\mathbf{v}} = \frac{D(x,y)+z}{D(x,y)} \begin{pmatrix} 1 \\ 0.1 \end{pmatrix}, \qquad v_3 = 0, \quad p_{hs} = -\rho_c g\, z, \qquad \theta = 278 + \tilde{\theta}, \qquad S = 0.033 + \tilde{S}.$$

Again we use SI units. Functions $\tilde{\theta}$ and $\tilde{S}$ denote small oscillations in each space dimension.

In steps *(i)* and *(iv)* of Algorithm 7 systems of three dimensional convection diffusion equation with two solution components each are solved. These steps are parallelized as described in Section 3. In step *(iii)* a two dimensional Poisson equation has to be solved. Here we use no parallelization since the overall share of work is negligible, see Figure 9. In steps *(ii)* and *(iv)* a three-dimensional transport equation is solved. Actually, this equation can be split into lines in the z-direction and the problem resolves into a set of ordinary differential equations. These equations are solved in parallel. We alter the mesh distribution in Section 3.4 in a way, that every ode can be solved without communication. For this, the meshes are decomposed in the $x-y$ plane only, see Figure 8. The pressure and density update in step *(vi)* is of the same type and calculated using a set of decoupled ode's.

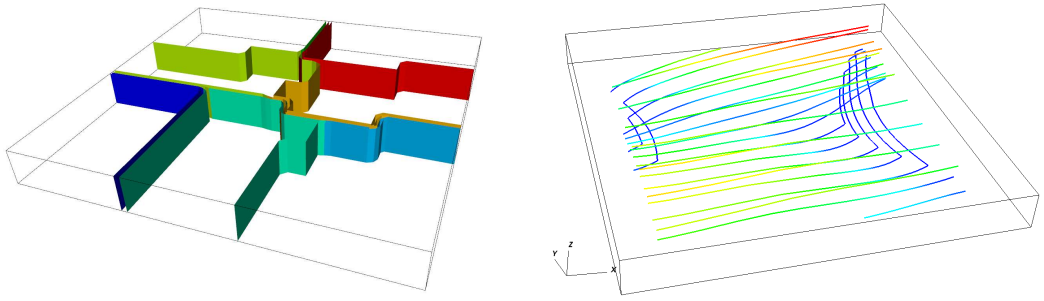

Figure 8. Left: partitioning of the domain into 7 subdomains. Right: streamlines of the solution.

In Tables II and III we collect running times for the example mentioned above. The times are given on two structured meshes and are times for one time-step. The iteration is split into the steps of Algorithm 7. The calculations in Table II where done on a quad oct-core Xeon machine running at 2.4 Mhz. The calculations from Table III have been performed on the Linux cluster *helics II*, see [20]. *helics II* is a cluster with 156 nodes connected with a

Table II. Running times for the hydrostatic approximation on the shared memory system.

elements	#CPU	*(i)*	*(ii)*	*(iii)*	*(iv)*	*(v)*	*(vi)*	total
131 072	1	103.1	3.8	0.41	4.0	101.1	4.5	216.9
131 072	2	54.9	2.0	0.44	2.0	53.7	2.3	115.3
131 072	4	31.1	1.1	0.47	1.1	28.1	1.3	63.0
131 072	8	16.8	0.6	0.41	0.6	15.9	0.7	35.0
131 072	16	12.8	0.5	0.45	0.5	10.3	0.6	25.1
1 198 372	1	982.1	30.9	4.01	31.1	940.1	38.9	2027.2
1 198 372	2	499.4	16.9	4.23	16.9	488.3	20.2	1045.9
1 198 372	4	263.8	8.7	4.10	8.7	253.5	11.1	549.9
1 198 372	8	131.0	4.3	3.23	4.4	145.3	5.7	294.0
1 198 372	16	75.2	2.5	2.98	2.5	85.5	3.6	172.3

Table III. Running times for the hydrostatic approximation on the pc-cluster *helics II*.

elements	#CPU	*(i)*	*(ii)*	*(iii)*	*(iv)*	*(v)*	*(vi)*	total
1 198 372	16	56.2	2.7	3.6	2.7	54.9	4.0	124.0
1 198 372	32	30.2	1.7	3.9	1.7	29.6	3.1	70.0
1 198 372	64	23.0	1.5	4.3	1.5	21.9	3.0	55.0

10G Myrinet highspeed network. Each node is dual dual-core AMD Opteron running at 2.8 GHz. For comparison we give the running times for the full Navier-Stokes system (16) on a sequential machine for one iteration:

elements	running time
16 384	143
131 072	1 107
1 048 576	6 986

These computations where done on the shared memory system (using 1 cpu). When using the splitting scheme, the computation on the mesh with 131 072 elements took only $216s$, nearly six times less than doing the full computation, see Table II.

In the left sketch of Figure 9 we plot the strictly sequential share of work in the overall algorithm used for solving the two dimensional Poisson problem. In the right sketch we show the parallel efficiency of the overall algorithm. For the computations on the Linux cluster *helics II* we use the sequential running time from Table II since we could not perform a sequential calculation on *helics II* due to limited memory resources. The nodes of *helics II* run at a higher cpu speed and the local memory connection is better.

On the large mesh, the overall parallel performance is very good using up to 32 cpu's on *helics II* and up to 8 cpu's on the shared memory system.

6. Conclusion

In this work we have presented the finite element toolbox *Gascoigne* using a parallel multigrid method on locally refined meshes. Focus of the software is the solution of very complex three

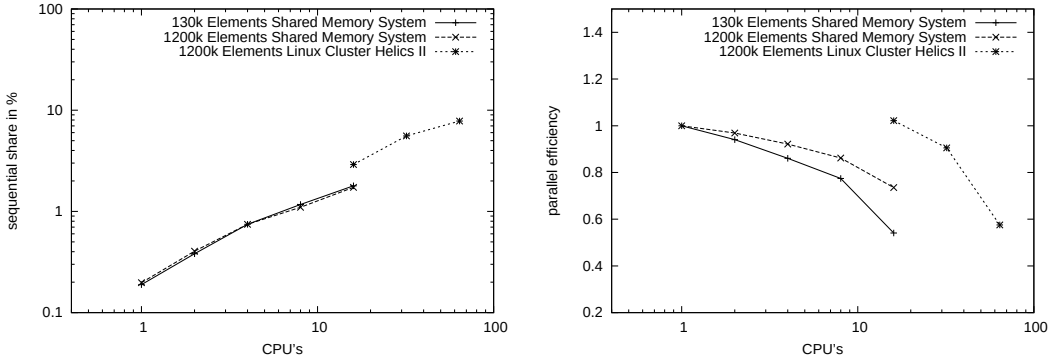

Figure 9. Left: sequential share of work for the 2D Poisson problem. Right: parallel efficiency of the complete algorithm.

dimensional (flow) problems. Especially when strong nonlinearities and local perturbations govern the character of the equations, the efficiency and strength of the implementation gets obvious. While other approaches aim at obtaining optimal parallel performance by using simple and fast numerical algorithms, we rely on robust implicit methods allowing for large time steps and local mesh adaptation. Our approach results in optimal parallel performance for very complex problems (like reactive flow simulations) and is still feasible and efficient for pure flow simulations like demonstrated in the last example.

REFERENCES

1. P. Bastian, *Parallele adaptive Mehrgitterverfahren*, Teubner Skripten zur Numerik, Stuttgart (1996)
2. R. Becker, M. Braack, *Multigrid techniques for finite elements on locally refined meshes*, Numerical Linear Algebra with Applications, vol 7, pp 373-379 (2000)
3. R. Becker and R. Rannacher, *An optimal control approach to error control and mesh adaptation in finite element methods*, Acta Numerica 2001 (A. Iserles, ed.), Cambridge University Press (2001)
4. L.C. Berselli, T. Iliescu and W.J. Layton, *Mathematics of Large Scale Simulation of Turbulent Flows*, Springer (2006)
5. M. Braack, *Adaptive finite elements for stationary compressible flows at low Mach number*, 8. Int. Conf. on Hyperbolic Problems: theory, numerics, applications, ed.: Freisthler and Warnecke, ISNM vol. 140, Birkhuser, p. 169-178 (2001)
6. M. Braack, T. Richter, *Solutions of 3D Navier-Stokes benchmark problems with adaptive finite elements*, Computers and Fluids, vol 35, no 4, pp 372-392 (2006)
7. M. Braack, T. Richter, *Stabilized finite elements for 3-D reactive flows*, Int. J. Numer. Meth. Fluids, 51, pp. 981-999 (2006)
8. A. Brandt, *Multigrid solvers on parallel computers*, Academic Press, New York (1981)
9. P.G. Ciarlet, *Finite Element Methods for Elliptic Problems*, North-Holland, Amsterdam (1978)
10. R. Becker, M. Braack, D. Meidner, T. Richter, B. Vexler, *The Finite Element Toolkit Gascoigne*, http://www.gascoigne.uni-hd.de
11. S. Griffies et al., *Ocean Modelling with MOM* , Clivar Exchanges, 12(3), 3-5, 13 (2007)
12. J.L. Guermond, P. Minev, Jie Shen *An overview of projection methods for incompressible flows*, Comput. Methods Appl. Mech. Engrg. 195, pp.6011-6045 (2006)
13. J. Pedlosky, *Geophysical Fluid Dynamics*, Springer (1986)
14. D. Olbers, *A Gallery of Simple Models from Climate Physics* Chorin Workshop on Stochastic Climate Models, Birkhäuser, pp. 3-63 (2001)

15. A. Prohl, *Projection and Quasi-Compressibility Methods for Solving the Incompressible Navier-Stokes Equations*, B.G. Teubner Stuttgart (1997)
16. R. Rannacher, *On Chorin's projection method for the incompressible Navier-Stokes Equations*, in The Navier-Stokes Equations II - Theory and Numerical Methods, pp.167-183, Springer Berlin/Heidelberg (1992)
17. T. Richter, *Parallel Multigrid Method for Adaptive Finite Elements with Application to 3D Flow Problems*, Doctoral Dissertation, University of Heidelberg (2005)
18. B. Schupp, *Entwicklung eines effizienten Verfahrens zur Simulation kompressibler Strömungen in 3D auf Parallelrechnern*, Doctoral Dissertation, University of Freiburg (1999)
19. C.A. Severijns, W. Hazeleger, *The efficient global primitive equation climate model SPEEDO* , Geosci. Model Dev. Discuss., 2. pp. 1115 - 1155 (2009)
20. Helics, *HEidelberg LInux Cluster System II*, http://helics.iwr.uni-heidelberg.de, 2007
21. J. Xu, *Iterative methods by space decomposition and subspace correction*, SIAM Review, vol 34, no 4, pp. 581 - 613 (1992)

Index

Bibliography

[AC00] M. Ainsworth and P. Coggins. The stability of mixed hp-finite element methods for Stokes flow on high aspect ratio elements. *SIAM J. Numer. Anal.*, 38:1721–1761, 2000.

[AF03] R.A. Adams and J.J. Fournier. *Sobolev spaces*. Pure and Apllied Mathematics. Academic Press, New York, 2003.

[AG94] C. Amrouche and V. Girault. Decomposition of Vector Spaces and Application to the Stokes problem in arbitrary dimension. *Csechoslovak Math. Journ.*, 44(119):109 – 140, 1994.

[AG01] P. Azerad and F. Guillén González. Mathematical justification of the hydrostatic approximation in the primitive equations of geophysical fluid dynamics. *SIAM J. Math. Anal.*, 33(4):847 – 859, 2001.

[AL94] T. Apel and G. Lube. Local inequalities for anisotropic finite elements and their applications to convection-diffusion problems, 1994. Preprint SPC94-26, TU Chemnitz-Zwickau.

[AM08] Th. Apel and G. Matthies. Non-conforming, anisotropic, rectangular finite elements of arbitrary order for the Stokes problem. *SIAM J. Numer. Anal.*, 46:1867–1891, 2008.

[Ape98] Th. Apel. Anisotropic Interpolation Error Estimates for Isoparametric Quadrilateral Finite Elements, 1998.

[Ape99] Th. Apel. Anisotropic finite elements: local estimates and applications, 1999.

[AR01] Thomas Apel and H. M. Randrianarivony. Stability of discretizations of the Stokes problem on anisotropic meshes, 2001.

[BB01] R. Becker and M. Braack. A finite element pressure gradient stabilization for the Stokes equations based on local projections. *CALCOLO*, 60(2):173 – 199, 2001.

[BB02] R. Becker and M. Braack. Solution of a stationary benchmark problem for natural convection with large temperature difference. *Int. J. Therm. Sci.*, 41:428–439, 2002.

[BB06] M. Braack and E. Burman. Local Projection Stabilization for the Oseen Problem and its Interpretation as a Variational Multiscale Method. *SIAM J. Numer. Anal.*, 43:2544–2566, January 2006.

[BBC+94] R. Barrett, M. Berry, T. F. Chan, J. Demmel, J. Donato, J. Dongarra, V. Eijkhout, R. Pozo, C. Romine, and H. Van der Vorst. *Templates for the Solution of Linear Systems: Building Blocks for Iterative Methods, 2nd Edition*. SIAM, Philadelphia, PA, 1994.

[BBJL07] M. Braack, E. Burman, V. John, and G. Lube. Stabilized finite element methods for the generalized Oseen problem. *Comput. Methods Appl. Mech. Eng.*, 196:853 – 866, 2007.

[BC08] S. Badia and R. Codina. Algebraic pressure segregation methods for the incompressible Navier-Stokes equations. *Archives of Computational Methods in Engineering*, 15:343–369, 2008.

[Bec95] R. Becker. An Adaptive Finite Element Method for the Incompressible Navier-Stokes Equations on Time-dependent Domains, 1995.

[BFH06] E. Burman, M.A. Fernández, and P. Hansbo. Continuous Interior Penalty Finite Element Method for Oseen's Equations. *SIAM J. Numer. Anal.*, 44:1248–1274, March 2006.

[BH06] E. Burman and P. Hansbo. Edge stabilization for the generalized Stokes problem: a continuous interior penalty method. *Comput. Methods Appl. Mech. Eng.*, 195(19-22):2393–2410, 2006.

[BL92] O. Besson and M.R. Laydi. Some estimates for the anisotropic Navier-Stokes equations and for the hydrostatic approximation. *Math. Modelling and Num. Anal. 26*, 7:855–865, 1992.

[BL09] M. Braack and G. Lube. Finite elements with local projection stabilization for incompressible flow problems. *Journal of Comput. Math.*, 27(2-3):116 – 147, 2009.

[Bla07] Jordi Blasco. An anisotropic pressure-stabilized finite element method for incompressible flow problems. *Computers and Mathematics with Applications*, 53(6):895 – 909, 2007.

[Bla08] Jordi Blasco. An anisotropic gls-stabilized finite element method for incompressible flow problems. *Comput. Meth. Appl. Mesh. Engrg.*, 197:3712 – 3723, 2008.

[BMP+06] Barnier B., G. Madec, T. Penduff, J.-M. Molines, A.-M. Treguier, J. Le Sommer, A. Beckmann, A. Biastoch, C. Böning, J. Dengg, C. Derval, E. Durand, S. Gulev, E. Remy, C. Talandier, S. Theetten, M. Maltrud, J. McClean, and B. De Cuevas. Impact of partial steps and momentum

advection schemes in a global ocean circulation model at eddy permitting resolution. *Ocean Dynamics*, 4, 2006.

[BP84] F. Brezzi and J. Pitkäranta. On the stabilization of finite element approximations of the Stokes equations. *W. Hackbusch (ed.), Notes on Numerical Fluid Mechanics: Efficient Solutions of Elliptic Systems*, 10, 1984.

[BR01] R. Becker and R. Rannacher. An optimal control approach to error control and mesh adaptation in finite element methods. *Acta Numerica 2001 (A. Iserles, ed.), Cambridge University Press*, 2001.

[Bra06] M. Braack. Anisotropic H1-stable projections on quadrilateral meshes. *Enumath 2005 Proc., eds.: Bermudez de Castro et al., Springer*, pages 495–503, 2006.

[Bra07] D. Braess. *Finite elements. Theory, fast solvers and applications in solid mechanics*. Cambridge: Cambridge University Press, 2007.

[Bra08a] M. Braack. A stabilized finite element scheme for the Navier-Stokes equations on quadrilateral anisotropic meshes. *ESAIM: Mathematical Modelling and Numerical Analysis*, pages 903–924, 2008.

[Bra08b] M. Braack. Local Projection Stabilization for the Oseen System on Anisotropic Cartesian Meshes. *Springer Heidelberg*, pages 441 – 448, 2008.

[BS11] M. Braack and F. Schieweck. Equal-order fininte elements with local projection stabilization for the Darcy-Brinkman equations. *Comp. Meth. Appl. Mech. Eng.*, 200:1126 – 1136, 2011.

[BSLB12] E. Behrens, F. U. Schwarzkopf, J. F. Lübbecke, and C. W. Böning. Model simulations on the long-term dispersal of 137 Cs released into the Pacific Ocean off Fukushima. *Environmental Research Letters*, 7(3):034004, 2012.

[BT06a] M. Braack and T.Richter. Local projection stabilization for the Stokes system on anisotropic quadrilateral meshes. *Enumath Proc. 2005, eds.: Bermudez de Castro et al., Springer*, 27(2-3):770 – 778, 2006.

[BT06b] M. Braack and T.Richter. Stabilized finite element for 3D reactive flows. *Intern. Journal for Numerical Methods in Fluids*, 51, Issue 9-10:981 – 999, 2006.

[Car86] D. Carlson. What are Schur Complements, Anyway? *Linear Algebra and its Applications*, 74(0):257 – 275, 1986.

[Cat61] L Cattabriga. Su un problema al contoro relativo al sistema di equazioni di Stokes. *Rend. Sem. Mat. Univ. Padova*, 31:308–340, 1961.

[CG00] T. Chacón Rebollo and F. Guillén González. An intrinsic analysis of existence of solutions for the hydrostatic approximation of Navier-Stokes equations. *Comptes Rendus de l'Academie des Sciences - Series I - Mathematics*, 330(9):841 – 846, 2000.

[CGS12] T. Chacón Rebollo, M. Gomez Marmol, and I. Sanchez Munoz. Numerical solution of the Primitive Equations of the ocean by the Orthogonal Sub-Scales VMS method. *Applied Numerical Mathematics*, 62(4):342 – 359, 2012. Third Chilean Workshop on Numerical Analysis of Partial Differential Equations (WONAPDE 2010).

[Cha] T. Chacón Rebollo. Numerical Approximation of Hydrodynamic Geophysical Flows.

[Cho68] A.J. Chorin. Numerical Solution of the Navier-Stokes Equations. *Mathematics of Computation*, 22(104):pp. 745–762, 1968.

[CLC00] T. Chacón Rebollo, R. Lewandowski, and E. Chacon Vera. Analysis of the hydrostatic approximation in oceanography with compression term. *ESAIM: Mathematical Modelling and Numerical Analysis*, 34:525–537, 2000.

[Con95] P. Constantin. A few results and open problems regarding incompressible fluids. *Notices Amer. Math. Soc.*, 42:658–663, 1995.

[CR02] T. Chacón Rebollo and D. Rodriguez Gomez. Prismatic finite element solution of the primitive equations of the ocean. Cours CEA-EDF-INRIA *Problemes Non Lineaires Appliques* Ecoulements peu profond a surface libre, 2002.

[CR04] T. Chacón Rebollo and D. Rodriguez Gomez. Numerical investigation of the regularity of the pressure for the primitve equations of the ocean. *Comput. Methods Appl. Mech. Engrg.*, 193:4457–4474, 2004.

[CRB11] B. Cushman-Roisin and J.-M. Beckers. *Introduction to Geophysical Fluid Dynamics. Physical and Numerical Aspects*. Academic Press, 2011.

[CRM03] C.Hu, R.Temam, and M.Ziane. The primitive equations on the large scale ocean under the small depth hypothesis. *Discrete and Contin. Dynam. Systems 9*, 1:97–131, 2003.

[CT07] C. Cao and E. Titi. Global Well-Posedness of 3D Primitive Equations. *Ann. Math. 166*, 1:245–267, 2007.

[CT08] C. Cao and E. Titi. Regularity Criteria for the three-dimensional Navier–Stokes Equations. *Indiana Univers. Mathem. J.*, 57(6):2643–2661, 2008.

[DB04] C. R. Dohrmann and P. B. Bochev. A stabilized finite element method for the Stokes problem based on polynomial pressure projections. *International Journal for Numerical Methods in Fluids*, 46:183 – 201, 2004.

[DG04] Ch. R. Doering and J. D. Gibbon. *Applied Analysis of the Navier-Stokes Equations*. Cambridge University Press, 2004.

[DHP03] I. Danaila, F. Hecht, and O. Pironneau. Simulation numerique en c++. *Dunod, Paris*, 2003.

[DKS04] S. Danilov, G. Kivman, and J. Schröter. A finite-element ocean model: principles and evaluation. *Ocean Modelling*, 6(2):125 – 150, 2004.

[Dob03] M. Dobrowolski. On the LBB constant on stretched domains. *Mathematische Nachrichten*, 254-255(1):64–67, 2003.

[dR60] G. de Rham. *Varietes Differentiables*. Hermann, 1960.

[DW89] J. Douglas and J. Wang. An Absolutely Stabilized Finite Element Method for the Stokes Problem. *Mathematics of Compuation*, 52(186):495 – 508, 1989.

[EG04] A. Ern and J.-L. Guermind. *Theory and Practice of Finite Elements*, volume 159. Springer, 2004.

[Fef] Ch. L. Fefferman. Existence and Smoothness of the Navier-Stokes Equation.

[FHS93] L.P. Franca, T.J.R. Hughes, and R. Stenberg. Stabilized finite element methods for the Stokes problem. *M.D. Gunzburger, R.A. Nicolaides(Eds.), Incompressible Computational Fluid Dynamics — Trends and Advantages, Cambridge University Press*, pages 87 – 107, 1993.

[FS02] S. Friedlander and D. Serre. *Handbuch for Mathematical Fluid Dynamics, Vol. 1/2*. North Holland: Amsterdam, 2002.

[GHPR07] S. Griffies, M.J. Harrison, R.C. Pacanowski, and A. Rosati. Ocean Modelling with MOM. *Clivar Exchanges*, 12(3), 3-5, 13, 2007.

[Gil82] A. E. Gill. *Atmosphere-ocean dynamics / Adrian E. Gill* . Academic Press, New York :, 1982.

[GMR01] F. Guillén González, N. Masmoudi, and M. A. Rodríguez Bellido. Anisotropic estimates and strong solutions of the Primitive Equations. *Diff. and Int. Eq.*, 14:1381–1408, 2001.

[GMS06] J.L. Guermond, P. Minev, and J. Shen. An overview of projection methods for incompressible flows. *Comput. Methods Appl. Mech. Engrg.*, 195:6011–6045, 2006.

[God79] K. Goda. A multistep technique with implicit difference schemes for calculating two- or three-dimensional cavity flows. *J. Comput. Phys.*, 30:76–95, 1979.

[GR86] V. Girault and P.-A. Raviart. *Finite Elements for the Navier Stokes Equations*. Springer Berlin, 1986.

[GR02] F. Guillén González and M.A. Rodríguez Bellido. On the strong solutions of the 2D Primitive Equations problem. *Nonlinear Analysis*, 50:621–646, 2002.

[GR04] F. Guillén González and M.A. Rodríguez Bellido. On the uniqueness and regularity of the Primitive Equations imposing additional anisotropic regularity. *Applied Mathematics Letters*, 18:783 – 789, 2004.

[GR05a] F. Guillén González and M.A. Rodríguez Bellido. A review on the improved regularity for the Primitive Equations. *Banach Center Publications*, 70:85 – 103, 2005.

[GR05b] F. Guillén González and D. Rodríguez Gómez. Bubble finite elements for the primitive equations of the ocean. *Numer. Math*, 2005.

[GS03a] J. L. Guermond and J. Shen. A new class of truly consistent splitting schemes for incompressible flows. *J. Comput. Phys.*, 192:262–276, 2003.

[GS03b] J. L. Guermond and J. Shen. Velocity-correction projectin methods for incompressible flows. *SIAM J. Numer. Anal.*, 41(1):112–134, 2003.

[GS04] J. L. Guermond and J. Shen. On the error estimates for the rotational pressure-correction projection methods. *Math. Comput.*, 73(248):1719–1737, 2004.

[Gue99] J. L. Guermond. Un resultat de convergence d'ordre deux en temps pour l'approximation des equations de Navier-Stokes par une technique de projection incrementale. *M2AN Math. Model. Numer. Anal.*, 30(1):169–189, 1999.

[Hac93] W. Hackbusch. *Iterative Lösung grosser schwachbesetzter Gleichungssysteme*. Teubner Verlag, 1993.

[Har02] Ph. Hartmann. *Ordinary Differential Equations*. Society for Industr. and Appl. Math., 2002.

[Her01] M. Hermann. *Numerische Mathematik*. Oldenbourg, 2001.

[HFB86] T. Hughes, L. Franca, and M. Balestra. A new finite element formulation for computational fluid dynamics: V. circumvent the Babuska-Brezzi condition: A stable Petrov-Galerkin formulation for the Stokes problem accommodating equal order interpolation. *Comput. Methods Appl. Mech. Engrg.*, 59:89–99, 1986.

[HK00] P. Hajlasz and P. Koskela. *Sobolev met Poincare*. Number 688. Memoirs of the American Mathematical Society, 2000.

[HR82] J.G. Heywood and R. Rannacher. Finite element approximation of the nonstationary Navier-Stokes problem. I. Regularity of solutions and second order error estimates for statial discretization. *SIAM J. Num. Anal.*, 19:275–311, 1982.

[Ist01] I.V. Istratescu. *Fixed Point Theory: An Introduction*. D. Reidel Publiching Company, 2001.

[JM86] J.-M.Ghidalaglia. On the fractal dimension of attractors for viscous incompressible fluid flows. *SIAM J. Math. Anal.*, 17(5):1139–1157, 1986.

[Jos98] J. Jost. *Partielle Differentialgleichungen: Elliptische (und parabolische) Gleichungen*. Springer, 1998.

[KB12] M. Kimmritz and M. Braack. Equal-order finite elements for the hydrostatic Stokes problem. *Computational Methods in Applied Mathematics*, 12:306–329, 2012.

[Kim12] M. Kimmritz. Symmetric Stabilization of Equal-Order Finite Element Discretized Hydrostatic Flow Problems. submitted, 2012.

[KOI91] G.E. Karniadakis, S.A. Orszag, and M. Israeli. High-order splitting methods for the incompressible Navier-Stokes equations. *J. Comput. Phys.*, 97:414–43, 1991.

[KR11] M. Kimmritz and Th. Richter. Parallel multigrid method for finite element simulations of complex flow problems on locally refined meshes. *Numerical Linear Algebra with Applications*, 18(4):615–636, 2011.

[Lad69] O.A. Ladyzhenskaya. *Mathematical Theory of Viscous Incompressible Flow*. Gordon and Breach, New York, 2nd, english translation edition, 1969.

[LAK06] G. Lube, Th. Apel, and T. Knopp. Stabilized Finite Element Methods with Anisotropic Mesh Refinement for the Oseen problem. *Int. Conference on Boundary and Interior Layers BAIL*, 2006.

[Lat11] Mojib Latif. Uncertainty in climate change projections. *Journal of Geochemical Exploration*, 110: Sustainability of Geochemical Cycling, 19th International Symposium on Environmental Biogeochemistry "Environmental Changes and Sustainability of Biogeochemical Cycling"(1):1–7, 2011.

[LBC+98] S. Levitus, T.P. Boyer, M.E. Conkright, T. O' Brien, C. Stephens J. Antonov and, L. Stathoplos, D. Johnson, and R. Gelfeld. *NOAA Atlas NESDIS 18, World Ocean Database 1998: VOLUME 1: INTRODUCTION*. U.S. Gov. Printing Office, Wash., D.C., 1998.

[Ler33] J. Leray. Etude de diverses quations intgrales non linaires et de quelques problmes que pose l'hydrodynamique. *J. Math. Pures Appl.*, 12:1–82, 1933.

[LQ86] U. Langer and W. Queck. On the convergence factor of Uzawa's algorithm. *Journal of Computational and Applied Mathematics*, 15(2):191 – 202, 1986.

[LR02] P.G. Lemarie-Rieusset. *Recent Developments in the Navier-Stoeks problem*. Chapman & Hall, 2002.

[LTW92] J.L. Lions, R. Temam, and S. Wang. On the equations of the large scale ocean. *Nonlinearity*, 5:1007–1053, 1992.

[Mei11] A. Meister. *Numerik linearer Gleichungssysteme: Eine Einführung in moderne Verfahren*. Vieweg + Teubner Verlag, 4 edition, 2011.

[MPP02] St. Micheletti, S. Perotto, and M. Picasso. Some remarks on the stability coefficients and bubble stabilization of FEM on anisotropic meshes, 2002.

[MS02] P. Ming and Z.-C. Shi. Quadrilateral mesh revisited. *Comput. Methods Appl. Mech. Engrg.*, 191:5671–5682, 2002.

[MSB+04] J. M. Murphy, D. M. H. Sexton, D. N. Barnett, G. S. Jones, M. J. Webb, M. Collins, and D. A. Stainforth. Quantification of modelling uncertainties in a large ensemble of climate change simulations. *Nature*, 430:768 – 772, 2004.

[MST07] G. Matthies, P. Skrzypacz, and L. Tobiska. A unified convergence analysis for local projection stabilizations applied to the Oseen problem. *M2AN Math. Model. Numer. Anal.*, 41:713–742, 2007.

[NP05] R.H. Nochetto and J.-H. Pyo. The Gauge-Uzawa Finite Element Method. Part I: The Navier-Stokes Equations. *SIAM J. Numer. Anal.*, 43:1043–1068, March 2005.

[Oue81] D. V. Ouellette. Schur complements and statistics. *Linear Algebra and its Applications*, 36(0):187 – 295, 1981.

[OWE12] D. Olbers, J. Willebrand, and C. Eden. *Ocean Dynamics*. Springer, 2012.

[Ped86] J. Pedlosky. *Geophysical Fluid Dynamics*. Springer, 1986.

[Pet65] W.V. Petryshyn. Constructional proof of Lax-Milgram Lemma and Its Application to Non-K-P.D. Abstract and Differential Operator Equations. *J.SIAM Numer. Anal. Ser. B*, 2(3):404 – 420, 1965.

[Pro97] A. Prohl. *Projection and Quasi-Compressibility Methods for Solving the Incompressible Navier-Stokes Equations*. B.G. Teubner Stuttgart, 1997.

[Pro08] Andreas Prohl. On Pressure Approximation via Projection Methods for Nonstationary Incompressible Navier-Stokes Equations. *SIAM J. Numer. Anal.*, 47(1):158–180, October 2008.

[PTW04] M. Petcu, R. Temam, and D. Wirosoetisno. Existence and regularity results for the primitive equations in two space dimensions. *Communications on Pure and Applied Analysis (CPAA)*, 3:115 – 131, 2004.

[Ran92] R. Rannacher. On Chorin's projection method for the incompressible Navier-Stokes Equations. *The Navier-Stokes Equations II - Theory and Numerical Methods, Springer Berlin/Heidelberg*, pages 167 – 183, 1992.

[Ric05] T. Richter. Parallel Multigrid Method for Adaptive Finite Elements with Application to 3D Flow Problems. Doctoral Dissertation, University of Heidelberg, 2005.

[RJ08] T. Reichler and K. Junsu. How Well Do Coupled Models Simulate Today's Climate? *Bulletin of the American Meteorological Society*, 89(3):303–311, 03/2008 2008.

[RST08] H.-G. Roos, M. Stynes, and L. Tobiska. *Robust Numerical Methods for Singularly Perturbed Differential Equations – Convection-Diffusion-Reaction and Flow Problems*, volume 24. Springer Series in Computational Mathematics, 2nd edition, 2008.

[Saa03] Y. Saad. *Iterative methods for sparse linear systems*. SIAM, 2003.

[Sca67] H. Scarf. The Approximation of Fixed Points of a Continuous Mapping. *SIAM J. Appl. Math.*, 15(5):1328 – 1343, 1967.

[SDT06] P. Sagaut, S. Deck, and M. Terracol. *Multiscale and Multiresolution Approaches in Turbulence*. Imperial College Press, 2006.

[Ser63] J. Serrin. The initial value problem for the Navier-Stokes equations. *Nonlinear Problems, R.E. Langer ed.*, pages 69–98, 1963.

[SH09] C.A. Severijns and W. Hazeleger. The efficient global primitive equation climate model SPEEDO. *Geosci. Model Dev. Discuss.*, 2:1115 – 1155, 2009.

[She92] J. Shen. On error estimates of the projection methods for the Navier-Stokes equations: first-order schemes. *SIAM J. Numer. Anal*, 29:57–77, 1992.

[She96] J. Shen. On error estimates of the projection methods for the Navier-Stokes equations: second-order schemes. *Math. Comp.*, 65(215):1039 – 1065, 1996.

[Sma63] J. Smagorinsky. General circulation experiments with the primitive equations. i. the basic experiment. *Mon. Wea. Rev.*, 91:99 – 164, 1963.

[Soh01] H. Sohr. *The Navier-Stokes equations. An Elementary Functional Analytic Approach*. Birkhäuser Verlag, Basel, 2001.

[Sol68] V.A. Solonnikov. Estimates for solutions of a non-stationary linearized system of Navier-Stokes equations. *A.M.S. Translations*, 75:1–116, 1968.

[Son09] T. Sonar. *Turbulenzen um die Fluidmeshanik*. Spektrum der Wissenschaft Verlagsgesellschaft mbH, 2009.

[SS98] D. Schötzau and C. Schwab. Mixed hp-FEM on anisotropic meshes. *Math. Models Methods Appl. Sci.*, 8:787–820, 1998.

[SSS99] D. Schötzau, C. Schwab, and R. Stenberg. Mixed hp-FEM on anisotropic meshes II: Hanging nodes and tensor products of boundary layer meshes. *Numer. Math.*, 83:667 – 697, 1999.

[Tem68] R. Temam. Une méthode d'approximation de la solution des équations de Navier-Stokes. *Bulletin de la S.M.F.*, 96:115–152, 1968.

[Tem69] R. Temam. Sur L'approximation de la solution des equations de Navier-Stokes par la methode des pas fractionaires ii. *Arch. Rat. Mech. Anal.*, 33:377–385, 1969.

[Tem79] R. Temam. *Navier-Stokes Equations. Theory and Numerical Analysis*. North Holland, 1979.

[Tem00] R. Temam. Some developments on Navier-Stokes equations in the second half of the 20th century. *Development of Mathematics 1950-2000, Birkhäuser, Basel*, pages 1049–1106, 2000.

[TMV96] L.J.P. Timmermans, P.D. Minev, and F.N. Van De Vosse. An approximate projection scheme for incompressible flow using spectral elements. *Int. J. Numer. Methods Fluids*, 22:673–688, 1996.

[TS01] A. Toselli and C. Schwab. Mixed hp-finite element approximations on geometric edge and boundary layer meshes in three dimensions. *SAM Report 2001-02, ETH Zürich*, 2001.

[Ver00] F. Verhulst. *Nonlinear Differential Equations and Dynamical Systems*. Springer, 2000.

[vK86] J. van Kan. A second-order accurate pressure-correction scheme for viscous incompressible flow. *SIAM J. Sci. Stat. Comput.*, 7:870–891, 1986.

[Wan10] K. Wannert. *Stabilie Algorithmem für die Magnetotomographi an Brennstoffzellen*. Forschumszentrum Jülich, 2010.

[WCd+11] M. Wade, G. Caniaux, Y. duPenhoat, M. Dengler, H. Giordani, and R. Hummels. A one-dimensional modeling study of the diurnal cycle in the equatorial Atlantic at the PIRATA buoys during the EGEE-3 campaign. *Ocean Dynamics*, 61:1–20, 2011.

[Wer05] D. Werner. *Funktionalanalysis*. Springer, 5th, extended edition, 2005.

[Yos80] K. Yoshida. *Functional Analysis*. Springer, 1980.

[Zia95] M. Ziane. Regularity results for Stokes type systems. *Applicable Analysis*, 58:263–292, 1995.

[Zia97] M. Ziane. Regularity results for the stationary primitive equations of the atmosphere and the ocean. *Nonlinear Anal.*, 28(2):289–313, January 1997.

Acknowledgements

This work has partially been supported by the DFG Excellence Cluster "Future Ocean" within the mini-proposal CP0721.

First of all I'd like to thank Prof. Dr. Malte Braack for the possibility to work on this interesting topic belonging to the challenging field of climate research, as well as for enabling the participations in conferences in Kiel and abroad, not forgetting for the assured financing throughout the entire time. Regarding the financial support I'd like to mention the great opportunity to give lessons in different fields of mathematics.

Further, I'd like express deep gratidute to Thomas Richter for always being welcome with my questions, the engaged answering of those, and the reading of my manuscript.

As well, my thanks are addressed to Prof. Dr. Steffen Börm for helpful discussions and to his team for the possibility to participate in students research activities taking place in this group.

Moreover, I'd like to thank Benjamin and Nico for the possibility of discussions.

The numerical examples have been implemented using the software library *gascoigne*. Thanks to Malte Braack, Roland Becker, Dominik Meidner, Thomas Richter and Boris Vexler for development, maintenance and enabling the work with this library.

Thomas Apel, Francisco Guillen, Isabel Munoz and Edriss Titi are thanked for the willing answering of my inquiries. I'd moreover like to thank Dudley Chelton for the kind permission to use his figure on the scales of oceanic processes.

For their great offering of the vast variety of courses not only concerning the oceanic issue I'd like to thank the organizors of the Integrated School of Ocean Sciences (ISOS).

In addition, I heartly thank the team of "Ocean circulation and climate dynamics" at the IfM Geomar for always being a welcome guest. In particular, I express my gratitude to Erik Behrens for lots of talks on physical issues, for the enduring answering my questions and for reading the physical concerns of this work.

For well-meaningness and carefree talks, also in stressing times, I'd like to thank Martin and Stephan. As well, my thanks are addressed to Ulrike Zander for the brightening little somethings.

Enabling nice times beside university I'd like to thank Petra for the nice coffee breaks, Gerhard for being there, anytime, Franziska and Erik inter alia for the refreshing mornings, Thorsten and Frank for the refreshing evenings, Olav for the enlightning in a dark moment, Daniel for the encouragements, as well as the Uni BigBand Kiel for their colorful notes. Claudia, Thomas, Stef, Barbara and André I would like to thank for being friends and family.
Last but not least, I heartfelty thank Tom and Doreen Rother for their inspirings, confidences and lots more.

Eidesstattliche Erklärung

Hiermit bestätige ich, dass die Abhandlung - abgesehen von der Beratung durch den Betreuer Prof. Dr. M. Braack - nach Form und Inhalt meine eigene Arbeit ist.

Die vorliegende Arbeit hat keiner anderen Stelle im Rahmen eines Prüfungsverfahrens vorgelegen. Teile der Arbeit sind wie folgt veröffentlicht beziehungsweise eingereicht:

- *Equal-order finite elements for the hydrostatic Stokes problem*
  Autoren: Madlen Kimmritz, Malte Braack
  Journal: Computational Methods in Applied Mathematics **12**(3)
  Jahr: 2012 (veröffentlicht)

- *Parallel multigrid method for finite element simulations of complex flow problems on locally refined meshes*
  Autoren: Madlen Kimmritz, Thomas Richter
  Journal: Numerical Linear Algebra with Applications **18** (4)
  Jahr: 2011 (veröffentlicht)

- *Symmetric Stabilization of Equal-Order Finite Element Discretized Hydrostatic Flow Problems*
  Autor: Madlen Kimmritz
  Journal: Computer Methods in Applied Mechanics and Engineering
  (eingereicht)

Die vorliegende Arbeit ist unter Einhaltung der Regeln guter wissenschaftlicher Praxis der Deutschen Forschungsgemeinschaft entstanden.

Ort, Datum	Madlen Kimmritz